

A STUDY OF COMPUTER MODELING  
FORMULATION AND SPECIAL ANALYTICAL  
PROCEDURES FOR EARTHQUAKE  
RESPONSE OF MULTISTORY BUILDINGS

A Report to the  
National Science Foundation

by

Carl F. Neuss  
Bruce F. Maison  
Jack G. Bouwkamp

J.G. BOUWKAMP, INC.  
Berkeley, California

January 1983

Any opinions, findings, conclusions  
or recommendations expressed in this  
publication are those of the author(s)  
and do not necessarily reflect the views  
of the National Science Foundation.



<b>REPORT DOCUMENTATION PAGE</b>	<b>1. REPORT NO.</b> NSF/CEE-83006	<b>2.</b>	<b>3. Recipient's Accession No.</b> PB83-204339
<b>4. Title and Subtitle</b> Study of Computer Modeling Formulation and Special Analytical Procedures for Earthquake Response of Multistory Buildings			<b>5. Report Date</b> January 1983
<b>7. Author(s)</b> C.F. Neuss, B.F. Maison, J.G. Bouwkamp			<b>6.</b>
<b>9. Performing Organization Name and Address</b> J.G. Bouwkamp, Inc. 1930 Shattuck Avenue Berkeley, CA 94704			<b>8. Performing Organization Rept. No.</b>
<b>12. Sponsoring Organization Name and Address</b> Directorate for Engineering (ENG) National Science Foundation 1800 G Street, N.W. Washington, DC 20550			<b>10. Project/Task/Work Unit No.</b>
<b>15. Supplementary Notes</b> Submitted by: Communications Program (OPRM) National Science Foundation Washington, DC 20550			<b>11. Contract(C) or Grant(G) No.</b> (C) (G) CEE7926734
<b>16. Abstract (Limit: 200 words)</b> The results of correlative analytical studies performed on five multistory buildings located in seismically active regions of the United States are presented. Several models of each building are formulated to assess the influence of various structural and nonstructural modeling aspects on dynamic properties and seismic response. Aspects such as two-dimensional versus three-dimensional frame modeling, rigid joint zone effects, participation of secondary framing systems, nonstructural slab-girder interaction, infill block walls, and mass modeling variations are considered. Effects of different modeling approaches on analytical results are evaluated and the relative importance of various modeling reinforcements is noted. It is determined that the natural periods and mode shapes determined from small amplitude vibration tests can be accurately predicted using practical analytical modes of limited complexity based upon the actual detailed physical characteristics of the building. Modeling various secondary features such as core frame systems is found to be important in predicting accurate small amplitude periods. It is noted that although the fundamental mode is generally the primary contributor to earthquake response of multistory buildings, the contributions of higher modes are also significant.			<b>13. Type of Report &amp; Period Covered</b>
<b>17. Document Analysis a. Descriptors</b> Earthquake resistant structures Dynamic structural analysis Computer programs Buildings  <b>b. Identifiers/Open-Ended Terms</b> Los Angeles (California) San Francisco (California) Seattle (Washington) SUPER-ETABS computer program  <b>c. COSATI Field/Group</b>			<b>14.</b>
<b>18. Availability Statement</b> NTIS			<b>19. Security Class (This Report)</b>
			<b>20. Security Class (This Page)</b>
			<b>21. No. of Pages</b> 455
			<b>22. Price</b>



## ABSTRACT

This report is intended to serve as a reference for practicing engineers involved in computer seismic analysis of multistory buildings. The purposes of the study reported herein are: (1) to summarize the methodology underlying current state-of-the-art in practical seismic analysis of buildings; (2) to investigate the degree to which practical mathematical models of limited complexity can accurately reflect true dynamic properties; (3) to identify the general dynamic characteristics of multistory buildings and show how these contribute to response induced by earthquakes; (4) to assess the influence of various detailed modeling aspects on the prediction of dynamic properties and analytical response; (5) to compare earthquake response based on dynamic theory with "equivalent static" response based on lateral load provisions as recommended by current building codes; and (6) to develop and apply special analytical techniques which lead to improved seismic response predictions of multistory buildings.

This report presents the results of correlative analytical studies performed on the following five multistory buildings located in seismically active regions of the United States: the Alcoa Building (San Francisco), the Transamerica Building (San Francisco), the University of California Medical Center Building (San Francisco), the Ranier Tower Building (Seattle), and the Century City Theme Tower Building (Los Angeles). Each of these structures has been the subject of a previous study in which the building's actual dynamic characteristics were established by experimental testing. The results of the previous studies have been used as a data base for developing numerical models that reflect the observed linear dynamic properties. In this study, each of these buildings has been extensively reanalyzed. Several models of each building have been formulated to assess the influence of various structural and nonstructural modeling

aspects on dynamic properties and seismic response. Aspects such as two-dimensional versus three-dimensional frame modeling, rigid joint zone effects, participation of secondary framing systems, nonstructural slab-girder interaction, infill block walls, and mass modeling variations are considered. The effects of different modeling approaches on analytical results are evaluated and the relative importances of various modeling refinements are identified.

In addition, the following three special topics of interest for multistory building analysis are addressed: (1) a formulation to account for the  $P-\Delta$  effect in dynamic or static seismic analysis; (2) the comparative performance of different modal combination schemes for response spectrum analysis applications; and (3) a procedure for performing approximate dynamic analysis for use in preliminary design based on the actual dynamic properties of the different multistory buildings studied. For each of these topics one of the study buildings is used to illustrate application of the respective analytical techniques.

In carrying out the objectives of this study, it has been necessary to perform several modifications to the ETABS computer analysis program. In order to make the modified program available to practicing engineers, this enhanced version of the ETABS program has been developed and documented as part of this project.

### ACKNOWLEDGEMENT

The funding for this work was provided by the National Science Foundation under Grant PFR-7926734. This support is most gratefully acknowledged.

The authors acknowledge the efforts of Mr. Steve Eder and Mr. Kazuhiko Kasai in performing much of the detailed analyses supporting this study. The authors are most appreciative of the contributions of Mr. John Skilling and Mr. Robert St. Germain of Skilling, Helle, Christiansen and Robertson, Engineers, Inc., Dr. Alex Tarics of Reid and Tarics Associates, Mr. Eric Tryde of Skidmore, Owings and Merrill, Inc., and Mr. Dennis Oh of Chin and Hensolt, Inc. in providing the interest and materials necessary for this work. Consultations with Prof. Edward L. Wilson of the University of California at Berkeley are gratefully acknowledged. Also, the authors would like to thank Ms. Martha Ashton for her diligent efforts in preparing the manuscript and Ms. Elsa Calero for her services in preparing the graphics for this report.

INTENTIONALLY BLANK

## TABLE OF CONTENTS

CHAPTER/ SECTION	TITLE	PAGE
	ABSTRACT . . . . .	i
	ACKNOWLEDGEMENT . . . . .	iii
	TABLE OF CONTENTS . . . . .	v
1	PROJECT OVERVIEW . . . . .	1
1.1	BACKGROUND AND OBJECTIVES . . . . .	1
1.2	USE OF EXPERIMENTAL STUDIES AS A BASIS FOR CORRELATIVE ANALYSIS . . . . .	3
1.3	PRACTICAL SEISMIC ANALYSIS OF BUILDINGS . .	4
1.4	COMPUTER PROGRAM DEVELOPMENT . . . . .	6
1.5	DOCUMENT ORGANIZATION . . . . .	6
2	APPLICATION OF THE RESPONSE SPECTRUM APPROACH AND LINEAR ELASTIC MODELING FOR SEISMIC ANALYSIS OF BUILDINGS . . . . .	9
2.1	INTRODUCTION . . . . .	9
2.2	DEVELOPMENT OF EARTHQUAKE RESPONSE SPECTRA . . . . .	11
2.2.1	Development of Response Spectra from Earthquake Records . . . . .	11
2.2.2	Development of Smoothed Design Response Spectra . . . . .	13
2.2.3	Development of Site Specific Response Spectra . . . . .	20
2.3	BACKGROUND ON THE APPLICATION OF RESPONSE SPECTRA FOR SEISMIC DESIGN OF BUILDINGS. .	23
2.4	BACKGROUND ON THE APPLICATION OF LINEAR ELASTIC STRUCTURAL MODELING FOR EARTHQUAKE RESPONSE . . . . .	29
2.5	INFLUENCE OF STIFFNESS AND MASS UNCERTAINTIES ON RESULTS OF RESPONSE SPECTRUM ANALYSIS . . . . .	34
	Tables and Figures . . . . .	45
3	ANALYTICAL STUDIES OF THE EARTHQUAKE RESPONSE OF SEVERAL MULTISTORY BUILDINGS BASED ON EXPERIMENTALLY DETERMINED DYNAMIC CHARACTERISTICS . . . . .	61

3.1	INTRODUCTION . . . . .	61
3.1.1	Scope and Purpose . . . . .	61
3.1.2	Approach Used for Analyses of the Study Buildings . . . . .	65
3.1.3	Computer Programs Used for Structural Analysis . . . . .	72
	Figures . . . . .	74
3.2	ALCOA BUILDING . . . . .	77
3.2.1	Description of the Structural System . . . . .	77
3.2.2	Results of Experimental Studies . . . . .	78
3.2.3	Description of Analytical Models . . . . .	80
3.2.4	Comparison of Analytical and Experimental Dynamic Properties . . . . .	82
3.2.5	Influence of Modeling Approach on Design Quantities . . . . .	84
3.2.6	Comparison of Dynamic Analyses and Code Equivalent Static Procedures . . . . .	88
3.2.7	Comparison of Code Design Forces with Dynamic Forces Induced by Actual Earthquake Spectra . . . . .	91
3.2.8	Summary . . . . .	92
	Tables and Figures . . . . .	96
3.3	TRANSAMERICA BUILDING . . . . .	127
3.3.1	Description of the Structural System . . . . .	127
3.3.2	Results of Experimental Studies . . . . .	128
3.3.3	Description of Analytical Models . . . . .	130
3.3.4	Comparison of Analytical and Experimental Dynamic Properties. . . . .	134
3.3.5	Influence of Modeling Approach on Design Quantities . . . . .	137
3.3.6	Comparison of Dynamic Analyses and Code Equivalent Static Procedures . . . . .	141
3.3.7	Comparison of Code Design Forces with Dynamic Forces Induced by Actual Earthquake Spectra . . . . .	144
3.3.8	Summary . . . . .	145
	Tables and Figures . . . . .	149
3.4	UNIVERSITY OF CALIFORNIA MEDICAL CENTER BUILDING . . . . .	169
3.4.1	Description of the Structural System . . . . .	169
3.4.2	Results of Experimental Studies . . . . .	171
3.4.3	Description of Analytical Models . . . . .	174
3.4.4	Comparison of Analytical and Experimental Dynamic Properties. . . . .	177
3.4.5	Influence of Modeling Approach on Design Quantities . . . . .	180
3.4.6	Comparison of Dynamic Analyses and Code Equivalent Static Procedures . . . . .	183
3.4.7	Comparison of Code Design Forces with Dynamic Forces Induced by Actual Earthquake Spectra . . . . .	185
3.4.8	Summary . . . . .	187
	Tables and Figures . . . . .	190

3.5	RAINIER TOWER BUILDING . . . . .	213
3.5.1	Description of the Structural System . . .	213
3.5.2	Results of Experimental Studies . . . . .	214
3.5.3	Description of Analytical Models . . . . .	216
3.5.4	Comparison of Analytical and Experimental Dynamic Properties. . . . .	220
3.5.5	Influence of Modeling Approach on Design Quantities . . . . .	223
3.5.6	Comparison of Dynamic Analyses and Code Equivalent Static Procedures . . .	228
3.5.7	Comparison of Code Design Forces with Dynamic Forces Induced by Actual Earthquake Spectra . . . . .	231
3.5.8	Summary . . . . .	233
	Tables and Figures . . . . .	236
3.6	CENTURY CITY THEME TOWER BUILDING . . . . .	255
3.6.1	Description of the Structural System . . .	255
3.6.2	Results of Experimental Studies . . . . .	257
3.6.3	Description of Analytical Models . . . . .	259
3.6.4	Comparison of Analytical and Experimental Dynamic Properties. . . . .	262
3.6.5	Influence of Modeling Approach on Design Quantities . . . . .	265
3.6.6	Comparison of Dynamic Analyses and Code Equivalent Static Procedures . . .	269
3.6.7	Comparison of Code Design Forces with Dynamic Forces Induced by Actual Earthquake Spectra . . . . .	272
3.6.8	Summary . . . . .	273
	Tables and Figures . . . . .	277
3.7	OBSERVATIONS AND CONCLUSIONS FROM THE CORRELATIVE ANALYTICAL STUDIES . . . . .	303
3.7.1	Period and Mode Shape Correlation . . . . .	303
3.7.2	Comparative Dynamic Properties of the Study Buildings . . . . .	305
3.7.3	Influence of Secondary Modeling Aspects on Stiffness Properties . . . . .	308
3.7.4	Influence and Interpretation of Secondary Modeling Aspects on Seismic Response Analysis . . . . .	311
3.7.5	Relative Significance of Various Modes on Seismic Response . . . . .	314
3.7.6	Comparison of ATC and UBC Period Estimates with Experimental and Analytical Results . . . . .	317
3.7.7	Comparative Magnitudes of Selected Response Spectrum Dynamic and Code Equivalent Static Loading Procedures . . . . .	319
3.7.8	Comparative Seismic Response Distributions for Dynamic and Code Equivalent Static Loading Procedures . . . . .	323
	Tables and Figures . . . . .	327

4	SELECTED TOPICS RELATING TO ANALYTICAL PROCEDURES FOR EARTHQUAKE RESPONSE OF MULTISTORY BUILDINGS . . . . .	333
4.1	ANALYSIS FOR P- $\Delta$ EFFECTS IN SEISMIC RESPONSE OF BUILDINGS. . . . .	335
4.1.1	Introduction . . . . .	335
4.1.2	Linear Analysis Approach . . . . .	336
4.1.3	Torsional P- $\Delta$ Effect . . . . .	344
4.1.4	Application of P- $\Delta$ Analysis in Design . . . . .	347
4.1.5	Results of Example Analyses . . . . .	350
4.1.6	Summary and Conclusions . . . . .	353
	Tables and Figures . . . . .	356
4.2	THE COMPARATIVE PERFORMANCE OF MODAL COMBINATION RULES IN RESPONSE SPECTRUM ANALYSIS . . . . .	363
4.2.1	Introduction . . . . .	363
4.2.2	Response Spectrum Modal Combination Rules . . . . .	364
4.2.3	Building Models Used for Example Analyses . . . . .	370
4.2.4	Earthquake Inputs Used for Example Analyses . . . . .	372
4.2.5	Results from Regular Building Analyses . . . . .	372
4.2.6	Results from Irregular Building Analyses . . . . .	374
4.2.7	Summary and Conclusions . . . . .	378
	Tables and Figures . . . . .	382
4.3	A METHOD FOR PERFORMING APPROXIMATE SEISMIC ANALYSIS OF MULTISTORY BUILDINGS . . . . .	401
4.3.1	Introduction . . . . .	401
4.3.2	Matrix Relationships for Gross Response Calculation Based on Dynamic Properties . . . . .	403
4.3.3	Observed Dynamic Properties of Actual Buildings . . . . .	408
4.3.4	Comparison with Uniform Shear Beam Idealization . . . . .	410
4.3.5	Development of Empirical Mode Shapes . . . . .	412
4.3.6	Example Analyses . . . . .	416
4.3.7	Summary and Conclusions. . . . .	423
	Tables and Figures . . . . .	425
5	GENERAL SUMMARY AND CONCLUSIONS . . . . .	439
	REFERENCES . . . . .	449

**INTENTIONALLY BLANK**

Page Intentionally Left Blank

# CHAPTER 1

## PROJECT OVERVIEW

### 1.1 BACKGROUND AND OBJECTIVES

Over the past two decades, significant advancements in the study of dynamic behavior of structures and in the field of earthquake seismology have been made. During this same period, there has been a rapid growth in computer technology and the application of this technology in the solution of engineering problems. Armed with an improved understanding of the earthquake phenomenon, a greater knowledge of complex structural behavior and the computational power of the computer, the structural engineering profession has moved steadily toward a more exacting and deterministic approach in the aseismic design of multistory buildings. In the past, aseismic design of buildings has been carried out using relatively simple methods for establishing earthquake loading and performing structural analyses based on equivalent static procedures as specified by building codes. However, current building design practice often requires more precise determination of local seismicity and critical ground motion characteristics, development of detailed numerical models for representing structural behavior, and application of advanced dynamic analysis techniques using sophisticated computer programs.

Although the use of more advanced analysis techniques and more representative descriptions of earthquake excitations generally lead to improved accuracy in predicting structural response, several difficulties arise in the implementation of these procedures for practical design. Often, the design engineer lacks background in the specialities of structural dynamics and earthquake seismology and, therefore, has difficulty understanding analysis procedures and interpreting results. This difficulty is further amplified by the apparent inconsistencies that exist between traditional codebook

working stress design criteria used with equivalent static analysis procedures and newer inelastic design criteria often used with dynamic analysis procedures. Also, because of the need for development of a numerical model of the building which closely reflects actual behavior, it may be necessary to include certain detailed modeling aspects which are generally not considered by the engineer in the structural design process. The design engineer may lack experience in assessing the relative importance of these aspects or may overlook their potential significance in affecting dynamic response predictions.

In order to assist the engineer in overcoming these difficulties, guidelines for performing seismic structural analysis by computer have been published (43) which outline the general mathematical formulations of the structural dynamics problem, give general descriptions of different analytical techniques, point out potentially significant modeling considerations, and review pertinent technical terminology. However, the information supplied by these general guidelines gives little insight into the dynamic behavior of actual structures and does not demonstrate the application of specific modeling and analytical techniques which best predict actual behavior. The purpose of this report is to provide a further reference which will serve as an aid to engineers in the development of computer models and in the interpretation of analytical results relating to the dynamic seismic analysis of multistory building systems. The objectives of the study reported herein are:

- (1) to summarize the methodology underlying current state-of-the-art in practical seismic analysis of buildings;
- (2) to investigate the degree to which practical mathematical models of limited complexity can accurately reflect the true linear dynamic properties of multistory buildings;
- (3) to identify general dynamic characteristics of multistory

buildings and show how these contribute to response induced by earthquakes;

- (4) to assess the influence of various detailed modeling aspects on the predictions of dynamic properties and analytical response;
- (5) to compare earthquake response based on dynamic theory with "equivalent static" response based on lateral load provisions as recommended by current building codes; and
- (6) to develop and apply special analytical techniques which lead to improved seismic response predictions of multistory buildings.

## **1.2 USE OF EXPERIMENTAL STUDIES AS A BASIS FOR CORRELATIVE ANALYSIS**

The foremost objective in the development of computer models of buildings for seismic analysis is to accurately represent actual building behavior. In this respect, comparison of experimental results obtained from full-scale ambient and forced vibration tests with analytically predicted results provide a valuable basis for evaluation of computer analysis procedures. During the last twenty years, ambient and forced vibration studies have been performed on a number of different multistory buildings (29, 31, 32, 39, 40) in which the small amplitude dynamic properties of the respective buildings were determined. The existence of this data base of experimental findings offers a unique opportunity to evaluate modeling procedures and analytical techniques that may be applied in seismic analysis of buildings.

In this study, the results of the previous experimental work are used as a basis for developing numerical models which reflect the observed dynamic properties of the following five study buildings:

1. ALCOA BUILDING, San Francisco (32)
2. TRANSAMERICA BUILDING, San Francisco (39)
3. UNIVERSITY OF CALIFORNIA MEDICAL CENTER, San Francisco (31)
4. RANIER TOWER BUILDING, Seattle (40)
5. CENTURY CITY THEME TOWER BUILDING, Los Angeles (29)

All five of the study buildings are of steel framed construction and range from 15 to 60 stories in height. Significant differences in design features exist among the buildings. Although all of the buildings studied are of steel construction, their behaviors are believed to be representative of multistory buildings having reinforced concrete frame construction as well. However, it should be noted that the behavior of these buildings is not necessarily representative of low-rise buildings nor multistory shear wall buildings.

### **1.3 PRACTICAL SEISMIC ANALYSIS OF BUILDINGS**

The overall approach used in this study is aimed at assisting the engineer/analyst in performing practical seismic analysis of building systems. In keeping with this objective, the methods used are intended to be representative of the current state-of-the-art analysis approaches as applied by practicing engineers for which certain fundamental analytical assumptions are commonly made.

For most buildings, inelastic response may be expected to occur during a major earthquake. Although nonlinear inelastic analysis programs are available, these are rarely employed because: (1) their proper use often requires the analyst to have special background and training; (2) results produced are difficult to interpret and apply to traditional design criteria; and (3) the costs associated with the substantial computational effort required are often prohibitively high. In practical analysis, linear elastic behavior is generally assumed in the calculation of member design forces and ductility demands. Thus, analyses performed for this study are based on linear elastic response. Further background on the application of the linear elastic behavior assumption for building analysis is discussed in section 2.4.

For linear elastic analysis, dynamic earthquake loads may be applied using the time-history, the frequency domain, or the response spectrum methods. Both the time-history and frequency domain methods require prescription of a specific ground motion record. However, determination of an appropriate earthquake record is problematic because it is difficult to predict future critical seismic ground motions that may occur at a given site. Therefore, it is prudent to base seismic design on a range of possible earthquake ground motions. The response spectrum method has the advantage that the spectral curve may represent an envelope of upperbound responses based upon several different ground motion records. Also, the response spectrum method is generally more cost effective than the alternative methods. For these reasons, the response spectrum method is the most widely used approach for representing dynamic earthquake loading and is the approach which has been used for the dynamic analyses performed in this study. Further background and discussion of the response spectrum approach is presented in sections 2.2 and 2.3.

In performing seismic analysis of multistory buildings, certain special modeling assumptions (e.g., rigid floor diaphragm behavior, lumped mass modeling) and solution schemes (e.g., substructuring techniques, superelement formulations) can be applied to simplify modeling procedures and to improve computational efficiency. The ETABS (49) computer program is a special purpose tool developed specifically for the analyses of building systems which takes advantage of these aspects in its modeling and solution procedures. ETABS is widely used by practicing engineers and for this reason it is the primary analysis program used in this study. A detailed description of the theoretical background and use of ETABS can be found in reference 49.

#### **1.4 COMPUTER PROGRAM DEVELOPMENT**

In carrying out this project, several modifications to the ETABS computer program have been made in order to extend analytical capabilities and produce results in a form most useful for the purposes of this study. Capabilities of this modified ETABS program include: analysis for gross response quantities including story shears, torques, overturning moments, deflections and drifts; improved modal combination schemes for response spectrum analysis; analysis for P- $\Delta$  effects in static and dynamic analysis; ability to perform preliminary dynamic and static analysis prior to member design based on approximate dynamic properties; automatic generation of UBC and ATC equivalent static loads; effective mass calculation for model verification; and, member stress checks.

It is felt that the added capabilities significantly enhance the ETABS program and may be useful to the practicing engineer in performing seismic analysis. Therefore, a modified version of the ETABS program and user manual (23) have been supplied to the National Information Service for Earthquake Engineering (NISEE) to be made available for public distribution. Inquiries regarding this program can be made to:

NISEE/Computer Applications  
Davis Hall  
University of California  
Berkeley, California 94720

(415) 642-5113

#### **1.5 DOCUMENT ORGANIZATION**

This report has been written in such a way as to facilitate its use as a reference document which can be reviewed in part rather than requiring a full reading. To this end, the remainder of the report is divided into three main chapters (Chapters 2, 3 and 4) covering different general areas with specific topics being addressed in

separate subsections. By referring to the Table of Contents, the reader may selectively choose those particular sections he/she may wish to review.

Chapter 2 presents a general background for understanding the basic principles of seismic analysis of multistory buildings. Sections 2.2 and 2.3 describe the general characteristics of earthquake response spectra, the various methods used for the development of representative spectra, and application of response spectrum analysis in state-of-the-art design. In section 2.4, background on the rationale for linear elastic structural modeling is discussed from the perspective of current practice and building code recommendations. In section 2.5, basic interrelationships that exist between structural modeling and earthquake response spectrum shape in dynamic analysis are presented and discussed.

In Chapter 3, the detailed correlative analyses performed on the study buildings are described and results are presented. These results show the influence of different modeling assumptions and analytical approaches on the predicted seismic response of the different buildings. In section 3.1, the methodology used for the analysis of all of the buildings is discussed. In sections 3.2 through 3.6, the modeling approaches and analytical results for each of the five study buildings are reported. In section 3.7, general observations and conclusions from the analytical studies are presented.

In Chapter 4, three special topics pertaining to analytical techniques applicable for the seismic analysis of multistory buildings are presented. In section 4.1, a method which accounts for the P- $\Delta$  effect in seismic analysis is presented. In section 4.2, the comparative performances of different modal combination rules in seismic analysis are investigated. In section 4.3, a method for performing approximate dynamic analysis at the preliminary design

stage is developed. For each of these topics, sample analyses have been performed on one of the study buildings to demonstrate the various analytical techniques and potential influence on analytical results.

## CHAPTER 2

### APPLICATION OF THE RESPONSE SPECTRUM APPROACH AND LINEAR ELASTIC MODELING FOR SEISMIC ANALYSIS OF BUILDINGS

#### 2.1 INTRODUCTION

In performing computer analyses of buildings for earthquake response, there are two main modeling aspects to be considered: (1) structural modeling of the stiffness and mass properties; and, (2) representation of the earthquake ground motions. Significant uncertainties exist in treating both of these modeling aspects and, therefore, several assumptions and simplifications are made in performing practical analysis for design purposes.

The assumption of linear elastic behavior is usually made for performing seismic analyses of buildings. Although nonlinear analysis computer programs are available, these are rarely employed in building design practice because they not only are difficult to use and interpret and but also costly to perform due to the great computational effort required. Even with the assumption of linear elastic behavior, care must be exercised in developing a numerical model of a building in order to capture the true dynamic properties. Aspects such as secondary structural systems and/or nonstructural components may have to be considered to develop a computer model that will accurately capture actual structural behavior.

Prescribing an appropriate earthquake input is problematic because it is very difficult to accurately predict future seismic ground motions that may occur at a given site during the useful life of a structure. Therefore, seismic design of buildings is generally based on analysis reflecting a range of possible earthquake ground motions. The response spectrum method is the most widely used

approach for representing earthquake excitations in dynamic analysis and is generally considered as "state-of-the-art" among building design engineers. The method employs superposition of a limited number of modal maximum responses as determined from a spectral curve for a prescribed dynamic excitation. Linear elastic structural behavior is a basic assumption of the response spectrum approach. The response spectrum method is computationally much more efficient than the more exact time history technique and, with appropriate modal combination schemes, can yield results that show excellent comparison with time history analysis as is demonstrated in section 4.2 of this report.

In sections 2.2, 2.3, and 2.4 of this chapter, fundamentals involving the development and application of response spectra and linear elastic structural models are reviewed. In section 2.5, the relationship between response spectrum modeling and structural modeling is explored in order to give a better understanding of how these modeling aspects affect analytical response.

## 2.2 DEVELOPMENT OF EARTHQUAKE RESPONSE SPECTRA

There are several approaches which can be used for developing response spectra to represent earthquake ground motions for design purposes. These fall into the following three general categories:

- (1) the use of actual earthquake spectra based on recorded ground motions
- (2) the use of recommended procedures for the development of smoothed design spectra
- (3) performance of a site specific study resulting in unique design spectra reflecting the actual site conditions.

The basic aspects of these three approaches are presented in the subsections that follow.

### 2.2.1 Development of Response Spectra from Earthquake Records

The generation of a response spectrum curve can be idealized by subjecting a series of damped single degree-of-freedom mass-spring systems with continuously varying natural periods to a given ground excitation. The absolute value of the peak displacement response (relative to the ground) occurring during the excitation for each system is represented by a point on the relative-displacement spectrum curve. In Figure 2.1, the generation of the response spectrum for the El Centro 1940 earthquake is illustrated. Using the ground acceleration record as input, (Figure 2.1(a)) a family of response spectrum curves can be generated for various levels of damping (Figure 2.1(b)) where higher damping values generally result in lower spectral response. The response spectrum curves may also be represented in terms of pseudo-velocity or pseudo-acceleration where these pseudo-values are based on the relative displacements as follows:

$S_d =$  spectral relative displacement  
 $S_v = \omega \cdot S_d =$  spectral pseudo-velocity  
 $S_a = \omega \cdot S_v = \omega^2 \cdot S_d =$  spectral pseudo-acceleration  
 where  $\omega =$  natural frequency (radians/second).

The pseudo-velocity and pseudo-acceleration spectra do not reflect true maximum values of velocity and acceleration but, rather, provide a direct means of evaluating the true relative displacement. The pseudo-velocity and pseudo-acceleration may be viewed as approximations to the true maxima for relative velocity and absolute acceleration.<sup>1</sup> Spectra for the true maxima for relative velocity and absolute acceleration can be calculated in addition to the true relative displacement curve. However, for the purpose of structural design, spectra based on true relative displacement are of most interest because these spectral displacements control the force levels induced in the structure. Response spectra are often represented showing  $S_d$ ,  $S_v$  and  $S_a$  ordinates on a single tripartite logarithmic plot. In Figure 2.2, a tripartite plot of the El Centro 1940 response spectrum for 5% critical damping is shown.

Spectra curves developed from actual earthquake records are quite jagged, being characterized by sharp peaks and troughs (Figure 2.1(b)). Because the magnitude and locations of these peaks and troughs can vary significantly for different earthquake records and because of the uncertainties inherent in predicting future seismic ground motions, it is wise to consider several possible earthquake spectra in the evaluation of structural response for design purposes.

---

<sup>1</sup> It should be noted that the pseudo-acceleration is in theory equal to the true maximum absolute acceleration ("absolute" meaning relative to a fixed reference point) for a system with no damping. For this reason, the terms "pseudo-absolute acceleration" or "absolute acceleration" are often used in place of "pseudo-acceleration" although the true absolute acceleration results only for zero damping.

Thus, if response to actual recorded earthquakes is to serve as a design basis, analyses should be performed using several selected spectra that are believed to be representative of critical ground motions that may occur at the site.

### **2.2.2 Development of Smoothed Design Response Spectra**

To provide an alternative to the use of several earthquake spectra for design, much work has been done to develop smoothed design spectra that represent approximate upperbound response envelopes based on expected critical levels of ground motion (Newmark (26,27), Blume (9), Seed (37), Trifunac (45)). Some code writing bodies such as the American Petroleum Institute (API), the Veterans Administration (VA), the Applied Technology Council (ATC), and the Nuclear Regulatory Commission (NRC) have incorporated recommendations for the development of design response spectra in their respective regulations (2,48,5,46) for construction and design practices. (Note that ATC guidelines have not yet been adopted by actual building codes.) To illustrate this general approach for developing response spectra, refer again to Figure 2.2, where the values of maximum ground acceleration, velocity and displacement for the El Centro 1940 record are plotted along with the spectrum curve. Comparison of the spectrum profile with the lines of ground motion maxima reflect the following important characteristics:

- (1) In the very low period range, the spectrum curve approaches the line of maximum ground acceleration, becoming virtually coincident for periods less than about 0.03 seconds.
- (2) In the low period range between 0.10 and 0.50 seconds, the variation of the spectrum curve tends to show

correlation with the line of maximum ground acceleration.

- (3) In the medium period range between 0.50 and 3.0 seconds, the variation of the spectrum curve tends to show correlation with the line of maximum ground velocity.
- (4) In the higher period range between 3.0 and 10.0 seconds, the variation of the spectrum curve tends to show correlation with the maximum ground displacement.
- (5) In the very high period range (greater than 10.0 seconds), the spectrum curve gradually approaches the line of maximum ground displacement (not shown in Figure 2.2).

Based on the above characteristics, a rough upperbound approximation for the El Centro response spectrum can be drawn using a few straight lines over different period ranges on the logarithmic tripartite plot. If lines parallel to the ground motion maxima are used, an approximate smoothed spectrum curve can be constructed as shown in Figure 2.2 by applying factors of proportionality to the peak values of ground acceleration, velocity and displacement. (Note that the use of lines parallel to the ground motion maxima is consistent with Newmark's recommendations (26,27) whereas other design spectra use lines non-parallel to the ground motion maxima.) In this way, a smoothed response spectrum curve can be constructed using various factors of proportionality applied to the ground motion maxima over different period ranges. However, the proportionality factors required to produce reasonable approximations to actual spectra vary significantly for different earthquake records. To illustrate this point, the pseudo-acceleration spectra for six different earthquake records

normalized to a peak ground acceleration of 0.4g are plotted in Figure 2.3. As can be seen from the significant variations in response among these normalized spectra, there is no unique correlation between peak ground acceleration and spectral amplitude for different ground motions. Similar variations in spectral profiles result if ground motions are normalized to peak velocity or peak displacement. Therefore, it can be concluded that ground motion maxima alone are an inadequate parameter set to accurately predict response spectrum profiles. Other characteristics of the ground motion histories that are important in determining the response spectrum shape and that should be considered in developing design spectra include, among others: frequency content of the ground motion, duration of strong motion shaking, mean values of individual acceleration peaks.

However, reasonable smoothed design spectra based on enveloping the spectral response of several earthquake records of similar intensity and site conditions can be constructed from a limited number of "base line" parameters that reflect the influences of expected ground motion maxima as well as other ground motion characteristics. In recent codified recommendations for the development of response spectra (5,48), these base line parameters have been termed "effective" ground motion maxima. For example, the ATC recommendations (5) incorporate the use of the seismicity parameters "effective peak acceleration" (EPA) and "effective peak velocity" (EPV) in the development of response spectrum curves. The following interpretation of EPA and EPV is given in the commentary of the ATC provisions:

To best understand the meaning of EPA and EPV, they should be considered as normalizing factors for construction of smoothed elastic response spectra for ground motions of normal duration.

The EPA and EPV thus obtained are related to peak ground acceleration and peak ground velocity but are not necessarily the same as or even proportional to peak acceleration and velocity...

Thus the EPA and EPV for a motion may be either greater or smaller than peak acceleration and velocity, although generally the EPA will be smaller than peak acceleration while the EPV will be larger than the peak velocity. Despite the lack of precise definitions, the EPA and EPV are valuable tools for taking into consideration the important factors relating ground shaking to the performance of a building.

Since smoothed design spectra are generally normalized to peak ground motions values, the engineer may be misled to believe that there is a direct theoretical correspondence between peak ground motions and overall spectral magnitude. The engineer should realize the difference between peak acceleration and effective peak acceleration, being aware of the broader interpretation of the latter. It should be noted that Trifunac (45) has made preliminary suggestions for developing design spectra based on more general, and routinely available parameters, eliminating the difficulties of specifying peak ground motion parameters for development of response spectra.

Different recommended procedures base construction of the response spectrum on different sets of peak ground motion parameters. For instance, Newmark's recommended spectrum (26) is normalized with respect to peak acceleration, velocity and displacement values. The ATC recommendations (5) are based on peak acceleration and velocity only. The NRC regulations<sup>1</sup> (46) are based on peak acceleration and displacement. The Blume (9), API (2), and Veterans Administration (48) recommended spectra are based on peak acceleration only. Because Newmark's spectrum is normalized with respect to three ground motion parameters, it allows greater flexibility in the development of a response spectrum curve. A tripartite plot of the Newmark spectrum with 5% critical damping normalized to a 0.4g peak ground acceleration is shown in Figure 2.4 (respective peak velocity and displacement values of 1.60 ft/sec and 1.20 ft are used for the construction of the

---

<sup>1</sup>It should be noted that the NRC regulations were developed largely from recommendations made in the Newmark (27) and Blume (9) studies.

spectrum as recommended by Newmark as reasonable values consistent with the 0.4g peak acceleration). For a comparison of this recommended design spectrum versus actual earthquake spectra, the Newmark pseudo-acceleration spectrum is plotted in Figure 2.3. As can be seen from this figure, smoothed design spectra such as the Newmark spectrum reflect an upperbound envelope of actual spectrum curves and, consequently, will generally produce more conservative levels of induced forces than would normally be expected from an actual earthquake having the same peak ground acceleration.

Response spectra may be viewed as being composed of four parts spanning different period ranges shown as zones A, B, C, D in Figures 2.3 and 2.4. Most design spectra use the following general relationship to represent the variation of spectral acceleration with period:

$$S_a \propto (1/T)^p$$

where the value of  $p$  will vary depending upon the design spectrum used and the various zones of the curve. In general, the characteristics of the spectral acceleration curves (Figure 2.3) for the various zones are as follows:

**Zone A: Very low period range, peak acceleration related.**

Spectral accelerations start from the peak ground acceleration value at  $T = 0$ , and rise to the maximum spectral acceleration values in zone B. The periods in this range are generally smaller than the periods corresponding to the maximum frequency content of the ground motion. Values of  $p$  in the neighborhood of  $-1.0$  are often used in this zone. A  $p$  value of  $-1.0$  results in spectral acceleration varying linearly with period.

**Zone B: Low period range, peak acceleration related.** In this

zone, the maximum spectral accelerations result because the predominant periods of the ground acceleration lie in this period range. Many recommended design spectra (including Newmark's) specify a line of constant acceleration,  $p = 0$ , to represent this zone.

**Zone C: Medium period range, peak velocity related.**

Spectral accelerations begin to decrease rapidly with increasing period and taper off to a more gradual decrease. For this zone,  $p$  values ranging between 0.5 and 1.0 are recommended by various design spectra. Newmark recommends  $p = 1.0$ .

**Zone D: Long period range, peak displacement related.**

In this zone, the periods are several times greater than the predominant periods of the ground accelerations and the resulting dynamic amplifications are relatively small. In this zone, the rate of descent of the acceleration spectrum is greater than that in zone C. Newmark recommends a value of  $p = 2.0$  for this zone.

In Figure 2.5, the Newmark (26), Blume (9), API (2), VA (48), ATC (5), and NRC (46) recommended smoothed design spectra are plotted for a 0.4g peak acceleration and 5% critical damping. In Table 2.1,  $p$  values used in the various spectrum zones are shown for these spectra. Also values corresponding to the Uniform Building Code (UBC) (20) equivalent static spectrum are given. (In section 2.3.2, the influence of the different spectral relationships ( $p$  values) on analytical response is discussed.) As may be noted from Figure 2.5 and Table 2.1, not all recommended design spectra incorporate all four zones as described above. The VA and ATC spectra do not include zone A separately since these spectra have been developed for building design applications where response in this very low period range is

usually not significant. However, for other types of facilities (e.g. nuclear power plants), very low period response may be important, and thus, zone A should be included as a separate portion as is done in the Newmark, Blume, API and NRC spectra. Also, zone D is omitted from some of these recommended spectra resulting in more conservative (larger) spectral amplitudes in the higher period ranges. Table 2.1 shows that the ATC, VA, and UBC recommended spectra include only zones B and C, that the API and Blume recommended spectra include only zones A, B, and C, and that the Newmark and NRC recommended spectra include all four zones A, B, C, D.

Local soil characteristics can have an important influence on the relative spectral amplifications in these zones by influencing the surface ground motions that result from a given base rock excitation (Seed(37)). For this reason, many recommended design spectra make allowance for the influence of soil type on the shape of the spectrum curve. The general tendency of overlying soil is to push the spectra response curve further out along the period scale, causing greater amplification in the longer period range as shown in Figure 2.6. Greater effective peak ground velocity and displacement are expected for sites with softer soil conditions. For the Newmark spectrum, estimates of these peak values can be directly used to modify the spectrum for various soil conditions. For other recommended spectra, such as ATC and API, local soil conditions are accounted for by classifying the site into one of a limited number of soil type categories and by applying different spectrum modifications for each category.

It can be seen from Figure 2.5 that significant differences exist among the various recommended spectrum profiles although all are based on the same peak ground acceleration and damping. For this figure, the normal or default soil condition was assumed for each

recommended smoothed design spectrum. These differences are especially significant in the longer period range where larger relative variations in spectral amplitude are noted. For instance, at a period of 4 seconds, Figure 2.5 shows the ATC spectral amplitude is about twice that of Newmark. Because of these differences, care must be taken in choosing an appropriate smoothed response spectrum for use in design.

### **2.2.3 Development of Site Specific Response Spectra**

For especially important structures or where local soil conditions are not amenable to simple classification, the use of recommended smoothed spectrum curves may be considered inadequate for final design purposes. In such cases, site specific studies are performed to determine more precisely the expected intensity and character of seismic motions. The development of site specific ground motions is generally the responsibility of geotechnical engineering consultants working within the structural engineer's design criteria. The Structural Engineers Association of California (SEAOC) has published guidelines (42) for developing site specific seismic ground motions in which the following general steps are recommended:

Step 1: Geological and Seismology Study

Step 2: Establish Average Recurrence Rates and  
Probabilistic Description of Earthquake Events  
for Each Source

Step 3: Determine Ground Motion Characteristics

(A full description of the recommended procedures and a bibliography of related publications are given in reference 42.)

In step 1, a study of the geology and seismology of the area is made to identify the types and locations of earthquake faults that may

have significant effects at the site. A historical study of past earthquakes is made to form a data base for projecting future seismic activity and estimating maximum capable Richter magnitudes.

In step 2, recurrence rates and probabilities of exceedence are established for various earthquake magnitudes based on the data from step 1. Recurrence rates can be represented by a logarithmic plot of number of events exceeding a given magnitude versus the magnitude value for a given time span as shown in Figure 2.7. Using this recurrence curve, probabilities of occurrence for various earthquake magnitudes can be calculated through the application of a given probability distribution law (Poisson, Bayesian, etc.). A typical plot of probability of occurrence versus magnitude for different structure design lives is shown in Figure 2.8.

From the accumulated geological data and seismologic history, peak ground accelerations in the base rock can be estimated using attenuation functions. Typically, these functions are empirical relationships based on various attenuation data where estimates of peak acceleration (A) are calculated as a function of Richter magnitude (M), distance to causative fault (d), and focal depth (h) of the source (i.e.,  $A = f(M, d, h)$ ). Using the attenuation functions and the information from steps 1 and 2, a relationship can be developed showing probabilities of occurrence for various levels of peak acceleration for an assumed project life span (e.g., 50 years) as shown in Figure 2.9. Given the expected life and importance of the structure, an appropriate probability of exceedence can be chosen and design levels of earthquake magnitude and corresponding base rock ground motion parameters (e.g., peak acceleration, frequency content, duration) can be specified.

In step 3, design ground motions at the surface level are developed for the local soil conditions. Empirical relationships may be used to develop free-field ground motion parameters resulting from

the expected base rock excitations. Alternatively, full time history computer analyses of the vertical propagation of seismic waves from the base rock through the soil can be performed to obtain a history of motion at the ground surface level. Computer programs have been developed to perform this type of analysis for linear (35) and non-linear (24) horizontally layered soil models. With programs such as these, one or more appropriate ground acceleration histories (recorded or artificially generated) whose characteristics roughly match expected critical base rock motions can be input to predict free-field surface motions which can then be used to develop smoothed response spectra curves to be used in design. In Figure 2.10, an example of site specific spectra developed in this way are shown.

### 2.3 BACKGROUND ON THE APPLICATION OF RESPONSE SPECTRA FOR SEISMIC DESIGN OF BUILDINGS

Once an approach for development of response spectra has been chosen and representative critical ground motions have been developed, there still remains a difficulty in applying spectrum analysis to the design of buildings. This difficulty arises from the fact that although response spectra are formulated based on linear elastic behavior, buildings in seismically active areas are generally designed to respond inelastically in a major earthquake. Before practical design can be carried out, further modification of the elastic response spectrum is required.

Several factors must be considered in determining the level of earthquake excitation that a structure is to be designed to resist. Apart from the local seismicity, factors reflecting the relative functional importance of the facility and the inherent toughness, ductility, and redundancy of the structural system are critical in assigning appropriate levels of earthquake induced loads for design purposes. Generally, the objectives in earthquake-resistant design are as follows:

- (1) to insure that no significant structural damage results from a moderate earthquake having a reasonable likelihood of not being exceeded during the life of the structure;
- (2) to insure against collapse or major structural failure for a rare severe earthquake.

Design codes for buildings and other types of structures generally incorporate the above two-level design philosophy in their

provisions, either explicitly or implicitly.

The first design objective can be met by sizing the structural members such that their yield strengths will not be significantly exceeded in an earthquake of moderate intensity. At this design level, the behavior is essentially linear elastic and application of elastic response spectrum analysis can be used to arrive at critical member forces.

In meeting the second design objective, the inelastic deformation capacity of the structure must be considered. At this design level, adequate energy absorption in the form of ductility and toughness must be provided for in the design of the structural system. Due to inelastic behavior, elastic response spectrum analysis is not directly applicable for this design objective. A full nonlinear time history analysis would be required for a "theoretically correct" analytical result. A full nonlinear analysis, however, is usually considered to be too costly and time consuming for practical design, especially for building analysis. As an alternative, an approximate technique for applying the response spectrum method to nonlinear analysis has been suggested by Newmark (26). This method is based upon the use of an inelastic response spectrum arrived at by reducing the elastic spectrum by a factor reflecting an assumed permissible ductility ratio. In using this technique, the forces resulting from linear analysis using inelastic spectra are presumed to be correct but corresponding displacements must be factored by the value of the ductility ratio. Procedures for practical application of inelastic spectra in the design of buildings have been suggested (4). However, it has been found that application of inelastic design spectra predicts nonlinear earthquake response with limited reliability (8). Moreover, being based on yielding single degree-of-freedom systems, the technique is especially suspect for multiple degree-of-freedom systems such as multistory buildings (22). Thus, although the

technique is convenient for preliminary design, it has not found general acceptance in the engineering design profession. Consequently, the second design objective of insuring against a major structural failure is often met qualitatively by employing connection and member design details that ensure ductile behavior. Recommendations for ductile design using reinforced concrete and steel are outlined in building codes (20, 41). Elastic response spectrum analysis is sometimes used to predict deformations and resulting ductility demands for a severe earthquake excitation. In this case, the implicit assumptions are that ductile behavior is well distributed throughout the structure and that the inelastic deformation response will be approximately equivalent to the elastic response. Results from this type of analysis may be used to predict approximate ductility demands and to perform story drift and overall stability (P- $\Delta$ ) checks for deformation levels expected to result from a major earthquake.

The term "dual spectrum approach" is used if two distinct levels of prescribed earthquake excitation are employed to meet the two aforementioned design objectives. The higher intensity motion is often called "maximum credible earthquake" (or ductility level earthquake) and the lower level motion is referred to as "maximum probable earthquake" (or strength level earthquake). The maximum credible earthquake spectrum reflects an envelope of response values which have a high probability (e.g., 85-95%) of not being exceeded during the lifetime of the structure. The maximum probable earthquake spectrum has a moderate probability (e.g., 50-60%) of not being exceeded. An example of dual response spectra developed from a site specific study is shown in Figure 2.10. Differences in magnitude and shape of these two spectra reflect differences in the characteristics of potentially critical earthquake sources. Also contributing to the differences between the spectra are the relative probabilities of

exceedance and damping values applied which, in turn, may depend on the social or economic importance of the facility being designed, and the type of structural system and construction materials used.

The social and economic importance of a facility influences the degree to which design response spectra are reduced from elastic response spectra corresponding to a maximum credible earthquake. In this regard, different industries require different levels of reduction (factors of safety) due to the varying importance of the structures that they design. For instance, in the nuclear industry, critical components of nuclear power plants may be designed to withstand a maximum credible earthquake in purely elastic response due to the functional importance of the facility. In the offshore oil industry, a lesser reduction of spectra is used than in the building industry because of importance considerations, the lack of structural redundancy and absence of nonstructural (energy absorbing) components in offshore towers as compared to buildings. Generally, buildings are designed using spectra corresponding to elastic limit level design which are more greatly reduced from maximum credible levels than would be the case for other types of structures (e.g., nuclear power plants, offshore oil platforms). This reduction in design force can be seen from Figure 2.11 where the El Centro 1940 (north-south component, 5% damping) acceleration spectrum is plotted along with an "equivalent" spectrum corresponding to static lateral force coefficients as specified by the UBC (20) for a ductile moment resisting frame structural system. Current UBC recommendations do not explicitly develop reduced force coefficients from a maximum credible earthquake level but, several factors contribute to justification for these relatively low level forces used for earthquake resistant design. Among these are the safety factor resulting from working stress design, the ductile capacity of the lateral force resisting system, energy dissipation contributed by nonstructural elements, and

increased damping that will be brought into action during an earthquake of major intensity. However, the underlying justification for this reduction lies in the fact that buildings designed for UBC static force levels have generally performed satisfactorily over the years when subjected to earthquake excitations.

The ATC recommendations (5) take a somewhat more rigorous approach than UBC in developing design response spectra for dynamic analysis starting with an excitation level corresponding roughly to a maximum credible earthquake for the site where:

the probability that the ordinates of the design elastic response spectrum will not be exceeded during a 50-year interval is roughly 90 percent, at least in the general range of 80 to 95 percent.

For zones of highest seismicity, this elastic response spectrum is based on an effective peak acceleration (EPA) of 0.4g and an effective peak velocity (EPV) of 12 in/sec. A plot of this elastic spectrum is shown in Figure 2.11. The ATC provisions recommend various factors of reduction ranging from 1.25 to 8.0 to be applied to the elastic response spectra depending on the type of structural system that will be employed. A plot of the ATC elastic spectrum with a reduction factor of 8.0 (corresponding to a ductile moment resisting frame system) is also shown in Figure 2.11. Using this reduced spectrum, ATC states that:

design is based on internal forces resulting from a linear elastic analysis using the prescribed forces and assumes that the structure as a whole under these prescribed forces should not deform beyond a point of "significant yield."

Here significant yield is defined as that level causing complete plastification of at least the most critical region of the structure.

As can be concluded from the above discussion, application of earthquake response spectrum analysis in the design of buildings

relies heavily on engineering judgment and experience from past performance. Development of appropriate design spectra for elastic analysis and corresponding force levels for elastic limit design is based on expected inelastic behavior and reserve strength capacity of the particular structural system.

## 2.4 BACKGROUND ON THE APPLICATION OF LINEAR ELASTIC STRUCTURAL MODELING FOR EARTHQUAKE RESPONSE

As discussed in the previous section, in earthquake resistant design of buildings, a "maximum credible" seismic event is expected to induce nonlinear (inelastic) response of the primary lateral force resisting structural system. Nonlinearities in response also occur at lower levels of excitation due to participation of various secondary and nonstructural elements that are typically present in building systems. Nevertheless, analysis procedures based on elastic periods and mode shapes generally can provide a practical and effective approach for developing dynamic response quantities to be used in design.

Modern earthquake engineering philosophy emphasizes that structural systems which do not have sudden discontinuities in stiffness, strength or mass and that have sufficient redundancy and ductility are desirable for earthquake resistant design. Investigators have shown that structures exhibiting these qualities tend not to show catastrophic changes in overall stiffness at higher levels of response and tend to retain their basic elastic vibration patterns (mode shapes) even after significant structural damage has occurred. For this reason, mode shapes derived from linear analysis are usually considered to be appropriate for the purpose of defining the dynamic distribution of force and deflection quantities.

In contrast to mode shapes, the natural periods of buildings may demonstrate significant variation at different levels of response whereby periods increase at higher levels of dynamic excitation. At large response levels corresponding to very severe earthquake excitations, inelastic softening of the primary lateral force resisting system results in significant period elongation. However, response based on elastic periods will more accurately represent force

levels from earthquakes of moderate intensity and will better reflect at least the initial response to a very severe earthquake. At moderate response levels, it has been observed in actual structures that periods become larger than those indicated by small amplitude testing even where no major structural damage has occurred. This period elongation is caused by various losses in stiffness. Possible sources of stiffness loss at moderate response levels include:

- (1) the loss of stiffness due to the nonparticipation of nonstructural systems with increasing deflection response;
- (2) a "loosening up" of the foundation primarily by nonlinear soil behavior;
- (3) in reinforced concrete structures, cracking of concrete reducing the effective section properties of members; and,
- (4) in steel structures, some yielding due to residual stresses resulting in reduced stiffness.

In developing a mathematical model for dynamic analysis by computer, care must be taken in assessing the influence of the above factors and to include or omit various stiffening aspects in the model of the building in order to arrive at natural periods that are appropriate for use in design. To make this assessment, the analyst should have an understanding of the functions and behaviors of the different components that make up the total building system.

Buildings are composed of various structural and nonstructural systems that perform different functions. The structural system's function is to safely transmit applied gravity, occupancy, wind and

earthquake loads to the foundation of the building. Thus, the structural system must have the ability to carry vertical and lateral loads. Separate vertical and lateral systems may be used to carry each of these types of loads, or a single system may be used to carry both. Components of vertical load systems may include floor slabs (in bending), supporting beams and girders, and columns and/or bearing walls. Lateral load carrying systems may include floor slabs (in diaphragm action), moment resistant frames composed of girders and columns, braced frames and/or shear walls. In some cases, a primary lateral load carrying system is backed up by a secondary system which can help support loads if a partial failure of the primary system occurs. Nonstructural systems may serve architectural or electromechanical functions and generally are designed to carry loads required for self support only. Nonstructural systems may include architectural features such as partitions, exterior cladding, curtain walls, infill block walls, ceilings and stairwells, as well as mechanical features such as plumbing, air conditioning, electrical ducts and elevators.

In developing an appropriate model for predicting earthquake response, the structural analyst should consider all aspects that may significantly influence the dynamic properties (periods and mode shapes) of the building regardless of whether these serve a structural or nonstructural purpose. In this regard, the SEAOC (41) lateral force commentary states that the period should be:

derived from the representative properties and dimensions of a mathematical model of the entire structure including those elements contributing to the stiffness of the structure, even though these elements may not be part of the designated lateral force resisting system.

The commentary further warns that if the period is calculated based on the lateral force resisting system acting alone:

the period may be too long since the contribution of nonstructural elements or assumed non-participating frames tends to shorten the period.

And, an overestimated period will result in less conservative design forces. However, explicit inclusion of all nonstructural or non-participating elements in the structural model would present a nearly impossible task for the analyst. In reality, for modern high rise construction, most nonstructural and non-participating elements do not affect dynamic behavior to any significant degree due to their lack of stiffness at small deflection and/or their lack of strength at larger deflections. Relating to this, the Applied Technology Council (ATC) tentative provisions (5) states that:

Because the periods of the modes contemplated in the provisions are those associated with moderately large, but still essentially linear response of the building, the period calculations should include only those elements which are effective at these amplitudes.

In formulating an analytical model, the analyst generally can safely neglect components such as plumbing, piping, and other electromechanical equipment along with non-moment resisting or light framing that may be part of the vertical load carrying system unless these are composed of non-isolated rigid elements of significant strength. The small influence of systems such as these may be more appropriately reflected by using an increased overall damping value in the calculation of response.

It may, however, be prudent to account for features such as secondary lateral systems, bending interaction of slab and girders, three dimensional (non-planar, tube-type) interaction, block walls and rigid stairwells, among others. Although appropriate to include features such as these for period determination, in some cases it may be inappropriate to distribute resulting forces back to these components. In this regard, the SEAOC commentary states that:

When calculating a structure's capacity to resist the seismic forces that are attracted, it may be necessary to assume that only those elements detailed as ductile and designated as part of the lateral load resisting system contribute resistance capacity. It may be necessary to ignore nonstructural or nonductile elements when assigning resistance capacity.

This suggests that the analyst may be required to develop forces based on one model and then distribute these forces to the structural elements of a somewhat different model. In some cases, this may be troublesome but often will involve only local redistribution of forces, if any.

In summary, linear elastic analysis by computer can provide very useful results to aid the engineer in earthquake resistant design. However, care must be taken to use a rational approach in developing a mathematical model of the structure in order to produce results consistent with design criteria.

## 2.5 INFLUENCE OF STIFFNESS AND MASS UNCERTAINTIES ON RESULTS OF RESPONSE SPECTRUM ANALYSIS

In linear elastic dynamic analysis, the natural periods and mode shapes are the most important properties governing structural response. For seismic analysis of buildings, gross design quantities such as story shears, overturning moments, deflections and story drifts are determined from these dynamic properties. The mode shapes govern the distribution of the design quantities over the height of the building and the natural periods (being directly related to spectral amplitudes) govern the magnitudes of these design quantities. The natural periods and mode shapes are analytically derived by performing an eigensolution of the stiffness and mass matrices and therefore are directly dependent on the properties of these matrices. Alterations to the stiffness and/or mass matrices will vary the natural periods and modes and thus change the magnitude and distribution of design quantities. In developing a mathematical model, the engineer may wish to make certain mass and stiffness assumptions in order to yield conservative analytical response. However, the degree of conservatism in the resulting response depends not only on the mass and stiffness assumptions made but also on the response spectrum chosen and analytical approach used. For instance, in the UBC static equivalent approach, a 20% mass overestimate will result in a 20% increase in forces and deflections. However, in dynamic analysis using the Newmark spectrum, a 20% mass overestimate may yield no increase in resulting forces or deflections. Because of the uncertainties involved in modeling and the resulting need for conservatism in analysis, it is important to understand how stiffness and mass variations will influence design quantities.

Often, uncertainties in modeling involve a roughly uniform variation in stiffness or mass properties over the height of the structure. For instance, effects such as rigid end zones, slab-girder

interaction, participation of secondary systems and nonstructural elements often cause a relatively uniform stiffening throughout the building. Likewise, mass modeling considerations such as dead weight estimates and the participation of live (occupancy) loads and partition loads may result in a uniform overestimate or underestimate of actual floor weights. Modeling variations such as these can cause a significant change in the natural periods of the structure but often do not result in a significant variation in mode shapes. For these types of modeling variations, the resulting influences on gross design quantities can be predicted by applying a simple factor to the stiffness and/or mass matrices, representing a uniform increase or decrease of these properties.

Relationships for changes in design quantities contributed by each mode resulting from factoring the stiffness and/or mass matrices can be derived mathematically for a planar model of a building as shown below.

Given  $\underline{K}$  = initial stiffness matrix (n x n)  
 $\underline{M}$  = initial mass matrix (n x n)  
 where n = number of stories in building

the resulting eigenproblem is formulated as:

$$[\underline{K} - \omega^2 \underline{M}] \underline{\phi} = \underline{0} \quad (2.1)$$

where  $\omega$  = a natural frequency for initial  
 stiffness and mass matrices  
 $\underline{\phi}$  = a mode shape (vector) for initial  
 stiffness and mass matrices (n x 1)

The resulting maximum modal story forces are given by:

$$\underline{F} = \underline{M} \underline{\phi} \frac{\underline{\phi}^T \underline{M} \underline{r}}{\underline{\phi}^T \underline{M} \underline{\phi}} Sa \quad (2.2)^1$$

and modal story displacements are given by:

$$\underline{D} = \underline{\phi} \frac{\underline{\phi}^T \underline{M} \underline{r}}{\underline{\phi}^T \underline{M} \underline{\phi}} \frac{Sa}{\omega^2} \quad (2.3)^1$$

where  $\underline{F}$  = initial modal story force vector (n x 1)  
 $\underline{D}$  = initial modal story displacement vector (n x 1)  
 $\underline{r}$  = unit vector of ones (n x 1)  
 $Sa$  = spectral acceleration for modal frequency in

Now, if the stiffness and mass matrix are factored, the eigenproblem becomes:

$$[\underline{K}^* - \omega^{*2} \underline{M}^*] \underline{\phi}^* = \underline{0} \quad (2.4)$$

where  $\underline{K}^* = a \underline{K}$  = the factored stiffness matrix (2.5a)

and  $\underline{M}^* = b \underline{M}$  = the factored mass matrix (2.5b)

Substituting (2.5a) and (2.5b) into (2.4), we have:

$$[a \underline{K} - \omega^{*2} b \underline{M}] \underline{\phi}^* = \underline{0}$$

or (2.6)

$$[\underline{K} - \omega^{*2} \frac{b}{a} \underline{M}] \underline{\phi}^* = \underline{0}$$

Comparing eigenproblems (2.6) and (2.1), we see that the frequency and mode shapes will vary according to:

$$\omega^{*2} \frac{b}{a} = \omega^2 \quad \text{or} \quad \omega^* = (a/b)^{1/2} \omega \quad (2.7)$$

---

<sup>1</sup>see Clough (11) for the derivation of expressions 2.2 and 2.3 .

and 
$$\underline{\phi}^* = b^{-1/2} \underline{\phi} \quad (2.8)$$

assuming 
$$\underline{\phi}^T \underline{M} \underline{\phi} = \underline{\phi}^{*T} \underline{M}^* \underline{\phi}^*$$

for mass normalized eigensolution.

The resulting design quantities for the factored stiffness and mass matrices are:

$$\underline{F}^* = \underline{M}^* \underline{\phi}^* \frac{\underline{\phi}^{*T} \underline{M} \underline{r}}{\underline{\phi}^{*T} \underline{M}^* \underline{\phi}^*} S_a^* \quad (2.9)$$

and

$$\underline{D}^* = \underline{\phi}^* \frac{\underline{\phi}^{*T} \underline{M} \underline{r}}{\underline{\phi}^{*T} \underline{M}^* \underline{\phi}^*} \frac{S_a^*}{\omega^2} \quad (2.10)$$

Substituting (2.5b), (2.7) and (2.8) into (2.9) and (2.10) we find that:

$$\underline{F}^* = b \frac{S_a^*}{S_a} \underline{F} \quad (2.11)$$

and

$$\underline{D}^* = \frac{b}{a} \frac{S_a^*}{S_a} \underline{D} \quad (2.12)$$

The value of the ratio  $S_a^*/S_a$  depends upon the variation in spectral amplitude resulting from the shift in natural period. For recommended smoothed design spectra, this ratio can be explicitly represented if the original natural period,  $T$ , and the shifted period,  $T^*$ , both lie in the same zone of the spectrum. Recalling that for most recommended design spectra:

$$S_a \propto (1/T)^P$$

we have

$$\frac{S_a^*}{S_a} = \left[ \frac{1/T^*}{1/T} \right]^P = (T/T^*)^P = (\omega^*/\omega)^P \quad (2.13)$$

and substituting (2.7) into (2.13),

$$\frac{S_a^*}{S_a} = (a/b)^{p/2} \quad (2.14)$$

Using (2.14) in (2.11) and (2.12), we now have:

$$\underline{F}^* = b (a/b)^{p/2} \underline{F} \quad (2.15)$$

and

$$\underline{D}^* = (b/a) (a/b)^{p/2} \underline{D} \quad (2.16)$$

Story shears (V) and overturning moments (OTM) vary in direct proportion to the story forces (F), and story drifts (d) vary in direct proportion to story deflections (D). Thus, at every story we have:

$$V^*/V = OTM^*/OTM = b (a/b)^{p/2} \quad (2.17)$$

and

$$D^*/D = d^*/d = (b/a) (a/b)^{p/2} \quad (2.18)$$

Expressions (2.17) and (2.18) represent the variations in gross design quantities that result for the response of a single mode due to factors of "a" and "b" being applied to the stiffness and mass matrices respectively. The value of "p" will depend upon which smoothed design spectra is used and in which spectrum zone the natural period of the mode lies. In Figure 2.5, various recommended smoothed design spectra are plotted and, in Table 2.1, "p" values for these spectra are shown for the different spectrum zones. Generally,

tall multistory buildings will have their most significant natural periods lying on the descending portions ( $p > 0$ ) of smoothed design spectrum curves represented by zones C and D in Figure 2.3. Therefore, the  $p = 0$  portion of spectrum curves are often of secondary significance for dynamic analysis of tall buildings. However, it is of interest to note that if equivalent static analysis methods as suggested by UBC or ATC are used and the fundamental period is calculated based on the code equations, variation in design quantities is identical to the  $p = 0$  condition in dynamic analysis. To illustrate the different relationships for spectral acceleration, plots of  $S_a^*/S_a$  versus  $T^*/T$  according to expression (2.13) are shown in Figure 2.12 for the different "p" values corresponding to the ATC ( $p = 0.667$ ), Newmark ( $p = 1.0, 2.0$ ), Blume ( $p = 0.794$ ), API ( $p = 1.0$ ) and VA ( $p = 1.0$ ) spectra.

In order to contrast the influence of different spectral shapes on design quantities, the following three cases are considered:

Case 1: variation of stiffness holding mass constant  
( $a = ?, b = 1.0$ );

Case 2: variation of mass holding stiffness constant  
( $a = 1.0, b = ?$ );

Case 3: equal variation of both mass and stiffness  
( $a = b = ?$ ).

The different "a" and "b" values for these cases are applied to expressions (2.17) and (2.18) in order to plot relationships for the variation of design quantities.

#### Case 1

In Figure 2.13, the variations in modal story shears, overturning moments, deflections and drifts for case 1 are plotted versus the

stiffness matrix multiplying factor, "a," for different "p" values. The influence of stiffness variation on modal design force quantities (story shears and overturning moments) is shown in Figure 2.13(a) and Table 2.2. As can be seen from the figure, significant differences in design force quantities result for different p values. For all p values except  $p = 0$ , increasing stiffness results in increased modal story shears and overturning moments. The reason for this is that increasing stiffness decreases the natural period which, for  $p > 0$ , results in larger spectral acceleration values and thus larger forces. For  $p = 0$ , the spectral acceleration remains constant and no force increase results. For  $p = 2.0$ , stiffness and force increases are directly proportional where, for instance, a 20% increase in stiffness results in a 20% increase in design forces (Figure 2.13(a):  $p = 2.0$ ,  $a = 1.20$ ,  $V^*/V = OTM^*/OTM = 1.20$ ). For  $p = 0.667, 0.794, 1.0$ , a given degree of stiffness increases results in a lesser degree of force increase where, for instance, if  $p = 0.667$  a 20% increase in stiffness results in a 6.3% increase in forces (Figure 2.13(a):  $p = 0.667$ ,  $a = 1.20$ ,  $V^*/V = OTM^*/OTM = 1.063$ ). As p values become progressively larger, greater rates of increase in design forces are observed.

In Figure 2.13(b), the variation of modal story deflection and drifts with stiffness changes is shown. As can be seen from the figure, changes in deflections resulting from stiffness variations are reversed from changes observed in force quantities. For all p values except  $p = 2.0$ , increasing stiffness results in decreased drifts. The reason for this is that for a given degree of stiffness increase, a lesser degree of force increase results. Therefore, the stiffness increase predominates over the force increase and a net decrease in corresponding deflections result. As p values become progressively larger, smaller rates of decrease in deflections are observed. For  $p = 2.0$ , the stiffness increase is equivalent to the force increase and deflections remain constant.

Thus, different spectra will yield significantly different results. If stiffness is increased by 20% in a long period building (e.g.,  $T = 4.0$  sec.) the Newmark spectrum (zone D,  $p = 2.0$ ) yields a 20% increase in fundamental modal forces and no change in deflections whereas the ATC spectrum (zone C,  $p = 0.667$ ) yields a 6.3% increase in modal forces and an 11.4% decrease in deflections (see Table 2.2). If the UBC static approach ( $p = 0$ ) is used, the fundamental period based on the code equation remains unchanged and no change in applied forces occurs but a 16.7% decrease in deflections results (Table 2.2).

### Case 2

In Figure 2.14, the variations in design quantities for case 2 are plotted. In this case, stiffness is held constant and mass is factored by "b". The first important observation that can be made for this case is that identical changes in modal story shears, overturning moment, deflection and drift quantities result due to variations in mass and, thus, can be represented by a single plot. For all  $p$  values except  $p = 2.0$ , increasing mass results in increased design forces and deflections. For  $p = 2.0$ , design quantities remain constant with increasing mass. Two offsetting influences affect design quantities as follows: (1) increasing mass results in higher internal forces being applied to the structure tending to increase design quantities; (2) increasing mass causes an increase in natural period which results in decreased spectral amplification (for  $p > 0$ ) tending to reduce design quantities. For  $p < 2.0$ , the influence of (1) above outweighs (2) and increasing design quantities result from larger masses. For  $p = 0$ , design quantities are directly proportional to the mass factor,  $b$ , where a 20% increase in mass results in a 20% increase in modal forces and deflections (Figure 2.14:  $p = 0$ ,  $b = 1.20$ ,  $V^*/V = OTM^*/OTM = D^*/D = d^*/d = 1.20$ ). For  $p = 0.667, 0.794, 1.0$ , a given degree of mass increase results in a lesser degree of

force and deflection increase where, for instance, if  $p = 0.667$  a 20% increase in mass results in a 12.9% increase in design quantities (Figure 2.14:  $p = 0.667$ ,  $b = 1.20$ ,  $V^*/V = OTM^*/OTM = D^*/D = d^*/d = 1.129$ ). As  $p$  values become progressively larger, smaller rates of increase in design quantities are observed for increasing mass.

Thus, for a long period buliding(e.g.  $T=4.0$  sec.), a 20% increase in mass results in no change in fundamental modal forces or deflections using the Newmark spectrum (zone D,  $p = 2.0$ ) whereas the ATC spectrum (zone C,  $p = 0.667$ ) yields a 12.9% increase in both forces and deflections (see Table 2.2). The UBC static approach ( $p = 0$ ) will result in a 20% increase in both forces and deflections (Table 2.2).

### Case 3

This case is a combination of cases 1 and 2 where the stiffness and mass are factored equally ( $a = b$ ). For this case, the factored mode shapes and natural periods are identical to the unfactored values. Since there is no period shift, spectral amplitudes are unchanged and variation of design force quantities results from changes in mass induced inertial forces only. As can be seen in Figure 2.15, identical variation in design quantities results for all values of  $p$ . In Figure 2.15(a), it is seen that modal design force quantities increase in direct proportion to the stiffness-mass increase where a 20% increase in stiffness and mass results in a 20% increase in modal shears and overturning quantities. In Figure 2.15(b), modal deflection variations are plotted. It is seen that an increase in stiffness and mass results in no change in deflections and drifts. This result can be reasoned from the fact that the increased inertial forces are resisted by an equally increased stiffness resulting in no change in modal deflections.

Thus, for a 20% increase in mass and stiffness, dynamic analysis

using any of the various spectra shown in Table 2.2 will result in a 20% increase in modal forces and no increase in deflection. Likewise, the UBC static approach also yields this same result.

The following general observations can be made from Figures 2.13, 2.14 and 2.15 and Table 2.2:

- (1) In dynamic analysis, if only the stiffness is varied, greater variation in story shears and overturning moments will result for higher  $p$  values. If UBC equivalent static approach is used ( $p = 0$ ) no change in design force quantities results (Figure 2.13(a)). For deflections, dynamic analysis results in lesser variations in for higher  $p$  values. For  $p = 2.0$ , no variation in deflections results with changing stiffness. If the UBC static approach is used, the greatest variation in deflections results (Figure 2.13(b)).
- (2) For changing mass only, dynamic analysis results in lesser variations in story shears, overturning moments, deflections and drifts for higher  $p$  values. If the UBC static approach is used ( $p = 0$ ), the greatest variation in design quantities results (Figure 2.14).
- (3) If stiffness and mass are both factored equally, the same variations in design quantities result for all  $p$  values including the UBC ( $p = 0$ ) equivalent static method.
- (4) For all  $p$  values, the most conservative (largest) story shears and overturning moments result from the stiffest and most massive idealization and the most conservative

deflections and drifts result from the least stiff and most massive model.

In the above observations, it is assumed that the UBC results are based on approximate code formulae for period calculation and not on the actual stiffness properties of the structure.

In summary, assumptions for modeling mass and stiffness properties will yield varying degrees of conservatism in response quantities depending on the spectrum (Newmark, Blume, ATC, etc.) and approach (dynamic or code equivalent static) used. Expressions (2.17) and (2.18) relate changes in mass and stiffness modeling to resulting variations in design quantities. These expressions, along with Table 2.1 and Figures 2.13, 2.14 and 2.15, can be used to predict the influence of various modeling assumptions on analytical response and to assess the degrees of conservatism that result for different response spectra and analytical approaches.

Table 2.1: P-Values Used by Various Recommended Design Spectra

Design Spectrum	Spectrum Zones			
	A	B	C	D
Newmark	-0.91	0	1.0	2.0
Blume*	-1.0	-1.0	0.794	---
NRC	-0.74	-0.14	0.822	2.0
API	-1.0	0	1.0	---
ATC	---	0	0.667	---
VA	---	0	1.0	---
UBC**	---	0	0.5	---

\*Recommended spectrum for 84% probability of not being exceeded.

\*\*UBC equivalent static spectrum.

$$S_a \propto (1/T)^p$$

Table 2.2: Variations in Modal Design Quantities Resulting from Factoring Stiffness and Mass Matrices

P	Spectrum	Zone	Design Quantity Ratio <sup>(1)</sup>	Case 1 Stiffness Variation Only			Case 2 Mass Variation Only			Case 3 Mass and Stiffness Variation		
				a =			b =			a = b =		
				0.8	1.0	1.2	0.8	1.0	1.2	0.8	1.0	1.2
2.0	Newmark	D	V*/V, OTM*/OTM	0.80	1.0	1.20	1.0	1.0	1.0	0.8	1.0	1.2
			D*/D, d*/d	1.0	1.0	1.0	1.0	1.0	1.0	1.0	1.0	1.0
1.0	Newmark, API, VA	C	V*/V, OTM*/OTM	0.894	1.0	1.095	0.894	1.0	1.095	0.8	1.0	1.2
			D*/D, d*/d	1.118	1.0	0.913	0.894	1.0	1.095	1.0	1.0	1.0
0.794	Blume	C	V*/V, OTM*/OTM	0.915	1.0	1.075	0.874	1.0	1.116	0.8	1.0	1.2
			D*/D, d*/d	1.144	1.0	0.896	0.874	1.0	1.116	1.0	1.0	1.0
0.667	ATC	C	V*/V, OTM*/OTM	0.928	1.0	1.063	0.862	1.0	1.129	0.8	1.0	1.2
			D*/D, d*/d	1.160	1.0	0.886	0.862	1.0	1.129	1.0	1.0	1.0
0.0	UBC static <sup>(2)</sup>	C	V*/V, OTM*/OTM	1.0	1.0	1.0	0.80	1.0	1.20	0.8	1.0	1.2
			D*/D, d*/d	1.250	1.0	0.833	0.80	1.0	1.20	1.0	1.0	1.0

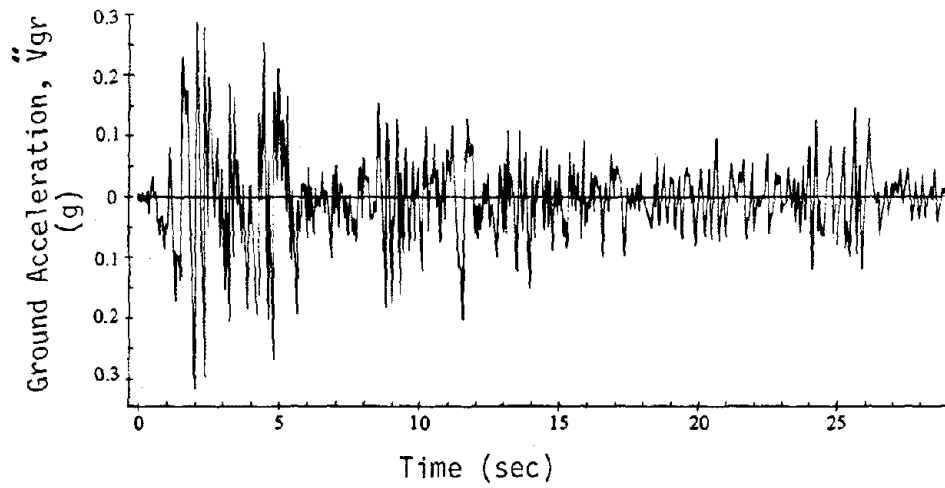
(1) Given  $\underline{K}^* = a\underline{K}$ ,  $\underline{M}^* = b\underline{M}$

Design quantity correspondence is

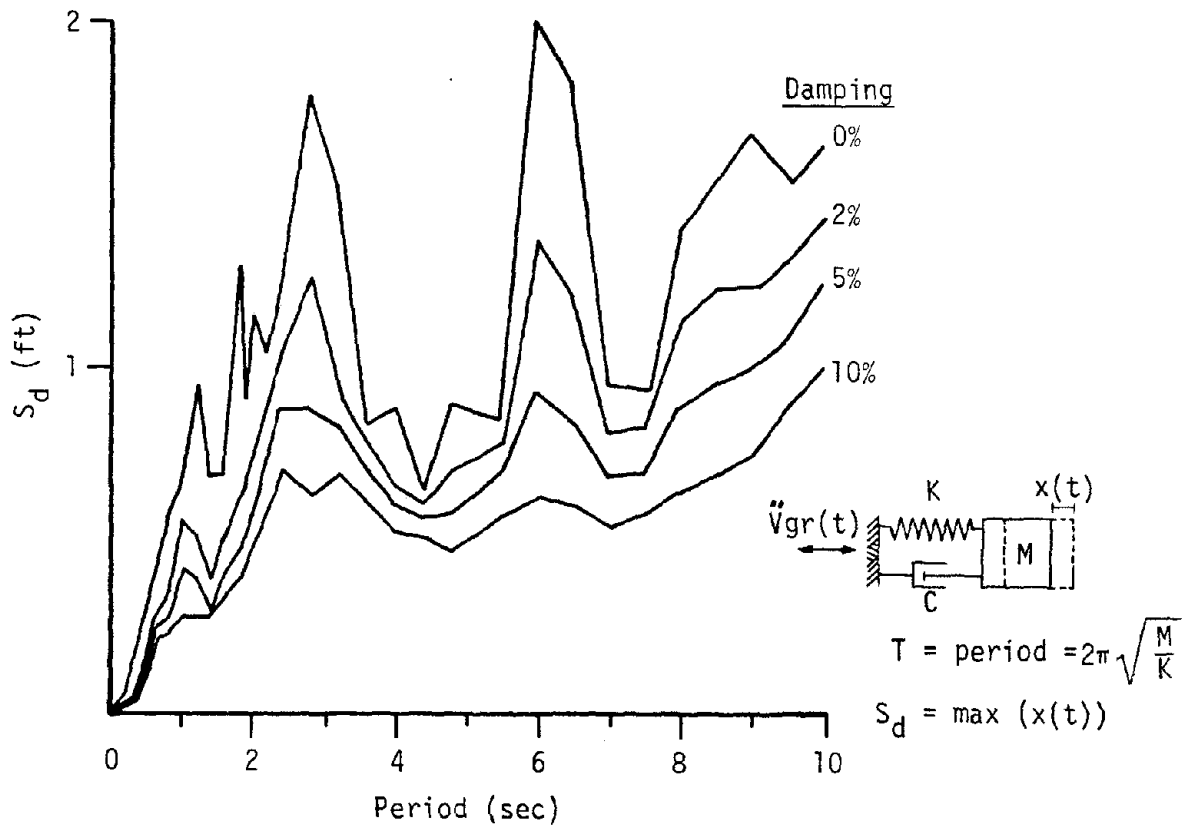
V, OTM, D, d:  $\underline{K}$ ,  $\underline{M}$

V\*, OTM\*, D\*, d\*:  $\underline{K}^*$ ,  $\underline{M}^*$

(2) Assumes period based on UBC equations.



(a) Ground Acceleration History from El Centro 1940 Record (N-S Component)



(b) Relative Displacement Response Spectra for El Centro 1940

Figure 2.1: Development of Response Spectra from Recorded Ground Motions

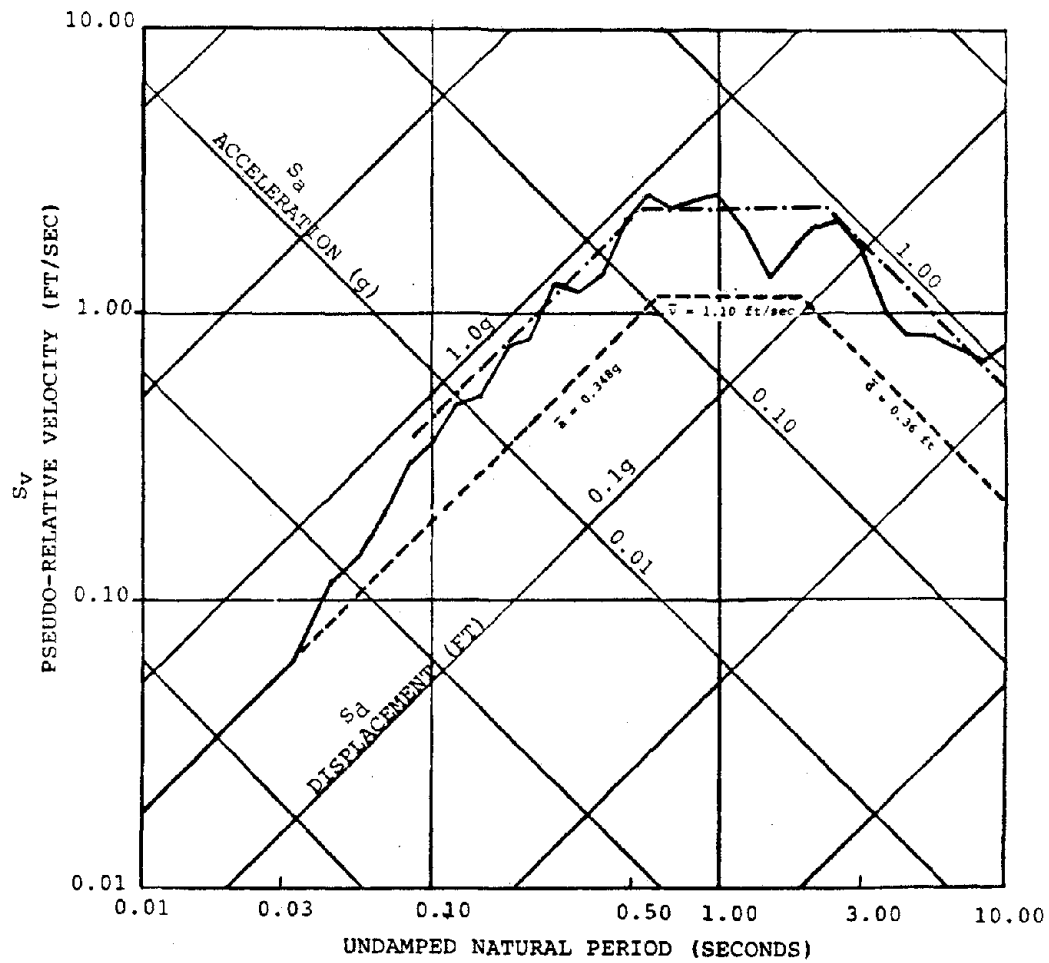


Figure 2.2: Tripartite Plot of El Centro 1940 Response Spectrum (5% damping, N-S Component)

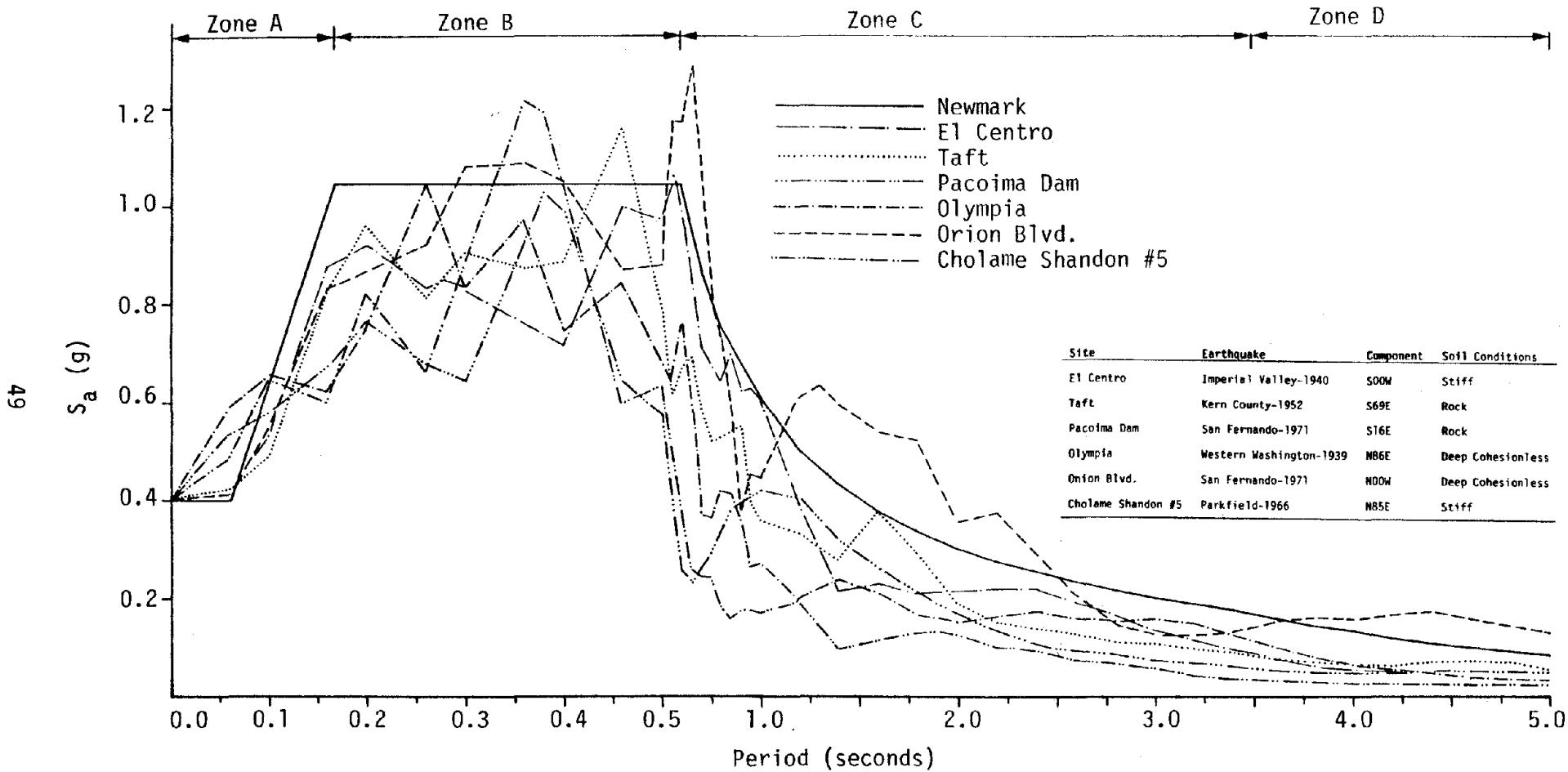


Figure 2.3: Several Earthquake Response Spectra Normalized to 0.4g Peak Ground Acceleration  
(All Spectra Are For 5% Critical Damping)

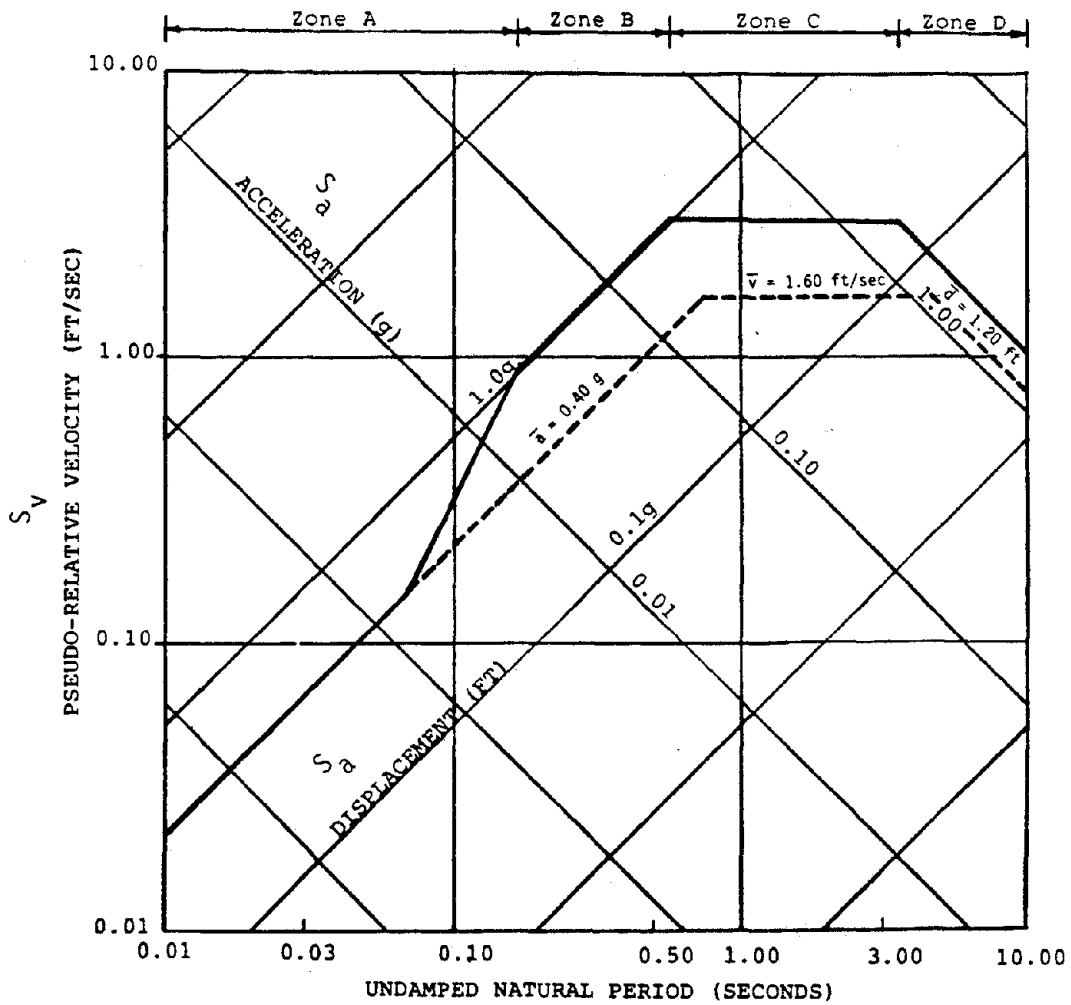


Figure 2.4: Tripartite Plot of Newmark Design Spectrum (peak gr. acc. 0.4 g, peak gr. vel. 1.60 ft/sec, peak gr. displ. 1.20 ft.)

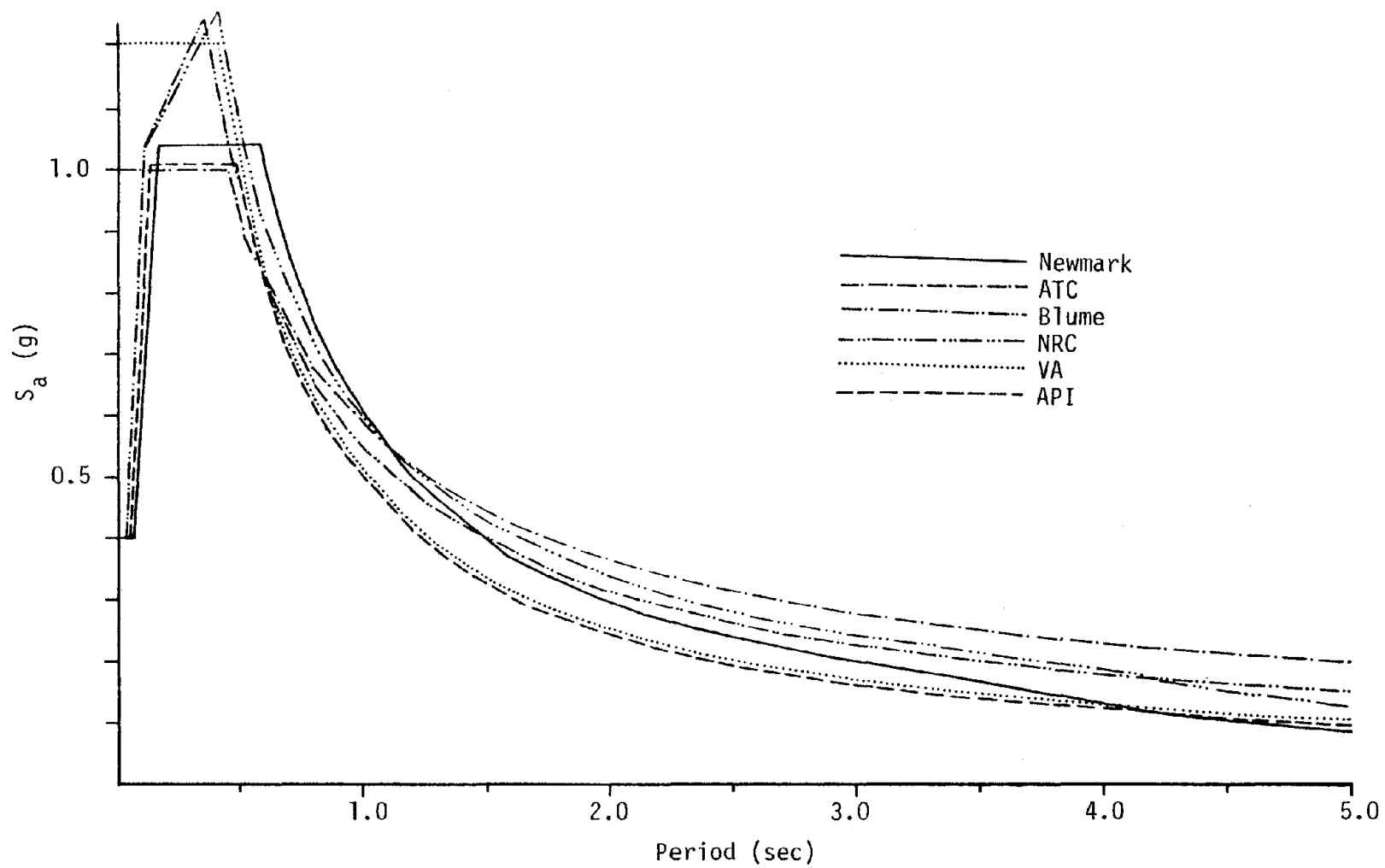


Figure 2.5: Various Recommended Smoothed Design Spectra  
(5% damping, 0.4 g peak gr. acc.)

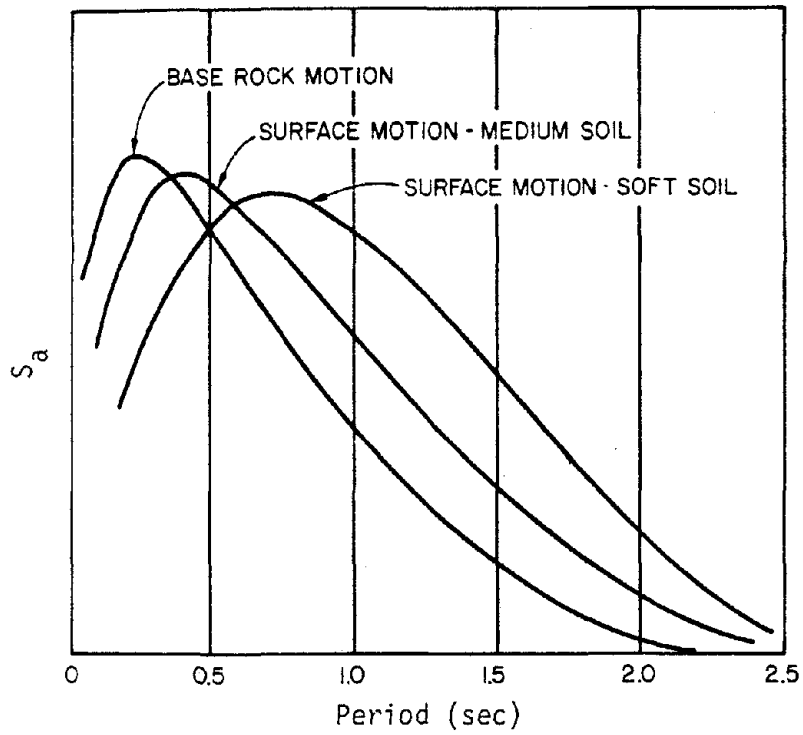


Figure 2.6: Influence of Soil Conditions on Response Spectra

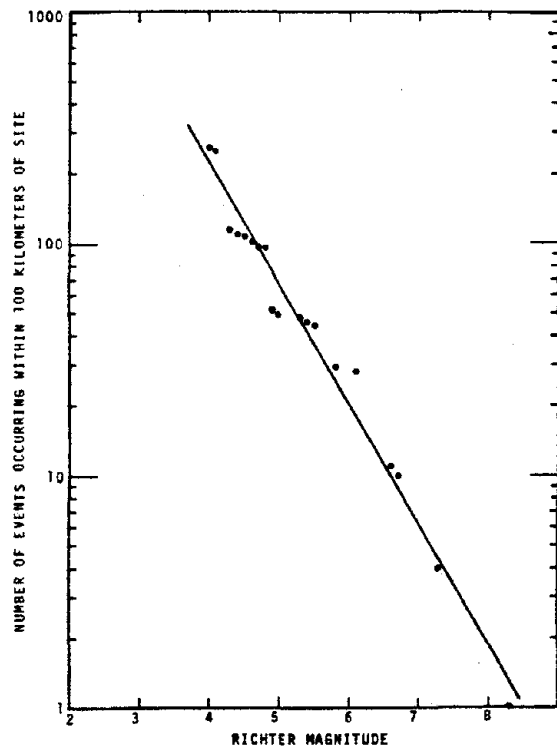


Figure 2.7: Earthquake Magnitude Recurrence Plot (San Francisco site, based on a 163 year time span)

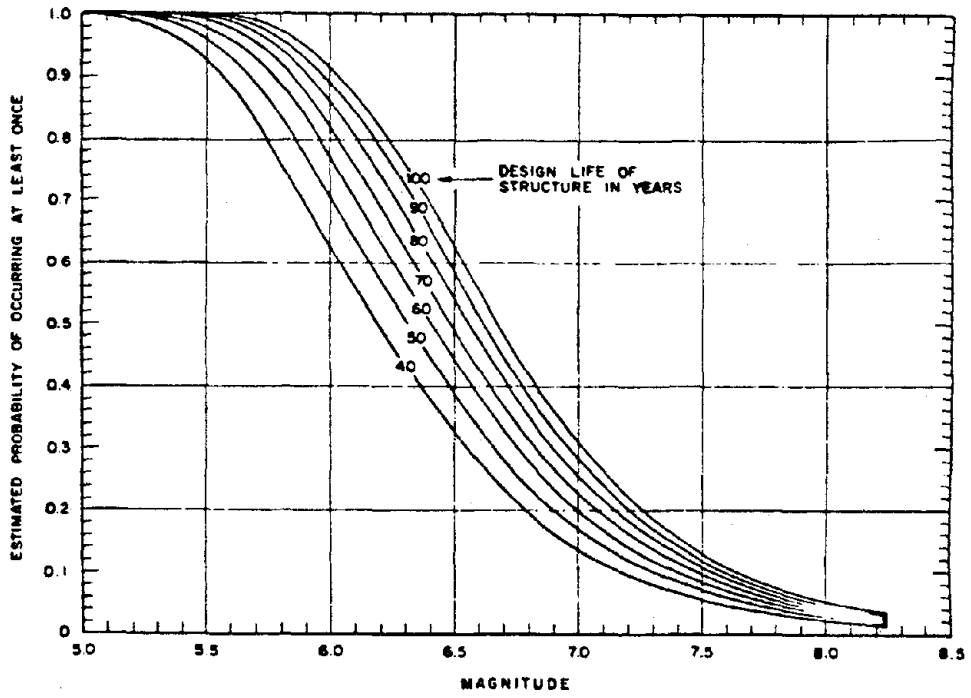


Figure 2.8: Earthquake Magnitude Probability Plot for Different Design Lifetimes

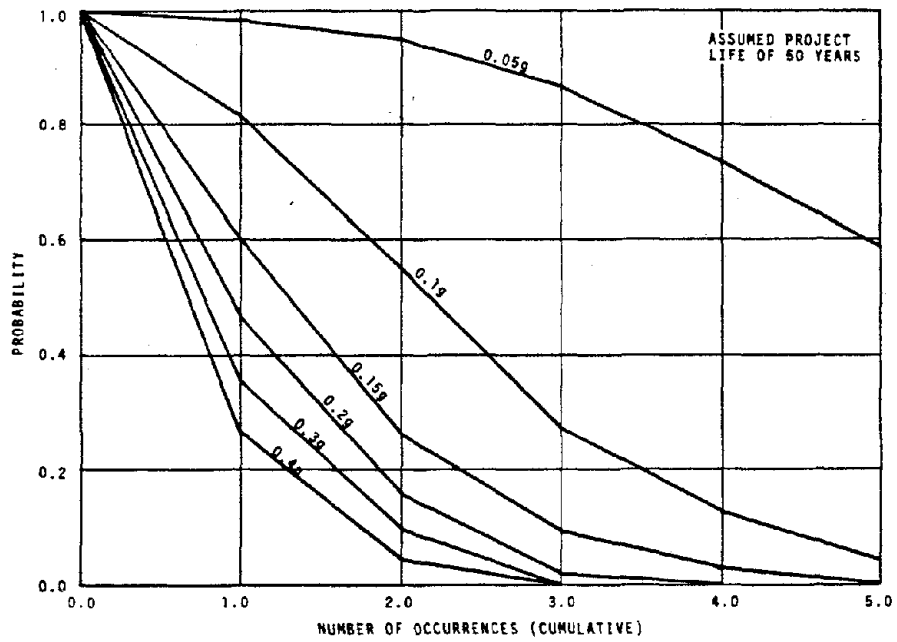


Figure 2.9: Peak Ground Acceleration Probability Plot

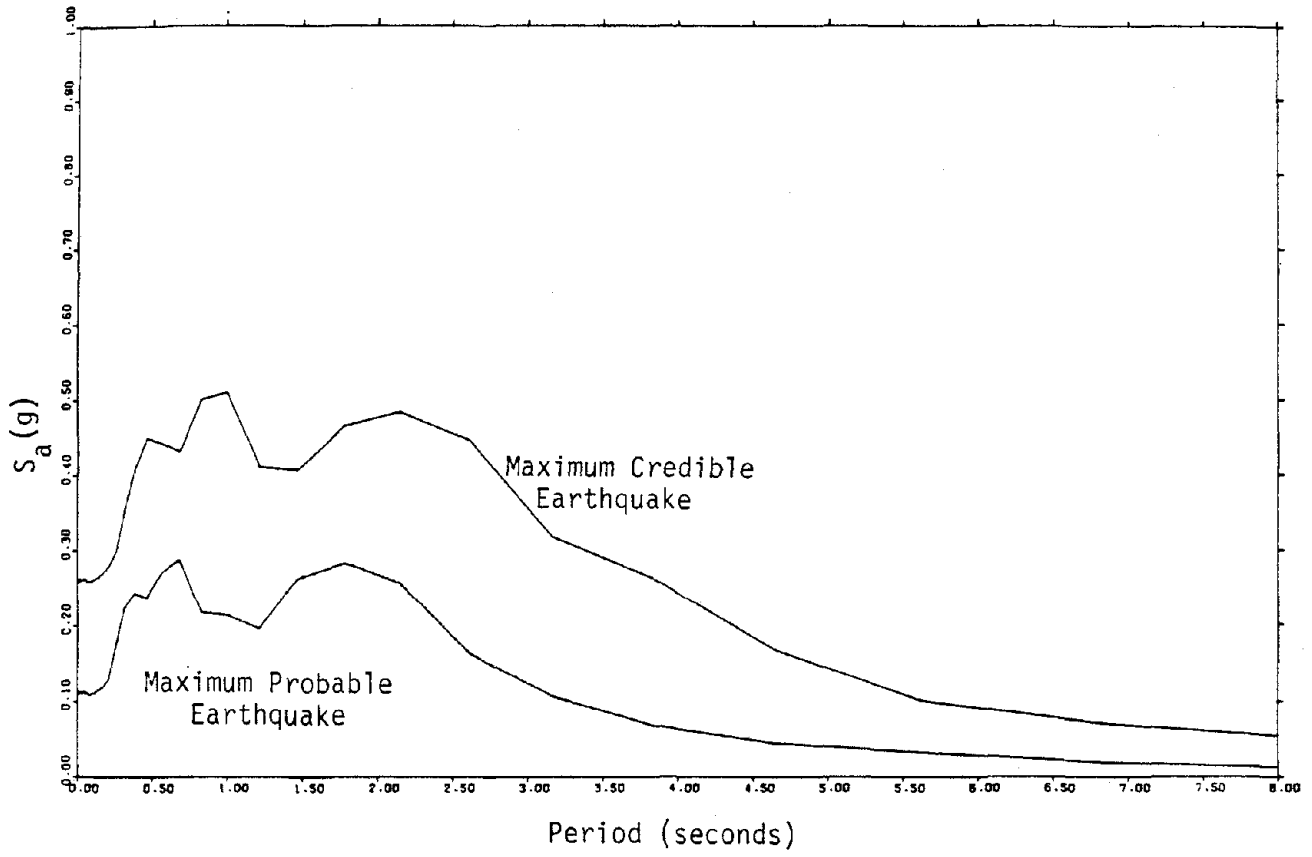


Figure 2.10: Site Specific Study Design Spectra

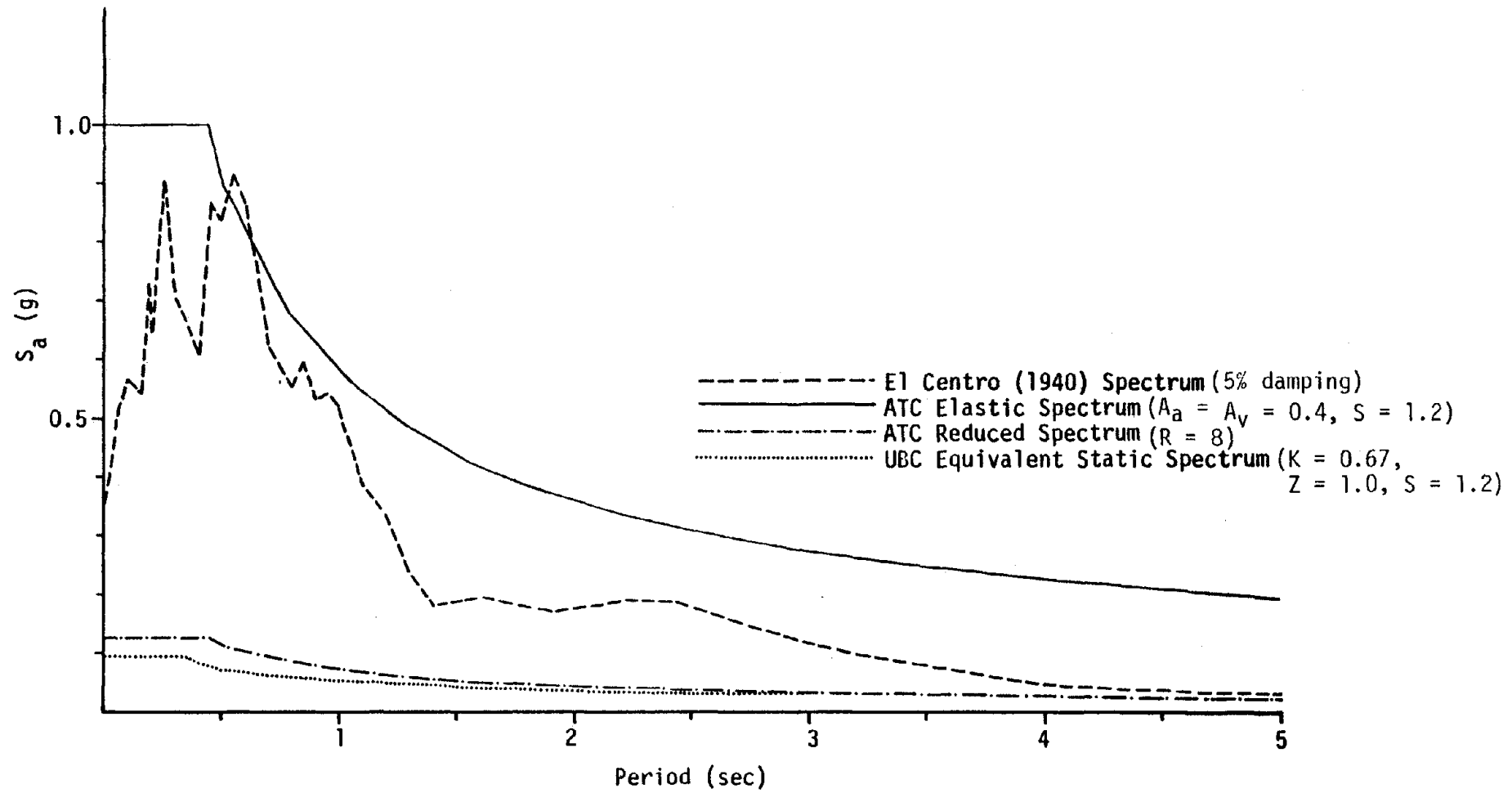


Figure 2.11: Comparative Acceleration Spectra: Elastic vs. Design

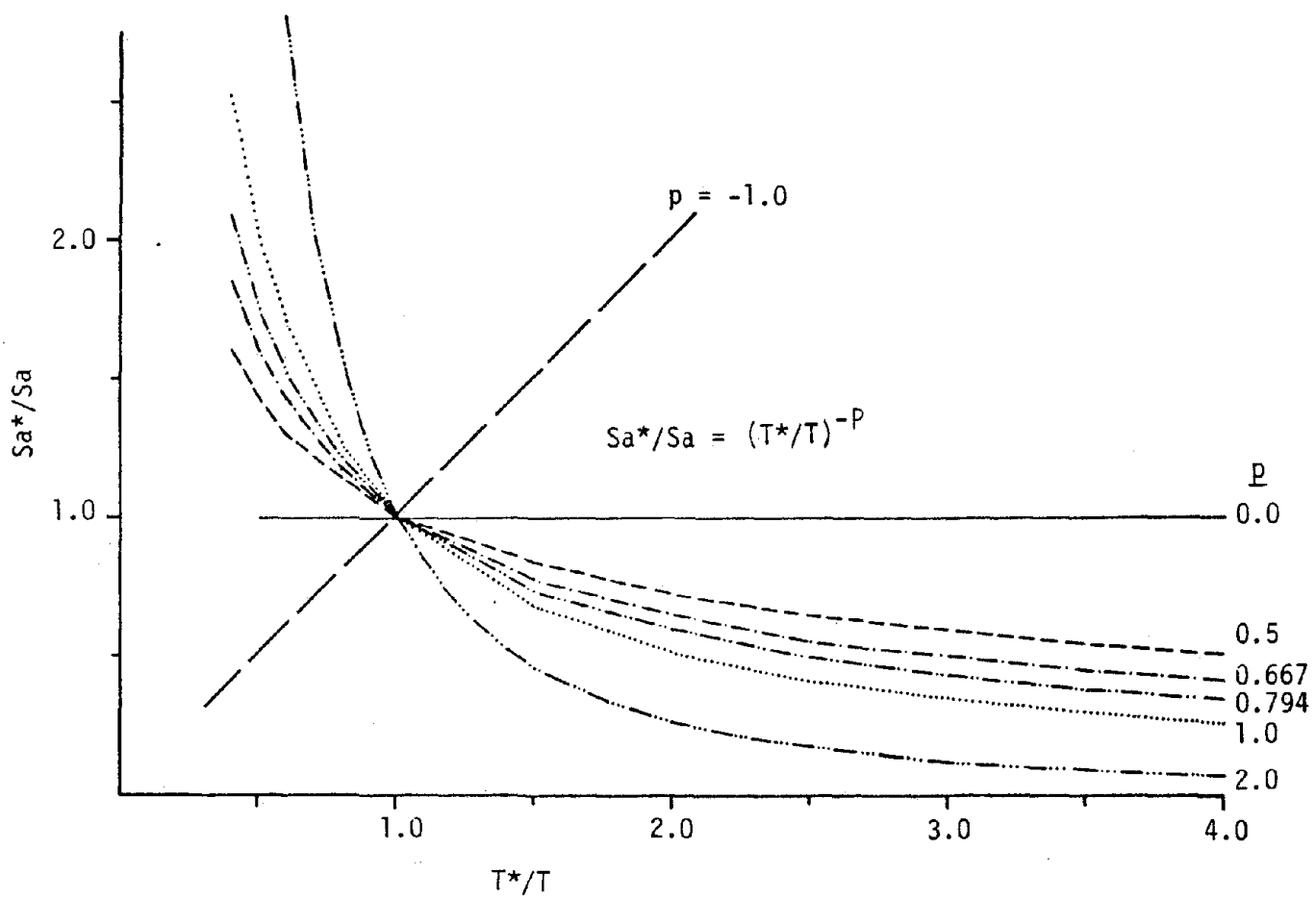
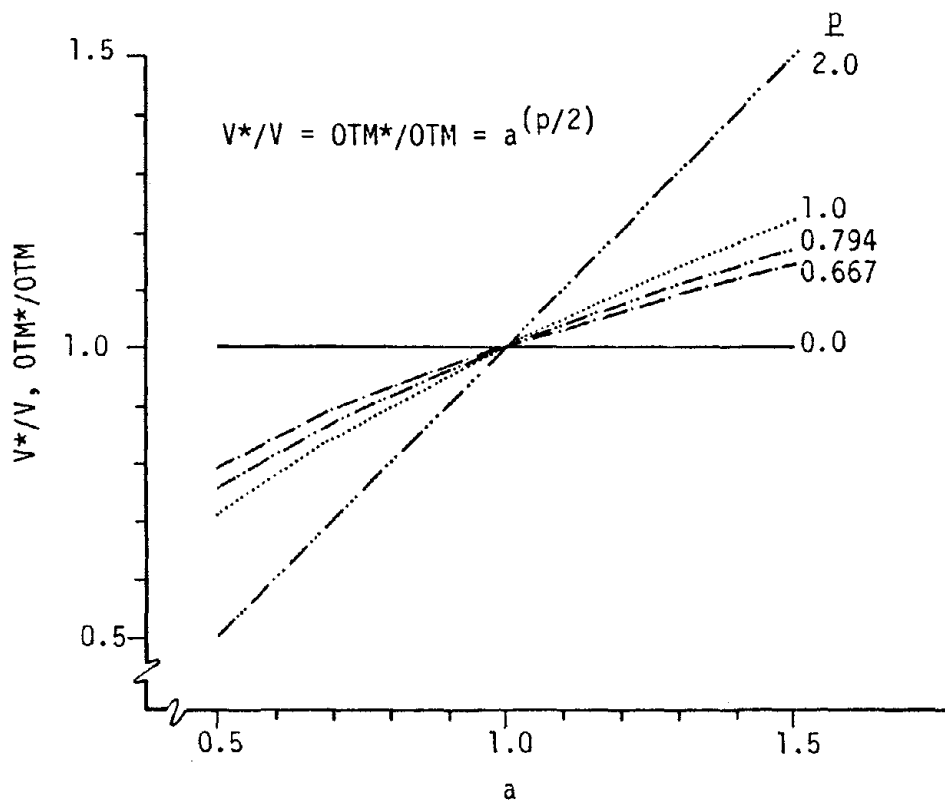
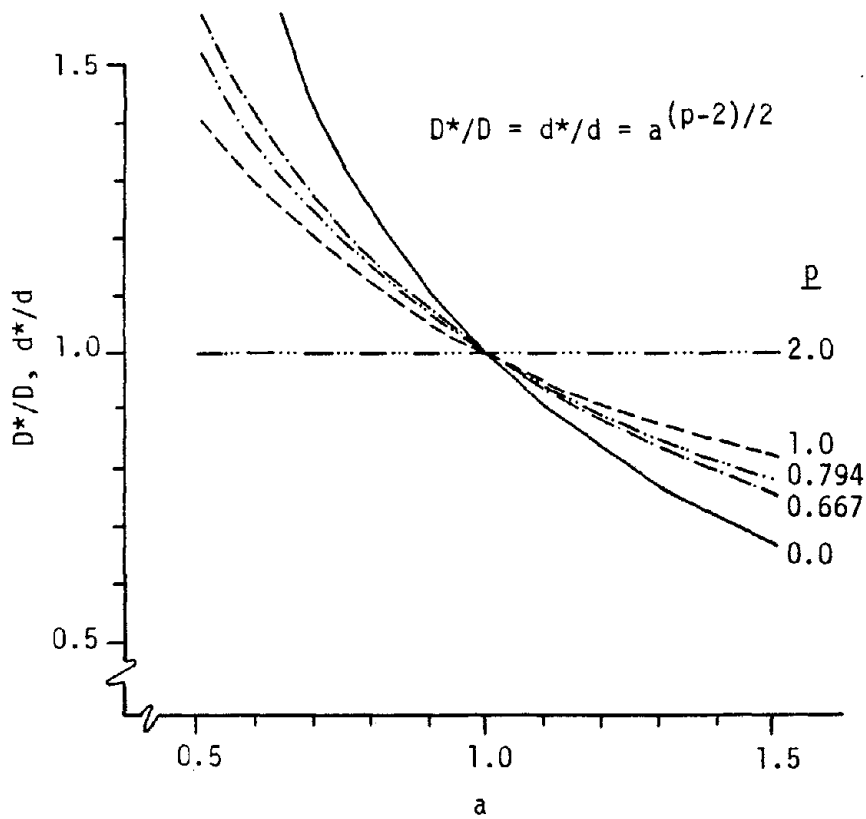


Figure 2.12: Variation of Spectral Acceleration with Period for Different P-values



(a) Modal Story Shear and Overturning Variations



(b) Modal Story Deflection and Drift Variations

Figure 2.13: Variation in Modal Design Quantities for Factored Stiffness, Constant Mass ( $K \rightarrow aK, M$  constant)

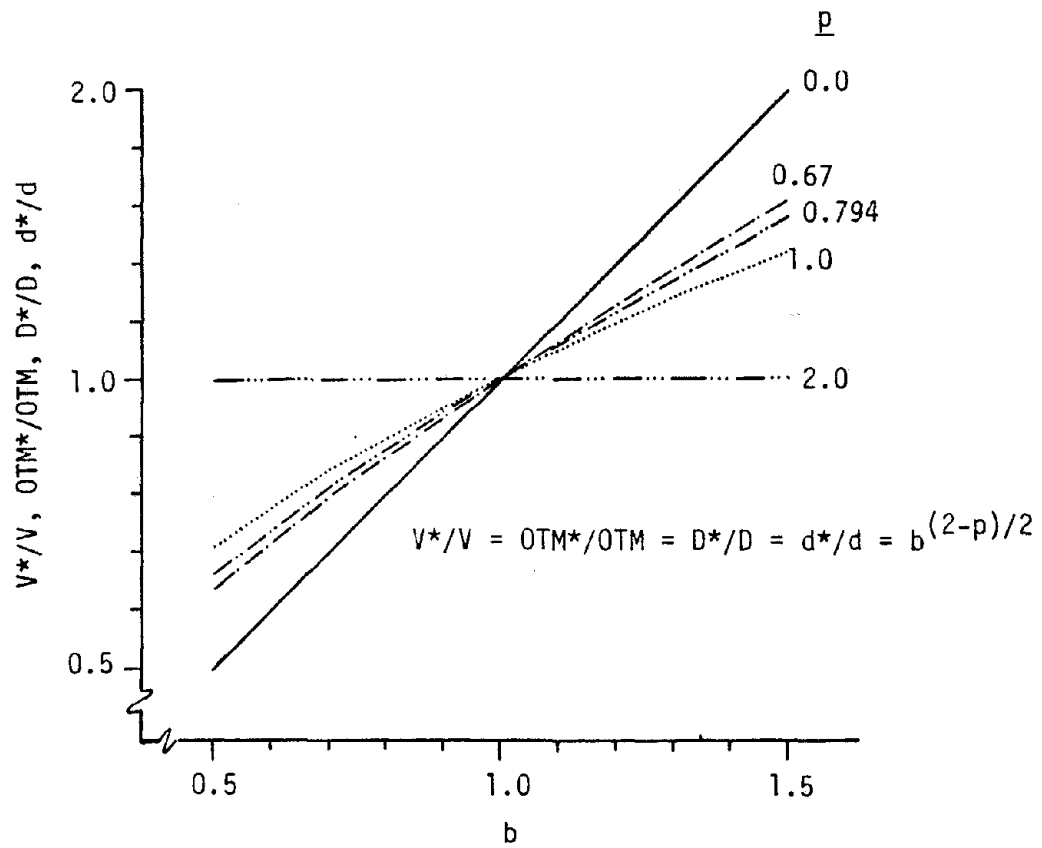
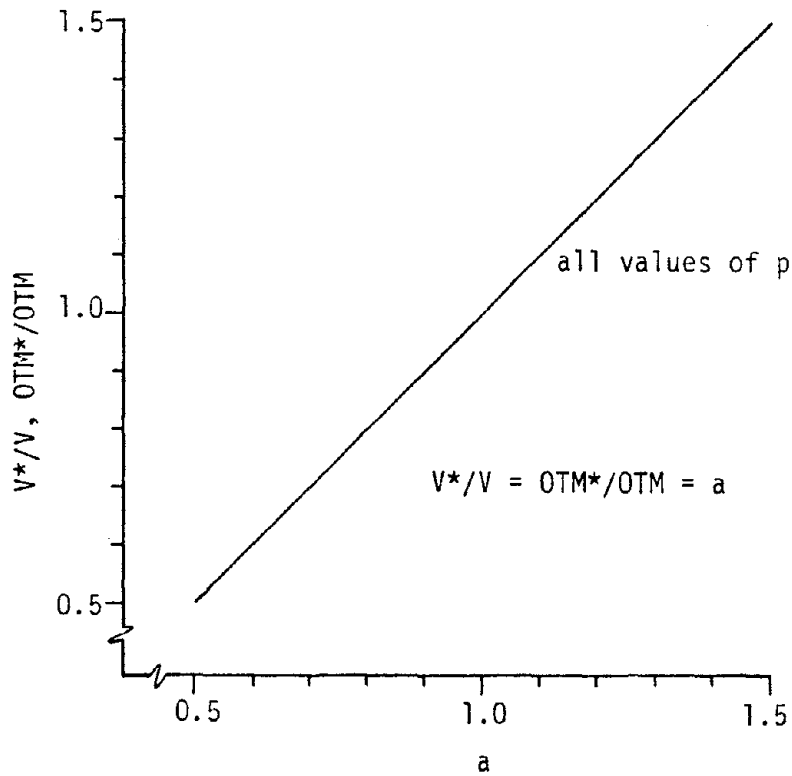
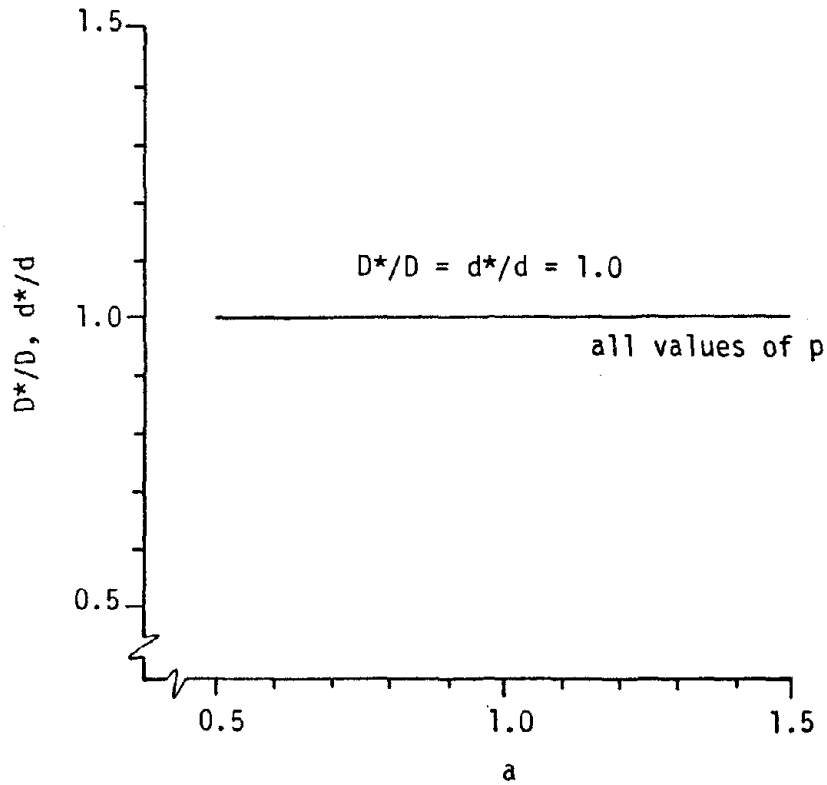


Figure 2.14: Variation in Modal Design Quantities for Constant Stiffness, Factored Mass ( $K$  constant,  $M \rightarrow bM$ )



(a) Modal Story Shear and Overturning



(b) Modal Story Deflection and Drift

Figure 2.15: Variation in Modal Design Quantities for Equally Factored Stiffness and Mass ( $\underline{K} \rightarrow a\underline{K}, \underline{M} \rightarrow a\underline{M}$ )

Page Intentionally Left Blank

## CHAPTER 3

### ANALYTICAL STUDIES OF THE EARTHQUAKE RESPONSE OF SEVERAL MULTISTORY BUILDINGS BASED ON EXPERIMENTALLY DETERMINED DYNAMIC CHARACTERISTICS

#### 3.1 INTRODUCTION

##### 3.1.1 Scope and Purpose

Since the magnitude and distribution of earthquake induced loadings depend upon the dynamic properties (periods and mode shapes) of a given structure, determination of these properties is an essential part of the seismic design process. With the aid of computers, numerical models of complex structures can be constructed and analyzed to give estimates of natural periods and mode shapes. However, numerical models based on an unrefined representation of the primary lateral force system acting alone often predict structural periods that are significantly larger than those that would be observed in small amplitude response studies due to the omission of various structural and nonstructural modeling aspects. Although periods based on small amplitude tests of buildings tend to be somewhat lower than those expected during moderate earthquake excitation (discussed in section 2.4), the development of analytical models whose dynamic properties correlate well with small amplitude tests is important in order to identify those modeling aspects that can significantly influence response. Armed with an understanding of the relative importance of these modeling aspects, the engineer/analyst can make a better assessment as to which of these aspects should or should not be considered in developing a computer model to meet his design objectives.

This chapter contains results of analytical studies performed on five multistory buildings located in seismically active regions of the

United States. Each building has been the subject of a previous study in which the building's overall dynamic characteristics were established by experimental testing using forced vibration and, in some cases, ambient motion techniques. The results of the previous studies are used as a data base for developing numerical models that reflect the true small amplitude dynamic properties. Earthquake analyses are then performed on several models of each building to assess the influence of various modeling assumptions. Predicted dynamic responses are compared with responses resulting from application of standard equivalent static analysis procedures recommended by current building codes.

The five buildings studied, their important construction features, and the references reporting the original experimental dynamic test results are as:

<u>Building</u>	<u>Construction Features</u>	<u>Ref.</u>
1. ALOCA BUILDING, San Francisco	diagonally braced frames with secondary moment frame	(32)
2. TRANSAMERICA BUILDING, San Francisco	moment frame, pyramid shaped	(39)
3. UNIVERSITY OF CALIFORNIA MEDICAL CENTER BUILDING, San Francisco	moment frame with long span girders	(31)
4. RANIER TOWER, Seattle	moment frame with concrete pedestal base	(40)
5. CENTURY CITY THEME TOWER, Los Angeles	moment frame, triangular plan	(29)

In the original studies referenced above, limited correlative computer analyses were performed where, in order to reflect observed behavior, the analytical models often incorporated stiffness and mass modeling assumptions of general nature without incorporating the actual detailed characteristics of the buildings. Therefore, practical guidelines for appropriate modeling approaches were not derived as

this was not the purpose of these studies.

In the current work, each of the study buildings has been extensively reanalyzed in order to develop computer models based on the actual detailed characteristics of the structure that reflect the the observed dynamic properties. The purposes of the analyses of the study buildings presented in this chapter are:

- (1) to investigate the degree to which practical mathematical models of limited complexity can accurately reflect true linear dynamic properties;
- (2) to understand the dynamic characteristics of the buildings and how these contribute to the response induced by earthquake;
- (3) to assess the influence of various modeling aspects on dynamic properties and analytical response;
- (4) to compare earthquake response based on dynamic theory with "equivalent static" response based on lateral load provisions as recommended by current building codes; and,
- (5) to draw general conclusions regarding the above considerations, (1) through (4), pertaining to the earthquake analysis of multistory buildings.

It should be noted that the superstructures of all five buildings studied are primarily of steel construction. Nevertheless, the general behaviors of these buildings are believed to be representative of multistory, high-rise buildings constructed of reinforced concrete as well.

It is realized that dynamic properties themselves along with the detailed analytical models used to capture these properties are of secondary interest to the design engineer. Of primary concern are the resulting force and displacement quantities for which he must design the structure in order to resist the earthquake excitation. In order to enhance the applicability of this work to engineering design, an effort has been made to present results in terms of gross engineering quantities most important for building design (i.e. gross shears, overturning moments, deflections, and drifts resulting in each story) and to keep the detailed modeling techniques consistent with current building design practice.

### **3.1.2 Approach Used for Analyses of the Study Buildings**

The analytical studies of the five buildings are reported separately in sections 3.2, 3.3, 3.4, 3.5, and 3.6. In order to enable direct comparison of results, a single analytical approach comprised of a six step procedure was used to investigate each of the study buildings and the discussion of each building is organized according to these steps. The background and intent of each step of this analytical approach is presented in the following descriptions.

#### **Step 1: Identification of the Structural System.**

A review of the building system based on the structural and architectural drawings and, if available, on design calculations is carried out. Various systems and components potentially contributing to the lateral resisting system are identified.

#### **Step 2: Results of Experimental Studies.**

Each building has undergone experimental dynamic testing by forced vibration and/or ambient motion methods. In this step, results of these studies are reviewed and significant aspects of overall dynamic behavior are identified.

#### **Step 3: Analytical Model Development and Comparison with Experimental Results.**

For each building, a series of detailed analytical models is developed to investigate the influence of various modeling aspects on dynamic properties (periods and mode shapes). Analytical results are compared with the dynamic properties observed in the experimental studies. Both translational and torsional modes of vibration are examined. It is recognized that arbitrary variations in stiffness and mass can easily be used to obtain a close match between experimental and analytical periods. However, in the analysis of the five study

buildings, all stiffness and mass modeling changes are explicitly accounted for. Between 4 and 6 detailed models are formulated for each building. The first model (Model 1) generally includes only the primary lateral force resisting system acting alone. Here, an unrefined model is used where simplifying conditions such as two dimensional (planar) frame behavior and center-to-center member dimensions are assumed. In subsequent models, aspects such as three dimensional (non-planar) frame action, rigid joint zones, vertical and/or secondary lateral systems, nonstructural slab-girder interaction, infill block walls, and refined estimates of mass are incorporated. Extraneous structural and nonstructural elements (e.g. floor beams with non-moment connections, architectural cladding, electromechanical ducts and piping, etc.) are not included in the models since it is usually not practical to model these components and since these generally do not contribute significant lateral resistance. The last model formulation for each building is the most refined and generally shows the best correlation with small amplitude results.

#### **Step 4: Influence of Modeling Approach on Results of Dynamic Analysis.**

The objective in this step of the analysis is to investigate the influence of the various assumptions used to develop the models of each building on overall engineering design quantities. For each of the models, a response spectrum dynamic analysis is performed for a unidirectional earthquake input. Comparative results are presented in the form of engineering quantities generally used in building design including story shears, story overturning moments, total deflections and story drifts. An envelope of maximum responses for each design quantity is calculated over the height of the building based on the square root of the sum of the squares (SRSS) modal combination method. The SRSS method provides good estimates of peak response for the

uncoupled modal responses of the five study buildings as discussed in section 4.2. The Newmark elastic spectrum (26) was used to perform the dynamic analyses since it is well known and is more representative of actual earthquake spectra than, for instance, the ATC (5) recommended spectrum. In order to yield results that are comparable to those that would be used for elastic limit design, the Newmark spectrum is scaled to reflect the peak ground acceleration level recommended by the ATC Tentative Provisions. ATC specifies a 0.4g effective peak ground acceleration for geographical areas of highest seismicity. The 0.4g scaled Newmark spectrum is shown in Figure 3.1.1. This spectrum is then reduced by the ATC recommended response modification factor,  $R$ , appropriate for the particular type of structural system (e.g.,  $R = 8$  for a moment resisting frame system;  $R = 6$  for a braced frame dual system). In addition to demonstrating the influence of modeling assumptions on the magnitudes of design quantities, the relative contributions of the various modes to these design quantities are also examined in this step in order to enhance understanding of the dynamic response of each building.

#### **Step 5: Comparison of Design Spectra Dynamic Analysis with Building Code Provisions.**

In this step, the object is to compare the analytical responses resulting from various dynamic and "equivalent static" recommended applications of earthquake loading. Two different smoothed design spectra are used for dynamic analysis: the Newmark spectrum and the ATC recommended spectrum. Also, two different equivalent static earthquake loading procedures are used: the UBC-1979 regulations and the ATC tentative recommendations. In order to have a common basis for comparison of these different loading methods, a single model of each building is analyzed. Generally, the model used for this analysis is the one that reflects the best correlation with the

observed small amplitude dynamic properties and/or produces the most conservative force quantities in dynamic response (i.e., the model having the lowest natural periods of vibration).

In order to allow direct comparison of response quantities resulting from the different seismic load procedures, the following assumptions are made:

- (1) Soil Conditions. Both the UBC and ATC provisions make allowance for soil effects on response using an "S" factor whose value ranges from 1.0 to 1.5. For consistency, the ATC recommended default value of  $S = 1.2$  is assumed for calculation of both the ATC and UBC spectral values representing stable deposits of sands, gravels or stiff clays. Specific recommended variations for soil conditions are not made for the Newmark spectrum but the data upon which the spectrum is based is representative of firm ground, soft rock, or competent sediments which are assumed to roughly correspond to the  $S = 1.2$  condition.
- (2) Peak Ground Acceleration. Both the Newmark and ATC recommended spectra are based on a peak ground acceleration value. ATC specifies effective peak acceleration, EPA, values ranging from 0.05g to 0.40g depending upon geographic locality. An EPA value of 0.4g was used for analysis of all of the study buildings. For consistency of ground motion magnitudes, the Newmark spectrum is scaled to this same 0.4g peak ground acceleration value. To yield force levels consistent with elastic limit design, both spectra are then reduced by the appropriate ATC specified response modification factor, R ( $R = 8$  for ductile moment frames;  $R = 6$  for

braced frame, dual system). A structural damping value of 5% is used in development of the ATC spectrum and is therefore also used for the Newmark spectrum.

- (3) Elastic Limit Design Factor for UBC. The ATC provisions use elastic limit design as a basis for developing magnitudes of earthquake loading where the strength of structural steel members is determined using a factor of 1.7 times the working stress levels allowed by AISC (1). The UBC, however, uses an allowable stress increase factor of 1.33 for earthquake loading. Therefore, to make a consistent comparison of UBC versus ATC equivalent static methods, earthquake UBC specified static loadings are factored by  $1.70/1.33 = 1.278$ .

In Figure 3.1.1, the reduced ATC spectrum is shown corresponding to an EPA value of 0.40g and an R value of 8 (for moment resisting frame construction) resulting in a reduced equivalent EPA value of 0.05g (=  $EPA/R = 0.4g/8$ ). Also shown in this figure is the Newmark spectrum scaled to the same 0.05g peak ground acceleration. As can be seen from the figure, ATC recommends more conservative values of spectral amplitude in longer period ranges and less conservative values in shorter period ranges. Since the multistory buildings being studied have relatively long periods, the ATC spectrum will generally produce higher levels of response than the Newmark spectrum for corresponding levels of ground motion amplitude. The Newmark spectrum, however, is more representative of actual earthquake spectra and, in fact, yields more conservative results than would generally be expected from an actual earthquake with the same peak acceleration (Figure 2.3). Also shown in Figure 3.1.1 is the UBC equivalent static spectrum for moment resisting frame multiplied by the 1.278 factor. As can be seen, the UBC recommends the largest

spectral amplitudes at longer periods and will generally result in the most conservative force levels for tall multistory buildings.

In the application of static load procedures, the UBC and ATC recommendations supply approximate empirical formulae for calculating the fundamental periods of buildings. However, period calculation based on a more detailed analysis is recommended. Therefore in this study, response results for the UBC and ATC equivalent static procedures are determined using two fundamental periods: (1) the approximate fundamental period as calculated by codebook formula; and, (2) the fundamental period corresponding to the analytical model used for the dynamic analyses. The difference between these two periods often results in significant variation in equivalent static response quantities.

In comparing the various static and dynamic analyses, both the magnitude and distribution of response quantities are examined. Firstly, the magnitude of design quantities (story shear, overturning moment, deflection, and story drift) resulting from the different earthquake loading approaches are compared. Then, these quantities are normalized with respect to base shear and the differences in the distribution of response over the height of the building are illustrated.

#### **Step 6: Comparison of Code Design Forces with Dynamic Forces Induced by Actual Earthquake Spectra**

In this step, force response predicted by dynamic analysis using real earthquake spectra are compared to equivalent static forces that would be used for the design of the building in accordance with UBC. The purpose is to examine, qualitatively, the ductility demand in the study buildings when subjected to major earthquakes. For each building two different computer models of the building are chosen from the 4 to 6 models developed and are used to predict elastic force

response. One model is composed only of structural elements contributing stiffness and strength to the primary lateral force resisting system. The relatively high natural periods of this model generally result in lower bound approximations to induced elastic dynamic forces. The second model includes various secondary and nonstructural (if any) elements and is, generally, the model that best reflects experimentally observed small amplitude behavior. The lower natural periods of this model usually result in conservative estimates of induced forces. Together, results from the two models serve to bound a range of force response that may be expected if the structure were to respond elastically to actual earthquakes. Two earthquake spectra were used for dynamic analysis, El Centro 1940 and Taft 1952. These two earthquake spectra are shown in Figure 3.1.2. Data pertaining to these earthquakes is as follows:

Site	Taft	El Centro
Date	7/21/52	5/18/40
Earthquake	Kern County	Imperial Valley
Richter Magnitude	7.6	6.6
Source Distance	56 km	8 km
Component	S69E	S00E
Soil	rock	stiff
Peak Gr. Acc.	0.179g	0.348g

Due to proximity of the source, the El Centro spectrum reflects greater intensity of ground motion than the Taft spectrum and will produce larger analytical force response quantities.

The UBC provisions are used to approximate the level of forces that the buildings have been designed to resist elastically where the lateral loads actually calculated by the design engineers are used, if available. The UBC forces are again multiplied by the factor 1.278 to correspond to elastic limit force levels. For comparison with the two earthquake spectra, the factored UBC equivalent static spectrum for moment resisting frames is also shown in Figure 3.1.2.

### 3.1.3 Computer Programs Used for Structural Analysis

The dynamic analyses of the study buildings are performed using a modified version of the ETABS program (23) and the SAP-IV (7) structural analysis program. Both of these programs are publicly available and distributed by the National Information Service for Earthquake Engineering located at the University of California, Berkeley.

ETABS is a special purpose program for the analysis of building systems. The following assumptions are incorporated in its analytical procedure:

- (1) floor slabs are assumed to behave as rigid diaphragms in their own plane,
- (2) only lateral translational and rotational lumped mass degrees of freedom are allowed,
- (3) column lines are vertical.

These assumptions enable ETABS to perform dynamic analysis of buildings with greater numerical efficiency than could be achieved using a general purpose program. The program is an adequate analysis tool for the majority of multistory buildings. However, ETABS' modeling capabilities are limited due to its assumptions and its fairly small element library. Most of the analyses of the study buildings are performed using ETABS. However, for special modeling situations, the SAP-IV general purpose analysis program is used. The SAP-IV program can perform analyses identical to ETABS, but with lesser efficiency (and greater cost). These programs were chosen for use in this study since they are publicly available and are relatively inexpensive to purchase and use. Several other commercially available programs are also able to perform analyses such as those described in this chapter. A modified version of the ETABS program able to produce

results in the form of gross engineering quantities has been used for this study.

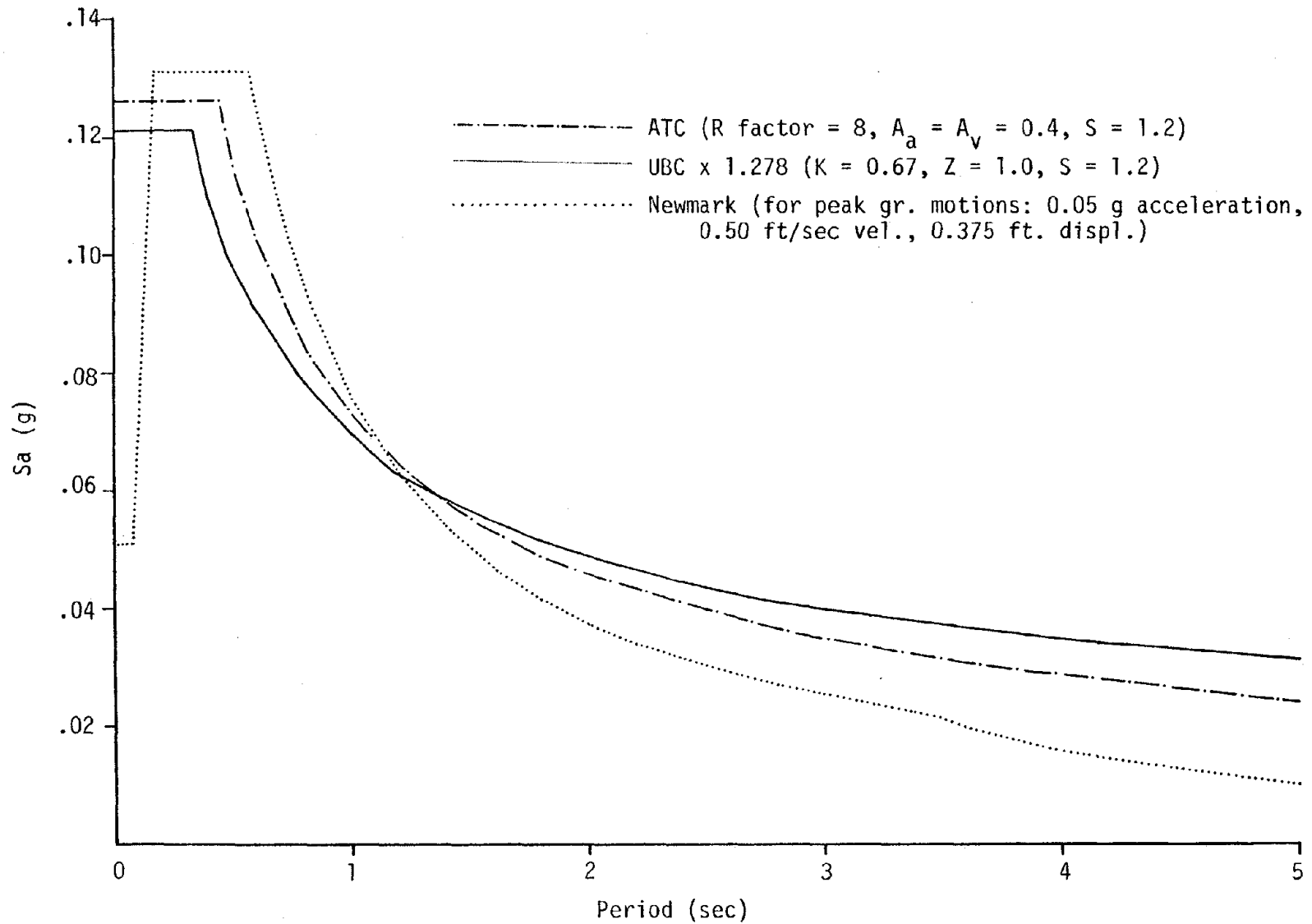


Figure 3.1.1: Response Spectra Recommended by ATC, UBC, and Newmark Scaled to Correspond to Elastic Limit Design

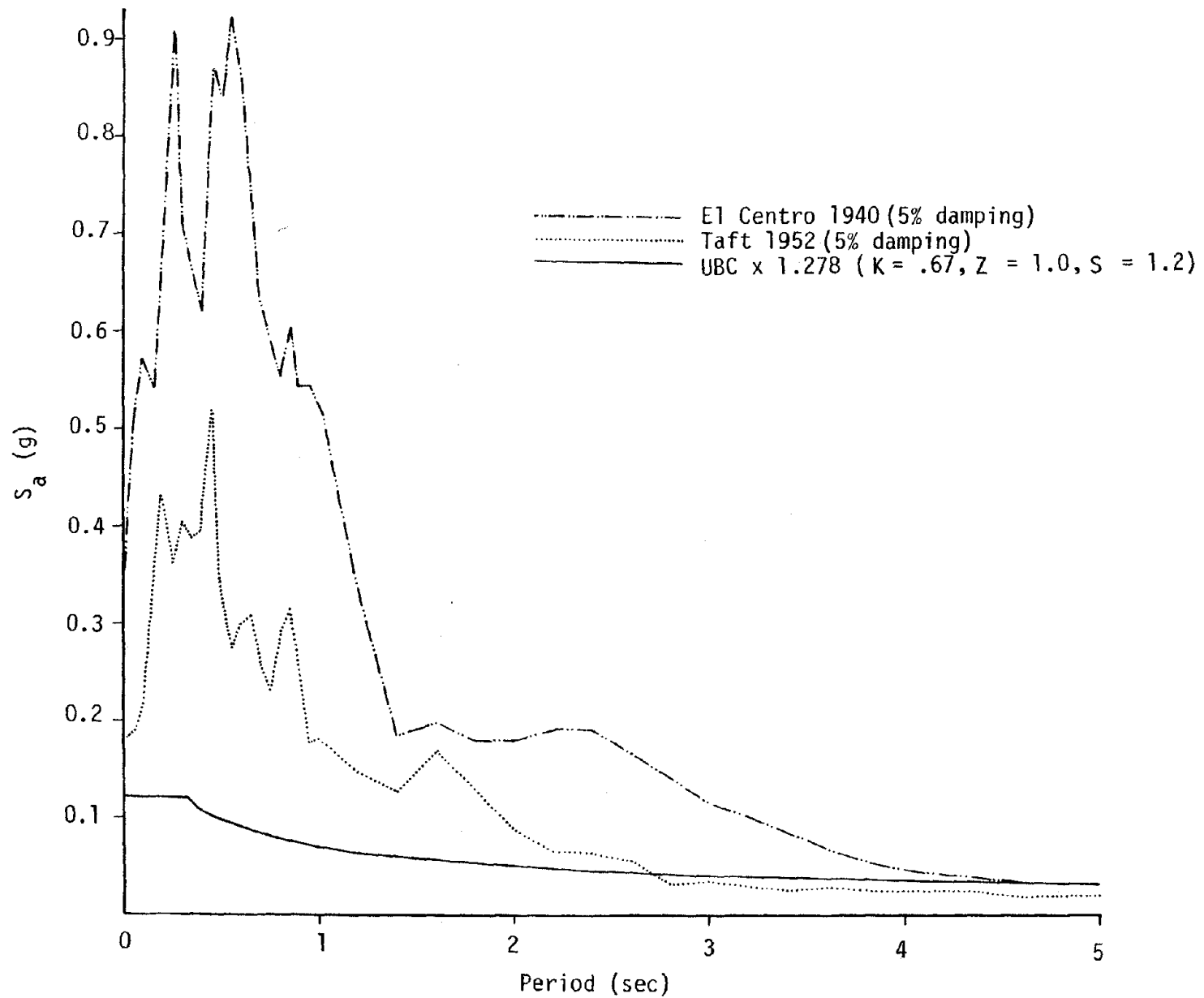


Figure 3.1.2: Comparison of Actual Earthquake Spectra with Factored UBC Equivalent Static Spectrum

Page Intentionally Left Blank

## 3.2 ALCOA BUILDING

The Alcoa Building is a multistory office building located in San Francisco, California. The structure was designed by Skidmore, Owings and Merrill, Architects and Engineers, Inc. of San Francisco. The construction of this building was completed in 1967. The 27-story building has base dimensions of 112 feet by 212 feet and rises to a height of 373 feet. A photograph of the building is shown in Figure 3.2.1.

### 3.2.1 Description of the Structural System

The primary lateral force resisting system consists of four braced frames located at the exterior walls of the building (two in the E-W direction, two in the N-S direction). Between the 2nd and 26th floors a truss bracing system is used with load transfer points every three stories (Figure 3.2.2). In the first story, lateral forces are resisted by moment frames in the N-S direction and by two shear walls in the E-W direction. Vertical hanger elements are used to carry floor loads to the transfer points. The corner columns and intermediate columns are box-sections constructed of welded steel plates. The outer dimensions of these columns are constant throughout the height of the building with the thickness of the plates being reduced with increasing height (Figure 3.2.3). The diagonal bracing members are also welded steel plate box sections.

In addition to the primary system, a central core ductile moment frame extends over the full height of the building as a secondary lateral resisting system (Figure 3.2.4(a)). The core columns and girders are wide flange sections, most of which are encased in concrete for fire protection. The girders are wide flange sections

with welded haunches as shown in Figure 3.2.5(a).

The E-W interior frames are linked to the exterior columns at frame lines C and D by girders spanning from the core to the exterior frame. Several bays of the interior frame are infilled with 8" concrete block walls enclosing stairwells and elevator shafts, as shown in Figure 3.2.4 (b). At the 1st story, the core frames are embedded in the two E-W shear walls at frame lines C and D (Figure 3.2.4 (a)). Each shear wall is 20 inches in thickness and about 42 feet in length.

The floor slab between the central core and the exterior frames consists of 2.5 inches of concrete cover over 1.5 inch concrete filled corrugated steel decking. Inside the core area, the floor typically consists of a 5 inch thick solid slab. In Figure 3.2.5 (b), typical floor slab construction for core and non-core areas are shown. The slabs are supported by secondary floor beams throughout.

Below the 1st floor level, lateral loads are resisted by a massive shear wall foundation system extending down through 3 levels (40 feet). The walls are continuous around the building periphery with additional E-W walls along frame lines C and D. The foundation is supported by a system of pile groups located under the foundation walls as shown in Figure 3.2.6.

### **3.2.2 Results of Experimental Studies**

In June 1967, small amplitude forced vibration tests of the Alcoa Building were carried out by the Earthquake Engineering Research Center of the University of California at Berkeley. For a detailed discussion of this study see reference 32. The forced vibration system was able to excite the first two modes in each of the two translational directions and in torsion. In Figure 3.2.7, the experimental results for the first two mode shapes and periods for each of the three directions of motion are shown.

The experimental results reflect several aspects of dynamic behavior of the building. Firstly, comparing results for the two translational directions, it is seen that the E-W fundamental period of 2.21 sec. is significantly larger than the 1.67 sec. period in the N-S direction. This reflects the greater stiffness that exists in the N-S direction owing to the larger plan dimension. A second aspect of dynamic behavior can be seen by comparing the two translational fundamental mode shapes in Figure 3.2.7. The N-S fundamental mode demonstrates shear beam type of response whereby the deflected shape can be reasonably approximated by a straight line of constant slope. This response indicates that the N-S lateral deflections are caused primarily by shearing distortions caused by axial deformations in the diagonal bracing. However, the E-W fundamental mode demonstrates more cantilever type behavior especially in the lower half of the building where the deflected shape shows an increasing slope with height. This response indicates that, in addition to shearing distortions, the E-W lateral deflections are significantly influenced by bending action due to large overturning moments near the base which cause substantial axial deformations in the columns.

Another significant aspect of behavior demonstrated in Figure 3.2.7 is foundation flexibility. As can be seen from the translational mode shapes, small deflections are induced at the base of the foundation. This indicates some lateral pile flexibility results even at the low levels of response. However, the foundation shear wall system responds essentially as a rigid body in the translational modes due to its relative stiffness.

In the torsional modes, no pile flexibility is noted but a greater relative flexibility in the foundation wall system is indicated compared to translational modes. This probably results from the fact that the E-W shear walls attract most of the torsional forces at the first story and, when transmitted to the foundation, the

peripheral walls are not fully participating in providing resistance. And, due to the small lever arm of the interior walls relatively greater torsional than shear flexibility results in the foundation system.

### 3.2.3 Description of Analytical Models

Dynamic analyses of the Alcoa Building are performed using a modified version of the ETABS program. The mass values used in the analyses were based on dead load calculations supplied by the design engineers. The 20 psf partition load required by UBC was subtracted from the dead load as this weight increase is believed to overestimate the actual weight of the building during the experimental testing. Also, the roof weight was reduced since it appeared to be significantly overestimated in the design calculations. The final weight values used in the analyses are shown in Table 3.2.1. Five computer models of the building were formulated to investigate the influence of various structural modeling aspects on overall response. Detailed descriptions of the various models are given below. Rigid floor diaphragm behavior is assumed for all models.

#### Model 1

In Model 1, only the primary lateral force resisting system consisting of the N-S braced frames of the exterior walls is modeled. Two analytical models are used to perform separate analyses of E-W and N-S frames act independently with no structural coupling. Beam-column and pin-ended brace elements are used to model the exterior wall truss system. This model can be represented using only 10 story levels over the height of the building since truss work points are located every three stories in the braced portion of the structure. Consequently, mass values for three stories are lumped at a single level where appropriate. The E-W concrete shear walls at the first level are modeled using an equivalent spring with stiffness equal to the

calculated shear stiffness of the walls. A schematic of the two frames of Model 1 is shown in Figure 3.2.8.

#### Model 2

The objective in the formulation of Model 2 is to account for the three-dimensional behavior of the exterior frame allowing full continuity at the intersections of the E-W and N-S frames. Inclusion of this three-dimensional behavior induces shear lag around the corners of the building allowing the N-S frame to contribute resistance to E-W response. A schematic of Model 2 is shown in Figure 3.2.9. The shear walls at the first floor level are modeled using ETABS' shear panel elements. As in Model 1, the structure is represented using lumped floor mass at 11 levels only.

#### Model 3

The objective in the formulation of Model 3 is to account for the effects of the interior core moment resistant frame in the building response. The core frame is modeled as a separate 26 story frame consisting of two frame lines in each direction. Rigid joints zones and haunched girder ends were accounted for in formulating member stiffnesses. Also, nonstructural slab-girder interaction is included assuming full composite action where equivalent section properties are calculated according to AISC specifications, section 1.11.5. Roughly 100% increase in moments of inertia resulted in the core girders due to this effect. Concrete encasement of some of the core columns was also accounted for causing equivalent increases in moment of inertia ranging from 10% to 120%. The exterior frame is linked to the interior frame only at levels where work points exist (every 3 stories over the braced portion of the structure). The floor masses are distributed over the 26 stories. A schematic of Model 3 is shown in Figure 3.2.10.

#### Model 4

Model 4 includes the nonstructural effect of the infill block

walls in the core frame system. A typical layout of the block wall locations is shown in Figure 3.2.4(b). Only those walls infilling the moment framing along frame lines C,D,G and H are included in the model. ETABS shear panel elements are used to model the infill walls using a shear modulus of 600 psi calculated in accordance with the Reinforced Masonry Engineering Handbook (3). A schematic of model 4 is shown in Figure 3.2.11.

#### Model 5

The main objective in the formulation of Model 5 is to include the effects of foundation and pile flexibility. Based on the results of the experimental tests, equivalent lateral springs were used to model pile flexibility in the two translational direction. The spring stiffness used reflects an average lateral stiffness of about 300 k/in. per pile. Finite elements are used to model the foundation wall system. A schematic of Model 5 is shown in Figure 3.2.12.

#### **3.2.4 Comparison of Analytical and Experimental Dynamic Properties**

Analyses were performed to extract the natural periods and mode shapes of the five models described in the previous section. In 3.2.13 and 3.2.14, the first two modes for translation in each direction and for torsion are shown for models 1,4, and 5. As can be seen from these figures, the analytical mode shapes compare very well with experimental values. In Figure 3.2.13, the fundamental translational modes resulting from analyses verify the shear type behavior in the N-S direction and the cantilever type behavior in the E-W direction that were noted in the experimental response. Model 5 gives a good representation of the relative stiffness of the foundation wall system and the pile flexibility at the base of the building that were noted in the experimental results.

In Table 3.2.2, analytical periods for the four models are compared with experimental values. Model 1 is the most flexible

idealization of the building consisting of the exterior braced frames acting as planar frames. As is seen from the table, this model produces fundamental periods of 2.42 sec. in the E-W and N-S directions, respectively, being 9.6% and 19.4% greater than experimental values.

In Model 2, three dimensional modeling of the exterior frame brings the fundamental periods down to 2.24 sec. and 1.95 seconds, respectively. As shown in Tables 3.2.3, these period reductions correspond to increases in fundamental modal stiffnesses of 16% and 5% for the E-W and N-S directions respectively. Since the shear lag resulting from the three dimensional modeling causes a flange effect inducing axial forces in the columns of the orthogonal frames, the E-W stiffness increased more than the N-S due to the longer effective flange provided by the N-S walls. The first two torsional periods of 1.12 sec. and 0.42 sec. are in excellent agreement showing variations from experimental values of less than 1.2%.

Addition of the core frame in Model 3 and the block walls in Model 4 causes further reductions in period to 2.00 sec. and 1.68 sec. for the E-W and N-S directions, respectively. Model 4 is the stiffest model and, having the lowest periods, will lead to the largest dynamic forces in seismic analysis. Inclusion of the pile flexibility in Model 5 results in periods which show the best overall comparison with experimental values. As seen in Table 3.2.2, Model 5 yields periods of the first two modes in the translational and torsional directions that are all within 5% of experimental values.

Also shown in Table 3.2.2 are UBC, ATC values for the fundamental period of this building based on codebook formulae. As can be seen, the code book periods of 1.69 sec. and 1.23 sec. for the E-W and N-S directions respectively underestimate the small amplitude experimental periods by approximately 25%.

In Table 3.2.3, the relative significance of various secondary

modeling assumptions on the modal stiffnesses is shown. In E-W translation, 3-dimensional modeling, participation of the core frame and addition of the nonstructural block walls contribute 16%, 19% and 11% increases, respectively, with respect to the Model 1 lateral stiffness. In the N-S direction, 3-dimensional modeling is not very significant showing only a 5% increase in the fundamental modal stiffness, but the core framing and block wall modeling cause stiffness increases of 13% and 24%, respectively. The total stiffness increases of Model 4 over Model 1 are shown in the last column of Table 3.2.3. Note that the translational modal stiffnesses show increases ranging from 42% to 58%. However, the torsional modal stiffnesses show increases of 8% and 10% indicating that the torsional stiffness is relatively insensitive to the modeling refinements made.

Overall, excellent correlation of the analytical and experimental dynamic properties is achieved by accounting for the various structural and nonstructural effects that might normally be omitted. Especially notable is the fact that the single formulation of Model 5 is able to predict the first two modes in each translation direction and in torsion with such good accuracy.

### **3.2.5 Influence of Modeling Approach on Design Quantities**

In this section, results of response spectrum dynamic analysis of each of the five models are presented to demonstrate the influence of different modeling approaches on gross design quantities. The Newmark spectrum scaled to 0.05g peak ground acceleration is used which corresponds to the ATC recommended reduced spectrum peak acceleration level. Four analytical modes which account for over 90% of the effective mass are used to calculate response in each of the two translational directions.

In Figures 3.2.15 through 3.2.18, predicted peak story shear, overturning, deflection and drift envelopes for the various models are

plotted over the full height of the building. Some significant aspects of response can be seen in these figures. In Figures 3.2.15 and 3.2.16, shear and overturning moment distributions are shown for the different models. In general, shear values increase with the stiffer model formulations. However, careful inspection of Figure 3.2.15 shows that in the uppermost 2 or 3 stories, shears from Model 3 are somewhat less than those from Models 1 and 2 for both the E-W and N-S directions. This is due to the core frame's role as a primary lateral force resisting system between the mechanical and roof levels causing reduced inertial forces at this level. Thus, omission of the core frame in Models 1 and 2 results in overly flexible response of the uppermost story producing overestimations of shear at this level. At the base, Model 4 predicts the greatest shear and overturning values, being the stiffest formulation. Addition of lateral pile flexibility in Model 5 results in slightly reduced force response values as is seen in the figures due to increased periods and accompanying lower spectral acceleration amplitudes.

In Figure 3.2.17, the deflection response envelopes are plotted for the various models. As would be expected, lesser deflections result with increasingly stiff models. As was noted in the mode shape response, the E-W deflections reflect a significant degree of cantilever type response whereas the N-S deflections show shear type deflection response. Another difference in deflection response of the two directions occurs at the first story where much smaller deflectionals result in the E-W direction due to concrete shear walls present at this level. These differences in deflection response are more dramatically illustrated in the drift responses shown in Figure 3.2.18. Again, cantilever type behavior is noted in the E-W direction (Figure 3.2.18(a)) evidenced by the increasing drift with greater height whereas the N-S response shows roughly constant drift reflecting shear type behavior. It is evident from Figure 3.2.18(a)

that inclusion of the structural core in Models 4 and 5 tend to reduce the E-W drifts caused by cantilever action in the upper part of the building as compared to the Model 1 response demonstrating the significant contribution of the core to the stiffness of this portion of the structure. Also, action of the core frame as a primary lateral force resisting system in the mechanical and roof levels and in the N-S first story substantially reduces drifts at these levels.

In Table 3.2.4, selected values of shear, overturning, deflection and drift are shown for the different models along with percent changes from Model 1. As can be seen from this table, base shear increases only slightly, due to the three dimensional idealization of Model 2 increasing 2.9% (from 2539k to 2612k) in the E-W direction and 1.9% (from 3031k to 3089k) in the N-S direction. An increase of 7.7% (from 6079 to 6545 x 10<sup>3</sup> k in.) in base overturning results for the E-W direction and a 2.9% increase (from 7967 to 8199 x 10<sup>3</sup> k in.) results in the N-S direction. Inclusion of the core moment frame in Model 3 causes further increases in force quantities bringing the story shears and overturning moments up an additional 5% to 10% over most levels of the building. In Model 4, where the stiffening effect of the core frame's infill block walls are accounted for, the largest base force quantities and smallest deflection quantities result. The E-W base shear of 3054k and base overturning of 7441 x 10<sup>3</sup> k in. are increases of 20.3% and 22.4% over Model 1 values. In the N-S direction, values of 3525k and 9211 x 10<sup>3</sup> k in. result, being respective increases of 16.3% and 15.6% over Model 1 values. Deflections and drifts are smallest for Model 4 being about 20% less than Model 1 in the EW direction and about 16% less in the N-S direction. Inclusion of lateral pile flexibility in Model 5 results in slightly smaller force quantities and slightly larger deflection quantities compared to Model 4 as seen the the table.

Greater understanding of the dynamic behavior of the Alcoa

Building can be gained by reviewing modal contributions to gross design quantities. Relative modal contributions to the total sum of the squares values of story shears, overturning moments, deflections and drifts over the full height of the building are shown in Figures 3.2.19 and 3.2.20 for Model 4. In Figure 3.2.19(a) and (b), the significance of the higher translational modes (2nd through 4th) are seen to contribute substantially to shear and overturning moment in the upper stories of the building. The second modes are dominant in shear and overturning response in the top 5 or so stories in both the E-W and N-S directions. Near the midheight of the building, shear response is dominated by the first mode only but overturning still has a significant contribution from the second mode. At the base, the first mode dominates overturning response with higher modes being insignificant. The second modes contribute significant shear force at the base especially in the E-W direction where the second mode contribution is nearly as great as the first. Figure 3.2.20(a) shows that deflections are dominated by the first mode, especially in the upper regions, but the second mode contributes significantly near the base. Like the shear response, modal contributions to drift in Figure 3.2.20(b) show the greatest contribution of higher modes near the top and base of the structure but the first mode is the largest contributor to drift at all levels of the building.

As seen from Figures 3.2.19 and 3.2.20, modal contributions to the various design quantities are quite similar in both the E-W and N-S direction. In general, however, higher modes have a somewhat greater influence in E-W response due to the greater flexibility and resulting longer periods in this direction.

### 3.2.6 Comparison of Dynamic Analyses and Code Equivalent Static Procedures

In this section, a comparison is made of the Alcoa Building's response to different recommended static and dynamic seismic loading approaches ( see section 3.1.2 for discussion). The ATC and Newmark spectra are used for dynamic analyses. Both of these spectra are based on the ATC recommended 0.067g reduced peak ground acceleration for dual system construction. The UBC equivalent spectrum is multiplied by 1.278 to correspond to elastic limit design. Model 4 is used as a basis for the comparative analysis since this model will yield the most conservative force results being the most stiff representation of the structure. Both the Model 4 analytical fundamental periods (2.00 sec. E-W and 1.68 sec. N-S) and the UBC, ATC codebook calculated periods (1.69 sec. E-W ; 1.23 sec. N-S) as shown in Table 3.2.2 are used to calculate equivalent static response. Gross design quantity responses are summarized in Figures 3.2.21 through 3.2.24 and in Table 3.2.5.

Comparing the dynamic analyses, Figures 3.2.21 through 3.2.24 show that the ATC spectrum produces somewhat larger response values than Newmark for this building. As summarized in Table 3.2.5, the ATC spectrum yields about 7% greater base shear, 20% greater base overturning moment, and 20-25% greater drifts and deflections in the E-W direction. In the N-S direction, about 7% increase in base shear is again noted along with increases in base overturning, deflection and drift of about 15%. In moving from the Newmark to ATC spectrum the base shear shows lesser variation than the other design quantities due to the significant participation of the higher modes in base shear response whereas the other tabulated response quantities are dominated by the first mode (see Figure 3.2.19 and 3.2.20). And, as can be seen in Figure 3.1.1, the ATC spectrum gives greater spectral accelerations than Newmark at periods longer than about 1.1 sec. but lower values at

lesser periods. Therefore, the reduced amplification of the second mode which contributes significantly to shear response partially offsets the base shear increase due to fundamental mode amplification. Results from equivalent static analyses are also shown in Figures 3.2.21 through 3.2.24. The shaded portion of these figures emphasizes the variation in static equivalent response quantities resulting from the use of the analytically derived fundamental periods from Model 4 versus the fundamental periods calculated from codebook formulae. The differences between codebook and analytical periods produce significant variations in predicted response, where the longer analytical periods yield smaller response values. For UBC static analysis, use of the codebook periods result in increases of about 9% and 17% over response quantities based on the analytical periods in the E-W and N-S directions respectively (e.g. as shown in Table 3.2.5, E-W base shear increases from 4026 k to 4386 k when codebook rather than analytical period is used). For ATC static analysis, use of the codebook periods result in increases of about 12% and 23% in the E-W and N-S directions over static results based on the analytical periods. Note that for this building, the UBC approach yields smaller story shears, drifts and deflections than the ATC static approach but greater base overturning moments due to the 0.8 reduction factor allowed by ATC.

It is of particular interest to compare the dynamic and equivalent static responses as recommended by ATC since these are derived from the same response spectrum. In Figures 3.2.21 and 3.2.22, the shear and overturning results for both the static and dynamic ATC approaches using the analytical fundamental periods are shown. Note that the ATC dynamic response quantities are all significantly less than the corresponding values obtain from equivalent static analysis. From Table 3.2.5, it is seen that the E-W base shear resulting from ATC dynamic analysis is 3273 k being only 78% of the static value of 4210k using the same 2.00 sec. fundamental

period. Similarly, the E-W dynamic base overturning is  $8892 \times 10^3$  k in. or 81% of the static value of  $10885 \times 10^3$  k in. This discrepancy between ATC equivalent static and dynamic results is due to the relative conservatism in the static solution introduced by assuming the full mass of the building participates in the response of the fundamental mode. This result is further discussed in section 3.7.

In Figures 3.2.25 through 3.2.28, the story shear, overturning moment, deflection and drift responses normalized to base shear are shown for the different static and dynamic analysis approaches. The dynamic analyses using Newmark and ATC spectra show similar trends in response distribution over the height of the building. In Figure 3.2.25, the story shear distribution show fairly close agreement between these two spectra but compared to the ATC results, the Newmark results indicate somewhat lesser relative shears in the lower two thirds of the building and higher relative shears in the upper third. This is due to the greater relative contribution of the higher (shorter period) modes in the Newmark response due to the spectrum shape (Figure 3.1.1). The ATC and UBC static response shear distributions show further variations from the dynamic distributions. The UBC and ATC static distributions result in larger relative shears in the lower two thirds of the building since these are based on the response of the fundamental mode only. The ATC static distribution gives the largest relative shears in the lower two thirds of the building (as much as 30% greater than the Newmark dynamic value at midheight in the E-W direction since it is based on a cantilever type (nonlinear) fundamental mode shape rather than a shear type (linear) mode shape as assumed by UBC. At the top of the building, the UBC distribution gives the greatest relative shear value due to the required top load and the ATC static distribution gives the lowest value. For the overturning moment distributions shown in Figure 3.2.26, UBC static gives the largest relative overturning at the base

but the ATC static results are more in line with the dynamic values due to the applied 0.8 reduction factor. Figure 3.2.27 shows the overestimated deflection response for the static methods since both distribute a greater portion of the load to the upper part of the structure than are indicated by the dynamic analyses. The drift distributions (Figure 3.2.28) also show larger relative response of the static approaches. It is interesting to note the greater separation of static and dynamic drift distributions in the E-W direction than in the N-S. This result is due to the fact that, in E-W direction, a large portion of the deflection response is due to cantilever action caused by overturning moments whereas in the N-S direction the deflection response is dominated by shear distortion. Thus, the overestimated overturning moments resulting from the static approaches cause greater relative increases in E-W direction deflection and drifts than in the N-S direction.

### **3.2.7 Comparison of Code Design Forces with Dynamic Forces Induced by Actual Earthquake Spectra**

The UBC story shears and overturning moments used for the seismic design of the Alcoa Building were provided by the design engineers. To approximate forces corresponding to yield level for this building, the UBC loads are factored by  $1.7/1.33=1.278$  and are shown in Figures 3.2.29 and 3.2.30. (Note that the design engineers used fundamental periods of 1.93 sec. and 1.41 sec. to calculate UBC loads in the E-W and N-S directions, respectively, and used dead weight estimates that included partition load resulting in somewhat larger values than those shown in Table 3.2.1.). Also shown in Figures 3.2.29 and 3.2.30 are the predicted dynamic responses to the Taft (1952) and El Centro (1940) earthquakes for 5% damping (see Figure 3.2.2 for a plot of these spectra) using both Model 2 and Model 4 to represent the building.

For the E-W direction, Figures 3.2.29(a) and 3.2.30(a) show that

the Taft earthquake induces forces that are comparable to the factored UBC forces . The Taft spectra yields somewhat higher shears near the top and base of the building than does UBC but also gives lesser overturning moments near the base. The El Centro spectra results in shears that are between 2.5 to 3.0 times and overturning values that are about 2.5 times the factored UBC values.

In the N-S direction, the Taft earthquake induces a relatively greater response than in the E-W direction and shows a wider variation between the Models 2 and 4 due to a spike in spectrum curve. Taft shears and overturning moments are 1.2 to 1.8 times the factored UBC values. The El Centro spectra results in forces values ranging from 2.0 to 2.8 times the UBC values.

### **3.2.8 Summary**

The results presented in the previous sections lead to the following observations regarding the behavior and analysis of the Alcoa Building:

- (1) Rational development of the numerical models leads to excellent agreement between the dynamic properties resulting from computer analysis and the dynamic properties determined from small amplitude experimental testing. Experimental and analytical mode shapes compared very well (Figures 3.2.13 and 3.2.14) and the final numerical model (Model 5) predicted the first six translational and rotational natural periods within 5% of experimental values (Table 3.2.2).
- (2) Analysis indicates that the various structural modeling aspects considered may significantly influence the response of the building. Inclusion of three dimensional modeling of the exterior frame, addition of the secondary core frame system, and addition of the

nonstructural infill block walls will leads to increaes in base shear and overturning moment ranging from 15% to 22% using the Newmark spectrum (Figure 3.2.15 - 3.2.18, Table 3.2.4).

- (3) As indicated by the analyses, this building exhibits shear beam type behavior in the N-S translational direction, but cantilever beam type behavior in the E-W direction. Thus the deflection and drift response characteristics differ in the two orthogonal directions (Figures 3.2.17 and 3.2.18).
- (4) In dynamic analysis, the influences of the higher modes (2nd and 3rd translational) contribute significantly to response especially in the upper portion of the building (Figures 3.2.19 and 3.2.20).
- (5) For this building, dynamic analysis shows that the ATC response spectrum yields more conservative results than the 0.05g Newmark spectrum resulting in 7% greater base shears and 15-20% greater base overturning moments due to the conservatism in the ATC spectrum in the longer period range.
- (6) Experimental periods are 30 to 35% greater than the values predicted by UBC and ATC code formula (Table 3.2.2). These period differences lead to large variations in the calculated in equivalent static response (Figures 3.2.21 - 3.2.24).
- (7) Comparing the UBC and ATC equivalent static approaches for this building, ATC leads to larger shears but smaller overturning values at the base of the building than UBC. In the uppermost portion of the building UBC yields larger shears and overturning moments due to the required top load.

- (8) Using the ATC recommended approaches for dynamic and equivalent static analyses and using the same fundamental period (2.0 sec.) for both, force quantities resulting from the dynamic analysis approach are significantly less than those resulting from the equivalent static analysis approach. Dynamically derived base shear and overturning moment are 80-90% of static values and roof deflection and typical drifts are 65-75% of static values (Table 3.2.5, Figures 3.2.21 - 3.2.24).
- (9) Regarding the distribution of equivalent static forces compared to dynamic force envelopes, ATC tends to substantially overestimate the shear relative forces in the lower two thirds of the building and underestimate shear near the top. The UBC distribution tends to overestimate shears in the lower portion to a lesser degree but overestimate shear at the top (Figure 3.2.25). The ATC distribution of overturning moment compares quite well with dynamic distributions whereas UBC overestimates base overturning forces (Figure 3.2.26). Both UBC and ATC equivalent static approaches overestimate deflection and drift for a given base shear compared to dynamic results (Figure 3.2.27 and 3.2.28).
- (10) Based on the earthquake loads used by the engineers in design, results based on the numerical models indicate that the building would have an essentially elastic response to the Taft (1952) earthquake in the E-W direction but, in the N-S direction, would have elastic responses 1.2 to 1.8 times the factored UBC loads. If subjected to the El Centro (1940) record, elastically derived forces of 2.0 to 2.8

times the factored UBC values would result.

Table 3.2.1: Dead Load Weights Used for Analytical Models

Floor	Weight(kips)	psf
roof	2800	135
mech	6500	314
25	2500	121
24	2500	121
23	2500	121
22	2500	121
21	2500	121
20	2500	121
19	2500	121
18	2500	121
17	2500	121
16	2500	121
15	2500	121
14	2500	121
13	2500	121
12	2500	121
11	2500	121
10	2500	121
9	2500	121
8	2500	121
7	2500	121
6	2500	121
5	2500	121
4	2500	121
3	2500	121
2	2821	136
Total	69621	

Table 3.2.2: Experimental vs. Analytical Natural Periods

Direction	Mode No.	Exp. Period(sec)	Model 1		Model 2		Model 3		Model 4		Model 5		UBC, ATC*	
			Period	%	Period	%	Period	%	Period	%	Period	%	Period	%
E-W	1	2.21	2.42	+9.6	2.24	+1.4	2.08	-5.9	2.00	-9.7	2.12	-4.0	1.69	-23.5
	2	0.71	0.79	+11.0	0.77	+8.5	0.72	+1.2	0.66	-7.5	0.69	-3.6		
N-S	1	1.67	2.00	+19.4	1.95	+16.6	1.84	+10.2	1.68	+0.2	1.76	+5.0	1.23	-26.3
	2	0.59	0.73	+23.3	0.71	+20.3	0.68	+14.2	0.58	-1.6	0.60	+1.7		
Torsion	1	1.12			1.12	+0.5	1.11	-1.1	1.08	-3.8	1.12	+0.3		
	2	0.43			0.42	-1.2	0.43	+0.8	0.40	-5.7	0.42	-2.4		

% = percent variation from experimental period.

\*Code periods calculated as follows:

UBC (eqn. 12-3A), ATC (eqn. 4-5):  $T = .05h/\sqrt{D}$  ;  $h = 358.5'$  1st floor to roof

$T_{EW} = .05 \times 358.5 / \sqrt{172} = 1.69$

$T_{NS} = .05 \times 358.5 / \sqrt{212} = 1.23$

Table 3.2.3: Influence on Modeling Aspects on Modal Stiffnesses

Direction	Mode	Stiffness Increase with Respect to Model 1			
		Three Dimensional Modeling	Addition of Core Frame	Addition of Block Walls	Total (Model 4)
E-W TRANS.	1	16%	19%	11%	46%
	2	5	15	23	43
N-S TRANS.	1	5	13	24	42
	2	6	9	43	58
TORSION	1	---	2	6	6
	2	---	0	10	10

Table 3.2.4: Influence on Modeling Variations on Design Quantities

Direction	Design Quantity	Model 1 %	Model 2 %	Model 3 %	Model 4 %	Model 5 %
E-W	Base shear(k)	2539 0	2612 + 2.9	2801 +10.3	3054 +20.3	3040 +19.7
	Base OTM( $\times 10^3$ k-in)	6079 0	6545 + 7.7	7117 +17.1	7441 +22.4	7155 +17.7
	Roof deflection(in)	3.61 0	3.31 - 8.4	3.03 -16.1	2.89 -20.0	3.08 -14.7
	14th floor drift(in)	0.16 0	--- ---	--- ---	0.13 -17.8	0.13 -15.3
N-S	Base shear(k)	3031 0	3089 + 1.9	3259 + 7.5	3525 +16.3	3513 +15.9
	Base OTM( $\times 10^3$ k-in)	7967 0	8199 + 2.9	8650 + 8.6	9211 +15.6	8996 +12.9
	Roof deflection(in)	2.79 0	2.71 - 3.0	2.53 - 9.1	2.33 -16.3	2.45 -12.1
	14th floor drift(in)	0.12 0	--- ---	--- ---	0.10 -15.6	0.11 -13.9

% = percent change from Model 1.

Table 3.2.5: Comparison of Design Quantities for Dynamic and Equivalent Static Analysis

Direction	Design Quantity	Dynamic				Static							
		Newmark		ATC		ATC				UBC*			
		Value	%	Value	%	Codebook Value	%	Analytical Value	%	Codebook Value	%	Analytical Value	%
E - W	Fundamental Period	2.00	0	2.00	0	1.69	-15.5	2.00	0	1.69	-15.5	2.00	0
	Base shear(k)	3054	0	3273	+7.2	4708	+54.1	4210	+37.9	4386	+43.6	4026	+31.8
	Base OTM( $\times 10^3$ k-in)	7441	0	8892	+19.5	12171	+63.5	10885	+46.3	13768	+85.0	12640	+69.9
	Roof deflection(in)	2.89	0	3.61	+24.6	6.27	+117.0	5.61	+93.8	5.79	+100.3	5.31	+83.5
	14th floor drift(in)	0.13	0	0.16	+22.5	0.27	+108.0	0.24	+88.4	0.24	+80.8	0.22	+70.5
N - S	Fundamental Period	1.68	0	1.68	0	1.23	-26.8	1.68	0	1.23	-26.8	1.68	0
	Base shear(k)	3524	0	3778	+7.2	5804	+64.7	4729	+34.2	5130	+45.6	4392	+24.6
	Base OTM ( $\times 10^3$ k-in)	9211	0	10545	+14.5	14608	+58.6	11904	+29.2	15857	+72.1	13577	+47.4
	Roof deflection(in)	2.34	0	2.72	+16.5	4.76	+103.4	3.88	+65.9	4.21	+79.9	3.60	+54.0
	14th floor drift(in)	0.10	0	0.12	+15.5	0.21	+110.0	0.17	+62.1	0.17	+71.0	0.15	+43.7

% = percent change from Newmark spectrum dynamic analysis.

\*UBC response values are factored by 1.70/1.33 = 1.278 for correspondence with ATC elastic limit load levels.

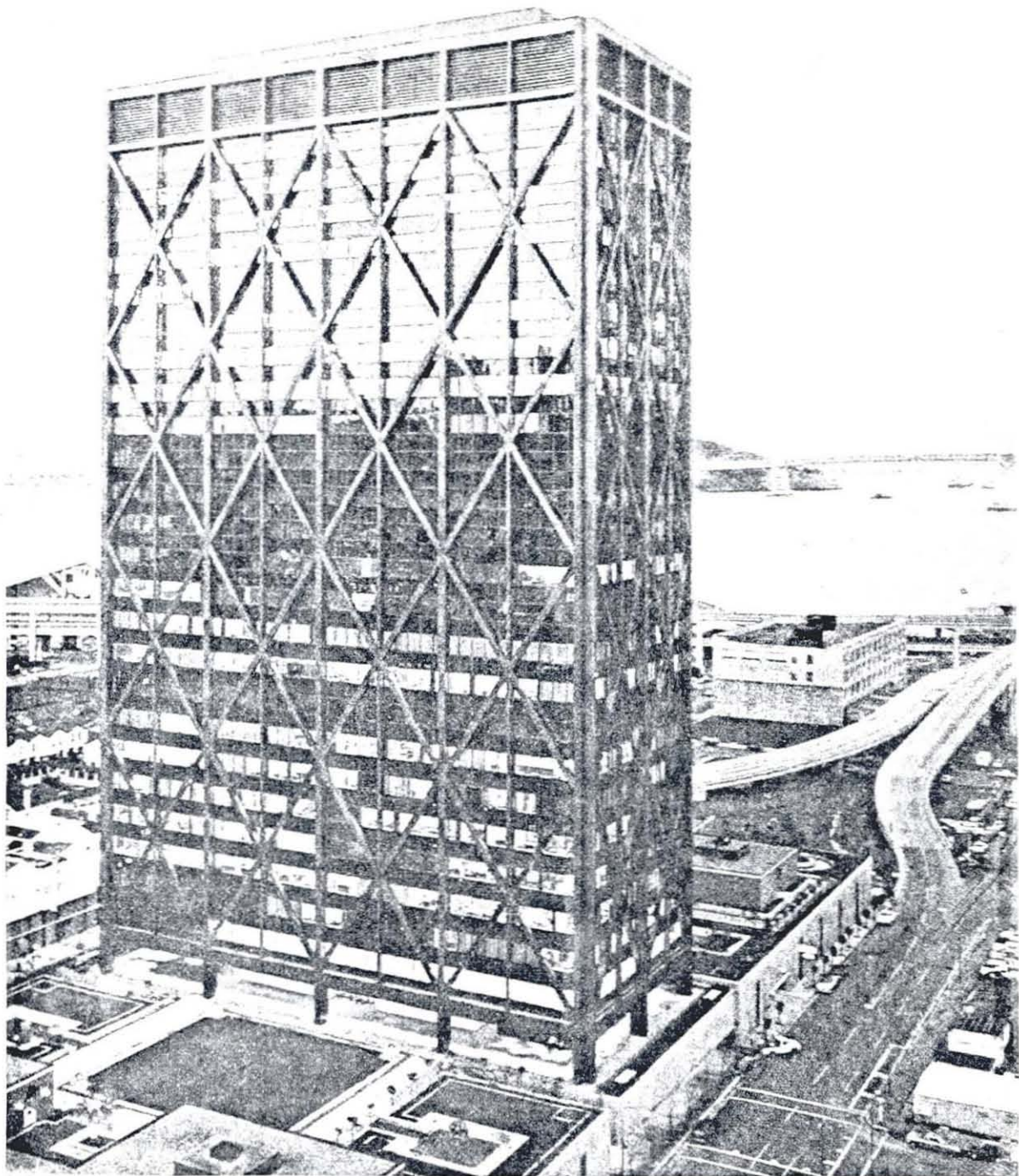


Figure 3.2.1: Alcoa Building  
San Francisco, California

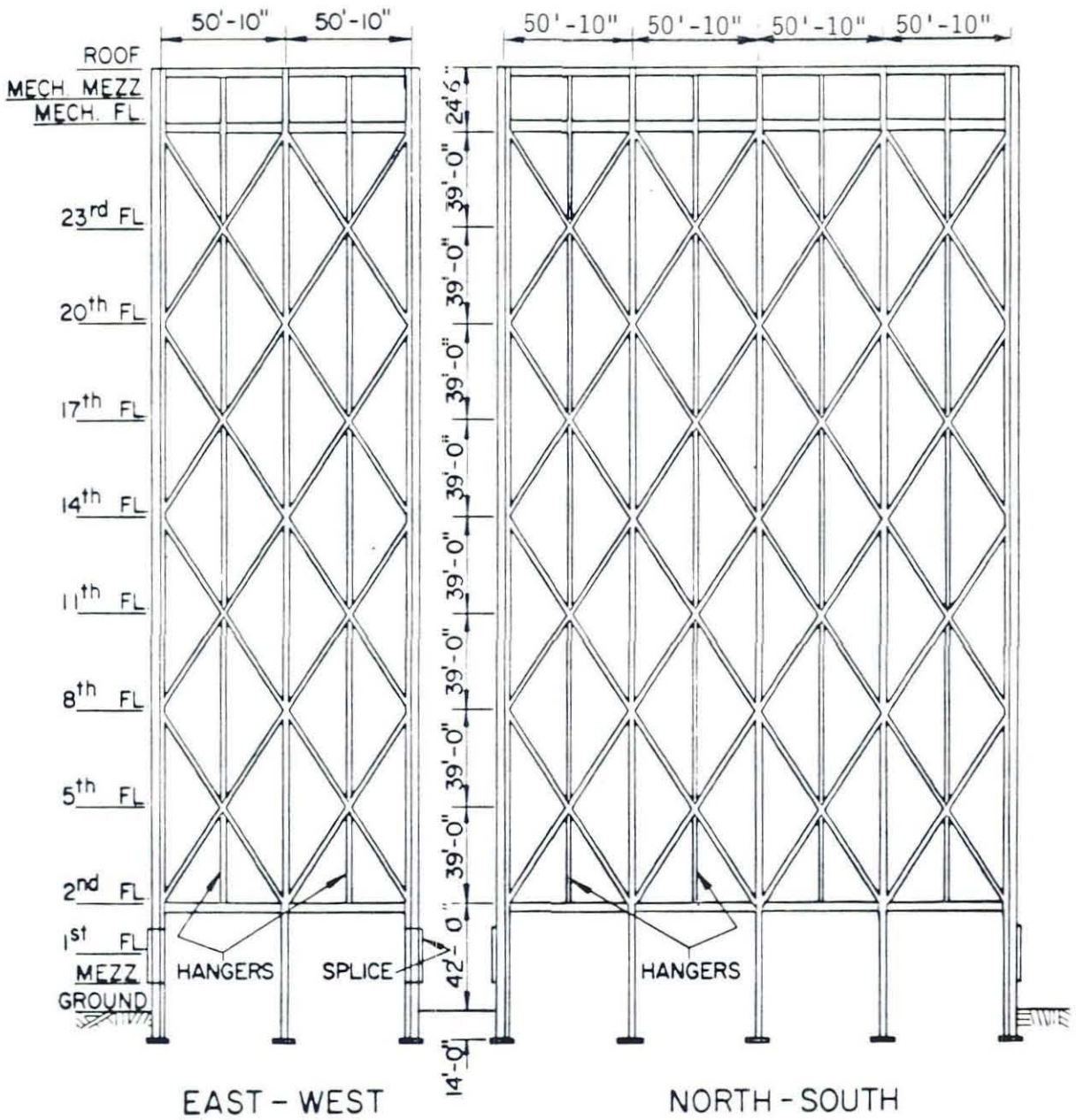
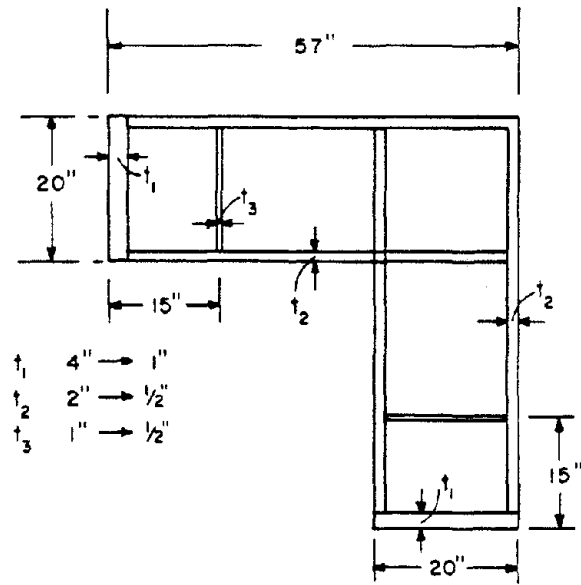
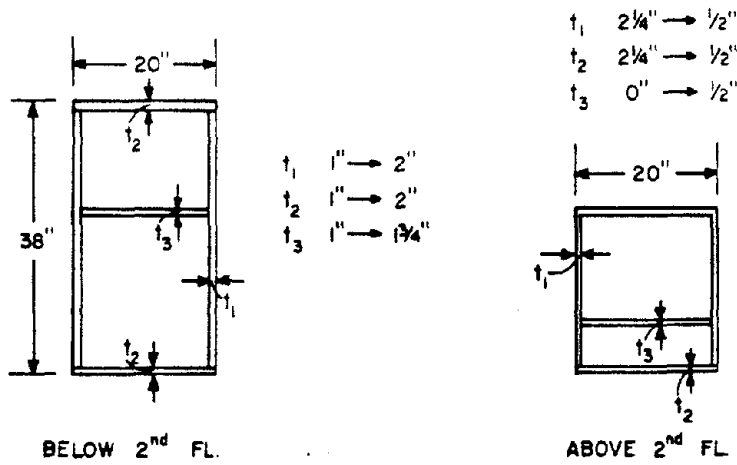


Figure 3.2.2: Elevation of Exterior Wall Braced Frame System

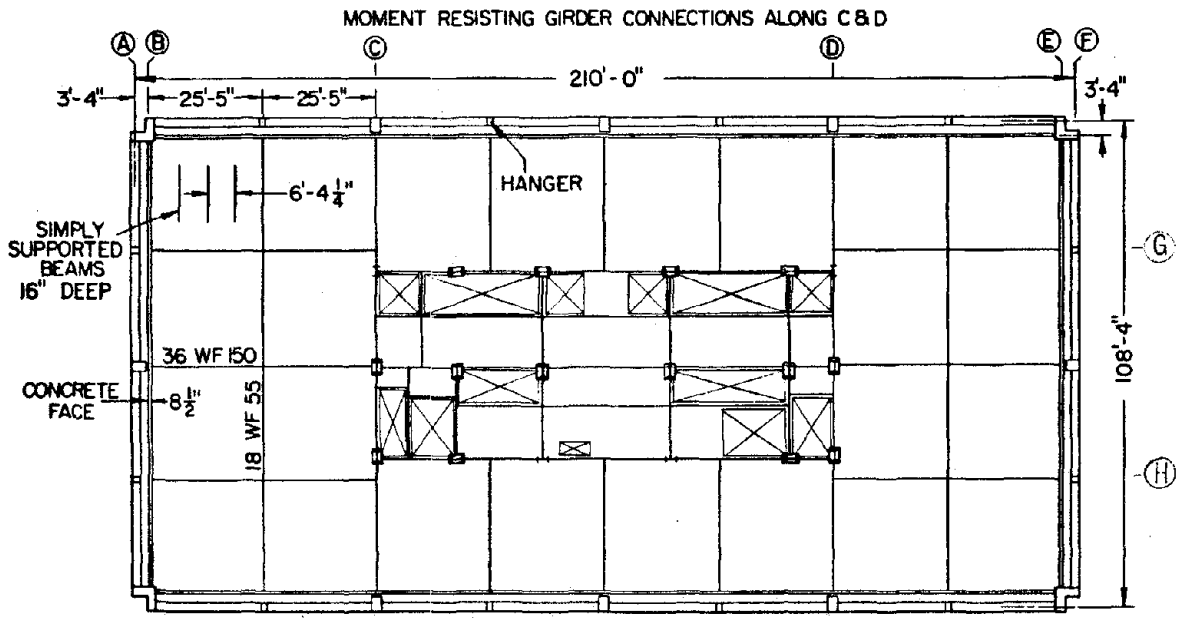


**CORNER COLUMNS**

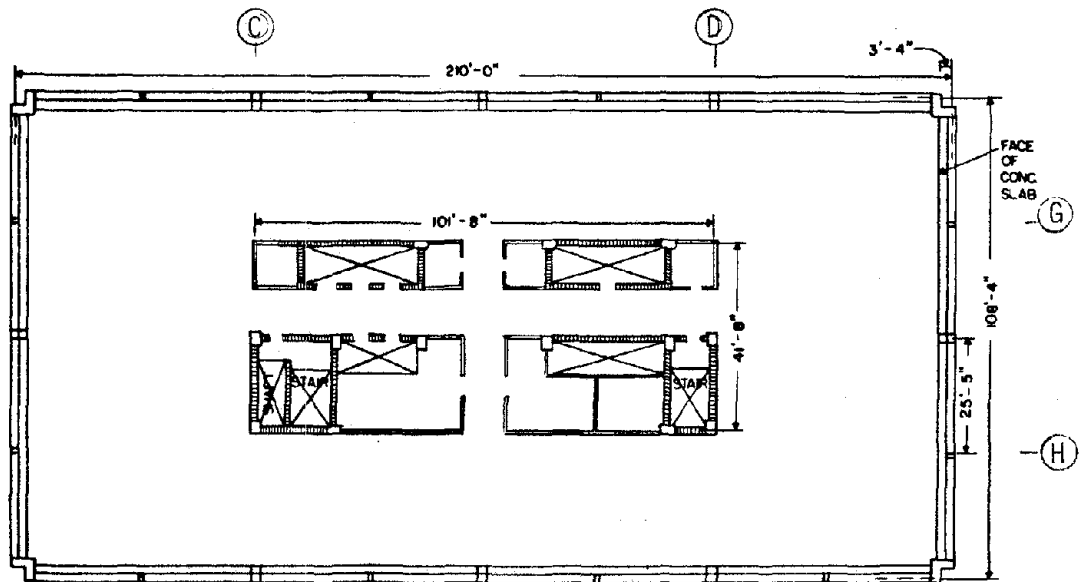


**INTERMEDIATE COLUMNS**

Figure 3.2.3: Built-up Column Sections Used in Exterior Walls

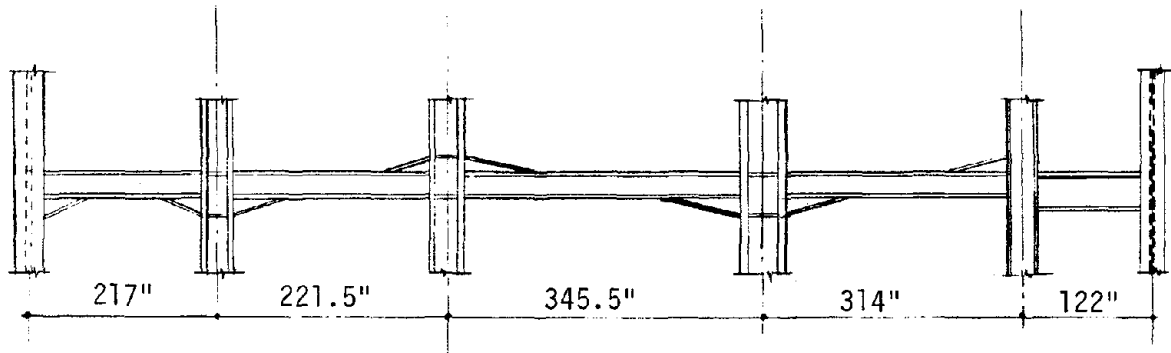


(a) Typical Floor Framing Plan

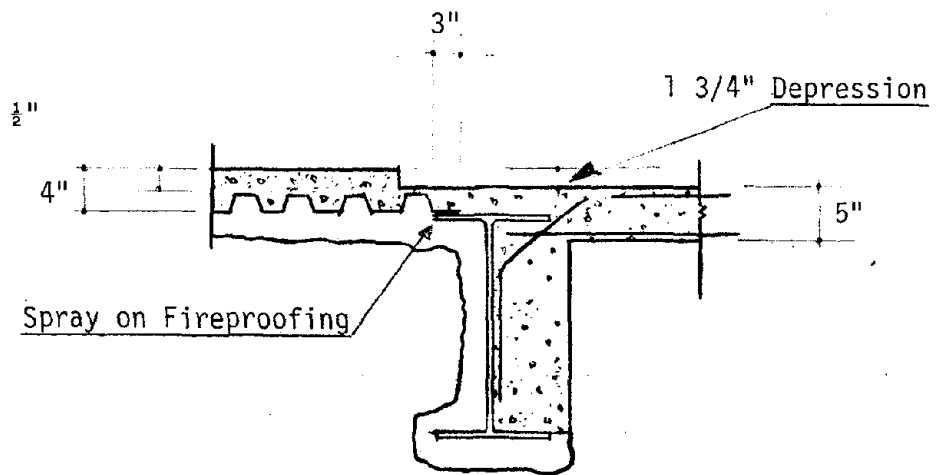


(b) Typical Location of Block Walls in Core

Figure 3.2.4: Plan Views of Alcoa Building



(a) Haunched Girders in N-S Direction Between Lines C and D



(b) Floor Slab Construction

Figure 3.2.5: Core Frame Details

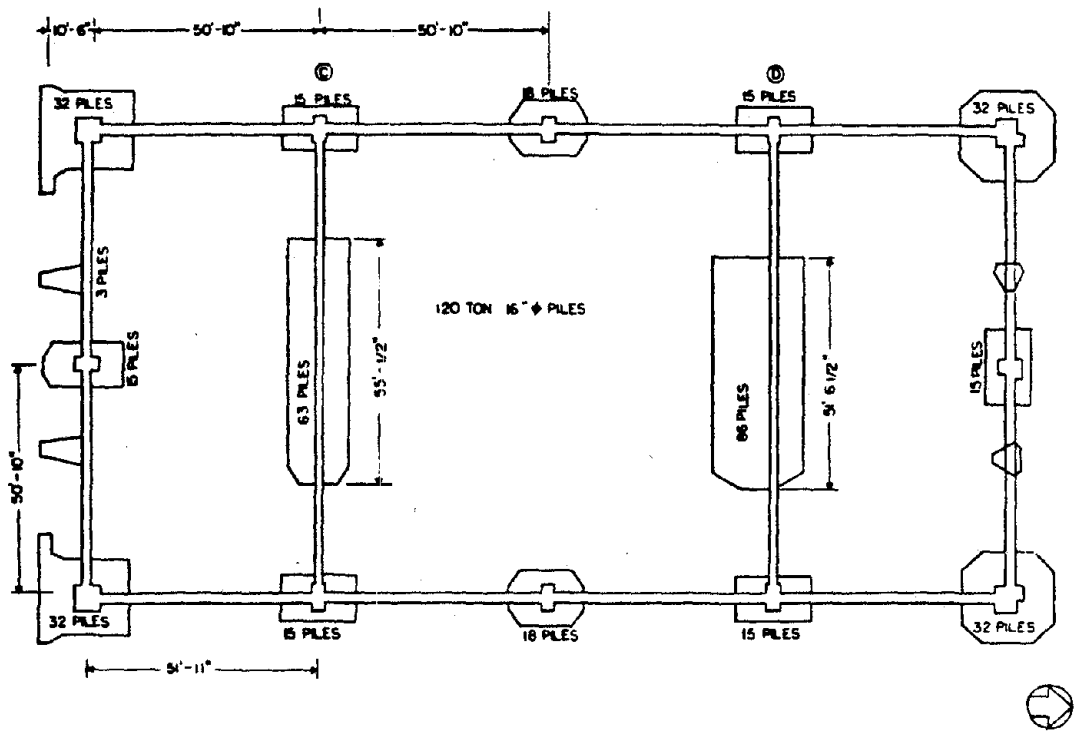


Figure 3.2.6: Pile Supported Foundation

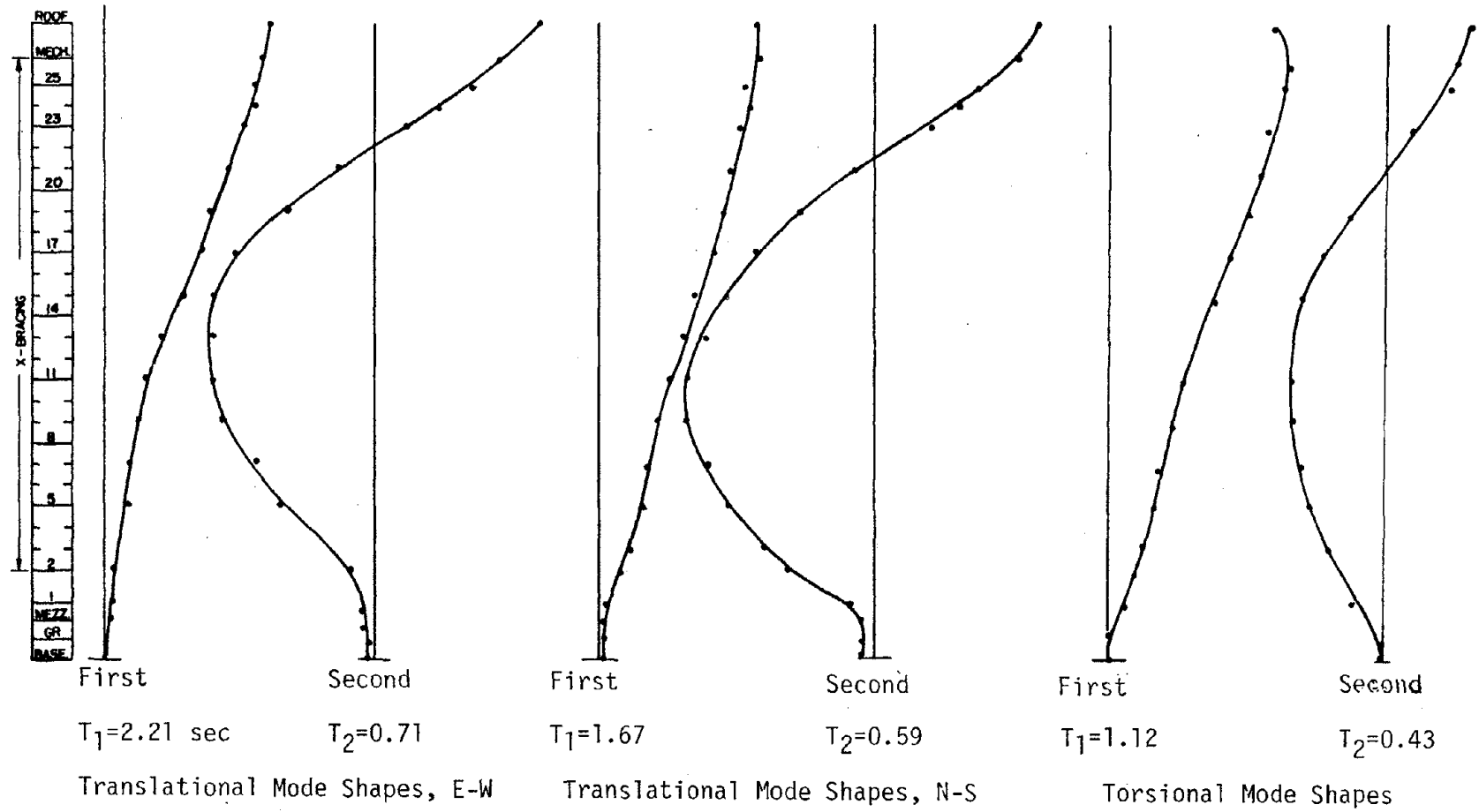


Figure 3.2.7: Experimental Mode Shapes

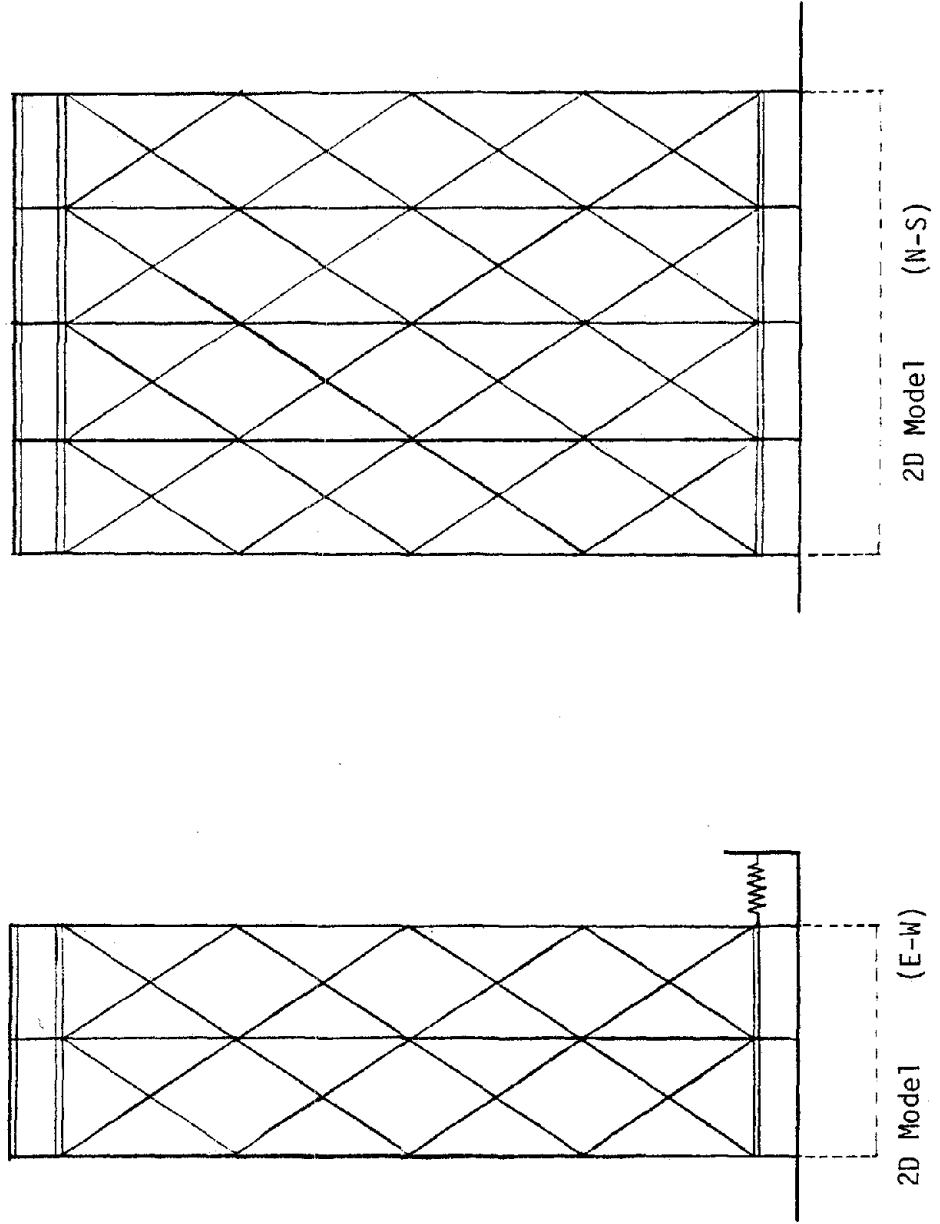


Figure 3.2.8: Model 1 Schematic

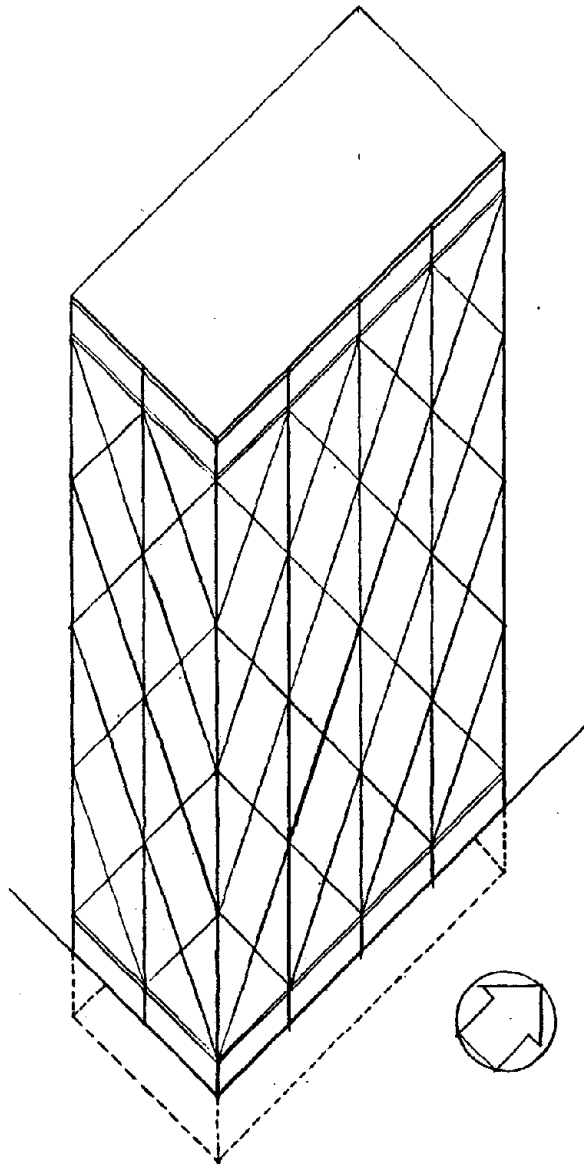


Figure 3.2.9: Model 2 Schematic  
(3-Dimensional Frame)

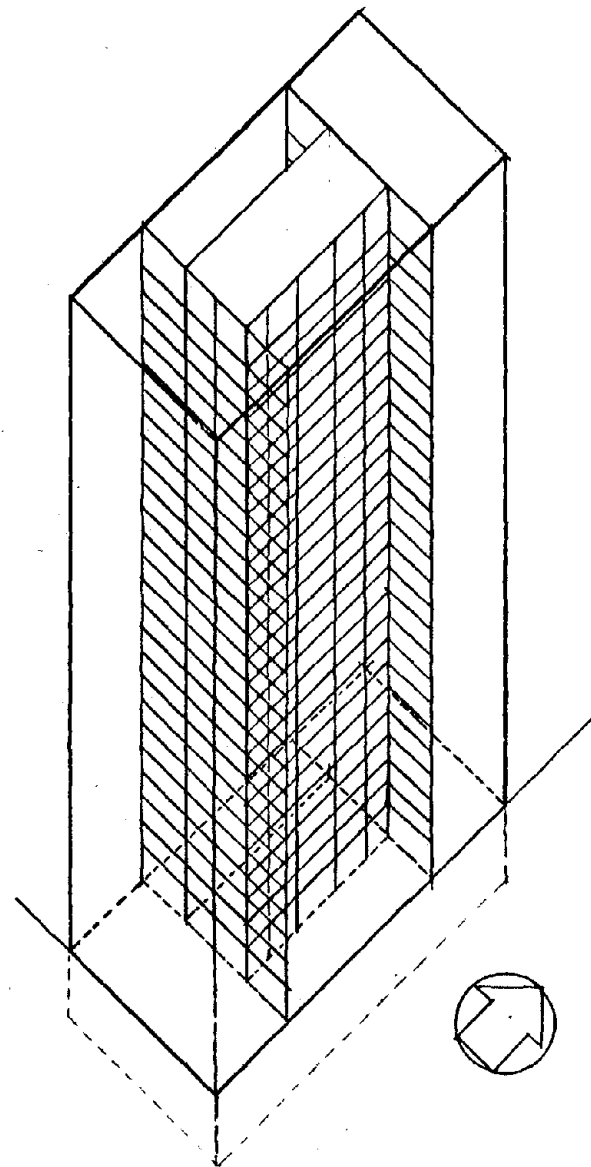


Figure 3.2.10: Model 3 Schematic  
(Includes Core Frame)

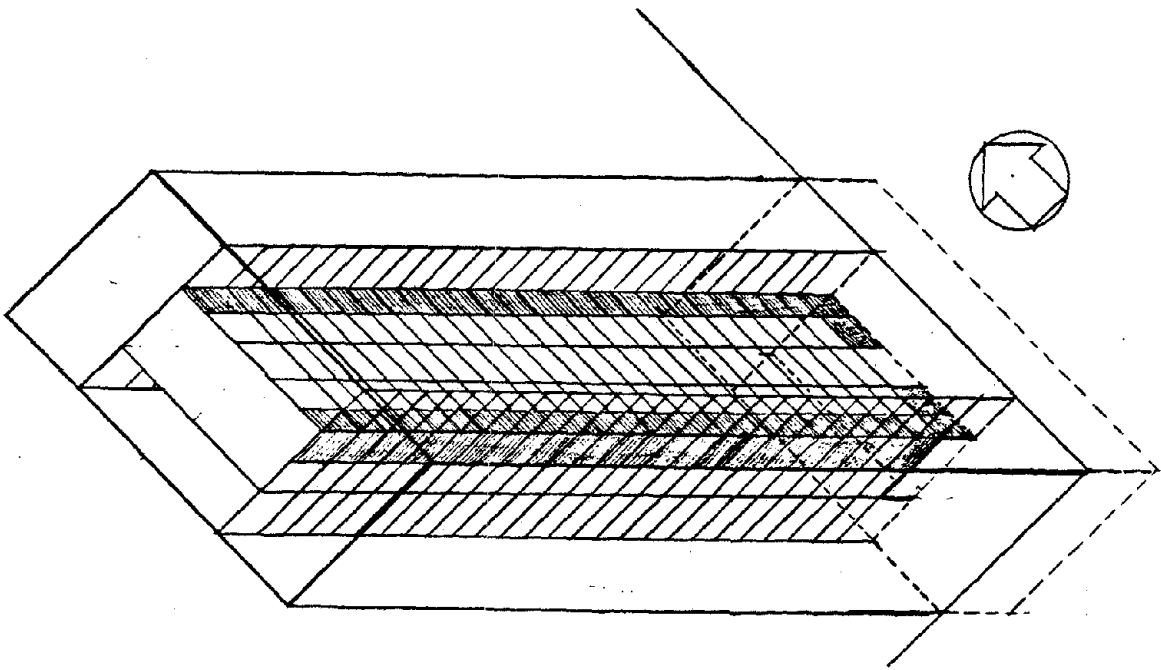


Figure 3.2.11: Model 4 Schematic  
(Includes Block Walls)

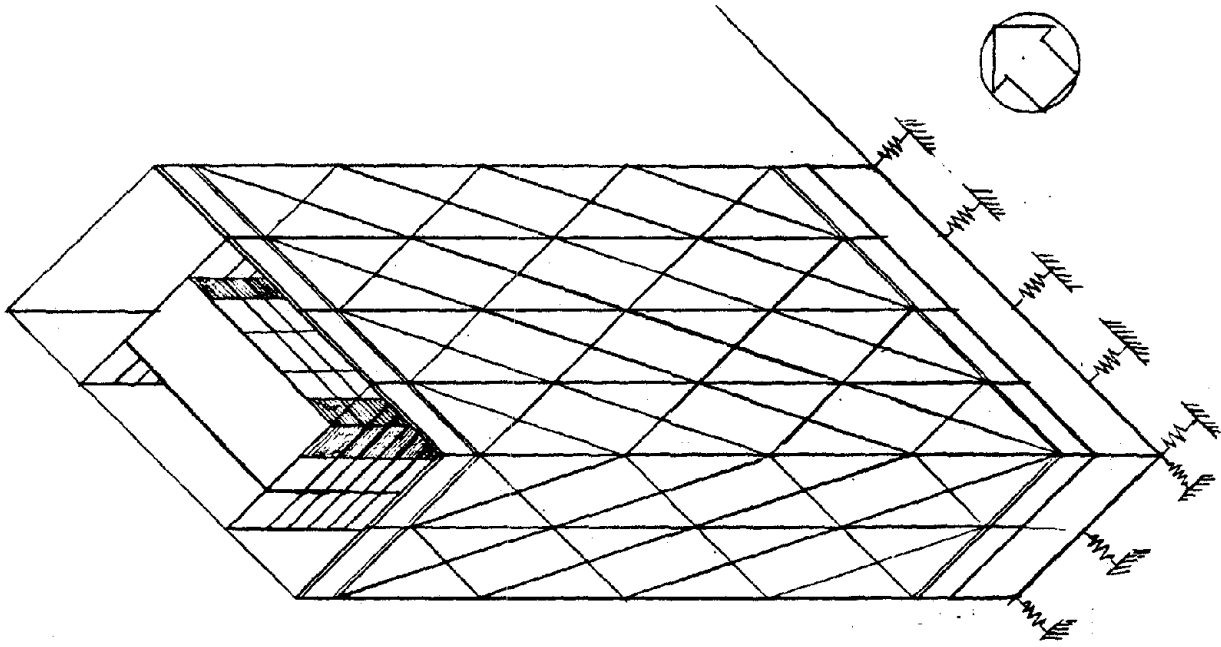
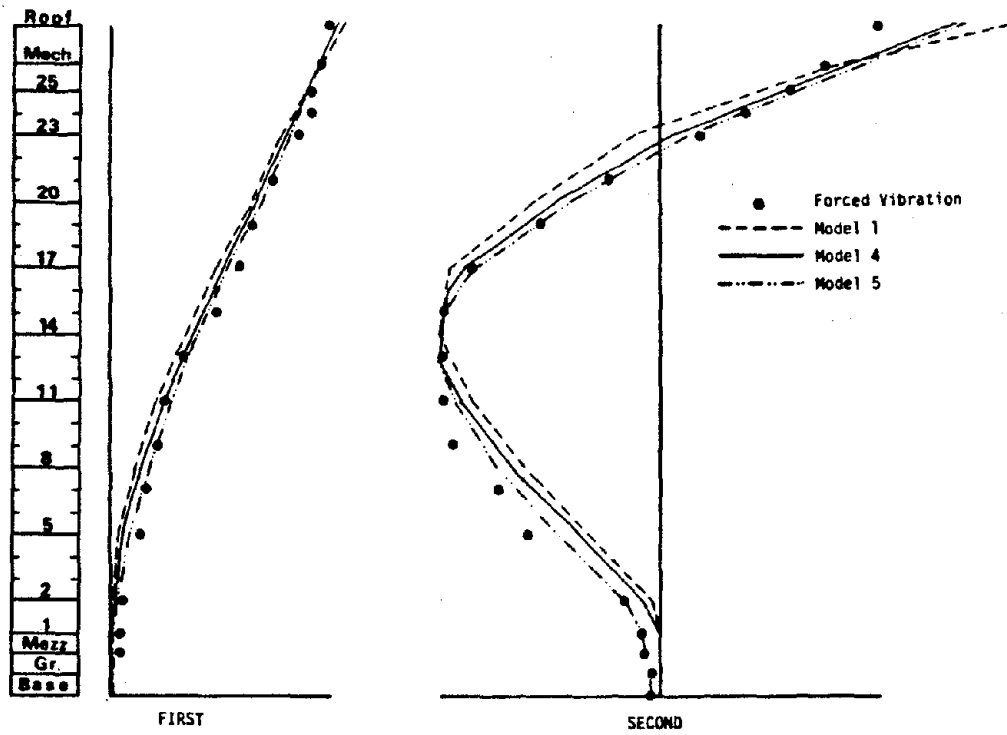
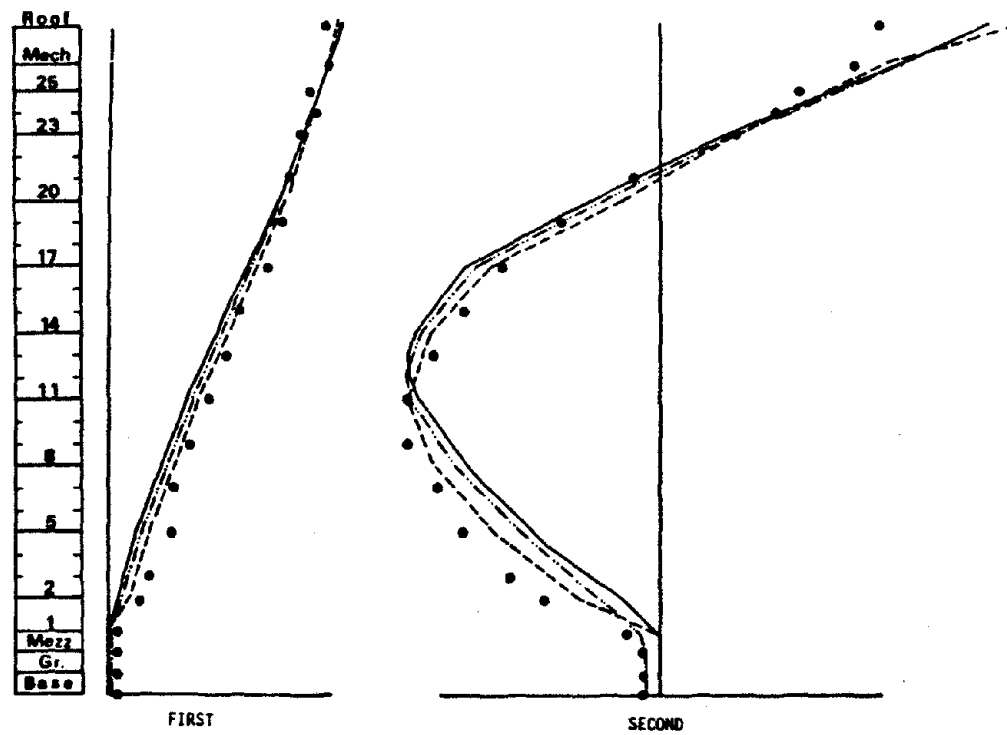


Figure 3.2.12: Model 5 Schematic  
(Includes Foundation Flexibility)



(a) E-W Direction



(b) N-S Direction

FIGURE 3.2.13: Analytical vs. Experimental Translational Mode Shapes

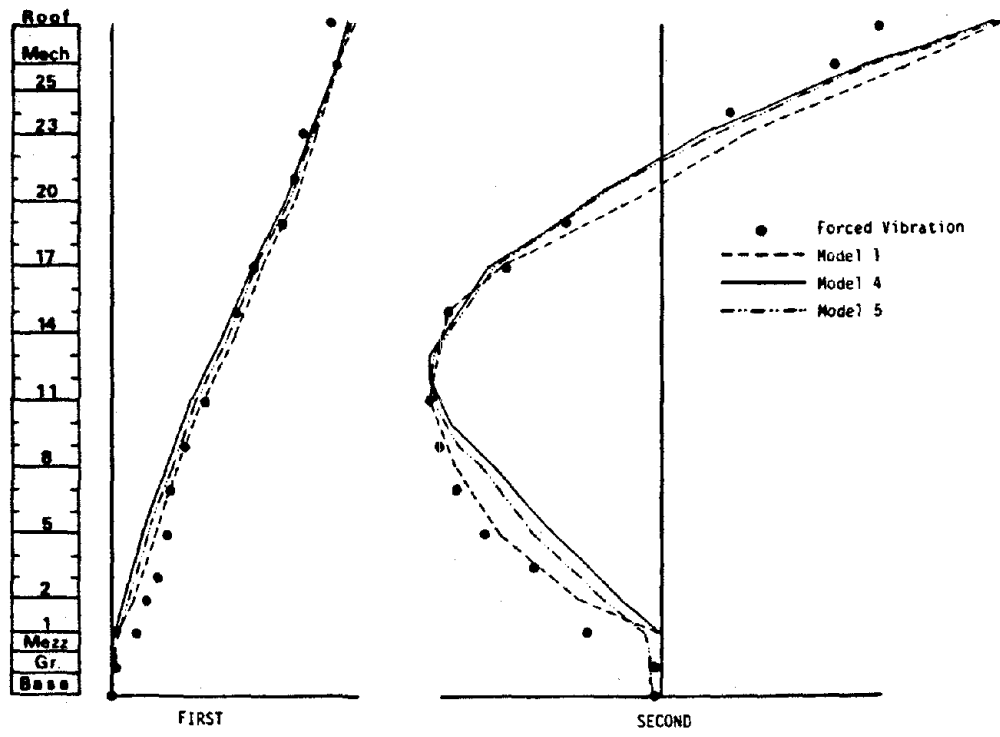
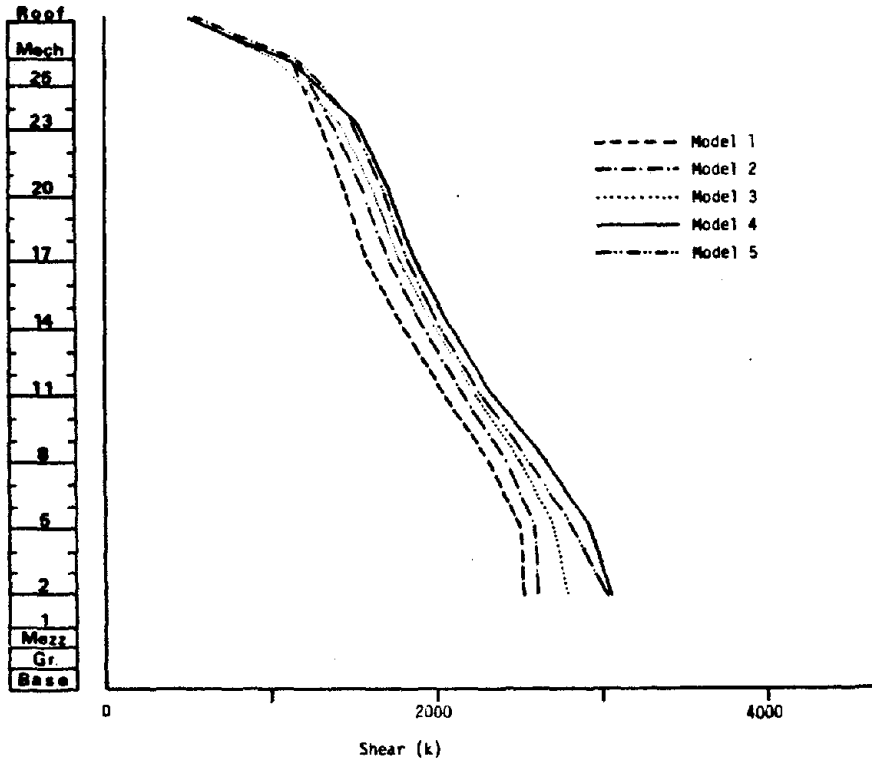
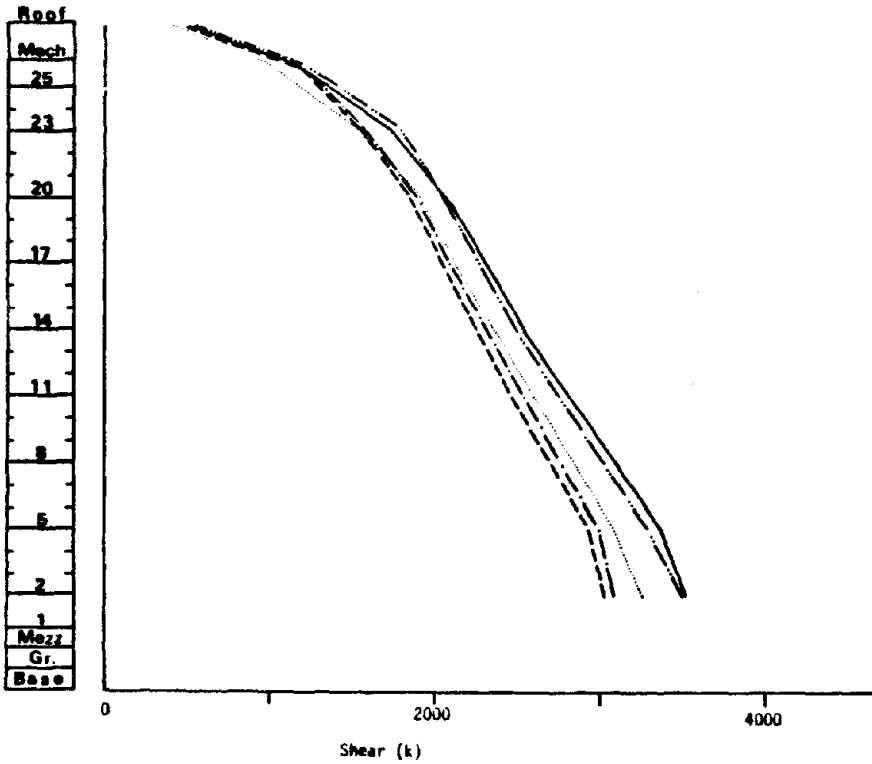


FIGURE 3.2.14: Analytical vs. Experimental Torsional Mode Shapes

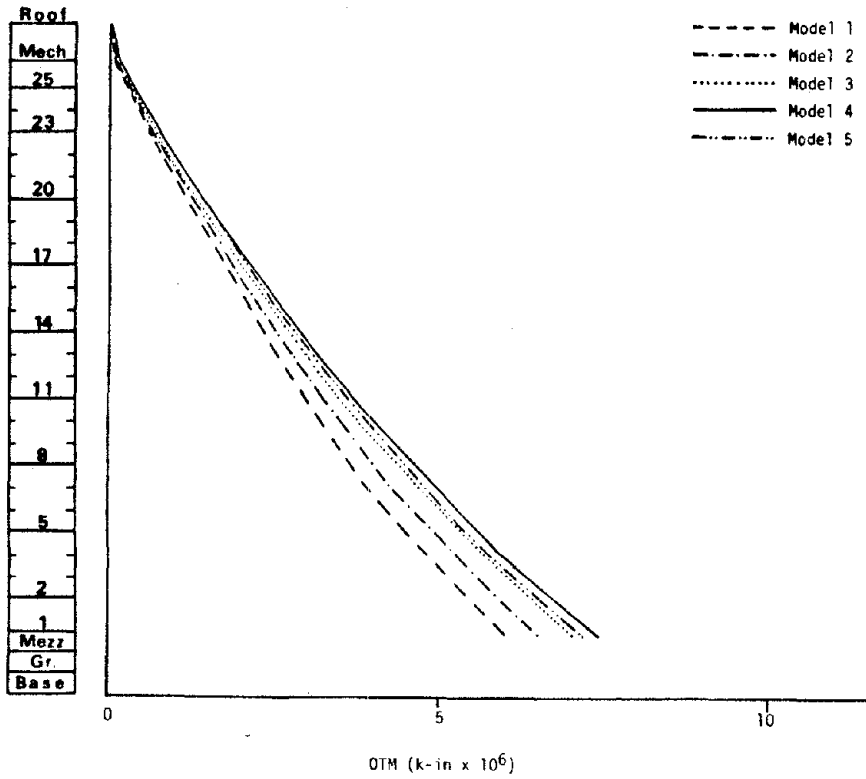


(a) E-W Direction

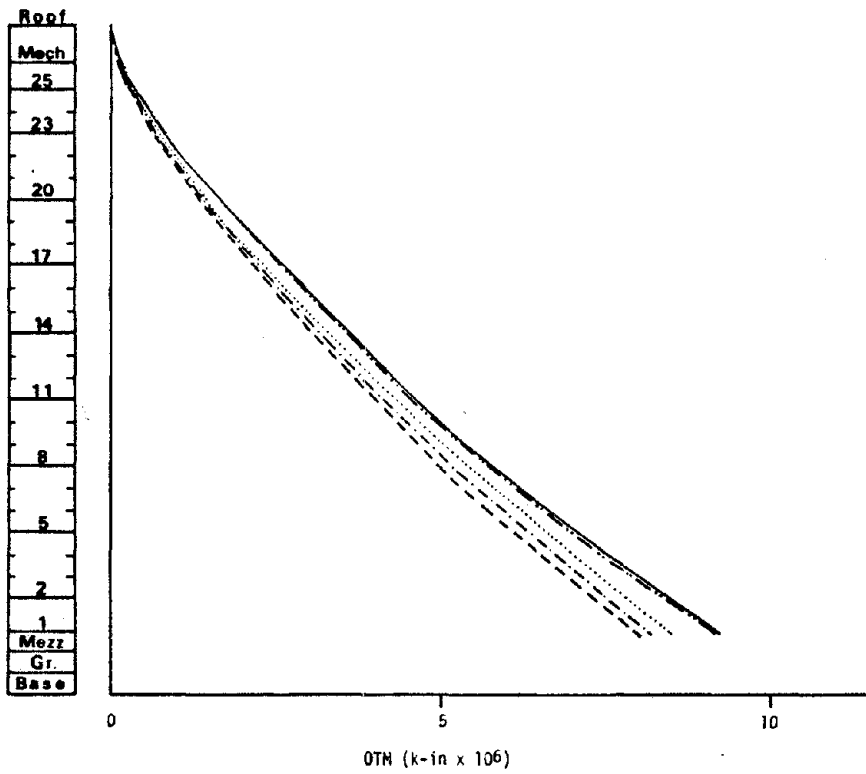


(b) N-S Direction

FIGURE 3.2.15: Influence of Modeling Approach on Story Shears

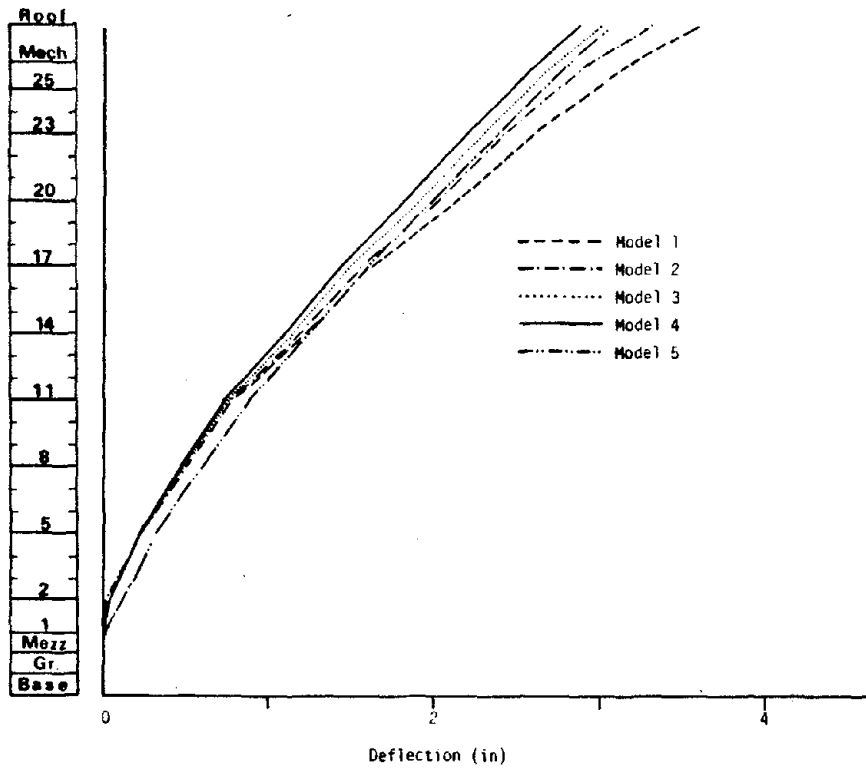


(a) E - W Direction

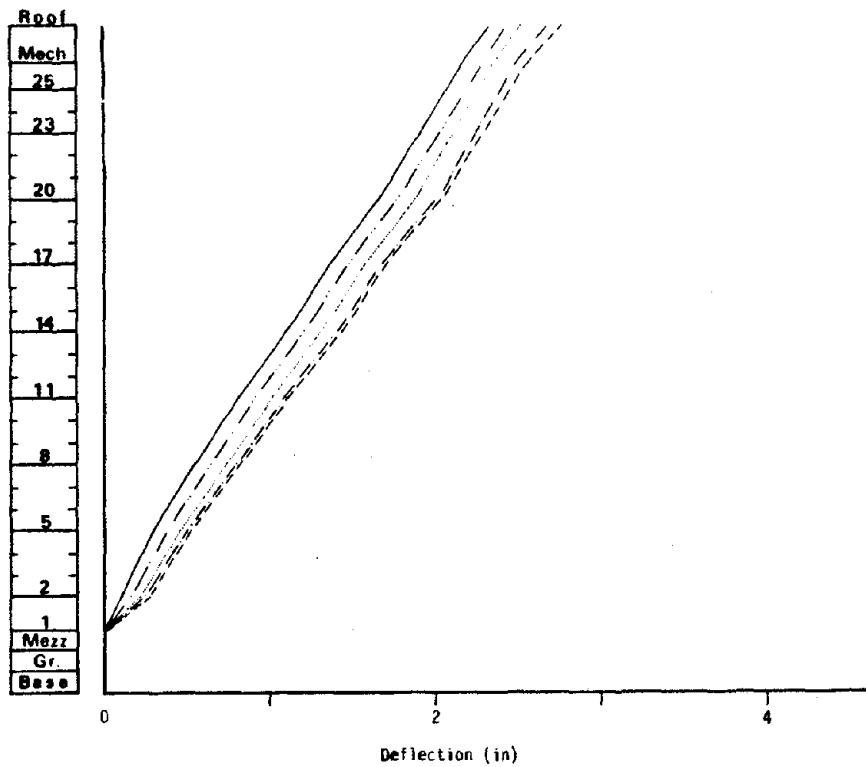


(b) N - S Direction

Figure 3.2.16: Influence of Modeling Approach on Story Overturning Moments

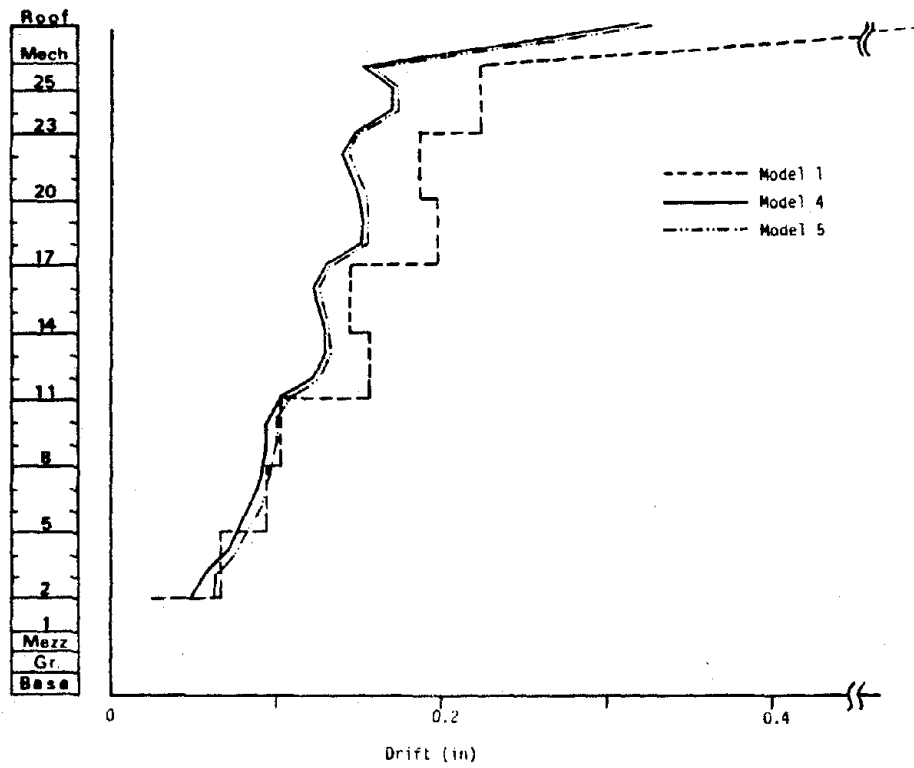


(a) E-W Direction

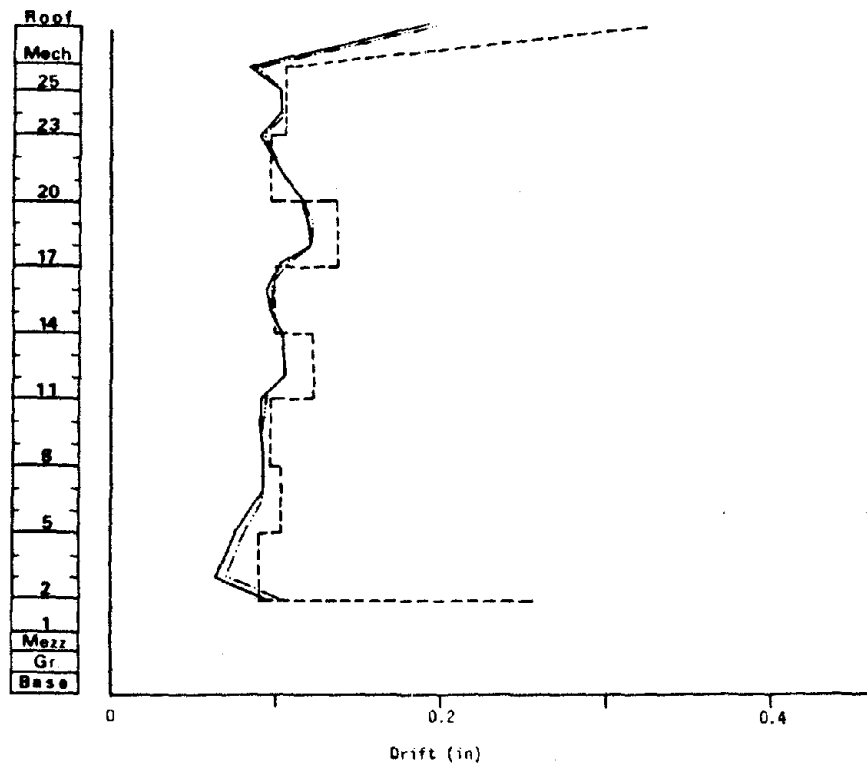


(b) N-S Direction

FIGURE 3.2.17: Influence of Modeling Approach on Story Deflections

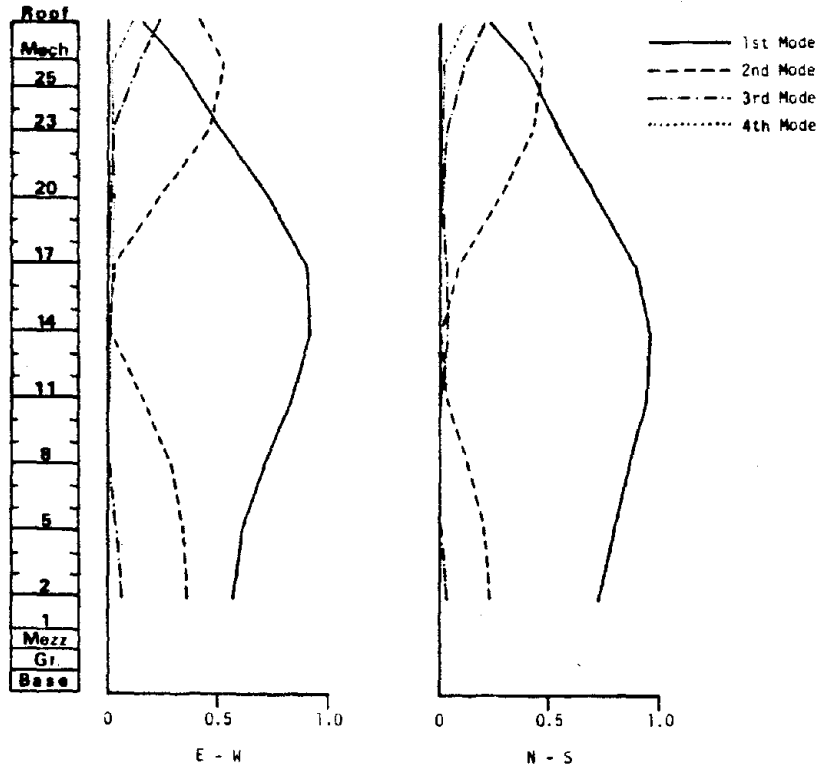


(a) E-W Direction

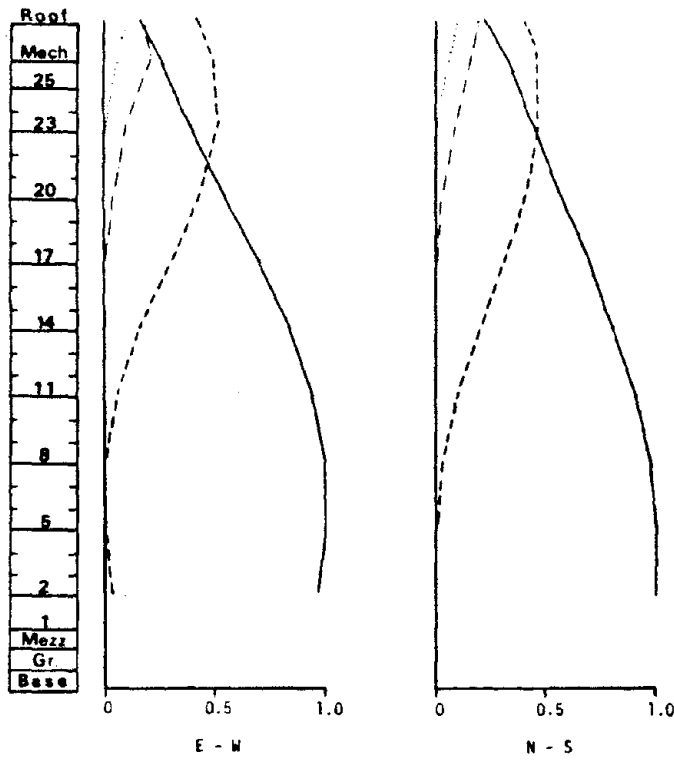


(b) N-S Direction

FIGURE 3.2.18: Influence of Modeling Approach on Story Drifts

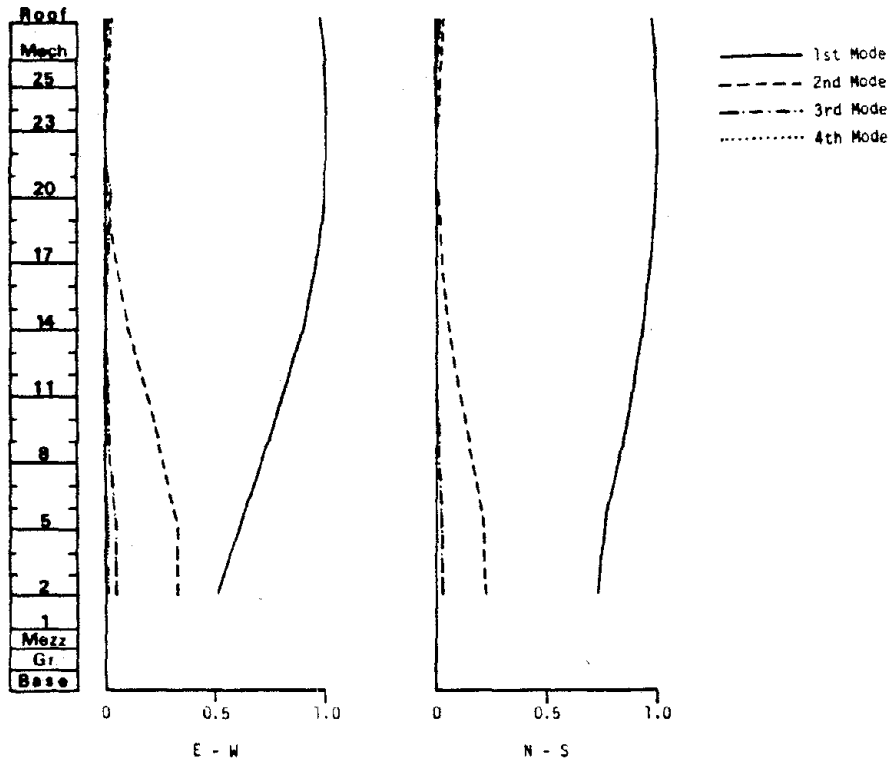


(a) Story Shear

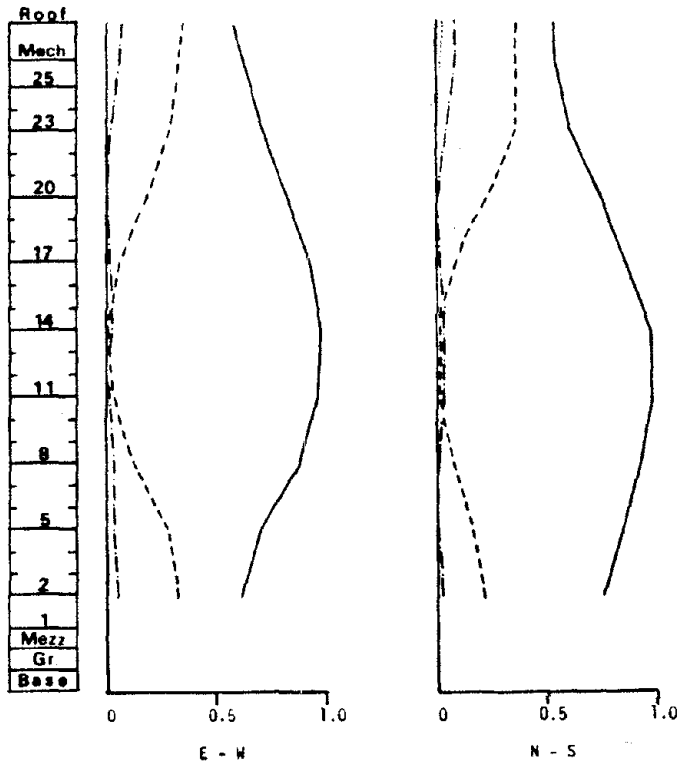


(b) Story Overturning Moment

FIGURE 3.2.19: Modal Contributions to Design Force Quantities

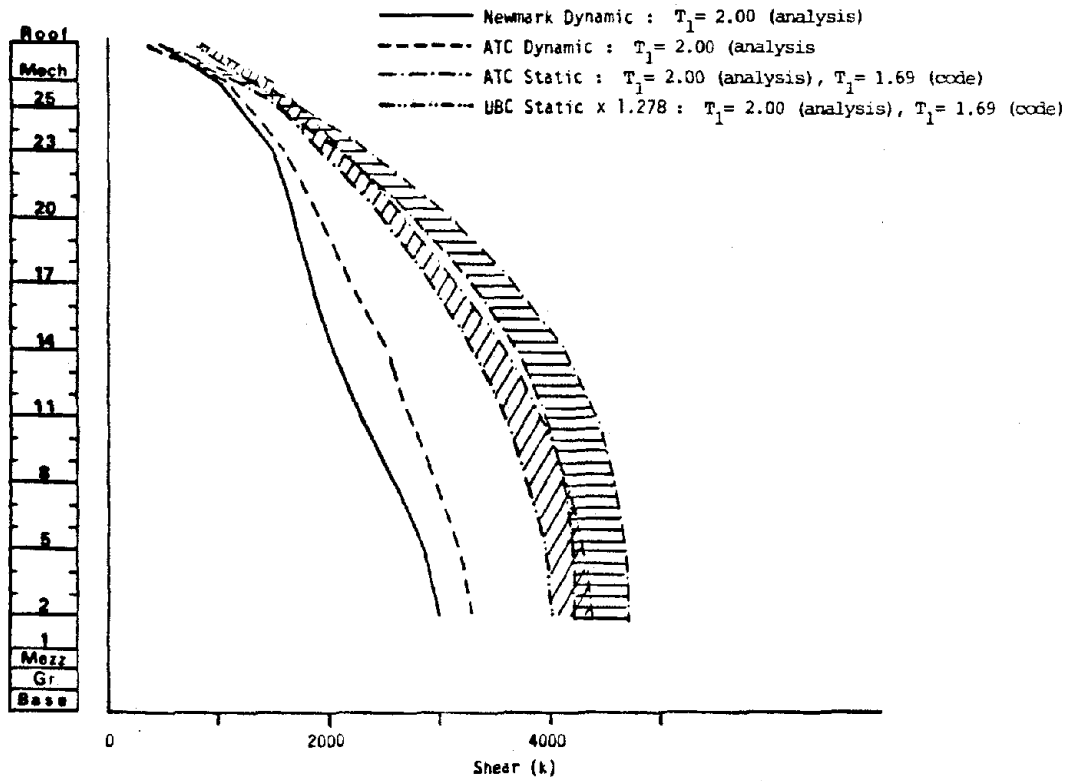


(a) Story Deflection

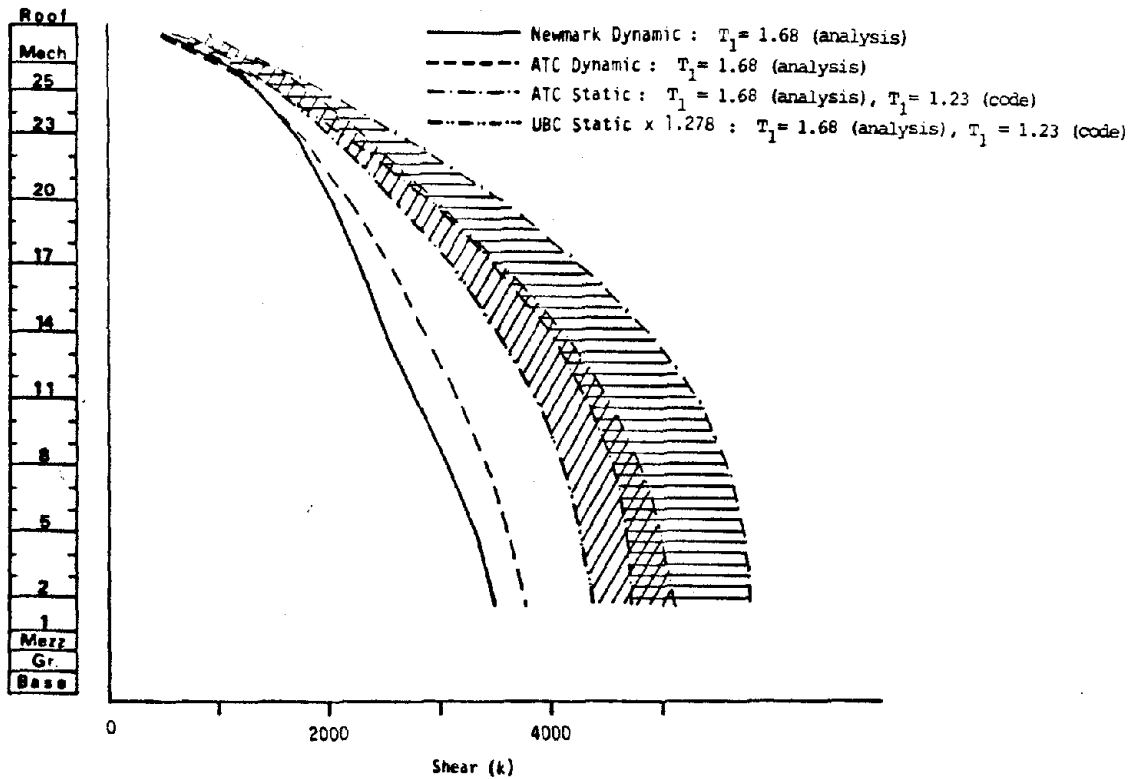


(b) Story Drift

FIGURE 3.2.20: Modal Contributions to Design Deflection Quantities

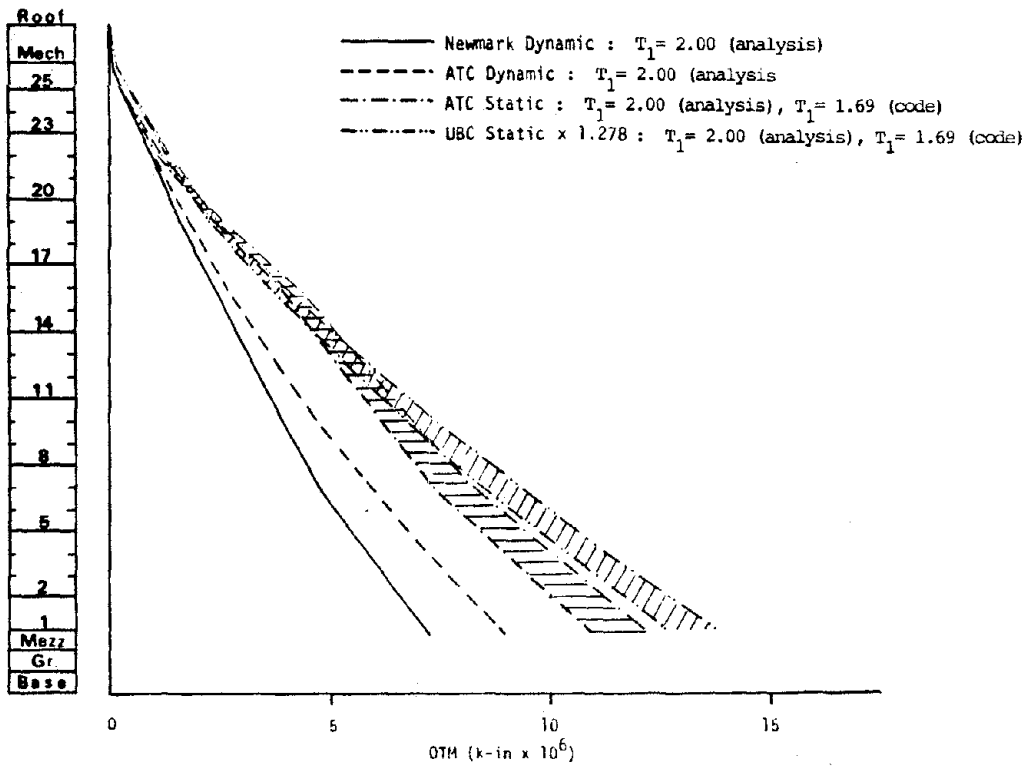


(a) E-W Direction

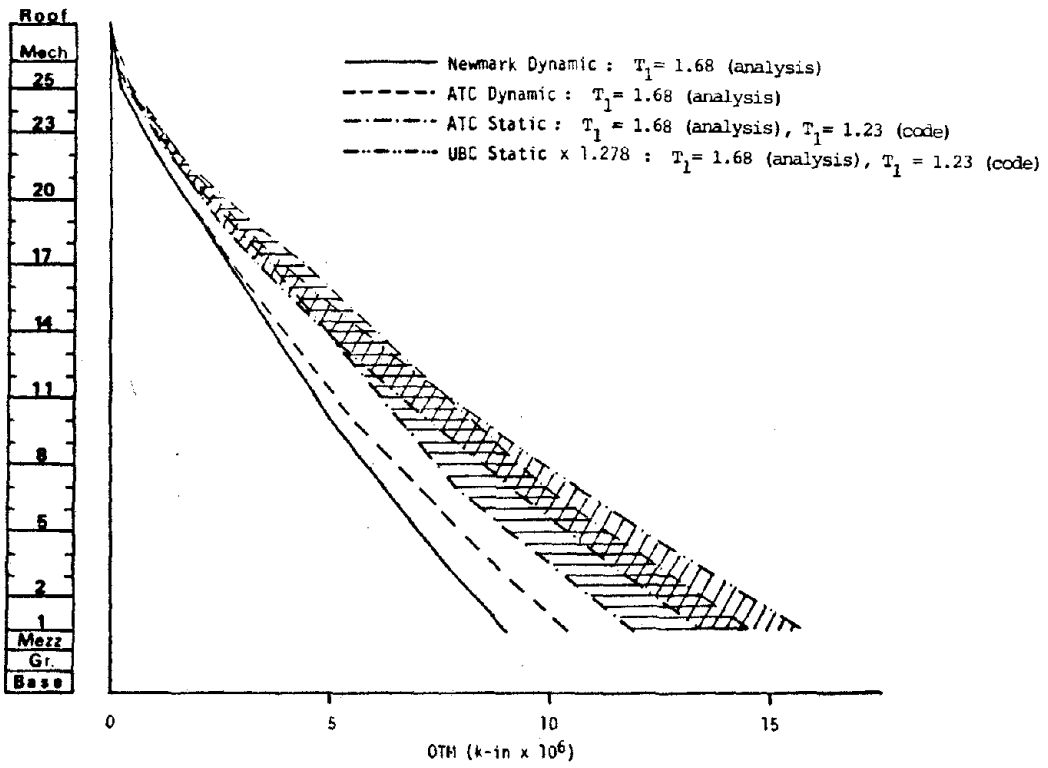


(b) N-S Direction

Figure 3.2.21: Story Shears Resulting from Dynamic and Equivalent Static Analyses

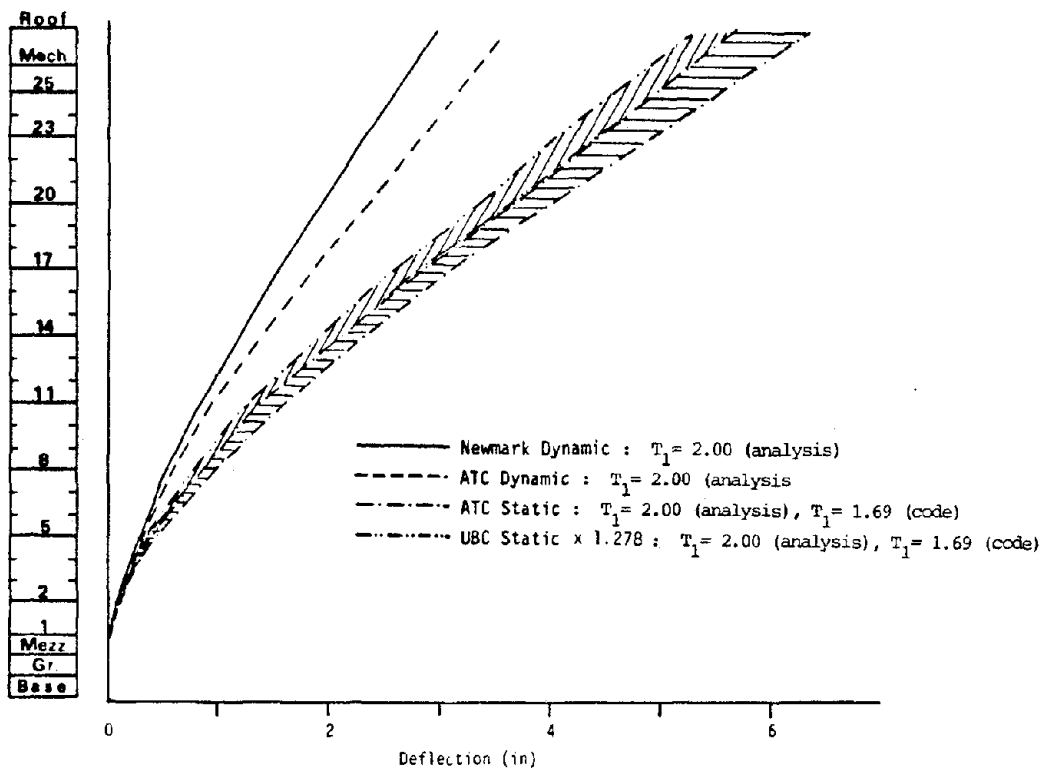


(a) E-W Direction

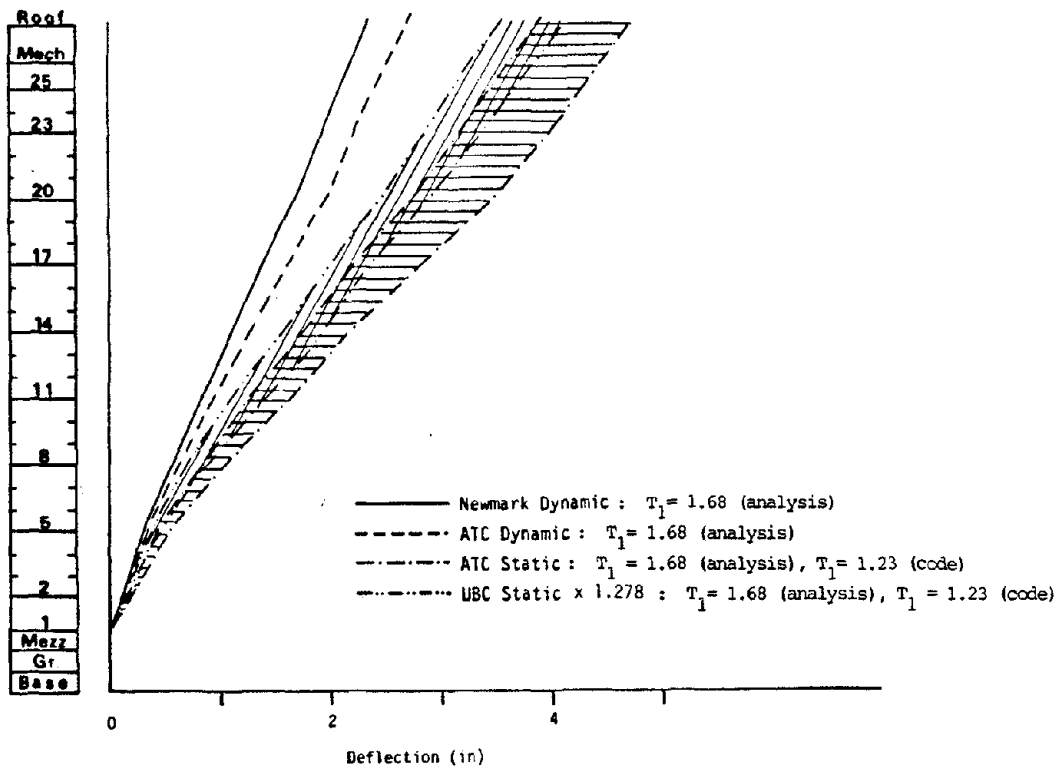


(b) N-S Direction

Figure 3.2.22: Story Overturning Moments Resulting from Dynamic and Equivalent Static Analyses

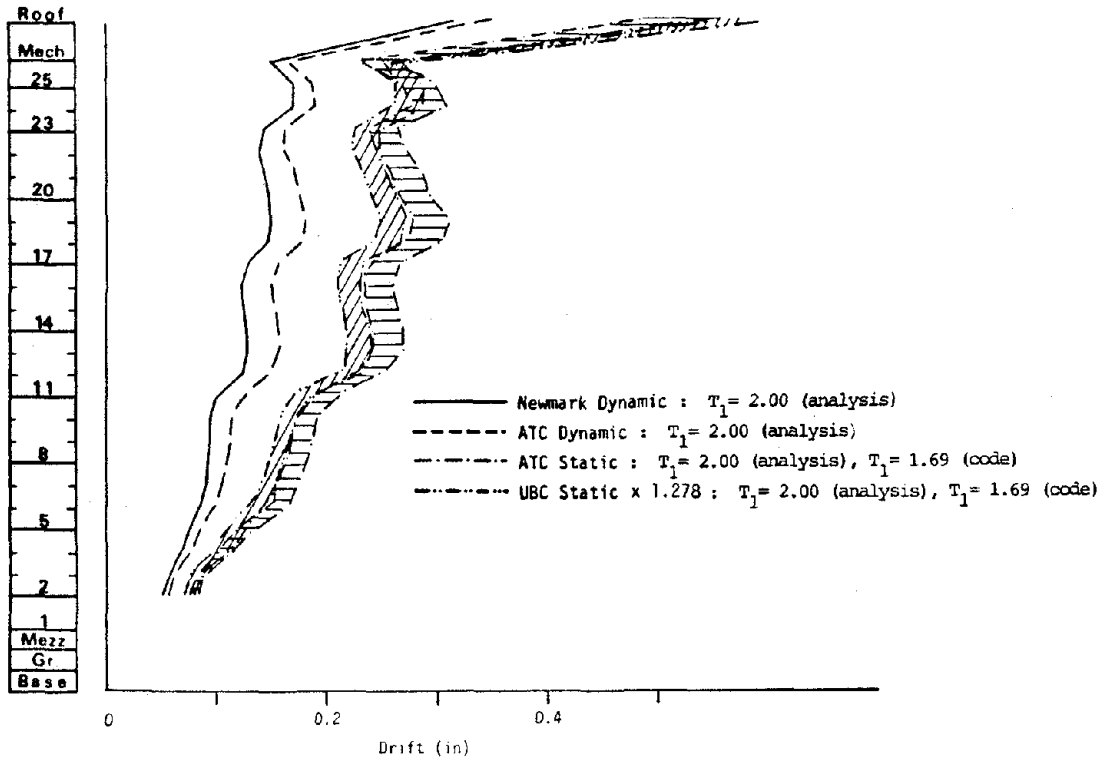


(a) E-W Direction

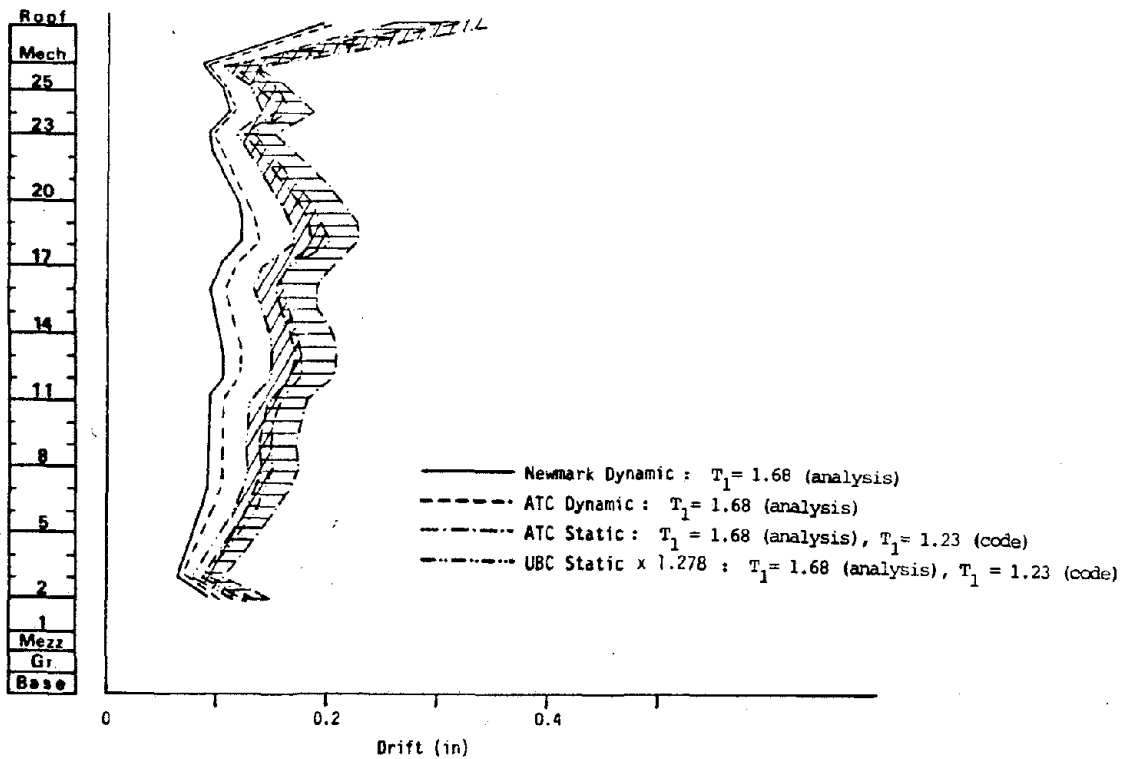


(b) N-S Direction

Figure 3.2.23: Story Deflections Resulting from Dynamic and Equivalent Static Analyses

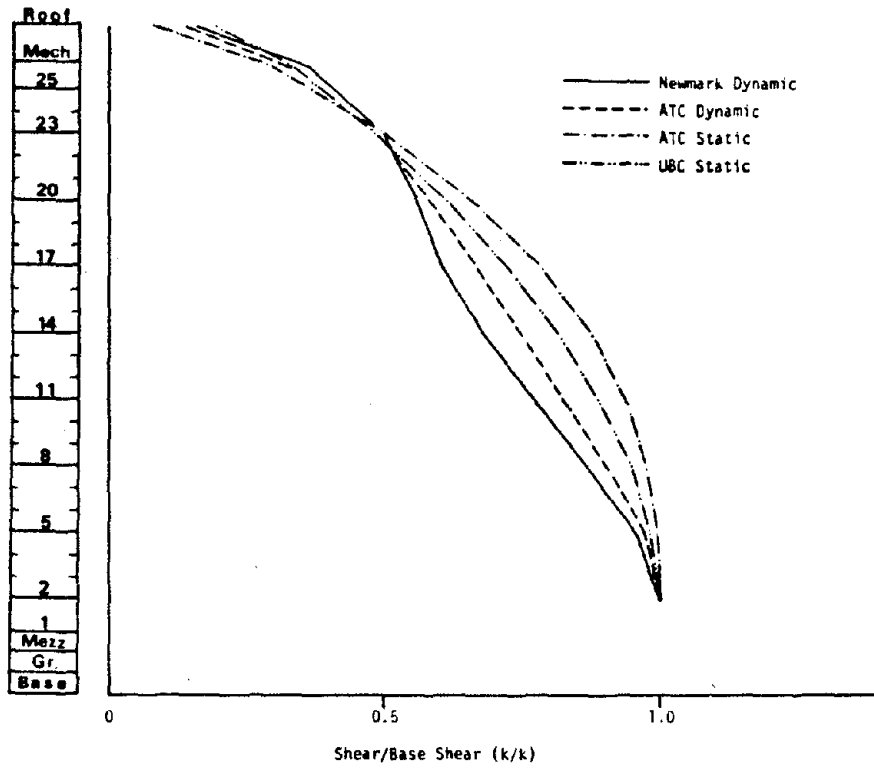


(a) E-W Direction

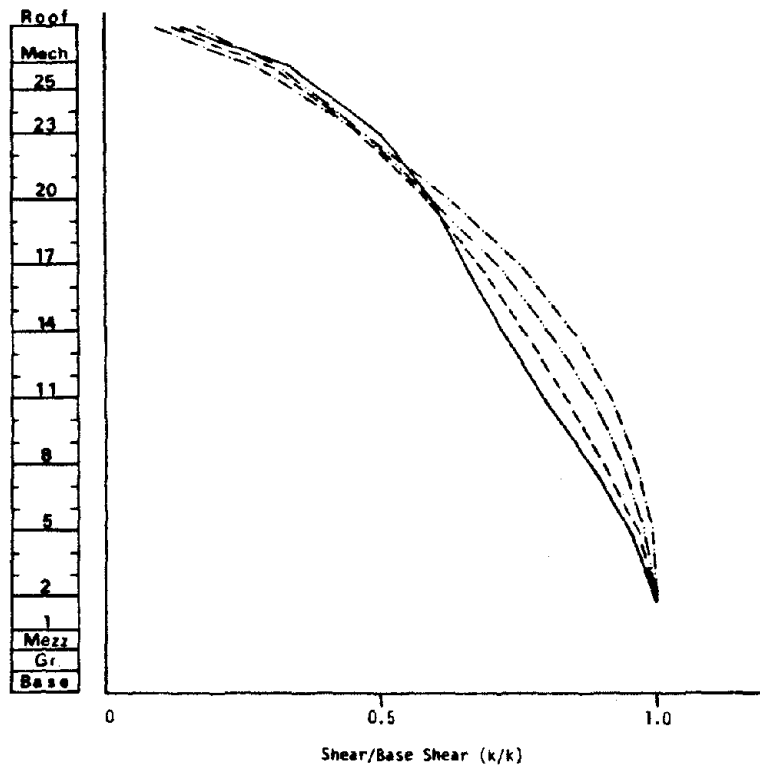


(b) N-S Direction

Figure 3.2.24: Story Drifts Resulting from Dynamic and Equivalent Static Analyses

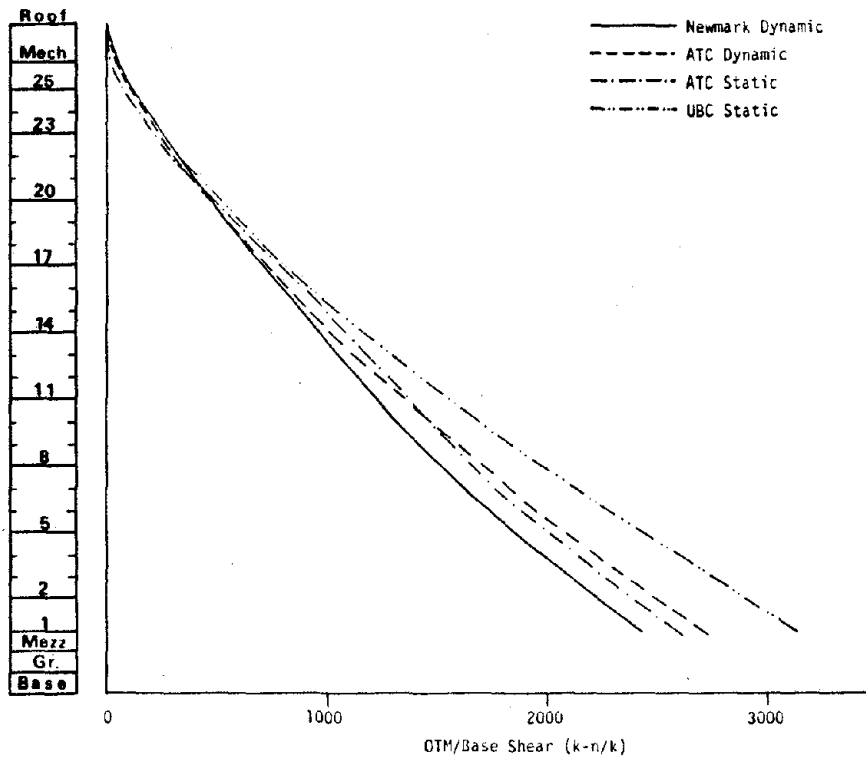


(a) E-W Direction

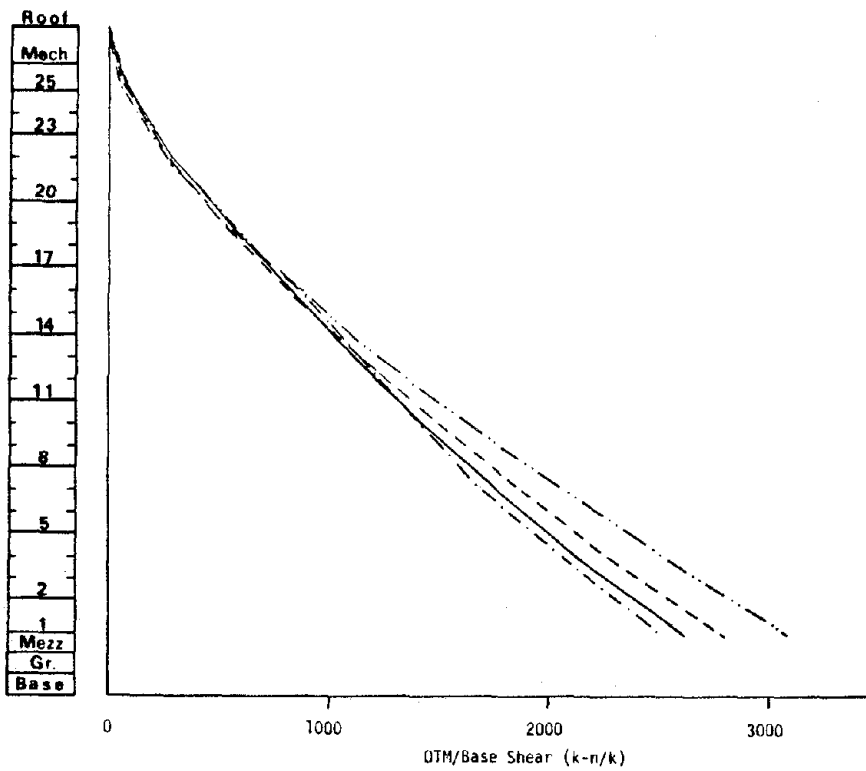


(b) N-S Direction

FIGURE 3.2.25: Story Shear Distributions Normalized to Base Shear

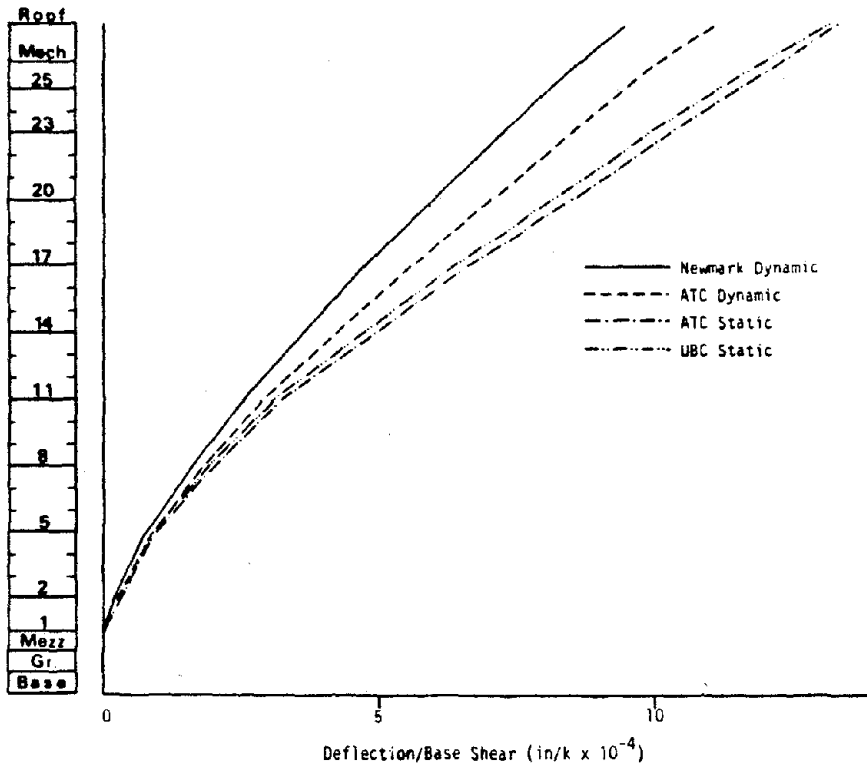


(a) E-W Direction

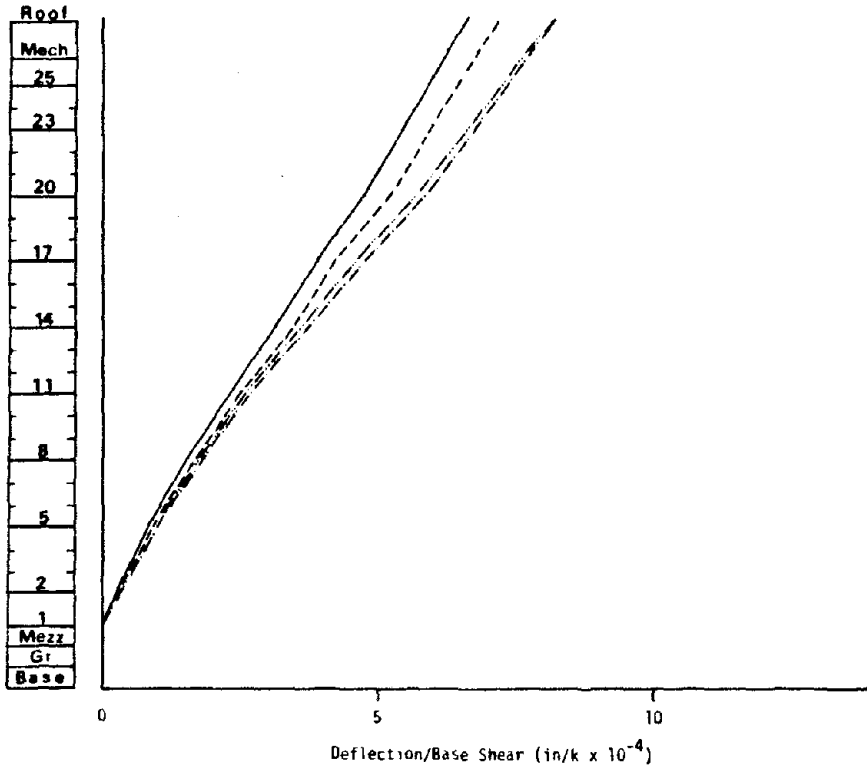


(b) N-S Direction

Figure 3.2.26: Story Overturning Moment Distributions Normalized to Base Shear

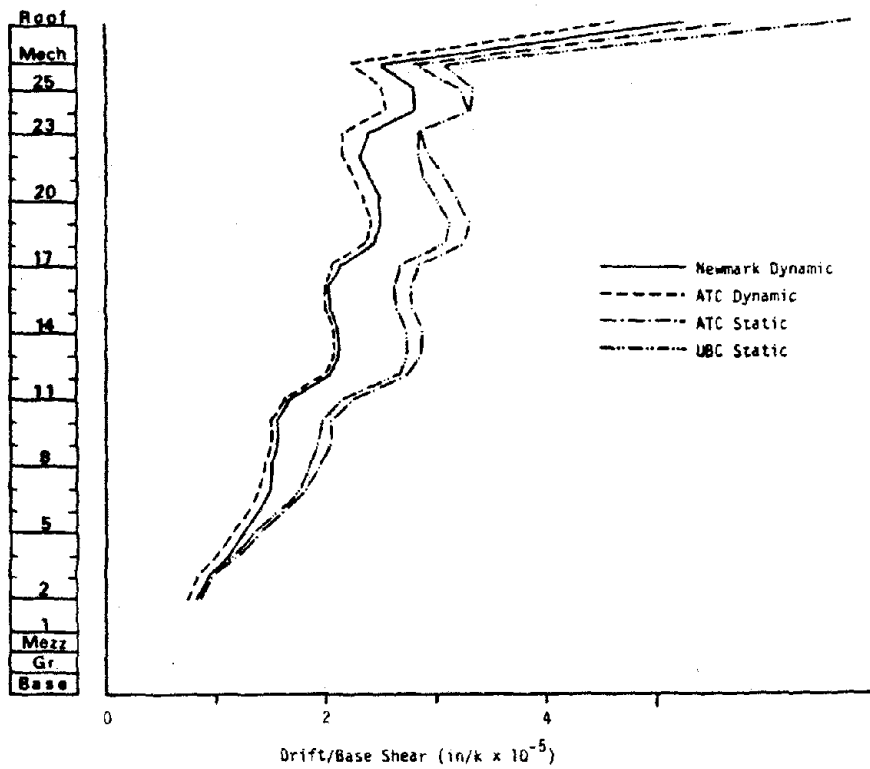


(a) E-W Direction

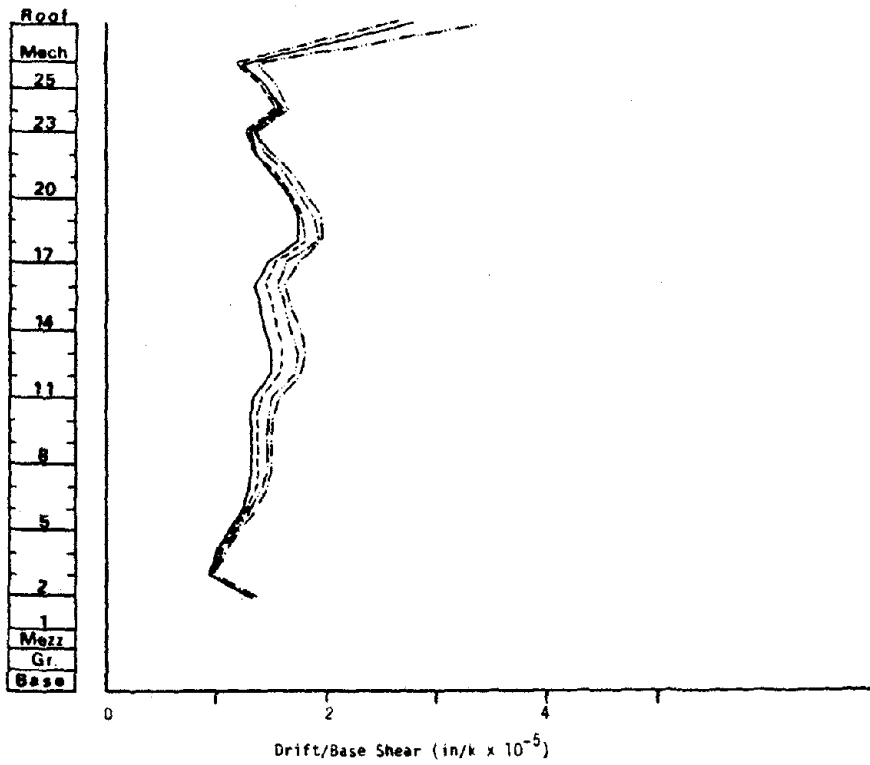


(b) N-S Direction

FIGURE 3.2.27: Story Deflection Distributions Normalized to Base Shear

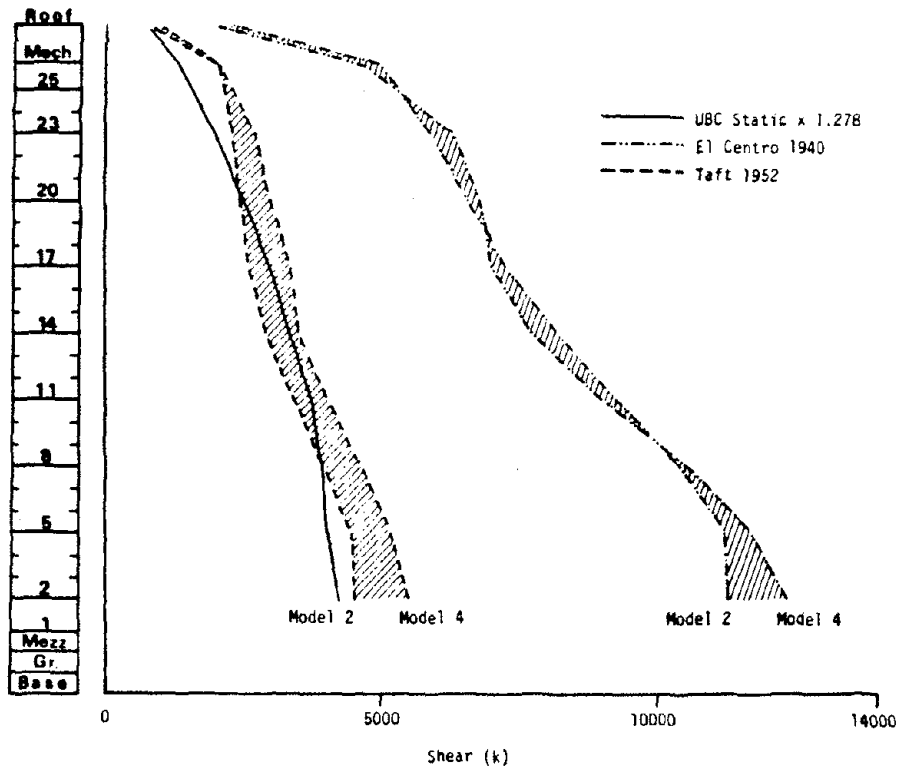


(a) E-W Direction

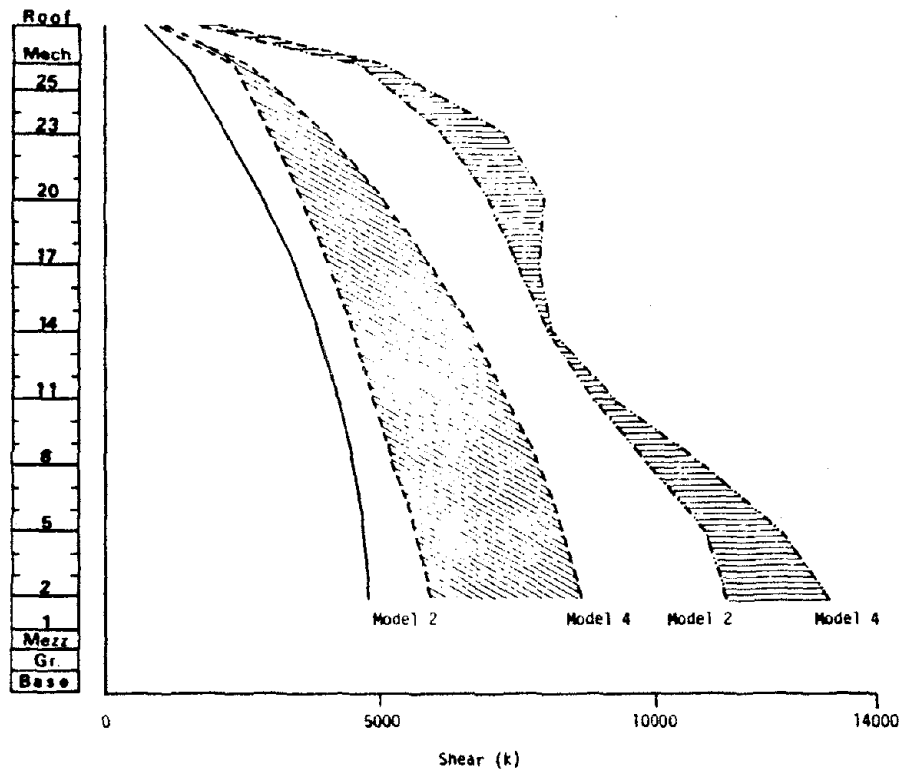


(b) N-S Direction

FIGURE 3.2.28: Story Drift Distributions Normalized to Base Shear

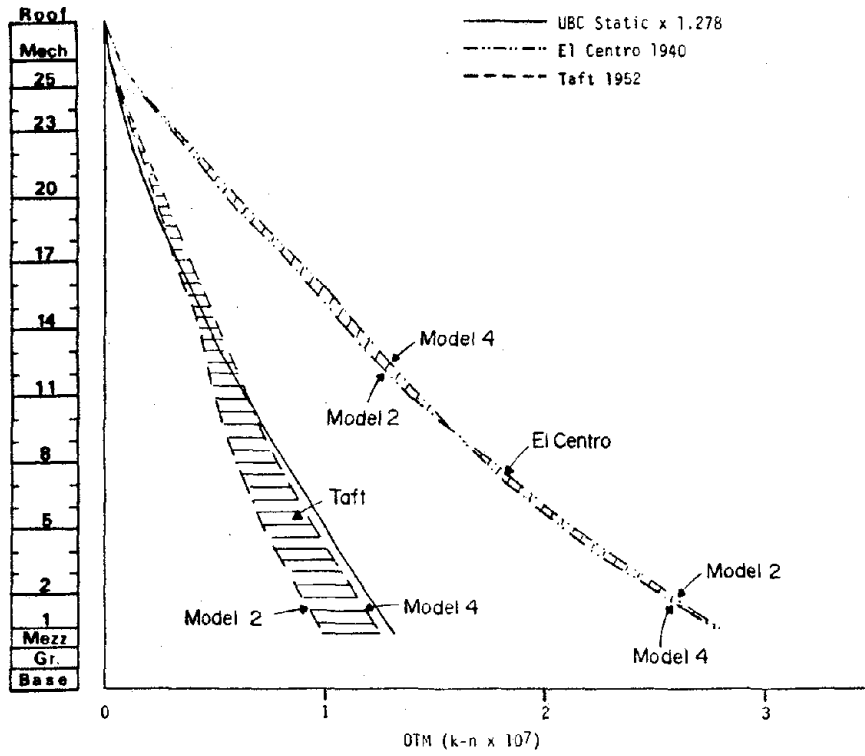


(a) E-W Direction

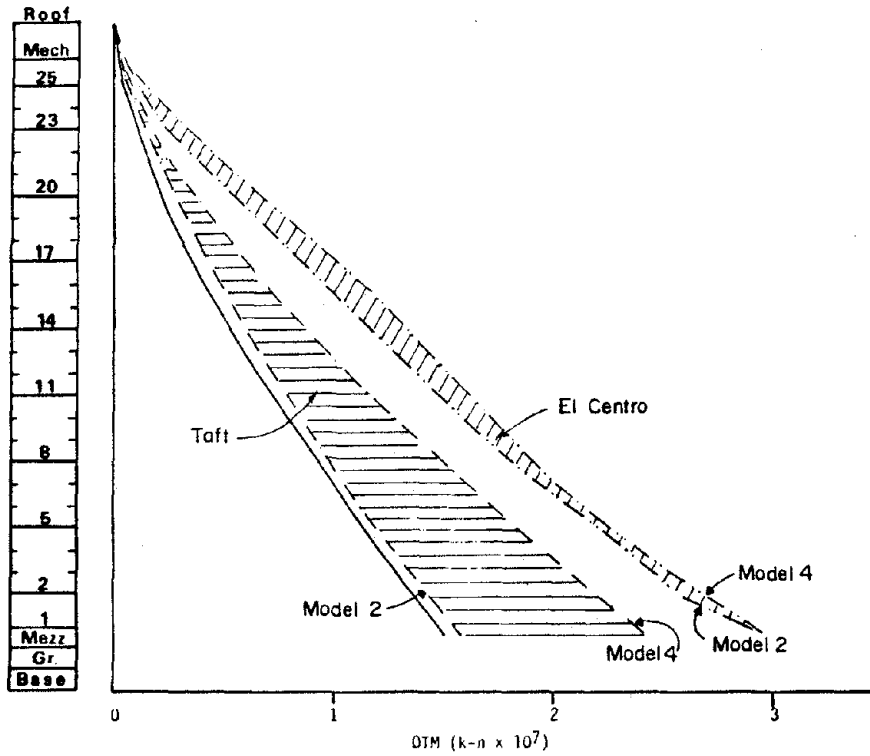


(b) N-S Direction

FIGURE 3.2.29: Comparison of UBC Design Shears versus Elastic Shears Induced by Actual Earthquake Spectra



(a) E-W Direction



(b) N-S Direction

Figure 3.2.30: Comparison of UCB Design OTM's versus Elastic OTM's Induced by Actual Earthquake Spectra

### **3.3 TRANSAMERICA BUILDING**

The Transamerica Building is a multistory pyramid shaped office building located in San Francisco, California. The structure was designed by Chin and Hensolt Engineers, Inc., also of San Francisco. The 60 story tower has a base dimension of 174 feet square at street level and rises to a height of 844 feet. A photograph of the building is shown in Figure 3.3.1.

#### **3.3.1 Description of the Structural System**

The primary lateral force resisting system consists of a steel moment resisting space frame with peripheral columns inclined at a slope of approximately 1 to 11. This moment frame begins at the 5th floor and extends over the full height of the building. Between the 2nd and 5th floors, lateral resistance is provided by a space truss system located at the periphery of the building spanning three stories. At the 2nd floor, a horizontal bracing system spans between the base of the peripheral space truss and the interior frames, redistributing lateral loads to the moment resisting frames of the 1st story. These frames extend down through three below grade parking levels to a 9 foot thick reinforced concrete mat foundation. Elevation and plan views of the structural system are shown in Figures 3.3.2 and 3.3.3.

The north-south (N-S) and east-west (E-W) lateral force resisting systems are nearly identical with the exception of secondary bracing in the protruding elevator shafts in the N-S direction between the 29th and 50th floors. Also, between the 30th and 40th floors, girders in the exterior N-S moment frames are omitted to make room for the elevator shafts (see Figure 3.3.3, floors 30-40). Otherwise, the columns and girders are symmetric in plan about the center of each

level. Through the first 17 stories there are twelve frame lines (six in each of the two directions) which include four exterior inclined planar frames and eight interior vertical planar frames (Figure 3.3.3, floors 5-17). At the 18th floor, four of the interior frame lines are terminated, leaving eight frame lines (four in each of the two directions) continuing up through the 45th story. At the 46th level, the four remaining interior vertical frames are discontinued leaving only the four exterior primary structural frames (consisting of four column lines and four adjoining beams) continuing over the remaining height of the building. The top ten stories (floors 51 to 60) serve only as an architectural cap and are not occupied, having no floor slabs. In these cap levels, cross bracing is used to provide stiffness in the horizontal plane (see Figure 3.3.3, floors 51-57).

All of the primary system columns are built-up box sections ranging from 30 inches square at the first level to 18 inches square in the top ten stories. The main girders are rolled sections varying from W14 to W36 (see Figure 3.3.2). The second floor horizontal braces are 36 inch built-up box sections. The floor construction typically consists of 2 1/2 inches of concrete cover over 3-inch concrete filled corrugated steel decking. The decking is spot welded to the floor beams. On the 5th and mechanical floors (19th and 49th), there is a 6 inch thick reinforced concrete floor slab. Below the second floor are heavier 8 inch reinforced concrete floor slabs. The exterior face of the building consists of precast concrete cladding (nonstructural) attached with clip angles and rods to secondary members. Above the 50th floor, precast facing is fixed to the columns and louvered aluminum panels are used as infill.

### **3.3.2 Results of Experimental Studies**

In June and November of 1972, forced vibration tests of the structurally complete Transamerica Building were carried out by the

Earthquake Engineering Research Center of the University of California at Berkeley. Also, an ambient motion study was performed by Kinematics, Inc., of San Gabriel, California. For a detailed discussion of these two studies see reference 39.

The forced vibration testing was performed using forced vibration generators fixed to the 48th floor of the building. The forcing system was able to excite N-S translational, E-W translational, and torsional vibration modes. To record response, 14 accelerometers were placed at vertical spacings of 3 to 6 floors over the height of the building. In Figure 3.3.4(a) and (b) ambient and forced vibration results for the first four natural periods and mode shapes are shown for the N-S and E-W directions, respectively. Note that the third translational mode could not be excited in the forced vibration tests and, thus, corresponding data is not included in Figure 3.3.4. This was due to the fact that the force generators on the 48th floor were near a nodal point for the third mode. Natural periods of 2.94, 1.68, 1.14 and 0.88 were determined for the first four N-S translational modes, respectively. In Figure 3.3.5, results for the first two torsional modes are shown. Periods of 2.24 and 1.23 seconds were determined for the first and second modes, respectively. Forced vibration data are missing from Figure 3.3.5 due to inability to excite these torsional modes.

The experimental results reflect several fundamental aspects of the dynamic behavior of this building. First, the dynamic properties in both the N-S and E-W direction were found to be essentially identical. This indicates that the elevator shafts and accompanying N-S direction bracing have negligible effect on the overall response of the building. For this reason, only the N-S direction will be considered for comparison with analytical results. The relative rigidity of the first four stories is evident from the mode shapes.

This is due to the stiff space truss that provides lateral support for this part of the building. No significant deflections at ground level are observed in the experimental results. So the building behaves as though it were fixed at the ground level with no foundation flexibility. Another interesting aspect of behavior is the relative flexibility of the ten story architectural cap (floors 51-60) evidenced by the much larger deflections (whiplash behavior) occurring in this part of the structure. The shape of the first translational mode indicates that a mixture of cantilever and shear type deflection behavior controls the overall response of the building.

### 3.3.3 Description of Analytical Models

Dynamic analyses of the Transamerica Building are performed using both the SAP-IV (7) and modified ETABS (23) computer programs. The SAP program is used for period and mode shape determination because the inclined exterior columns can not be modeled using ETABS. However, the modified ETABS program is used as a post-processor to calculate gross response quantities using dynamic properties from the SAP analyses as input. For computational efficiency, rules of symmetry are applied to reduce the size of the SAP model to a quarter segment of the building. Appropriate boundary conditions are imposed along the two lines of symmetry. Separate analyses for translational and torsional modes are performed since the symmetry of the structure results in uncoupled translational and torsional modes.

Floor diaphragms are assumed to be infinitely rigid in-plane. At each floor level, a master node along a central vertical axis (center of mass) is assigned. The local horizontal translational degrees of freedom and local vertical axis rotational degree of freedom at each column line are slaved to the master nodes to impose the rigid floor idealization. The three remaining degrees of freedom are allowed at each node except when constrained by boundary conditions. The master

node is allowed only one degree of freedom corresponding to the translational or torsional direction of motion being considered. The modeling scheme and symmetric boundary conditions used at each floor are shown in Figure 3.4.6. Since no foundation flexibility is apparent in the experimental results, fully fixed boundary conditions are imposed at the ground level. Four models are presented for comparative analysis. Refinements were progressively made in developing each subsequent model in order to evaluate the influence of various modeling assumptions and to better capture the experimentally observed behavior.

#### Model 1

Model 1 consists entirely of 3-D beam-column elements using center-to-center member dimensions. Only the primary lateral force resisting steel space frame is modeled. Element properties are based on the bare steel column and girder sections. Elevator shaft bracing is neglected, being considered a secondary system that acts independently of the floor diaphragm (experimental results showed this to be the appropriate analytical assumption). The final quarter building model included 638 nodal points, 947 elements and 1355 degrees of freedom. With the nodal numbering scheme used, the bandwidth of the stiffness matrix was limited to 142.

The lumped mass values at each floor are based on the dead load calculations supplied by the structural designer. The total floor weights used in Model 1 are given in Table 3.3.1. The 20 psf partition load required by UBC (12) was subtracted from the dead loads as this weight increase is believed to overestimate the actual weight of the buildings during the experimental testing. Torsional mass moments of inertia are based on the assumption that the mass is distributed evenly over each floor. For consistency with the quarter building model, the values of mass and mass moment of inertia used for the analyses correspond to 1/4 of the weight values shown in the

Table 3.3.1.

Model 2

The main objective in the formulation of Model 2 is to account for the rigidity of joint regions at the column-girder intersections. The mass values are the same as those used for Model 1.

In this model, the entire joint panel zone is assumed to be infinitely rigid, whereby the element stiffnesses are calculated based on the clear height of the columns (being reduced by the girder depth) and the clear spans of the girders (being reduced by the column width). The SAP IV beam-column element has no explicit allowance for rigid end zone effects as does ETABS. To account for this effect without the costly addition of extra nodal points around each joint slaved to a master joint node, a parameter study was performed on a partial frame of the building to determine an appropriate modeling approach. In this study, a model with one node per joint was compared with a model having five nodes per joint, with the four additional nodes at distances corresponding to clear heights and spans of the intersecting column and girders. In the model with one node per joint, the column and girder moments of inertia were modified as follows:

$$I^* = I (L/L-d)^3$$

where  $I$  = actual moment of inertia

$I^*$  = modified moment of inertia

$L$  = center-to-center length of column or  
girder member

$d$  = depth of adjoining column or girder  
element

This increase in moment of inertia is based on the assumption that the member ends undergo relative lateral translational displacements only

with no relative rotational displacements. Neglecting this relative rotational flexibility results in a slight overestimate of stiffness. However, the results of the parameter study showed that this modeling approach is reasonably accurate for this building. Applying this technique to member properties of the full building, increases the moments of inertia by 35 to 75% for columns and by 15 to 20% for girders.

As a sidelight to Model 2, an additional model was formulated which included the rigid zone effect in the columns only. An analysis was performed on this model in order to assess the relative importance of column versus girder rigid end zone effects on the dynamic properties of the building.

### Model 3

The objective in the formulation of Model 3 is to account for the stiffening effects of the floor slabs on frame action in the building. This formulation includes the rigid end zones as described in Model 2 and also accounts for slab-girder interaction by further increasing girder moments of inertia based on composite steel-concrete section properties. Mass values are the same as those used for Model 1.

The floor slab is constructed of concrete filled steel decking. No shear connectors are provided since the girders are not designed to act compositely with the slab. However, the steel deck was spot welded to the girders and therefore, some composite action may be expected for moderate levels of deformation. For the stiffness formulation of this model, full composite action is assumed with section properties calculated according to the AISC Specifications (1), section 1.11.5. All decking is assumed to run perpendicular rather than parallel to the girders resulting in lower values of moment of inertia. A typical composite section based on effective slab width and thickness as recommended by AISC is shown in Figure

3.3.7. The increase in girder moments of inertia ranged from 90 to 115% by including composite action.

#### Model 4

A review of the dead weights provided by the structural designers indicated that these values were somewhat conservative. After performing detailed mass calculations at various floors, a dead weight reduction of 15 psf was indicated for all levels of the building to give a better estimate of the true building weight at the time of experimental testing. Also, the design weights for the architectural cap were found to be overestimated by a factor of approximately two. For Model 4, mass values are changed from previous models in accordance with these findings resulting in the values shown in Table 3.3.1. The structural stiffness modeling is the same as for Model 3.

#### **3.3.4 Comparison of Analytical and Experimental Dynamic Properties**

Analyses were performed to extract the natural periods and mode shapes of the four models described in the previous section. In this section, results of these analyses are presented and compared with results of the experimental study.

In Figures 3.3.8 and 3.3.9 the first four N-S translational and first two torsional mode shapes are shown for models 1 and 4, representing the simplest and most refined models, respectively. As can be seen from this figure, the analytical mode shapes compare very well with experimental results. Both the nodes (neutral points) and anti-nodes (points of maximum displacement) are predicted with good accuracy. It is noted that the mode shapes change only slightly for the different models, indicating that the mode shapes are relatively insensitive to the modeling variations. As in the experimental results, the relative stiffness of the first five stories is reflected

in the analytical mode shapes. Due to the large relative flexibility of the 10-story architectural cap, the analytical mode shapes did not show as good agreement with experimental results in this part of the structure. However, analysis showed that the behavior of the cap does not significantly influence the overall response of the main portion of the building. Therefore, the detailed response of the cap is omitted from the figures. An interesting aspect of behavior due to the discontinuities of stiffness over the height of the building can be observed in the first translational mode (Figure 3.3.8). As noted in section 3.3.1, interior frames are discontinued at level 18. Also, girders from the center bay of the exterior frame are omitted from levels 30 to 40. Careful inspection of the first translational mode shows sudden increases in the slope of deflection at levels 18 and 30 corresponding to these structural discontinuities. The experimental results also appear to show this behavior. It will be seen that these discontinuities significantly affect the interstory drift in the building.

In Table 3.3.2, analytical periods for the four models are compared with experimental values. As can be seen, significant variations in natural periods result for the different models. Model 1 is the most flexible idealization of the buildings consisting of only the bare steel frame with center-to-center member dimensions. As can be seen from the table, the first analytical translational period is 3.77 sec., or 28.2% greater than the experimentally determined period of 2.94 sec. The higher modes show greater variations from experimental values with the largest difference resulting in the second mode where the analytical period is 37.3% greater than experimental. The torsional modes show 38.8 and 33.3% variations for the first and second modes, respectively.

In Model 2, the addition of rigid end zones improves correlation of the analytical and experimental periods significantly where the

fundamental translational period is reduced to 3.49 second and variations in analytical versus experimental periods range from 18.7 to 27.2%. These period reductions correspond to increases in modal stiffnesses ranging from approximately 15% to 23% for the different translational and torsional modes as shown in Table 3.3.3. Thus, the rigid joint zones have a roughly uniform stiffening effect on these modes. Separate analyses were performed to study the relative importance of the girder and column rigid end zones effects. Although the influence of both were significant, it was found that the girder rigid end zone effect had the greater influence on the natural periods of the building.

In Model 3, the addition of slab-girder interaction further improves correlation with experimental results. Here, the fundamental translational period is reduced to 3.13 sec. and variation with respect to experimental period values for all modes ranges from 4.1 to 15.8% as shown in Table 3.3.2. These periods indicate that the slab-girder interaction effect causes increases in modal stiffnesses ranging from 18% to 44% of the Model 1 stiffnesses as shown in Table 3.3.3. The slab-girder interaction is seen to have a non-uniform effect on the modal periods and stiffnesses whereby the fourth translational and torsional modes show the greatest changes and the third translational mode shows the least change. Slab girder interaction has a somewhat greater effect on the natural periods than does the rigid joint zone effect for this building. The combined effects of both of these modeling aspects cause increases in modal stiffnesses ranging from 33 to 67% (Table 3.3.3) with the fundamental mode showing a 45% increase in stiffness.

The dead weight reductions included in Model 4 (15 psf in each level and 50% in the cap) further improved analytical and experimental period correlation. The fundamental translational period is reduced to 3.00 sec. which is within 2% of the experimental period of 2.94 sec.

The higher translational and torsional modes also show excellent agreement ranging from -1.4 to +5.3% variation from experimental results (Table 3.3.2).

Also shown in Table 3.3.2 are UBC and ATC values for the fundamental period based on the respective codebook formulae. As can be seen, these values (5.0 sec. for UBC, 4.64 sec. for ATC) err significantly from the experimental and analytical results overestimating the periods by 70% and 58%, respectively. These large discrepancies are primarily due to the pyramid configuration of the building which results in much larger decreases in stiffness and mass with increasing height than would occur in a building of regular configuration upon which the code formulae are based.

Overall, excellent correlation of the analytical and experimental dynamic properties of the building is achieved by accounting for the stiffening effects of rigid joint zones and slab-girder interaction and minor refinement of dead weight values. Especially notable is the fact that a single model formulation (Model 4) is able to predict the first four translational and two torsional periods and mode shapes with such good accuracy.

### **3.3.5 Influence of Modeling Approach on Design Quantities**

In this section, results of response spectrum dynamic analysis of each of the four models are presented to demonstrate the influence of the different modeling approaches on gross design quantities. The Newmark spectrum scaled to 0.05g peak ground acceleration is used which corresponds to the ATC recommended reduced spectrum peak acceleration level. The first four translational modes are included in the analyses which account for approximately 80% of the effective mass.

In Figure 3.3.10(a), predicted peak story shear envelopes for the various models are plotted over the full height of the building. As

can be seen from this figure, significant increases in story shears result from the inclusion of the rigid joint zone and slab girder interaction effects in Models 2 and 3. In Table 3.3.4, the values of base shear are shown for the different models along with percent changes from Model 1. As can be seen from this table, base shear increases from 766k in Model 1 to 980k in Model 3 (a 28% increase) due to the smaller natural period and resulting increases in spectral magnitude in the latter model. The slight mass reduction in Model 4 decreases the base shear slightly to a value of 969k or a 26.5% increase over the Model 1 values. It should be noted that due to the relative stiffness of the first five stories of the building, the full contribution of these stories to the total base shear is not captured by the first four translational modes. Therefore, the shear envelopes of Figure 3.3.10(a) are slightly truncated in these stories. This effect can be corrected by including additional modes in the analysis.

In Figure 3.3.10(b), peak story overturning moments are shown for the different models. Table 3.3.4 shows that variations in overturning moments closely follows shear variations whereby the  $3180 \times 10^3$  k-in. base overturning moment of Model 1 increases to  $4055 \times 10^3$  k-in. in Model 4, being an increase of 27.5%.

Peak story deflections are shown in Figure 3.3.11(a). From this figure, it is seen that decreased deflections result in the stiffer models. Model 1 yields a peak 50th floor deflection of 18.6 in. where Model 4 yields a 17.3 in. deflection, being a decrease of 7.3%. The smaller changes in deflection are primarily due to the fact that the first mode of Model 1 lies on zone D ( $p = 2.0$ ) of the Newmark spectrum and it has been shown (section 2.5, Figure 2.13) that for this zone, modal shear and overturning moment vary linearly with changing stiffness but that modal deflections remain constant. The relatively small 7.3% decrease in deflection in Model 4 is due to shifting of the fundamental period from zone D to zone C, overall reduction in mass

values and some participation of higher modes in the deflection response. Also seen in Figure 3.3.11(a) is the influence of the stiffness discontinuities at levels 18 and 30 where sudden changes in the slope of the deflection envelopes are noted.

In Figure 3.3.11(b), peak story drifts are shown for the different models. Overall, comparison of the drifts in Models 1 and 4 showed the same trends as the deflections where reductions on the order of about 10-15% result over most of the building for Model 4. However, in the region between the 18th and 30th floors, larger reductions in drift are observed with the addition of slab-girder interactions in Model 3. This is due to the fact that the overall stiffness of this region of the structure is more sensitive to girder moments of inertia owing to the longer girder spans (see Figures 3.3.2 and 3.3.3). In Table 3.3.4, this effect is shown by the 0.59 in. drift of Model 1 being reduced by 30.5% in Model 4 to 0.41 in. The influence of the stiffness discontinuities is most dramatically illustrated in Figure 3.3.11(b) where the drifts seem to reflect the behavior of three shear beams having different properties spanning between the points of discontinuity at floors 18, 30 and 45. This figure also demonstrates the overall cantilever (bending) action of the building reflected by increasing drifts in upper levels over the height. This would indicate that a significant component of the drifts in upper levels results from rigid body rotation.

Insight into the dynamic behavior of the Transamerica Building can be gained by studying the modal contributions to the gross design quantities. Relative modal contributions to story shears, overturning moments, deflections and drifts over the full height of the building (including the cap portion) are plotted in Figure 3.3.12. In Figure 3.3.12(a), it is seen that higher modes contribute significantly to story shear near the base of the building. The 1st through 4th modes contribute 59.0, 28.6, 8.9 and 3.5% to the total sum of the squares

value, respectively. Thus the higher modes contribute 41% to the square of the total base shear value. At the 25th floor, the fundamental mode dominates the story shear response, where the contributions of the 1st through 4th modes are 88.6, 0.7, 6.3 and 4.4%, respectively. In the architectural cap, story shear is dominated by higher modes where the contributions of the first four modes at the 51st level are 6.6, 21.8, 46.8 and 24.8%, respectively. From this figure it is seen that higher modes contribute most significantly to shear response in the upper and lower portions of the building and not very significantly near the building's midheight. In Figure 3.3.12(b), modal contributions to story overturning moments indicate that the first mode dominates overturning in the lower portion of the building but higher modes are significant to dominant in the upper portions of the building. Figure 3.3.12(c) shows that the first mode makes the largest contribution to total story deflections throughout the building where higher modes are significant only in the lower portion of the building and in the architectural cap. In Figure 3.3.12(d), it is seen that for story drifts the first mode dominates response in the lower portion of the building but the higher modes become dominant in the upper portion. If corrected for rigid body rotations, the higher modes would show greater contributions to drifts throughout the building.

In summary, the modeling of rigid joint zones and slab-girder interaction effects significantly influence the analytical response of the building and leads to higher values of story shears and overturning moments and somewhat lower deflections and drifts. It is seen that higher modes contribute significantly to the total response and that the relative importance of the various modes depends upon the particular response quantity and location over the height of the building.

### 3.3.6 Comparison of Dynamic Analyses and Code Equivalent Static Procedures

In this section, a comparison is made of the Transamerica Building's response to different recommended static and dynamic seismic loading approaches (see section 3.1.2 for further description). The ATC and Newmark spectra are used for the dynamic analyses. Both of these spectra are based on the ATC recommended 0.05g reduced peak ground acceleration for moment resisting frame construction. The ATC and UBC guidelines are used for equivalent static analyses. The UBC equivalent spectrum is multiplied by 1.278 to correspond to elastic limit design. In Figure 3.1.1, the ATC, Newmark and scaled UBC spectra are shown for comparison. Model 4 is used as a basis for the comparative analysis since this model best represents the observed dynamic properties. Both the Model 4 analytical fundamental period (3.0 sec.) and the codebook calculated fundamental periods (4.64 sec. for ATC; 5.0 sec. for UBC) as shown in Table 3.3.2 are used to calculate equivalent static responses. It should be noted that the recommended UBC (1979 edition) load that is usually applied at the top of the building is omitted since it would greatly overestimate response in the upper stories due to the decreasing story weights with increasing height that are characteristic of this building. (Note also that this top load was not required in the original UBC design). Gross design quantity responses for the different analytical approaches are summarized in Figures 3.3.13, 3.3.14 and in Table 3.3.5.

Comparing the dynamic analyses, Figures 3.3.13 and 3.3.14 show that the ATC spectrum produces significantly larger response values than the Newmark spectrum. As shown in Table 3.3.5, compared to Newmark, the ATC spectrum yields 29.4% greater base shear, 40.2% greater base overturning moment, 37.4% greater deflection at the 50th floor, and 34.1% greater 25th story drift. This result is due to the

conservatism built into the ATC spectrum in the longer period range where at 3.0 sec. the ATC spectrum has a 40% larger spectral amplitude (see Figure 3.1.1). Note that since overturning response is dominated by the 3.0 sec. fundamental mode, the ATC spectrum induces this same 40% increase in base overturning moment over the Newmark result. Greater participation of the higher modes in shear response results in a smaller increase (29.4%) of the ATC base shear over the Newmark result.

Results from equivalent static analysis are also shown in Figures 3.3.13 and 3.3.14. The shaded portions of these figures emphasize the variation in static equivalent response quantities resulting from the use of the analytically determined fundamental period (3.0 sec.) versus the fundamental periods calculated using the codebook formulae. The relatively large differences between codebook and analytical periods produce large variations in predicted response where the shorter analytical period yields greater response values. For UBC analysis, use of the analytical 3.0 sec. period results in an increase of 29% over response quantities based on the 5.0 sec. codebook period (e.g., base shear increases from 8522k to 11001 k as shown in Table 3.3.5). ATC static analysis shows a 34% increase in response quantities resulting from the 4.64 sec. to 3.0 sec. period shift. Note that compared to the ATC static loads, the UBC approach (with top load omitted) yields smaller story shears and overturning moments in the upper portion of the building and higher shears and overturning moments in the lower portion.

It is of particular interest to compare the dynamic and equivalent static responses as recommended by ATC since these are derived from the same response spectrum. In Figures 3.3.13(a) and (b), the shear and overturning moments resulting from both of these ATC approaches are shown for the same 3.0 sec. fundamental period. The base shear resulting from dynamic analysis is 1253k or 61% of the

2068k static base shear and the base overturning moment is  $5682 \times 10^3$  k-in or 61% of the static value of  $9300 \times 10^3$  k-in. Here, the static overturning moments have been reduced as allowed by ATC. The rather large discrepancy between the equivalent static and dynamic results is due to the relative conservatism in the static solution introduced by the implicit assumption that the full mass of the building participates in the response of the fundamental mode. This result is further discussed in section 3.7.

In Figures 3.3.15 and 3.3.16, the story shear, overturning moment, deflection and drift responses normalized to base shear for the different dynamic and static analyses are shown. As can be seen from these figures, the ATC and Newmark dynamic analyses yield very similar response quantity distributions for a given value of base shear. However, the static response distributions show significant variations from the dynamic predictions. As can be seen from the story shear distribution in Figure 3.3.15(a), the ATC static approach gives greater shear values (as much as 20-25% greater around the midheight of the building) over most of the building than would be predicted by dynamic analyses and gives somewhat lower values near the top of the building. The UBC static approach compares well with dynamic analyses in the lower half of the building but yields significantly lower shears in the top half of the building due in part to the omission of the top loading as discussed earlier. As for overturning moment distribution, Figure 3.3.15(b) shows that both the UBC and ATC static approaches compare fairly well with dynamic results near the base of the building but UBC gives substantially lower values in the upper part of the building. These observations on force distribution indicate that design based on equivalent static approaches (ATC and UBC) would tend to make the upper stories of this building more susceptible to structural damage from earthquake ground shaking.

In Figure 3.3.16(a), deflections normalized to base shear show

that the UBC results compare fairly well with dynamic predictions. However, the ATC static results give significantly larger deflections in the upper stories because greater overall bending action occurs due to the fact that the overturning moments are not reduced for deflection calculations. In Figure 3.3.16(b), the ATC static approach gives larger drifts than dynamic results in the middle region of the building primarily due to the larger normalized shears and unreduced overturning moments in this portion of the building relative to dynamic values. Near the top, the normalized ATC static drifts compare well with dynamic values since expected increases in drifts due to greater bending action are offset by lesser shear deformations. The UBC static drift distribution compares well with dynamic values in the lower stories but shows significantly smaller drifts in the upper stories due to underestimation of shear forces in this region.

### **3.3.7 Comparison of Code Design Forces with Dynamic Forces Induced by Actual Earthquake Spectra**

The UBC story shears and overturning moments used for the seismic design of the Transamerica Building were provided by the design engineers and are shown in Figure 3.3.17 after application of the 1.278 factor to bring the UBC working stress loads up to the elastic limit level. These values are based on a fundamental period of 4.07 sec. and the designers' dead weight estimates (including partition loads) which are somewhat larger than those shown in Table 3.3.1. Also shown in Figure 3.3.17 are the predicted dynamic responses to the Taft (1952) and El Centro (1940) earthquakes for 5% damping using both Model 2 and Model 4 to represent the properties of the building (see Figure 3.1.2 for a plot of the spectra).

These figures indicate that only relatively minor inelastic response, if any, would result from the Taft excitation and that most of this would occur between the 30th and 50th floors where both story

shears and overturning moments exceed the factored UBC (elastic limit) levels. This result agrees with observations made from Figures 3.3.15(a) and (b) which indicate the relative underestimation of UBC design forces in the upper portion of the structure. Remembering that the Taft spectra is representative of a 7.6 magnitude earthquake occurring at a distance of 56 km. from the building site and producing a peak ground acceleration of 0.179g, it is reassuring to find that this building should have a primarily elastic response.

Analyses for the El Centro earthquake indicate elastic force levels ranging between 1.5 and 2.3 times the factored UBC levels as seen in Figure 3.3.17. Assuming these elastic analyses give a reasonable approximation for ductility demand, El Centro excitation would induce overall ductility ratios ranging from 1.5 to 2.3.

### 3.3.8 Summary

The results presented in the previous sections lead to the following observations regarding the behavior and analysis of the Transamerica Building:

- (1) Rational development of the numerical models leads to excellent agreement between the dynamic properties resulting from computer analysis and the dynamic properties determined from small amplitude experimental testing. Close correlation of results is achieved for several modes. (Figures 3.3.8, 3.3.9 and Table 3.3.2)
- (2) Analysis indicates that the effects of both rigid joint zones and nonstructural slab-girder interaction significantly influence the small amplitude response of the building. Inclusion of these effects may lead to increases of about 30% (using the Newmark spectrum) in base shear and base overturning moment values compared

to results based on a model of the bare steel frame alone using center-to-center dimensions. (Figure 3.3.10 and Table 3.3.4)

- (3) The sudden discontinuities in stiffness that occur in this building are shown to be important in deflection and drift response whereby the termination of frames at various levels causes irregular drift response over the height of the building (Figure 3.3.11).
- (4) In dynamic analysis, the influence of higher modes (2nd, 3rd, 4th) on design quantities is seen to be significant (Figure 3.3.12). In order to fully capture inertial forces produced in the relatively stiff first four stories, more than four translational modes for each direction must be included in the analysis.
- (5) For this building, dynamic analysis shows that the ATC response spectrum yields more conservative results than the 0.05g Newmark spectrum resulting in approximately 30% greater base shear and 40% greater base overturning (Figure 3.3.13 and Table 3.3.5) due to the conservatism of the ATC spectrum in the longer period range.
- (6) Application of the UBC and ATC codebook formulae results in significantly greater values of the fundamental period than are indicated by the small amplitude tests and corresponding analysis leading to wide variations in the response from equivalent static analysis depending upon the period used. (Figures 3.3.13, 3.3.14 and Table 3.3.5)
- (7) Comparing the UBC and ATC equivalent static approaches

for this building, ATC leads to smaller shears and overturning moments than UBC at the base but yields larger values in the upper portion of the building (Figure 3.3.13).

- (8) Using the ATC recommended approaches for dynamic and equivalent static analyses and using a 3.0 sec. fundamental period for both, force quantities resulting from the dynamic analysis approach are substantially less than those resulting from the equivalent static analysis approach. Dynamically derived base shear and overturning values are only 61% of the corresponding values resulting from equivalent static analysis. (Figure 3.3.13 and Table 3.3.5)
- (9) Regarding the distribution of equivalent static design forces compared to dynamic force envelopes, ATC tends to overestimate the relative magnitude of shear forces in the lower portion of the building and both UBC and ATC underestimates shear near the top. The UBC shear distribution compares well with dynamic distribution in the lower half of the building but substantially underestimates the relative shear in the upper half of the building. ATC static overturning moment distribution shows somewhat better comparison with the dynamic distribution than does UBC (Figure 3.3.15).
- (10) Based on the UBC seismic loads used by the engineers in design, results based on the numerical models indicate that the building would have an essentially elastic response if subjected to the Taft (1952) earthquake record. If subjected to the El Centro (1940) record, elastic story shears 1.5 to 2.3 times greater and

elastic story overturning moments 1.4 to 2.0 times greater than factored UBC design values result.

Table 3.3.1: Dead Load Weights Used for the Analytical Models

Floor	Models 1,2,3		Model 4	
	Weight(kips)	psf	Weight(kips)	psf
60	73	3890	37	1970
59	53	986	27	502
58	63	540	32	300
57	68	383	34	191
56	73	274	37	127
55	78	209	39	104
54	83	166	42	84
53	88	137	44	69
52	93	116	47	59
51	98	100	49	50
50	511	433	493	418
49	526	377	505	362
48	541	326	516	311
47	558	299	530	284
46	576	277	545	262
45	596	259	561	244
44	616	242	578	227
43	637	228	595	213
42	659	216	613	201
41	682	205	632	190
40	707	196	653	181
39	732	187	673	172
38	758	180	695	165
37	785	173	717	158
36	814	167	741	152
35	842	162	764	147
34	874	157	791	142
33	904	152	815	137
32	937	149	842	134
31	970	145	870	130
30	1041	147	935	132
29	1056	141	943	126
28	1107	139	988	124
27	1152	138	1026	123
26	1200	136	1068	121
25	1251	134	1118	120
24	1303	134	1157	119
23	1355	132	1201	117
22	1408	131	1239	116
21	1463	130	1294	115
20	1519	129	1343	114
19	1575	128	1391	113
18	1632	127	1440	112
17	1691	126	1490	111
16	1751	126	1542	111
15	1811	125	1593	110
14	1881	124	1654	109
13	1936	123	1700	108
12	1998	122	1753	107
11	2063	122	1809	107
10	2128	121	1864	106
9	2195	120	1922	105
8	2263	120	1980	105
7	2342	120	2049	105
6	2501	124	2197	109
5	2691	129	2377	114
4	1645	217	1531	202
3	1645	217	1531	202
2	1767	58	1313	43
<b>Total</b>	<b>64365</b>		<b>56965</b>	

Table 3.3.2: Experimental vs. Analytical Natural Periods

Direction	Mode No.	Exp. Period(sec)	Model 1		Model 2		Model 3		Model 4		UBC*		ATC*	
			Period	%	Period	%	Period	%	Period	%	Period	%	Period	%
N-S	1	2.94	3.77	+28.2	3.49	+18.7	3.13	+ 6.5	3.00	+ 2.0	5.0	+70.1	4.64	+57.8
	2	1.58	2.17	+37.3	2.01	+27.2	1.83	+15.8	1.65	+ 4.4				
	3	1.14	1.49	+30.7	1.39	+21.9	1.29	+13.2	1.08	+ 5.3				
	4	0.88	1.20	+36.7	1.09	+24.1	0.95	+ 7.7	0.87	- 1.4				
Torsion	1	2.24	3.11	+38.8	2.82	+25.9	2.41	+ 7.6	2.36	+ 5.4				
	2	1.23	1.64	+33.3	1.48	+20.3	1.28	+ 4.1	1.25	+ 1.6				

% = percent variation from experimental period.

\*Code periods calculated based on 50-story height as follows:

UBC (eqn. 12-38):  $T = 0.10 N = 0.10 \times 50 = 5.0$  sec.

ATC (eqn. 4-4):  $T = C_T h_n^{3/4} = .035 \times (676.33)^{3/4} = 4.64$  sec.

Table 3.3.3: Influence of Modeling Aspects on Modal Stiffnesses

Direction	Mode	Stiffness Increase with respect to Model 1		
		Rigid Joint Zone	Slab-Girder Interaction	Total
N-S Trans.	1	17%	28%	45%
	2	17	23	40
	3	15	18	33
	4	21	39	60
Torsional	1	22	38	60
	2	23	44	67

Table 3.3.4: Influence of Modeling Variations on Design Quantities

Design Quantity	Model 1		Model 2		Model 3		Model 4	
		%		%		%		%
Base shear(k)	766	0	867	+13.3	980	+28.0	969	+26.5
Base OTM( $\times 10^3$ k-in)	3180	0	3640	+14.5	4105	+29.1	4055	+27.5
50th floor deflection(in)	18.6	0	18.8	+ 0.8	18.2	- 2.2	17.3	- 7.3
25th floor drift(in)	0.59	0	0.54	- 8.3	0.42	-28.8	0.41	-30.5

% = percent change from Model 1.

Table 3.3.5: Comparison of Design Quantities for Dynamic and Equivalent Static Analyses

Design Quantity	Dynamic				Static							
	Newmark		ATC		ATC				UBC*			
		%		%	Codebook	%	Analytical	%	Codebook	%	Analytical	%
Fundamental Period	3.0	0	3.0	0	4.64	54.7	3.0	0	5.0	66.7	3.0	0
Base shear(k)	968	0	1253	29.4	1547	59.8	2068	113.6	1831	89.2	2364	144.2
Base OTM( $\times 10^3$ k-in)	4054	0	5682	40.2	6956	71.6	9300	129.4	8522	110.2	11001	171.4
50th floor deflection(in)	17.4	0	23.9	37.4	37.7	116.7	50.4	189.7	31.0	78.2	40.1	130.5
25th floor drift(in)	0.41	0	0.55	34.1	0.78	90.2	1.04	153.7	.73	78.1	.95	131.2

% = percent change from Newmark spectrum dynamic analysis.

\*UBC values are factored by 1.70/1.33 = 1.278 for correspondence with ATC elastic limit load levels.

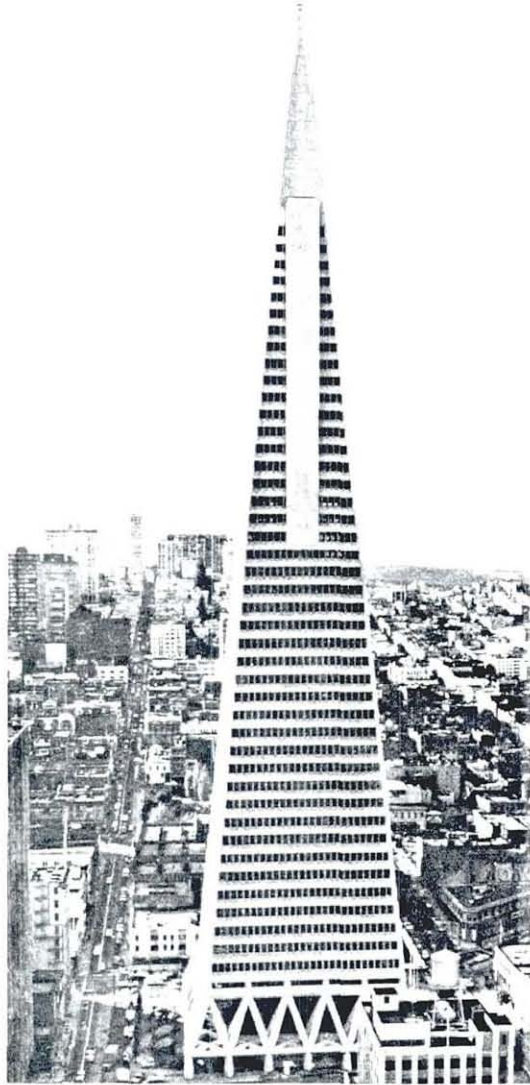


Figure 3.3.1: Transamerica Building  
San Francisco, California

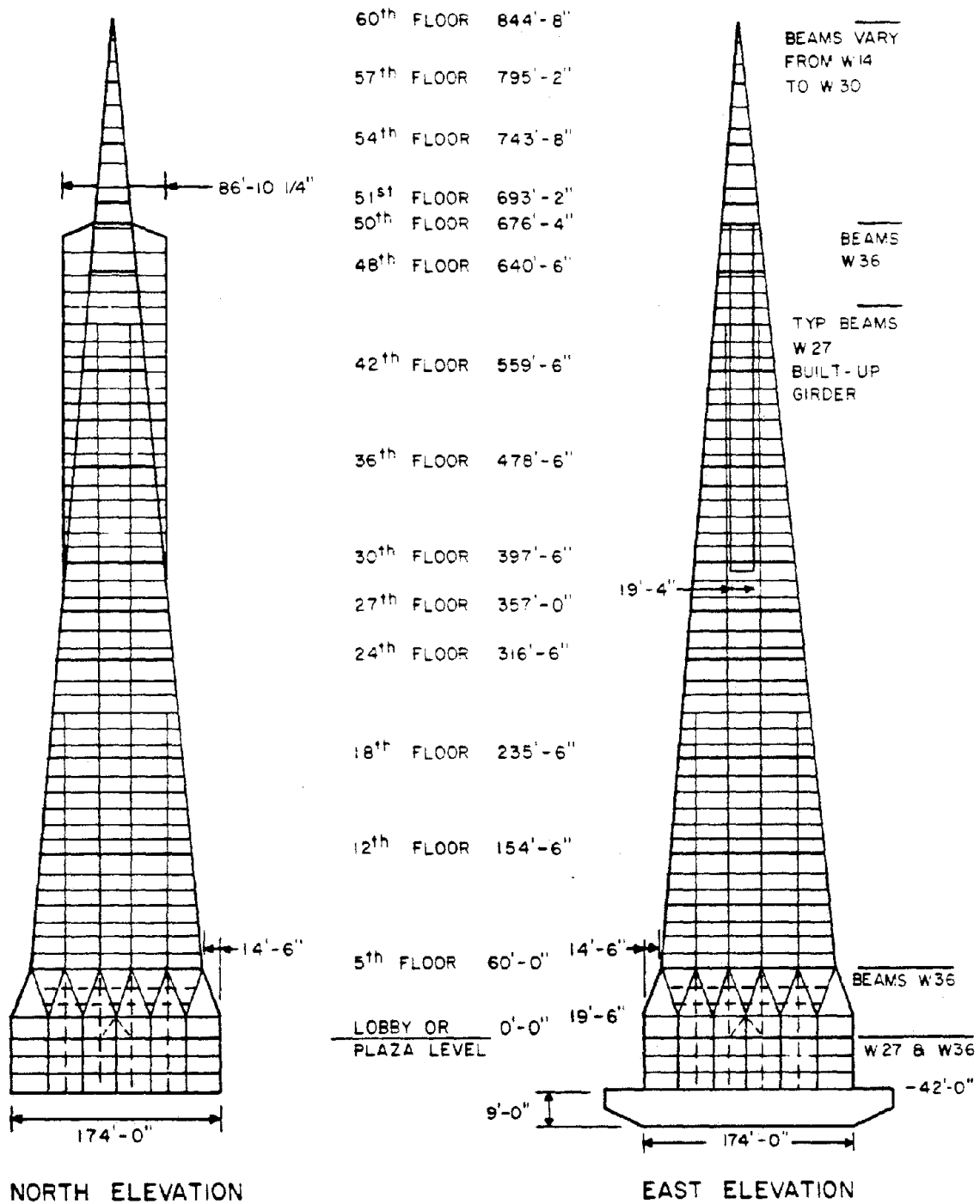


FIGURE 3.3.2: Elevation Views of Transamerica Building

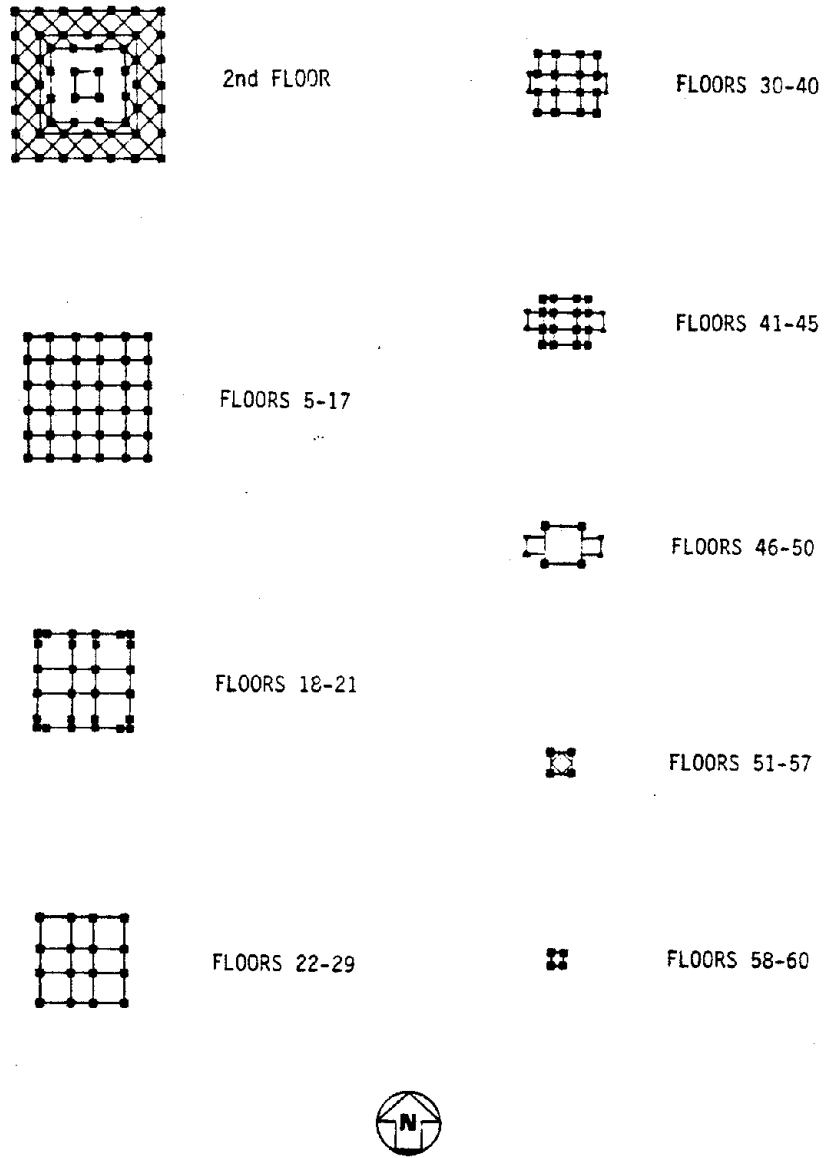
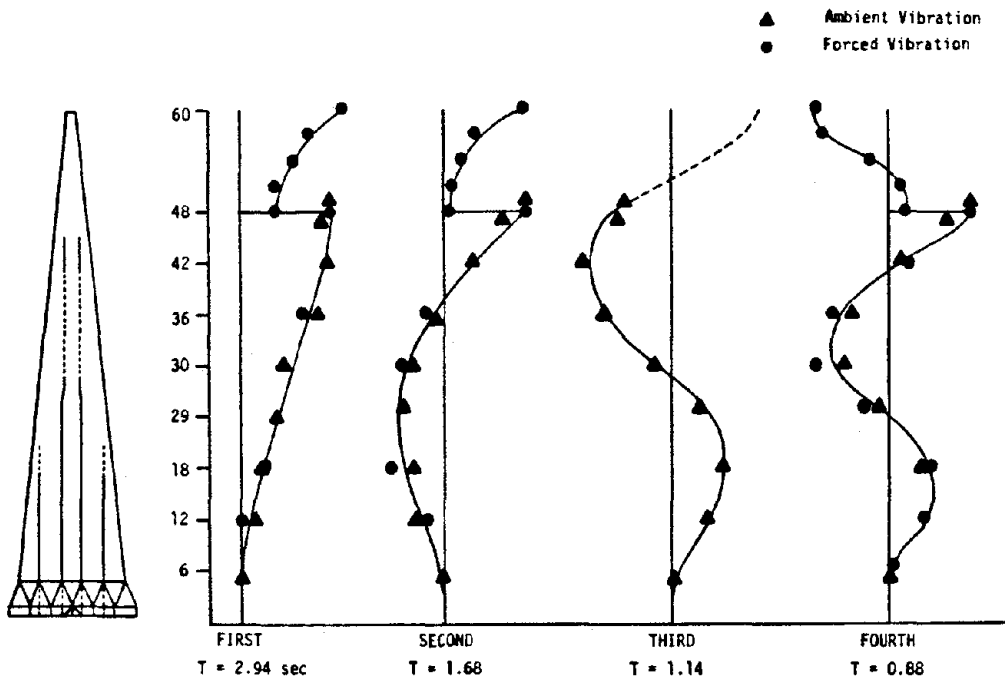
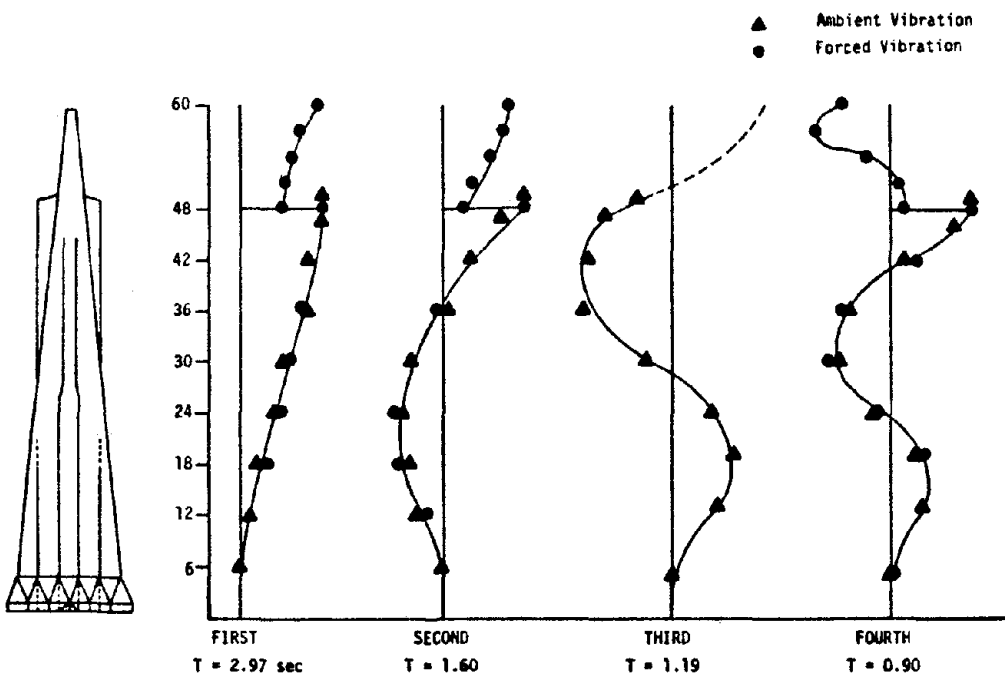


FIGURE 3.3.3: Plan Views of Transamerica Building



(a) N-S Direction



(b) E-W Direction

FIGURE 3.3.4: Experimental Translational Mode Shapes

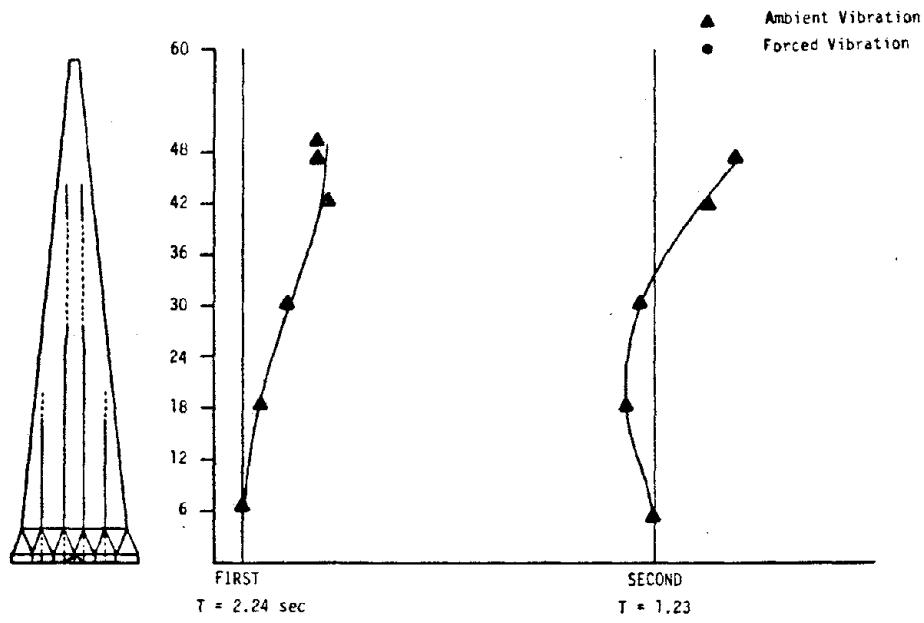
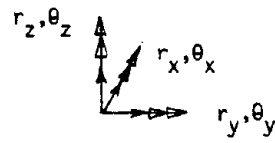
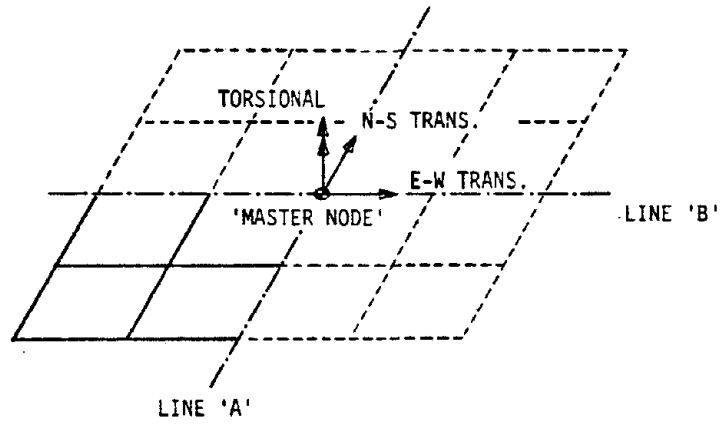


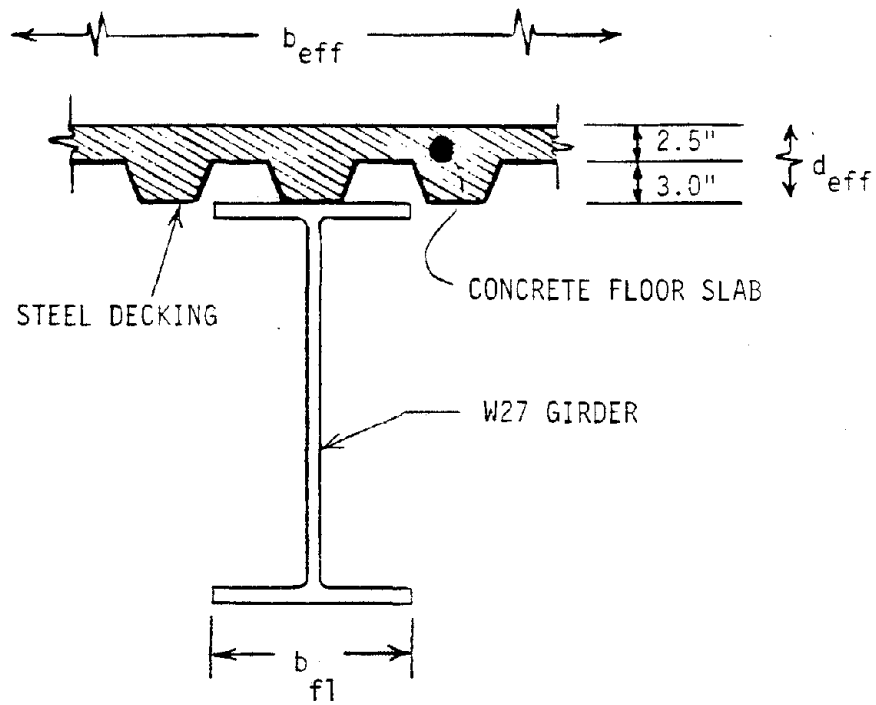
FIGURE 3.3.5: Experimental Torsional Mode Shapes



MOTION	LINE 'A'						LINE 'B'					
	$r_x$	$r_y$	$r_z$	$\theta_x$	$\theta_y$	$\theta_z$	$r_x$	$r_y$	$r_z$	$\theta_x$	$\theta_y$	$\theta_z$
N-S TRANS.	S	S	0	1	0	S	S	S	1	1	0	S
E-W TRANS.	S	S	1	0	1	S	S	S	0	0	1	S
TORSIONAL	S	S	0	1	0	S	S	S	0	0	1	S

1 = FIXED , 0 = FREE  
 S = SLAVED TO 'MASTER NODE'

FIGURE 3.3.6: Boundary Conditions  
 for Symmetric Modeling



EFFECTIVE SLAB THICKNESS (AISC 1.11.5)

ribs parallel to girder :  $d_{eff} = 2.50$  in.

ribs perpendicular to girder:  $d_{eff} = 3.44$  in.

EFFECTIVE SLAB WIDTH (AISC 1.11.1)

$$b_{eff} = b_{fl} + (16 \times d_{eff})$$

FIGURE 3.3.7: Modeling Approach for Slab-Girder Interaction

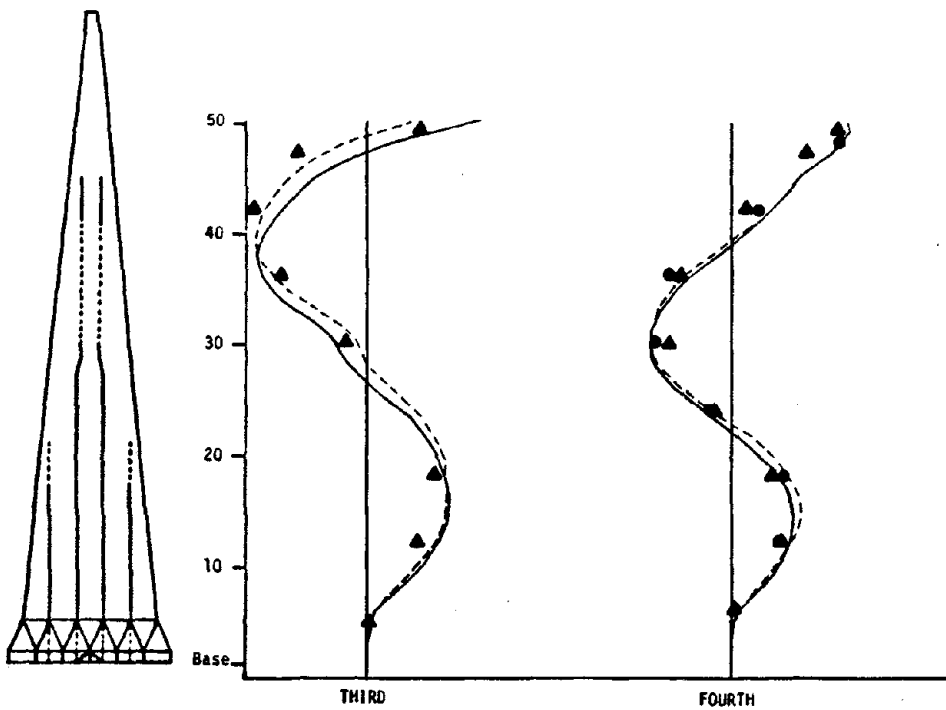
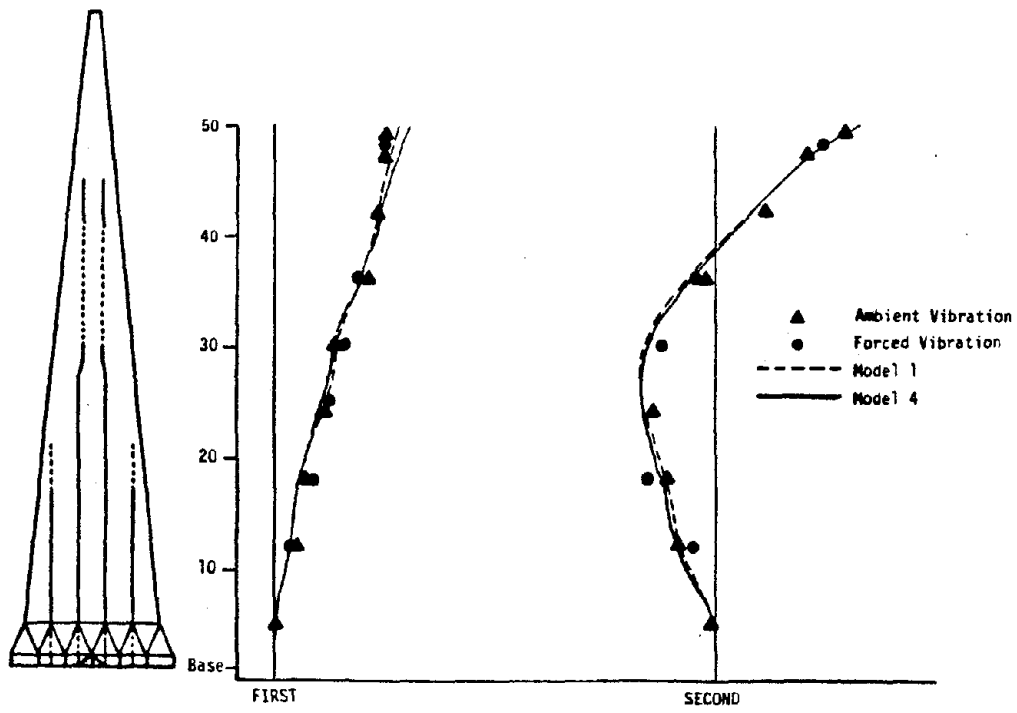


FIGURE 3.3.8: Analytical vs. Experimental Mode Shapes (N-S Translational)

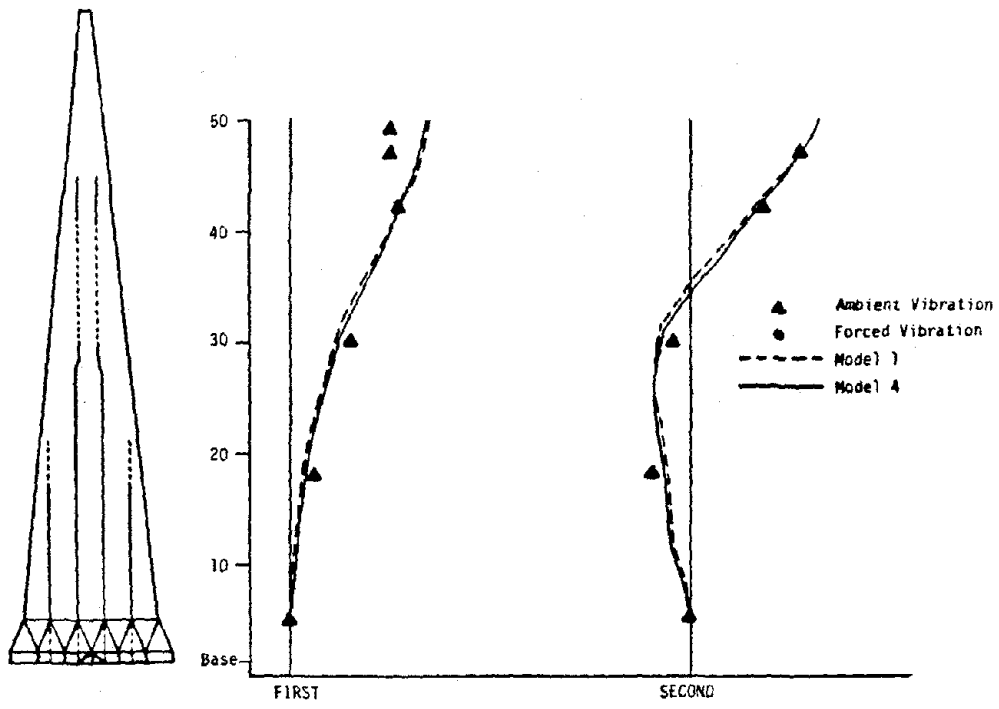
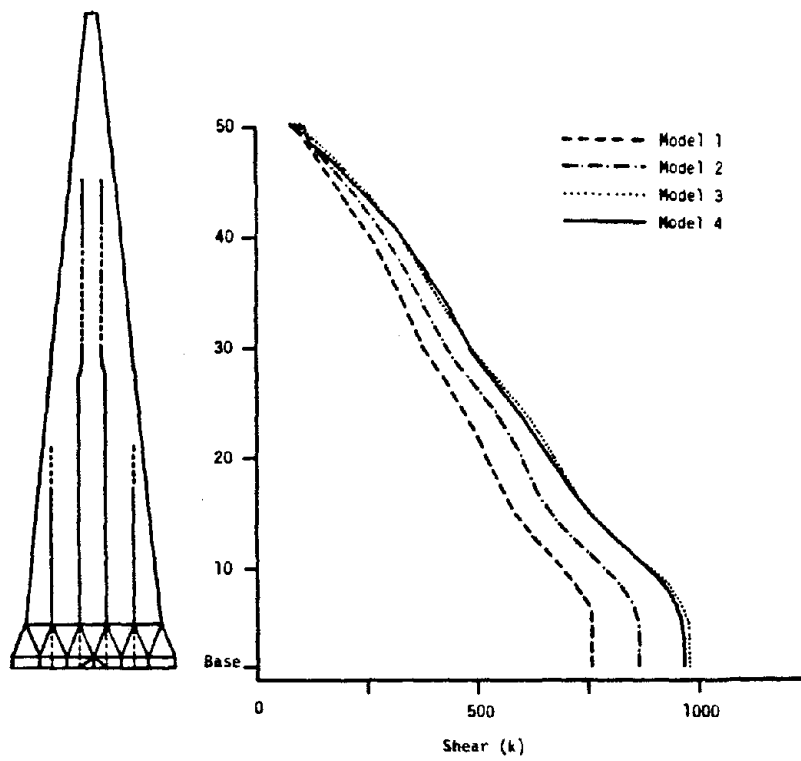
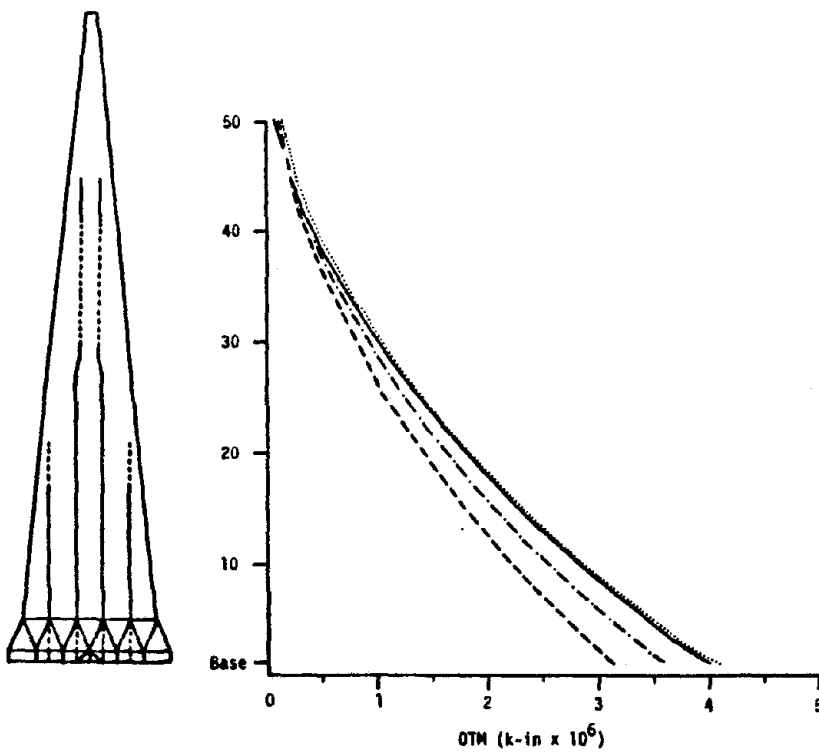


FIGURE 3.3.9: Analytical vs. Experimental Mode Shapes (Torsional)

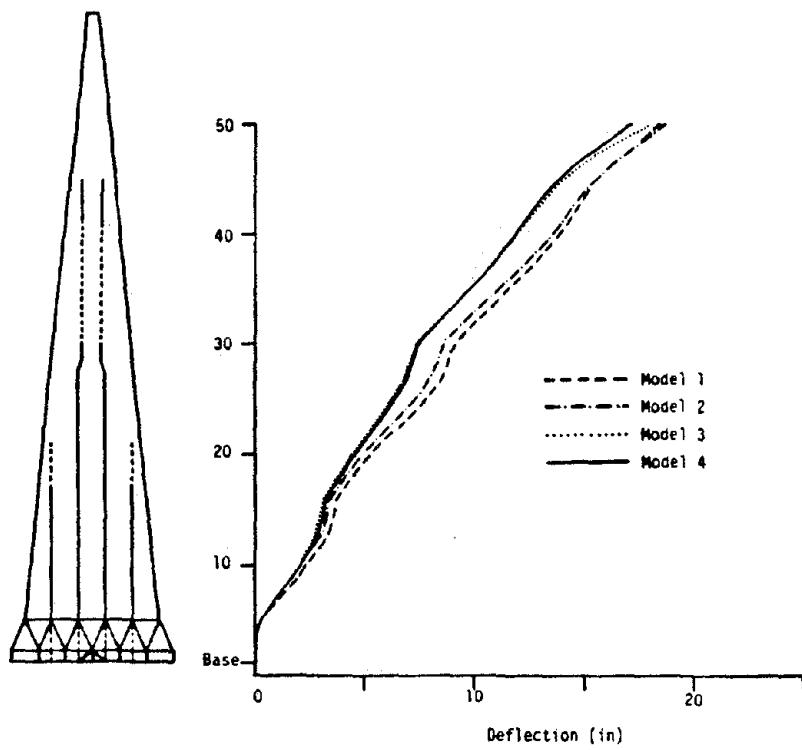


(a) Story Shear

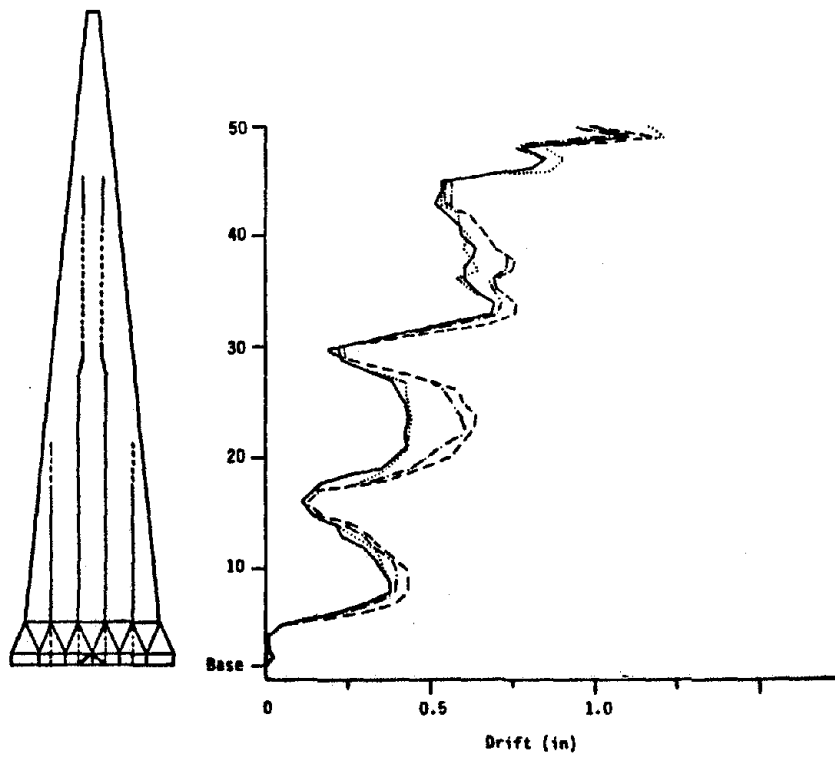


(b) Story Overturning Moment

FIGURE 3.3.10: Influence of Modeling Approach on Story Force Quantities



(a) Story Deflection



(b) Story Drift

FIGURE 3.3.11: Influence of Modeling Approach on Story Deflection Quantities

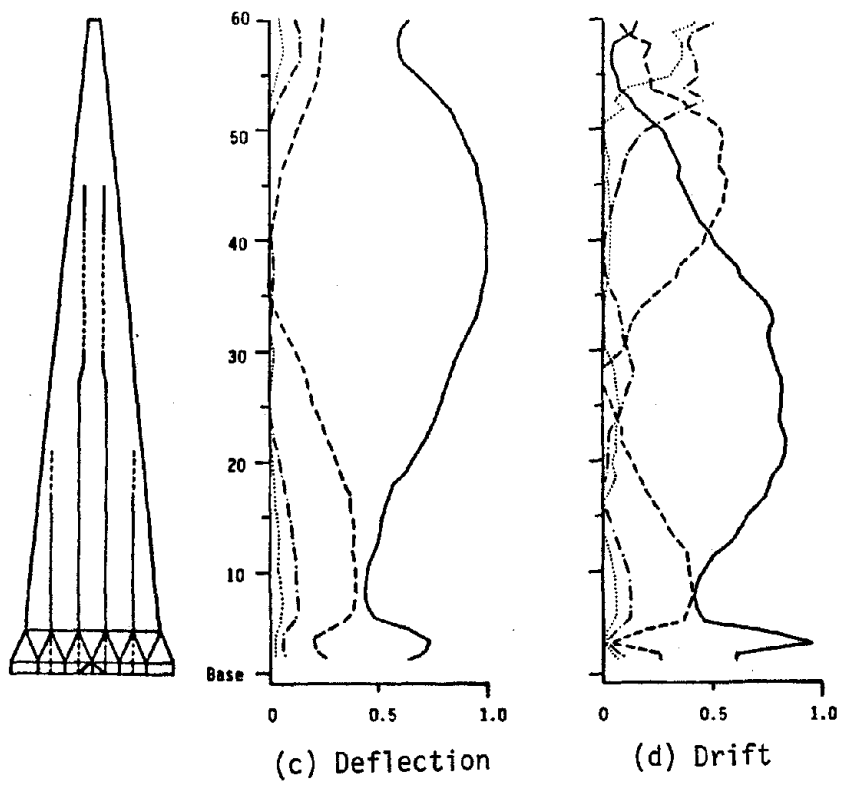
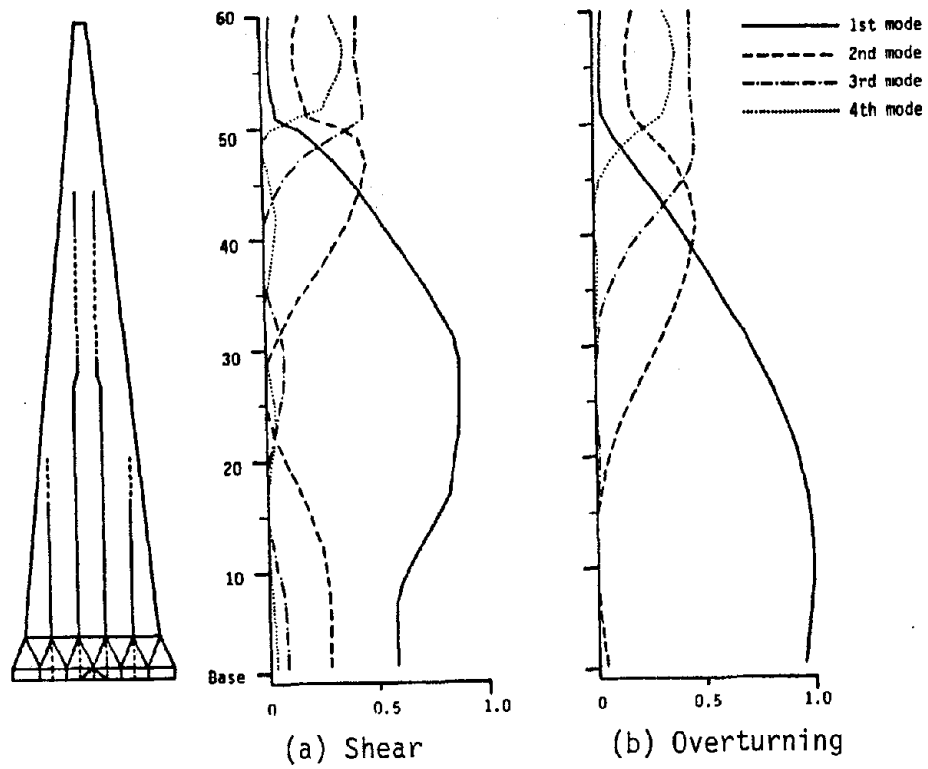
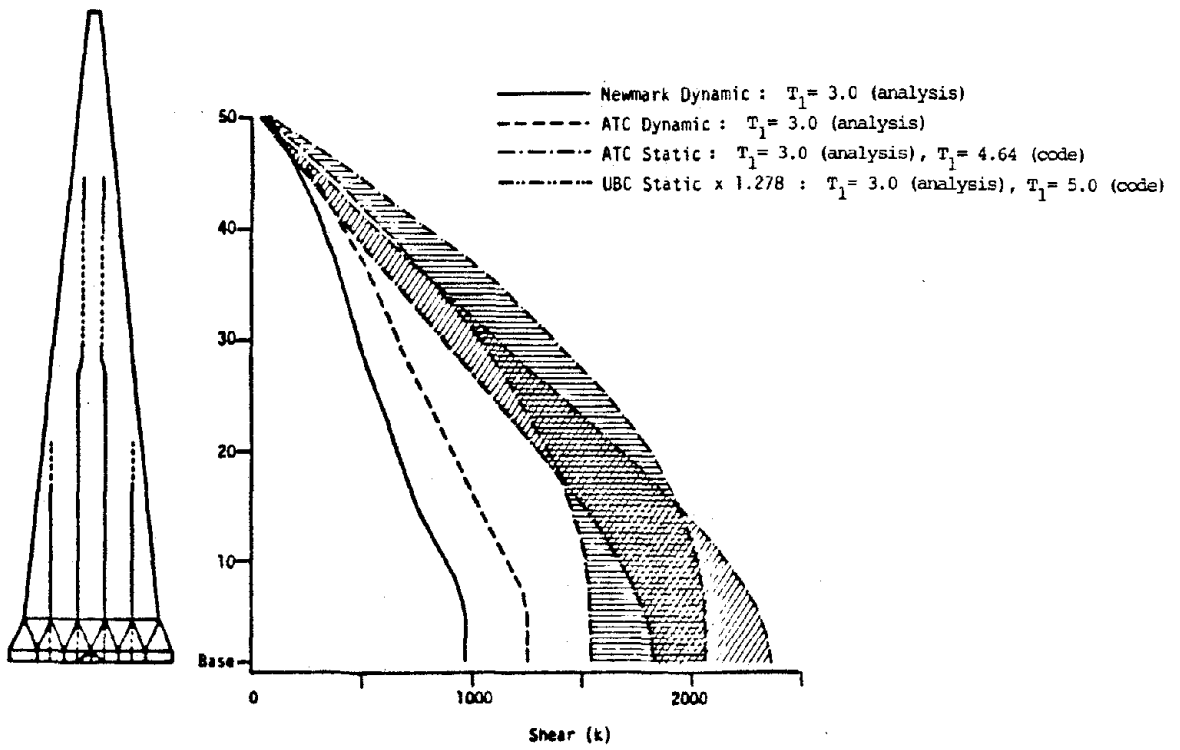
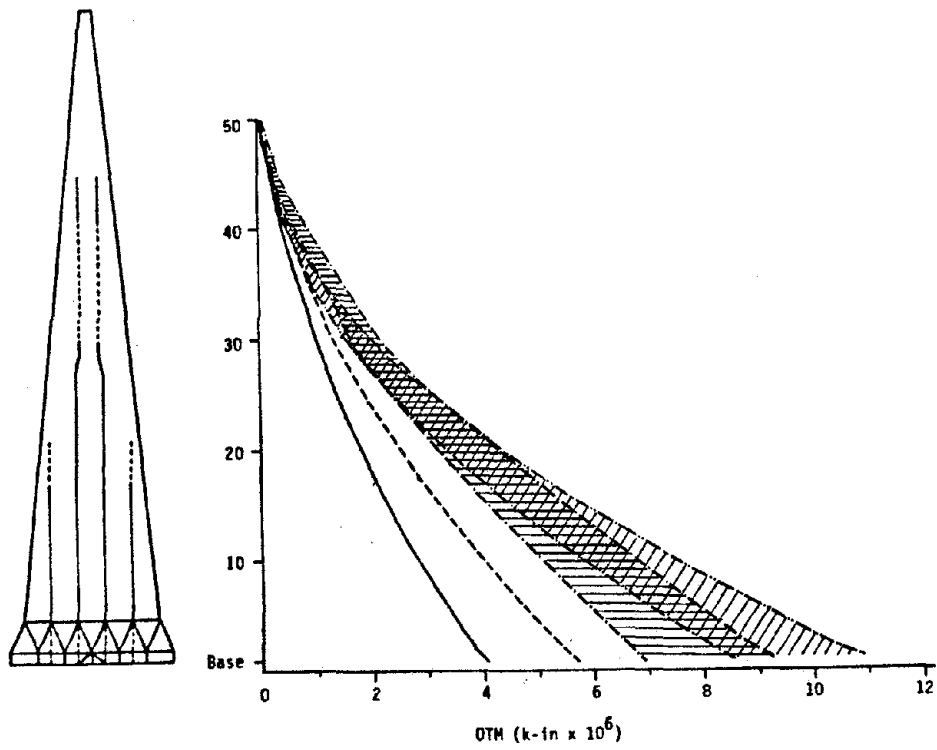


FIGURE 3.3.12: Modal Contributions to Design Quantities

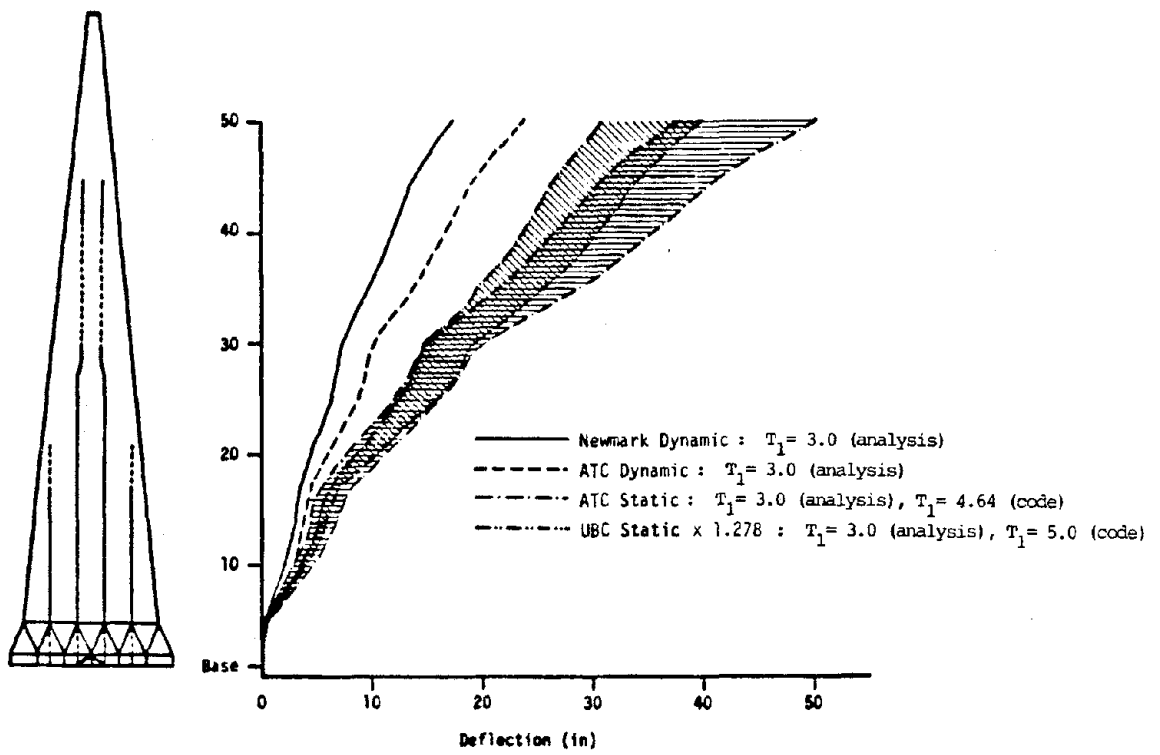


(a) Story Shear

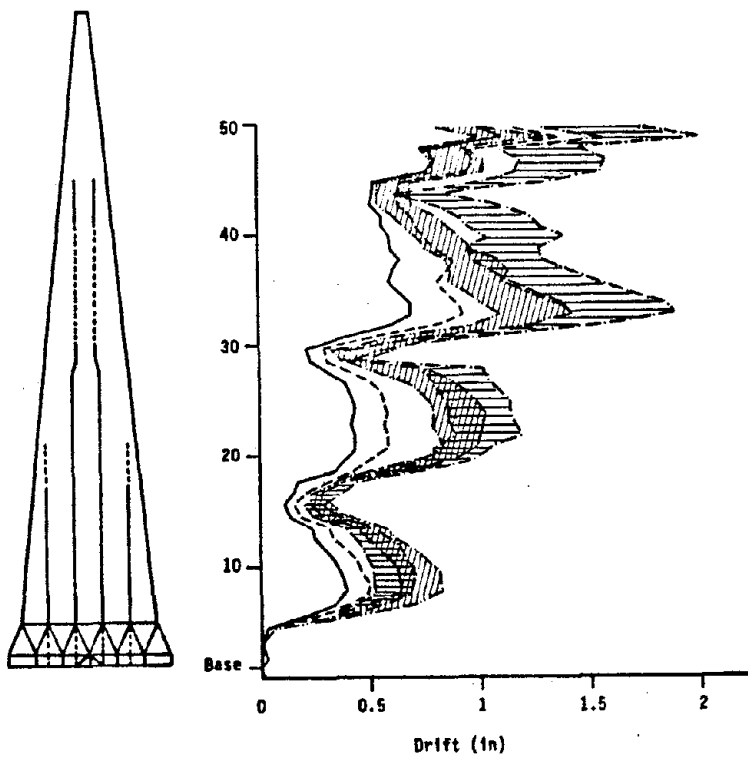


(b) Story Overturning Moment

FIGURE 3.3.13: Force Quantities Resulting from Dynamic and Equivalent Static Analyses

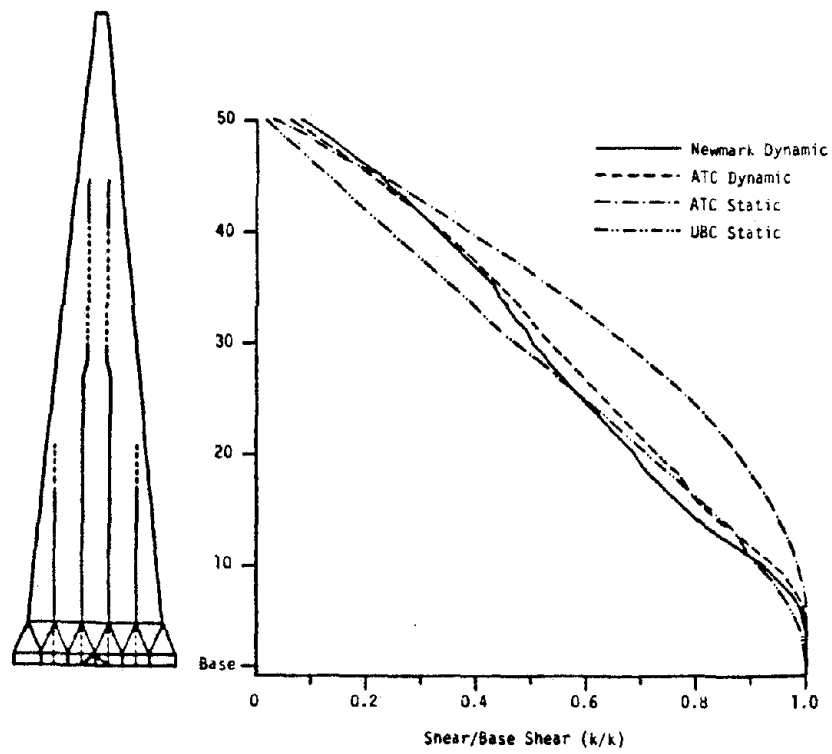


(a) Story Deflection

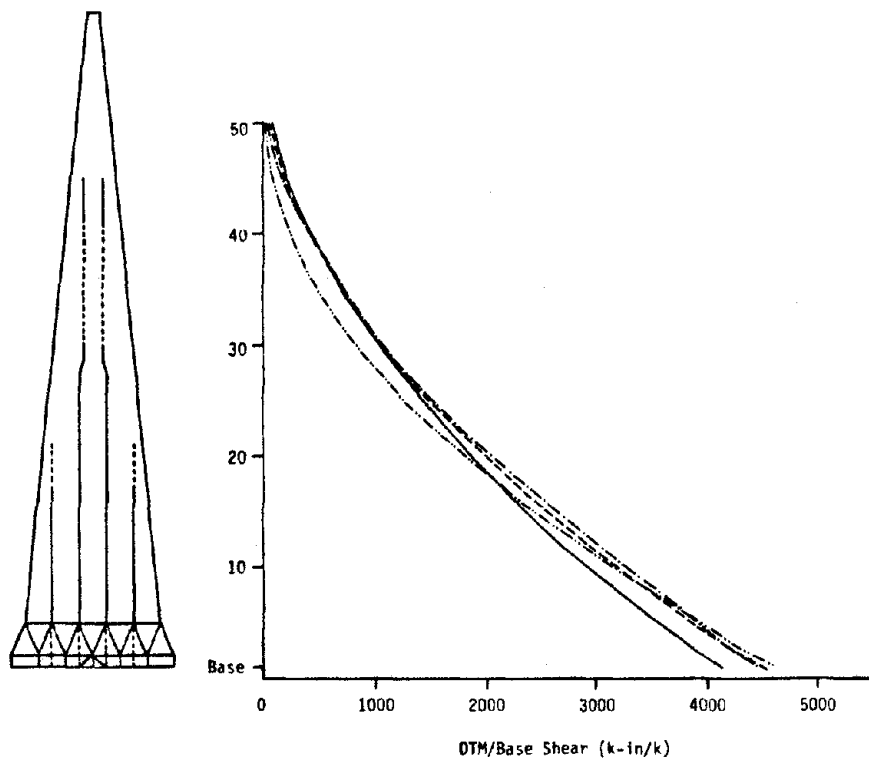


(b) Story Drift

FIGURE 3.3.14: Deflection Quantities Resulting from Dynamic and Equivalent Static Analyses

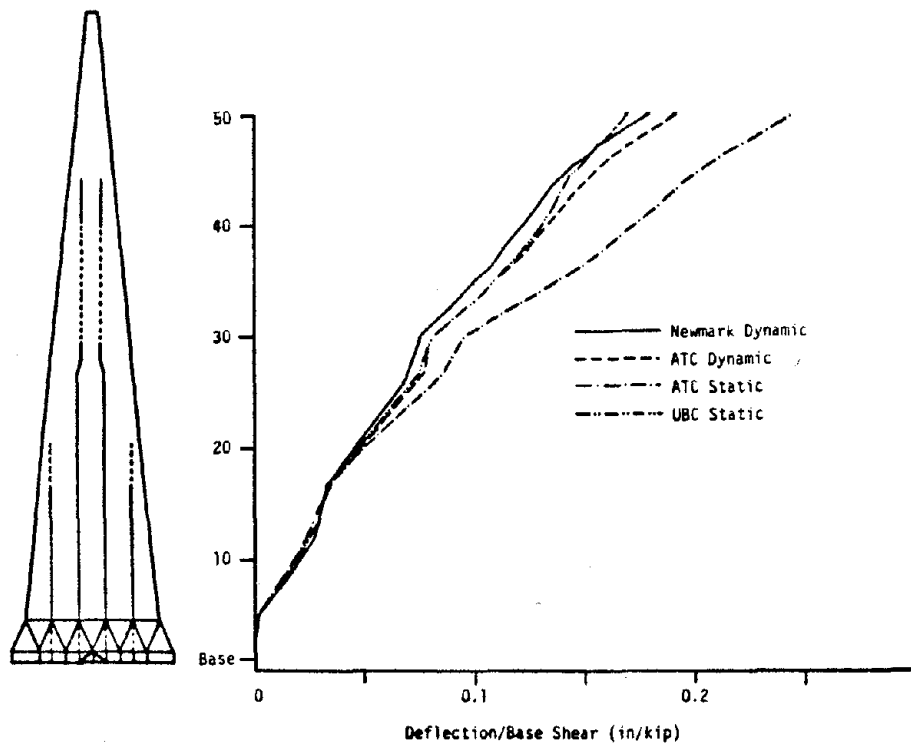


(a) Story Shear

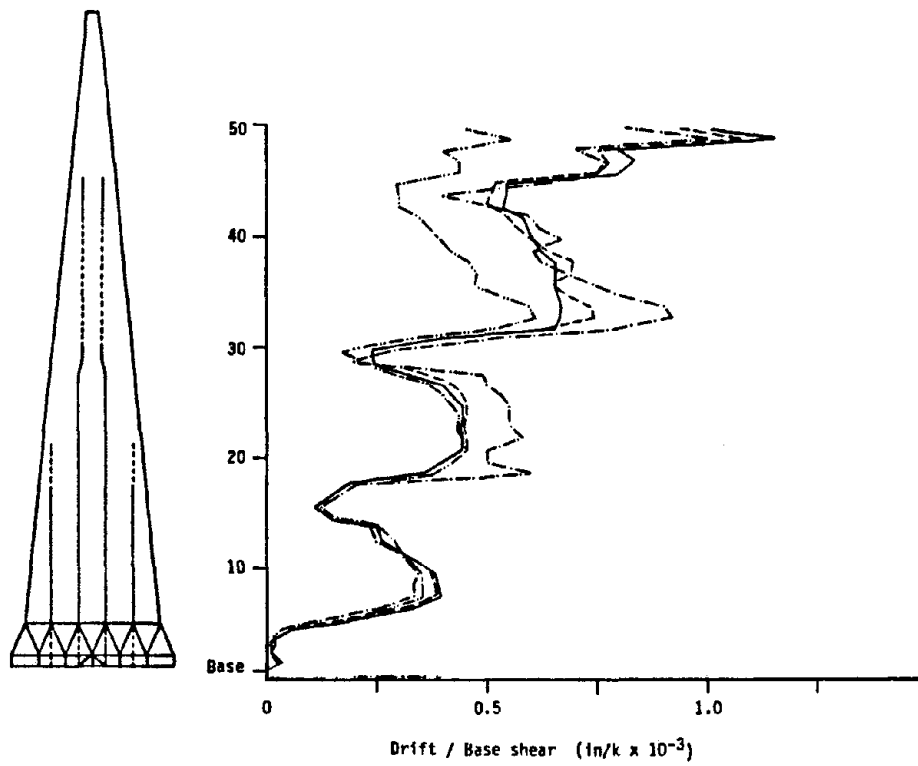


(b) Story Overturning Moment

FIGURE 3.3.15: Force Quantity Distributions Normalized to Base Shear

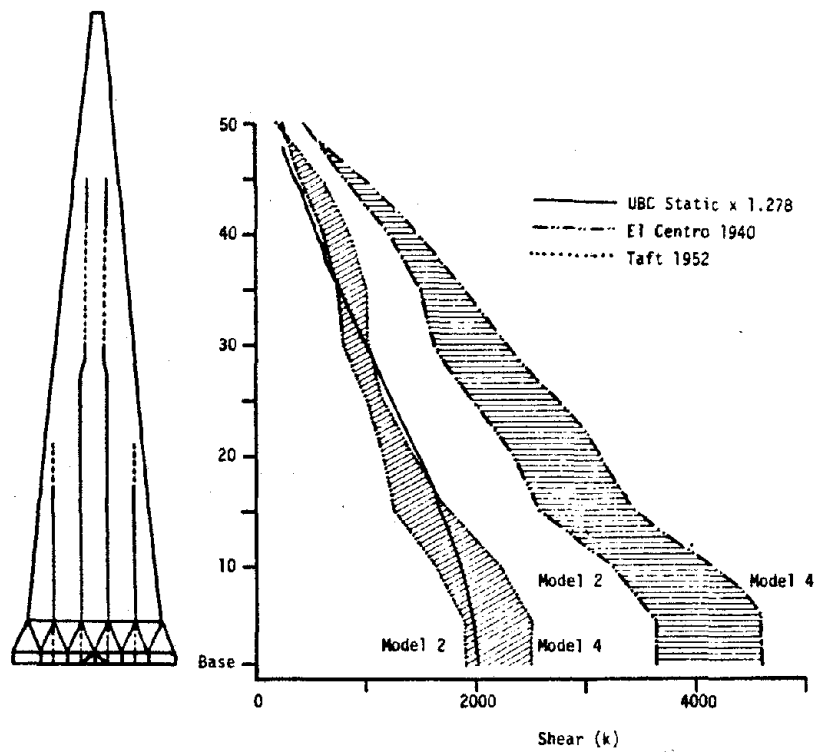


(a) Story Deflection

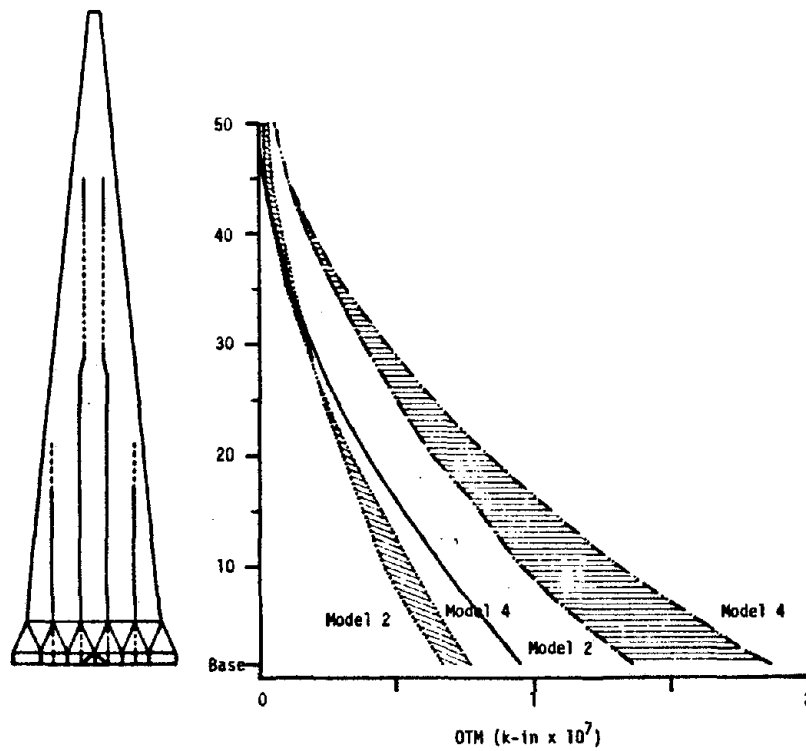


(b) Story Drift

FIGURE 3.3.16: Deflection Quantity Distributions Normalized to Base Shear



(a) Story Shear



(b) Story Overturning Moment

FIGURE 3.3.17: Comparison of UBC Design Forces versus Elastic Forces Induced by Actual Earthquake Spectra

### 3.4 UNIVERSITY OF CALIFORNIA MEDICAL CENTER BUILDING

Located in the San Francisco Medical Center complex, the 15 story (above grade) Health Sciences East Building houses classrooms, laboratories, a library and related facilities for medical instruction and research. Designed in the early 1960's by Reid, Rockwell, Banwell, and Tarics, Architects and Engineers, San Francisco, the Health Sciences buildings (East and West), associated service towers and elevator tower were constructed during the period 1963-1965.

The East Building (Figure 3.4.1) has a column free interior core area (about 92 feet square depending upon floor elevation) subdivided with non-structural partitions as function warrants. Corridors lie between the core area perimeter and the exterior glass window walls. The columns are located just outside the interior core within the corridors. The East Building is nonstructurally connected at each floor level to adjacent structures: a mechanical service tower and a connecting corridor that provides access to other buildings (Figure 3.4.2).

#### 3.4.1 Description of the Structural System

The Health Sciences East Building is 195 feet high and has a square floor plan with an outside dimension of 115'-3". The structural system is a steel moment resisting type frame with four frames each in the North-South and East-West directions. Twelve H type columns built up with plates and angles, connected by rivets, are located on lines 10'-10" inward from the perimeter of the building. The column center-to-center distances are 30'-1 1/2", 33'-4" and 30'-1 1/2" along each side. The depth and flange width of the corner column sections vary from  $d = 29"$ ,  $b_f = 24"$  at the top, to  $d = 32.5"$ ,  $b_f = 30"$  at the ground level. The intermediate column sections vary from  $d = 33"$ ,  $b_f = 36"$  at the top, to  $d = 37.5"$ ,  $b_f = 36"$  at ground level. All girders have a depth of 42". The girder sizes in the exterior

frames increases toward the base (noncomposite moment of inertia  $I = 11000 \text{ in}^4$  at the top, to  $I = 39000 \text{ in}^4$  at the bottom). The interior girders all have a constant section ( $I = 23000 \text{ in}^4$ ). The girder web plates are perforated to allow passage of piping and ventilation ducts. Inclined angles are welded around openings to reinforce the web. The typical girder-column connections are composed of plates and T sections that are welded and bolted. The girders' flanges are connected to the column flanges (column strong axis connection) by T sections (from W36 x 300) with high strength bolts used in both the column and girder flanges. Girder flanges are connected by bolts to connection plates which are welded between the web and column flanges (column weak axis connection). Girder webs are connected to the column by bolted shear plates. Additional description of the girder-column connection is found in ref. 10. The floor framing including floor beams and purlins are shown in Figure 3.4.3. A cast-in-place 5 1/2 inch thick light weight aggregate concrete slab rests on top of the steel floor framing. Nelson studs provide shear transfer (composite action) between the slab and floor framing.

Below the ground floor level, the steel columns are cast integrally into reinforced concrete columns that extend through the basement level to reinforced concrete caissons. Between the basement and ground floor levels are reinforced concrete walls 24 inches thick which are located along the frame column lines, thus forming a grid. Interconnecting the caissons and supporting the basement floor slab and shear walls are reinforced concrete grade beams (about 8 feet deep). The caissons for the corner and intermediate columns have 6 foot diameters, and extend to a maximum depth of about 67 feet below the basement level. Because the service tower was found to have some influence (31) on the East Building's dynamic behavior, a brief description of this structure along with the interbuilding connections follows. The mechanical service tower has plan dimensions 20 feet by

36 feet and is 220 feet in height. The tower contains a stairwell with openings on either side for piping and ventilation ducts. It is a vertical steel truss system encased in reinforced concrete. At the basement and ground floor a levels reinforced concrete slab and beams structurally connect the service tower to the East Building (Figure 3.4.4).

At each floor level two types of nonstructural connections exist between the East Building and adjacent structures (service tower and connecting corridor). Bellows-type aluminum ducts (Figure 3.4.5) run the entire height of the building to provide weatherproofing; and, steel plates span the gap between buildings (about 3 feet) to allow traffic between buildings at each story level. The plates are bolted to the service tower only, and rest freely on the East Building floor slabs.

#### **3.4.2 Results of Experimental Studies**

Experimental studies to determine the dynamic properties of the U.C. Medical Center were conducted by the Department of Civil Engineering of the University of California at Berkeley between the Summer of 1964 and the Fall of 1965. The natural periods, mode shapes and damping capacities were determined by small amplitude forced vibration test procedures in which the building was excited by a rotating eccentric mass and the vibration response was measured by accelerometers located at various floor levels. Four series of tests were conducted: Summer 1964, Summer 1965, Fall 1965 I, and Fall 1965 II. The Summer 1964 tests were conducted when the East Building steel frames and concrete slabs were in place, and the service tower frames in place but not yet encased in concrete. The Fall 1965 tests were conducted on the nearly completed building with exterior window walls erected and most of the ventilation ducts, piping and partitions in place. Between the Summers of 1964 and 1965, the service tower was encased in concrete. For a detailed discussion of the experimental

studies see ref. 31.

The experimental translational and torsional periods are presented in Table 3.4.1. Several interesting features regarding the dynamic characteristics of the building are apparent. For any test series, the North-South and East-West periods agree closely. The largest percentage difference between the N-S and the corresponding E-W experimental period is 10% for the second mode from the Summer 1965 tests. Most of the N-S periods are within 5% of the corresponding E-W values. The N-S and E-W period agreement is expected because the building is square in plan and has the same structural system type in each direction, although the building does not have identical stiffness properties in each principal direction because of the orientation of the corner columns (Figure 3.4.2). The natural periods of the Summer 1965 tests and thereafter are shorter than the periods as determined during the Summer 1964. Also, the Summer 1965, Fall 1965 I and Fall 1965 II tests yield periods that are somewhat constant. Comparing the periods from the Summer 1964 study to the later tests, most periods shorten by less than 15%, however a maximum period shortening of 23% occurs in the N-S fundamental period between the Summer 1964 and the 1965 tests. The decrease in periods was attributed primarily to the effects of the service tower interacting dynamically with the East Building (31). It was believed that the bare steel frame of the service tower had very little effect on the dynamic behavior of the East Building in the Summer of 1964 tests, and the building was tested in isolation. When the steel frame had been encased in concrete, the service tower did effect the behavior of the East Building; both buildings then formed a new structural system resulting in the observed shorter periods. After the Summer 1964 tests, no experimental results for the fourth mode are reported. This is because the force generators were located on the 15th floor rather than on the roof as in the Summer 1964 tests. As a neutral point for

the fourth mode coincided with the 15th floor level, the fourth mode could not be excited. A dramatic decrease in the torsional periods between the Summer 1964 and the Fall 1965 tests is apparent (Table 3.4.1). However, no discussion explaining the large period shifts is presented in the original report.

The first four N-S and E-W translational mode shapes are shown in Figures 3.4.6 and 3.4.7. Note that the results from all the test series tend to agree favorably. This indicates that the translational mode shapes were not significantly effected by the construction sequence nor by the building coupling after the Summer 1964 as noted previously. For any mode, the N-S translational mode shape is similar to the corresponding E-W mode shape. The similarity of the N-S and E-W dynamic properties may be expected because the building has the same structural system type in each direction. The first mode has a characteristic straight line deflection pattern. The second mode has a neutral point (node) at about the 13th floor level and the third mode has nodes at about the 9th and 15th floor levels. Because only the Summer 1964 test was able to determine the fourth mode shape and this test recorded accelerations at only five floor levels, the actual mode shape is not clearly defined. The first two torsional mode shapes are shown in Figure 3.4.8. Only the torsional mode shapes as determined in the 1965 tests were reported. The fundamental torsional mode has constant rotational amplitudes above the 13th floor level. No discussion is presented in the original report as to possible reasons for this observed behavior. However, it may result from a coupling of the East Building and the associated structures via friction between the slabs and the steel plates (Figure 3.4.5). The second torsional mode has more of the expected smooth curve shape with a node point near the 12th floor level.

The natural periods as determined from the Summer 1964 tests are used for comparison with the analytical study results. Regarding mode

shapes, both the Summer 1964 and Fall 1965 II test results are used in comparison with the analytical model results. The Summer 1964 tests have floor acceleration measured at only 5 floor levels; therefore, the Fall 1965 II results are included because the accelerations are recorded at many floor levels thus defining the higher mode shapes accurately. As shown in Figures 3.4.6 and 3.4.7, the mode shapes are somewhat invariant among the test series.

### **3.4.3 Description of Analytical Models**

A modified version of the ETABS (23) computer program is used for the dynamic analysis of the U.C. Medical Center. Inherent in the ETABS model formulation is the assumption that building floors are rigid in plan, which is appropriate for this building since it has a square floor plan with concrete floor slabs. The models are assumed fixed at the ground floor level (2nd floor). Below this level, the steel columns are cast integral into the concrete basement columns and a grid of concrete wells connect the basement columns (Figure 3.4.1). The foundation consists of grade beams under the walls and caissons supporting the columns. The basement and foundation make for a very stiff system with respect to the steel superstructure and the experimental results indicate this by showing insignificant movements at the ground floor level in the mode shape plots. No attempt is made to model the building interaction with the adjacent structures although this effect was believed to contribute to the observed period shifts. Also, with respect to design applications, it was considered unfeasible to develop a model of the coupled building system in which sufficient confidence could be placed. Five building models are examined in order to evaluate the influence of various modeling assumptions on the dynamic characteristics and seismic response.

### Model 1

With Model 1, the exterior frames alone are assumed to constitute the lateral stiffness of the structure. The exterior frames have four bays each and can be expected to have much larger stiffness than the interior large span single bay frames. The model consists of the two exterior E-W frames (Figure 3.4.9(a)). Each frame is composed of beam and column elements with the center-to-center dimensions used for element stiffness formulation. This implies the assumption that the joint flexibility is equivalent to the stiffness of short beam or column segments within the joint region. The beam elements have a moment of inertia that accounts for the composite action of the floor slabs. The slab effective width is assumed to be  $b + 16t$  ( $b$  = flange width;  $t$  = slab thickness) as per AISC recommendations ( a steel-concrete modular ratio of 12 is used). The moment of inertia of the composite girder is about twice as large as that of the noncomposite girder. A uniform mass equivalent to 100 psf distributed uniformly over the floor is assumed. Because the original design mass calculations were not available, this load was estimated from review of the structural drawings. Since only the exterior E-W frames are considered, the model has a single translational mass degree of freedom at each of the 15 floor levels. No N-S or torsional dynamic properties are computed.

### Model 2

Because the girder-to-column connection region has an inherent rigidity which may be expected to be significantly greater than equivalent short beam or column segments, the effects of stiffening these region are examined in Model 2. This model is the same as Model 1 except fully rigid connection zones are provided. For beams, the regions at each end of the beam equal to half the column width are

assumed rigid; and, for columns, the regions at each end equal to half the beam depth are assumed rigid. This reduces the effective length of the columns and beams by 27 and 8%, respectively.

#### Model 3

Model 3 is a fully three dimensional model which includes the exterior and interior frames in both the E-W and N-S directions (Figure 3.4.9 (b)). The N-S and E-W interior frames have girders that intersect at "missing" column locations. The effects of the N-S interior girders vertically supporting the E-W girders (and vice versa) at the "missing" column locations are included in this model. As with the previous model, slab-girder composite action and fully rigid end zones are incorporated. Each floor level has 3 mass degrees of freedom consisting of N-S, E-W translations, and rotations about a vertical axis. Because the three dimensional nature of the model, torsional as well as translational dynamic properties are calculated.

#### Model 4

This model investigates the effective composite slab width assumption by increasing the effective slab width. Developed from Model 3, the assumed effective slab width is increased from  $b + 16t$  to  $b + 32t$ , and the girder moment of interias are adjusted accordingly. This increases the moment of interias by about 15% over those used in Model 3.

#### Model 5

Since the actual floor mass at the time of the experimental testing is not known, Model 5 examines the effects resulting from an increase in floor weight from 100 psf to 110 psf. Developed from Model 3, the translational mass and floor rotational interias are increased by 10% at each story level.

#### 3.4.4 Comparison of Analytical and Experimental Dynamic Properties

In this section, the natural periods and mode shapes for the 5 analytical models are calculated and compared with the experimental results. Comparison of the first four analytical and experiment E-W translational mode shapes are shown in Figure 3.4.10. Both the Summer 1964 and Fall 1964 II experimental mode shapes are presented. The analytical mode shapes show very close agreement and are within 5% of each other at most story levels; thus only one curve is drawn to represent them. The invariance of the mode shapes is somewhat expected because the modeling features incorporated basically produce uniform changes in the stiffness or mass matrices which does not effect the mode shapes. The first two analytical mode shapes have excellent correlation with the experimental results. The second mode shape node point (location of zero modal displacement) near the thirteenth floor is correctly predicted by the models. The analytical third mode shape agrees favorably with the experimental, however, the neutral (node) points are predicted slightly higher up than actual and the amplitudes of the lower story antinodes (points of maximum modal displacements) are larger than actual (when mode shapes are normalized to the roof displacement). Because only the Summer 1964 fourth mode shape results were reported, the actual mode shape is not accurately defined, although the analytical shapes capture the general trends as shown.

The first two analytical torsional mode shapes are compared with the Fall 1965 II test results in Figure 3.4.11. The experimental first torsional mode has an irregular shape with an apparent sharp increase in rotation around the twelfth floor level and an almost constant rotation above that level; whereas, the analytical shape has the characteristic smooth curve. The analytical mode shapes indicate the general shape. Considering the second torsional mode, the analytical mode shape agree favorably with the experimental data,

having the same antinode amplitudes (when normalized to roof rotation), but predicting the node point about one story higher than experimentally observed.

The analytical natural periods are compared with the experimental values from the Summer 1964 test series in Table 3.4.2. Note the variation of the natural periods among the different models. Model 1 with the building lateral stiffness based on only the exterior moment resisting frames that are formulated with member center to center dimensions and composite slab girder action, has a fundamental period of 1.61 seconds which is 36.4% larger than the experimental value of 1.18 seconds. The analytical periods for the higher modes are also larger by about 30%.

Introduction of fully rigid end zones in Model 2 increases the lateral stiffness, and reduces the periods significantly. The fundamental period of 1.25 seconds is 5.9% longer than the experimental value and the higher modal periods are within 2% of the actual values. As shown in Table 3.4.3 the rigid end zones increase the effective modal stiffnesses by an average 71%. This large increase is primarily due to the change in column stiffnesses since the effective length of the column is reduced by 27% versus only 8% for the girders.

The fully three dimensional Model 3 with all N-S and E-W frames incorporated, gives a fundamental E-W period of 1.13 seconds which is 4.2% less than the actual value. The higher E-W modal periods are about 11% less than the actual periods. Comparison of the analytical periods indicate that the interior frame effects result with an average modal stiffness increase of 46% over the Model 1 values (Table 3.4.3). Because Model 3 is three dimensional the torsional periods are extracted and compared with the actual periods. The analytical fundamental torsional period is .802 seconds, 4.3% longer than the experimental value of .769 seconds. The second torsional period is

15.7% less than the actual value.

Model 4 is developed from Model 3 by increasing the girder moment of inertias to represent a larger effective slab width. As a result, the fundamental E-W period is 1.09 seconds, or 7.6% less than the actual experimental value. The higher modal periods are also less, by about 14%. The analytical fundamental torsional period of .770 seconds agrees within 1% of the actual value; however, the second period is 19.1% less than the actual value. The larger effective slab width increased the effective modal stiffnesses of Model 4 over Model 3 by an average of only 7% (calculation using the period shifts from Table 3.4.3).

Model 5 investigates the effects from using a larger floor weight of 110 psf versus the 100 psf used in the previous models. It is developed from Model 3 by increasing the translational and torsional mass values by 10%. This model has a fundamental E-W period of 1.19 seconds which agrees within 1% of the actual value. The higher modal periods are smaller than the actual values by about 7%. The fundamental torsional period of .841 seconds is 9.4% larger than and the second modal period is 11.6% smaller than the experimental values.

Based on the observed natural period variations resulting from the different modeling assumptions, several conclusions can be drawn regarding effective model formulation.

(1) The effects of joint rigidity should be modeled. Because of the large shift in natural periods between Models 1 and 2, it is apparent that a fully rigid connection zone is a better assumption than using center-to-center dimensions in the stiffness formulation (effectively assuming the joint flexibility to be equivalent to short beam or column segments within the joint region). Without this assumption, any model formulation would be too flexible and its natural periods larger than actual. The concept of using a rigid zone smaller than the actual joint region to account for some inherent joint flexibility

could potentially provide a better model; however, the selection of the reduced joint size is arbitrary.

(2) The interior frames possess a significant amount of lateral stiffness as compared to the exterior frames and should be included in the model formulation.

(3) The composite action of the concrete slab with the steel girders should be accounted for when determining girder section properties. Although a model ignoring composite action was not analyzed, it should be noted that the composite steel girder-concrete slab moment of inertia is about twice that of the steel girders alone. By ignoring composite action, any model would be too flexible. In Model 4, the effective slab width is assumed to be  $(b + 32t)$ , a 90% increase over the value used in Model 3  $(b + 16t)$ . However, this results with only an 8% increase in the composite moment of inertia. This produced about a 4% decrease in the natural periods (Table 3.4.2). Apparently, the stiffness (thus dynamic properties) are not sensitive to the assumed slab width, provided a reasonable assumption is made (e.g. AISC recommendations).

Also included in Table 3.4.3 are the fundamental natural periods as estimated by the UBC and ATC formulae. The UBC formula yields a period of 1.50 seconds which is 27.1% larger; and, the ATC method gives a value of 1.82 seconds which is 54.2% larger than the actual period. Note that any of the models studied provide better fundamental period estimates than the ATC formula and Models 2 to 5 yield better period estimates than the UBC formula would calculate.

#### **3.4.5 Influence of Modeling Approach on Design Quantities**

In this section, response spectrum dynamic analyses are performed on each of the models to evaluate the effects of the modeling features on the design forces and displacements resulting from dynamic response spectrum analyses. The Newmark response

spectrum scaled to .05g is used as the earthquake excitation. The earthquake direction is parallel to the E-W building axis. SRSS combination using four modes is used for the solution of story envelope shears, overturning moments, deflections, and drifts.

The peak response envelopes plotted along the height of the building are shown in Figures 3.4.12 and 3.4.13. The characteristic shapes of the response envelope curves are similar for all models. The amplitudes of the response envelope curves vary according to the model.

The peak story shear envelopes are shown in Figure 3.4.12(a). The peak story shears progressively increase in Models 1 to 5. As the lateral stiffness is progressively increased in Models 1 to 4, the natural periods decrease (Table 3.4.2), resulting with larger spectral accelerations, therefore larger inertia forces and resulting story shears. Model 5 is developed from Model 3 by increasing the floor mass. The increase in mass lengthens the natural periods which yields smaller spectral accelerations, however this is offset by the larger mass, thus resulting with larger story inertia forces in Model 5 versus those in Model 3. This effect is explained in Section 2.5 (Figures 2.13, 2.14) whereby the story shears increase as the mass increases for modes that lie on zone C ( $p = 1.0$ ) of the Newmark response spectrum. In Table 3.4.4, the values of base shear are presented for each model along with the percentage change from Model 1. Model 5 with a base shear of 1101 kips represents a 42.1% increase over the Model 1 shear of 775 kips. The single modeling feature that produced the largest increase in story shears is the introduction of rigid joint zones in Model 2. This increased the shears by 24.5% over the Model 1 values.

The envelope values of story overturning moments for the various models are shown in Figure 3.4.12(b). The trends are similar as for the story shears with the most flexible Model 1 having the smallest

overturning moment values and Models 4 and 5 having the largest values. As shown in Table 3.4.4, the overturning moments follow the shear variation with Model 5 having the largest base overturning moment of  $1683 \times 10^3$  k-in which is a 49.6% increase over the Model 1 value of  $1125 \times 10^3$  k-in.

Lateral story deflection envelopes are shown in Figure 3.4.13(a). As the models become progressively stiffer from Model 1 to 4 the lateral deflections decrease. Model 5 with increased mass over Model 3 has larger lateral displacements than Model 3 due to the larger inertia forces. Table 3.4.4 contains the roof deflections for each model. Model 1 has the largest roof deflection of 1.62 in. and Model 4 has the smallest deflection with 1.10 in., a decrease of 32.1%.

Peak story drifts are shown in Figure 3.4.13(b). Note that the drifts are fairly uniform between the 4th and 15th floors, suggesting a shear beam type of deformation pattern along the building height. The trends are similar to deflection envelope plots; that is, smaller drifts in the stiffer models. The 10th floor story drifts for each model are presented in Table 3.4.4. Model 1 has the largest drift (.132 in.) which is 31.8% larger than the Model 4 drift (.090 in.).

To illustrate the relative influence of the various modes on the total computed response, the relative modal contributions of to the total peak design quantity response plotted along the building height for model 3 are shown in Figure 3.4.14. At any story level, the relative contribution is represented as the square of the individual modal contribution divided by the total sum of the squared modal contributions. The first mode is the primary contributor to the total responses. For story shears, the higher modes have some influence near the base and a significant effect toward the roof where the higher modes contribute about 50% to the total sum of the squared modal shears at the roof level. For overturning moments, a similar pattern as for the story shears is apparent. The contribution of the

higher modes increase toward the top of the building where they contribute about 50% to the total sum of the squared modal overturning moments near the roof. The story deflections are completely dominated by the first mode, the higher modes contribute only 9% of the total sum of squared modal of the deflections near the base. The story drifts show similar trends as the shears; that is, higher modes have some influence near the base and increased influence toward the top of the building.

In summary, the various models yield response quantity envelope curves which are similar in shape, but differing in amplitude. Because the models basically involve uniform refinements in stiffness (Models 1-4) or mass (Model 5), the mode shapes are somewhat invariant, and the natural periods have considerable variation. Since the spectral accelerations and displacements are determined from the natural periods, the variation in the amplitudes of the response quantity envelope curves are primarily dependent upon the variation of the natural periods among the models. The response quantities are dominated by the fundamental mode with higher mode effects more pronounced toward the top of the building.

#### **3.4.6 Comparison of Dynamic Analysis and Code Equivalent Static Procedures**

The seismic responses of the U.C. Medical Center Building in terms of the gross design quantities as calculated by dynamic response spectrum procedures and equivalent static methods are compared in this section. For the dynamic analysis, both the ATC and Newmark response spectrums are used. The spectra are scaled to .05g peak ground acceleration as per the ATC recommendation for moment resisting frame structures. The ATC and UBC guidelines are used for the equivalent static methods. The UBC spectra is scaled by a factor of 1.278 to represent the elastic limit intensity. Model 3 is used for the comparative analysis. The equivalent static responses are computed

using both the ATC and UBC approximate fundamental period estimations (1.82 sec. for ATC; 1.5 sec. for UBC) and the analytical period value (1.13 sec.). Results from these analyses are presented in Table 3.4.5 and Figures 3.4.15 and 3.4.16.

The dynamic response spectrum analyses with the ATC and Newmark response spectra yield nearly identical results and are represented by a single curve in the Figures. This is because the first mode dominates the building response (Figure 3.4.14) and the spectral acceleration values from the ATC and Newmark spectrums at the fundamental period (1.13 sec.) are virtually identical (Figure 3.1.1).

The equivalent static analysis results are also presented in Figures 3.4.15 and 3.4.16. The shaded portions in these figures illustrate the variation in the response quantities resulting from the use of the analytically determined fundamental period (1.13 sec.) versus the fundamental periods calculated using the approximate estimation formulae. The relatively large variation in the ATC and UBC equivalent static results from using the approximate and analytical periods is expected since the spectral accelerations set the response amplitudes and are determined from the periods. In general, the shorter periods result in higher spectral accelerations. The fundamental period as estimated by the ATC formula (1.82 sec.) is 61% longer than the analytical period value (1.13 sec.). Accordingly, the responses as calculated using the analytical period are over 30% greater than the values when the approximate period is used (Table 3.4.5). A similar effect is shown for the UBC equivalent static analysis in which the response values using the analytical period are over 15% greater than the values using the UBC approximate period estimation (1.5 sec.).

Comparing the dynamic and equivalent static (using  $T = 1.13$  sec.) results using the ATC response spectra illustrates the

conservatism inherent to the equivalent static procedure introduced by using the full building mass as the effective fundamental modal mass. The equivalent static story shears and base overturning moments are about 25% larger (Table 3.4.5) than the dynamic response spectrum values. The static overturning moments have been reduced as allowed by ATC.

In Figures 3.4.17 and 3.4.18, the story peak shear, overturning moment, deflection and drift responses normalized to the base shear for the different dynamic and static analyses are shown. Equivalent static analysis methods have a story shear distribution which overestimates the shears at the building midheight (Figure 3.4.15 (a)) as compared to a dynamic analysis distribution (about 14% overestimate by the ATC and 5% for UBC). Normalized overturning moments indicate that for a given base shear, the ATC equivalent static procedure agrees well with the dynamic analysis results, whereas the UBC procedure overestimates the base overturning moment by 9%. The deflections and drifts normalized to base shear show that the equivalent static procedures yield distributions that agree favorably with those resulting from dynamic analyses. The normalized ATC and UBC equivalent static roof deflections are 7 and 3% greater than the normalized dynamic analysis results respectively.

#### **3.4.7 Comparison of Code Design Forces with Dynamic Forces Induced by Actual Earthquake Spectra**

In this section, the story shears and overturning moments resulting from the Taft 1952 (peak ground acceleration .179g) and El Centro 1940 (peak ground acceleration .348g) earthquakes are compared with the UBC elastic limit design quantities. Four modes are used in the analysis and 5% critical damping assumed. The UBC forces are calculated using the analytical period value of 1.13 sec. and are multiplied by 1.278 to represent the elastic limit force levels. Two models are examined with each of the actual earthquake spectra. The

first being Model 3 which has periods that agree well with the small amplitude experimental values, and the second is Model 1 which has periods about 40% longer than actual. The purpose of evaluating the response with two models for each earthquake excitation is to illustrate the range (shaded regions in Figure 3.4.19) of response values resulting from the simplest and most refined analytical models. Also, because the building's natural periods can be expected to effectively lengthen during an actual major earthquake, the response from Model 1 provides an indication of how the actual earthquake response may differ from the elastic response (Model 3). However, it is recognized that the apparent "period lengthening" of buildings during major earthquakes is a consequence of inelastic activity and representing this behavior by an elastic model with lengthened periods does not rigorously conform to a theoretically correct solution.

The peak story shear and overturning moment envelopes are shown in Figure 3.4.19. For the Taft excitation, Model 1 has larger peak responses than Model 3. This is because the actual spectra is irregular and happens to have larger spectral accelerations at the Model 1 fundamental period ( $S_a = .165g$ ) than the Model 3 fundamental period ( $S_a = .138g$ ). This behavior is not possible when using smooth design type spectra since the spectral acceleration decrease with increasing period (except in the very short period range for some spectra, see Figure 2.5). For the El Centro excitation, the story shear envelopes from Models 1 and 3 have considerable variation (Figure 3.4.19 (a)). The waviness of the shear envelope in model 1 is from the contribution of the higher modes. The ratio of the fundamental spectral acceleration to the second modal acceleration for Model 1 is 1:4.6, whereas the ratio for Model 3 is 1:1.7. Also shown in Figure 3.4.19 are the story shears and overturning moments from the UBC equivalent static analysis procedures (scaled by 1.278 to reflect elastic limit force levels). The UBC forces presented are based upon

an assumed floor weight of 100 psf as this weight is judged to be the representative of the actual floor dead load. As noted in the analyses of the other study buildings, the actual design dead loads are believed to overestimate the actual floor weights. Therefore, the forces presented may be less than those using the actual design loads. The story shears and overturning moments from both the Taft and the El Centro excitations exceed the elastic limit UBC results along the entire building height. If the building is designed according to the UBC criteria presented and assuming the elastic earthquake analysis results can be used to approximate the ductility demand, then the Taft excitation produces overall ductility ratios ranging from about 1.7 to 2.1 and the El Centro excitation induces ductility ratios from about 2.7 to 4.4.

#### **3.4.8 Summary**

Five analytical models of the University of California Medical Center Building are analyzed to investigate the relative influence of various modeling assumptions on the dynamic characteristics and seismic response behavior. The models are developed by the progressive addition of various features. The effects of rigid girder-column connection regions, slab-girder composite action, interior frames, and floor mass variation are evaluated. From the analysis of the five models, the following observations are made:

(1) Several building models have dynamic properties that agree favorably with the experiential values. Models 2, 3 and 5 have E-W translational natural periods that are within 12% of the experimental periods (Table 3.4.2).

(2) The mode shapes from the models are somewhat invariant and agree well with the experimental results (Figure 3.4.10). The natural periods from the models vary significantly depending upon the modeling features incorporated. Model 1 has natural periods that are about 50%

larger than those from Model 4 (Table 3.4.2).

(3) The characteristic shapes of the peak force and displacement envelopes (using the Newmark spectrum) are the same for all models (Figures 3.4.12 and 3.4.13). Models 1 to 4 have increasing modal stiffnesses (Table 3.4.3). Accordingly, the amplitudes of the peak story shear and overturning moment envelopes increase (due to increased spectral accelerations resulting from the decreased periods), and the peak story deflection and drift envelopes decrease progressively from Models 1 to 4 (Table 3.4.4).

(4) The fundamental mode dominates the peak design response quantities when using the Newmark spectrum (Figure 3.4.14). The higher modes have some influence toward the building top for story shears, overturning moments, and drifts.

(5) For this building, dynamic analysis using the Newmark and ATC spectrum yield similar peak response quantity values (Table 3.4.5). This is because the building fundamental period is close to the period value at which the spectral curves intersect (Figure 2.5).

(6) The design force and displacement quantities from both equivalent static procedures (using the analytical fundamental period) are greater than those from the dynamic analyses (Figures 3.4.15 and 3.4.16). For base shear, the static UBC and ATC procedures give values that are 22 and 25% greater than the dynamic analysis results, respectively (Table 3.4.5). For base overturning moment, the static UBC and ATC procedures yield values 33 and 25% greater than dynamic analysis results, respectively.

(7) The UBC and ATC approximate periods are significantly larger than the actual (or analytically calculated) fundamental period (Table 3.4.2). The use of these periods in the equivalent static analysis procedures results with smaller forces and displacements than those using the actual period (Figures 3.4.15 and 3.4.16).

(8) The normalized peak response quantities indicate that the

distributions from the equivalent static procedures agree favorably with those from the dynamic analysis results for the story deflections and drifts (Figure 3.4.18). However, for story shears the static procedures overestimate the shear distribution near the building midheight and overestimate the overturning moments toward the base (Figure 3.4.17). The overturning moment reduction as allowed in the ATC static procedure improves the overturning moment distribution as compared to the dynamic analysis distribution.

(9) The story shears and overturning moments from both the Taft and the El Centro excitations exceed the elastic limit UBC forces along the entire building height (Figure 3.4.19). The overall ductility ratios range from about 1.7 to 2.1 for the Taft earthquake and are from about 2.7 to 4.4 for the El Centro earthquake. This observation assumed that the building is designed only to the UBC equivalent static force criteria.

Table 3.4.1: Experimental Natural Periods  
from All Test Series

Direction	Mode No.	Experimental Periods in Seconds			
		Summer 1964	Summer 1965	Fall 1965 I	Fall 1965 II
N-S	1	1.18	.91	.91	1.0
	2	.44	.38	.40	.42
	3	.26	.23	.22	.23
	4	.18	---	---	---
	5	.14	---	.13	.13
E-W	1	1.18	1.00	1.00	1.05
	2	.44	.42	.40	.43
	3	.26	.22	.22	.22
	4	.18	---	---	---
	5	.14	.13	.13	.13
Torsion	1	.77	---	---	.38
	2	.34	---	---	.22
	3	.20	---	---	.16

Table 3.4.2: Comparison of Experimental and Analytical Natural Periods

Direction	Mode No.	Exp. * Period(sec)	Model 1		Model 2		Model 3		Model 4		Model 5		UBC**		ATC**	
			Period	%	Period	%	Period	%	Period	%	Period	%	Period	%	Period	%
E-W	1	1.18	1.61	+36.4	1.25	+5.9	1.13	-4.2	1.09	-7.6	1.19	+0.8	1.50	+27.1	1.82	+54.2
	2	0.444	0.574	+29.3	0.444	-0.9	0.395	-11.0	0.380	-14.4	0.415	-6.5				
	3	0.256	0.339	+32.4	0.258	+0.8	0.229	-10.5	0.221	-13.7	0.241	-5.9				
	4	0.180	0.243	+35.0	0.183	+1.7	0.159	-11.7	0.154	-14.4	0.167	-7.2				
Torsion	1	0.769				0.802	+4.3	0.770	+0.1	0.841	+9.4					
	2	0.345				0.291	-15.7	0.279	-19.1	0.305	-11.6					

% = percent variation from experimental period.

\* Experimental periods from Summer 1964.

\*\*Code periods calculated based on a 15 story height as follows:

UBC (egn. 12-3B):  $T = 0.10N = 0.10 \times 15 + 1.5$  sec.

ATC (egn. 4-4):  $T = C_T h_n^{3/4} = .035 \times (195)^{3/4} = 1.82$  sec.

Table 3.4.3: Influence of Modeling Aspects on Model Stiffnesses

Direction	Mode	Stiffness Increase with Respect to Model 1			Total
		Rigid Joint Zone	Interior Frame	Increased Slab-Girder Interaction*	
E-W Trans.	1	66%	37%	15%	118%
	2	67	44	17	128
	3	73	46	16	135
	4	76	58	15	149
Average		71%	46%	16%	108%

\*Stiffness increase resulting from effectively doubling the composite slab width participating with girders.

Table 3.4.4: Variation of Design Quantities Resulting from Analytical Models

Design Quantity	Model 1		Model 2		Model 3		Model 4		Model 5	
		%		%		%		%		%
Base Shear (k)	775	0	964	+24.4	1053	+35.9	1095	+41.3	1101	+42.1
Base OTM( $\times 10^3$ k-in)	1125	0	1458	+29.6	1619	+43.9	1690	+50.2	1683	+49.6
Roof Deflection (in)	1.62	0	1.26	-22.2	1.14	-29.6	1.10	-32.1	1.18	-27.2
10th floor drift (in)	0.132	0	0.101	-23.5	0.093	-29.5	0.090	-31.8	0.097	-26.5

% = percent change from Model 1.

Table 3.4.5: Comparison of Design Quantities for Dynamic and Equivalent Static Analyses

Design Quantity	Dynamic				Static							
	Newmark		ATC		ATC		UBC*					
		%		%		%		%		%		
Fundamental Period	1.13	0	1.13	0	1.82	+61.1	1.13	0	1.50	+32.7	1.13	0
Base Shear (k)	1053	0	1060	+0.7	959	-8.9	1318	+25.2	1114	+5.8	1283	+21.8
Base OTM ( $\times 10^3$ k-in)	1619	0	1628	+0.6	1480	-8.6	2030	+25.4	1876	+15.9	2160	+33.4
Roof Deflection (in)	1.139	0	1.145	+0.5	1.112	-2.4	1.528	+34.2	1.239	+8.8	1.427	+25.3
10th floor drift (in)	0.093	0	0.093	0	0.090	-3.2	0.124	+33.3	0.097	+4.3	0.112	+20.4

% = percent change from Newmark spectrum dynamic analysis.

\*UBC values are factored by  $1.70/1.33 = 1.278$  for correspondence with ATC elastic limit load levels.

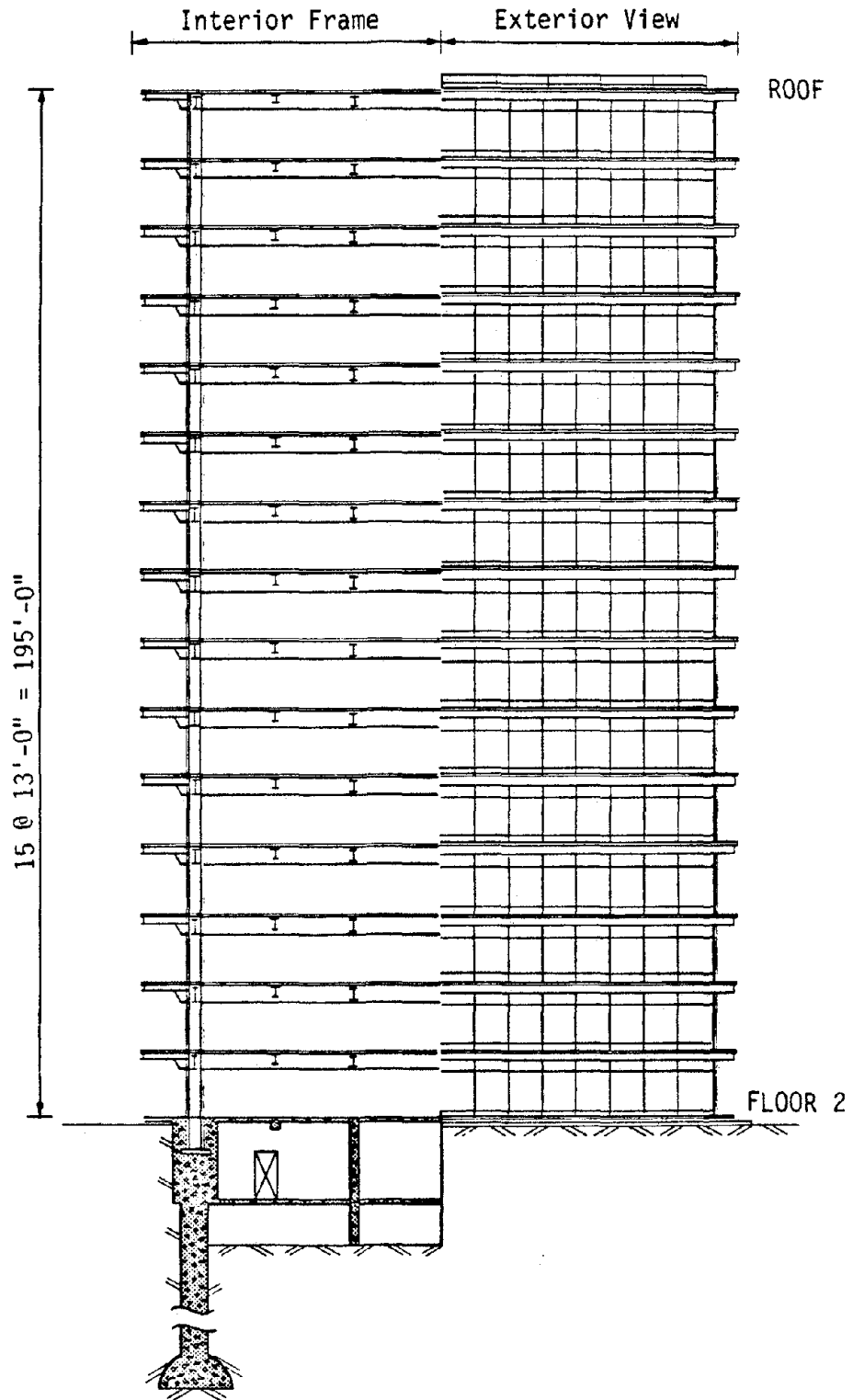


Figure 3.4.1: Elevation View of the East Building of the University of California Medical Center

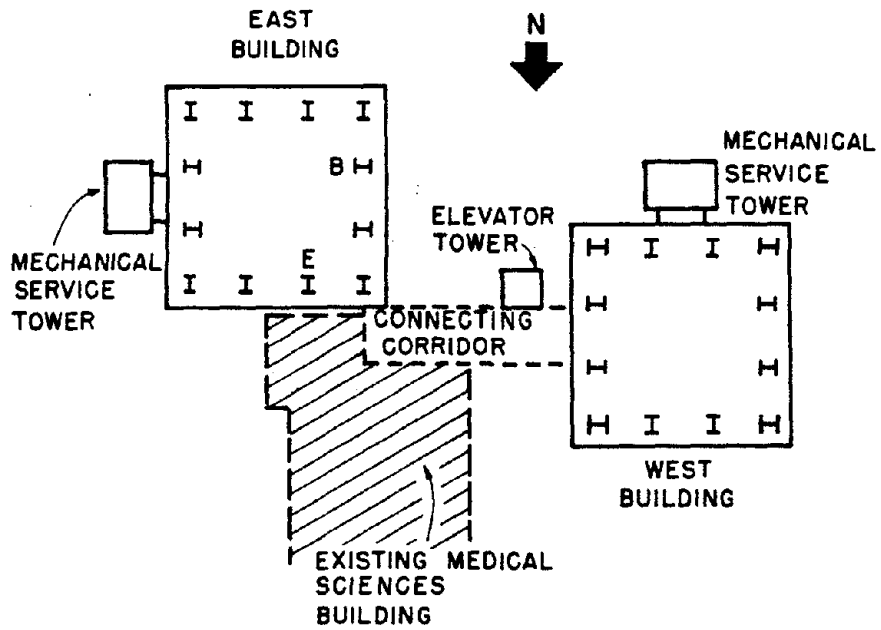


Figure 3.4.2: General Plan View of Buildings



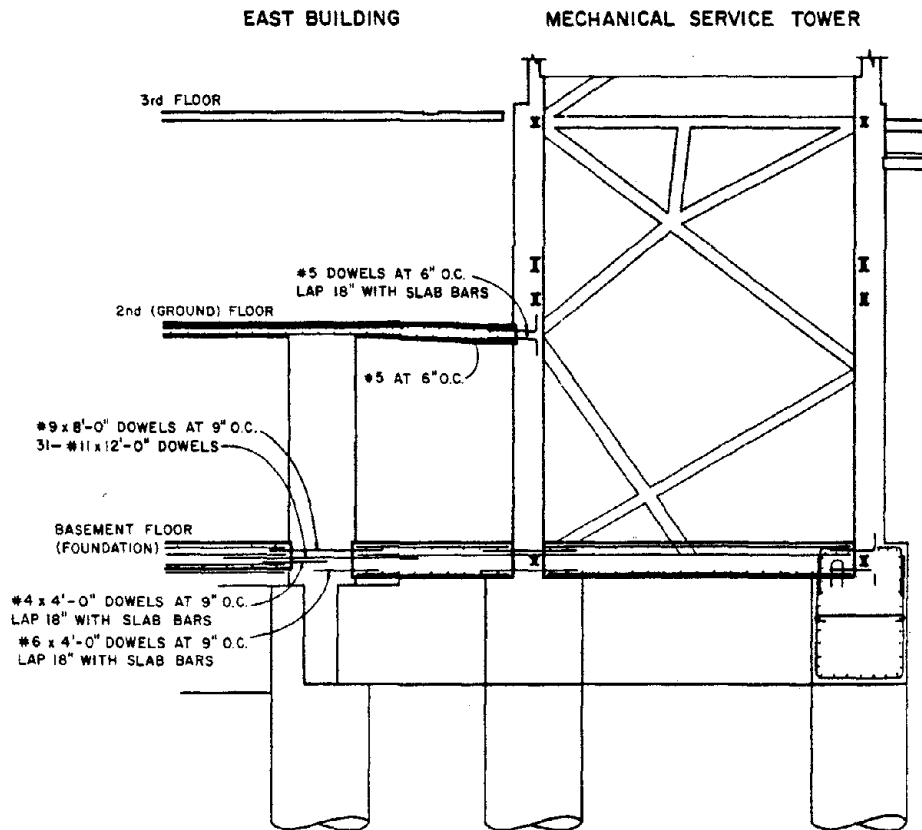
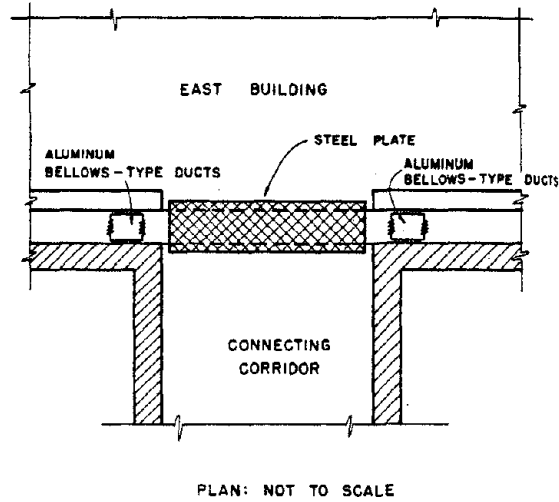
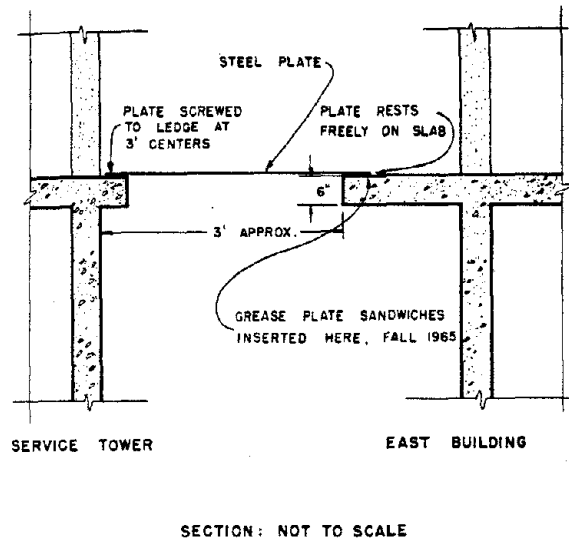


Figure 3.4.4: Structural Connections Between East Building and Service Tower



(a) Connection to Connecting Corridor



(b) Connection to Service Tower

Figure 3.4.5: Nonstructural Connections Between East Building and Adjacent Structures

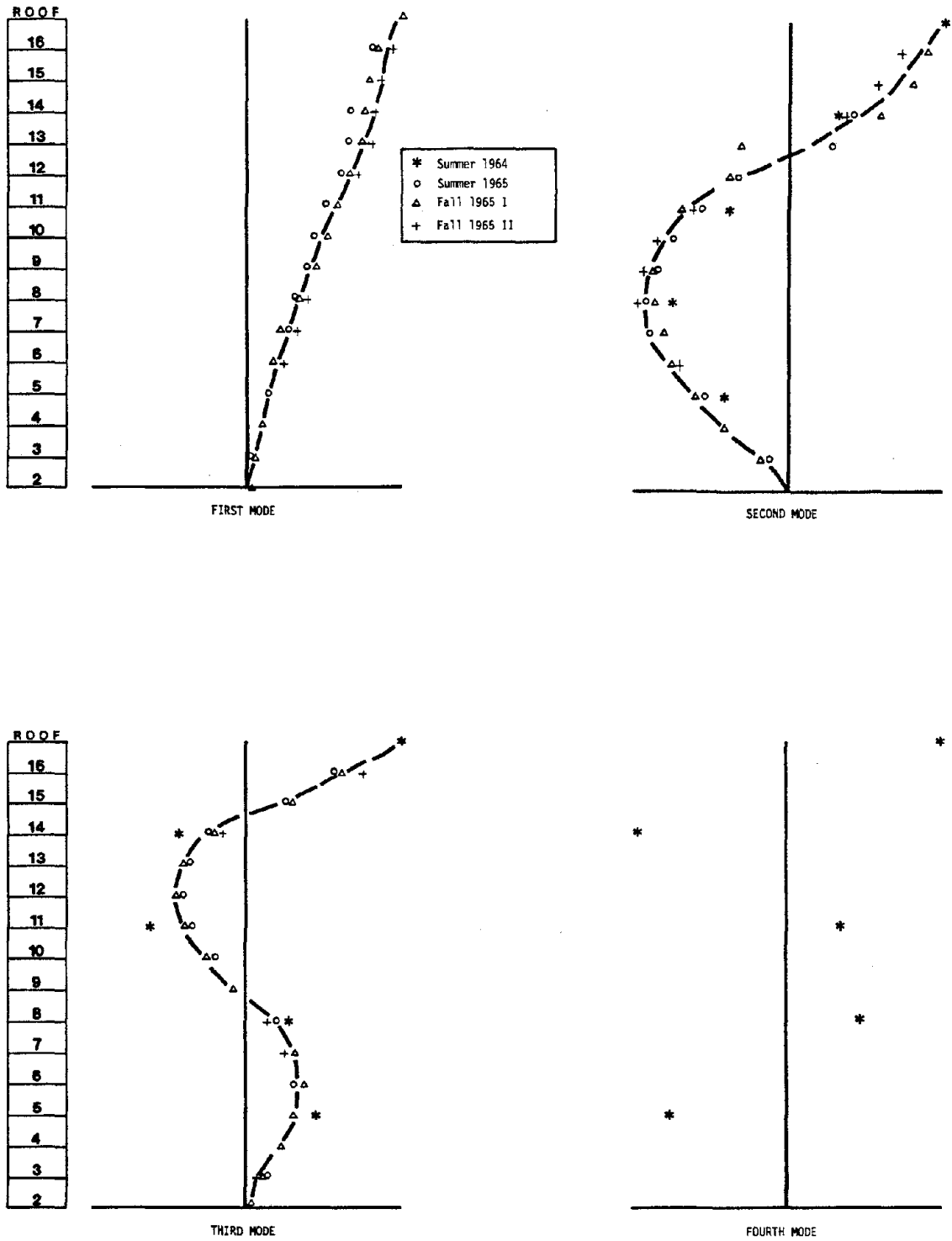


Figure 3.4.6: North-South Experimental Mode Shape

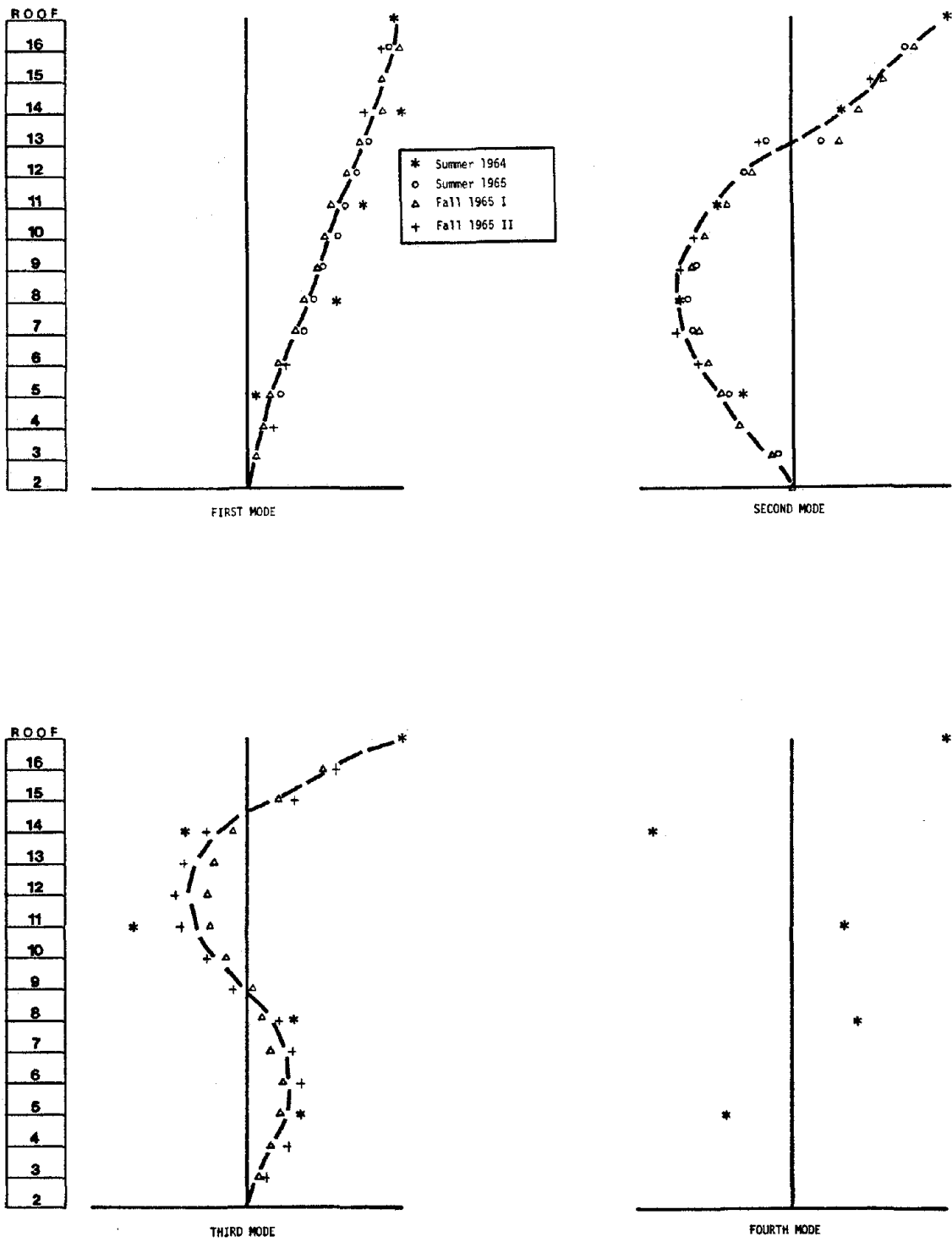


Figure 3.4.7: East West Experimental Mode Shapes

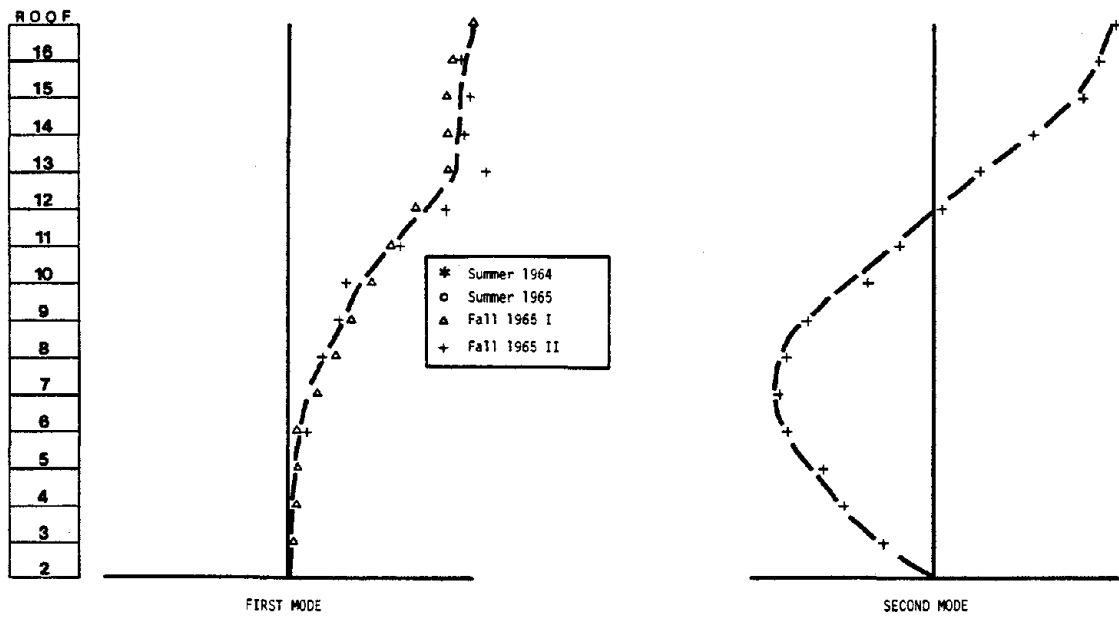


Figure 3.4.8: Torsional Mode Shapes

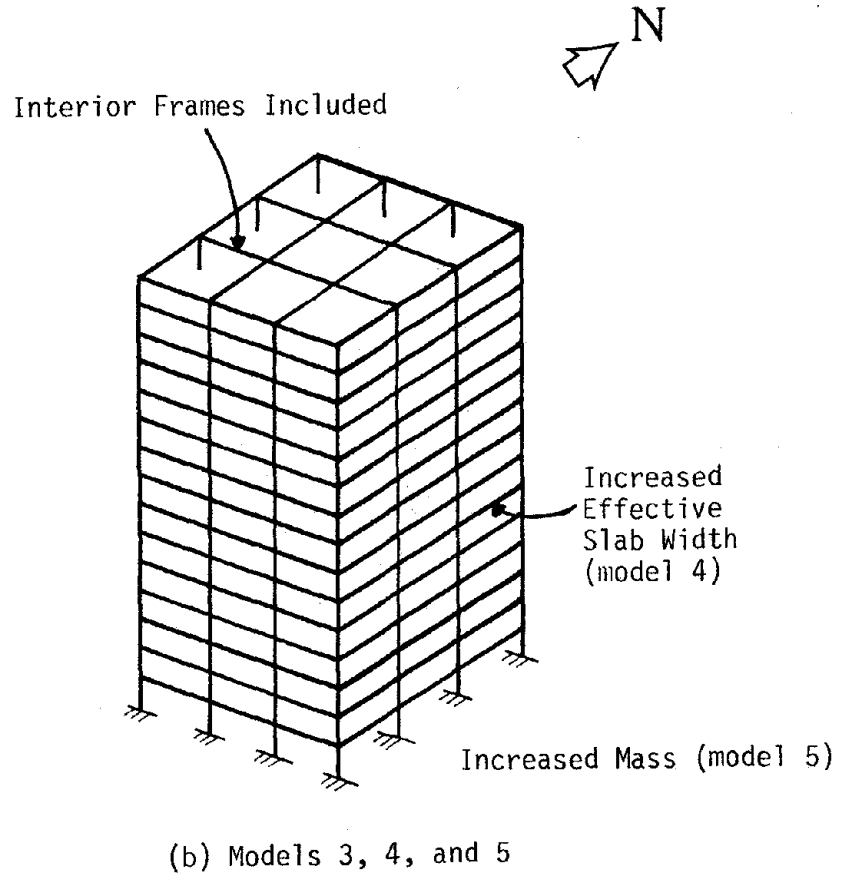
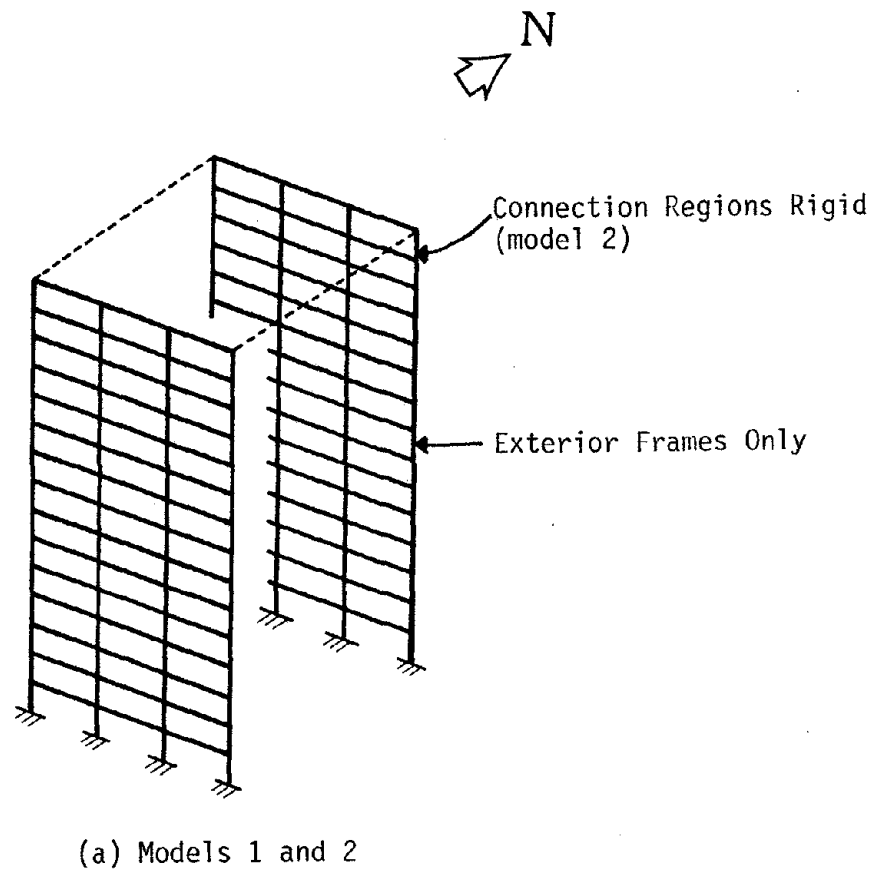


Figure 3.4.9: Analytical Models

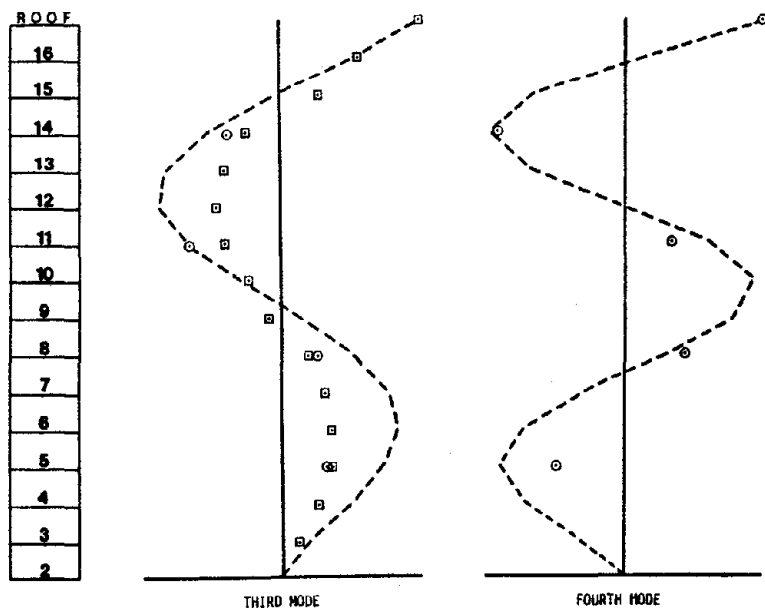
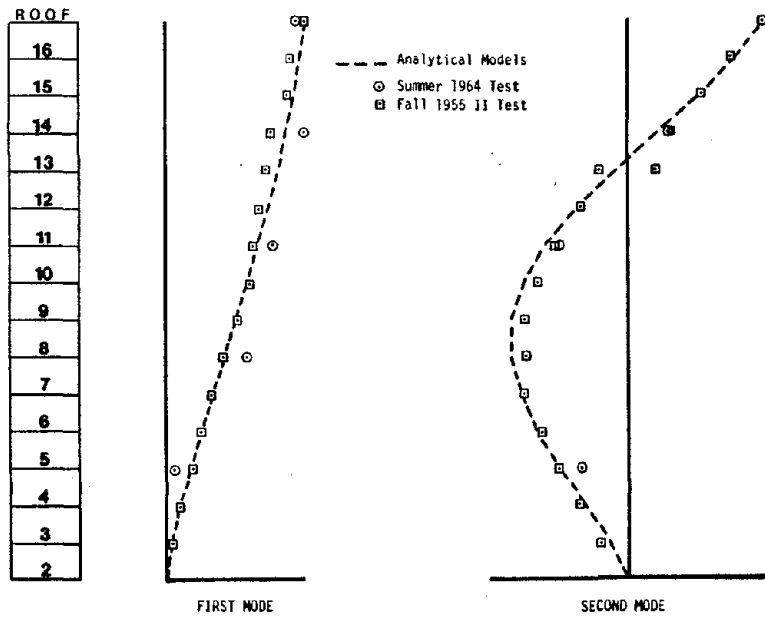


Figure 3.4.10: Comparison of Analytical and Experimental Mode Shapes (E-W Translational)

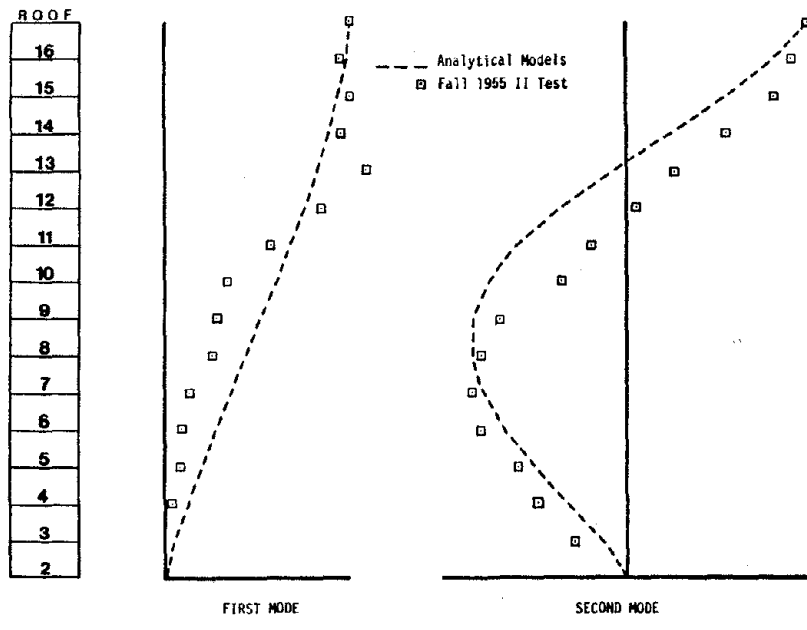
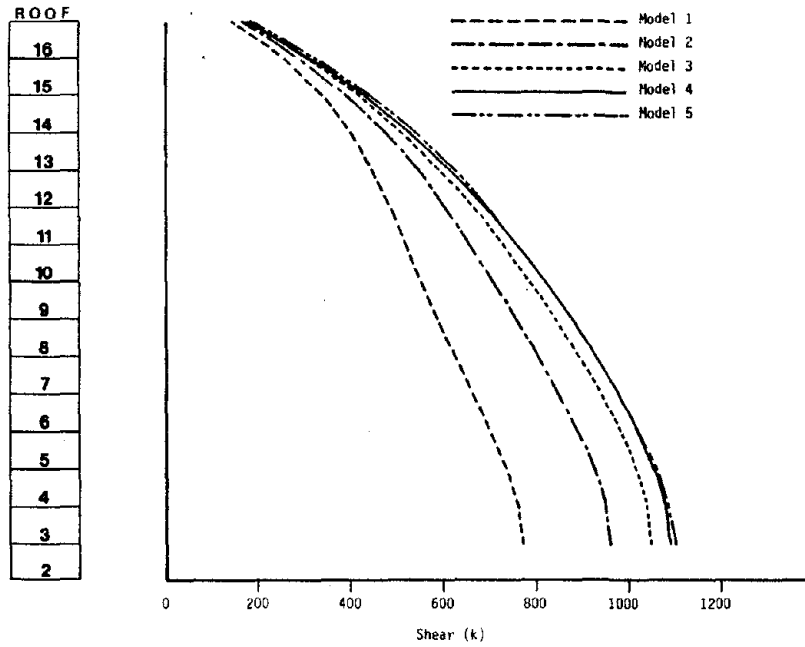
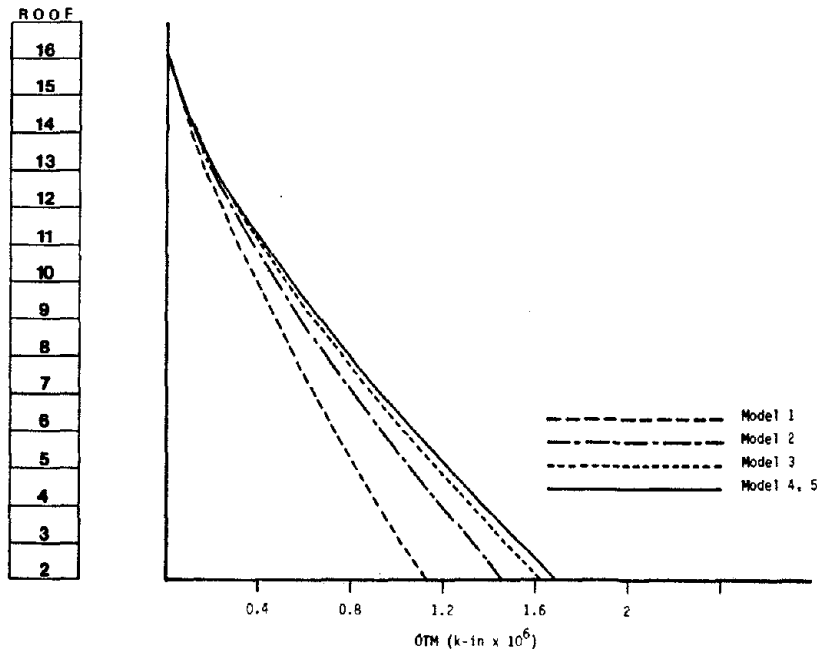


Figure 3.4.11: Comparison of Analytical and Experimental Mode Shapes (Torsional)

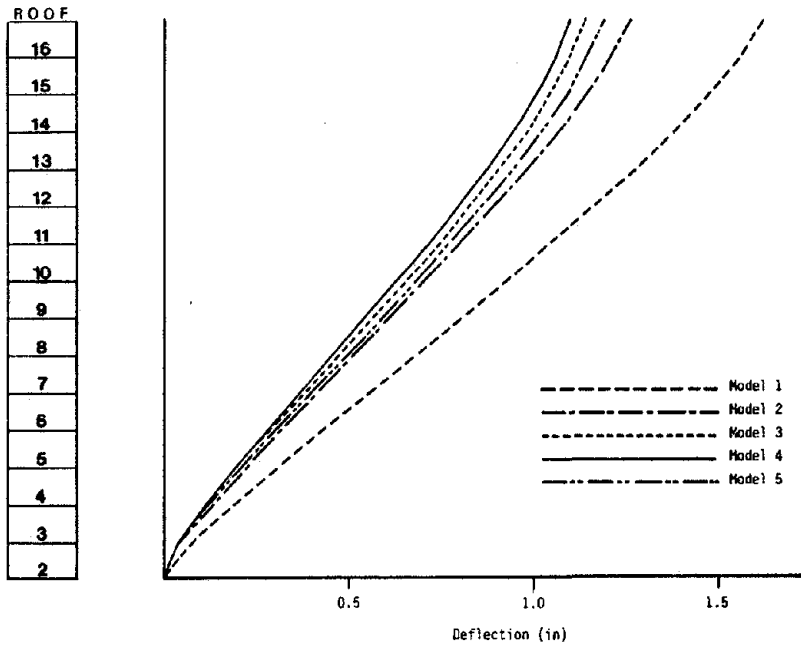


(a) Story Shears Envelopes

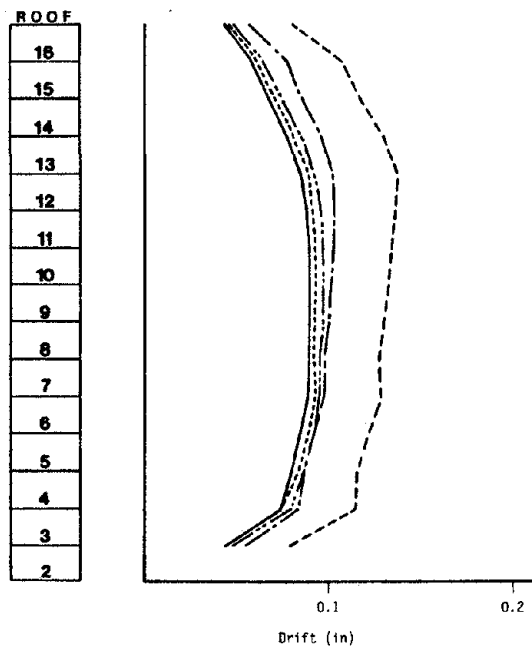


(b) Story Overturning Moment Envelopes

Figure 3.4.12: Comparison of Story Force Quantities from the Various Analytical Models

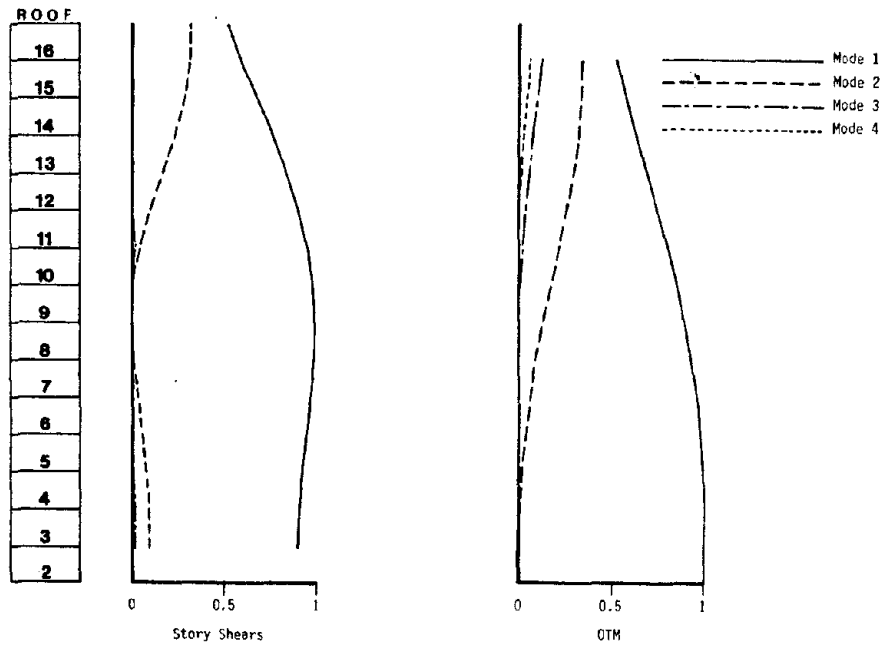


(a) Story Deflection Envelopes



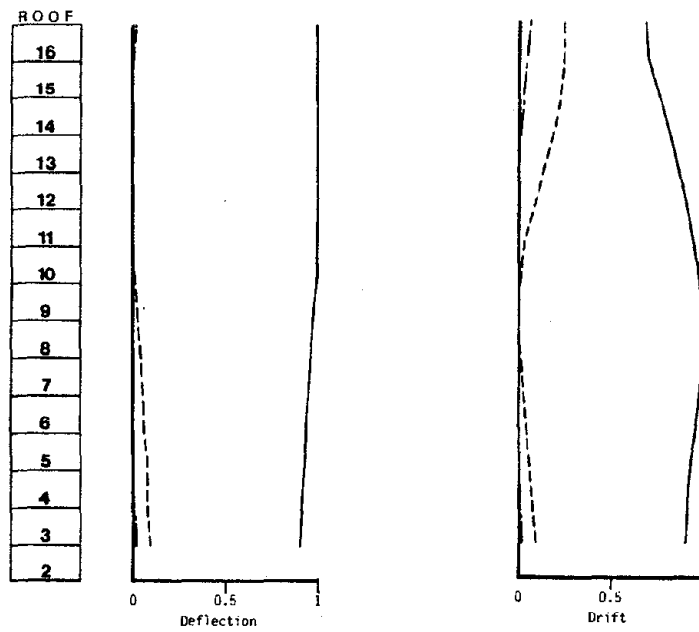
(b) Story Drift Envelopes

Figure 3.4.13: Comparison of Story Displacement Quantities from the Various Analytical Models



(a) Shear

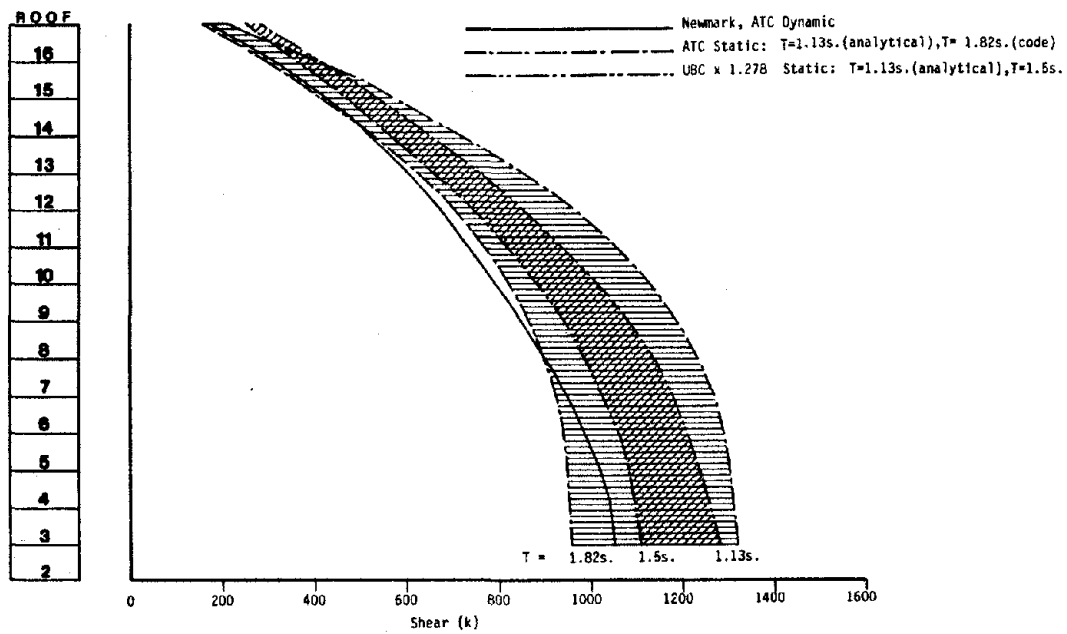
(b) Overturning Moment



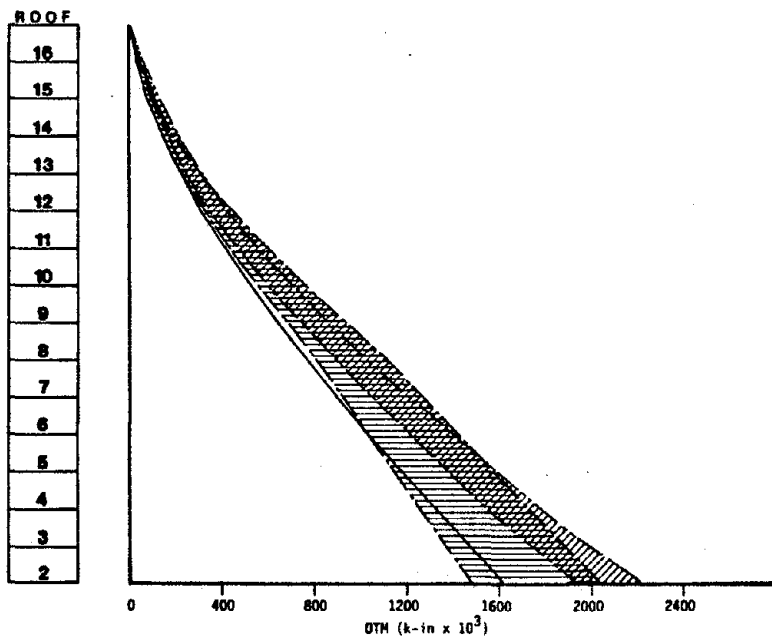
(c) Deflection

(d) Drift

Figure 3.4.14: Modal Contributions to Design Quantities

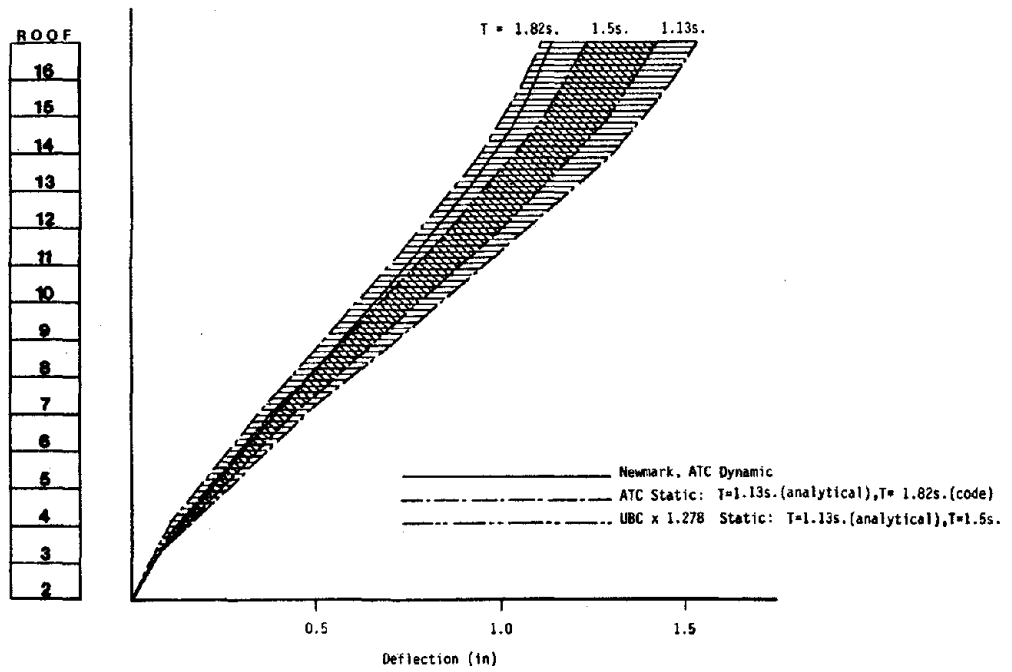


(a) Story Shear Envelopes

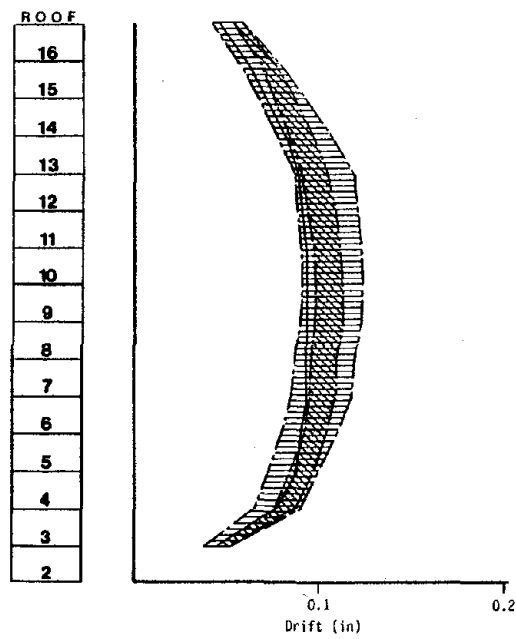


(b) Story Overturning Envelopes

Figure 3.4.15: Story Force Quantities Resulting from Dynamic and Equivalent Static Analyses

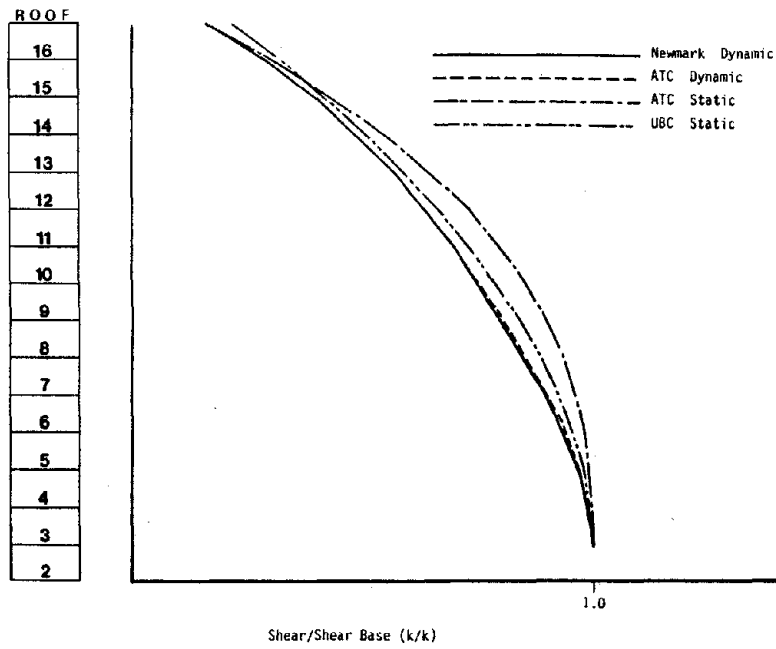


(a) Story Deflection Envelopes

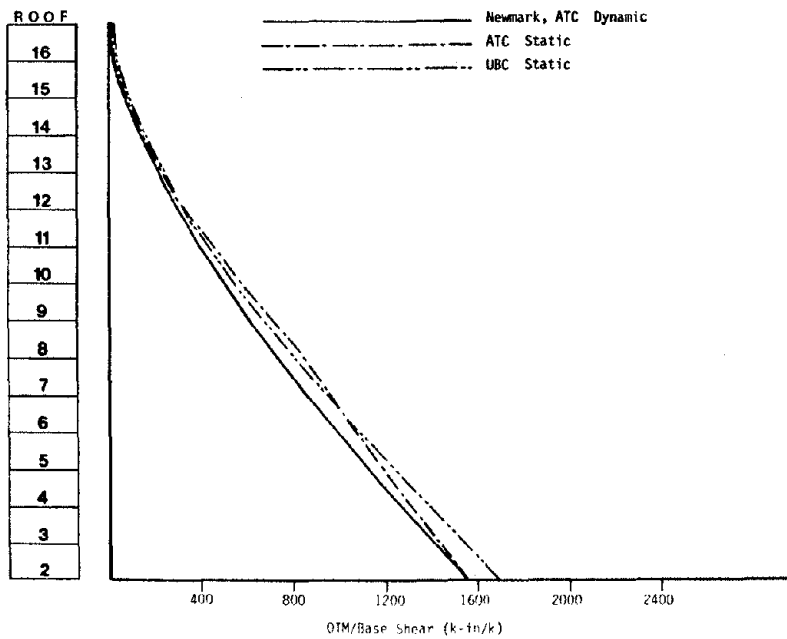


(b) Story Drift Envelopes

Figure 3.4.16: Story Displacement Quantities from Dynamic and Equivalent Static Analyses

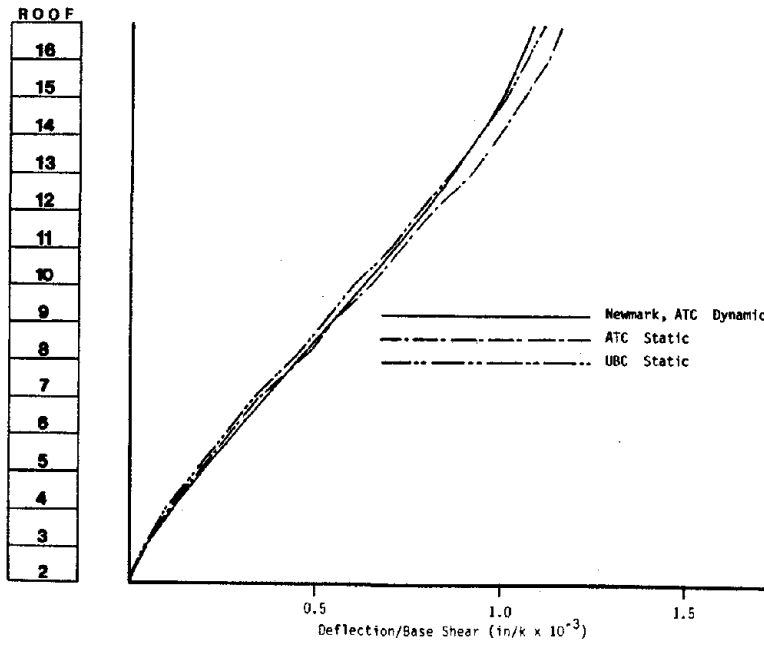


(a) Story Shears

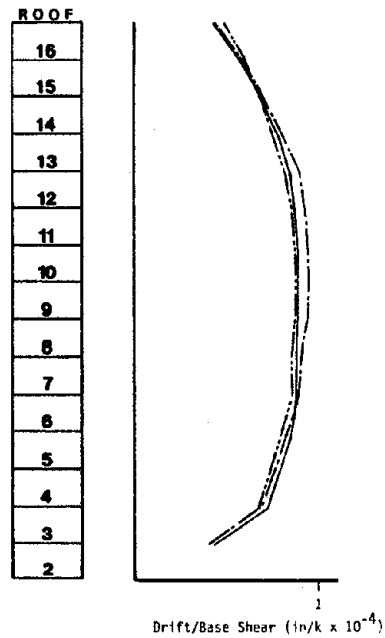


(b) Story Overturning Moments

Figure 3.4.17: Story Force Quantities Normalized to Base Shear

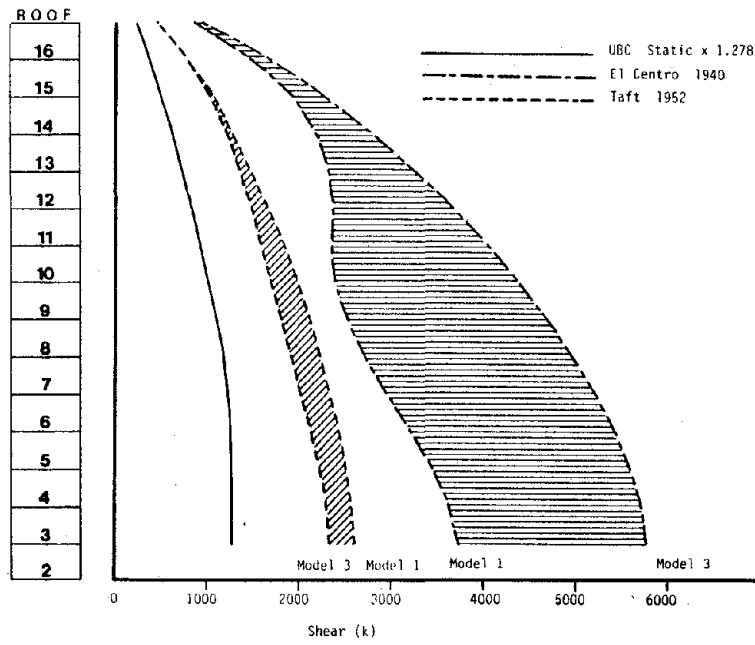


(a) Story Deflections

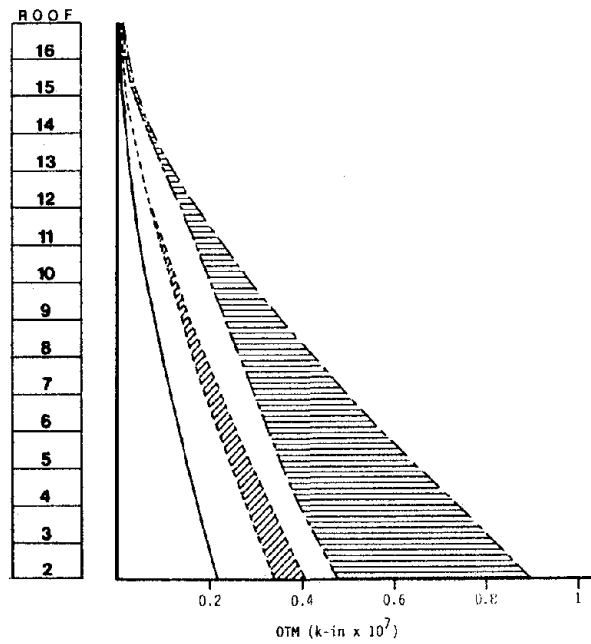


(b) Story Drifts

Figure 3.4.18: Story Displacement Quantities Normalized to Base Shear



(a) Story Shear Envelopes



(b) Story Overturning Moment Envelopes

Figure 3.4.19: Comparison of UBC Design Forces and Elastic Forces Induced by Actual Earthquake Spectra

### 3.5 RANIER TOWER BUILDING

The Ranier Tower is a multistory office building located in Seattle, Washington. The structural design of this building was performed by Skilling, Helle, Christiansen, Robertson, Inc. of Seattle. The building features a novel architectural design in which a 30 story steel office tower is supported by a tapered 12 story reinforced concrete pedestal base. The office tower is square in plan with a side dimension of 139 feet. The pedestal base is also square in plan but has a varying side dimension decreasing from 139 feet at the 12th story to approximately 68 feet at ground level. The total height of the building is 373 feet. A photograph of Rainer Tower is shown in Figure 3.5.1.

#### 3.5.1 Description of the Structural System

Elevation and plan views of the structural system are shown in Figure 3.5.2. The primary lateral force resisting system of the steel tower (13th to 42nd story) consists of four identical moment resisting frames located at the exterior walls of the building. Each exterior frame contains seven equally spaced column lines and has full symmetry of column and girder sections about the central column line. The exterior frames do not share common corner columns but are joined at the four corners by intersecting girders cantilevered from adjacent columns. In the exterior frames, all columns are W14 sections and all girders are W30 sections. At levels 13, 24, 25 and 26, the W30 girders are additionally reinforced with welded flange plates. Girders in the exterior frames are designed to act compositely with the floor slab having shear studs welded to their top flanges.

In the pedestal base, lateral force resistance is provided by the curved exterior reinforced concrete walls (see Figure 3.5.2(a)). These walls have varying thickness ranging from a minimum of 2 feet near the 10th floor level to a maximum of 5 feet 10 inches at the base. At the top of the pedestal (12th floor level), the wall

thickness is 5 feet 4 inches. At this level, a 2 foot thick heavily reinforced and post-tensioned concrete slab ties the four pedestal walls together and resists lateral spreading that would otherwise be caused by the vertical loads carried by the peripheral columns. At lower levels in the pedestal base, ordinary reinforced concrete slabs act as horizontal stiffeners for the pedestal walls. The pedestal walls extend down through two below grade levels to a 12 foot thick reinforced concrete mat foundation which is 106 feet square in plan.

In addition to the primary lateral system described above, a central core frame is provided in the steel tower to carry vertical dead loads. However, this frame is not designed as a ductile moment resisting system. The core frame is supported by reinforced concrete columns and bearing walls located in the pedestal core. The layout of the core framing system is shown in Figure 3.5.2 (b).

The floor construction in the tower typically consists of a 3 1/4 inch lightweight concrete cover over 3 inch concrete filled corrugated steel decking giving a total thickness of 6 1/4 inches. However, in the top three stories, 5 and 8 inch thick slabs are used. All floor slabs are supported by simply supported floor beams which span between the exterior walls and the central core.

The typical story height in the office tower is 12 feet except for stories 24 and 40 where the heights are 15 feet. Also, the mechanical levels corresponding to stories 41 and 42 have taller story heights of 15 feet 6 inches and 19 feet 6 inches, respectively.

### **3.5.2 Results of Experimental Studies**

In April and May of 1977, forced vibration and ambient motion tests of the structurally complete Ranier Tower Building were conducted by the Earthquake Engineering Research Center of the University of California at Berkeley. For a detailed discussion of these tests see reference 40.

The forced vibration tests were performed using two forced vibration generators fixed to the 39th floor of the building. This forcing system was able to excite six N-S translational modes, six E-W translational modes, and five torsional modes of vibration. Response was recorded by 12 accelerometers vertically spaced at 2 to 5 story intervals over the height of the building. In Figure 3.5.3, the forced and ambient vibration results for the first four N-S translational modes are shown. Natural periods of 4.44, 1.39, 0.76, and 0.55 seconds were determined for the first, second, third and fourth (N-S translational) modes, respectively. In Figure 3.5.4, the results for the first four torsional modes are shown whose periods were found to be 2.65, 0.95, 0.54 and 0.38 seconds, respectively.

The experimental results reflect several fundamental aspects of the dynamic behavior of this building. Firstly, the dynamic properties in both the N-S and E-W translational directions were found to be virtually identical. Slight differences (less than 5%) between the translational periods of the N-S and E-W directions were noted. These differences are attributable to the non-symmetric core frame which is somewhat stiffer in the N-S direction than in the E-W due to the greater number of columns in the N-S frames (see Figure 3.5.2 (b)). Because the dynamic properties in the two translational directions are essentially the same, only the N-S direction will be considered for comparison with analytical results. A second important aspect of the dynamic behavior is the relative rigidity of the pedestal base. As can be seen in Figure 3.5.3, the pedestal does not participate substantially in the dynamic response of the first three translational modes because of its large relative stiffness. In the fourth mode, however, more significant pedestal deflections are noted. Therefore, participation of the pedestal in dynamic response probably will occur primarily in the fourth and higher modes. A third aspect worth mentioning is the greater relative pedestal deflection in the

fourth translational mode compared to the fourth torsional mode. This behavior suggests that overturning deformation may occur in the underlying soil for the translational modes and that this effect could be potentially significant in translational response analysis.

Regarding the overall behavior of the tower portion of the building, the approximately linear shape of the first translational mode indicates that shear type deflection behavior controls overall response with no significant cantilever type behavior being apparent.

### **3.5.3 Description of the Analytical Models**

Analyses of the Ranier Tower Building have been performed using the ETABS and SAP-IV computer programs. The SAP program was used to make an assessment of the stiffness properties of the reinforced concrete pedestal. These properties were then incorporated in the form of an equivalent column in the final ETABS models used for dynamic analyses. In the ETABS analyses, floor diaphragms are assumed to be infinitely rigid and mass is lumped at the center of each floor. In total, seven different models of the Rainer building have been formulated and analyzed. These models are described in the following.

#### **Model 1**

Model 1 is a two dimensional ETABS model of a single exterior planar frame of the steel office tower above the pedestal. Member properties are based on the bare steel column and girder sections. Center-to-center member lengths are used in this model. This planar model consists of 7 column lines and 6 bays and neglects the three-dimensional effects of the orthogonal frames. The model has 31 stories with a rigid base assumed at the 12th floor level (top slab of the pedestal). The mass values used correspond to 1/2 the weight of each story, based on dead load calculations supplied by the designer and an estimated 10% of the design live load for the lower 13 floors of the steel tower as used in reference 40. These story weights are

shown in Table 3.5.1. It should be noted that the slab-girder interaction effect resulting from the composite girder design is neglected in this model so that the influence of this modeling aspect may be assessed separately in a later model.

### Model 2

The main objective in the formulation of Model 2 is to account for the rigidity of joint regions at the column-girder intersections in the exterior steel frame. Model 2 is a planar frame model with section properties and mass values identical to Model 1. However, in Model 2, the entire joint panel zone is assumed to be infinitely rigid in flexure. In calculating element stiffness, the lengths of the girders are reduced by corresponding column widths and the column heights are reduced by corresponding girder depths. The ETABS program was modified to allow full axial column flexibility through the joint zone. As a sidelight to Model 2, an additional model was formulated which includes the rigid joint zone effect in the columns only. Analysis was performed on this model in order to evaluate the relative significance of column versus girder rigid joint zone effects on the dynamic properties of the building.

### Model 3

The objective in the formulation of Model 3 is to account for the stiffening effects of the composite floor slab design on the planar frame action in the steel tower. This formulation includes the rigid end zones as described in Model 2 and also accounts for composite behavior of the slab and girders in the exterior frame by increasing the girder moments of inertia in accordance with the composite section properties as given by the AISC Specifications (1), section 1.11.5. Where floor slabs consist of light weight concrete filled steel decking, the decking is assumed to run perpendicular to the girders resulting in lower values of moments of inertia. A typical

composite section based on effective slab width and thickness as recommended by AISC is shown in Figure 3.5.5. In all but the top stories, floor slabs consist of lightweight concrete filled steel decking where the increase in girder moments of inertia ranged from 74% to 91% by including composite action. In the top three stories, girder moments of inertia increased from 79% to 180% where 5 inch and 8 inch thick reinforced concrete floor slabs are used. Mass values are the same as those used for Model 1.

#### Model 4

This model is formulated to account for the three-dimensional effects of the four coupled exterior planar frames of the steel tower portion of the building. The model incorporates compatibility of the orthogonal exterior frames by including the cantilevered girders which join the frames at the four corners of the building. In all, 32 column lines and 32 bays are needed to define this model. Since Model 4 is three-dimensional, translational and torsional modes of vibration are determined. The lumped mass values at each floor are based on the story weights used in Model 1. Torsional mass moments of inertia are based on the assumption that the mass is distributed evenly over each floor. The formulation of Model 4 includes the rigid joint zone effects and the composite girder section properties used in Model 3.

#### Model 5

The main objective in the formulation of Model 5 is to account for the stiffening effect of the core frame on the steel tower. This model is formulated by adding the core columns and beams in a separate frame which is linked to the rigid floor diaphragms at each floor level. The beam column connections are assumed to have full moment resistance capacity. The core frame model includes flexurally rigid joint zones and nonstructural slab-girder interaction. The core model consists of 21 column lines and 27 bays. Also incorporated in Model 5

is a reduction in floor weights used for mass calculation. The 20 psf partition load required by UBC and the 10% live load in the lower portion of the tower are believed to overestimate the actual weight of the building during testing. Therefore, the 10% live load and 15 psf were subtracted from the floor loads used in the first four models. The new story weights used for this model are shown in Table 3.5.1.

As a sidelight to Model 5, a separate model was formulated including the story weight reduction but omitting the core frame. Analysis was performed on this model in order to evaluate the influence of the core frame alone on the dynamic properties of the building.

#### Model 6

Model 6 is formulated to account for the effects of the reinforced concrete pedestal on the dynamic behavior of the building. In this model, the 2 foot thick heavily reinforced and post-tensioned concrete floor slab is assumed to be infinitely rigid both in-plane and out-of-plane. Below the 12th floor, all exterior and core frame members are discontinued and only a single column line at the center of the building extends downward to a fully restrained base at the first floor. To obtain the shear, flexural, and torsional properties of this equivalent column, a SAP-IV finite element model of the pedestal was formulated. In the SAP model plane stress finite elements were used to represent the walls and floor slabs of the pedestal. The finite element model of the pedestal is shown in Figure 3.5.6. Static and dynamic analyses of the SAP model were performed to establish approximate properties for the single equivalent column used to represent the pedestal base in the ETABS model. The exterior and core frame modeling above the 12th floor is identical to that in Model 5. The lumped mass values at each floor level of the pedestal are based on dead load calculations supplied by the structural designer. Torsional mass moments of inertia for the pedestal are based on the

assumption that the mass is evenly distributed over each floor. The weight values used for calculation of mass properties of the pedestal are shown in Table 3.5.1.

#### Model 7

The objective in the formulation of Model 7 is to account for the potential overturning flexibility of the soil underlying the building's foundation. An elastic modulus of subgrade reaction ranging from 80 to 320 lb/in<sup>3</sup> was indicated from soils data as provided by the design engineers. Using these soil stiffnesses together with the assumption that the foundation slab is infinitely rigid, two analyses were performed incorporating base rotational flexibility. In order to model this rotational flexibility with ETABS, an extra story is added at the base of the building and a dummy column is inserted. The top of this dummy column is laterally restrained with stiff translational springs. The rotational stiffness properties of the dummy column correspond to the subgrade soil stiffnesses given above acting over the 106 foot square foundation slab.

#### **3.5.4 Comparison of Analytical and Experimental Dynamic Properties**

In Figures 3.5.7 and 3.5.8, respectively, the first four N-S translational modes and the first four torsional modes from Models 4 and 6 are shown. Only slight changes in mode shapes were noted among the seven different models analyzed. Therefore, only two of the models are presented which show the differences in mode shapes with (Model 4) and without (Model 6) consideration of the pedestal base. As can be seen from the figures, the analytical models show good correlation with the experimental mode shapes. In general, both nodes and antinodes are predicted with reasonably good accuracy. The relative rigidity of the pedestal base is seen in the analytical modes of Model 6. However, these results tend to underestimate the

relative deflection of this portion of the structure. For this reason, Model 7 was formulated to determine the degree to which rotational flexibility of the foundation may contribute to the larger pedestal deflections noted in the experimental results. For the subgrade modulus values provided by the engineer, however, foundation flexibility was found to have an insignificant effect on the analytical mode shapes.

In Table 3.5.2, analytical periods for the seven models are compared with experimental values. Model 7 results are not shown separately in this table since the foundation flexibility included in this model resulted in no change from Model 6 periods.

Model 1 is the most flexible idealization consisting of the bare planar exterior frame. The fundamental translational period of this model is 7.16 sec. which is 61.1% greater than the experimentally determined period of 4.44 sec. (Table 3.5.2). The higher translational modes show greater variations ranging from 74.9% to 97.8% greater than the experimental values. Clearly, this model is much more flexible than the actual structure.

In Model 2, the inclusion of rigid joint zone effects improves period correlation significantly. The fundamental analytical period is reduced to 6.18 seconds. As seen in Table 3.5.3, this change is primarily due to the reduced effective length of columns which, for the first mode, increases the stiffness by 25%. The reduced girder effective lengths also are significant contributing a 9% stiffness increase. However, the periods for this model are still between 39.1% and 66.0% higher than the experimental values (Table 3.5.2).

In Model 3, the effects of composite slab-girder interaction are incorporated in the planar frame model yielding a fundamental period of 5.59 seconds. This modeling aspect causes a 30% stiffness increase in the first mode (Table 3.5.3). In most practical applications, this model would be considered an accurate representation of the building

since it incorporates the important modeling aspects effecting the primary lateral force resisting system. However, as is seen from Table 3.5.2, the analytical period values for this model range from 25.8% to 48.2% greater than the experimental values indicating that this model is still significantly more flexible than the actual structure.

The Model 4 results show that consideration of three dimensional frame behavior further reduces period values. The fundamental period is reduced to 5.00 sec. being 12.4% greater than the experimental value. Inclusion of this modeling aspect increases the fundamental mode stiffness by 41% of the Model 1 stiffness. However, higher modes are stiffened to a lesser degree (9% to 20%) since the orthogonal frames brought into play primarily help to resist story overturning moments which are most significant in the fundamental mode. Model 4 is the first model which produces torsional periods. As can be seen from Table 3.5.2, the first analytical torsional period of 2.65 sec. for this model is virtually identical with the experimental value being only 0.3% less. The higher torsional periods do not show as close correlation being greater than the experimental values by 7.3% to 12.8%.

In Model 5, the inclusion of the core frame and slight reductions in mass values cause a further lowering of periods. The fundamental period for this model is 4.27 sec. which is 3.8% less than the experimental value. As seen in Table 3.5.3, inclusion of the core frame increases the fundamental mode stiffness by 33% of the Model 1 stiffness. Higher modes show greater stiffness increases ranging from 38% to 48%. The total stiffness increase resulting from the various modeling aspects included up to Model 5 is between 126% and 140% for the six modes shown in Table 3.5.3.

In Model 6, the addition of the pedestal base increases all periods slightly. The fundamental period of 4.35 sec. is only 2.2%

less than the 4.44 sec. experimental value. Higher analytical periods show greater variations with values ranging from 6.4% to 18.7% greater than experimental results. The fundamental torsional period for this model is 2.46 sec. which is 7.1% less than the experimental value of 2.65 sec. The higher torsional periods show excellent correlation with the analytical values being within 3.1% of experimental.

The inclusion of foundation flexibility in Model 7 has negligible effect on the dynamic properties resulting in periods and mode shapes which are virtually identical to Model 6. Therefore, Model 7 results are not shown in the tables and figures at the end of this section.

Overall, good correlation of the analytical and experimental dynamic properties of the Rainer Tower building is achieved by accounting for various stiffening effects including rigid joint zones, composite slab-girder interaction, three-dimensional frame action, the core framing system and the concrete pedestal base. The influence of foundation flexibility is negligibly small for the soil modulus values provided by the design engineers. Model 6 is able to predict the first six translational and four translational periods and mode shapes with good accuracy and provides the best analytical representation of the small amplitude dynamic properties.

For comparison with analytical and experimental values, the UBC and ATC period values as calculated from codebook empirical formulae are also shown in Table 3.5.2. Assuming the pedestal base is rigid, but UBC and ATC predict a fundamental translational period of 3.1 sec. which is 30.2% less than the experimental value indicating that the codebook formulae do not yield good estimates of fundamental period for this building.

### **3.5.5 Influence of Modeling Approach on Design Quantities**

In this section, results of response spectrum dynamic analysis for each of Models 1, 3, 4, 5 and 6 are presented to demonstrate the

influence of the different modeling approaches on gross design quantities. The Newmark response spectrum scaled to .05g peak ground acceleration is used which corresponds to the ATC recommended reduced spectrum peak acceleration level. Six translational modes are used in the analyses of Models 1 to 5. However, in Model 6, twelve translational modes are used in order to capture the response of the stiff pedestal base.

In Figure 3.5.9(a), predicted peak story shear envelopes for the various models are plotted over the height of the building. Note that the pedestal base is included only in Model 6 and, therefore, response in this portion of the structure is not shown for Models 1 to 5. As can be seen from the differences between Model 1 and Model 3 response, significant increases in story shears result from inclusion of rigid joint zones and composite girder behavior in the planar frame idealization. In Table 3.5.4, the variations in story shear at the 13th story (the first story above the pedestal base) are shown for the different models along with percent increases in shear with respect to Model 1. As can be seen from this table, the 13th story shear increases from 515k in Model 1 to 708k in Model 3 (a 37.5% increase) due to the shorter periods of Model 3 which cause increases in modal spectral amplitudes. The three dimensional frame modeling included in Model 4, increases the 13th story shear to 775k; and, addition of the core frame in Model 5 increases this value to 817k. In Model 6, inclusion of the pedestal base further increases story shears over the height of the building despite the fact that periods are slightly increased in this model (as seen in Table 3.5.2). This result is caused by the fact that the higher (2nd and above) mode shapes change enough to offset the decreased spectral amplitudes of this model with slightly larger modal participation factors. Thus, the 13th story shear for Model 6 is 845k, which is 64.1% greater than the Model 1 shear value of 515k. An important aspect of the building's behavior

is shown by the sudden increases in shear in Model 6 below the 13th story. This result reflects the greater stiffness and mass that is present in the concrete pedestal. The shear at the base of the pedestal is 2280k, about 2.7 times greater than the 845k shear at the base of the office tower.

In Figure 3.5.9(b), peak story overturning moments are shown for the different models. From this figure, it can be seen that the changes in overturning moment response among the different models are significantly greater than those observed in shear response. This is due to the fact that, whereas the shear response has substantial contributions from higher modes, the overturning response is dominated by the fundamental mode whose period lies on a portion of the Newmark spectrum where spectral amplitudes vary most rapidly (in proportion to  $1/T^2$ ). Thus as periods decrease in the more refined models, the overturning response increases more rapidly than does the shear response. This is seen in Table 3.5.4 where the overturning moment at the base of the 13th story increases from  $895 \times 10^3$  k in. in Model 1 to  $2050 \times 10^3$  k in. in Model 6 constituting a 129% increase in overturning compared to the 64% increase observed for shear.

Peak story deflections are shown in Figure 3.5.10(a). As can be seen from this figure, smaller variations in total deflection than in shear or overturning result as the models become progressively more stiff. Peak roof deflections for the different models are shown in Table 3.5.4. From this table, it is seen that the 3.83 inch roof deflection of Model 1 decreases to 3.63 inches in Model 6, a reduction of only 5.2% despite the 140% total modal stiffness increase (Table 3.5.3). This relatively small change in deflection is explained by the fact that deflection response is dominated by the fundamental mode and that the fundamental period lies on the portion of the Newmark spectrum where spectral amplitude varies as  $1/T^2$ . As shown in section 2.5, increases in stiffness modeling will result in no change in

deflection response of modes whose periods lie on this portion of the Newmark spectrum (see Equation 2.18, Figure 2.13(b) where  $p = 2$ ). Therefore, although the models become substantially stiffer, only small changes in deflection response are noted for this building and these changes are caused primarily by the participation of the higher modes whose periods lie on a different zone of the spectrum.

In Figure 3.5.10(b), peak story drifts are shown for the different models. Irregularities in drift values near the 25th and 40th levels result from the taller heights of these stories. It is noted that the drifts show somewhat greater changes with modeling variations than do deflections. For instance, as shown in Table 3.5.4, the 0.153 inch 28th story drift of Model 1 is reduced to 0.136 inches in Model 6, and 11.1% decrease compared to the corresponding 5.2% roof deflection decrease. This results from the fact that drifts are more influenced by the higher modes than are deflections. Another notable result seen in Figure 3.5.10(b) is that the drifts are more greatly reduced in the upper than in the lower stories. This results from the fact that, whereas the exterior frame (the primary lateral force resisting system) has substantial decreases in lateral story stiffness with increasing height, the secondary modeling aspects considered have a more uniform stiffness over the height. Thus, greater reductions in drift of the upper stories occur as the models are refined. It is also noted that the drifts of the pedestal base shown for Model 6 typify shear beam type deflection behavior with little cantilever effect.

A better understanding of the dynamic behavior of the Rainer Tower building can be gained by studying the modal contributions to the gross design quantities. Relative modal contributions to story shears, overturning moments, deflections and drifts over the full height of the building are shown in Figure 3.5.11 for Model 6. In

Figure 3.5.11(a), it is seen that higher modes contribute most significantly to shear response in the top several stories of the office tower and in the pedestal base. For this model, the 12th mode which has a period of 0.20 sec. dominates the shear response in the pedestal with the 5th through 11th modes also contributing significantly. Although the fundamental mode dominates the shear response over most of the height of the steel office tower, it contributes little to the total peak shear response of the pedestal. Thus for this model to accurately represent the shear forces in the pedestal, at least 12 modes must be considered in the analysis. In Figure 3.5.11(b), the modal contributions to overturning are shown. Unlike that for shear, the fundamental mode dominates the overturning response in the pedestal with the 12th mode having a significant but reduced contribution. Modal contributions to deflection are shown in Figure 3.5.11(c) where it is seen that the fundamental mode dominates deflection response in the office tower but the 12th mode contributes most significantly to the pedestal's deflections. In Figure 3.5.11(d), modal contributions for drift show similar trends as those for shear indicating that drifts are controlled primarily by those modes inducing the greatest shear forces at a given story.

In summary, the modeling of rigid joint zones, composite slab-girder interaction, three-dimensional frame compatibility and the core framing system significantly influence the analytical response of the building and lead to progressively higher values of story shears and overturning moments and somewhat lower values of deflections and drifts. Because of the rigidity of the pedestal base, its inclusion in the analytical model has only minor influence on the response of the office tower above. It is seen that higher modes contribute significantly to the total response especially in the pedestal base for which 12 translational modes must be included to capture the participation of the pedestal's mass in the dynamic analysis.

### 3.5.6 Comparison of Dynamic Analyses and Code Equivalent Static Procedures

In this section, a comparison is made of the Ranier Tower's response to different recommended static and dynamic loading approaches (see section 3.1.2 for further description). The ATC and Newmark spectra are used as ground motion inputs for the dynamic analyses. Both of these spectra are based on the ATC recommended 0.05g reduced peak ground acceleration for moment resisting frame construction. The ATC and UBC guidelines are used for the equivalent static analyses. The UBC equivalent spectrum is multiplied by 1.278 to correspond to elastic limit design level forces. In Figure 3.1.1, the ATC, Newmark and scaled UBC spectra are shown for comparison. Model 6 is used as a basis for the comparative analysis since this model best represents the experimentally observed dynamic properties.

Comparing the dynamic analyses, it can be seen from Figure 3.5.12(a) that the Newmark and ATC spectra yield virtually identical dynamic base shear values of 2280 and 2270k, respectively. However, the distributions of story shear over the height differ substantially. The ATC spectrum specifies a significantly greater spectral amplitude than Newmark at the 4.35 sec. fundamental period thereby resulting in higher shears in the steel office tower whose response is dominated by the fundamental mode. The Newmark spectrum, however, specifies larger amplitudes than does ATC for the higher modes which dominate the pedestal response and, consequently, leads to greater lateral inertial forces being induced in the pedestal by the Newmark spectrum. Since overturning response is dominated by the fundamental mode (see Figure 3.5.11(b)), the ATC spectrum gives larger overturning moments than Newmark throughout the structure as seen in Figure 3.5.12(b); the ATC base overturning is  $6600 \times 10^3$  k in. which is 57.5% greater than the Newmark value of  $4190 \times 10^3$  k in. (see Table 3.5.5). Since deflections and drifts are also dominated by the fundamental mode, the

ATC spectrum yields significantly greater response for these quantities as well as seen in Figures 3.5.13(a) and (b). As shown in Table 3.5.5, the ATC peak roof deflection is 7.15 inches or 97% greater than the Newmark result of 3.63 inches; and, the ATC 28th story drift is 0.256 inches or 86.9% greater than the Newmark value of 0.137.

The ATC and UBC equivalent static loads are determined using both the fundamental period of 3.1 sec. calculated from codebook formulae (both ATC and UBC formulae happen to lead to the same 3.1 sec period value for this building based on the height of the steel tower only) and the Model 6 fundamental analytical period of 4.35 sec. Results from these equivalent static analyses are shown in Figure 3.5.12 and 3.5.13. The ATC and UBC force distributions are based on the respective codebook procedures with no special consideration made for the pedestal's relatively large stiffness. As can be seen from these figures, substantial variations in the static responses result from use of the different fundamental periods. For the UBC analyses, use of the 4.35 sec. analytical period (same as experimental) results in all response quantities being reduced from those determined using the codebook period of 3.1 sec. (e.g. base shear decreases from 3987k to 3348k as shown in Table 3.5.5). The ATC static analyses show a 20.9% decrease in response quantities resulting from the same period shift (e.g. base shear decreases from 3450k to 2730k, Table 3.5.5). Note that the UBC static forces and deflections are significantly larger than the corresponding ATC static values due to the larger spectral amplitudes specified by UBC; for example, using the 4.35 sec. fundamental period, the ATC base shear is 2730k or 18.5% less than the 3384k UBC value (Table 3.5.5).

Aside from comparison of response magnitudes, it is of interest to compare the distributions of response for the various dynamic and equivalent static loading approaches. For this purpose, the shear,

overturning, deflection and drift responses over the height of the building normalized with respect to base shear are shown in Figures 3.5.14 and 3.5.15 where it is seen that wide variations in response distribution exist. In Figure 3.5.14(a), it can be seen that, for a given base shear, the ATC dynamic results show much higher relative shears over most of the building than do the Newmark results. As previously mentioned, this results from the difference in the ATC and Newmark spectra shapes whereby the greater amplification of the fundamental mode in the ATC spectrum curve causes larger relative inertial forces to be induced in the steel office tower portion of the structure. The UBC and ATC equivalent static force distributions show further variations from the dynamic distributions resulting in shears in the office tower which are as much as 2 to 3 times greater than the Newmark values. These large discrepancies result from the fact that the equivalent static methods of force distribution do not account for the discontinuities in mode shape caused by the large relative stiffness of the pedestal base. It should be noted that the UBC and ATC codes warn about applying the standard force distribution procedures for buildings with stiffness discontinuities; and, Figure 3.5.24(a) shows the force distribution errors that can result from ignoring this aspect. Comparing the UBC and ATC static shear distributions, UBC gives larger relative shears in the upper few stories of the building due to the required top load. However, ATC yields larger relative shears in lower levels due to the curved (cantilever type) fundamental mode shape assumed for equivalent static force distribution.

The normalized distributions of overturning moment, deflection and drift show results consistent with the shear distributions whereby Newmark dynamic gives somewhat larger relative response magnitude and the UBC and ATC equivalent static approaches lead to the largest relative responses. Again comparing the UBC and ATC static results,

note that the ATC normalized overturning is significantly less than that of UBC due to the ATC allowed overturning reduction factor (Figure 3.5.14(b)). Also note that the UBC story drifts in the upper few stories are about 1.5 to 3 times greater than the ATC drifts due to the UBC required top load.

In summary, large differences in both the magnitude and distribution of seismic response of the Ranier Tower result for the different dynamic and equivalent static loading approaches. The severe stiffness discontinuity existing in this building make the predicted dynamic response sensitive to spectrum shape and also invalidates the standard equivalent static force distribution procedures. The use of code formulae yields relatively poor estimates of fundamental period and, thus, also leads to significant discrepancies in equivalent static response prediction.

### **3.5.7 Comparison of Code Design Forces with Dynamic Forces Induced by Actual Earthquake Spectra**

The UBC story shears and overturning moments used for the seismic design of the Ranier Tower building were provided by the design engineers. These code forces, factored by 1.278 to bring the UBC working stress loads up to the elastic limit level are shown in Figure 3.5.16. These values are based on separate lateral load calculations for the steel tower and the concrete pedestal with assumed fundamental periods of 3.1 sec. and 0.7 sec., respectively. (Note that the code forces are plotted using the UBC moment frame K factor of 0.67 over the whole building to give an elastic force distribution that is comparable to dynamic analyses results. In the actual design, a K factor of 1.33 was used for the concrete pedestal.) Also, shown in the figure are the predicted analytical elastic responses of Model 6 to the Taft (1952) and El Centro (1940) earthquakes assuming 5% of critical damping (see Figure 3.1.2 for a plot of these spectra).

In Figure 3.5.16(a), it can be seen that the shear distributions

induced by the actual earthquakes differ significantly from the UBC design shear envelope. It is seen that, whereas the shear forces between the 12th and 31st stories resulting from the Taft earthquake are somewhat less than or equal to the factored UBC forces. However, the Taft shear forces above the 35th story and below the 12th substantially exceed the factored UBC forces. The response to the El Centro earthquake shows the same trend as that of Taft but is somewhat larger in magnitude. It is in the portions of the structure where higher modes are most important to response that the actual spectra give much greater relative shear magnitudes. The reason for these differences are: (1) the UBC top load was not required at the time this building was designed and thus, higher mode effects are not adequately captured in the upper stories; (2) compared to the El Centro and Taft spectra, the UBC spectra tends to underestimate spectral amplitudes in the shorter period ranges where higher modal periods lie (see Figure 3.1.2); and (3) the fundamental pedestal period of 0.7 assumed for the UBC pedestal force calculations is significantly higher than the periods of the modes in which the pedestal mass was most active and, thus, results in lower spectral amplitudes and induced inertial forces for this portion of the structure. The result is that, for the Taft record, top story shears are about 2 to 3 times greater than the factored UBC values and the base shear in the pedestal is about 1.6 times the UBC value; and for the El Centro record, top story shears range from 3 to 6 times and the base shear in the pedestal is about 2.5 times greater than the UBC values.

Figure 3.5.16 shows that like the shear response, the overturning moment responses in the upper portion of the structure resulting from the actual earthquake spectra are much larger than those for UBC. However, below the 25th floor, the UBC overturning values are significantly greater than the Taft values and are similar in

magnitude to the El Centro values. This results from the conservatism in overturning moment determination inherent to the UBC equivalent static procedure for lower portions of multistory buildings.

### 3.5.8 Summary

The results presented in the previous sections lead to the following observations regarding the behavior and analysis of the Ranier Tower building:

- (1) Rational development of the numerical models leads to good agreement between the dynamic properties resulting from computer analysis and the dynamic properties determined from small amplitude tests. Model 6 which includes various secondary structural modeling aspects achieves good correlation of the periods and mode shapes for several translational and torsional modes of vibration (Figures 3.5.7, 3.5.8 and Table 3.5.2).
- (2) Analysis indicates that various structural modeling aspects significantly influence the small amplitude dynamic behavior of the building including slab-girder interaction, rigid joint zone effects, three-dimensional frame behavior, and core frame modeling. Consideration of these effects increases the stiffness of the office tower portion of the structure by approximately 140% of the stiffness of the planar exterior steel frames acting alone. Using the Newmark response spectrum. These modeling refinements lead to increases of 64% in shear and 129% in overturning at the base of the office tower (Figure 3.5.9 and Table 3.5.4).
- (3) The finite element idealization used to model the concrete pedestal base appears to give an overly stiff representation of this portion of the structure (Figures 3.5.7 and 3.5.8). This is probably due to the coarseness of the finite element mesh of the pedestal, the overestimation of the shear

modulus of the concrete and the neglect of cracking in the concrete. However, since inclusion of the pedestal has only minor influence on the response of the steel tower portion of the structure, this modeling inaccuracy did not appreciably affect overall response.

- (4) In dynamic analysis, the higher modes (2nd and above) contribute significantly to response especially in the upper stories and in the pedestal base (Figure 3.5.11). Omission of higher modes may lead to serious underestimation of induced forces in these portions of the building.
- (5) For this building, dynamic analysis shows that the ATC response spectrum yields much greater response values than the 0.05g Newmark spectrum over most of the structure (approximately 65% greater shear and 100% greater overturning moment at the base of the office tower). These differences are due to the relative conservatism of the ATC spectrum in the longer period range.
- (6) Experimental and refined analytical fundamental periods are about 40% greater than the values predicted by UBC and ATC code formulae (Table 3.5.2). Use of codebook periods lead to substantially larger (19% for UBC, 26% for ATC) equivalent static responses than does use of the analytical periods (Figures 3.5.12, 3.5.13).
- (7) Comparing the UBC and ATC equivalent static approaches for this building, UBC leads to larger applied shears and overturning moments than ATC for the same fundamental period. Shear force and overturning moment differences are larger in the upper stories due to the UBC required top load. In the lower stories, UBC overturning moments are larger due to the overturning reduction allowed by ATC.
- (8) Regarding the distribution of response, application of the

UBC or ATC equivalent static methods without special consideration for the severe stiffness discontinuity caused by the pedestal base leads to gross overestimation of the relative force and deflection responses in the steel tower portion of this building. It is also seen that, in dynamic analysis, the distribution of response may vary substantially for different response spectra due to the significance of several modes which span a wide range of natural periods (Figures 3.5.14 and 3.5.15).

- (9) Based on the UBC seismic loads used by the design engineers, predicted responses of the analytical model indicate that dynamic loads induced by both the Taft and El Centro earthquake spectra may far exceed UBC levels in the top stories of the office tower and in the pedestal base. However, the forces induced in the lower two-thirds of the office tower are closer in magnitude to the UBC values (Figure 3.5.16).

Table 3.5.1: Dead Load Weights Used for the Analytical Models

Floor	Models 1,2,3,4		Models 5,6,7	
	Weight (kips)	psf	Weight (kips)	psf
Roof	2996	166	2725	151
42	3328	184	3031	168
41	3955	219	3658	203
40	2133	118	1838	102
39	2070	115	1780	99
38	2070	115	1780	99
37	2074	115	1782	99
36	2074	115	1782	99
35	2088	116	1792	99
34	2088	116	1792	99
33	2101	116	1806	100
32	2110	117	1812	100
31	2129	118	1823	101
30	2129	118	1823	101
29	2147	119	1837	102
28	2147	119	1837	102
27	2309	128	1994	110
26	2309	128	1994	110
25	2400	133	1867	103
24	2484	138	1943	108
23	2409	133	1867	103
22	2409	133	1867	103
21	2416	134	1869	104
20	2416	134	1869	104
19	2430	135	1878	104
18	2430	135	1878	104
17	2444	135	1887	105
16	2444	135	1887	105
15	2449	136	1887	105
14	2449	136	1887	105
13	2461	136	1898	105
<b>TOTAL (w/o base)</b>	<b>73898</b>		<b>61370</b>	
12			7560	419
10			6073	462
8			5027	561
6			6564	1128
4			6454	1109
2			8737	1871
1			4516	967
<b>TOTAL (w/base)</b>			<b>106301</b>	

Table 3.5.2: Experimental vs. Analytical Natural Periods

Direction	Mode No.	Exp. Period(sec)	Model 1		Model 2		Model 3		Model 4		Model 5		Model 6	
			Period	%										
N-S	1	4.44	7.16	+61.1	6.18	+39.1	5.59	+25.8	5.00	+12.4	4.27	-3.8	4.35	-2.2
	2	1.39	2.63	+89.3	2.23	+60.3	2.00	+43.9	1.86	+34.2	1.56	+12.0	1.56	+12.6
	3	0.76	1.50	+97.8	1.26	+66.0	1.12	+48.2	1.08	+42.2	0.89	+17.9	0.90	+18.7
	4	0.55	1.06	+91.7	0.88	+60.1	0.79	+43.3	0.77	+38.6	0.63	+14.9	0.64	+15.8
	5	0.47	0.82	+76.0	0.68	+46.5	0.61	+31.3	0.60	+27.4	0.49	+5.8	0.50	+6.4
	6	0.38	0.67	+74.9	0.56	+45.5	0.50	+31.4	0.49	+27.5	0.41	+6.3	0.41	+6.8
Torsion	1	2.65						2.65	-0.3	2.45	-7.8	2.46	-7.1	
	2	0.95						1.02	+7.3	0.93	-2.4	0.93	-1.6	
	3	0.54						0.60	+11.9	0.55	+1.5	0.55	+2.4	
	4	0.38						0.43	+12.8	0.39	+2.1	0.39	+3.1	

UBC*		ATC*	
Period	%	Period	%
3.10	-30.2	3.10	-30.2

% = percent variation from experimental period.

\*Code periods calculated based on 50-story height as follows:

UBC (eqn. 12-3B):  $T = 0.10 N = 0.10 \times 3.1 = 3.1$  sec.

ATC (eqn. 4-4):  $T = C_n h_n^{3/4} = .035 \times (393)^{3/4} = 3.1$  sec.

Table 3.5.3: Influence of Modeling Aspects on Modal Stiffnesses

Approximate Stiffness Increase with respect to Model 1							
Direction	Mode	Rigid Joint Zone		Slab-Girder Interaction	3-D Modeling	Core Framing	TOTAL (MODEL 5)
		Col.	Gird.				
N-S Trans	1	25%	9%	30%	41%	33%	138%
	2	28	11	34	26	41	140
	3	28	14	38	13	47	140
	4	29	16	35	11	48	139
	5	30	15	35	11	46	137
	6	30	13	36	9	38	126

Table 3.5.4: Influence of Modeling on Design Quantities

Design Quantity	Model 1		Model 2		Model 3		Model 4		Model 5		Model 6	
		%		%		%		%		%		%
13th story shear	515.	0.	600.	+16.5	708.	+37.5	775.	+50.5	817.	+58.6	845.	+64.1
13th story OIM ( $\times 10^3$ in-k)	895.	0.	1190	+33.0	1410	+57.5	1800	+101.	2110.	+136.	2050.	+129.
Roof deflection (in.)	3.83	0.	3.76	-1.8	3.79	-1.0	3.68	-3.9	3.63	-5.2	3.63	-5.2
28th story drift	0.153	0.	0.151	-1.3	0.144	5.9	0.141	-7.8	.135	-11.8	.136	-11.1

% = percent change from Model 1

Table 3.5.5: Comparison of Design Quantities for Dynamic and Equivalent Static Analyses

Design Quantity	Dynamic				Static							
	Newmark		ATC		ATC				UBC*			
	%		%		Codebook Period		Analytical Period		Codebook Period		Analytical Period	
					Period	%	Period	%	Period	%	Period	%
Fundamental Period (sec)	4.35	0.	4.35	0.	3.10	-28.7	4.35	0.	3.10	-28.7	4.35	0.
Base shear <sup>1</sup>	2280.	0.	2270.	-0.4	3450.	+51.3	2730.	19.7	3987	74.9	3348	46.8
Base OIM (x 10 <sup>3</sup> in-k) <sup>1</sup>	4190	0.	6600.	57.5	13300.	217.	10560	152.	18505	342.	15527	271.
Roof deflection (in.)	3.63	0.	7.15	97.0	19.1	426.	15.1	316.	22.6	522.	19.0	423.
28th story drift (in.)	.137	0.	.256	86.9	.661	383.	.524	283.	.684	291.	.574	319.

% = percent change from Newmark spectrum dynamic analysis.

\*UBC values are factored by 1.70/1.33 = 1.278 for correspondence with ATC elastic limit load levels.

<sup>1</sup>base shear and overturning values refer to base of concrete pedestal.

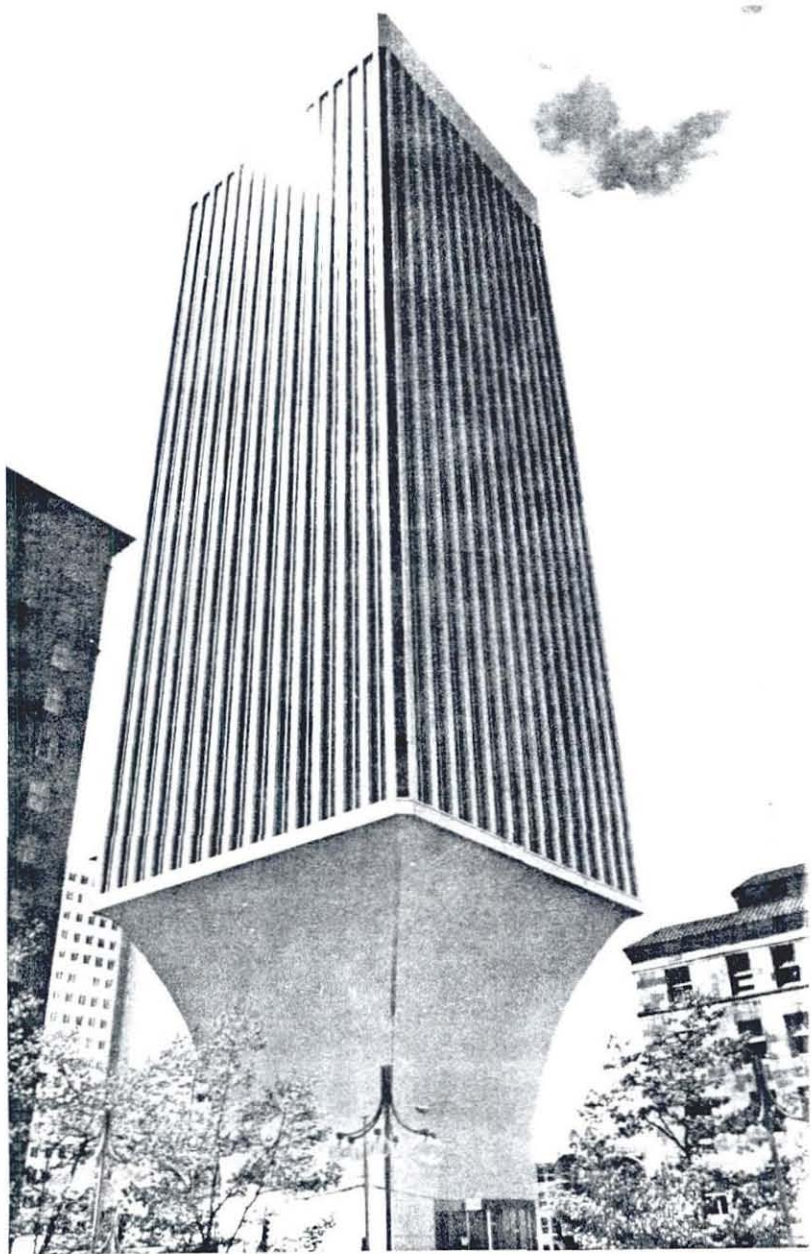
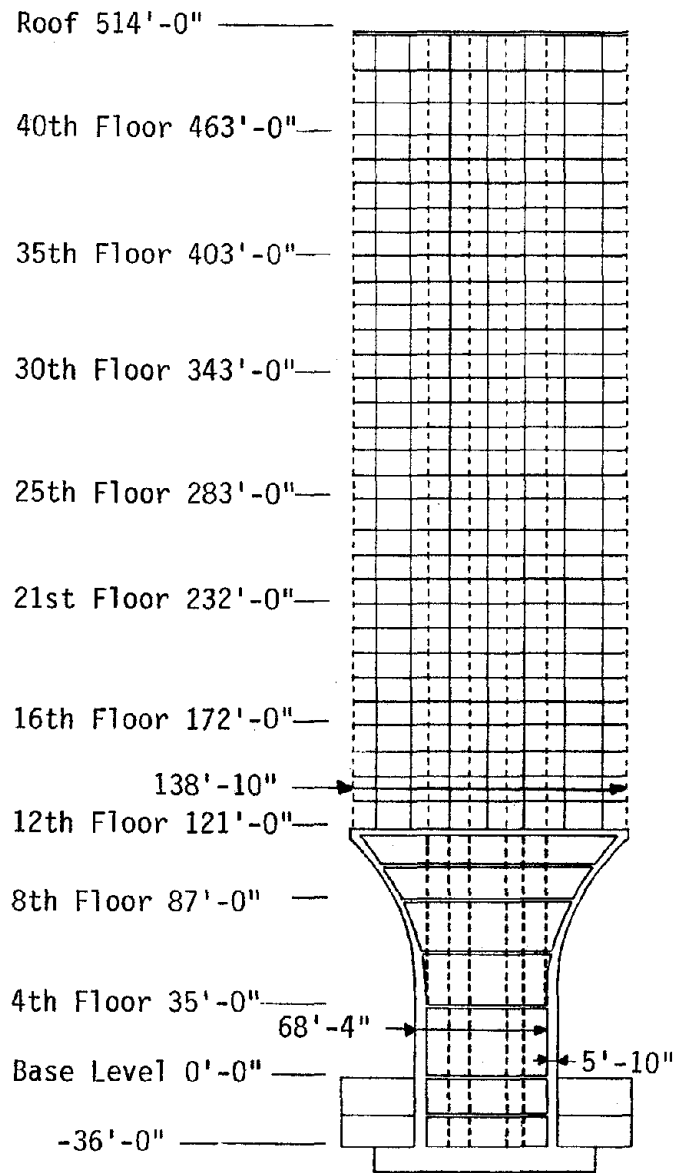
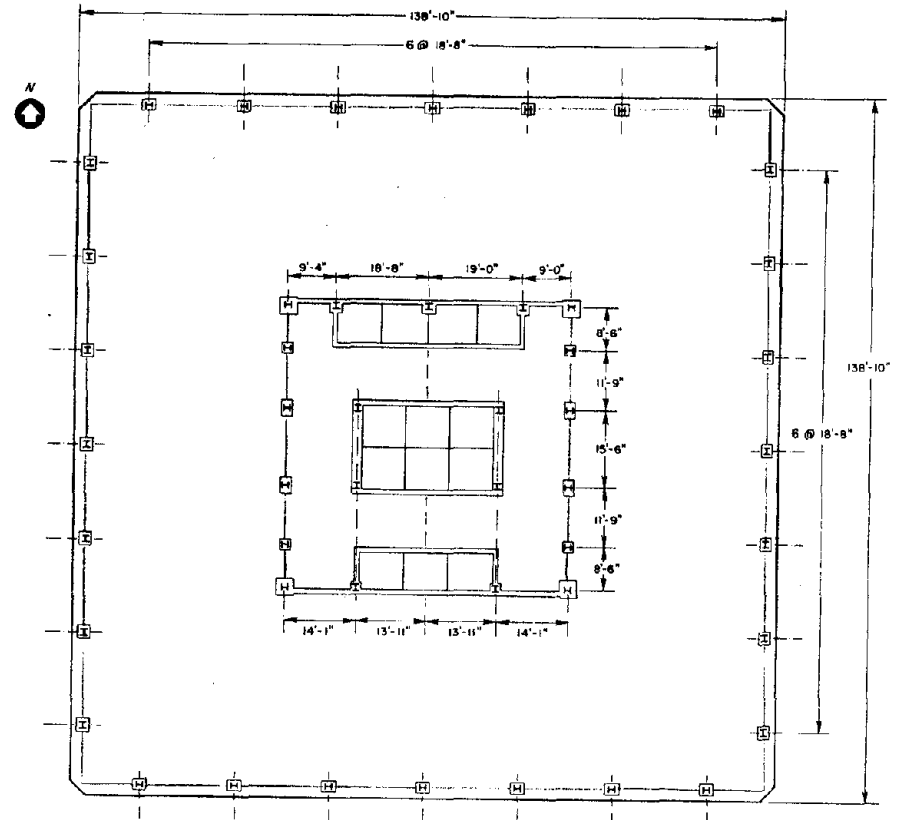


Figure 3.5.1: Ranier Tower Building  
Seattle, Washington



(a) East Elevation



(b) Plan

Figure 3.5.2: Elevation and Plan Views of Ranier Tower

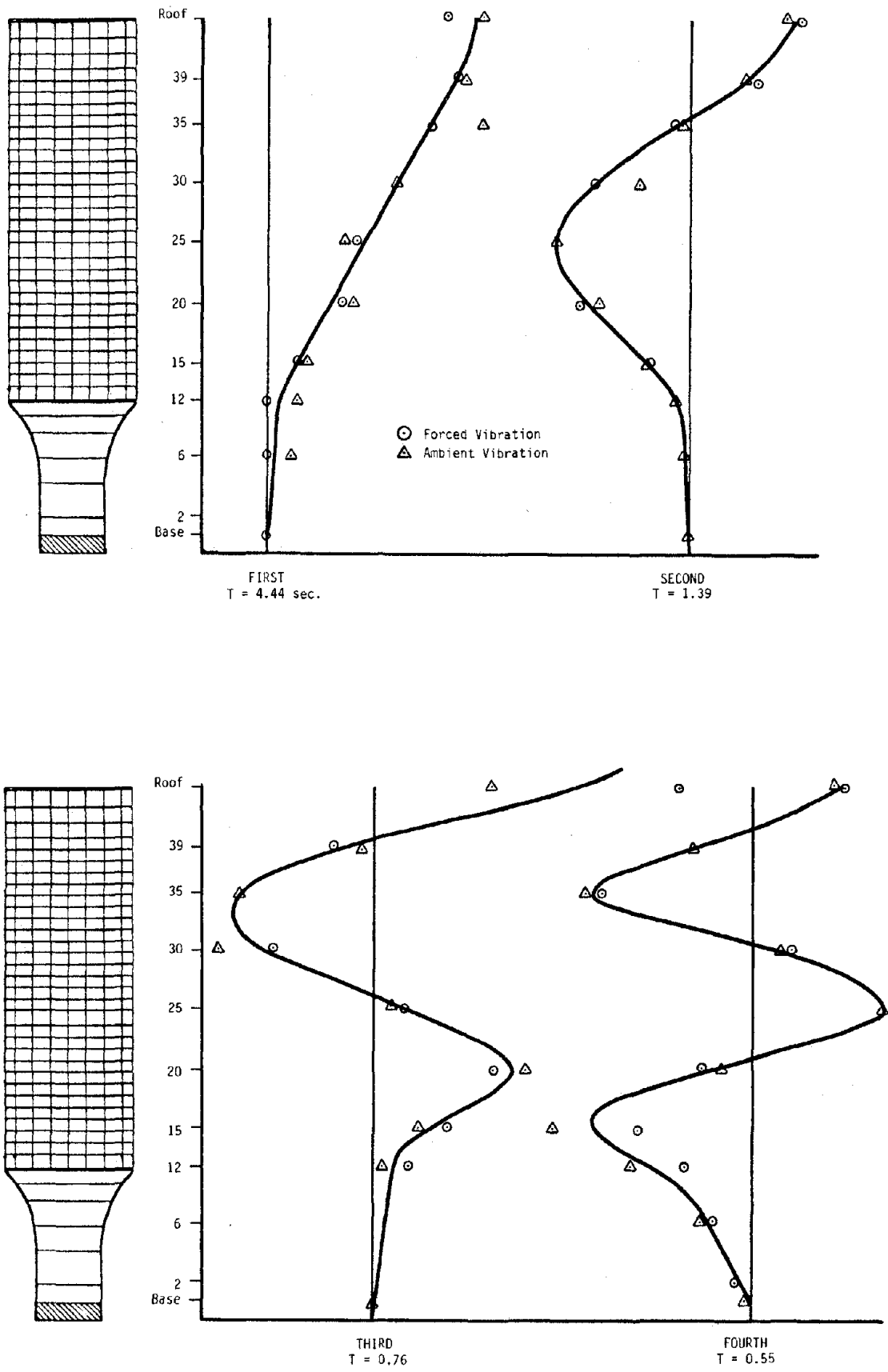


Figure 3.5.3: Experimental Translational Mode Shapes (N-S Direction)

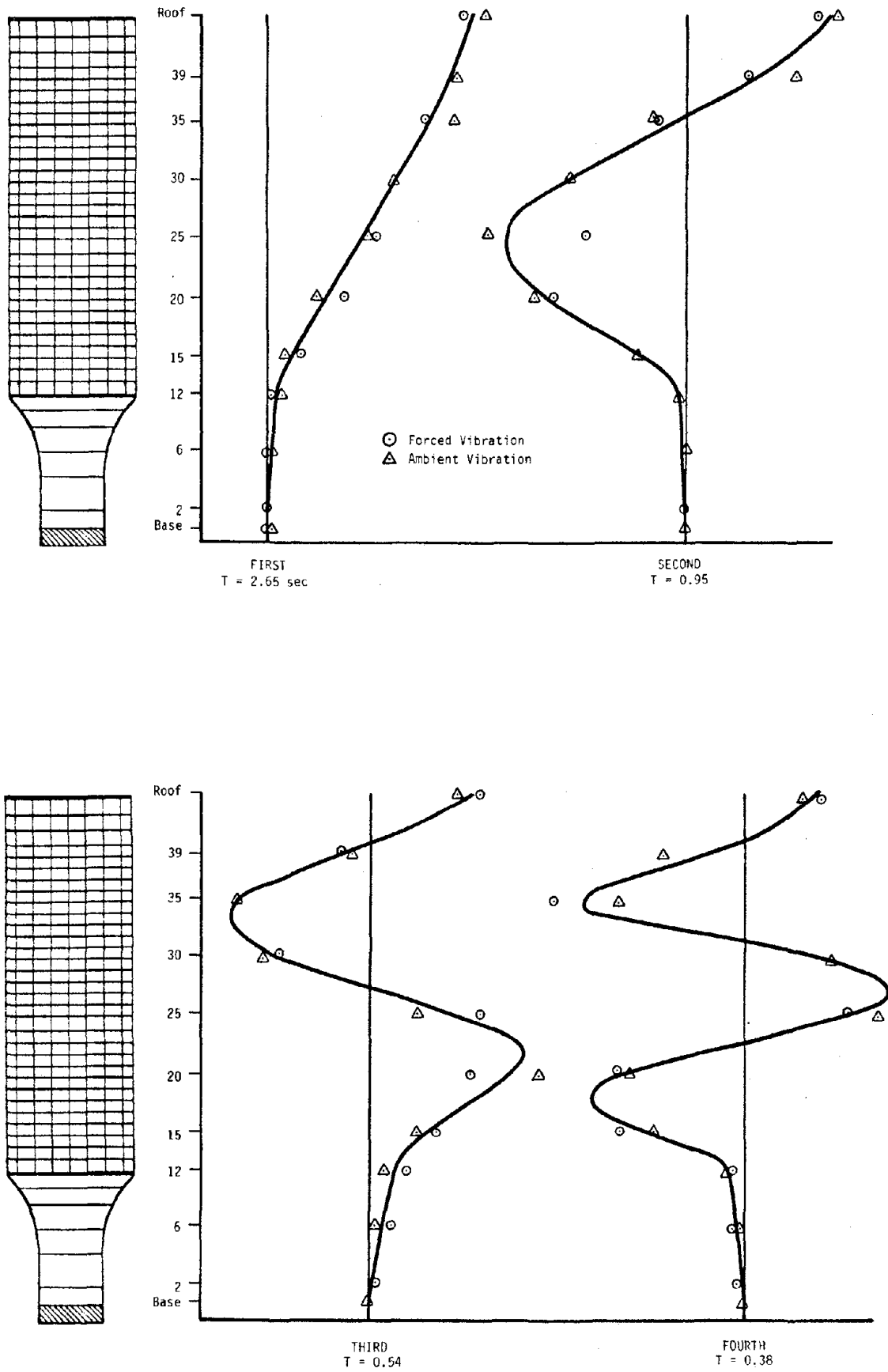


Figure 3.5.4: Experimental Torsional Mode Shapes

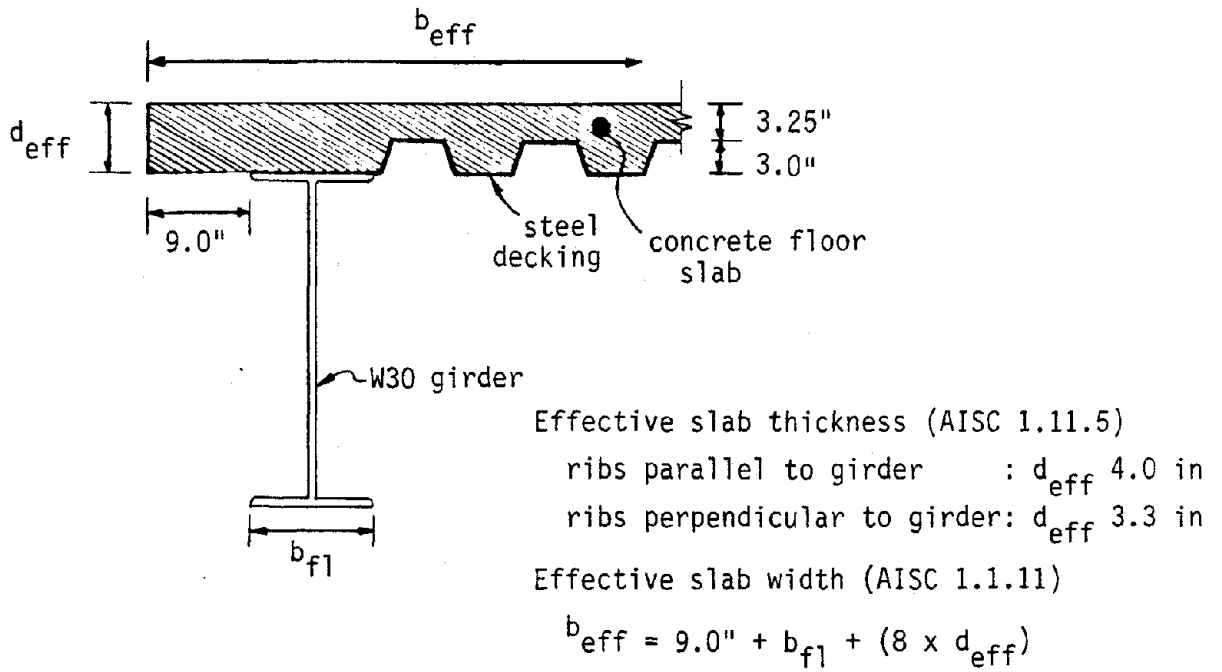


Figure 3.5.5: Modeling Approach for Slab-Girder Interaction

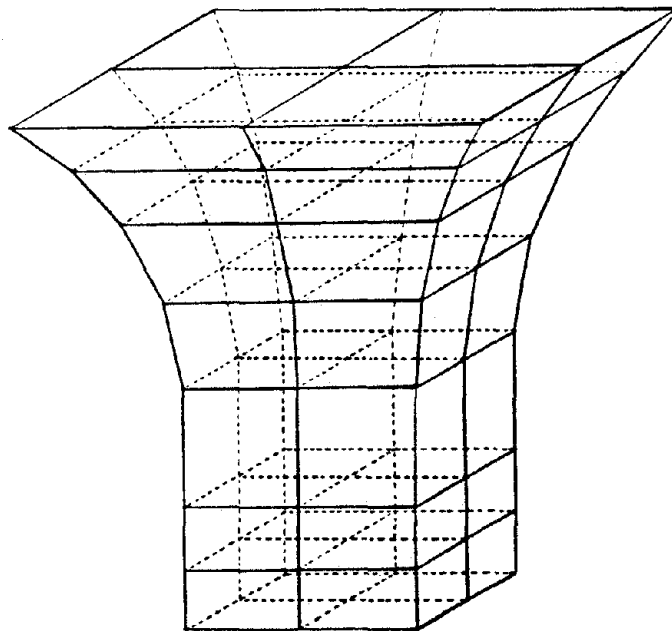


Figure 3.5.6: Schematic of Finite Element Model of Pedestal Base

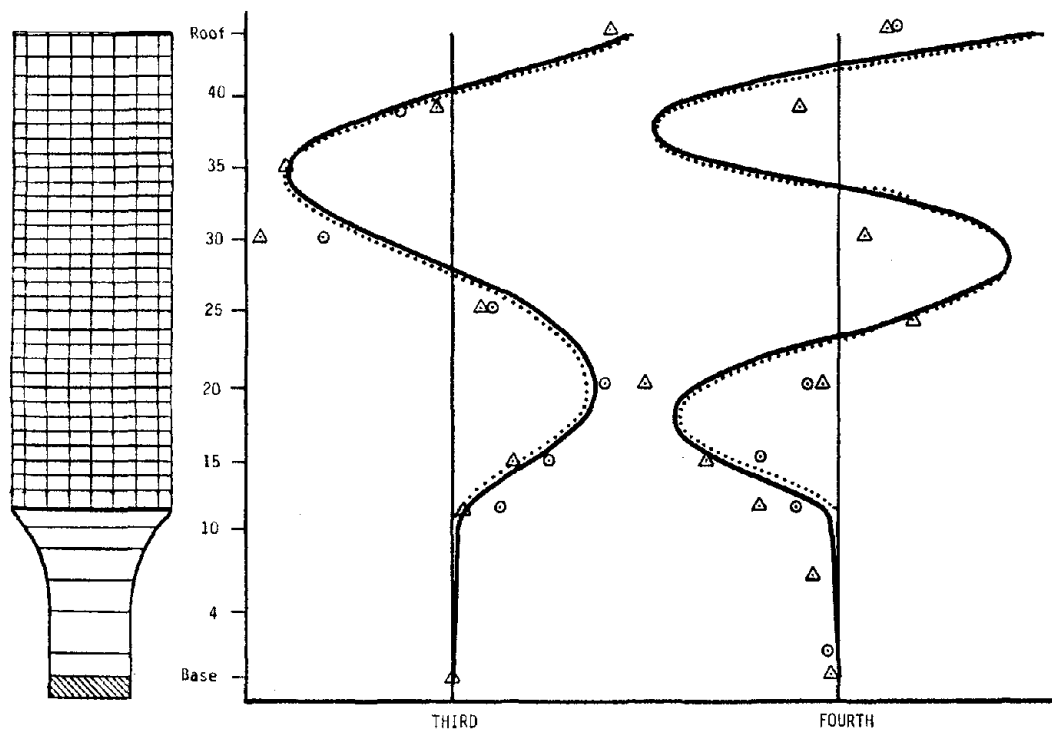
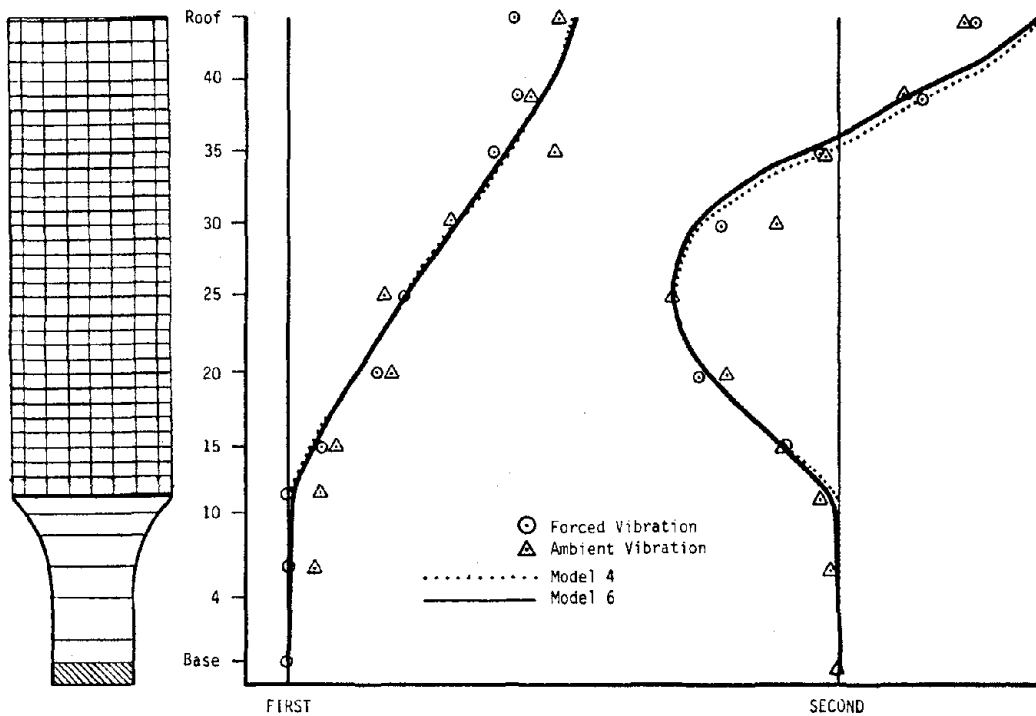


Figure 3.5.7: Analytical vs. Experimental Mode Shapes (N-S Translational)

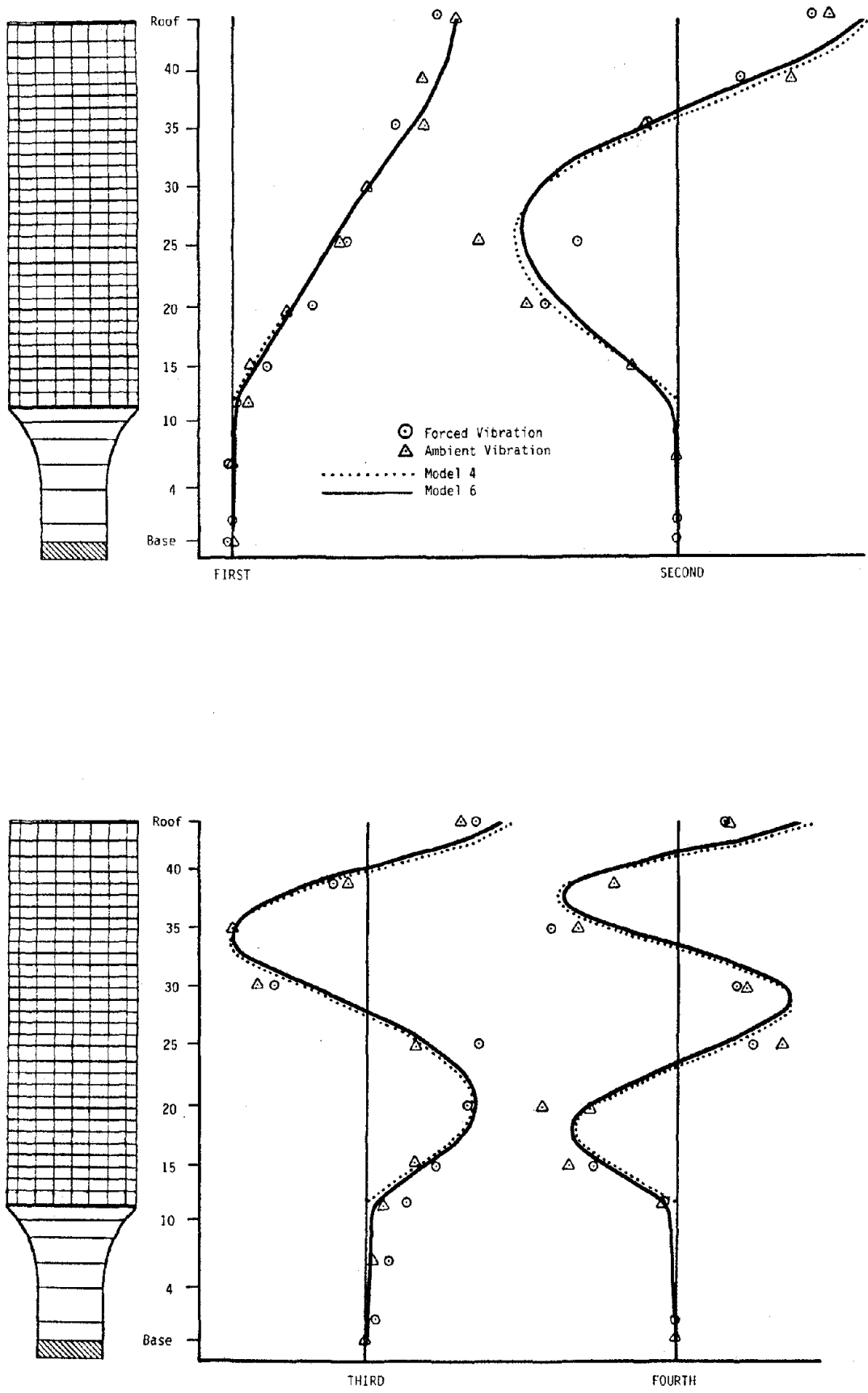
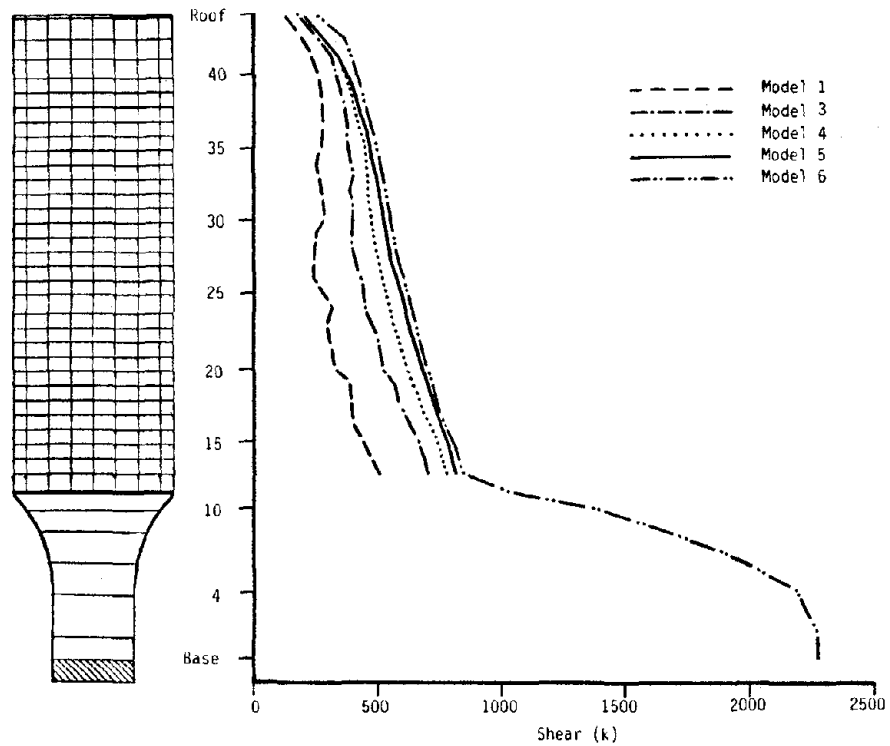
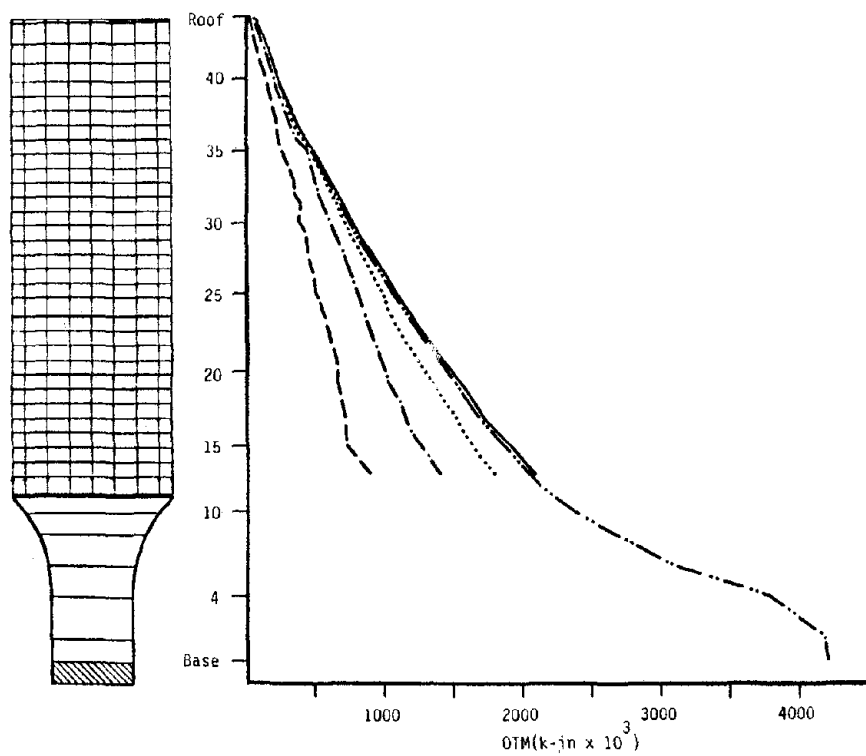


Figure 3.5.8: Analytical vs. Experimental Mode Shapes (Torsional)

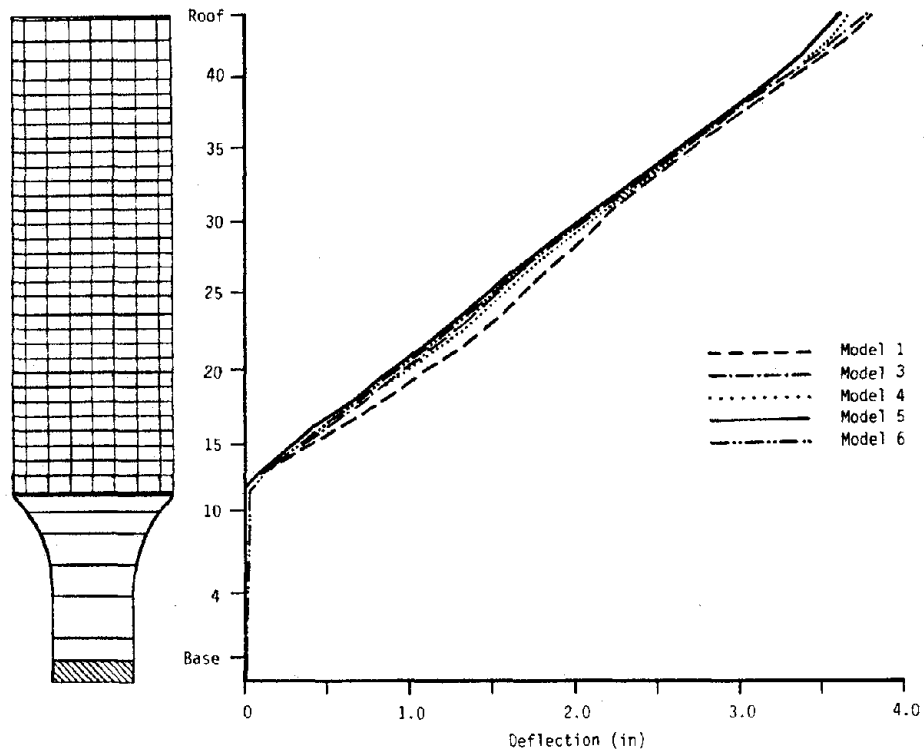


(a) Story Shear

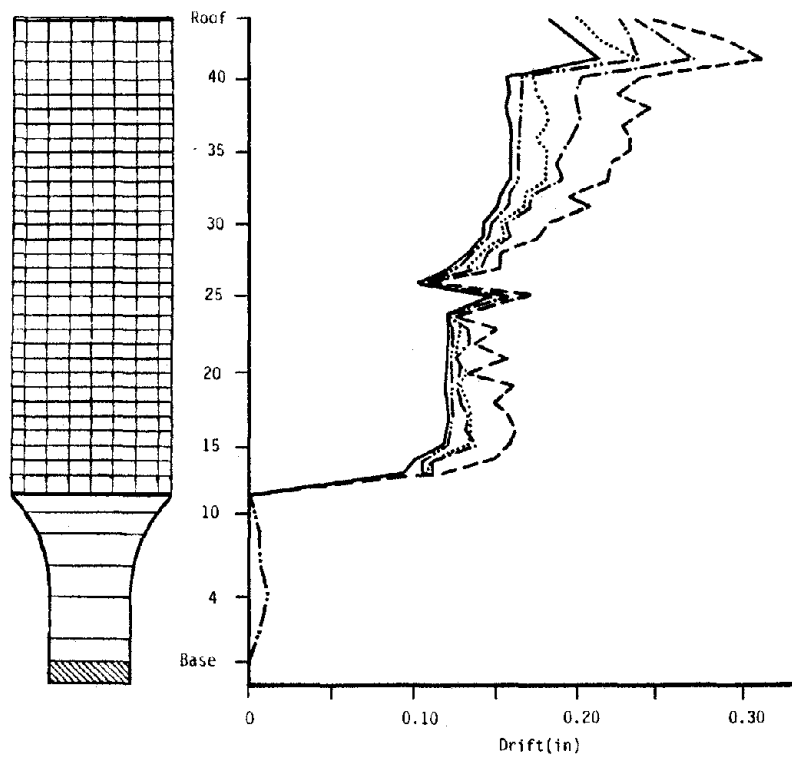


(b) Story Overturning Moment

Figure 3.5.9: Influence of Modeling Approach on Story Force Quantities



(a) Story Deflection



(b) Story Drift

Figure 3.5.10: Influence of Modeling Approach on Story Deflection Quantities

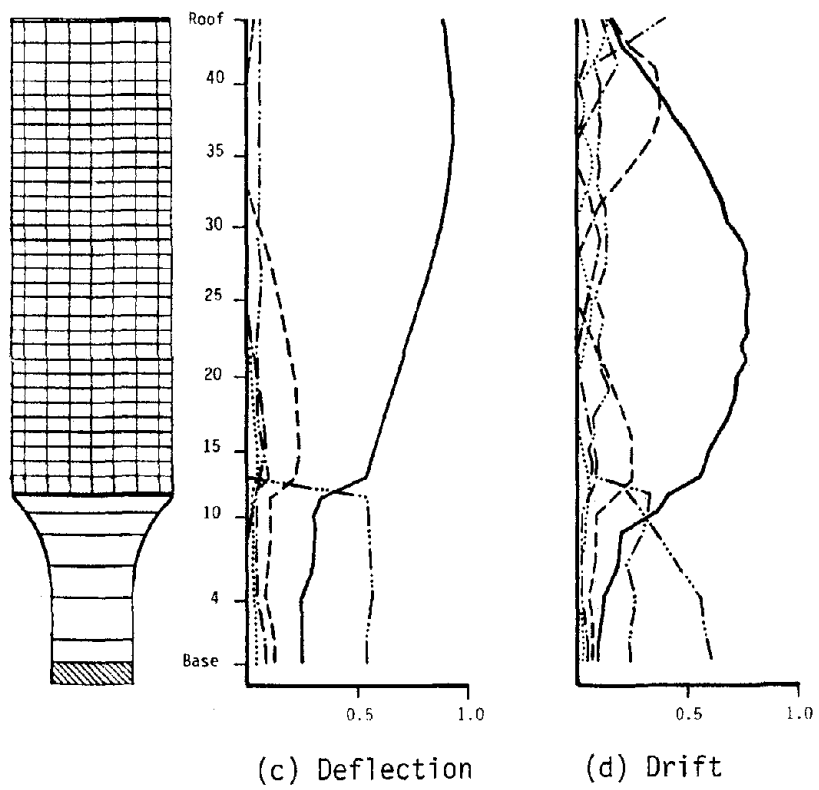
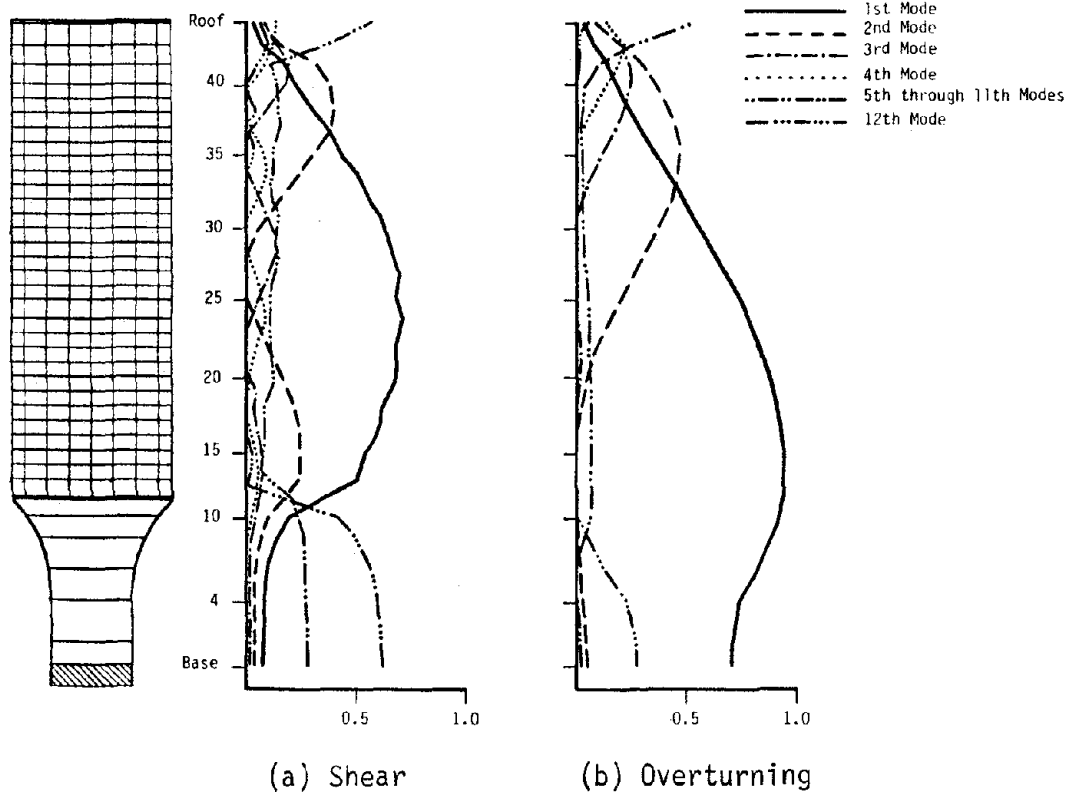
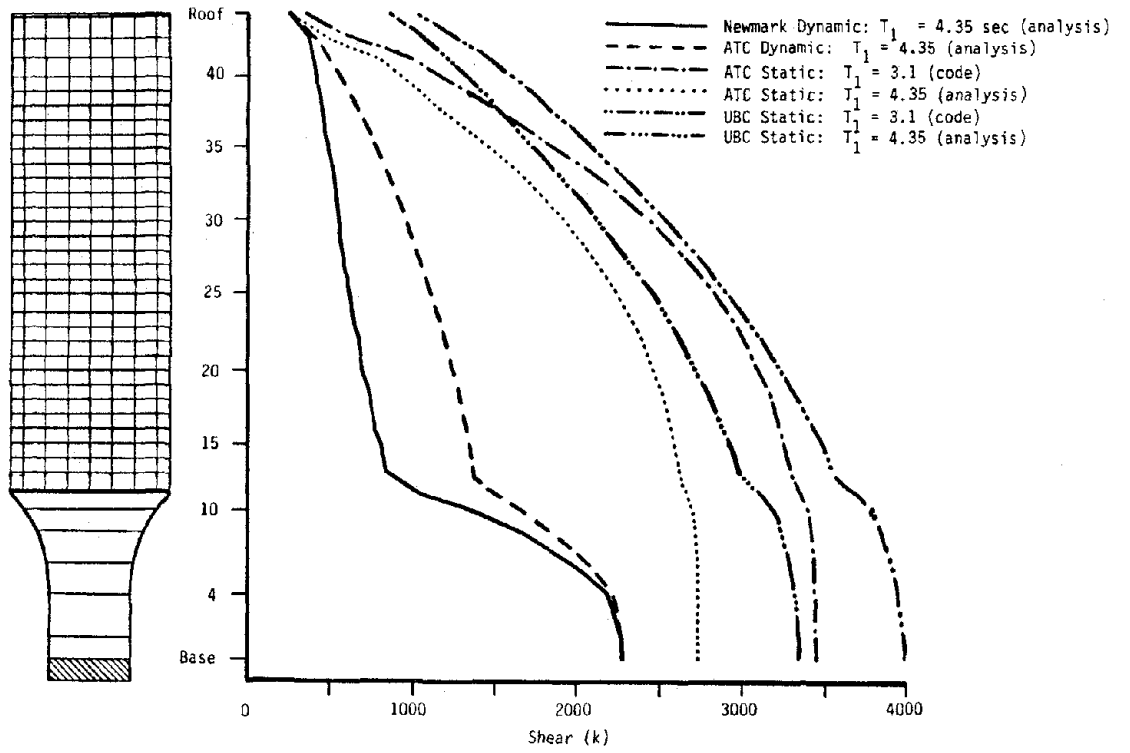
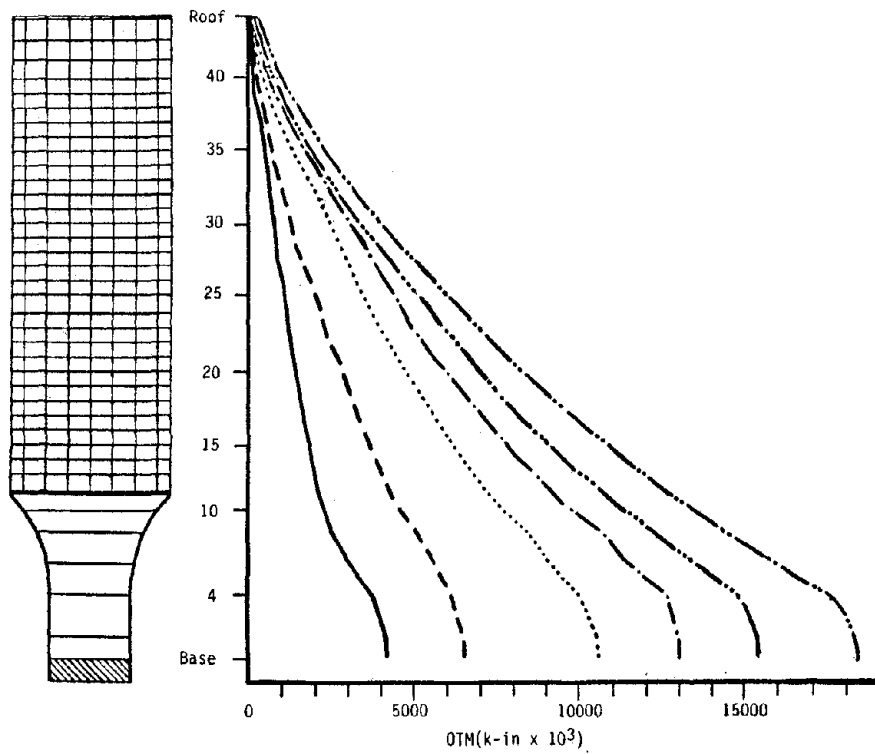


Figure 3.5.11: Modal Contributions to Design Quantities

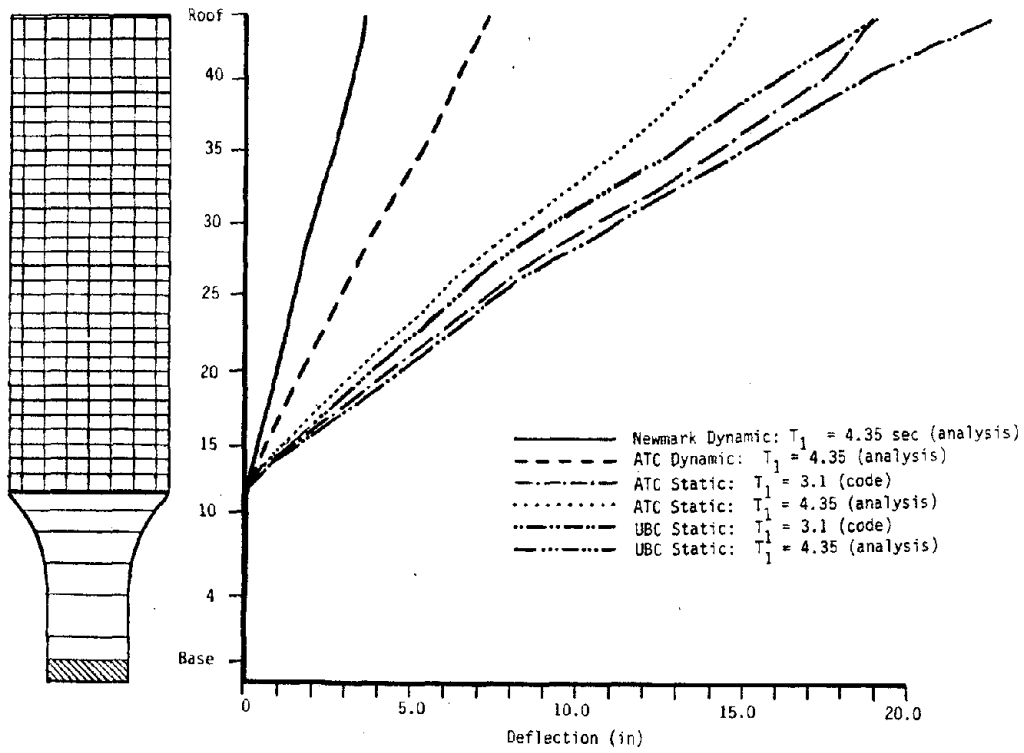


(a) Story Shear

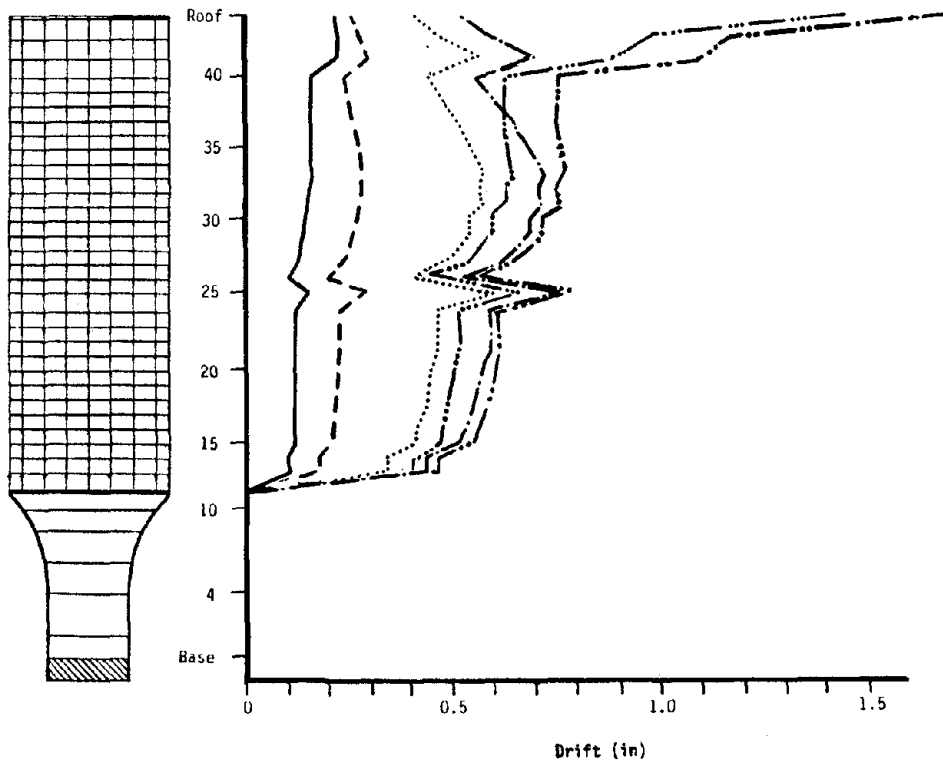


(b) Story Overturning Moment

Figure 3.5.12: Force Quantities Resulting from Dynamic and Equivalent Static Analyses

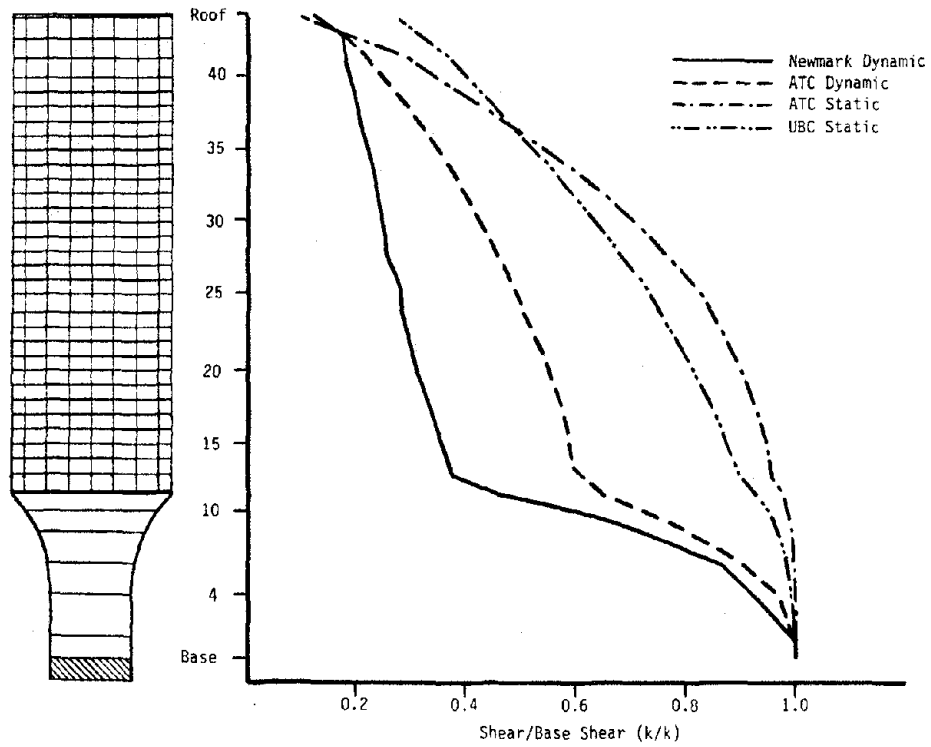


(a) Story Deflections

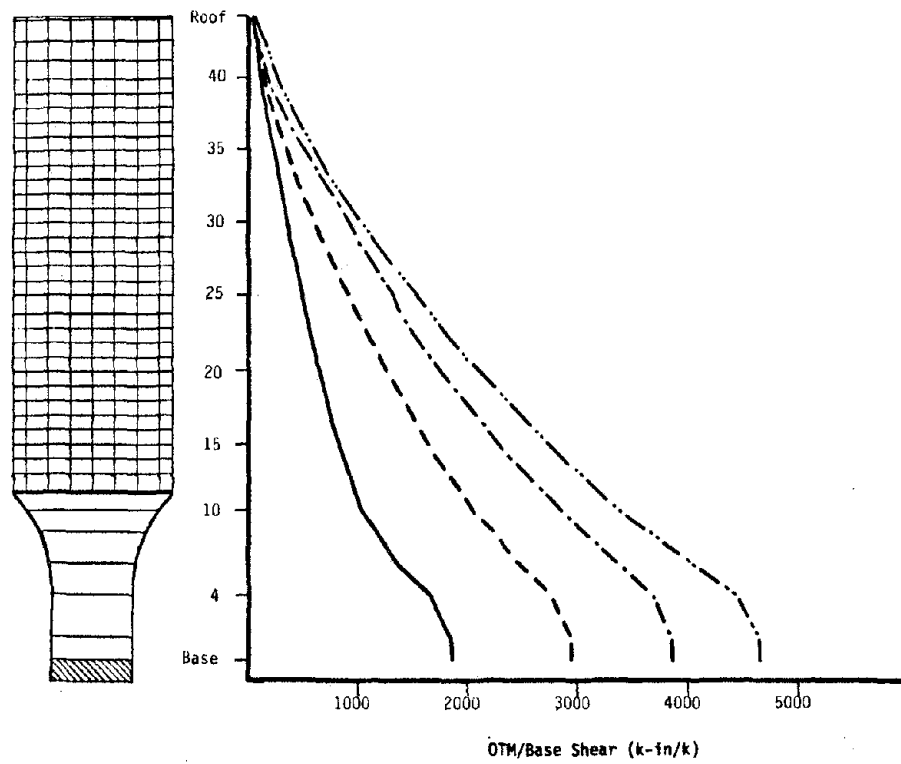


(b) Story Drifts

Figure 3.5.13: Deflection Quantities Resulting from Dynamic and Equivalent Static Analyses

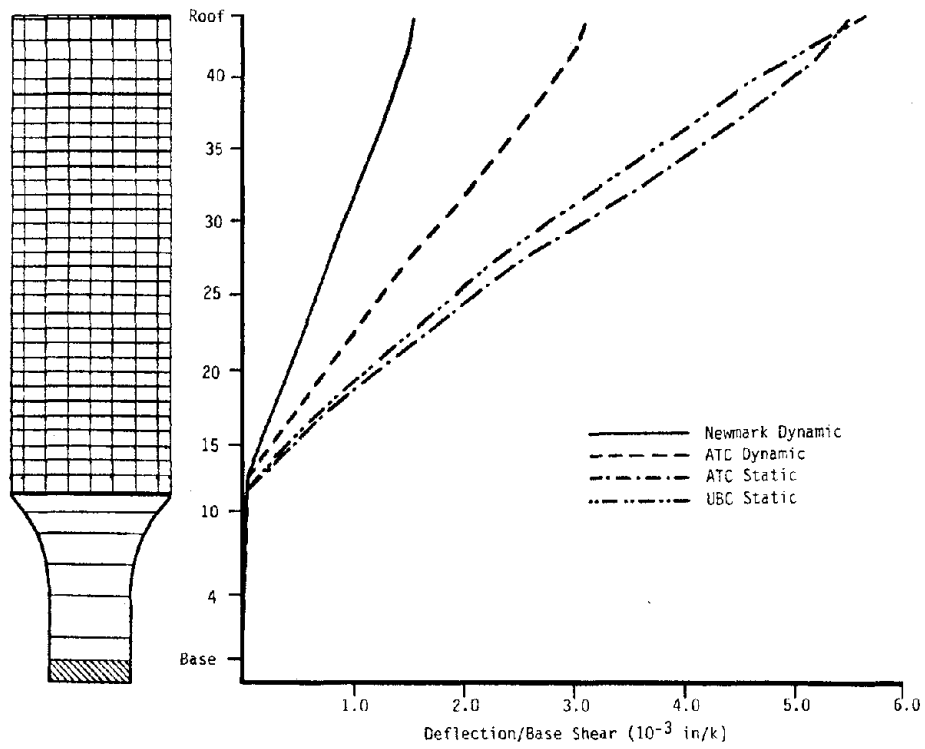


(a) Story Shear

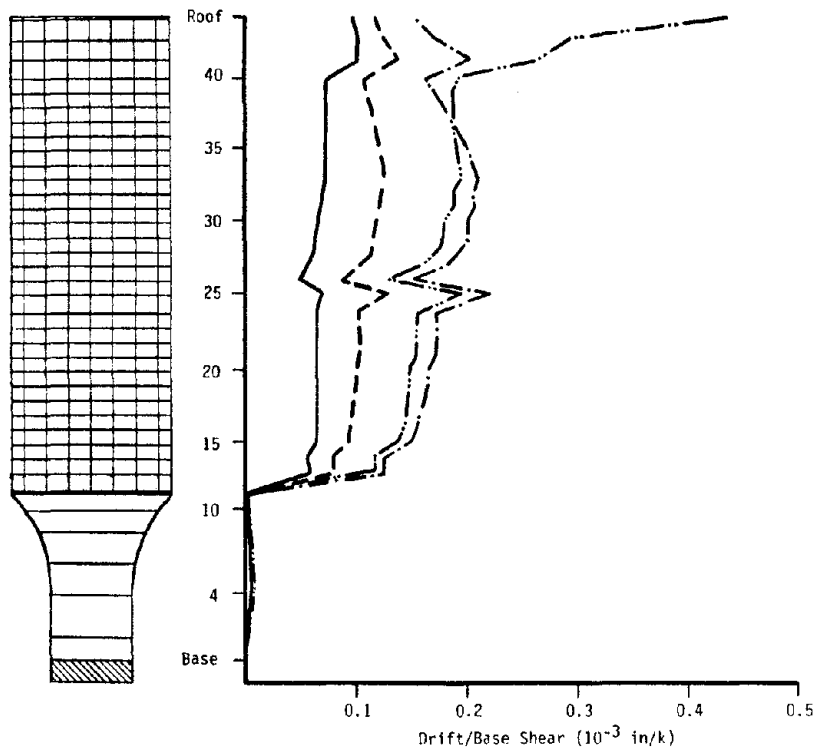


(b) Story Overturning Moment

Figure 3.5.14: Force Quantity Distributions Normalized to Base Shear

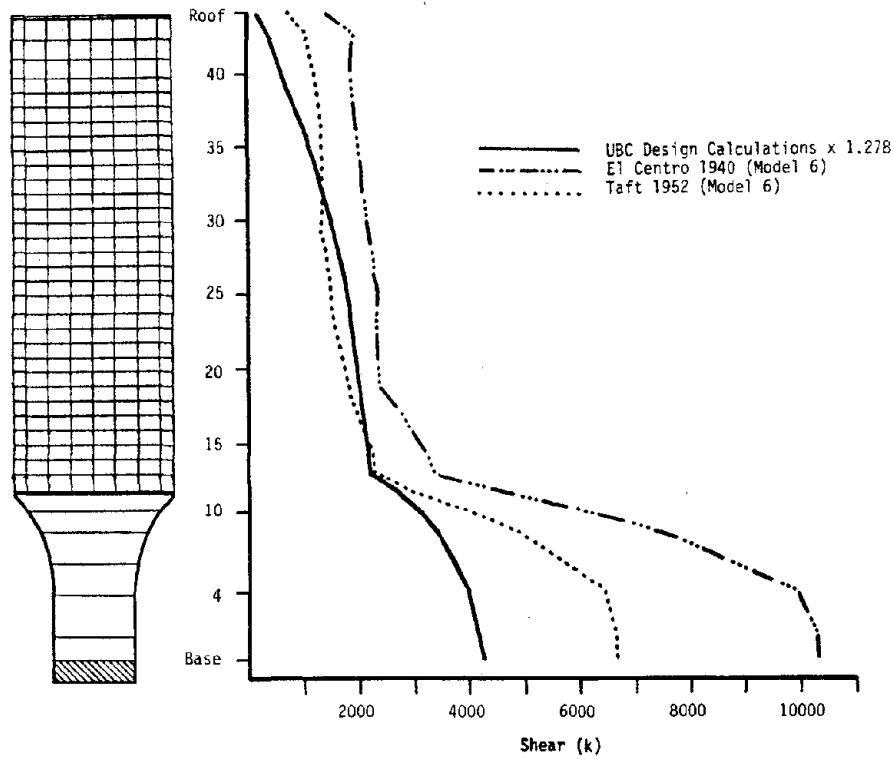


(a) Story Deflection

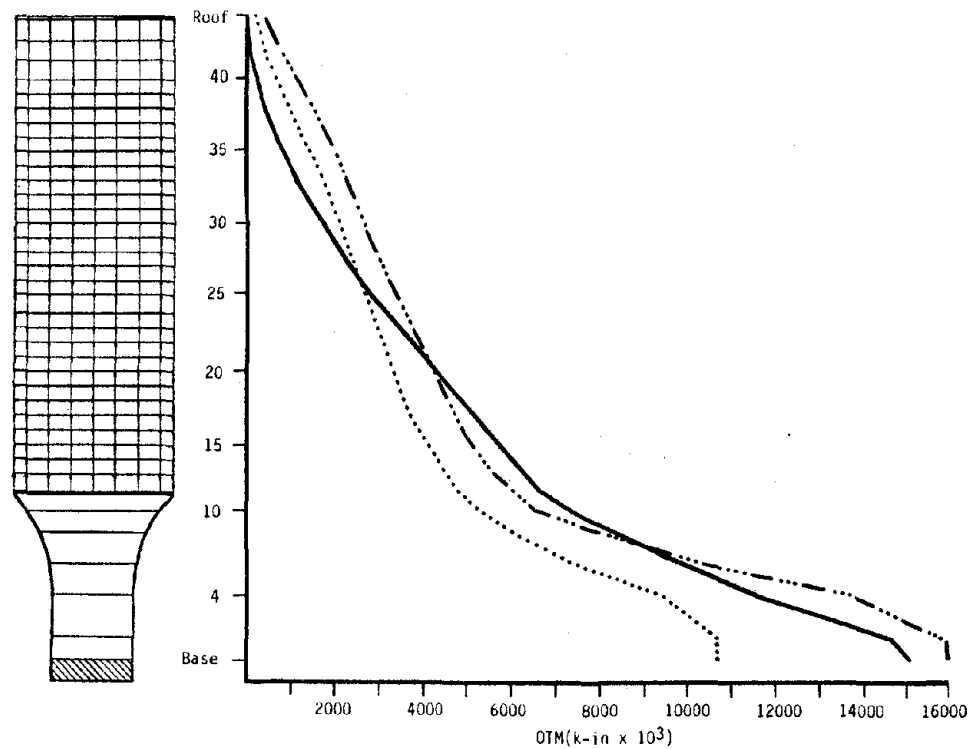


(b) Story Drift

Figure 3.5.15: Deflection Quantity Distributions Normalized to Base Shear



(a) Story Shear



(b) Story Overturning Moment

Figure 3.5.16: Comparison of UBC Design Forces vs. Elastic Forces Induced by Actual Earthquake Spectra

### **3.6 CENTURY CITY THEME TOWER BUILDING**

The Century City Theme Towers are twin multistory office buildings located in Los Angeles, California. Each tower is forty-four stories in height above the plaza level and has six underground parking levels. The buildings have equilateral triangular floor plans with side dimensions of 254 feet and are about 570 feet in height above the plaza level. The structural engineers are Skilling, Helle, Christiansen, Robertson of Seattle, Washington. The buildings were designed and constructed in the early 1970s and the South Tower was experimentally tested during November 1974 and March 1975. A picture of the South Tower is shown in Figure 3.6.1.

#### **3.6.1 Description of the Structural System**

The structure is composed of exterior wall and interior core framing systems (Figure 3.6.2). The exterior walls are moment resistant frames which resist vertical and lateral loads. Each exterior wall has twenty-three bays with columns located at 10'-2" centers (Figure 3.6.3). The columns are W21 shapes or built up sections ( $d=21$  inches), and the spandrel beams are built up sections with a depth of 48 inches (Figure 3.6.4). The corners are built up sections that vary according to the height along the building. Typical corner column sections are shown in Figure 3.6.5. Plate girders are located at the building top (depth of 28'-1 1/2") and at the second floor (depth of 7 feet) levels. The exterior frames terminate at the second floor level, however the corner columns extend below to the B level (Figure 3.6.6). At the second floor level (where the exterior frames terminate) is located a horizontal truss system that connects the exterior wall and interior core systems. Its function is to transfer the horizontal shears from the exterior walls to the interior core. Vertical loads in the exterior walls are transferred to the corner columns. The interior core system is primarily a vertical load carrying system above the second floor and a

vertical and lateral load resisting system below the second floor level. The interior framing consists of W shape columns (W14 section type) and beams (up to W30 section type). Between the second floor and the B level, the interior core perimeter framing is interconnected by steel plates thus forming a steel shear wall system to resist the horizontal shear forces that are transferred from the exterior walls to the interior core. The floor system typically consists of a 4 3/4 inch thick concrete slab placed over a 1 1/2 inch steel deck which is supported by steel floor beams which span between the exterior and interior core systems (steel decking omitted in the interior core region slabs). Shear connectors are provided for slab composite action with the floor framing including the exterior wall spandrel beam). From the B level down to the foundation (F level) the structural system consists of reinforced concrete elements. Underneath the interior core steel shear walls are concrete core walls 20 inches thick and concrete columns. The corner columns are also a reinforced concrete with a dimension of 20 feet square at the F level. Each parking level is constructed of reinforced concrete slabs. The foundation system consists of reinforced concrete mats. The interior core rests on a triangular shaped mat eight feet thick and the corner columns are supported by individual foundation mats with a thickness of 14 feet and plan dimensions about 40 feet by 45 feet. The foundation is placed on a silty sand layer.

The lateral force resisting behavior may be summarized as follows. In the upper portion of the structure the lateral forces are primarily resisted by the exterior moment resisting frames. At the second floor level, the lateral shear force is transferred from the exterior walls to the interior core shear walls via a horizontal truss system whereas the overturning moment is primarily resisted by axial forces in the corner columns.

### 3.6.2 Results of Experimental Studies

Experimental investigations of the South Tower were conducted by the Earthquake Engineering Research Center of the University of California at Berkeley during November 1974 (forced vibration study) and March 1975 (ambient vibration study). The building was structurally complete prior to the experimental testing. In addition, the exterior aluminum and glass covering was installed, as well as interior partition walls and installations in the interior core area.

The forced vibration testing was performed using two rotating mass vibration generators mounted on the 42nd floor. The natural periods are taken from a frequency-response curve which is determined by recording the acceleration response at various excitation frequencies. Once the natural periods are determined, the structure is excited at each natural frequency and the mode shapes are obtained by measuring the acceleration amplitudes at various floor levels. The ambient vibration study uses a different approach in which time segments of the building's ambient acceleration response are recorded. The ambient vibrations are produced by the movements of the occupants, equipment, and by wind pressures. These vibrational exciting forces tend to have a wide frequency spectrum, thus the structure responses in all its normal modes. The natural periods are determined by transforming the recorded acceleration time segments into the frequency domain via Fourier analysis techniques. The natural periods are identified as the frequencies with peaks in the plots of the Fourier amplitude spectra. The mode shapes are determined comparing the measured Fourier amplitudes of the natural periods at various floor levels. A detailed discussion of the test procedures may be found in reference 29.

The first four N-S and E-W translational mode shapes are shown in Figures 3.6.7 and 3.6.8. Note that the forced and ambient vibration results agree favorably thus providing an independent check ensuring

the validity of the results. The N-S mode shapes are virtually identical to the corresponding E-W shapes. The first mode has a somewhat straight line shape for the middle stories of the building. Only near the building top and bottom does it change to a curved shape. The second; third; and fourth modes have neutral (node) points at about the 33rd; the 20th and 37th; and, the 15th, 28th and 40th floor levels, respectively. The modal displacement components at the B level are very small thus indicating that the building behaves as fixed below this level. At the B level, the steel superstructure terminates at the top of a concrete substructure which continues to the mat foundation. Also apparent in the mode shape plots are the stiffening effects of the steel shear walls near the building base which can be seen by the slight reversed curvatures in the mode shapes below the 2nd floor level. The first two torsional mode shapes are shown in Figure 3.6.9. As noted with the translational node shapes, the forced vibration results agree closely with the ambient vibration study. The second mode has a neutral point at about the 30th floor level.

The experimental natural periods are presented in Table 3.6.1. The forced vibration periods and the corresponding ambient periods agree closely, with most values being within in 2%. Note that the N-S and E-W period values also agree closely. The N-S forced vibration periods (3.75, 1.28, .73, .51 seconds) are within 5% of the corresponding E-W values (3.75, 1.32, .76, .53 seconds). The same type of behavior is observed for the ambient period values. The similarity between the N-S and E-W dynamic properties is a result of the equilateral triangular arrangement of the lateral force resisting elements. It can be shown that the lateral stiffness of such a system is the same in all directions. As a result, the N-S and E-W directions have similar mode shapes and periods. An additional consequence is that the lateral translational modes do not have unique

principal axis direction. For example, if the Theme Tower were to be experimentally tested in the Northeast-Southwest and Northwest-Southeast directions (Figure 3.6.3), uncoupled modes oriented along these directions with natural periods similar to those observed for the N-S and E-W directions would be expected. However, slight differences may occur due to the nonsymmetry in the interior core region (Figure 3.6.3).

### 3.6.3 Description of Analytical Models

Dynamic analyses of the Century City Theme Tower South Building are performed using a modified version of the ETABS(49) computer program. Inherent in the model formulation is the assumption that floors are rigid in-plane thus allowing each floor to be idealized by three mass degrees of freedom (two translational and one torsional) located at the floor center of mass. Because of the relatively large number of vertical column lines (23 bays along each exterior frame), rules of symmetry are used to reduce the model size. Planar symmetry exists about the N-S building axis, therefore only one half of the building need be modeled. Structural elements which intersect the plane of symmetry are connected to fictitious columns located the plane of symmetry that have artificial stiffness properties to simulate the appropriate boundary conditions. For calculation of the N-S dynamic properties (periods and mode shapes), boundary conditions allowing symmetric behavior are imposed on the plane of symmetry (Figure 3.6.10). The E-W and torsional dynamic properties are calculated using boundary conditions allowing antisymmetric behavior (Figure 3.6.10). All models are assumed to be completely fixed at the B level. As observed in experimental results the actual building behaves as fixed at this level. The lumped mass values at each floor are based on the dead load calculations supplied by the structural engineer. The total floor weights used in all models are presented in Table 3.5.2. These weights are reduced from the actual values used in

the design because it is believed that they overestimated the actual building weights at the time of experimental testing. Notably, the partition and insulation loads were reduced. This effectively reduced the floor weights by about 10%. Torsional mass moments of inertia are based on the assumption that the mass is uniformly distributed over each floor. Because only one half of the building is modeled, the weight values presented in Tabel 3.5.2 are half of the total floor weights. Various models are examined for comparative analysis, with each model becoming progressively refined.

#### Model 1

Model 1 is formulated to represent the lateral behavior of the Century City Theme Building in the N-S direction. The model is composed of the exterior frame in the N-S direction and the interior core steel shear walls below the second floor level (Figure 5.6.11(a)). The exterior frame is modeled with 3-D beam-column elements with stiffness properties based on the center-to-center member lengths and the steel section properties (composite action ignored). The interior core steel shear walls are modeled by a single column having equivalent stiffness. Notable structural features omitted from this model are: the inherent rigidity in the beam-column connection regions; slab-spandrel beam composite action; the E-W exterior frame; and, the interior core framing above the second floor level. Each of these items will be progressively incorporated into the models that follow.

#### Model 2

Model 2 accounts for the stiffening effects caused by the inherent rigidity of the joint regions at the column-spandrel beam intersections. It is the same as Model 1 except that the exterior frame beam-column connection regions are assumed to be infinitely rigid, whereby the element stiffnesses are calculated using the clear spans of the columns and beams (Figure 3.6.11 (a)). The element ends

are connected to the nodes by rigid links. The spandrel beams are 48 inches deep versus a 12'-7" story height, therefore, the rigid end zones reduce the effective column height by 32%. The columns have a section depth of 21 inches and are located on 10'-2" centers, thus the effective beam lengths are reduced by 17%.

#### Model 3

Model 3 is developed from Model 2 by including the effects of slab-spandrel beam composite action. The floor slabs at the exterior frame are constructed of 1 1/2 inch steel decking and 4 3/4 inch slabs which are designed to act compositely with the floor framing beams. The spandrel section properties are calculated according to AISC Specifications in which an effective slab width of  $b_f + 16t_s$  is assumed ( $b_f$  is flange width and  $t_s$  is slab thickness). The increase in the beam moment of interias are about 40% on the average over those neglecting composite action.

#### Model 4

Model 4 includes the exterior E-W as well as the N-S frames. Like Model 3, both rigid end zones and composite action are incorporated into the exterior wall model formulation. The steel shear walls are modeled by a single column having equivalent N-S lateral, E-W lateral and torsional stiffness. A schematic illustration of the model is shown in Figure 5.6.11(b). Because this model is three dimensional (N-S, E-W and torsional stiffness) two separate analyses are performed to calculate first the N-S, then the E-W and torsional dynamic properties. As discussed previously, for the N-S analysis, symmetric behavior boundary conditions are imposed on the plane of symmetry and for the E-W/torsional analysis, antisymmetric behavior boundary conditions are used (Figure 3.6.10).

#### Model 5

Model 5 is developed from Model 4 by including the interior core framing system which is located above the steel shear walls and

extends to the roof. The framing interior core above the second floor level is primarily a vertical load carrying system which is composed of standard rolled beam and column shapes. Only the peripheral beam and columns of the interior core (along column lines parallel to the exterior walls) are included in the model. Although the interior core framing is not designed as a lateral moment resisting frame system, fully rigid connection regions and slab-beam composite action are assumed.

#### **3.6.4 Comparison of Analytical and Experimental Dynamic Properties**

In this section the natural periods and mode shapes as obtained from the previously discussed models are presented and compared with the experimental results. The first four North-South translational mode shapes for Models 1 and 4 are compared with the experimental results in Figure 3.6.12. Model 1 is the simplest whereas Model 4 represents a refined model. The various analytical model mode shapes are somewhat insensitive to the modeling features incorporated, however the differences among the mode shapes are more distinguishable with increasing mode number. The similarity of mode shapes among the models is because the various modeling features incorporated produce a roughly uniform change in stiffness which does not greatly effect the mode shapes. The analytical mode shapes agree well with the experimental results. The location of the nodal points (points of zero deflection) and the relative amplitudes of the antinodes (points of maximum deflection) are predicted accurately. The effects of the deep steel girder at the building top, and the interior core steel shear walls at the building base are reflected in both the experimental and the analytical mode shapes. The steel girder reduces the drifts in the top stories as compared to the drifts below the 44th level. This effect is shown in the mode shape plots by the change in curvature near the 44th level. In a similar manner, the shear walls

reduce drifts below the second floor level as compared to those above, and the mode shapes reflect this by the change in curvature near the building base. The first two torsional mode shapes from Model 4 are compared with the experimental results in Figure 3.6.13. The analytical torsional mode shapes agree closely with the experimental results.

The natural periods from the analytical models are compared with the experimental forced vibration values in Table 3.6.3. For any model, the natural period error percentages when compared to the experimental values are somewhat independent of mode number. This indicates that the ratios of the higher modal periods to the fundamental period (ratio  $T_1/T_i$ , where  $T_i$  is the  $i$ th period) among the analytical models and the experimental results are similar. Models 1 and 4 have period ratios of 1.00, 2.85, 4.93, 7.18; and, 1.00, 2.92, 5.12, 7.30, respectively. These compare closely with the experimental period ratios of 1.00, 2.93, 5.14, 7.35. It is of interest to note that these ratios correspond approximately to a uniform shear beam period ratios of 1.00, 3.00, 5.00, 7.00. Model 1 is the most flexible model, therefore, its natural periods are the longest. It has a fundamental period of 5.67 seconds which is 51.2% greater than the experimental value of 3.75 seconds. The use of rigid member joint zones in Model 2 has a significant stiffening effect which reduces the periods. The fundamental period of 4.16 seconds is 10.9% longer than the experimental value. Rigid joint zones have the effect of increasing the modal stiffnesses by an average of 94% over the Model 1 values as shown in Table 3.6.4. The large stiffness increase can be expected as a result of the significant shortening of the effective column heights (32%) and beam lengths (17%).

Model 3 includes the effects of slab-spandrel beam composite action which further stiffens the system and reduces the natural periods. Its fundamental period of 4.05 seconds is 8% larger than the

experimental value. As shown in Table 3.6.4, the composite action produces an average increase in modal stiffness of 10% when compared to Model 1.

The E-W exterior frame and the E-W core shear walls are included in Model 4. The E-W frame stiffens the system in the N-S direction by its frame out-of-plane stiffness (column weak axis bending) and by three-dimensional action with the N-S exterior frame whereby axial forces are generated in the E-W frame columns. This model has a fundamental E-W natural period of 3.94 seconds which is 5.1% larger than the experimental value (Table 3.6.3). This is reflected in Table 3.6.4 by an average increase in modal stiffness of 12% over when compared to Model 1. Because Model 4 is three-dimensional, a second analysis was performed with antisymmetric behavior boundary conditions to determine the E-W and torsional natural periods. The E-W analytical natural periods are similar to the N-S analytical periods and agree favorably with the experimental values. As discussed previously, the similarity of the N-S and E-W periods may be expected due to the equilateral triangular arrangement of the lateral force resisting systems. The analytical N-S and E-W periods were not identically equal because the artificial boundary columns have finite stiffness. The first two torsional periods are presented in Table 3.6.3. The torsional periods compare well to the experimental values with the fundamental torsional period of 2.76 seconds being within 1.4% of the experimental value of 2.80 seconds.

Although not presented in the Tables or Figures, the N-S dynamic properties of Model 5 were computed (this model was studied after the results from the previous models were tabulated and plotted). The resulting natural periods and mode shapes closely agree to those from Model 4 thus indicating that the interior core framing above the second floor has only a very small effect on the building's lateral stiffness. The N-S fundamental period from Model 5 is 3.92 seconds

which is within 1% of the Model 1 fundamental period of 3.94 seconds.

Also contained in Table 3.6.3 are the fundamental period values as calculated by the approximate UBC and ATC formulae. The UBC value of 4.6 seconds is 22.7% larger, and the ATC value of 4.19 seconds is 11.7% larger than the experimental fundamental period. Note that Models 2, 3 and 4 provide better estimates than either of the code type formulae.

In summary, it is observed that the analytical mode shapes are somewhat insensitive to the modeling features used whereas the natural periods show considerable variation. A model incorporating the exterior walls (N-S and E-W) and the interior core shear walls is found to predict the actual periods within 6%. Included in the element stiffness formulation is the effects of column-spandrel beam connection rigidity (rigid member end zones) and slab-spandrel beam composite action.

### **3.6.5 Influence of Modeling Approach on Design Quantities**

In this section the response spectrum dynamic analyses of models 1 to 4 are presented to demonstrate the influence of the different modeling approaches on the calculated seismic response. The Newmark spectrum scaled to 0.5g peak ground acceleration is used to represent the earthquake excitation. The first six N-S translational modes are included in the analyses and the total peak responses are estimated by using a SRSS combination of the individual modal responses.

Peak story shear envelopes from each model are shown in Figure 3.6.14(a). The shape of the envelope curves are similar for all models. This is because the mode shapes from the various Models are somewhat invariant (Figure 3.6.12). Therefore, the distribution of the design quantities among the models can be expected to be similar. The amplitudes of the shear envelopes increase from Models 1 to 4. This results from the increasing spectral accelerations that are a consequence of the decreasing natural periods from Models 1 to 4

(Table 3.6.3). The story inertia forces (and resulting story shears) are directly proportional to the spectral accelerations which are a function of the natural periods. Shown in Table 3.6.5 are the values of base shear from the various models and percentage change from Model 1. Model 1 composed of the bare steel N-S exterior frame and interior core shear walls has the largest natural periods with the smallest spectral accelerations and therefore the smallest story shears. The base shear progressively increases from 1030 kips in Model 1 to 1886 kips in Model 4, representing a 83% increase. The shear plateaus between the second floor and base levels indicate that the masses at these levels are not fully participating in the dynamic models. Below the second floor level are the steel shear walls which are stiffer than the superstructure (Figure 5.6.12). Apparently, the mass of the stiffer shear wall system is excited by modes higher than the six included in these analyses. This can be corrected by including additional higher modes in the analyses, however the changes in the resulting response quantities can be expected to be minor, (Figure 3.6.16).

Peak story overturning moment envelopes for the models are shown in Figure 3.6.14(b). The overturning moment envelopes exhibit similar trends as the story shear envelopes; that is, the envelopes have similar characteristic shapes but have different amplitudes. Model 1 has the smallest base overturning moment of  $3656 \times 10^3$  kip-inch, whereas Model 4 has the largest value of  $7506 \times 10^3$  kip-inch, being a 105% increase (Table 3.6.5).

Peak story deflection envelopes for Models 1 and 4 (other models have similar values) are shown in Figure 3.6.15(a). Note that the deflections are virtually identical for all models. This behavior can be explained by consideration of the Newmark response spectrum curve. Because the first mode dominates the deflection response, and for all models, the fundamental period is on zone D ( $p = 2.0$ ) of the Newmark

spectrum, the modal deflections remain constant independent of changing modal stiffness. In general, the increases in stiffness from Models 1 to 4 are offset by the increases in internal forces resulting in virtually no change in lateral deflections (see section 2.5). As shown in Table 3.6.5, Model 4 has a roof deflection of 3.42 inches which is only 1% smaller than the Model 1 value of 3.45 inches.

In Figure 3.6.15(b) peak story drifts are shown for Models 1 and 4. The other models have drift values in very close to the Model 4 envelope values. The decrease in drift at the third floor level (Model 4) is a result of a smaller story height above the second floor level. Note that the stiffer Model 4 has significantly reduced drifts as compared to those of Model 1, whereas for deflections the envelope values are virtually identical as noted previously. This is because for drifts, the higher modes contribute significantly to the total drift response (Figure 3.6.16) and these modes have their natural periods on zone C ( $p = 1.0$ ) of the Newmark spectrum. For this zone the modal drifts are reduced as the modal stiffness is increased. Table 3.6.5 contains the peak drifts values at the 30th floor level for all models. Model 4 has a drift of .098 inches which is 12% less than the Model 1 value of .111 inches.

The relative modal contributions to the total peak design quantity response (using four modes) plotted along the building height for Model 4 are shown in Figure 3.6.16. At any story level, the relative contribution is represented as the square of the individual modal contribution divided by the total sum of the squared modal contributions. Note that in this calculation, the square root is omitted (as used in SRSS combination) such that the sum of the modal contribution ratios will equal one. To determine the ratio of the individual modal responses to the total response represented by the SRSS combination, the square root of the values presented in Figure 3.6.16 is required; however, the sum of these ratios would be greater

than one. Regarding story shears (Figure 3.6.16(a)) the higher modes have significant contributions to the total response throughout the building height. The higher modes contribute 80, 10, and 35% to the total sum of the squared modal story shears at the top, at the 17th floor level and at the base, respectively. A similar trend is shown for story drifts (Figure 3.6.16(d)) in which the higher modes contribute 90, 10, and 35% of the total squared drifts near the top, at the 10th floor level and at the base, respectively. The sudden increase in the fundamental mode drift contribution at the top of the building is a result of the deep plate girder spanning the top two floor levels, which restricts the drifts because of its rigidity (Figure 3.6.16(d)). The small amount of drift in the top stories is primarily from the fundamental mode. For story overturning moments, the higher modes have significant affects increasing toward the top of the building; whereas, they have a negligible effect near the base and contribute 80% of the total squared overturning response toward the top (Figure 3.6.16(b)). A different trend is shown for the peak story deflections in which the higher modes have significant contributions (up to 35%) toward the base and negligible effects near the building top (Figure 3.6.16(c)).

In summary, the shapes of the peak response envelope curves are very similar because the mode shapes are somewhat invariant among the models. The amplitudes of the response curves from the various models have considerable variation due to the variation in spectral acceleration values as a result of the different natural periods among the models. Of the various modeling features incorporated, the introduction of rigid connection regions produced the greatest increase in design force quantities (Figure 3.6.14). The design displacement quantities are somewhat invariant among the models. This is a consequence of the stiffness increase being compensated by the increase in spectral accelerations as a result of decreased natural

periods. The relative individual modal contributions depend upon the particular response quantity and location along the height of the building. For this building, the higher modes have significant effects on each of the peak response quantities studied.

### **3.6.6 Comparison of Dynamic Analyses and Code Equivalent Static Procedures**

In this section a comparison of the Century City Theme Tower's design quantity response as computed by dynamic response spectrum and equivalent static analysis techniques are compared. Model 4 is used as the study building model as its dynamic properties agree well with experimental values. For the dynamic analyses, the ATC and Newmark spectra scaled to 0.05g peak ground acceleration are used as the earthquake input. The peak ground acceleration value of 0.05g is the ATC recommended value for moment resisting frame structures. For equivalent static analyses, the procedures as recommended by ATC and UBC are used. For comparison purposes, the UBC equivalent spectrum is multiplied by 1.278 to correspond to the elastic limit force levels. Both the analytical fundamental period (3.94 seconds) and the ATC and UBC recommended approximate period estimations (4.19 sec. for ATC; 4.6 sec. for UBC) are used in equivalent static analyses. The peak gross design quantities are presented in Figures 3.6.17, 3.6.18 and in Table 3.6.6.

Regarding the dynamic analyses, the gross design quantities as computed using the ATC spectrum are considerably larger than those computed by the Newmark spectrum (Figures 3.6.17, 3.6.18). This result is attributable to the differences in the spectra primarily in the long period range; whereby, the ATC spectral accelerations for the first two modes (3.94 sec., 1.35 sec.) are 76 and 8% larger than the Newmark spectral values, respectively. The base overturning moment and roof deflection are dominated by the fundamental mode (Figures 3.6.16(b)(c)) and comparison of the ATC and Newmark results (Table

3.6.6) reflect the difference in spectral acceleration at the fundamental period. The ATC values for the base overturning moment ( $13170 \times 10^3$  kip-inch) and roof deflection (5.96 inch) are about 75% greater than the values from the Newmark spectrum ( $7506 \times 10^3$  kip-inch and 3.42 inches, respectively). Because the higher modes have greater influence on the base shear and 30th floor level drift (Figure 3.6.16 (a)(d)) the ATC values (2893 kips., 0.153 inch) are about 55% (Table 3.6.6) larger than the Newmark results (1886 kips, 0.098 inch).

The equivalent static analysis results are also presented in Figures 3.6.17 and 3.6.18. The shaded regions illustrate the variation in design quantities dependent upon whether the approximate period estimations or the more accurate analytical periods are used in the calculations. For the UBC equivalent static analyses, the use of the approximate period value (4.6 sec.) yields design quantities (Table 3.6.3) that are about 8% smaller than those using the analytical period (3.94 sec.). The ATC approximate period value (4.19 sec.) results with design quantities (Table 3.6.3) about 5% smaller than those using the analytical period. Comparing the UBC and ATC equivalent static analyses, the UBC procedure has larger response values along the entire building height. This is because the UBC spectrum when scaled to the elastic limit design has larger spectral accelerations in the long period range than the ATC spectrum (Figure 3.1.1). The primary differences between the shapes of the response quantity curves is a result of the UBC top story force which is not included in the ATC formulation. This effect is most apparent in the story shear and drifts plots (Figures 3.6.17(a), 3.6.18(b)), whereby the UBC static method has significantly larger values near the top of the building.

A comparison of the ATC dynamic and equivalent static (with  $T_1 = 3.94$  sec.) analysis results (Figures 3.6.17, 3.6.18) illustrate the effects of the different formulations since the fundamental spectral

accelerations are the same in both cases. As discussed in section 3.7, the ATC static analysis uses an approximate first mode shape and assume the entire building mass participates in this mode. As a consequence, the ATC static base shear of 3659 kips is 26% greater than the dynamic analysis value of 2893 kips (Table 3.6.6).

In Figures 3.6.19 and 3.6.20, the story shear, overturning moment, deflection and drift responses normalized to base shear for the dynamic and static analyses are presented. Comparing the normalized shears from the dynamic analyses, the normalized distribution using the Newmark spectrum have larger shears toward the building top and reduced shears toward the bottom as compared to results using the ATC spectrum. This is because of the higher mode effects which are amplified greater in the Newmark spectrum than in the ATC spectrum at the long period range. The ratio of the fundamental mode spectral acceleration is 1:3.3 for the Newmark spectrum and the ratio is 1:2.0 for the ATC spectrum thus indicating more higher mode amplification in the Newmark spectrum results. Comparing the static analysis results, the UBC method has higher shear values toward the building top and reduced shears at the building midheight relative to the ATC static results (Figure 3.6.19 (a)). These differences are primarily because the UBC lateral top force used to account for higher mode effects is omitted in the ATC method. Both the static analysis response quantity shear distributions have significant variations from the dynamic results, most notably at the building midheight where the static analysis methods have greater shear values. Regarding overturning moment distribution (Figure 3.6.19(b)), the ATC static normalized distribution agrees favorably with the dynamic analysis results (ATC static overturning moment reduction included). The normalized deflections are presented in Figure 3.6.20(a). Both the static analysis methods yield deflection distributions which agree closely and are greater than the

dynamic analysis distributions. As shown in the normalized drift plots (Figure 3.6.20 (b)), the story drift distributions from both equivalent static analysis methods indicate larger drifts (along the entire building height) than those from dynamic analysis.

### **3.6.7 Comparison of Code Design Forces with Dynamic Forces Induced by Actual Earthquake Spectra**

In this section, the story shears and overturning moments resulting from the Taft 1952 (peak ground acceleration .179g) and El Centro 1940 (peak ground acceleration .348g) earthquake spectra (5% critical damping) are computed for Models 1 and 4. The purpose of evaluating the response with two models for each earthquake excitation is to illustrate the range (shaded regions in Figure 3.6.21) of response values resulting from the simplest and a more refined analytical model. In addition, because the building's natural periods can be expected to effectively lengthen during an actual major earthquake, the response from Model 1 provides an indication of how the actual earthquake response may differ from the elastic response (Model 4). Model 4 best represents the small amplitude dynamic properties of the actual building ( $T_1 = 3.94$  seconds, whereas Model 1 has longer periods ( $T_1 = 5.67$  seconds; 44% longer). However, it is recognized that the apparent "period lengthening" of buildings during major earthquakes results from inelastic response activity and representing this behavior by an elastic model with lengthened periods does not rigorously conform to a theoretically correct solution. As shown in Figure 3.6.21(a), the story shear envelopes from the dynamic analyses exhibit a waviness, especially those from the El Centro excitation. This behavior is a consequence of the higher mode effects that are amplified by the actual earthquake spectra. In the case of Model 4 using the El Centro spectrum, the ratio of the spectral acceleration at the fundamental mode to the value at the second mode is 1:4.2. The shear plateau below the second floor level (Figure

3.6.21(a)) indicates that the modes which excite the mass below this level are not included in the dynamic analysis. As noted previously, this is a result of the stiffness increase caused by the steel shear walls at these levels. Also shown in Figure 3.6.21 are the story shears and overturning moments from the UBC equivalent static analysis procedures scaled by 1.278 to reflect elastic limit load levels. Note that the floor masses used in the equivalent static procedure are the same as those used in the dynamic analyses and they do not include the partition loads that were judged to be overestimates of the actual mass. Therefore, the UBC values presented may be somewhat less than the values used for an actual building design. Comparing the story shears and overturning moments from the Taft excitation to the UBC values, the Century City Theme Tower would behave essentially elastically since the actual earthquake induced forces are less than the scaled elastic limit UBC values. This conclusion assumes that the building is designed to resist the 1979 UBC forces which are calculated according to the criteria selected for used in this study (see section 3.1.2). The actual design forces are not presented (based upon the Los Angeles building code which was similar to the 1967 UBC when the building was designed). For the El Centro excitation, the story shears exceed the UBC elastic limit values along the entire building height for Model 4, and near the building top for Model 1. The story overturning moments exceed the UBC elastic limit values in the upper building stories for both Models 1 and 4. Assuming the elastic analyses provide an approximation for the distribution of seismic forces in the inelastic range, the El Centro excitation would produce inelastic response in the upper stories where both the story shears and overturning moment exceed the elastic limit UBC design force quantities.

### 3.6.8 Summary

The dynamic properties and seismic response behavior of various

analytical models of the Century City Theme South Tower are investigated. The purpose is to develop analytical models that correlate to the actual building's dynamic properties as determined by experimental forced vibration studies; and, to evaluate the effects of the various modeling features on the computed dynamic properties and seismic response behavior. The basic model consists of the N-S exterior frame and the interior core shear wall below the second floor level. Additional models are developed by progressively incorporating various structural features to this basic model. The effects of rigid beam-column connection regions, slab-spandrel beam composite action, the E-W exterior frame, and the interior core framing system are evaluated. The results from the study of these models lead to the following observations:

(1) Analytical models representing the primary structural systems of the building have dynamic properties that agree well with the experimental values. Model 4 which incorporates the N-S and E-W exterior frames, rigid connection zones and slab-spandrel beam composite action has natural periods that are within 6% of the experimental values (Table 3.6.3).

(2) The mode shapes from all models agree favorably with the experimental results (Figure 3.6.12). The mode shapes are somewhat invariant to the modeling features. However, the natural periods from the analytical models are sensitive to the modeling features (Table 3.6.3). The natural periods of Model 4 are about 30% shorter than those of Model 1. The introduction of rigid joint zones produces the greatest period shift (stiffening effect) of the modeling features investigated (Table 3.6.4).

(3) The characteristic shapes of the peak response force and displacement envelopes from using the Newmark spectrum are similar for all models. The amplitudes of the peak story shear and overturning moment envelopes vary among the models and have increasing force

values from Models 1 to 4 (Figure 3.6.14). The amplitudes of the story deflection and drift envelopes are similar for all models (Figure 3.6.15).

(4) The higher modes have significant influence on the computed seismic response quantities (Figure 3.6.16). The importance of the higher modes contribution to the total peak response varies according to the location along the height of the building and with the response quantity type.

(5) Dynamic response spectrum analysis using the ATC spectrum yield shears and overturning moments that are over 50% greater than those as computed using the Newmark spectrum (Figure 3.6.17). The large variation is attributable to the differences in the spectra in the larger period range.

(6) The UBC equivalent static analysis procedure yields shears and overturning moments that are greater than the ATC equivalent static method (about 20% greater shears and about 45% greater overturning moments when using the same fundamental period). Both equivalent static analysis procedures result with forces and deflections that are significantly greater than a dynamic analysis using either the ATC or the Newmark spectra (Figures 3.6.17 and 3.6.18).

(7) The distribution of the static design forces as compared to dynamic force envelopes (when normalized) indicates that the static procedures overestimate the relative magnitude of shear forces in the lower portions of the building (Figure 3.6.19(a)). Toward the top of the building, the static UBC force distribution overestimates both the ATC and Newmark response spectrum dynamic distributions, whereas the ATC static force distribution is less than the dynamic Newmark and greater than the dynamic ATC results. Regarding normalized overturning moments, the static UBC results are greater than both the dynamic response spectrum results along the entire building height. However, the static ATC results (with overturning moment reductions)

agree favorably with the dynamic analysis values.

(8) A comparison of the force distributions from dynamic response spectrum analyses using actual earthquake spectra to force distributions from the equivalent static UBC (1979) criteria, indicate that the building would respond elastically if subjected to the Taft (1952) earthquake (Figure 3.6.21). However, if subject to the El Centro (1940) earthquake record, inelastic response may be expected because the computed story shears and overturning moments exceed the UBC elastic limit forces at many story levels. This observation assumes the building is designed to the UBC force criteria only.

Table 3.6.1: Experimental Natural Periods

Direction	Mode No.	Experimental Period in Seconds	
		Force Vibration Study	Ambient Vibration Study
N-S	1	3.75	3.66
	2	1.28	1.26
	3	.73	.72
	4	.51	.50
E-W	1	3.75	3.80
	2	1.32	1.32
	3	.76	.75
	4	.53	.52
Torsion	1	2.80	2.88
	2	1.01	1.00

Table 3.6.2: Dead Load Weights Used  
in Analytical Models

Floor	All Models	
	Weight(kips)	psf
44	4397	315
43	0	0
42	1333	95
41	1333	95
40	1333	95
39	1333	95
38	1333	95
37	1333	95
36	1333	95
35	1333	95
34	1333	95
33	1333	95
32	1333	95
31	1352	97
30	1352	97
29	1352	97
28	1352	97
27	1352	97
26	1352	97
25	1352	97
24	1352	97
23	1352	97
22	1352	97
21	1352	97
20	1352	97
19	1352	97
18	1352	97
17	1352	97
16	1352	97
15	1399	100
14	1399	100
13	1399	100
12	1399	100
11	1399	100
10	1399	100
9	1399	100
8	1399	100
7	1399	100
6	1399	100
5	1399	100
4	1399	100
3	1399	100
2	2964	212
Plaza	757	54
A	684	49
TOTAL	63284	

Table 3.6.3: Experimental vs. Analytical Natural Periods

Direction	Mode No.	Exp. Period(sec)	Model 1		Model 2		Model 3		Model 4	
			Period	%	Period	%	Period	%	Period	%
N-S	1	3.75	5.67	+51.2	4.16	+10.9	4.05	+8.0	3.94	+5.1
	2	1.28	1.99	+55.5	1.43	+11.7	1.39	+8.6	1.35	+5.5
	3	0.73	1.15	+57.5	0.82	+12.3	0.80	+9.6	0.77	+5.5
	4	0.51	0.79	+54.9	0.56	+9.8	0.55	+7.8	0.54	+5.9
Torsion	1	2.80							2.76	-1.4
	2	1.01							0.96	-5.1

UBC*		ATC*	
Period	%	Period	%
4.6	22.7	4.19	11.7

% = percent variation from experimental period.

\*Code periods calculated based on 46-story height as follows:

UBC (eqn. 12-3B):  $T = 0.10 N = 0.10 \times 46 = 4.6$  sec.

ATC (eqn. 4-4):  $T = C_T h_n^{3/4} = .035 \times (590.29)^{3/4} = 4.19$  sec.

\*Torsional analysis not performed.

Table 3.6.4: Influence of Modeling Features on Modal Stiffnesses

		Stiffness Increase with respect to Model 1			
Direction	Mode	Rigid Joint Zone	Slab-Girder Interaction	3-D Effects	Total
N-S Trans.	1	86%	10%	11%	107%
	2	94	11	12	117
	3	97	10	16	123
	4	99	7	8	114
	Average	94%	10%	12%	115%

Table 3.6.5: Influence of Modeling Features on Building Seismic Response

Design Quantity	Model 1		Model 2		Model 3		Model 4	
		%		%		%		%
Base shear (k)	1030.	0	1704.	65.	1782.	73.	1886.	83.
Base OTM (k-in x 10 <sup>3</sup> )	3656.	0	6764	85.	7160	96.	7506	105.
Roof deflection	3.45	0	3.41	-1.	3.41	-1.	3.42	-1.
30th level drift (in)	0.111	0	0.096	-14.	0.094	-15.	0.098	-12.

% = incremental percent from Model 1

Table 3.6.6: Comparison of Design Quantities from Dynamic and Equivalent Static Analyses.

Design Quantity	Dynamic				Static							
	Newmark		ATC		ATC				UBC*			
		%		%	Codebook		Analytical		Codebook	%	Analytical	%
Fundamental period (sec)	3.94	0	3.94	0	4.19	6	3.94	0	4.60	17	3.94	0
Base shear (k)	1886.	0	2893.	53	3505.	86	3659.	94	4025.	113	4348.	131
Base OTM (k-in x 10 <sup>3</sup> )	7506.	0	13170	75	15110.	101	15780.	110	21430.	186	23150.	208
Roof deflection (in)	3.42	0	5.96	74	8.76	156	9.15	168	9.91	190	10.7	213
30th level drift (in)	.098	0	.153	56	.227	132	.236	141	.249	154	.269	174

% = increment % from Newmark spectrum dynamic analysis

\* = UBC forces are factored by  $1.70/1.33 = 1.278$  for correspondence with ATC elastic limit load levels

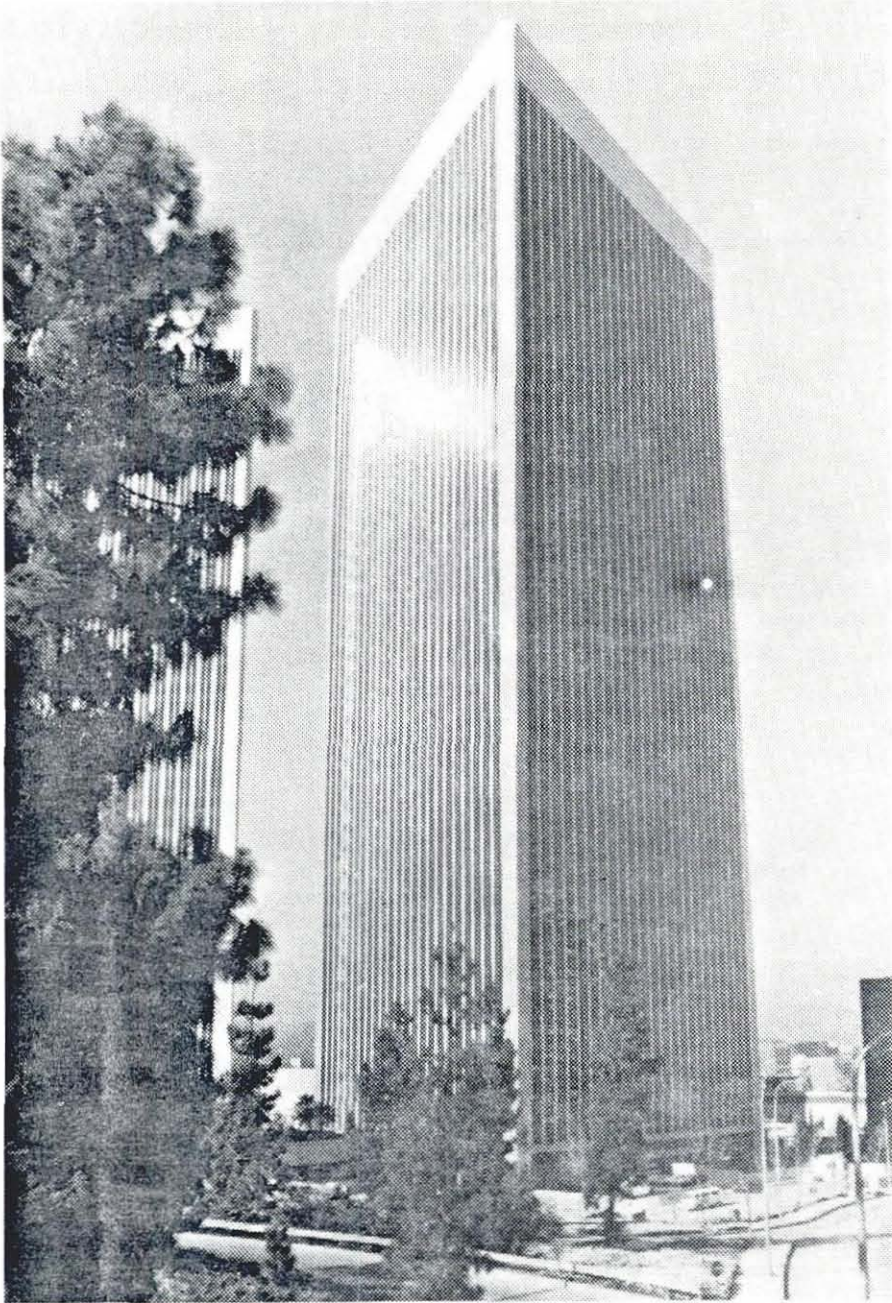


Figure 3.6.1: General View of the South Theme Tower Building

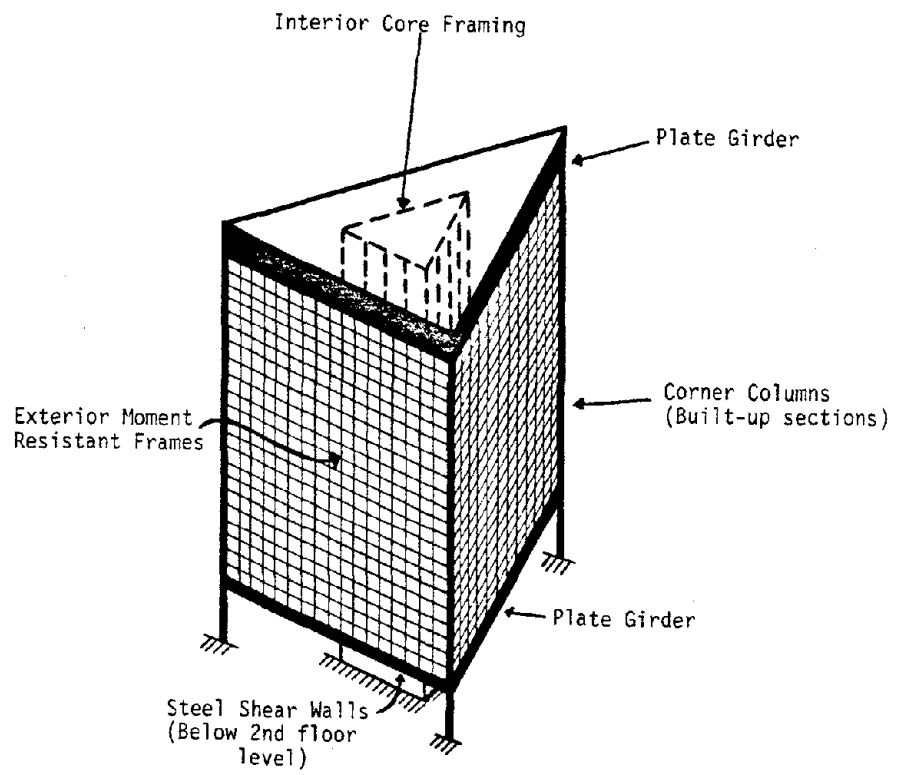


Figure 3.6.2: Structural Configuration

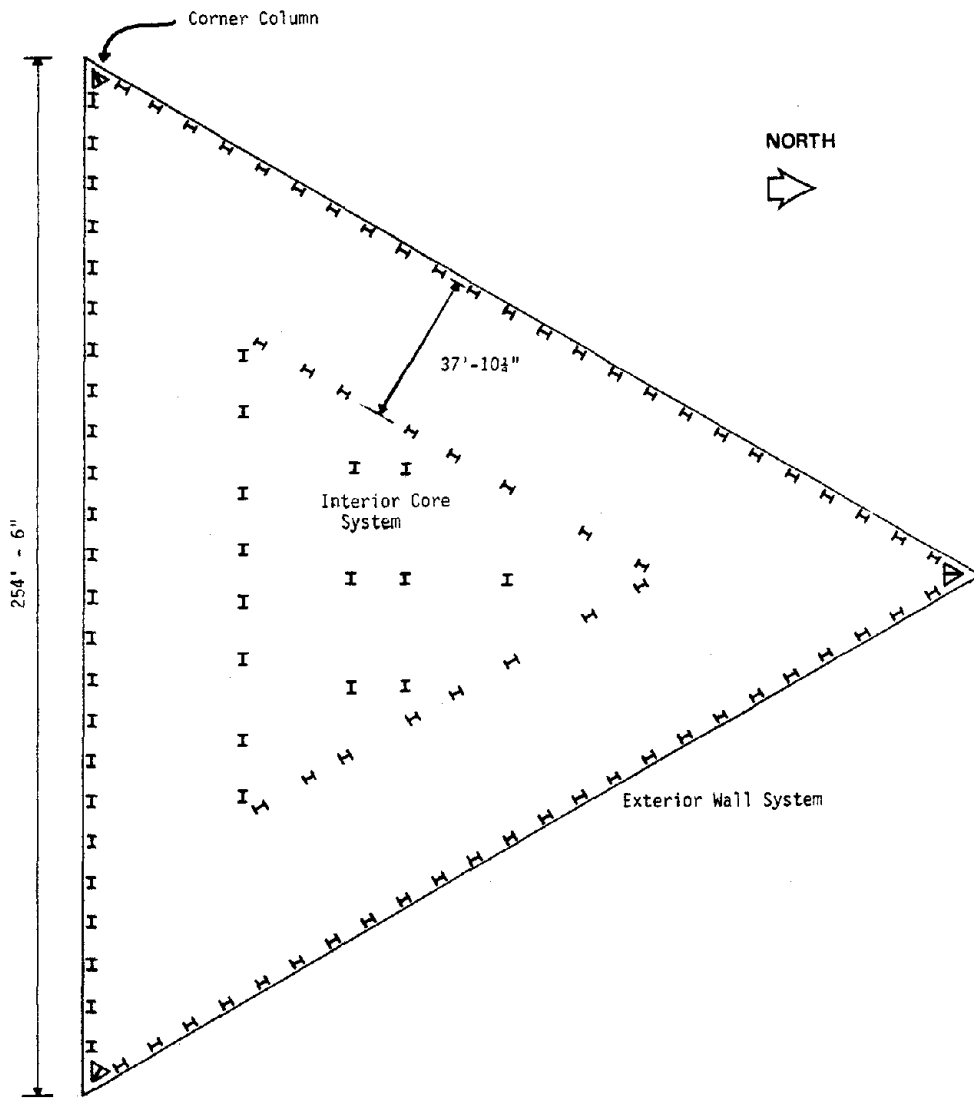


Figure 3.6.3: Building Plan View

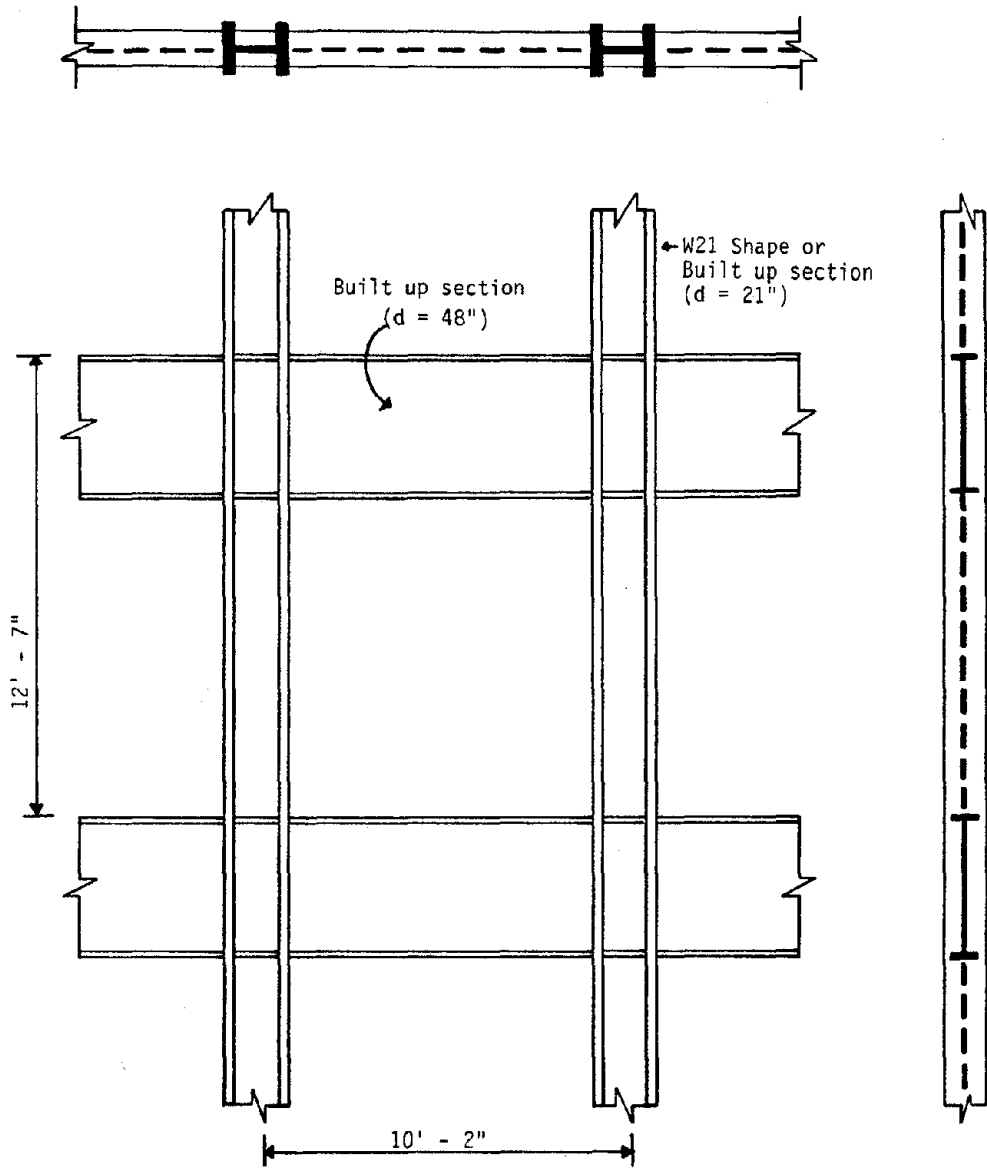
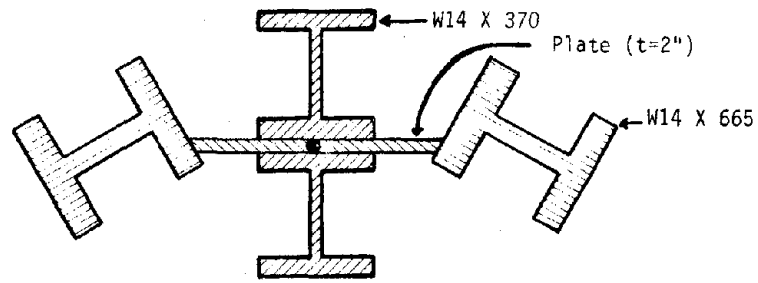
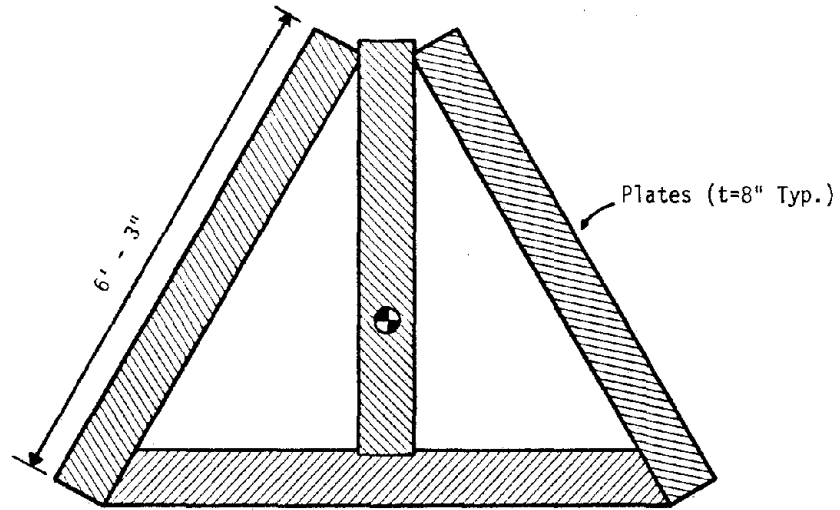


Figure 3.6.4: Exterior Wall Section



Section at the 14th floor level

(a) Corner Column Section Between 14th and 32nd Floor Levels (W14 shapes vary according to elevation)



(b) Corner Column Section Below 2nd Floor Level

Figure 3.6.5: Typical Corner Column Sections

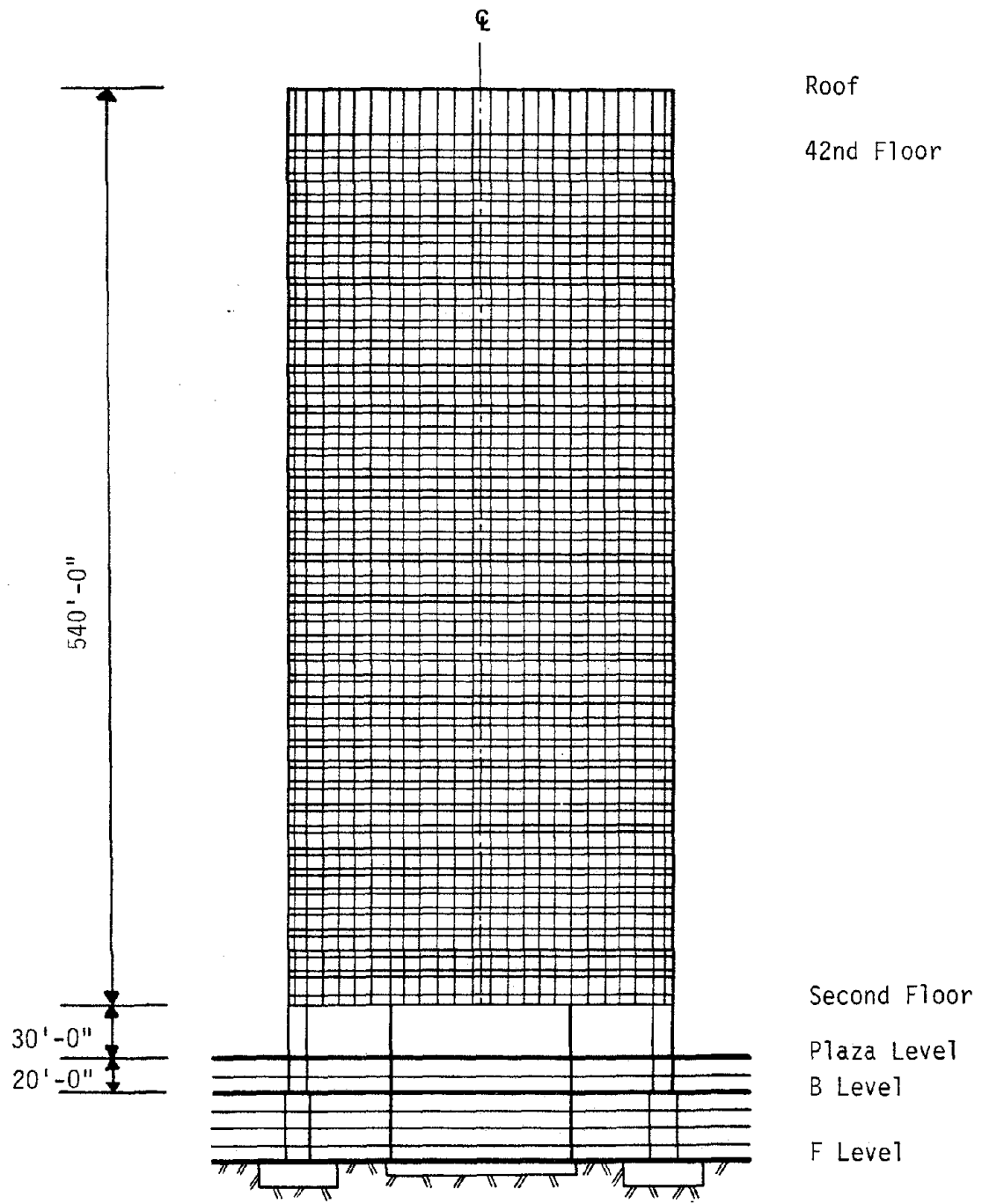


Figure 3.6.6: Building Elevation View

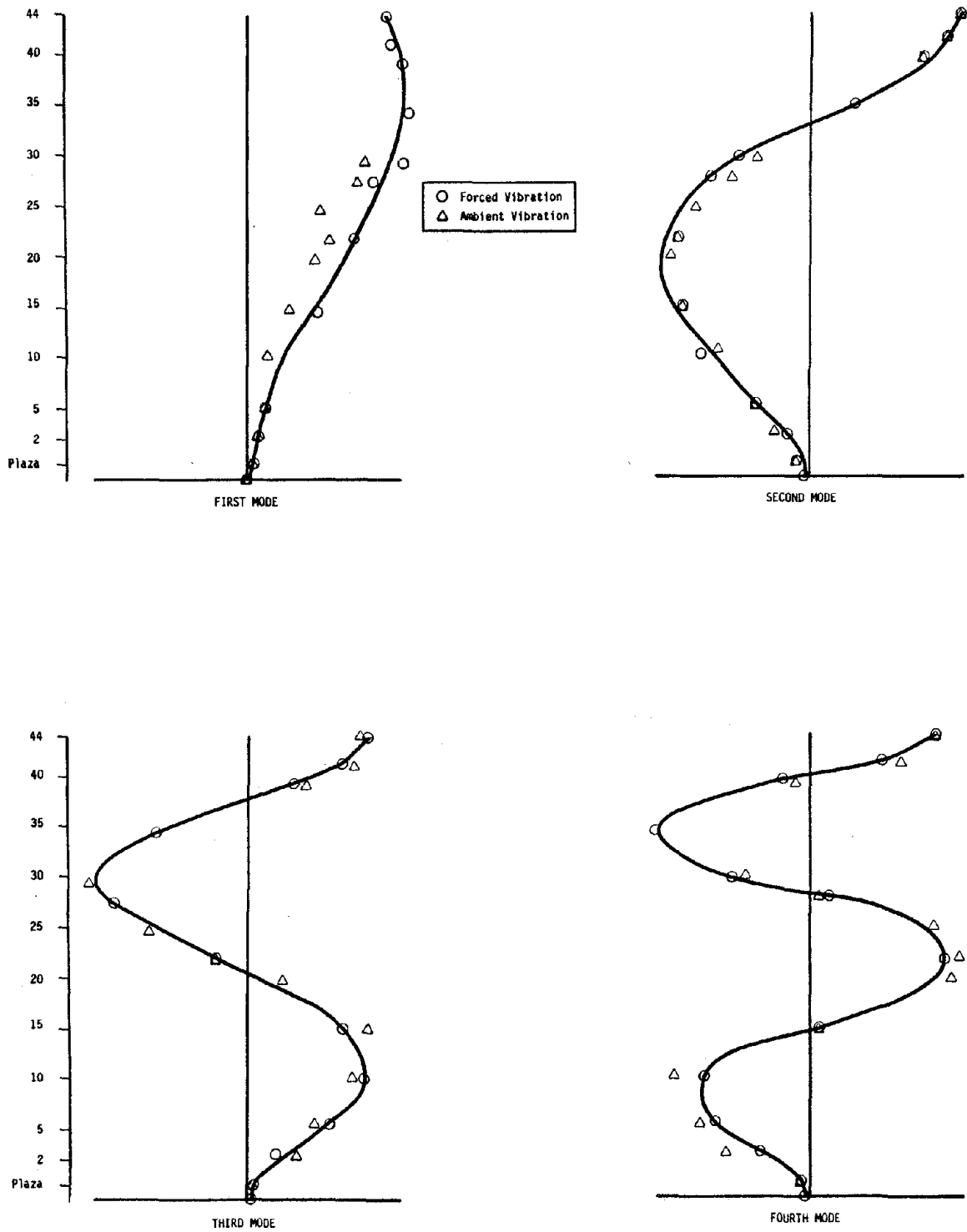


Figure 3.6.7: North-South Experimental Mode Shapes

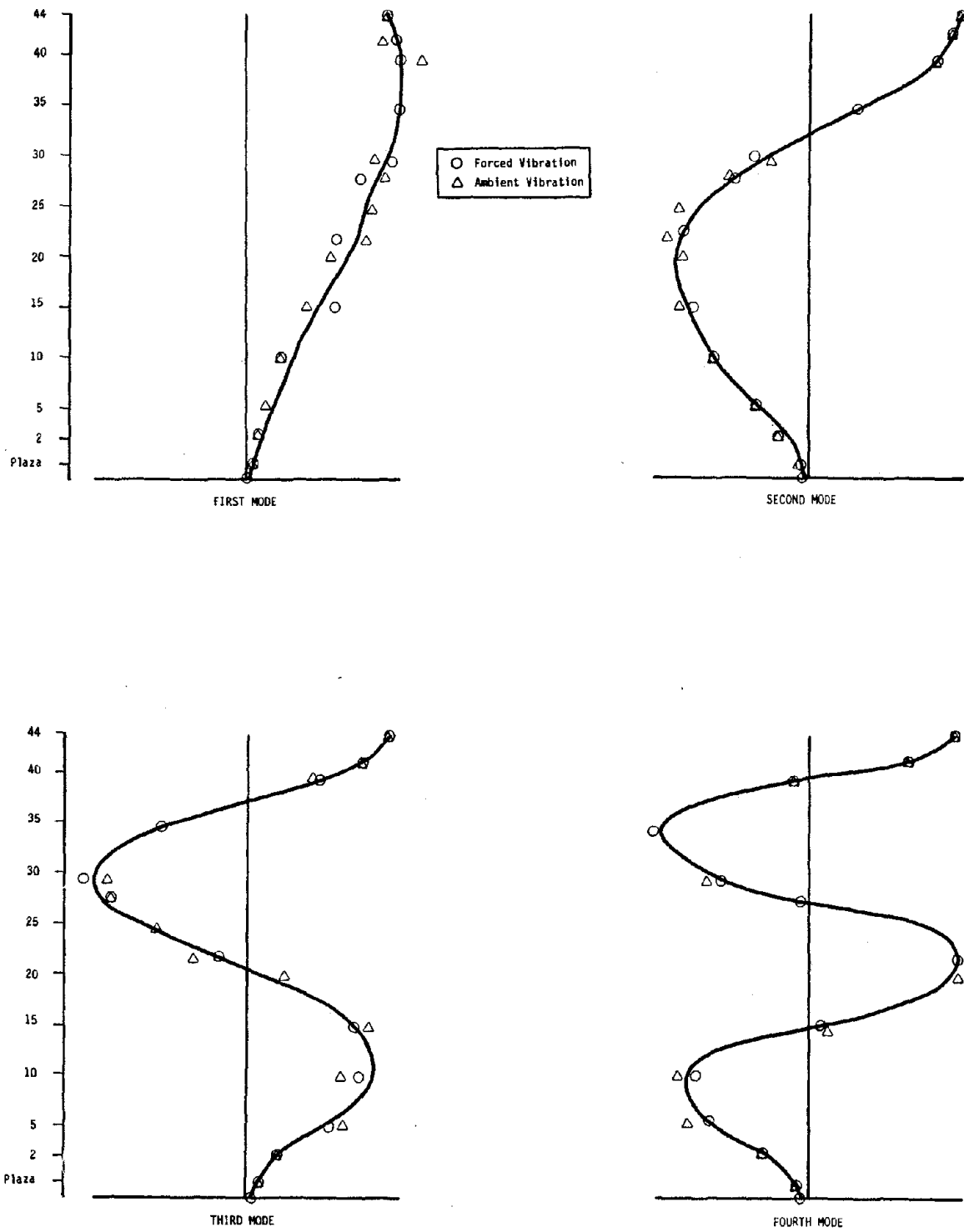


Figure 3.6.8: East-West Experimental Mode Shapes

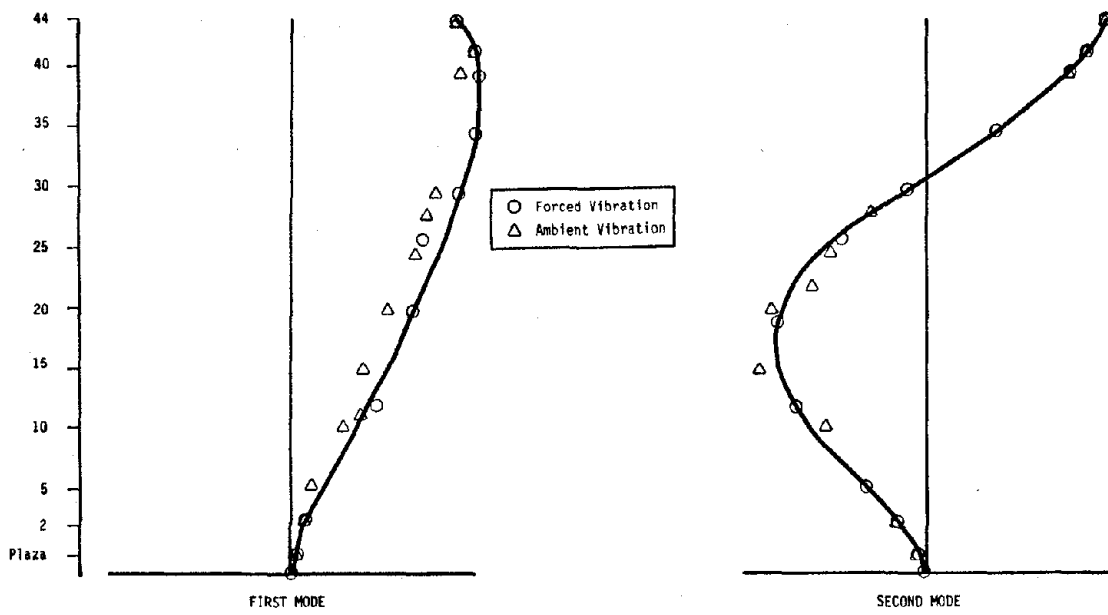
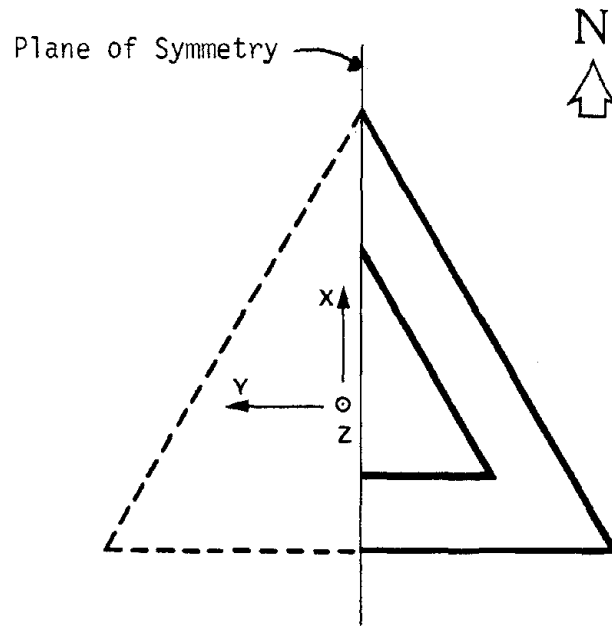


Figure 3.6.9: Torsional Experimental Mode Shapes



Building Plan View

Boundary Conditions on Plane of Symmetry

Analysis Type	Displacement Boundary Conditions*					
	Translations			Rotations		
	x	y	z	xx	yy	zz
Symmetric (N-S)	0	1	0	1	0	1
Antisymmetric (E-W and Torsion)	1	0	1	0	1	0

\* Boundary Condition Code:  
 0 = Displacement Allowed  
 1 = Displacement Constrained

Figure 3.6.10: Model Symmetry Boundary Conditions

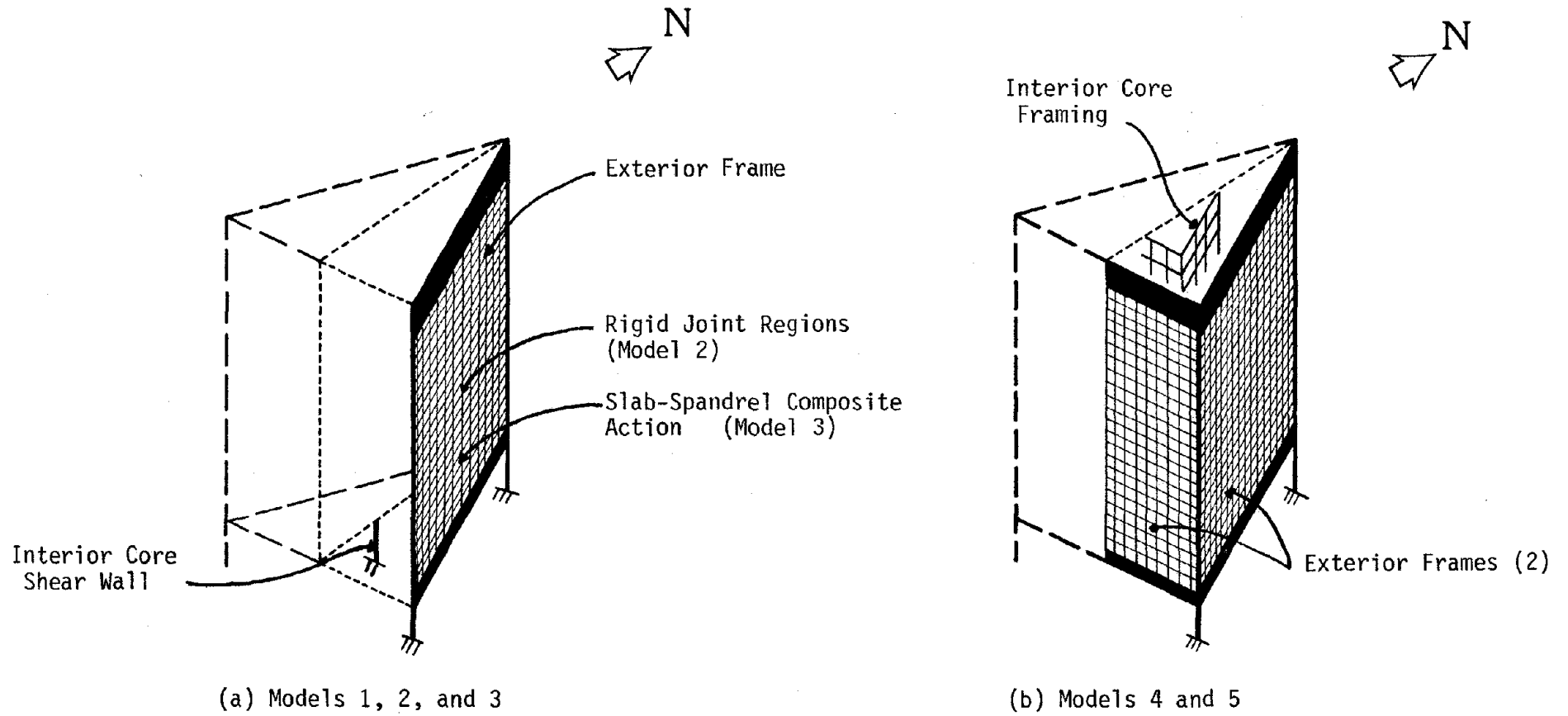


Figure 3.6.11: Building Model Idealizations

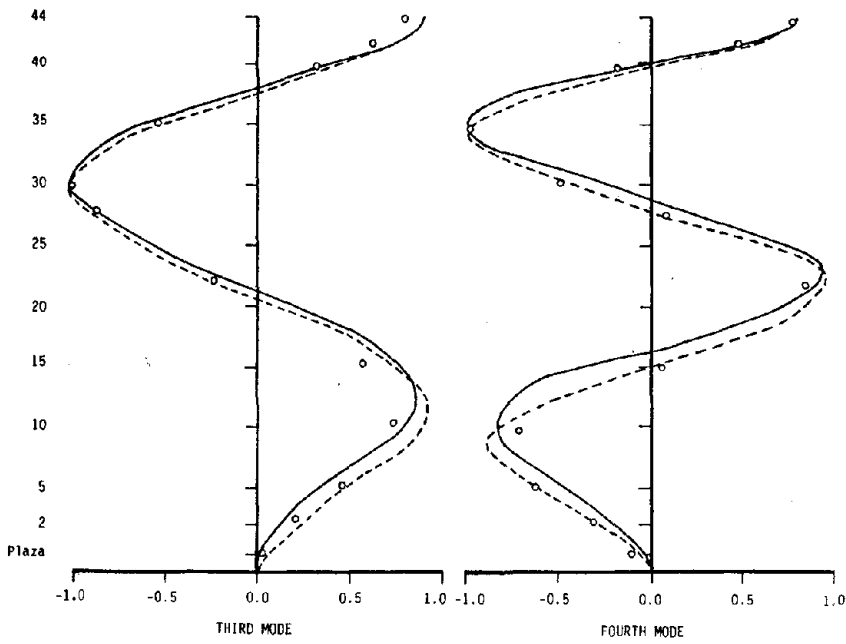
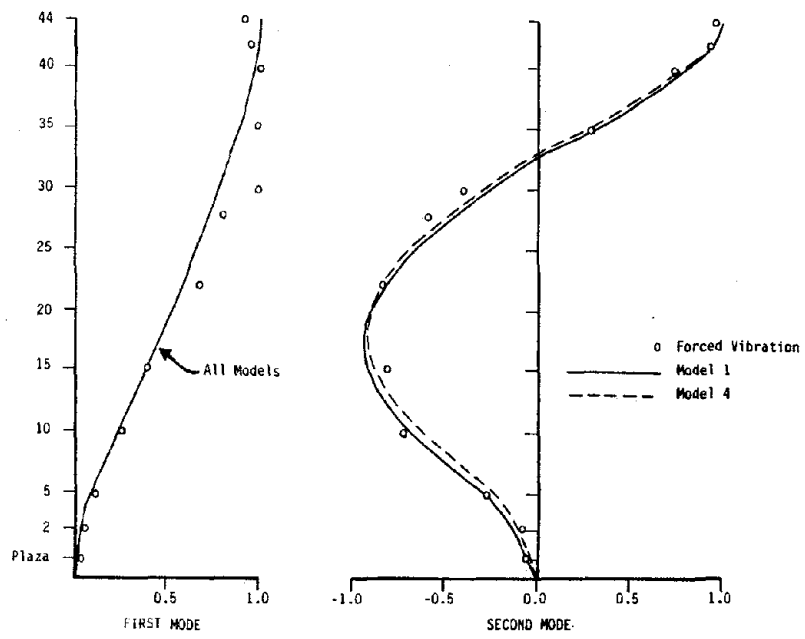


Figure 3.6.12: Comparison of Experimental and Analytical N-S Mode Shapes

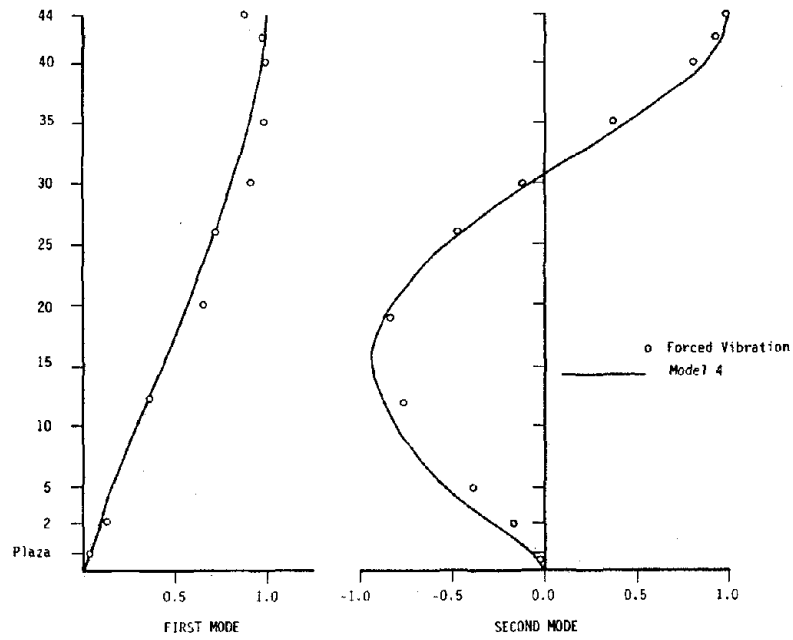
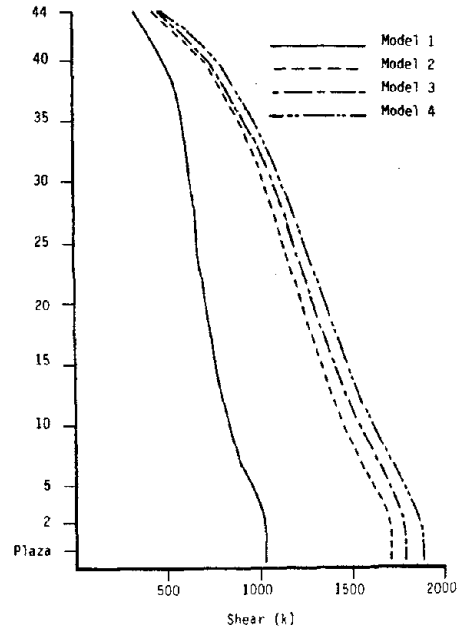
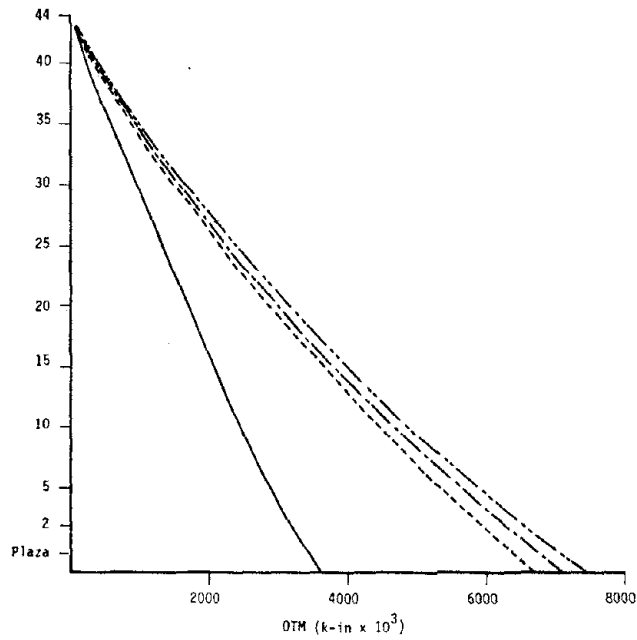


Figure 3.6.13: Comparison of Experimental and Analytical Torsional Mode Shapes

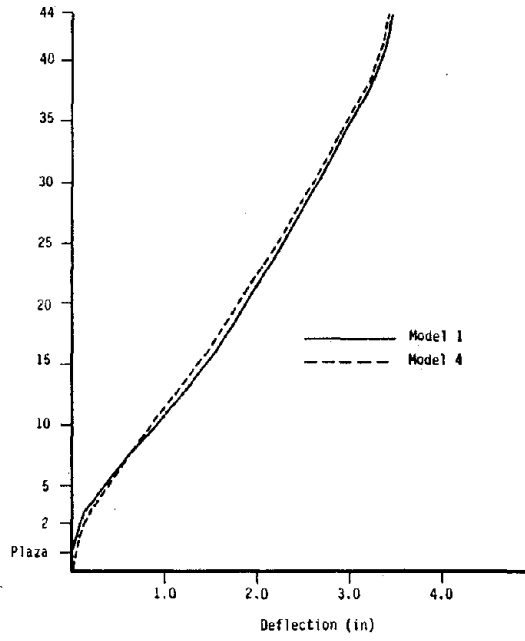


(a) Shears

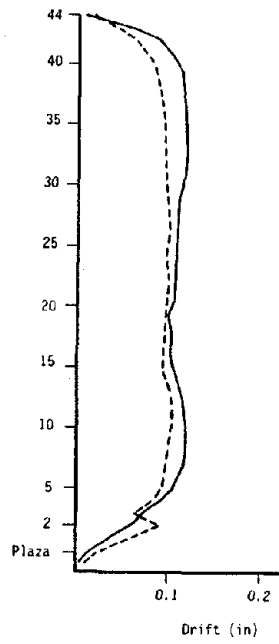


(b) Overturning moment

Figure 3.6.14: Story Force Quantities from the Analytical Models

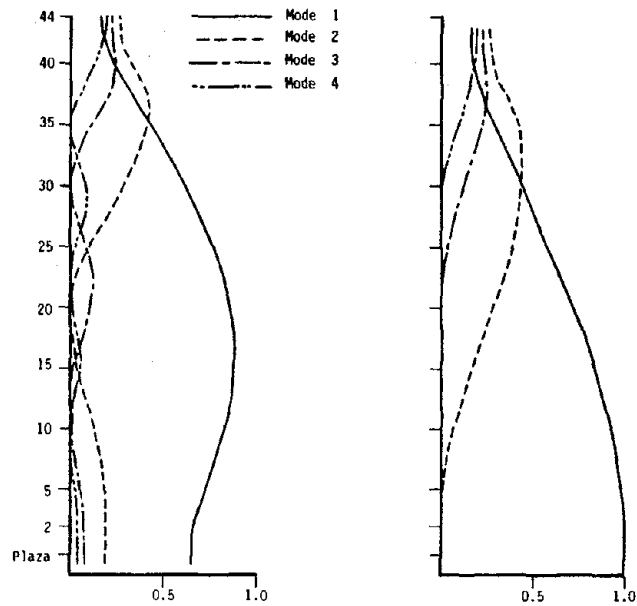


(a) Deflections



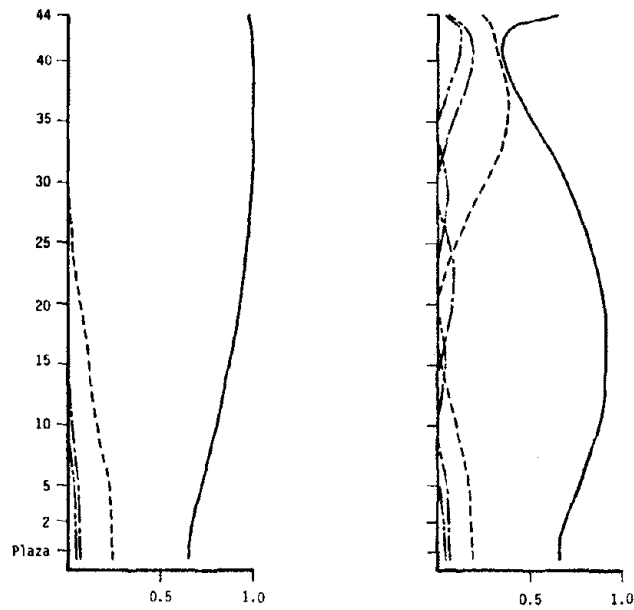
(b) Drifts

Figure 3.6.15: Story Displacement Quantities from the Analytical Models



(a) Shears

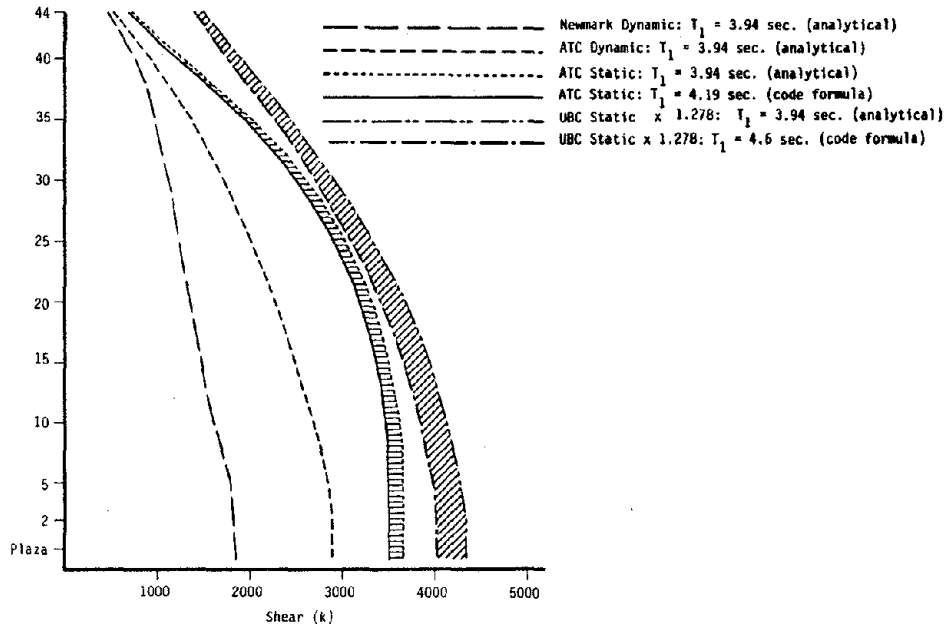
(b) Overturning moments



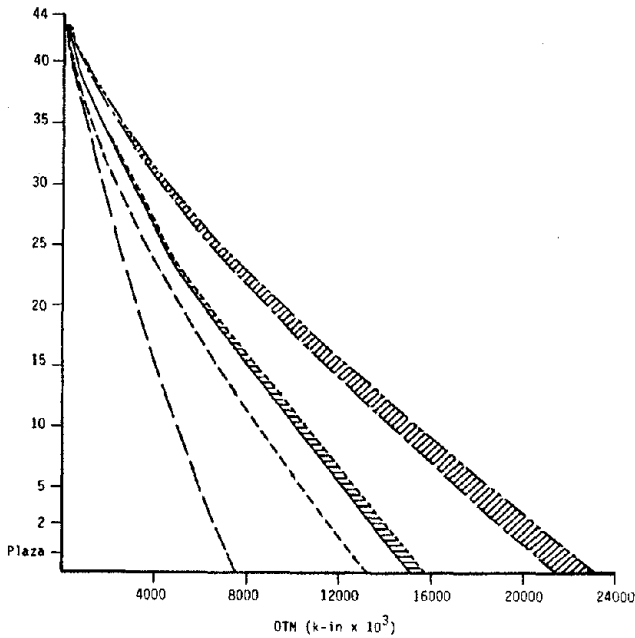
(c) Deflections

(d) Drifts

Figure 3.6.16: Modal Contributions to Design Quantities

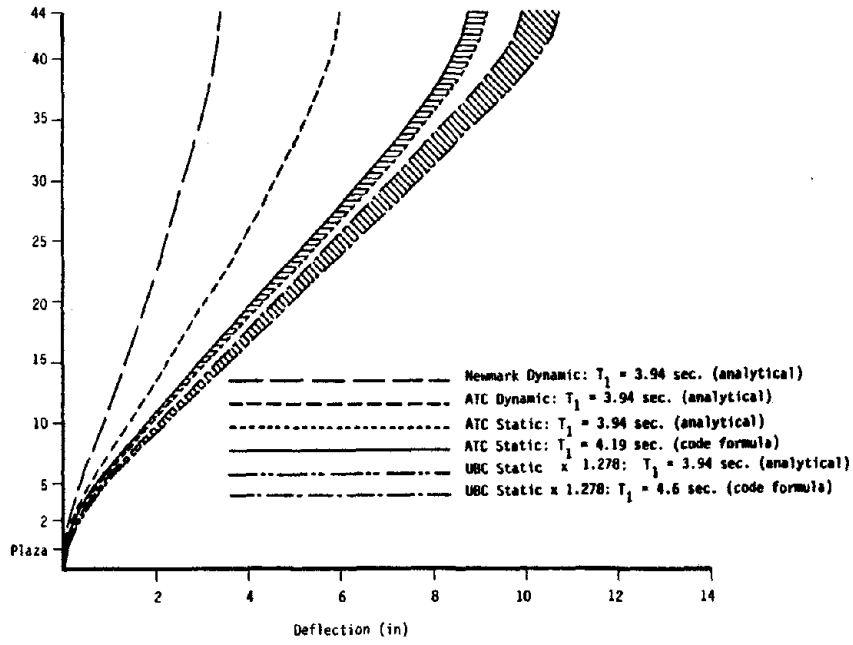


(a) Shears

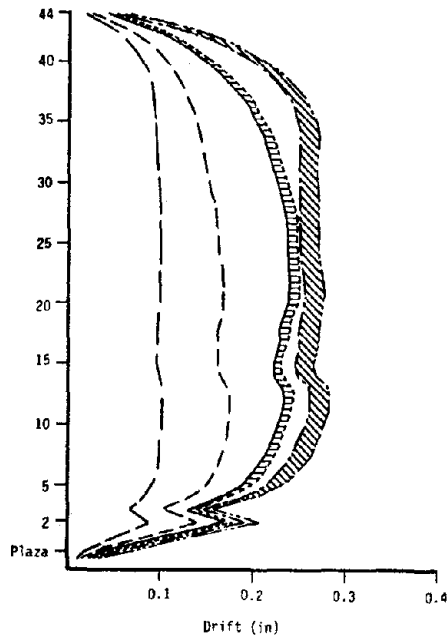


(b) Overturning moments

Figure 3.6.17: Story Force Quantities Resulting from Dynamic and Equivalent Static Analyses

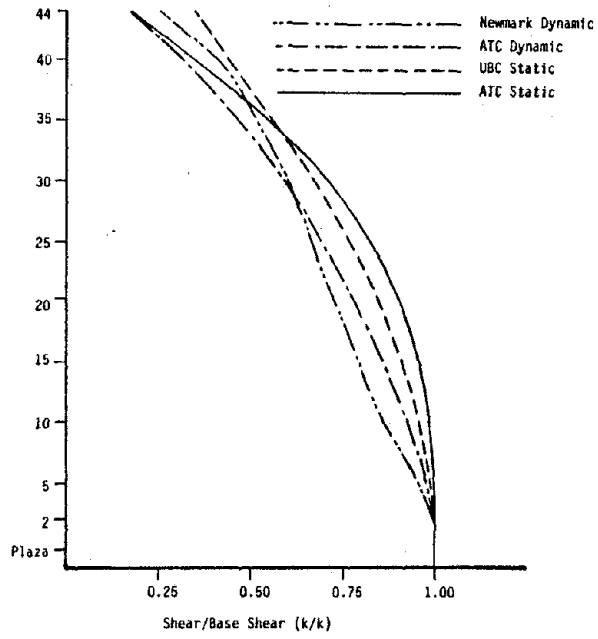


(a) Deflections

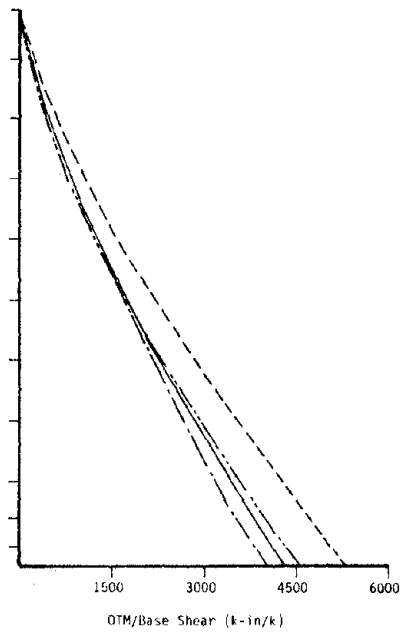


(b) Drifts

Figure 3.6.18: Story Displacement Quantities Resulting from Dynamic and Equivalent Static Analyses

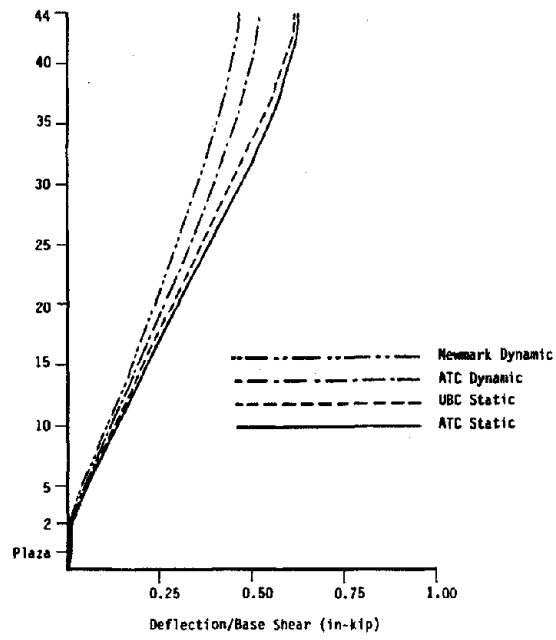


(a) Normalized Shears

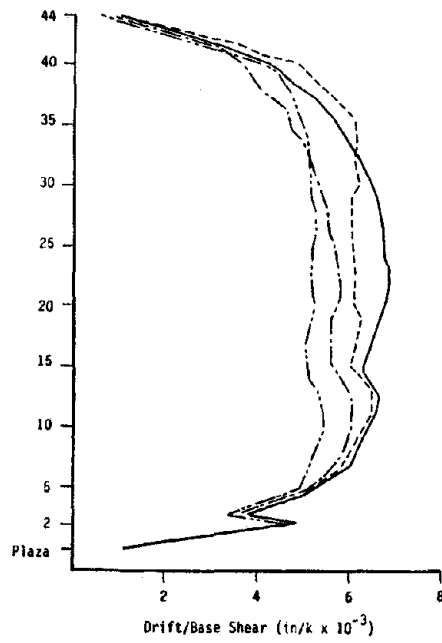


(b) Normalized Overturning Moments

Figure 3.6.19: Story Force Quantities Normalized to Base Shear

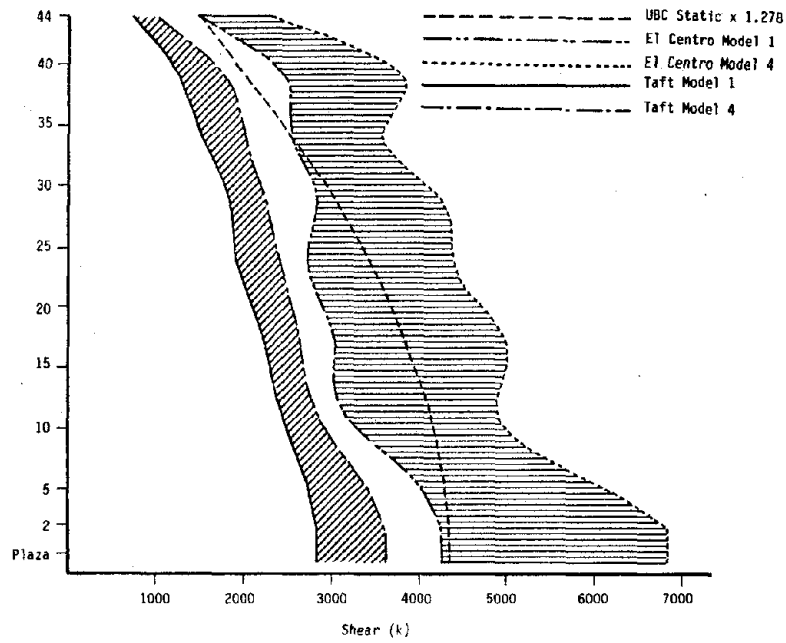


(a) Normalized deflections

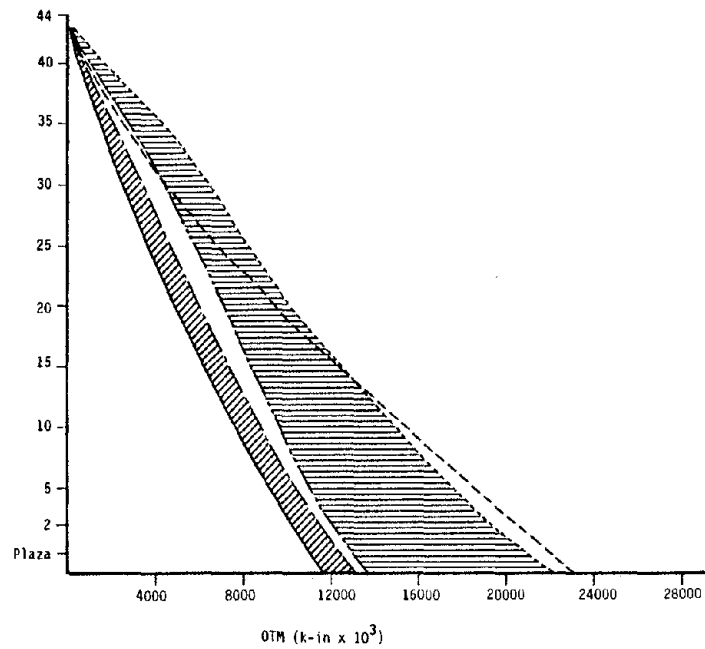


(b) Normalized drifts

Figure 3.6.20: Story Displacement Quantities Normalized to Base Shear



(a) Shears



(b) Overturning moments

Figure 3.6.21: Comparison of UBC Design Forces versus Elastic Forces Induced by Actual Earthquake Spectra

### **3.7 OBSERVATIONS AND CONCLUSIONS FROM THE CORRELATIVE ANALYTICAL STUDIES**

The correlative analyses of the five structures discussed in this chapter demonstrate several important aspects relating to seismic analysis of multistory buildings. From the results of these analyses, general observations and conclusions relating to modeling approaches, overall dynamic behavior characteristics, and expected variations in response due to different representations of seismic loading are made in the sections that follow. Detailed discussions of the analyses performed on each of the buildings are presented in sections 3.2 to 3.6.

#### **3.7.1 Period and Mode Shape Correlation**

Very good to excellent correlation of experimental and analytical periods was achieved for all of the buildings studied. Final analytical models were able to accurately predict fundamental and higher periods for both translational and torsional modes. However, initial analytical periods based on computer models of the primary lateral force resisting system acting alone were always higher than experimentally determined periods. As can be seen from the ratios of analytical to experimental periods in Table 3.7.1 (column 1), initial analytical translational fundamental periods were from 1.10 to 1.51 times larger than corresponding periods resulting from small amplitude vibration studies. However, by accounting for various secondary modeling aspects, period correlation was substantially improved. Final analytical fundamental periods (based on computer models of the primary lateral force resisting system acting in conjunction with secondary lateral and/or vertical force resisting systems and other significant structural and/or nonstructural aspects) were within 5% (period ratios between 0.96 and 1.05) for all of the buildings as can be seen from Table 3.7.1 (column 2). Analytical mass values which gave best correlation were somewhat smaller than corresponding values

typically used in design calculations; this is due to the fact that building code requirements tend to overestimate mass by including a 20 psf partition load and because design engineers often make other conservative assumptions in calculations of dead weight. However, mass variations, overall, had only a minor effect on the analytical periods.

In general, analytical mode shapes correlated very well with those derived from experimental studies. The location and relative deflection amplitudes of nodes and antinodes were predicted with good accuracy for fundamental and higher modes. For buildings where severe stiffness discontinuities occurred, resulting irregularities in analytical mode shapes matched experimental results well. Good correlation of experiment and analysis was observed even where only slight perturbations in mode shape occurred due to more moderate stiffness discontinuities (e.g. discontinued frames evidenced in first mode of Transamerica Building). The secondary modeling aspects that were included in the refined analytical models did not significantly influence the analytical mode shapes. This result indicates that the secondary aspects considered had more or less constant relative stiffening effects over height for the buildings studied and suggests that it may be appropriate to represent the influence of secondary effects by simply factoring the stiffness of the primary lateral force resisting system.

**SUMMARY:** The correlative analyses performed show that natural periods and mode shapes determined from small amplitude tests can be accurately predicted using practical analytical models of limited complexity based on actual detailed characteristics of the structure. However, to achieve correlation between analytical and experimental periods, various secondary aspects must be included in the models. Use of an analytical model that accounts for none of these secondary aspects will most likely result in natural period estimates that are

larger than those that would result during a moderate earthquake event.

### 3.7.2 Comparative Dynamic Properties of the Study Buildings.

Similar trends in the dynamic properties of the different buildings are apparent from the experimental and analytical results. In Table 3.7.2, ratios of analytical fundamental translational periods to higher translational periods are shown for the different buildings studied. As can be seen from this table, all of the buildings, except Transamerica, had nearly equivalent ratios of fundamental period to higher periods. The Transamerica building exhibited substantially lower period ratios than did the other buildings due to the vertical irregularity introduced by its tapered configuration. As shown in Table 3.7.2, average period ratios for the group of buildings studied (excluding Transamerica) are 2.89 for  $T_1/T_2$ , 5.06 for  $T_1/T_3$  and 7.18 for  $T_1/T_4$ . These average values compare closely with the theoretical uniform shear beam period ratios of 3.0, 5.0, and 7.0, respectively, also shown in the table. This result indicates that multistory buildings which are basically regular over their heights have period ratios that are approximately equivalent to uniform shear beam ratios. Thus, given the fundamental period, good approximations of higher mode periods can be made using the uniform shear beam relationship by dividing the fundamental period by three, five, seven, nine, etc., to estimate the second, third, fourth, fifth, etc., periods, respectively.

In Figure 3.7.1, the first four analytical translational mode shapes based on refined analytical models of the different buildings studied are shown for comparison. (Note that for the Transamerica and Rainer buildings, respectively, the architectural cap and pedestal base have been omitted from the plotted mode shapes.) As can be seen from this figure, some variations in mode shape exist among the different buildings. However, the following similar characteristics

are apparent:

- (1) The number of node points (points of zero deflection) for a given mode is equal to the mode number. For example, the first mode has one node point (at the base); the second mode has two node points; etc. This result generally occurs in multistory buildings unless flexibility of the floor slab allows substantial in-plane diaphragm deformation. For tall multistory buildings, diaphragm deformation is usually not significant. (Note that for Transamerica's fourth mode, the fourth node occurs in architectural cap and is not shown.)
- (2) Except at the top of the structure, all antinodes of the higher modes have nearly equal relative deflection amplitudes for each building. The antinodes at the tops of the buildings tend to have a less predictable relative amplitude but are of the same general magnitude as those below.
- (3) The location of node points relative to total height are roughly the same for the different buildings. For example, for each of the buildings studied, a node for the second mode occurs at a point located between 0.75 and 0.81 times the total height (see Figure 3.7.1). Because of the Transamerica building's vertical irregularity, the relative location of its node points varied significantly from the other buildings in the third and fourth modes.
- (4) The distances between node points of higher modes tend to decrease with increasing height above the base. For example, for the fourth mode in Figure 3.7.1, the average distances between the first (base) to second, second to third, and third to fourth nodes are approximately 0.37, 0.29 and 0.24 times the total height, respectively.

It is of interest to compare these observed mode shape characteristics with those of a uniform shear beam which are also shown in Figure 3.7.1. These modes are sine curves represented by

$$\phi_n (h) = \sin \left[ \left( \frac{2n-1}{2} \right) \pi \frac{h}{H} \right]$$

where  $n$  = the mode number. The most notable similarities seen in Figure 3.7.1 between the uniform shear beam idealization and the actual observed results are that the same number of nodes and antinodes result in respective modes and that the antinodes have a constant relative deflection amplitude. The most notable differences are that node points occur at lower points in the uniform shear beam idealization than are observed in the actual buildings and that the

distance between these node points is constant rather than decreasing with height. These differences between the uniform shear beam idealization and the actual building responses result from the fact that the actual buildings have decreasing lateral stiffnesses with height (rather than being uniform) and that some cantilever type deformation (in addition to shear type) is caused by axial extension or compression of the columns and other vertical force resisting elements. The Alcoa N-S, U.C. Medical Center, Ranier Tower, and Century City buildings, generally behave as nonuniform shear beams with little or no cantilever type response. However, the Alcoa E-W and Transamerica buildings demonstrate mixed cantilever beam and nonuniform shear beam behavior.

It should be noted that although the results that have been presented in Table 3.7.2 and Figure 3.7.1 are for translational modes, the torsional modes for the respective buildings demonstrate behavior that is very similar to the translational modes. That is, both torsional period ratios and mode shapes correspond very closely with corresponding translational results and have similar relationships with respect to uniform shear beam theory.

**SUMMARY:** The dynamic properties of the various buildings are very similar in nature in that the period ratios and mode shapes of the different buildings compare quite closely. Observed period ratios of the buildings compare very well with results from uniform shear beam theory. However, the observed versus uniform shear beam mode shapes showed significant differences. Based on the results of the buildings studied, it can be seen that multistory buildings which are basically regular over their heights will generally show similar trends in their dynamic properties. Also, it can be seen that, based on the behavioral trends observed in this study, the dynamic characteristics of several modes of vibration for a planned multistory building may be reasonably approximated before detailed design and/or analysis

proceeds. In section 4.3, an approach for performing preliminary dynamic analysis based on estimates of dynamic properties is presented.

### **3.7.3 Influence of Secondary Modeling Aspects on Stiffness Properties**

Results of the analytical studies presented earlier in this chapter show that secondary structural and nonstructural modeling aspects have a significant influence on the dynamic properties observed in the small amplitude experimental studies. The secondary aspects that were considered (where applicable) are rigid joint zone effects, three dimensional frame modeling, core frame modeling, nonstructural slab-girder interaction, and infill block wall modeling. In Table 3.7.3, the increases in the generalized stiffness of the fundamental mode caused by these different secondary aspects for each of the study buildings are shown. As can be seen from this table, the different secondary aspects had varying relative importance for each of the buildings studied. In the comments that follow, the term "stiffness" refers to the generalized fundamental modal stiffness determined from period values for the different analytical models formulated for each building.

Inclusion of flexurally rigid joint zones caused increases in stiffness ranging from 0% to 85% over that of the initial model of the primary lateral force resisting systems (Table 3.7.3, column 1). The greatest stiffness increases from rigid joint zone effects occurred in the Century City Tower (85%) due to the closely spaced columns in this building and in the U.C. Medical Center (66%) due to the deep girders required for the long span framing. Moderate increases in stiffness of 17% and 26% result in the Transamerica and Ranier Tower buildings, respectively. Rigid zones had no significant influence on the truss bracing system of the Alcoa building as is expected since bending deformations do not contribute significantly to the overall response.

Summarizing, rigid joint effects have a significant stiffening influence on moment resisting frame structures with a particularly larger influence in buildings with especially short or long spans.

Modeling of nonplanar, intersecting frames with full three-dimensional compatibility had a significant stiffening effect in some of the buildings. The Alcoa building showed a 16% (Table 3.7.3, column 2) increase in the E-W stiffness due to the participation of the N-S framing acting as flanges which increase the effective moment of inertia in the E-W direction. A lesser stiffness increase of 5% in the N-S direction is noted due to the smaller flange effect provided by the E-W framing. The Ranier Tower showed a 32% stiffness increase and the Century City building showed an 11% increase. In the above buildings, 3-D frame modeling brought into play the axial resistance of the columns in nonplanar intersecting frames. In the Transamerica building, 3-D modeling has negligible effect since all columns are common to perpendicular planar frames and, therefore, have full participation in 2-D frame modeling. In the U.C. Medical building, the girders are unable to transmit significant axial forces to columns of nonplanar frames due to the long spans and, consequently, 3-D frame modeling has negligible influence.

Nonstructural slab-girder bending interaction in the primary lateral resisting system was accounted for in the Transamerica and Century City buildings where stiffness increases of 28% and 11% resulted, respectively (Table 3.7.3, column 3). In the U.C. Medical and Ranier Tower buildings, the primary lateral systems are designed to act compositely with the concrete floor slabs and, therefore, the resulting interaction is included in the initial model results. Since the Alcoa building is a truss system, slab-girder bending interaction does not significantly influence the lateral stiffness of the primary lateral resisting system.

The influence of including the core frame (where appropriate) as

part of the analytical model is significant for some of the study buildings. The core frame models are comprised of primary vertical and/or secondary lateral force resisting framing with nonstructural slab-girder interaction effects included if appropriate. In the Alcoa building the core frame is a secondary (back-up) ductile moment resistant frame capable of carrying 25% of the code specified lateral load. Inclusion of the core frame caused stiffness increases of 19% and 13% in the E-W and N-S directions, respectively (Table 3.7.3, column 4). In the U.C. Medical building, the long span interior frames are designed primarily for vertical load but also contribute significantly to lateral stiffness as evidenced by the 37% stiffness increase shown in the table. In the Ranier Tower, a 25% stiffness increase is contributed by the primarily vertical load carrying core frame assuming full moment connections. In the Century City building, a 2% stiffness increase results from inclusion of the core frame; this stiffness increase is small because the lightweight beams that frame between the heavier columns are unable to provide sufficient stiffness to induce significant frame action even if full moment connections are assumed.

Concrete masonry block walls were used as an infill material in the core frame of the Alcoa building. Inclusion of these walls in the analytical model led to significant increases in stiffness of 11% and 24% in the E-W and N-S directions, respectively (Table 3.7.3, column 5).

**SUMMARY:** Total increases in the fundamental mode generalized stiffness due to secondary modeling aspects over that of the initial model of the primary lateral force resisting system range from 42% to 109% for the different study buildings (Table 3.7.3, column 6). These relatively large stiffness increases indicate the importance of including the various secondary modeling aspects to accurately predict small amplitude dynamic properties. In developing an analytical model

for larger amplitude motions, secondary nonstructural aspects such as slab-girder interaction and infill block walls may be neglected if it is judged that these components are unable to provide resistance at larger levels of displacement amplitude. Nevertheless, the secondary structural aspects such as rigid joint zones, 3-D frame modeling, and core frame modeling can still cause significant increases in stiffness as can be seen from Table 3.7.3 and will certainly be active at larger levels of response. Therefore, these aspects should be included in model development in order to obtain more accurate period estimates.

#### **3.7.4 Influence and Interpretation of Secondary Modeling Aspects on Seismic Response Analysis**

The impact that secondary modeling aspects have on predicted seismic response of a particular building depends not only upon the induced stiffness increases and accompanying shortening of natural periods but also upon the response spectrum used for the analysis and period zones of the spectrum to which significant modes correspond.

Dynamic analyses have been performed on each of the study buildings to compare responses resulting with and without inclusion of secondary modeling aspects using the Newmark response spectrum (shown in Figure 3.1.1). The stiffening influence and resulting period shortening caused by inclusion of secondary modeling aspects will generally produce increased design forces when smoothed design response spectra such as Newmark's are used. This is because smoothed design response spectra usually have increasing spectral amplitude with decreasing period in the period ranges that are most significant for multistory buildings. However, despite the increased forces, deflection responses tend to decrease or remain constant as a result of stiffening due to secondary modeling aspects. These trends are reflected in Table 3.7.4, where variations in base shear, base overturning moment, and roof deflection resulting from consideration of all secondary modeling aspects are shown for the different

buildings studied. As can be seen from this table, variations in base shear ranged from +16% to +87%; variations in overturning moment ranged from +13% to +112%; and, variations in roof deflection ranged from -1% to -27%. In order to better understand the reasons for these response variations, the responses of the Alcoa and Century City buildings are explained in more detail.

The Alcoa building showed the smallest variation in design forces because secondary modeling aspects had a lesser total effect on its stiffness than on the stiffnesses of most of the other buildings studied (42% and 46% in Table 3.7.3, column 6) and because its significant periods lie in zone C of the Newmark spectrum (see Figure 2.3) where spectral amplitude varies with period in proportion to  $1/T$ . These variations are consistent with predictions that can be made using the relationships developed in section 2.5 based on the stiffening observed in the fundamental mode. For example, Figure 2.13 (a) can be used to reason the variations in response quantities for the Alcoa E-W direction as follows: a 46% fundamental mode stiffness increase corresponds to a  $a = 1.46$  in Figure 2.13(a) and the Newmark spectrum zone C corresponds to the  $p = 1.0$  curve which predicts a 21% increase in shear and overturning response ( $V^*/V = OTM^*/OTM = 1.21$ ) of the fundamental mode. This compares well with the 20% and 18% increases in base shear and overturning that resulted in the detailed analyses (Table 3.7.4). Likewise, using Figure 2.13(b), a 17% decrease in fundamental mode deflection response ( $D^*/D = 0.83$  for  $a = 1.46$ ,  $p = 1.0$ ) is predicted which compares well with the 15% reduction shown in the table. The fact that the results from the detailed analyses compare so well with predicted fundamental modal response variation reflects the predominant influence of the fundamental mode in the overall response of the Alcoa Building.

The Century City building showed the greatest variation in design forces from secondary modeling aspects because it had the greatest

total secondary stiffening effect among the buildings studied (109% in Table 3.7.3, column 6) and because its fundamental period lies in zone D of the Newmark spectrum where spectral amplitude varies more rapidly with period (in proportion to  $1/T^2$ ). Increases in base shear and overturning of 87% and 112%, respectively, are seen in Table 3.7.4. Using Figure 2.13(a), the 109% stiffness increase due to secondary effects leads to a 109% predicted increase in the fundamental modal shear and overturning response ( $V^*/V = OTM^*/OTM = 2.09$  for  $a = 2.09$ ,  $p = 2.0$ ). This result agrees well with the actual base overturning increase (112%) but agrees less favorably with the actual base shear increase (87%). This discrepancy in base shear is due to the fact that although the fundamental mode dominates the base overturning response of this building, higher modes significantly influence the base shear response and the higher mode shear contributions will increase to a lesser extent since they lie on zone C of the Newmark spectrum. Using Figure 2.13(b), it can be seen that increasing stiffness due to secondary effects will result in no change in fundamental modal deflection response for  $p = 2.0$ . This 0% predicted variation agrees well with the slight 1% decrease shown in Table 3.7.4 reflecting the dominant influence of the fundamental mode in deflection response of this building.

**SUMMARY:** It can be seen that consideration of secondary modeling aspects can have significant and widely varying impact on analytical response of multistory buildings. The degree of variation in response will depend upon the amount of stiffness increase due to secondary aspects, the shape of the response spectrum used, the relative importance of fundamental versus higher modes, and the particular response quantity of interest. If an estimate of the stiffening effect of secondary modeling aspects can be made, the relationships of section 2.5 can be used to approximate resulting variations in response quantities.

### 3.7.5 Relative Significance of Various Modes on Seismic Response

As part of the response spectrum dynamic analyses performed on the subject buildings (using Newmark's spectrum), a study of the relative contributions of the various modes to the shear, overturning, deflection, and drift responses was carried out. For each of the buildings, the fundamental mode of vibration showed the greatest overall influence on the dynamic response. However, the contributions of higher modes were significant as well.

Since, for the response spectrum analyses performed in this study, the square-root-of-the-sum-of-the-squares modal combination rule is used to calculate peak responses, the contribution of each mode to peak response can be represented as a ratio of the square of the mode's peak response to the total sum of the squares of all modal peak responses. For example, the contribution of mode 'n' to total peak shear response may be represented by the ratio

$$\frac{(V_n)^2}{\sum_{i=1}^N (V_i)^2}$$

where

$V_i$  = peak shear in mode i

N = total number of modes considered

Modal contribution ratios calculated in this way for base shear response are shown in Table 3.7.5 for the different buildings analyzed. From this table, the relative importance of the fundamental mode in contributing to peak base shear is reflected by the high ratios observed in mode 1 for the Alcoa, Transamerica, U.C. Medical Center and Century City buildings. The contribution of higher modes decreases rapidly with increasing mode number for these buildings. As can be seen from the table, modes higher than the fourth contribute negligibly to base shear response for these four buildings which are

basically regular over their heights and have no severe discontinuities in lateral stiffness. However, the Ranier Tower shows completely different response behavior having very low contributions from the first four modes to total base shear. For this building, higher modes become dominant in the base shear response due to the very stiff and massive concrete pedestal upon which the steel superstructure of the building rests. It turns out that the pedestal's response is predominantly activated by the 12th mode whereas the steel superstructure's response is most influenced by the fundamental mode. Since base shear of this building is controlled by pedestal response, higher modes must be considered to fully capture the dynamic behavior.

It can also be seen from Table 3.7.5 that the taller buildings having longer fundamental periods tend to show greater relative contributions from the higher modes. For instance, the 195 ft. tall U.C. Medical Center building ( $T_1 = 1.13$ ) has modal contribution ratios of .89, .10, .01, and .00 from its 1st, 2nd, 3rd, and 4th modes, respectively, whereas the 576 ft. tall Century City building ( $T_1 = 3.94$ ) has corresponding modal contribution ratios of .68, .19, .08 and .04. The greater contributions from the higher modes in the Century City building result from the fact that as fundamental period increases and moves away from the spectrum zone containing peak dynamic amplifications (zone B in the Newmark spectrum between about 0.15 sec. and 0.50 sec.), higher modes become more greatly amplified relative to the fundamental mode.

Although the results shown in Table 3.7.5 are illustrative for demonstrating the relative importance of the various modes to response, these only reflect the modal contributions for one response quantity (story shear) at one location (base level) over the building's height. In Figures 3.2.19-20, 3.3.12, 3.4.14, 3.5.11, and

3.6.16, the modal contribution ratios are plotted for shear, overturning moment, deflection and drift at all story levels over the full heights of the different buildings. From a study of these figures, the following observations can be made regarding modal contributions to the various response quantities at different levels of the buildings:

- (1) Higher modes influence story shear response most significantly in the uppermost levels of the buildings. For most of the buildings, the 2nd, 3rd and 4th mode contribute more greatly to shear response at the top of the building than does the fundamental mode. However, the fundamental mode typically dominates shear response around the midheight of the buildings. Near the base of the buildings, the contribution of the higher modes again become more important but the fundamental mode is generally most significant. The Rainer Tower is an exception where the 12th mode dominates base shear response due to the massive concrete pedestal.
- (2) Like story shears, overturning moments are influenced most significantly by higher modes in the uppermost portions of the buildings. At lower levels of the buildings, the fundamental mode becomes progressively more dominant in controlling overturning forces. Unlike the case for story shears, higher modes generally contribute insignificantly to overturning at the bases and overturning response is dominated by the fundamental mode.
- (3) Total deflection response is generally dominated by the fundamental mode at all levels of the buildings with higher modes having only slight significance near the base. An exception to this is seen in the pedestal based Ranier Tower where the fundamental mode dominates the deflection response of the steel superstructure but the 12th mode contributes most to the deflection in the pedestal base.
- (4) Drift responses follow the same general trends as shear response whereby higher modes have the greatest influence near the top and base of the structures and the fundamental mode is dominant around midheight.

**SUMMARY:** Although the fundamental mode is generally the most dominant in seismic response of multistory buildings, higher modes are often significant contributors. The taller the building, the more significant the higher modes become. Generally, the first 4 to 6 modes occurring in a single translational direction are enough to capture all significant unidirectional response in a symmetric multistory building. If severe stiffness discontinuities exist, as in

the case of the Ranier Tower, enough modes must be considered to capture the full response in all regions of the structure. The relative importance of the higher modes in influencing response depends upon the fundamental periods of the building, the particular response quantity of interest, and the location being considered over the height of the building.

### **3.7.6 Comparison of ATC and UBC Period Estimates with Experimental and Analytical Results**

It is of interest to compare the fundamental periods predicted by the UBC and ATC codebook empirical formulae with the periods determined from the detailed analytical models and the experimental tests since the period values used will have a direct influence on the magnitude of applied seismic forces. In Table 3.7.1 (columns 3 and 4), the ratios of UBC and ATC empirically calculated periods to experimental small amplitude periods are shown for the different buildings. For all of the buildings except Transamerica, the UBC period estimates range from .70 to 1.27 times the experimentally determined values and the ATC period estimates range from .70 to 1.54 times as experimentally determined values. Thus, it is seen that, for the group of regular buildings studied, the empirical codebook predictions have limited accuracy and lead to as much as 30% underestimation and 54% overestimation of small amplitude fundamental periods. Most often, the codebook formulae will underestimate actual small amplitude periods for modern highrise construction. However, overestimates were noted in the U.C. Medical Center and Century City buildings due to the especially large stiffening influence of rigid joint effects resulting from the particularly long and short girder spans, respectively, used in the design of these buildings. For the Transamerica building, larger errors result from application of the codebook formulae as is seen from the period ratios of 1.70 and 1.58 for UBC and ATC, respectively, indicating that codebook estimates are

highly unreliable for buildings with significant vertical irregularity.

Since the fundamental periods from the experimental tests and from the final analytical models are nearly equal (see Table 3.7.1, column 2), the error ranges quoted above also apply for codebook versus final analytical periods. However, many of the secondary modeling aspects included in the final analytical models of this study are not typically considered by practicing engineers in the development of analytical models. Often, computer models, which include only the primary lateral force resisting system with none of these secondary aspects, are used and will lead to substantially higher estimates of natural period and, consequently, may cause further discrepancies between analytical and codebook periods. In columns 5 and 6 of Table 3.7.1, the ratios of the periods of the initial analytical models (including only the primary lateral force resisting system) to the UBC and ATC codebook periods are shown. For the regular buildings (Transamerica excluded), the initial analytical periods ranged from 1.07 to 2.01 times UBC estimates and from 0.88 to 2.01 times the ATC values. Generally, analytical periods based on the primary lateral force resisting system acting alone will be substantially larger than UBC or ATC codebook estimates and can be as much as 100% larger (e.g., Ranier Tower). However, this was not noted in the U.C. Medical Center and Century City buildings due to the large rigid joint zone stiffening effects mentioned earlier.

**SUMMARY:** UBC and ATC empirical formulae have limited accuracy in predicting actual small amplitude period. These formulae show especially poor overall correlation with periods derived from initial analytical models of the primary lateral force resisting systems acting alone. Since the natural periods of vibration ultimately control the magnitude of forces that will be induced in a building during earthquake excitation, the engineer should be wary of any large

differences that may occur between analytical versus codebook periods and be able to reconcile these differences based on the detailed characteristics of the structure and the particular design criteria being applied.

### **3.7.7 Comparative Magnitudes of Selected Response Spectrum Dynamic and Code Equivalent Static Loading Procedures**

In this study, analyses were performed on one model of each building using four different recommended seismic loading procedures: two equivalent static and two dynamic. The equivalent static methods used are those prescribed by UBC and ATC; the dynamic analyses response spectra used are those prescribed by ATC and Newmark. As described in section 3.1.2 (step 5), analytical responses resulting from application of the different procedures reflect a single set of assumptions relating to soil conditions, peak ground acceleration, and design force level (elastic limit rather than working stress level). Therefore, the calculated responses are in accordance with a common basis of comparison. In Figures 3.2.21-24, 3.3.13-14, 3.4.15-16, 3.5.12-13, and 3.6.17-18, the gross response quantities of shear, overturning, deflection and drift resulting from the four different seismic loading procedures are shown for the different buildings. From these figures, it may be seen that wide variations in the magnitude of the predicted seismic responses result for the different loading procedures despite the fact that they are based on ostensibly common assumptions. Responses for the dynamic analysis procedures (Newmark and ATC) are based on analytical models whose period values compare closely with the experimental test results. Responses for the equivalent static analysis procedures (UBC and ATC) are based on two periods, namely, the analytically derived values (same as in the dynamic analysis) and the codebook empirical formulae values. As can be seen from the figures, differences that occur between the analytical and codebook period values can lead to wide variations in

magnitude of response using the equivalent static methods (see section 3.7.6).

Putting aside the changes in equivalent static responses caused by use of codebook empirical period estimates, a general comparison of the results from the different seismic loading procedures can be made by comparing total base shears based on analytical period values only. In Table 3.7.6, base shear ratios resulting from the different analytical procedures are shown with respect to results of Newmark spectrum dynamic analysis of each building. Here, models that give analytical periods corresponding to the experimental results have been used for the response calculations of each building. The following observations can be made from examination of this table:

- (1) The results from UBC and ATC equivalent static approaches give comparable base shear magnitudes for the buildings studied. As can be seen from the table, UBC leads to larger base shears than ATC for the longer period buildings (i.e., Transamerica, Ranier Tower and Century City) but gives slightly smaller values for the shorter period buildings (Alcoa E-W, Alcoa N-S, and U.C. Medical Center). These results reflect the differences in the UBC and ATC response spectrum curves where, as can be seen from Figure 3.1.1, the UBC spectrum has higher amplitudes than ATC in the longer period range and lower amplitudes in the shorter period range. The largest difference between the two equivalent static base shears occurs in the Century City building where the UBC value is 19% greater than the ATC value ( $2.34/1.97 = 1.19$ ).
- (2) Another important observation is the large differences that occur between the ATC equivalent static and ATC dynamic results. Despite the fact that both ATC analyses are based on the same fundamental period and response spectrum curve, the dynamic approach leads to substantially lesser base shear quantities for all of the buildings. Two aspects of seismic force determination common to both ATC equivalent static and dynamic analyses procedures are, firstly, that the contribution of a given mode to total base shear can be represented as the effective modal mass of the particular mode times the spectral amplitude corresponding to the mode's natural period and, secondly, that the sum of the effective masses of all modes should equal the total mass of the building (as shown in Clough(11)). However, in the equivalent static approach, only the fundamental mode is used in the analyses and its corresponding effective modal mass is implicitly assumed to be equal to the total mass of the building whereas, in dynamic analyses, the true effective modal mass of the fundamental mode typically is only 60% to 75% of the total mass. Thus, since the fundamental mode generally dominates base shear response, ATC dynamic analysis

leads to base shear responses that are less than the equivalent static values as is observed in Table 3.7.6. For the buildings studied, the base shears calculated in accordance with the ATC dynamic analysis method ranged from 59% (for Ranier Tower,  $1.62/2.76 = .59$ ) to 80% (for the U.C. Medical Center,  $1.00/1.25 = .80$ ) of the base shears calculated using the ATC equivalent static method. These results put in question the prudence of the ATC recommendation of using the same response spectrum curve for both single mode equivalent static analysis and multiple mode dynamic analysis.

- (3) A third important observation is the fact that the dynamic analyses using the Newmark spectrum (scaled to .067g for the Alcoa building and .05g for the others) yield the lowest values for base shear for all of the buildings studied as seen in Table 3.7.6. This result is due to the fact that Newmark specifies a relatively rapid descent of spectrum amplitude with increasing period in proportion to  $1/T$  or  $1/T^2$  in longer period ranges whereas UBC and ATC specify slower descents in proportion to  $1/T^{.5}$  and  $1/T^{.67}$ , respectively. The UBC and ATC recommend conservatively high estimates of spectral amplitude in the longer period range whereas the Newmark spectrum gives lower values and is more in accordance with observed earthquake ground motions. In this regard, the ATC commentary states that the "elastic acceleration response spectrum for earthquake motions has a descending branch for longer values of  $T$  ...and it varies roughly as  $1/T$ . However, because of a number of reasons associated with structural behavior of long-period buildings, it was decided that ordinates of design spectra should not decrease as rapidly with  $T$ ; hence, the period  $T$  appears to the two-thirds power." Thus, both the UBC and ATC equivalent static and ATC dynamic results reflect this conservatism for the multistory buildings studied.

In addition to being subjected to the four loading procedures mentioned above, analytical models of each building were also subject to both the Taft and El Centro response spectra (with 5% of critical damping) as described in section 3.1.2 (step 6). Results of these analyses are shown in Figures 3.2.29-30, 3.3.19, 3.4.17, 3.5.16, and 3.6.21. In these figures, the forces induced (assuming linear elastic behavior) by the Taft and El Centro spectra are compared to UBC forces factored by 1.278 to approximate the minimum level of forces that could initiate yielding (elastic limit level) in the buildings. If available, the engineer's original UBC seismic forces applied in the actual design were used. For each building, one of the models analyzed is composed of the primary lateral force resisting system including secondary structural modeling aspects, if any, contributing

directly to the stiffness of the primary system (e.g. rigid joint zones). For this model, secondary aspects that are nonstructural or are not part of the primary system are not included. In Table 3.7.7, the ratios of the base shears resulting from Taft and El Centro are shown with respect to the factored UBC base shear. As can be seen from the table, the Taft earthquake induces base shears ranging from 0.83 to 1.86 times the UBC elastic limit forces. These results indicate that if all the buildings were designed to resist only the minimum seismic force levels as specified by the UBC, only the U.C. Medical Center (ratio of 1.86) would suffer severe overstress while the other buildings' responses would be primarily elastic. This result is somewhat reassuring considering the fact that the Taft record represents a 7.6 magnitude earthquake with a source distance of 56 km and a peak ground acceleration of 0.17g. The El Centro record (6.6 magnitude, 8 km source distance, 0.34g peak ground acceleration) represents a more intense ground motion than Taft and gives base shears that are 1.52 to 3.36 times the UBC elastic limit levels for the buildings studied as shown in Table 3.7.7. Although these values indicate the potential for substantial inelastic response in a major earthquake event they are much smaller than the comparable spectrum reduction factors of 6 to 8 (for the buildings studied) that would be applied to the elastic design spectrum (0.4g effective peak acceleration) recommended by ATC for elastic limit design.

**SUMMARY:** Although equivalent static load procedures recommended by UBC and ATC would appear to require design for only a relatively low level of seismic forces compared to those that could be induced by a major earthquake, many conservatisms are built in to these procedures for the design of multistory buildings. These conservatisms result from factors such as: fundamental period underestimation, mass overestimation, response spectrum amplitude overestimation in longer period ranges, fundamental mode effective mass overestimation, and

resistance of secondary structural or nonstructural systems. Thus, multistory buildings designed according to equivalent static procedures may often rely less on inelastic response and ductile behavior in resisting a major earthquake than may be inferred from codebook criteria.

### **3.7.8 Comparative Seismic Response Distributions for Dynamic and Code Equivalent Static Loading Procedures**

In section 3.7.7, relative magnitudes of responses using dynamic and equivalent static loading procedures are compared. In this section, the distribution of response over the heights of the buildings are contrasted for the different loading procedures used. In Figures 3.2.25-28 ,3.3.15-16, 3.4.17-18, 3.5.14-15, and 3.6.19-20, the distribution of shear, overturning, deflection and drift responses normalized to base shear are shown for the buildings studied.

From a review of these figures, it can be seen that dynamic analyses using the Newmark and ATC response spectra generally lead to similar distributions of responses over the heights of the buildings. The differences that occur between the dynamic responses using these two spectra result from the greater relative amplitudes of the higher modes in the Newmark results causing higher relative shears near the tops of the buildings and lower relative shears around midheight compared to the ATC distributions. The difference in shear distributions are generally not substantial at most levels of the buildings but can become more pronounced in the upper few stories. The longer the building's natural periods, the greater these differences become. The greatest differences in distribution of response predicted by these two spectra are seen in the Rainer Tower results. However, the large separation of the fundamental periods of the steel superstructure and the concrete base leads to larger than typical differences in relative spectral amplitude of the significant modes and causes large variations between the Newmark and ATC response

distributions.

Despite the differences in response distribution that may occur from dynamic analysis using different smoothed spectra (such as Newmark vs. ATC), larger distribution discrepancies are noted when these dynamically produced distributions are compared with response distributions resulting from UBC and ATC equivalent static analysis procedures. The most obvious discrepancy between dynamic and equivalent static results is seen in the Rainer Tower story shear distributions (Figure 3.5.14(a)). In this building, severe stiffness and mass discontinuities occurring at the interface of the steel superstructure and the concrete pedestal result in a sharp increase in the distribution of story shear in levels below when dynamic analysis is used. Whereas the mode shapes used in the dynamic analyses reflect these discontinuities, the approximate fundamental modes used in equivalent static analysis do not. In the ATC and UBC equivalent static analyses, the use of grossly inaccurate fundamental mode approximations cause a disproportionate part of the total inertial forces to be applied to the steel superstructure leading to relative story shears at the interface that are more than twice those indicated by Newmark dynamic analysis. Both the UBC and ATC recommendations warn against the use of standard equivalent static techniques for analysis of buildings with significant discontinuities of stiffness or mass; and, the Rainer Tower example demonstrates the large errors that may potentially result.

In addition to this gross discrepancy, other, more subtle differences demonstrated in all of the buildings are worth noting. Comparison of the dynamic and equivalent static response distributions indicates that both the UBC and ATC equivalent static force distribution methods tend to overestimate relative story shears near the midheights for all of the buildings studied. This results from the fact that these methods do not directly account for the effects of

higher modes which may contribute significantly to base shear response but, insignificantly to midheight shear response. The ATC shear distributions generally show larger variations from dynamic results than do UBC. For example, near the midheight (22nd story) of the Century City building, the ATC story shear (relative to base shear) is 25% higher than Newmark whereas the UBC story shear is 17% higher (Figure 3.6.19(a)). The ATC distribution leads to greater overestimations because of the nonlinear (cantilever type) fundamental mode shape that is assumed for taller buildings causing a greater proportion of the lateral forces to be applied in the upper stories. In addition to the midheight story shear overestimation, the UBC tends to overestimate shears in the top stories as well. This is a result of the special top load that is required by UBC to account for the greater contribution of higher modes to response in the uppermost portions of the structure. UBC equivalent static analysis leads to overestimations of relative story shear at the tops of all the buildings studied except the Transamerica building where the top load has been omitted. These discrepancies between equivalent static and dynamic shear force distributions at the midheight and uppermost story levels generally become larger for buildings having longer natural periods due to the increasing importance of higher modes in overall response.

Another difference in response distribution is noted in overturning moment results. Equivalent static methods attempt to represent peak shears that are induced over the height of a building from multiple modal responses with a single force distribution rule based on an assumed fundamental mode shape. As discussed in section 3.7.5, although higher modes may contribute significantly to shear forces at the base of a building, they generally contribute negligibly to base overturning. As a result, both the UBC and ATC equivalent static methods lead to higher base overturning moments relative to

base shear than do the dynamic analyses. The largest difference is noted in the Alcoa E-W results where UBC static analysis leads to a 30% greater base overturning relative to base shear than does Newmark dynamic analysis (Figure 3.2.26(a)). The ATC procedure, however, allows for a reduction of its equivalent static overturning moment by specifying a reduction factor of 0.7 to be applied at the lower stories of taller buildings. This reduction factor is reflected in the ATC equivalent static overturning responses presented for the different buildings and leads to improved comparisons with dynamic overturning distributions. For example, referring again to the Alcoa E-W response, the ATC equivalent static base overturning relative to base shear was only 7% greater than the Newmark result being a significant improvement over the UBC 30% overestimate.

**SUMMARY:** The equivalent static response distributions differ notably from dynamic response distributions in some respects. Compared to dynamic analysis, the UBC equivalent static method leads to relative overestimations of shear response in the midheight and upper story regions and, also, to relative overestimations of overturning response in the lower story regions of the buildings studied. The ATC equivalent static method consistently overestimates shear response in the midheight regions of the building but gives reasonably good estimates of base overturning by allowing application of an overturning reduction factor. In general, the differences noted above tend to become amplified as natural periods increase and, consequently, will be larger for taller buildings. In section 4.3, a method for approximate dynamic analysis is presented whereby potential differences between equivalent static and dynamic response distributions can be predicted at the preliminary design stage.

Table 3.7.1: Ratios of Analytical and Codebook Fundamental Periods with respect to Experimental Periods

Building	Fundamental Period Ratios					
	Analysis vs. Experimental		Codebook vs. Experimental		Analysis vs. Codebook	
	(1) $T_{initial}/T_{exp}$	(2) $T_{final}/T_{exp}$	(3) $T_{UBC}/T_{exp}$	(4) $T_{ATC}/T_{exp}$	(5) $T_{initial}/T_{UBC}$	(6) $T_{initial}/T_{ATC}$
Alcoa E-W	1.10	0.96	0.76	0.76	1.45	1.45
Alcoa N-S	1.20	1.05	0.74	0.74	1.62	1.62
Transamerica	1.28	1.02	1.70	1.58	0.75	0.81
Rainer Tower	1.41	0.98	0.70	0.70	2.01	2.01
U.C. Med Center	1.36	1.01	1.27	1.54	1.07	0.88
Century City	1.51	1.05	1.23	1.12	1.23	1.35

$T_{initial}$  is the fundamental analytical period resulting from the initial model of the primary lateral force resisting system.

$T_{final}$  is the fundamental analytical period resulting from the final model of the building including secondary modeling aspects.

$T_{UBC}$  is the fundamental period based on empirical UBC codebook formulae.

$T_{ATC}$  is the fundamental period based on empirical ATC codebook formulae.

$T_{exp}$  is the fundamental period determined from experimental test results.

Table 3.7.2: Ratios of Fundamental Analytical Periods to Higher Mode Periods

Building	Modal Period Ratios		
	$T_1/T_2$	$T_1/T_3$	$T_1/T_4$
Alcoa E-W	3.03	5.37	7.71
Alcoa N-S	2.89	5.07	6.97
Transamerica	1.82	2.78	3.45
Rainer Tower	2.74	4.80	6.78
U.C. Med. Center	2.86	4.94	7.13
Century City	2.92	5.11	7.29
Average*	2.89	5.06	7.18
Uniform Shear Beam	3.0	5.0	7.0

\*Average period ratios excluding Transamerica

Table 3.7.3: Increases in Fundamental Mode Stiffness due to Secondary Modeling Aspects

Stiffness increases with respect to the initial model of the primary lateral force resisting system						
	(1)	(2)	(3)	(4)	(5)	(6)
Building	Rigid Joint Zone	3-D Frame Modeling	Non-Structural Slab-Girder Interaction	Core Framing <sup>1</sup>	Infill Block Walls	TOTAL
Alcoa E-W	--	16%	--	19%	11%	46%
Alcoa N-S	--	5	--	13	24	42
Transamerica	17	0	28%	--	--	45
U.C. Med. Center	66	0	--	37	--	103
Rainer Tower <sup>2</sup>	26	32	--	25	--	83
Century City	85	11	11	2	--	109

<sup>1</sup> modeling includes rigid joint zone and slab-girder interaction effects in the core frame

<sup>2</sup> for Rainer Tower results differ from those shown in Table 3.5.3 because, here, slab-girder interaction is accounted for in model of primary lateral system

Table 3.7.4: Variation in Design Quantities due to Secondary Modeling Aspects (based on dynamic analysis using Newmark spectrum)

Response increases with respect to the initial model of primary lateral force resisting system			
Building	Base Shear	Base Overturning Moment	Roof Deflection
Alcoa E-W	+20%	+18%	-15%
Alcoa N-S	+16	+13	-12
Transamerica	+27	+28	- 7
U.C. Med. Center	+42	+50	-27
Rainer Tower <sup>1,2</sup>	+36	+84	- 6
Century City	+87	+112	- 1

<sup>1</sup> for Rainer Tower results differ from those shown in Table 3.5.4 because, here, slab-girder interaction is accounted for in model of primary lateral system

<sup>2</sup> base shear and overturning values refer to the base of the steel tower at the top of the concrete pedestal.

Table 3.7.5: Modal Contributions to Base Shear  
(based on dynamic analysis using Newmark spectrum)

Building	Analytical Fundamental Period (sec)	Total Height (ft)	Modal Contribution Ratios for Base Shear					Total
			Mode 1	Mode 2	Mode 3	Mode 4	Higher Modes	
Alcoa E-W	2.00	378	.58	.35	.06	.01	.00	1.00
Alcoa N-S	1.68	378	.74	.23	.03	.00	.00	1.00
Transamerica	3.00	845	.59	.28	.09	.03	.01	1.00
U.C. Med. Center	1.13	195	.89	.10	.01	.00	.00	1.00
Rainer Tower	4.35	551	.07	.04	.01	.01	.87	1.00
Century City	3.94	576	.68	.19	.08	.04	.01	1.00

Table 3.7.6: Ratios of Base Shears Resulting from Different Seismic Loading Approaches

Building	Analytical Fundamental Period (sec)	Total Height (ft)	Base Shear Ratios wrt. Newmark Spectrum Analysis			
			Dynamic		Equivalent Static	
			Newmark	ATC	ATC	UBC
Alcoa E-W	2.00	378	1.00	1.07	1.38	1.32
Alcoa N-S	1.68	378	1.00	1.07	1.34	1.25
Transamerica	3.00	845	1.00	1.29	2.14	2.44
U.C. Med. Center	1.13	195	1.00	1.00	1.25	1.22
Rainer Tower <sup>1</sup>	4.35	551	1.00	1.62	3.12	3.53
Century City	3.94	576	1.00	1.56	1.97	2.34

<sup>1</sup>For Rainer Tower, values refer to base of steel superstructure at top of concrete pedestal.

Table 3.7.7: Ratios of Base Shears Resulting from Actual Earthquake Spectra to UBC Elastic Limit Values

Building	Model	Base Shear Ratios wrt. UBC Base Shear		
		UBC <sup>1</sup>	Taft	El Centro
Alcoa E-W	2	1.00	1.06	2.63
Alcoa N-S	2	1.00	1.23	2.35
Transamerica	2	1.00	.94	1.80
U.C. Medical Center	3	1.00	1.86	3.36
Rainier Tower <sup>2</sup>	6	1.00	1.05	1.52
Century City	4	1.00	0.83	1.56

<sup>1</sup>UBC values are factored by 1.278 to reflect elastic limit force levels.

<sup>2</sup>For the Rainier Tower, values refer to base of the steel superstructure at top of concrete pedestal

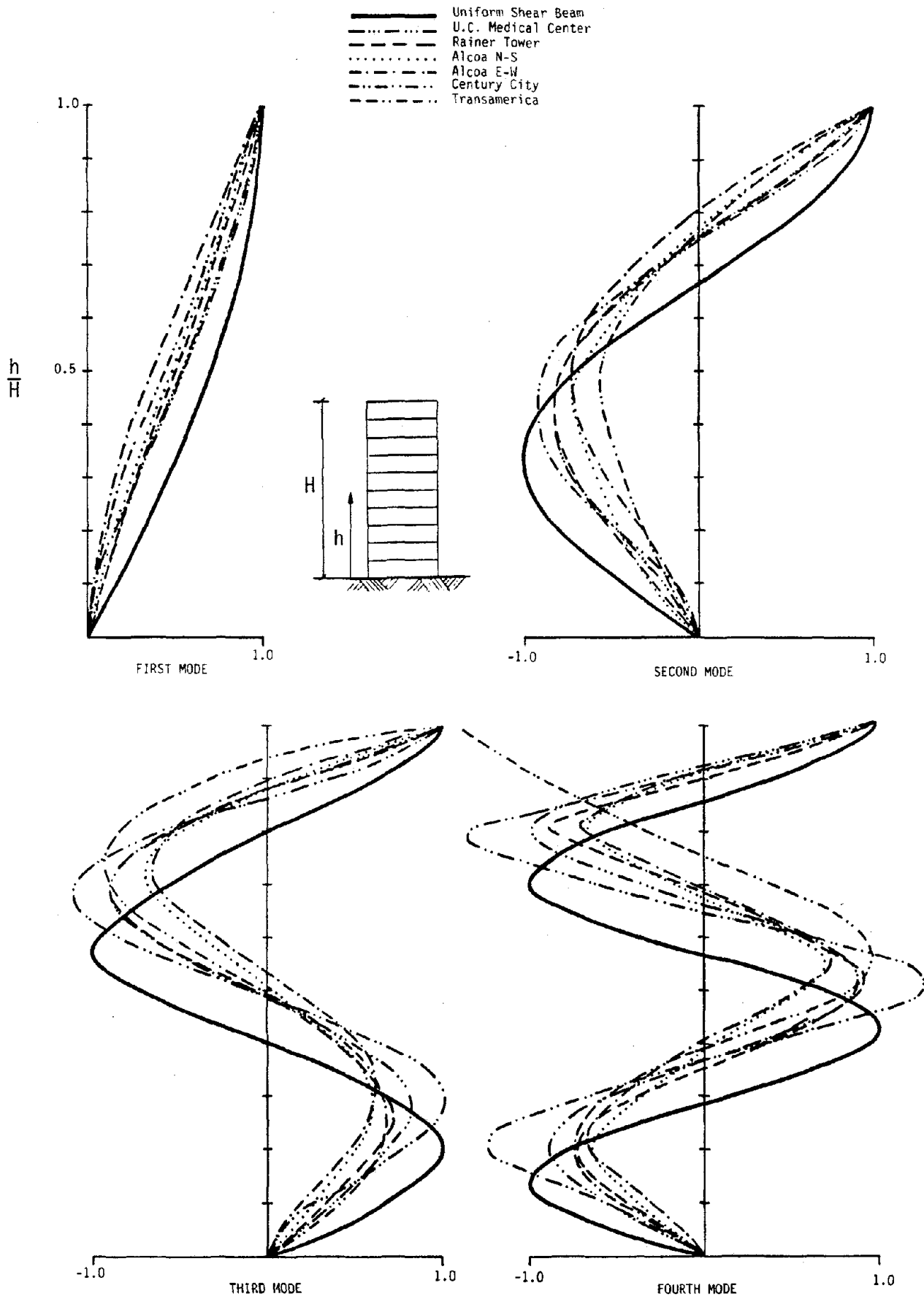


Figure 3.7.1: Comparative Analytical Mode Shapes

Page Intentionally Left Blank

**CHAPTER 4**  
**SELECTED TOPICS RELATING TO ANALYTICAL**  
**PROCEDURES FOR EARTHQUAKE RESPONSE**  
**OF MULTISTORY BUILDINGS**

In this chapter, three selected topics involving special analytical procedures for the seismic analysis of multistory buildings are presented. These topics are: (1) a method for accounting for the P- $\Delta$  effect in seismic analysis of buildings; (2) an investigation of comparative performances of different modal combination rules used in response spectrum analysis; and (3) a method for performing approximate dynamic analysis at the preliminary design stage. In the discussions that follow, sample analyses have been performed on one of the study buildings for each of the topics to demonstrate the analytical techniques and their potential influence on analytical results.

In order to investigate the topics discussed in this chapter, several modifications to the ETABS (49) program were required to extend its analytical capabilities. The new analytical features are incorporated in a modified version of the ETABS program (23) which has been made available for public distribution through the National Information Service for Earthquake Engineering (NISEE).

*Preceding page blank*

Page Intentionally Left Blank

## 4.1 ANALYSIS FOR P- $\Delta$ EFFECTS IN SEISMIC RESPONSE OF BUILDINGS

### 4.1.1 Introduction

Buildings are typically designed to resist two types of applied forces: stationary vertical (gravity) forces originating from dead weight, occupancy and equipment loads; and, transient lateral forces caused by earthquake or wind loading. These applied forces induce net vertical forces, horizontal shear forces, overturning moments and torsional moments which must be resisted at each story of the building. The vertical force and horizontal shear force acting at a given story are equivalent to the summations of the respective vertical and lateral loads applied above that story. The overturning and torsional moments acting at a given story have two contributing components: (1) primary moments resulting from the applied lateral and vertical loads acting over their respective lever arms measured from the points of application in the undeformed building configuration; and, (2) second-order moments caused by the vertical loads acting over their respective incremental lever arms resulting from the lateral deflection of the building. This latter second-order contribution to the overturning and torsional moments is commonly referred to as the P- $\Delta$  effect.

Current building codes(20) do not give specific recommendations for evaluating P- $\Delta$  effects in seismic analysis. However, in order to limit the influence of P- $\Delta$  effects, codes do specify design criteria for maximum allowable interstory drifts. Generally, P- $\Delta$  effects in low rise buildings are negligible since the total lateral deflections are kept relatively small by the story drift limitation. However, in taller mid-rise and high-rise buildings, where lateral deflections may be much larger, the maximum drift requirement does not ensure that the P- $\Delta$  effects will be negligibly small. For this reason, the proposed Applied Technology Council (ATC) recommendations (5) for

seismic design of buildings require a P- $\Delta$  check as a standard part of earthquake response analysis.

A study of an analytical approach which accounts for the P- $\Delta$  effects in buildings is described herein. The objectives are: (1) to illustrate how the P- $\Delta$  forces enter into the static and dynamic equations of equilibrium; (2) to present a consistent formulation of the P- $\Delta$  effect applicable for elastic seismic analyses of buildings; (3) to investigate an approximate approach to account for amplified P- $\Delta$  effects resulting from inelastic deformation levels; and (4) to demonstrate the application of P- $\Delta$  analysis in performing seismic response analysis of an actual building. In the discussion that follows, a matrix formulation for the linear solution of the P- $\Delta$  effect resulting from lateral deflection and torsional rotation response of buildings is presented. This formulation may be applied to reflect procedures suggested by ATC(5) in which P- $\Delta$  effects are calculated based on elastic limit deformation levels. The formulation also allows the ability to account for amplified P- $\Delta$  effects that may result from inelastic deformation levels caused by a major earthquake event as has also been suggested (13). The overall influences of P- $\Delta$  effects on results of static and dynamic analyses using these approaches are discussed. The formulation presented has been implemented in a computer program and results of sample analyses of a 31 story moment resisting frame building are reviewed.

#### **4.1.2 Linear Analysis Approach**

A common misconception among engineers is the belief that solution of the elastic P- $\Delta$  problem requires a nonlinear, large deflection analysis procedure. Theoretical solutions of the P- $\Delta$  phenomenon for simple beam columns based on the governing differential equations show that lateral deflections will vary linearly with applied lateral loads given unchanging axial load magnitude (44). In practical seismic analysis of buildings, the total vertical (gravity)

loads are calculated from dead weight estimates and are generally assumed to remain constant during earthquake excitation (i.e., vertical inertial loads resulting from vertical ground motions are not usually explicitly accounted for). The induced lateral inertial loads and resulting deflections are the quantities that must be determined for design. By analogy of these loading conditions with simple beam column problems, it can be seen that use of a linear solution technique to account for P- $\Delta$  effects in buildings is consistent with theory. However, in commonly used hand calculation procedures for determining P- $\Delta$  effects (12), the engineer performs an iterative solution procedure to solve a linear problem thereby avoiding the task of directly formulating and solving the governing simultaneous equations of equilibrium. In computer-aided analysis, direct solution of the simultaneous equations is easily carried out with no iteration.

In state-of-the-art computer programs used for linear elastic analysis of buildings, lateral seismic response is most efficiently calculated based on a reduced matrix formulation including only the lateral stiffness properties of the structure (49). Element-level non-lateral degrees of freedom may be condensed out by a forward reduction process and lateral degrees-of-freedom can be transformed to a single node per story by assuming in-plane rigidity of the floor diaphragm. This approach leads to the construction of a lateral stiffness matrix possessing only one (for planar frames) or three (for space frames) degrees-of-freedom per floor. P- $\Delta$  effects can be introduced into the linear matrix formulation at the element level before condensation to the lateral stiffness matrix by use of member geometric stiffness matrices (also called stability coefficient or initial stress stiffness matrices) (11,19,30). In this approach, the contribution of both interstory drifts and local column curvatures can be accounted for in the magnification of forces and deflections. However, the influence of the local column curvatures is generally

much smaller than that of the interstory drifts in producing second-order forces in buildings. If the influence of the column curvatures is considered to be negligible as is assumed in common hand methods (12), the P- $\Delta$  effect can be accurately accounted for after condensation to the lateral stiffness matrix. A description of this procedure for static and dynamic analysis is given below.

### Static Analysis

In Figure 4.1.1, the P- $\Delta$  effect is illustrated for a planar multistory building frame subjected to static lateral loading. If P- $\Delta$  effects are ignored, the deflections can be solved for by the direct stiffness matrix method as follows:

$$\underline{R} = \underline{K} \underline{r} ; \underline{r} = \underline{K}^{-1} \underline{R} \quad (4.1.1)$$

where

$\underline{K}$  = elastic lateral stiffness matrix (n x n)

$\underline{R}$  = applied static lateral forces (n x 1)

$\underline{r}$  = lateral deflections (n x 1)

and

n = the number of lateral displacement degrees of freedom.

As shown in Figure 4.1.1(a), if P- $\Delta$  effects are to be included in the analysis, an additional second-order overturning moment ( $M_i$ ) must be applied at each story (i) equal to the accumulated gravity forces ( $\sum_{j=i}^n P_j$ ) times the interstory drift ( $r_i - r_{i-1}$ ). These second-order overturning moments can be introduced by applying equivalent lateral force couples acting over each story. The equivalent lateral forces ( $F_i$ ) for each story are equal to the P- $\Delta$  story overturning moment ( $M_i$ ) divided by the story height ( $h_i$ ) as shown in Figure 4.1.1(b). Thus, in the formulation of the problem accounting for P- $\Delta$  moments, a fictitious lateral force set,  $\underline{F}$ , must be added to the applied lateral loads and Equation 4.1.1 now becomes

$$\underline{R} + \underline{F} = \underline{K} \underline{r} \quad (4.1.2)$$

where

$\underline{F}$  = equivalent lateral force vector resulting from  
the P- $\Delta$  effect (n x 1)

$$\underline{F} = \begin{bmatrix} F_n \\ F_{n-1} - F_n \\ F_{n-2} - F_{n-1} \\ \cdot \\ \cdot \\ \cdot \\ F_2 - F_3 \\ F_1 - F_2 \end{bmatrix}$$

and

$$F_i = M_i / h_i = \left( \sum_{j=i}^n P_j \right) (r_i - r_{i-1}) / h_i$$

Noting that the equivalent lateral forces,  $F_i$ , vary linearly with interstory drift,  $\underline{F}$  can be represented by the matrix product:

$$\underline{F} = \underline{K}_G \underline{r} \tag{4.1.3}$$



or

$$\underline{R} = [\underline{K} - \underline{K}_G] \underline{r} \quad ; \quad \underline{r} = [\underline{K} - \underline{K}_G]^{-1} \underline{R} \quad (4.1.5)$$

Thus, the P- $\Delta$  problem can be formulated and solved as a linear system whereby the elastic stiffness matrix,  $\underline{K}$ , is modified by a matrix,  $\underline{K}_G$ , which accounts for second order overturning moments caused by the interaction of the gravity loads with lateral displacements. The  $\underline{K}_G$  matrix may be termed the "lateral geometric stiffness matrix." In the solution of Equation 4.1.5, the lateral stiffness is decreased with the inclusion of  $\underline{K}_G$  and the resulting lateral displacements are increased. These increased displacements are used in the backsubstitution phase and will accordingly lead to increased local element deformations and corresponding member forces which will be in static equilibrium with the story overturning moments resulting from the applied lateral loads,  $\underline{R}$ , plus the lateral P- $\Delta$  forces,  $\underline{F}$ , as shown in Equation 4.1.2. It should be noted that the lateral P- $\Delta$  forces are fictitious lateral forces which have been introduced to approximate the second-order overturning moments. Despite the cancelation of these forces over the height of the building, an artificial residual lateral force equal to  $F_i$  will remain at each story,  $i$ , causing increased horizontal shear forces. Although not a true lateral load, this residual force represents an increase in story shear force acting normal to the deflected configuration of the building caused by the story vertical load. These increased story shears are generally considered appropriate for design (33).

### Dynamic Analysis

With P- $\Delta$  effects included, the matrix equation of dynamic equilibrium is:

$$\underline{M} \ddot{\underline{r}}(t) + \underline{C} \dot{\underline{r}}(t) + \underline{K} \underline{r}(t) = \underline{F}(t) - \underline{M} \underline{1} \ddot{r}_g(t) \quad (4.1.6)$$

where  $\underline{M}$ ,  $\underline{C}$  and  $\underline{K}$  are the mass, damping, and lateral elastic stiffness matrices, respectively, where  $\ddot{r}_g(t)$  is the ground acceleration at

time "t" due to the earthquake excitation and  $\underline{1}$  is a column vector (n x 1) of ones, and where  $\underline{F}$  is the equivalent lateral force vector introduced by P- $\Delta$ . Substituting Equation 4.1.3 into 4.1.6 we have

$$\underline{M} \ddot{\underline{r}}(t) + \underline{C} \dot{\underline{r}}(t) + \underline{K} \underline{r}(t) = \underline{K}_G \underline{r}(t) - \underline{M} \underline{1} \ddot{r}_g(t)$$

or

$$\underline{M} \ddot{\underline{r}}(t) + \underline{C} \dot{\underline{r}}(t) + [\underline{K} - \underline{K}_G] \underline{r}(t) = - \underline{M} \underline{1} \ddot{r}_g(t) \quad (4.1.7)$$

This equation can be transformed to normal coordinates in the same manner as if the P- $\Delta$  effect were not included. For the solution of mode shapes and frequencies which are used in the transformation to the uncoupled modal equations, the eigenproblem becomes

$$[\underline{K} - \underline{K}_G - \omega_i^2 \underline{M}] \underline{\phi}_i = \underline{0} \quad (4.1.8)$$

where

$$\omega_i = i^{\text{th}} \text{ mode natural frequency}$$

$$\underline{\phi}_i = i^{\text{th}} \text{ mode shape (n x 1) .}$$

Since modifying  $\underline{K}$  by  $\underline{K}_G$  effectively reduces the lateral stiffness, the resulting frequencies will be lower and the mode shapes will be slightly different than if the P- $\Delta$  effects are ignored. These lower frequencies and corresponding modes represent the actual free vibration responses that would be observed if the P- $\Delta$  influence is present as noted by Newmark, et al. (28).

Based on the dynamic properties resulting from Equation 4.1.8, a standard response spectrum analysis can be performed to evaluate the maximum modal displacements which can be backsubstituted to evaluate maximum modal member forces. These modal member forces can then be combined using an appropriate modal combination rule to approximate peak member force quantities which now will include forces contributions from the P- $\Delta$  effect. It is possible to calculate the peak modal story shear and overturning forces that will be in equilibrium with the peak modal member forces at each level. The usual matrix operations used for calculation of these peak story

forces must be modified to account for P- $\Delta$  . The peak modal story forces for the  $i$ th mode are calculated based on the lateral force vectors,  $\underline{f}_i$ , given by the expression:

$$\underline{f}_i = \underline{K} \underline{\phi}_i \frac{L_i}{M_i^*} \frac{S a_i}{\omega_i^2} \quad (4.1.9)$$

where  $L_i = \underline{\phi}_i^T \underline{M} \underline{1} =$  participation factor for mode  $i$

$$M_i^* = \underline{\phi}_i^T \underline{M} \underline{\phi}_i = \text{modal mass for mode } i$$

and

$S a_i =$  spectral acceleration amplitude for mode  $i$

From Equation 4.1.8, it can be seen that

$$\underline{K} \underline{\phi}_i = \omega_i^2 \underline{M} \underline{\phi}_i + \underline{K}_G \underline{\phi}_i \quad (4.1.10)$$

Substituting Equation 4.1.10 into 4.1.9, the modal lateral force vectors including P- $\Delta$  effects are of the form:

$$\underline{f}_i = (\omega_i^2 \underline{M} \underline{\phi}_i + \underline{K}_G \underline{\phi}_i) \frac{L_i}{M_i^*} \frac{S a_i}{\omega_i^2}$$

$$\underline{f}_i = \underline{M} \underline{\phi}_i \frac{L_i}{M_i^*} S a_i + \frac{1}{\omega_i^2} \underline{K}_G \underline{\phi}_i \frac{L_i}{M_i^*} S a_i$$

The second term of this equation can also be represented in terms of spectral displacements,  $S d$ , giving

$$\underline{f}_i = \underline{M} \underline{\phi}_i \frac{L_i}{M_i^*} S a_i + \underline{K}_G \underline{\phi}_i \frac{L_i}{M_i^*} S d_i \quad (4.1.11)$$

where

$$S d_i = \frac{S a_i}{\omega_i^2}$$

Thus, the first term in Equation 4.1.11 represents the modal lateral

inertial force contribution being proportional to spectral accelerations,  $S_a$ , and the second term represents modal P- $\Delta$  force contributions being proportional to spectral displacements,  $S_d$ . As in the case of static analysis, the internal resisting story shear forces will reflect the application of fictitious lateral forces which account for the P- $\Delta$  overturning moments. Total peak story responses can be estimated by operating on the peak modal responses with an appropriate modal combination rule.

#### 4.1.3 Torsional P- $\Delta$ Effect

Torsional earthquake response may result in a building if structural and/or mass eccentricity is present or from torsional ground motion components. If these conditions cause torsional response to be a significant aspect of behavior, a three dimensional analysis should be performed where three (two translational and one torsional) degrees-of-freedom are assigned at each story level. The lateral geometric stiffness matrix,  $K_G$ , must be formulated to reflect P- $\Delta$  effects for each of these three degrees of freedom. The  $K_G$  coefficients for lateral translational P- $\Delta$  effects are identical in each of the two translational directions and are formulated as shown in the preceding discussion. To develop the formulation for lateral torsional P- $\Delta$  effects, a separate idealization must be used.

The torsional P- $\Delta$  effect has been previously discussed by Rosenblueth (33) and is illustrated in Figure 4.1.2 for a single story building. As the rigid floor diaphragm is rotated through an angle,  $\theta$ , each column undergoes a translational displacement as shown in Figure 4.1.2(a). This translation introduces a local P- $\Delta$  effect in each column where the second order moment can be represented by an equivalent lateral force couple as shown in Figure 4.1.2(b). The equivalent lateral forces,  $F_i$ , for column  $i$  are

$$F_i = \frac{p_i d_i}{h} \theta$$

where

- $p_i$  = vertical force carried by column  $i$
- $d_i$  = distance of column  $i$  from the center of rotation
- $h$  = story height
- $\theta$  = an imposed torsional rotational displacement

The cumulative effect of the equivalent lateral force couples at each column introduces a second order story torque as shown in Figure 4.1.2(c) represented by

$$T = \Sigma (F_i d_i) = \Sigma (p_i d_i^2) \cdot \frac{\theta}{h} \quad (4.1.12)$$

where the summations are over the total number of columns. Equation 4.1.12 may also be represented by

$$T = \frac{PD^2}{h} \cdot \theta \quad (4.1.13)$$

where

$$D = \left( \frac{\Sigma (p_i d_i^2)}{P} \right)^{\frac{1}{2}}$$

$D$  = the radius of gyration of column forces about the floor center of rotation

and

$P$  = the total vertical force carried at a given story

$$P = \Sigma p_i \text{ over all columns.}$$

For a given building, the value of  $D$  can be estimated from inspection of the plan configuration of the vertical force resisting elements (e.g. columns) and knowledge of the approximate distribution of vertical loads to these elements. This formulation is consistent with that suggested by Rosenblueth (33).

If the structural system of a building provides roughly uniform vertical support over the plan area of the floor (e.g., regularly spaced columns over the floor area) and dead loads are evenly

distributed over the floor area, the radius of gyration of the column forces may be assumed to be approximately equal to the radius of gyration of the floor mass; that is,

$$D = (m_R / m)^{\frac{1}{2}} = (m_R \cdot g / P)^{\frac{1}{2}} \quad (4.1.14)$$

where  $m_R$  = the rotational mass moment of inertia of the floor

and  $m = P/g$  = the total mass of the floor.

Using this assumption, Equation 4.1.14 can be substituted into 4.1.13 giving

$$T = \frac{m_R \cdot g}{h} \cdot \theta \quad (4.1.15)$$

In general, the use of Equation 4.1.15 will give an adequate representation of torsional P-Δ effects without having to calculate D from the individual column forces. However, in cases where the assumption of uniform vertical load resistance distribution is not adequate (e.g., a building with peripheral columns supporting the entire vertical load), the more precise Equation 4.1.13 can be used. Thus, for three dimensional response including torsional effects, the  $K_G$  matrix (dimension 3 x 3 corresponding to the X-translational, Y-translational, and torsional rotational degrees of freedom respectively) for the single story building in Figure 4.1.3 becomes

$$\underline{K}_G = \begin{bmatrix} m & 0 & 0 \\ 0 & m & 0 \\ 0 & 0 & m_R \end{bmatrix} \cdot \frac{g}{h}$$

wherein the gravity loads are represented in terms of mass and

gravitational acceleration.

For a multistory building, the torsional geometric stiffness matrix containing torsional rotational degrees of freedom only is of the same form as translational geometric stiffness matrix as shown in Equation 4.1.4 with  $T_i^*$  being substituted for  $P_i^*$

where

$$T_i^* = \sum_{j=i}^n (P_j D_j^2)$$

or based on Equation 4.1.15,

$$T_i^* = \left( \sum_{j=i}^n m_{Rj} \right) \cdot g$$

A full three-dimensional geometric matrix (dimension  $3n \times 3n$ ) is constructed by appropriate insertion of terms from the  $x$  and  $y$  translational  $K_G$  matrices and from the torsional  $K_G$  matrix (all of dimension  $n \times n$ ). In this form, the geometric stiffness matrix can now be used for static and dynamic analysis (as previously described) to evaluate three dimensional  $P-\Delta$  influences including torsional effects.

#### 4.1.4 Application of $P-\Delta$ Analysis in Design

In geographic areas of high seismicity, multistory buildings are not generally designed to respond elastically to a maximum credible level of earthquake excitation. Despite the potential for inelastic behavior, member design is typically based on force levels corresponding to a more moderate earthquake and classical linear elastic analysis procedures are used to determine the distribution of forces to the resisting elements. In order to protect against collapse, building codes incorporate special provisions to insure that

substantial capacity for ductile response is provided in the design. In a major earthquake event, induced inertial forces will be effectively limited as yielding occurs and stiffness degrades but, corresponding lateral deflections may be several times larger than displacements corresponding to incipient yielding. Since the P- $\Delta$  forces increase linearly with deflection, they are not subject to the same type of limitation as the inertial forces. Tests on the ultimate strength of frames subjected to increasing monotonic lateral loading have shown that the P- $\Delta$  effect is critical in initiating structural instability and pursuant collapse (6,16). However, nonlinear analytical studies on frames subjected to transient earthquake loading have produced conflicting indications regarding the possible significance of P- $\Delta$  effects on inelastic dynamic stability (17,21). Currently, this aspect of structural behavior is not well understood and further research is needed to establish appropriate guidelines for aseismic design.

Current building codes (20) implicitly rely on drift limitations to protect against P- $\Delta$  instability. Alternative provisions recommended by the Applied Technology Council (5) require explicit treatment of P- $\Delta$  effects whereby secondary forces are calculated based on elastic limit lateral deflection levels. The ATC recommended analysis procedure corresponds to Equation 4.1.2 where applied lateral forces (  $R$  ) and P- $\Delta$  forces (  $E$  ) are determined based on the same elastic limit displacement level (  $\delta$  ). However, uncertainty remains as to whether this procedure will lead to an adequately conservative design; and, it has been suggested that a deflection amplification factor corresponding to expected inelastic displacement levels be applied to the ATC elastic limit deflections for the calculation of P- $\Delta$  forces (13).

Current ATC recommendations specify a deflection amplification factor,  $C_d$ , to be applied to elastic limit drifts for approximate

calculation of extreme inelastic drifts. Recommended  $C_d$  values vary from 1.25 to 6.5 depending upon the ductility of the structural system and the materials used in construction. If the amplified deflections used for the ATC drift criteria are also used for calculation of the P- $\Delta$  forces, the corresponding equivalent lateral force vector becomes

$$\underline{F} = \underline{K}_G \underline{r}_a = C_d \underline{K}_G \underline{r} \quad (4.1.16)$$

where  $\underline{r}_a$  = amplified displacements for inelastic response

$$\underline{r}_a = C_d \underline{r}.$$

With substitution of Equation 4.1.16 into Equations 4.1.2 and 4.1.6, the revised matrix formulations become

$$\underline{R} + C_d \underline{K}_G \underline{r} = \underline{K} \underline{r} \quad (4.1.17)$$

for static analysis, and

$$\underline{M} \ddot{\underline{r}}(t) + \underline{C} \dot{\underline{r}}(t) + \underline{K} \underline{r}(t) = C_d \underline{K}_G \underline{r}(t) - \underline{M} \underline{l} \ddot{r}_g(t) \quad (4.1.18)$$

for dynamic analysis. These equations can be solved in the same way as previously described but, now, a factored lateral geometric stiffness matrix ( $C_d \underline{K}_G$ ) is used to represent the amplified P- $\Delta$  forces resulting from expected inelastic displacements. Of course, these formulations do not rigorously represent the complex inelastic problem but, do provide a means for producing increased P- $\Delta$  forces for design purposes corresponding to inelastic displacement levels. Because the problem of inelastic dynamic stability is not well understood, choosing an appropriate value of  $C_d$  for use in design applications is a matter of conjecture. Significant variations in analytical response can result from the use of different  $C_d$  values as is shown in the results of the sample analyses that follow.

#### 4.1.5 Results of Example Analyses

The matrix formulation for the P- $\Delta$  effect as described in the preceding discussion has been implemented in a modified version of the the ETABS computer program (23). In order to produce representative results that may be expected in actual design situations, a model of an existing modern high-rise building has been analyzed. The building used for this example analyses is the Rainier Tower building located in Seattle, Washington. This building features a novel architectural design in which a 31 story, 393 foot tall office tower constructed in steel is supported by a tapered 12 story, 121 foot tall reinforced concrete pedestal base. A detailed three-dimensional analytical model of this structure has been previously developed (see section 3.5) whose dynamic properties correlate closely with experimental results observed in a small amplitude forced vibration study of the building (40). Both experimental and analytical results showed that the pedestal base has negligible influence on the response of the steel moment frame tower above due to the pedestal's large relative stiffness. Therefore, only the steel tower is modeled for this analyses with the assumption that a condition of full fixity exists at its base at the top of the pedestal. A schematic of the analytical model is shown in Figure 4.1.3. Typical story heights are 12 feet but, the 1st and 13th stories are 15 feet in height and the 29th,30th and 31st story heights range from 15 to 19.5 feet. The average dead weight per floor used in the analyses is 1980 kips which is about a 105 psf floor load and does not include code required 20 psf partition loads.

Both equivalent static and dynamic seismic (response spectrum) analyses have been performed in accordance with ATC recommendations. The ATC acceleration response spectrum is represented by

$$\frac{S_a}{g} = \frac{1.2 A_v S}{R T^{2/3}} \leq 2.5 A_a/R$$

where  $A_v$  is the effective peak velocity related acceleration;  $A_a$  is the effective peak acceleration;  $R$  is the response modification factor;  $S$  is the seismic soil coefficient; and,  $T$  is natural period. Analyses were performed assuming a spectrum corresponding to areas of highest seismicity where  $A_v = 0.4$  and  $A_a = 0.4$ . A value of  $S = 1.2$  was assumed and  $R = 8$  was used as is specified for moment resisting frame construction. The resulting strength level design spectrum is shown in Figure 4.1.4. The ATC recommended  $C_d$  values for inelastic drift calculation is 5.5. In order to compare the influence of different  $C_d$  values on analytical response quantities,  $P-\Delta$  effects were incorporated into the analyses using  $C_d$  factors equal to 0.0 ( $P-\Delta$  ignored), 1.0 ( $P-\Delta$  forces based on elastic limit deflection levels), 3.0 ( $P-\Delta$  forces based on intermediate inelastic deflection levels) and 5.5 ( $P-\Delta$  forces based on extreme inelastic deflection levels). The static and dynamic analyses performed using  $C_d = 1.0$  and  $C_d = 0.0$  are consistent with ATC recommendations for seismic analysis with and without consideration of  $P-\Delta$  effects, respectively.

### Static Analysis

The fundamental analytical period of 4.67 seconds was used to calculate static seismic loads according to ATC provisions. Story deflections, shears and overturning moments resulting from the static analyses are shown in Figures 4.1.5, 4.1.6, and 4.1.7, respectively, and corresponding values are tabulated for selected story levels in Table 4.1.1 (note that ATC allowed overturning moment reduction for static analysis is not reflected in these results). These results show that inclusion of  $P-\Delta$  effects lead to increases in the design quantities at all levels of the building for static analysis. With  $P-\Delta$  ignored ( $C_d = 0.0$ ), roof deflection is 11.9 in. and base shear and overturning are 1583k and  $5769 \times 10^3$  in-k, respectively. When  $P-\Delta$  forces are calculated based on elastic displacements using  $C_d = 1.0$ , increases over the  $C_d = 0$  case of 6.6%, 5.1% and 6.7% are observed in

roof deflection, base shear and base overturning, respectively (Table 4.1.1). For intermediate inelastic displacement levels ( $C_d=3.0$ ) increases of 22.9%, 17.1% and 23.9% are noted. P- $\Delta$  increases based on extreme inelastic displacement levels ( $C_d=5.5$ ) are 52.5%, 37.5% and 55.2% for roof deflection, base shear and base overturning, respectively. At amplified displacement levels ( $C_d = 3.0$  and  $C_d = 5.5$ ), irregularities in the story shear envelope result in the 14th story and in the 1st and 2nd story where significant dips in shear are noted. This effect results from the fact that the drifts in these stories are relatively smaller than those in adjacent stories due to larger column sections provided at these levels to compensate for greater than usual story heights of adjacent stories. The smaller drifts lead to smaller equivalent lateral P- $\Delta$  forces being applied and result in smaller relative story shears at these stories.

#### Dynamic Analyses

In Table 4.1.2, variations in natural translational periods and corresponding spectral amplitudes that result from the different  $C_d$  values are shown. Longer periods that result from increasing  $C_d$  values lead to decreased spectral amplitude. This effect tends to partially offset P- $\Delta$  magnifications in each mode. It should be noted from Table 4.1.2 that the first translational period is increased the most by P- $\Delta$  since overturning contributes more to the response of this mode than to the higher modes. This mode contributes most heavily to P- $\Delta$  magnification. Also, shown in Table 4.1.2 are the torsional periods for different  $C_d$  values. These periods show a smaller variation than the translation periods indicating a lesser influence of P- $\Delta$  on torsional response. Story deflections, shears and overturning moments from dynamic analyses are shown in Figures 4.1.8, 4.1.9, and 4.1.10, respectively, and corresponding values are tabulated in Table 4.1.3. These response quantities are calculated

based on the square root of the sum of the squares (SRSS) modal combination rule. With P- $\Delta$  ignored ( $C_d = 0.0$ ), roof deflection is 7.7 inches and base shear and overturning are 1181k and  $3831 \times 10^3$  in-k, respectively. For  $C_d = 3.0$ , increases of 13.4%, 8.2% and 14.3% are noted and, for  $C_d = 5.5$ , increases of 33.9%, 20.2% and 36.2% result. As in static analysis, dips in the shear envelopes are noted (Figure 4.1.9).

In contrast to the static analysis, decreases in story shear and overturning in the upper few stories result for  $C_d > 0.0$  since P- $\Delta$  effects are small near the top of the structure and the effect of decreased spectral amplitude controls. At the roof level, decreases in story shear and overturning of 1.3% result for  $C_d = 1.0$  and decreases of 6.3% result for  $C_d = 5.5$ .

#### 4.1.6 Summary and Conclusions

A matrix formulation to account for P- $\Delta$  effects in computer seismic analysis of multistory buildings has been presented. The method uses a linear solution approach requiring no iteration and can be used for performing static or dynamic elastic analyses. Amplified P- $\Delta$  effects resulting from inelastic displacement levels which may occur during a major earthquake can be accounted for in an approximate manner. The method has been implemented in a computer program and sample seismic analyses of a 31-story building model have been performed based on ATC seismic analysis procedures. From the results of these sample analyses, the following observations and conclusions are drawn:

1. The formulation presented provides a consistent and effective means for predicting the magnified deflections and overturning moments caused by P- $\Delta$  effects in static or dynamic analysis for elastic displacement levels using  $C_d = 1.0$ .
2. In static analysis, including the P- $\Delta$  effect will increase the

story drift, shear and overturning moment responses at all levels of a building for any value of  $C_d$  (Figures 4.1.5, 4.1.6 and 4.1.7). These increased response values will lead to a more conservative design throughout the building than if the P- $\Delta$  effect is ignored.

3. In dynamic analysis, including the P- $\Delta$  effect may increase or decrease the story drift, shear and overturning moment responses at a given story of a building (Figure 4.1.8, 4.1.9 and 4.1.10). Decreases in response can occur when spectral amplitude reductions resulting from the longer natural periods caused by P- $\Delta$  predominate over increases induced in modal responses before spectral factorization. Decreased responses are most likely to occur in upper portions of the building where P- $\Delta$  effects are relatively small. Consequently, inclusion of P- $\Delta$  effects in dynamic analysis may not necessarily lead to a more conservative design throughout the building than if P- $\Delta$  is ignored depending upon the degree of period shift and the response spectrum used. Design response spectrum curves which have a more rapid descent of spectral amplitude with increasing period in the longer period range will tend to produce greater decreases in response in the upper stories when P- $\Delta$  effects are included.

4. To account for P- $\Delta$  moments, fictitious lateral forces are introduced which approximate shear forces acting normal to the deformed building configuration. It should be remembered that the magnitude of these lateral forces depend directly on the interstory drifts and, if nonuniform drifts occur in a building, irregularities in the story shear envelope may result especially for larger values of  $C_d$  (Figures 4.1.6 and 4.1.9).

5. P- $\Delta$  magnifications corresponding to elastic displacement levels ( $C_d = 1.0$ ) may be viewed as unconservative for design purposes considering the larger inelastic displacement levels that may occur

during a major earthquake (13). For example, in the moment resisting frame building studied,  $C_d = 1.0$  yields base overturning increases of 6.6% and 3.6% over the  $C_d = 0.0$  case ( $P-\Delta$  ignored) for static and dynamic analyses, respectively. However, if extreme inelastic displacement levels are assumed in the calculation of  $P-\Delta$  effects, much larger increases in response may result. For example, base overturning increases of 55.2% and 36.2% result for static and dynamic analyses with  $C_d = 5.5$  (note that  $C_d = 5.5$  is specified by ATC for inelastic drift criteria of moment resisting frame buildings). In light of seismic force levels currently used in design practice,  $P-\Delta$  increases of this magnitude may be considered excessively large. An intermediate value of  $C_d = 3.0$  leads to more modest base overturning increases of 23.9% and 14.3% for static and dynamic analysis, respectively. As is seen from these results, large variations in response may occur from the use of different  $C_d$  values for the calculation of  $P-\Delta$  effects. Since inelastic dynamic instability is currently not well understood, choice of an appropriate  $C_d$  value for use in  $P-\Delta$  analysis remains a matter of conjecture. More research is needed to determine values of  $C_d$  that are appropriate for use in practical design applications.

Table 4.1.1: Results of ATC Static Analyses Using Different  $C_d$  Values

Story	Design Quantity	$C_d = 0.0$	$C_d = 1.0$ (%)	$C_d = 3.0$ (%)	$C_d = 5.5$ (%)
Roof (31st)	Deflection (in.)	11.9	12.7 (6.6)	14.7 (22.9)	18.2 (52.5)
	Shear (k)	194.2	198.2 (2.0)	207.1 (6.7)	221.2 (13.9)
	OTM (in-k x 10 <sup>3</sup> )	45.4	46.4 (2.1)	48.5 (6.7)	51.8 (13.9)
20th	Deflection	7.2	7.7 (7.3)	9.0 (25.5)	11.5 (59.3)
	Shear	1257.	1347. (7.2)	1572. (25.1)	1986. (58.1)
	OTM	1536.	1624. (5.7)	1837. (19.6)	2209. (43.8)
10th	Deflection	3.1	3.3 (7.5)	3.9 (26.5)	5.0 (62.3)
	Shear	1545.	1663. (7.6)	1959. (26.8)	2517. (62.9)
	OTM	3671.	3911. (6.5)	4505. (22.7)	5573. (51.8)
Base	Deflection	0.	0. --	0. --	0. --
	Shear	1584.	1664. (5.1)	1855. (17.1)	2178. (37.5)
	OTM	5769.	6164. (6.8)	7148. (23.9)	8955. (55.2)

% = percent variation with respect to  $C_d = 0.0$

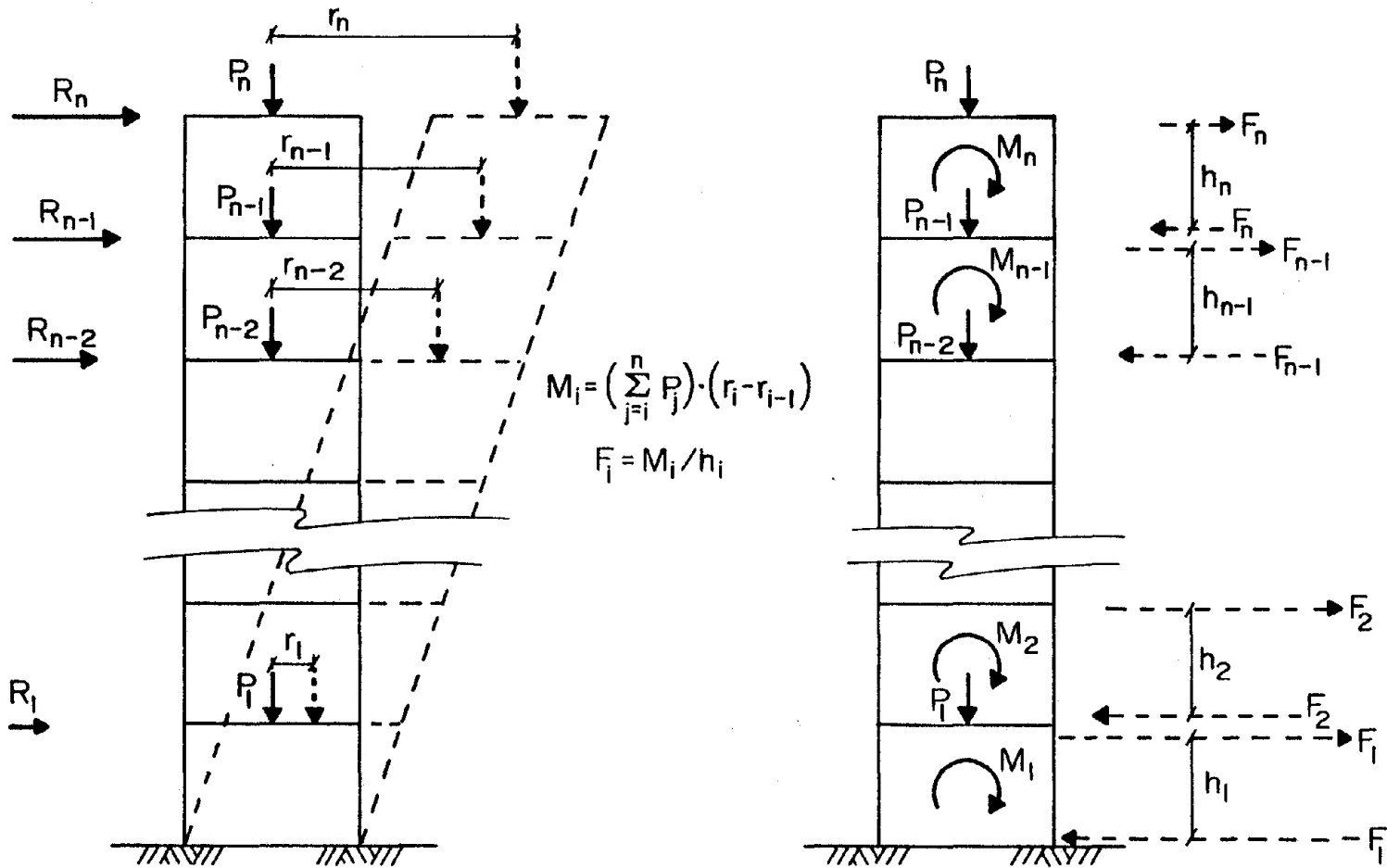
Table 4.1.2: Influence of P- $\Delta$  Effect on Natural Periods and Spectral Amplitudes

Direction	Mode	$C_d = 0.0$		$C_d = 1.0$		$C_d = 3.0$		$C_d = 5.5$	
		Period	Sa/g	Period	Sa/g	Period	Sa/g	Period	Sa/g
Translational	1	4.67	.0257	4.82	.0249	5.21	.0236	5.84	.0223
	2	1.71	.0508	1.76	.0498	1.87	.0476	2.05	.0445
	3	0.99	.0728	1.01	.0716	1.07	.0694	1.15	.0659
	4	0.70	.0921	0.72	.0906	0.76	.0870	0.82	.0821
Torsional	1	2.47	--	2.49	--	2.54	--	2.61	--
	2	0.93	--	0.94	--	0.96	--	0.98	--
	3	0.55	--	0.56	--	0.56	--	0.58	--
	4	0.35	--	0.40	--	0.40	--	0.41	--

Table 4.1.3: Results of ATC Dynamic Analyses Using Different  $C_d$  Values

Story	Design Quantity	$C_d = 0.0$	$C_d = 1.0$ (%)	$C_d = 3.0$ (%)	$C_d = 5.5$ (%)
Roof (31st)	Deflection (in.)	7.7	7.9 (3.4)	8.7 (13.4)	10.3 (33.9)
	Shear (k)	171.4	169.2 (-1.3)	165.2 (-3.7)	160.7 (-6.3)
	OTM (in-k x 10 <sup>3</sup> )	40.1	39.6 (-1.3)	38.7 (-3.6)	37.6 (-6.3)
20th	Deflection	4.9	5.1 (4.0)	5.7 (15.5)	6.8 (39.1)
	Shear	824.9	858. (4.0)	951.0 (15.3)	1136. (37.7)
	OTM	1004.	1030. (2.6)	1104. (10.0)	1249. (24.4)
10th	Deflection	2.3	2.4 (4.3)	2.7 (16.4)	3.2 (41.2)
	Shear	1116.	1163. (4.3)	1299. (16.5)	1576. (41.3)
	OTM	2352.	2431. (3.4)	2662. (13.2)	3127. (32.9)
Base	Deflection	0.	0. --	0. --	0. --
	Shear	1281.	1307. (2.1)	1386. (8.2)	1539. (20.1)
	OTM	3831.	3971. (3.6)	4381. (14.3)	5218. (36.2)

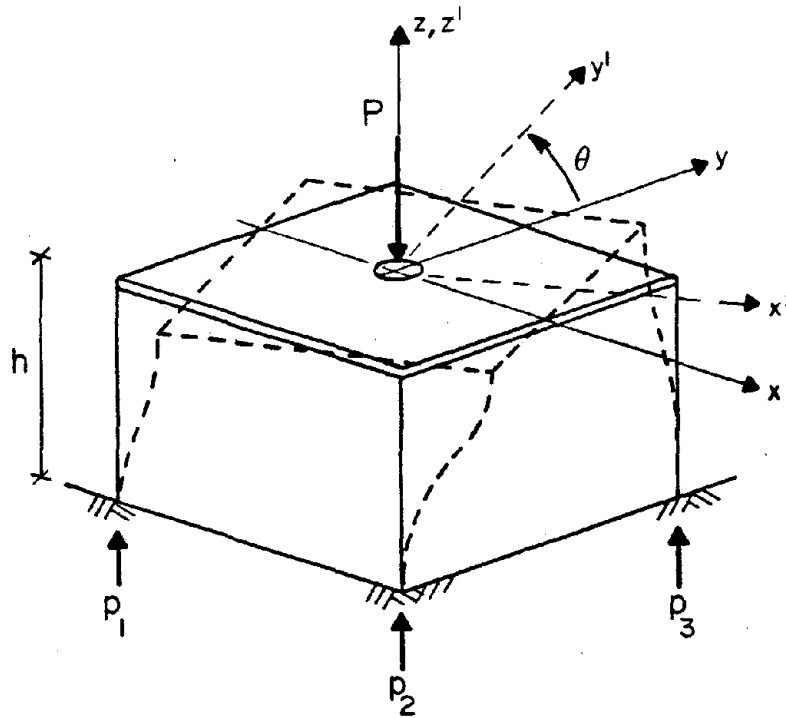
% = percent variation with respect to  $C_d = 0.0$



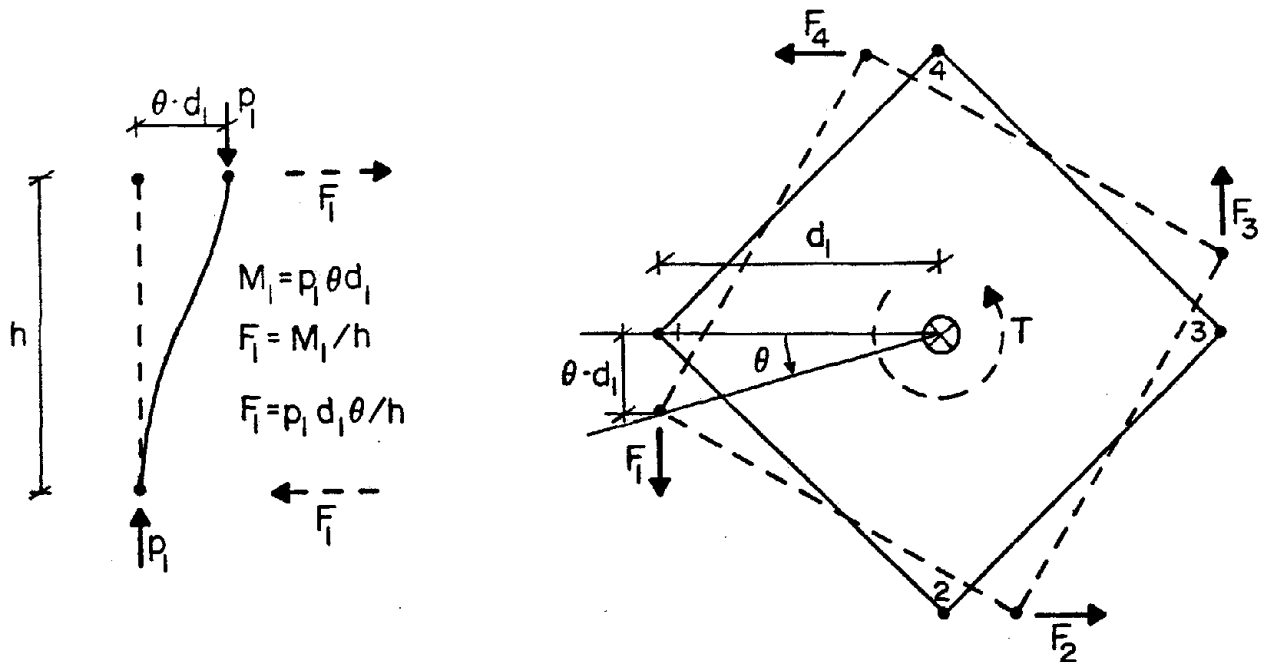
(a) Origin of P-Δ Overturning Moments

(b) Representation of P-Δ Moments with Equivalent Lateral Force Couples

Figure 4.1.1: Equivalent Lateral Force Formulation for P-Δ Analysis



(a) Deflected Shape due to Torsional Rotation



(b) P-Δ Forces Acting at Column 1

$$T = \sum (F_i d_i) = \sum (p_i d_i^2) \cdot \frac{\theta}{h}$$

(c) Torque Resulting from Cumulative P-Δ Forces

Figure 4.1.2: Torsional P-Δ Effect for a Single Story Building

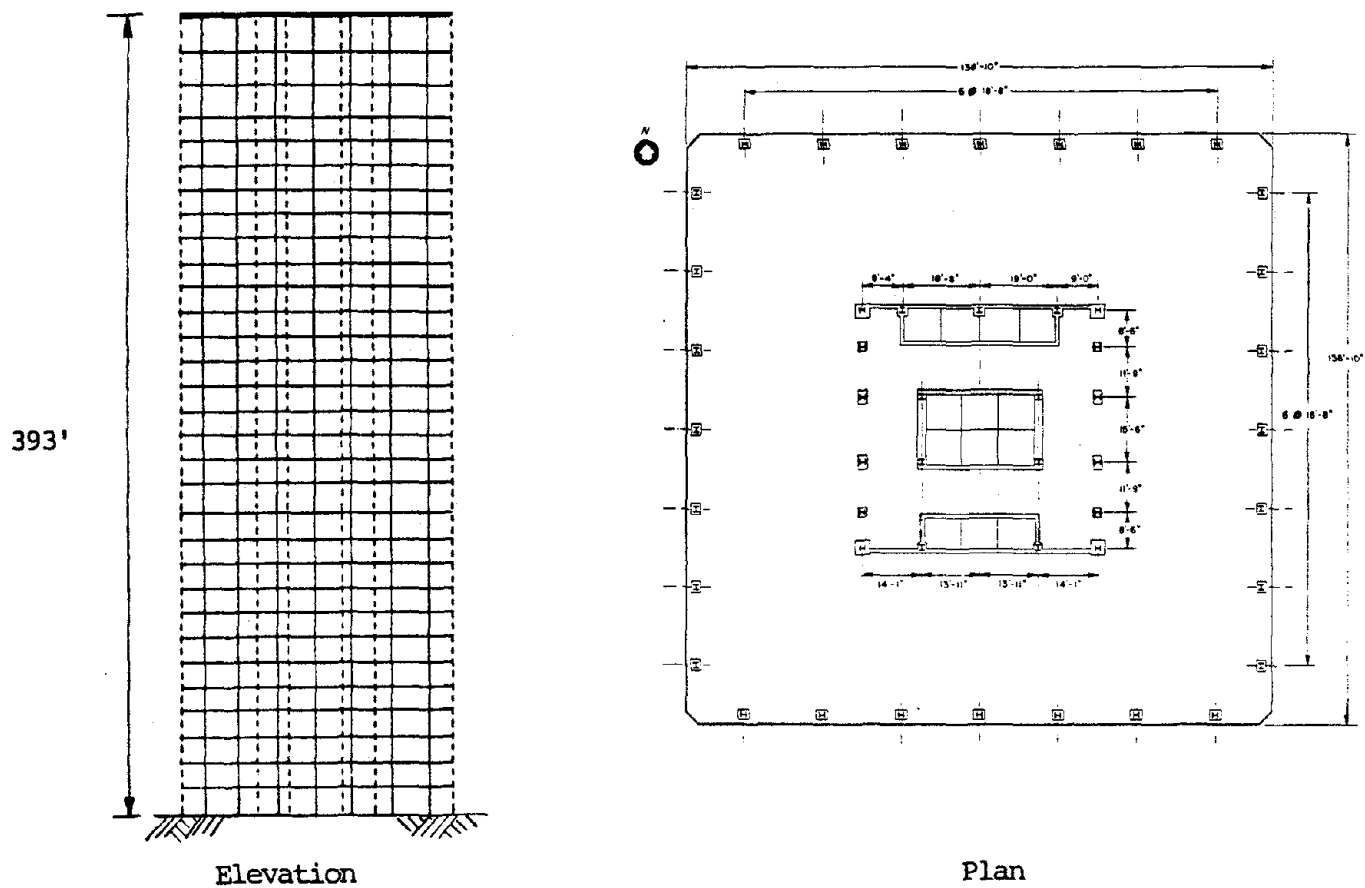


Figure 4.1.3: Rainer Tower Building (31-story superstructure)

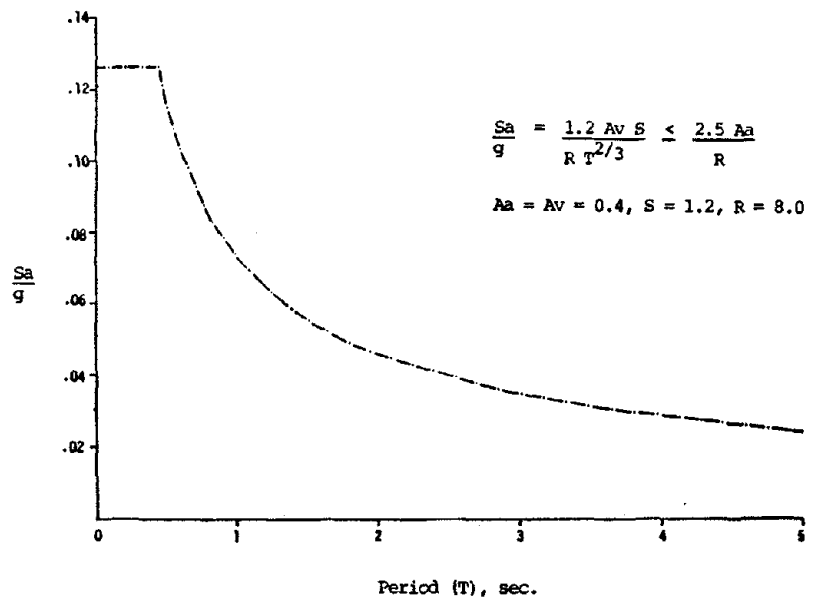


Figure 4.1.4: ATC Response Spectrum

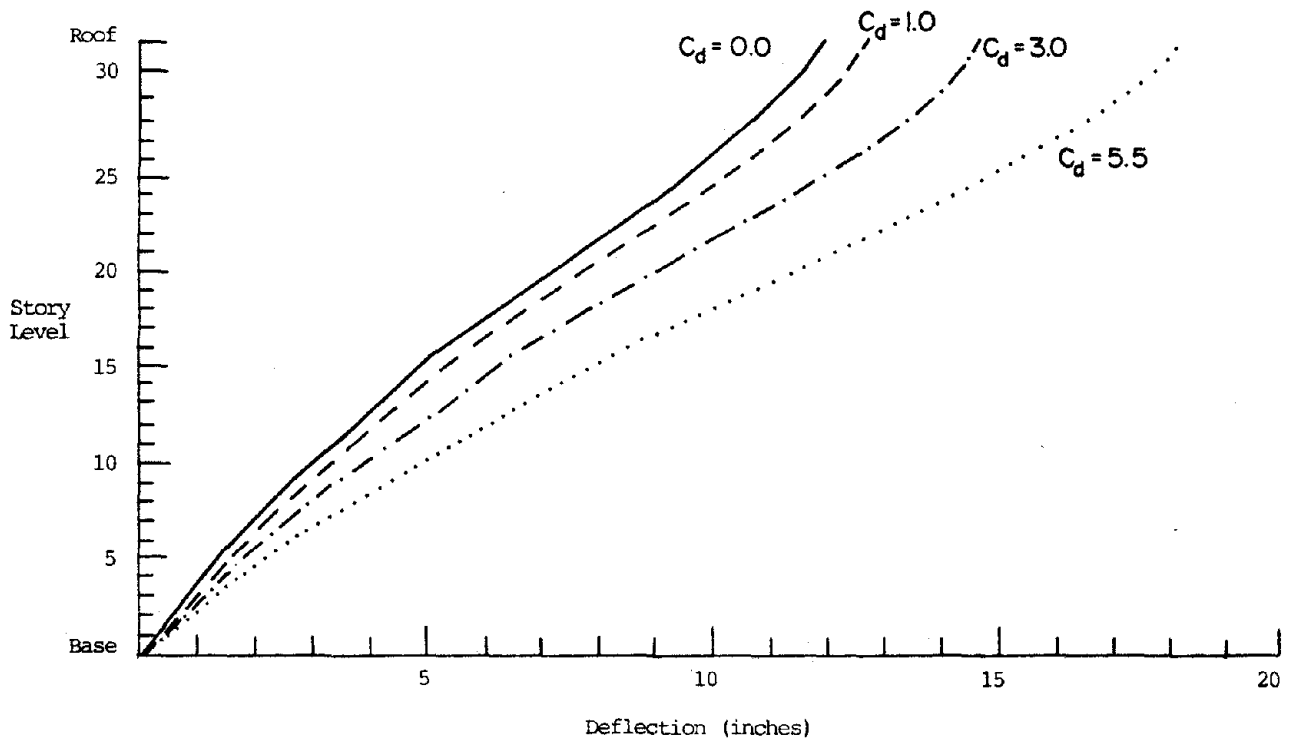


Figure 4.1.5: Story deflections resulting from ATC static analysis using different  $C_d$  values

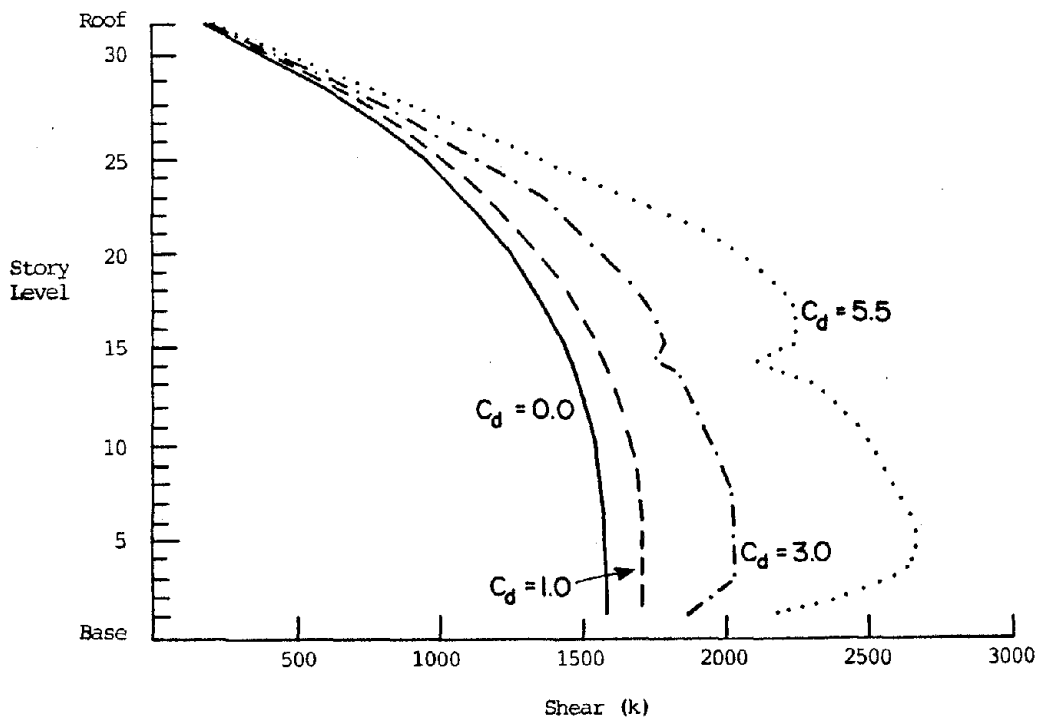


Figure 4.1.6: Story shears resulting from ATC static analysis using different  $C_d$  values

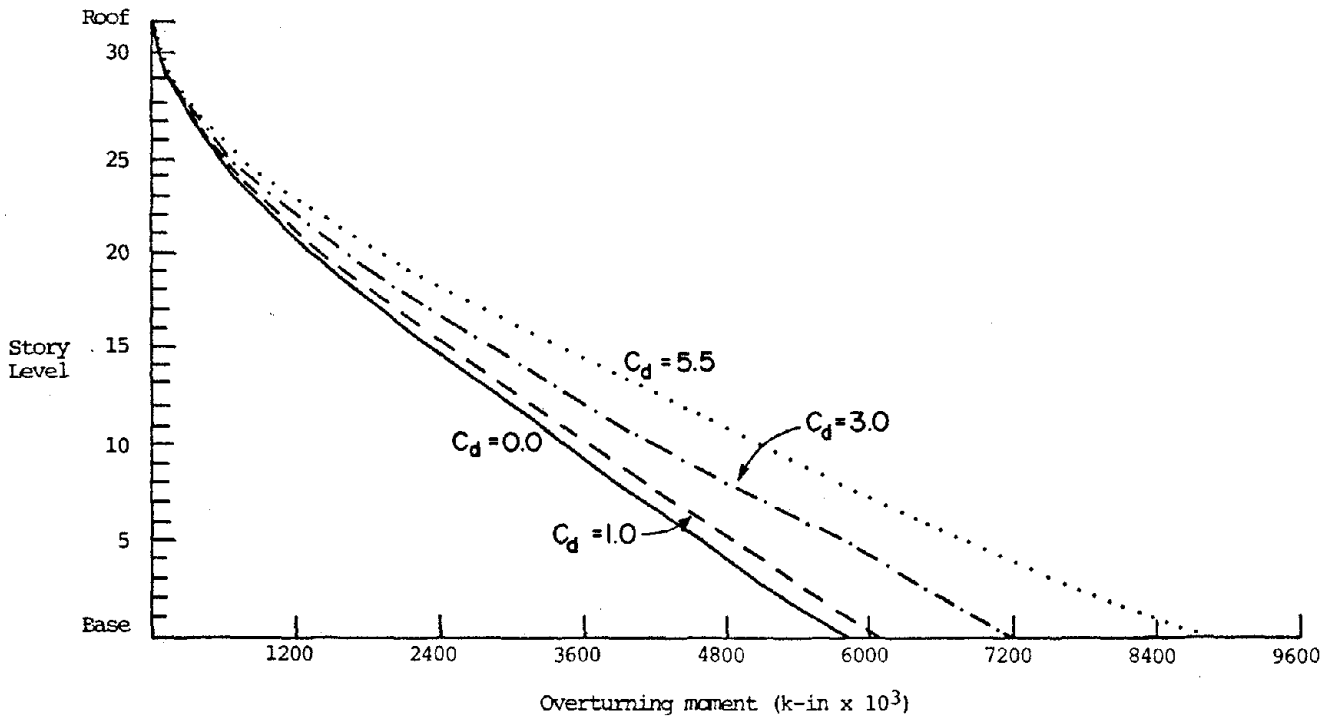


Figure 4.1.7: Story overturning moments resulting from ATC static analysis using different  $C_d$  values

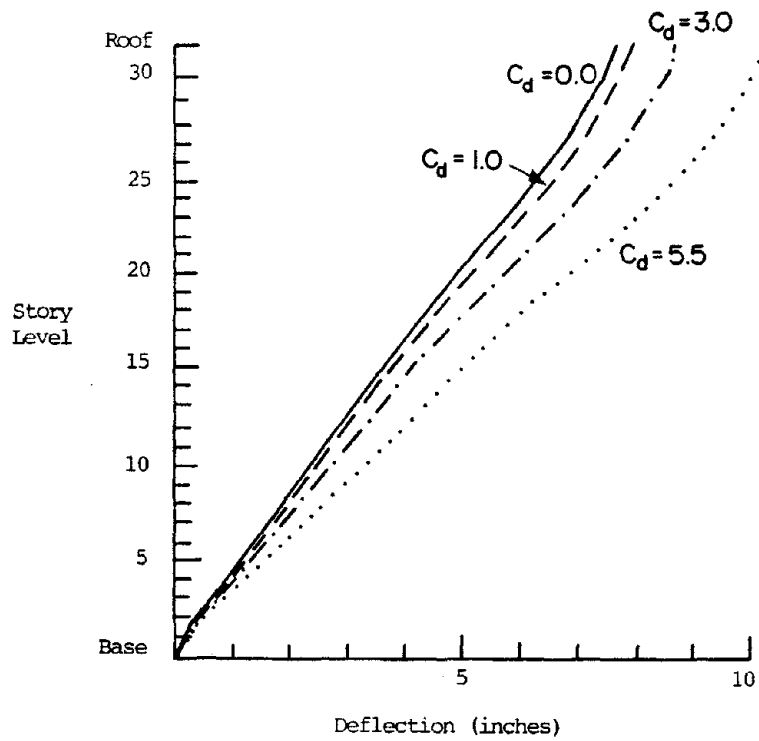


Figure 4.1.8: Story deflections resulting from ATC dynamic analysis using different  $C_d$  values

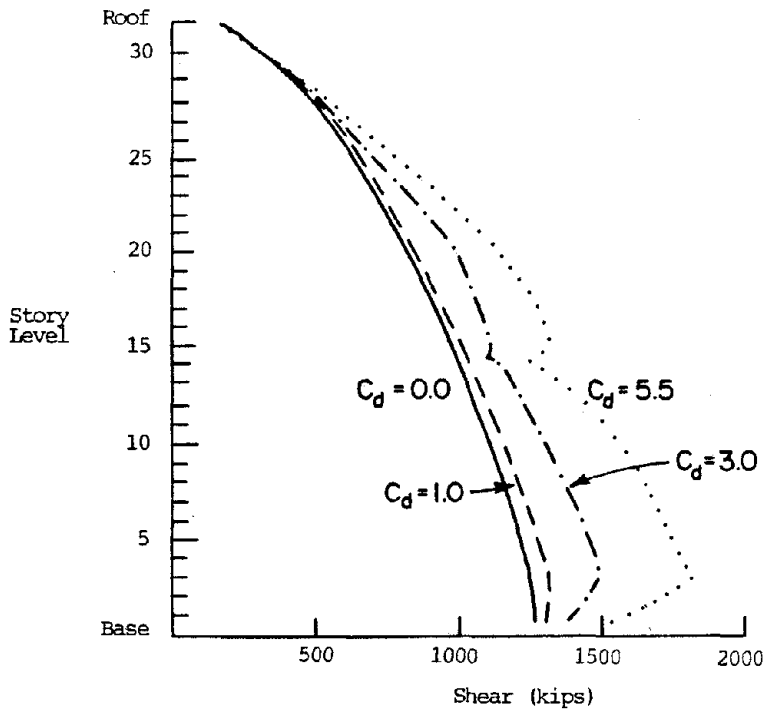


Figure 4.1.9: Story shears resulting from ATC dynamic analysis using different  $C_d$  values

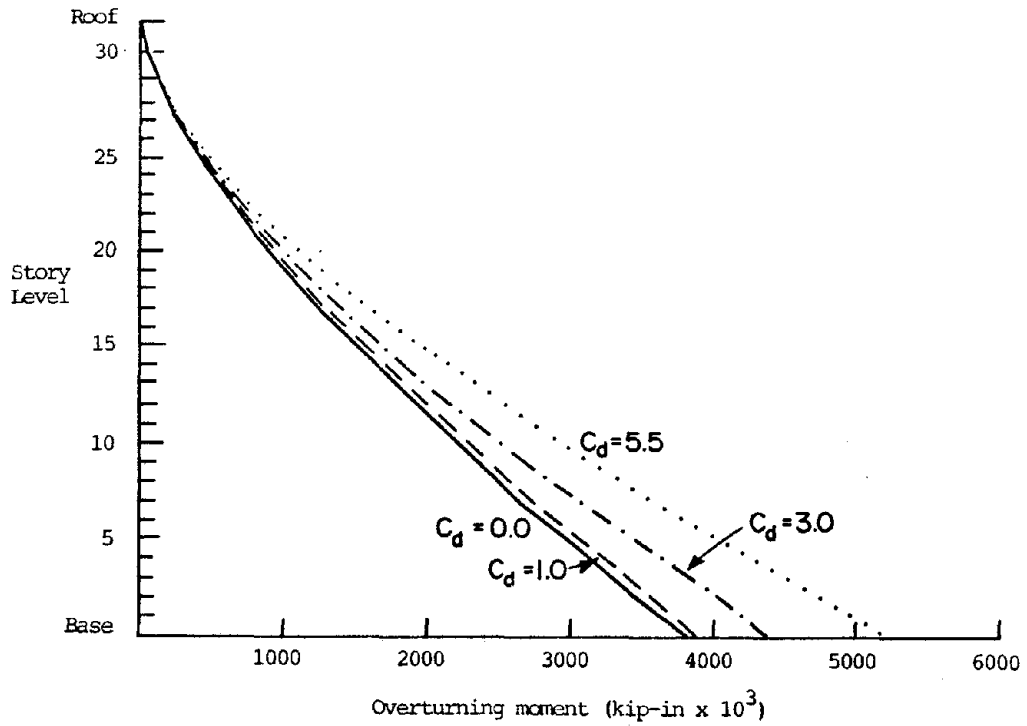


Figure 4.1.10: Story overturning moment resulting from ATC dynamic analysis using different  $C_d$  values

## 4.2 THE COMPARATIVE PERFORMANCE OF MODAL COMBINATION RULES IN RESPONSE SPECTRUM ANALYSIS

### 4.2.1 Introduction

The response spectrum method is a widely used procedure for performing elastic dynamic seismic analysis. The response spectrum, by definition, represents the set of the maximum acceleration, velocity or displacement responses of a family of single-degree-of-freedom (SDOF) damped oscillators, resulting from excitation by a specific earthquake ground motion. The application of response spectrum analysis procedures to structures which cannot be adequately described as SDOF system requires modal analysis techniques to transform the coupled multi-degree-of-freedom equations of motion to a set of uncoupled equations in normal coordinates. This transformation allows the response of each mode to be evaluated as a SDOF system. The response spectrum can be used to predict the individual modal response maxima, but lacks modal time phasing information. Therefore, the relative times at which each peak modal response occurs are unknown. To estimate the total peak response, techniques which combine the individual maximum modal responses are required. Numerous response spectrum modal combination rules have been proposed with the intent of minimizing the total peak response prediction errors when compared to the time history analysis values. The most common rule is the square root of the sum of the squares (SRSS) method, which is recommended for use in the nuclear power(47), offshore oil(2) and building industries (5). However, it is generally recognized that the SRSS method can be a poor estimator of peak responses when applied to systems with closely spaced natural periods. For these cases, various other rules have been suggested, but no single method has gained wide acceptance although a candidate may be the recently presented complete quadratic combination method(50). This method accounts for the influence of

modes with closely spaced periods using the principles of random vibration theory, and is relatively easy to use.

The performance of four different modal combination rules are investigated by sample seismic analyses of a structurally symmetric fifteen story highrise building. The four modal combination rules are: (1) the square root of the sum of the squares (SRSS) method, (2) the double sum combination (DSC) method (34), (3) the complete quadratic combination (CQC) method, and (4) the absolute sum (ABS) method. The SRSS and ABS methods are well known whereas the CQC method is a recent development similar in form to the earlier DSC method. The study includes buildings with concentric and eccentric mass idealizations to investigate the significance of one dimensional versus three dimensional vibration response on the accuracy of the rules. The maximum building response in terms of story deflections, shears, overturning moments and torques are computed by the response spectrum method using each rule and are compared with the time history results for three different single component translational earthquake records. The objectives are: (1) to illustrate situations where the commonly used SRSS rule performs less favorably; (2) to compare and highlight the lesser known DSC and CQC methods; (3) to show representative error magnitudes relative to the time history values; and (4) to make recommendations regarding the most appropriate combination rule for general use based on minimum average error criteria.

#### **4.2.2 Response Spectrum Modal Combination Rules**

In this section, the equation form of the modal combination rules are presented along with a brief discussion regarding their formulation and application.

Square root sum of the sum of the squares (SRSS) method

Form of combination rule(18):

$$R_{\max} = \sqrt{\sum_{i=1}^n R_i^2} \quad (4.2.1)$$

where,

$R_{\max}$  = estimated maximum response for quantity R.

$R_i$  = maximum response of quantity R in mode i.

n = number of modes considered.

Double sum combination\* (DSC) method

Form of combination rule(34,28):

$$R_{\max} = \sqrt{\sum_{i=1}^n \sum_{j=1}^n R_i P_{ij} R_j} \quad (4.2.2)$$

where,

$$P_{ij} = \left[ 1 + \left( \frac{(\omega_i^! - \omega_j^!)}{(\beta_i^! \omega_i + \beta_j^! \omega_j)} \right)^2 \right]^{-1} \quad (4.2.3)$$

in which,

$$\omega_i^! = \omega_i \sqrt{1 - (\beta_i^!)^2} \quad (4.2.4)$$

$$\beta_i^! = \beta_i + \frac{2}{S \omega_i} \quad (4.2.5)$$

---

\*Apparently the name "double sum" was introduced in ref. 38 for the combination rule developed by Rosenblueth et al. It should be noted that this rule differs from the NRC double sum method (47).

$\omega_i$  = natural frequency of the ith mode.

$\beta_i$  = critical damping ratio for the ith mode.

S = time duration of "white noise" segment of earthquake excitation. For actual earthquake records, this may be represented by the strong motion segment characterized by extremely irregular accelerations of roughly equal intensity.

### Complete quadratic combination (CQC) method

Form of combination rule(14,15):

$$R_{\max} = \sqrt{\sum_{i=1}^n \sum_{j=1}^n R_i P_{ij} R_j} \quad (4.2.6)$$

where,

$$P_{ij} = \frac{8 \sqrt{\beta_i \beta_j \omega_i \omega_j} (\beta_i \omega_i + \beta_j \omega_j) \omega_i \omega_j}{(\omega_i^2 - \omega_j^2)^2 + 4 \beta_i \beta_j \omega_i \omega_j (\omega_i^2 + \omega_j^2) + 4 (\beta_i^2 + \beta_j^2) \omega_i^2 \omega_j^2} \quad (4.2.7)$$

### Absolute sum of modal maxima (ABS) method

Form of combination rule:

$$R_{\max} = \sum_{i=1}^n |R_i| \quad (4.2.8)$$

The accuracy of each of the above modal combination rules in predicting the peak time history response depends upon the characteristics of the earthquake record and the structure's dynamic properties. The SRSS, DSC and CQC rules are based upon the theory of random vibrations. Two of the major assumptions used in the

development of these rules are: (1) the excitation is a a sample of a wide frequency band (covering the structure's natural frequencies) stationary Gaussian random process; and, (2) the vibration responses of the structure's normal modes are also stationary. In general, these assumptions are reasonably accurate if the earthquake has a time segment with extreme irregular accelerations of roughly equal intensity which is several times longer than the fundamental period of the structure(15). The simple form of the SRSS rule as compared to the DSC and CQC rules is a consequence of the additional assumption that the modal vibrations are statistically independent; that is, the vibration of any mode is not correlated to that of any other mode. In systems with closely spaced periods, the SRSS rule may be a poor estimator of the actual maximum response (38,50). By introduction of a modal cross-correlation coefficient matrix  $P_{ij}$ , the DSC and CQC rules account for the mutual reinforcement and/or cancellation of modes with closely spaced periods. In particular, the important quality of retaining the signs when combining the cross-modal components (allowing cancellation) can be most significant. Elements of the matrix  $P_{ij}$  can assume values ranging from zero to one (where zero represents no modal cross-correlation) depending primarily upon the relative proximity of the natural periods (Figure 4.2.1). If the periods are well separated, the off-diagonal elements (terms where  $i \neq j$ ) of the matrix  $P_{ij}$  become small and the DSC and CQC methods approach equivalence with the SRSS rule.

Both the DSC and CQC modal cross-correlation coefficient matrices are functions of the modal frequencies and damping ratios. In addition, the DSC formulation includes a parameter for the strong motion duration. To contrast the two methods, the effects of these parameters on the modal cross-correlation coefficient relating two modes are presented in Figure 4.2.1. For both the DSC and the CQC methods, modal cross- correlation coefficients increase as adjacent

modal periods approach the same value, and as the modal damping increases. In addition, for the DSC method, as the ratio of the natural period to the earthquake strong motion duration (ratio  $T_i/S$ ) increases, the modal cross-correlation coefficients increase. Therefore, for a given period ratio  $T_i/T_j$ , modes with the longest periods will have the largest cross-modal effects. When the DSC strong motion duration is set to infinity, the DSC and CQC methods become virtually identical.

As a guide to the approximate natural vibration period range in which random vibration theory based rules (i.e. SRSS,DSC,CQC) are most appropriate, it has been suggested (28) that structures having their most significant natural periods in the range bounded by the intersections of the a and v lines and the v and d lines that are used in the construction (26) of a tripartite logarithmic response spectrum earthquake plot are best suited for these types of combination rules (where a, v, d are the peak ground acceleration, velocity and displacement, respectively). For earthquake records associated with firm ground sites and moderate distances from the focus (El Centro 1940 record type), the corresponding period range is from about .5 seconds to 4 seconds. An example where an a combination rule not based on random vibration theory would be more effective is in the analysis of very short period (very stiff) structures where the spectral accelerations approach the peak ground acceleration. For this case, an algebraic sum of the modal responses will yield the best accuracy in a response spectrum analysis. This approach is equivalent to a static analysis using the peak ground acceleration times the structure's mass to develop external forces . In the analysis of highrise buildings, the modes contributing significantly to the response generally have periods greater than .5 seconds, therefore, the algebraic combination rule is not considered in this study. However, it should be noted that situations can arise where other

special rules are more appropriate.

The ABS rule is an upper bound estimate of the response. It assumes that all modes reach their maxima with the same sign at the same instant in time. In general, this method results in response estimates that are very conservative and is usually not used for design purposes. It is presented in this study because it is of interest to compare the other combination methods against the upper bound values for the response.

In the application of the four aforementioned combination rules, several properties regarding the peak response quantity estimations should be noted. First, the sign of the response quantity is lost; that is, the peak response may either be plus or minus. When combining the results with load cases of known signed responses (e.g., static gravity load cases) judgment must be exercised to formulate the appropriate loadings for design purposes. Secondly, a collection of response quantities produces an estimated maximum response envelope. When considering an envelope of maximum response quantities, it should be recognized that they do not necessarily occur at the same time, consequently if additional response parameters are generated from combinations of these envelope values, inconsistencies are introduced. For example, the use of a story inertia force envelope to calculate cumulative story shears results in values larger than the combined modal story shears. In addition, the use of a story displacement envelope to calculate story drifts results with values smaller than the combined modal drifts. Regarding design applications, the former case may be considered conservative, whereas the latter case is unconservative. Thus, to arrive at the best estimates of the peak response values, modal combinations should be performed separately for each of the response quantities that are to be considered.

### 4.2.3 Building Models Used for Example Analyses

In order to produce representative results that may be expected in actual design situations, a model of an existing modern high-rise building has been formulated for use in the comparative analyses. The fifteen-story steel moment resisting frame structure of the University of California Medical Center Health Sciences East Building (see section 3.4) is used as an example building for this study (Figure 4.2.2). The building is 195 feet in height and is square in plan with an outside dimension of 115 feet 3 inches. The columns are located near the periphery along frame lines 10 feet 10 inches from the building perimeter (twelve vertical column lines with no interior columns). Four moment resisting frames are located in each the North-South and East-West directions. Two building models are formulated. The first is a "regular" building in which the centers of stiffness and mass are coincident. The second is an "irregular" building with the mass offset from the stiffness center of the building. The building's actual dynamic characteristics (natural periods and mode shapes) have been determined from an experimental vibration study (31) and a detailed analytical model of the building has been developed which represents the small amplitude behavior with good accuracy (Model 3, see section 3.4 for detailed model description).

A modified version of the ETABS program (23) is used for the analytical study. Floor diaphragms are idealized as being rigid in their own plane allowing each floor level to be represented with three mass degrees of freedom (two lateral translational and one torsional). Both building models are assumed to be fixed at the ground level (floor 2) and to have 5% of the critical damping in all modes.

### Regular Building Model

A characteristic of this model due to symmetry, is that it has uncoupled translational and torsional modes; that is, each mode responds in a purely translational or torsional sense. This implies that that for translational earthquake ground motion input along either of the building's main axes only those translational modes parallel to the ground motion are excited. The orthogonal translational and torsional modes have zero participation factors. The structural response may be described as one-dimensional since the floor motions have only a single displacement component. The actual building was experimentally tested at various stages during the construction sequence. The East-West dynamic characteristics of the completed building are presented in Table 4.2.1 and Figure 4.2.3 for comparison with the analytical model properties. Comparing the analytical with experimental periods from Table 4.2.1, the first and third periods agree within 2% and the second period is within 11%. Note that the periods are well separated. In Figure 4.2.3, it can be seen that the analytical mode shapes fits the experimental results favorably.

### Irregular Building Model

The irregular building model is developed from the regular model by offsetting the center of mass at each story level by 10% of the plan dimensions of the exterior frame lines as shown in Figure 4.2.4. This results in coupled natural modes; that is, each individual mode contains both translational and torsional floor displacement components whereby earthquake excitation from any direction will cause three-dimensional response with all the modes participating. Representative mode shapes are shown schematically in Figure 4.2.5, and the natural periods are contained in Table 4.2.2. Modes containing predominantly translational components have closely

spaced periods.

#### 4.2.4 Earthquake Inputs Used for Example Analyses

Each building model is analyzed using three single component translational earthquake records input parallel to the East-West building axis. Data for the selected earthquake records (36) is as follows:

<u>Earthquake Record</u>	<u>Soil Type</u>	<u>Epicentral Distance</u>
San Fernando 1971 Pacoima Dam (S00E component)	Rock site	2 miles
Imperial Valley 1940 El Centro (S00E component)	Stiff soil	5 miles
San Fernando 1971 Orion Blvd. (N00W component)	Deep cohesionless soil	10 miles

As shown in Figure 4.2.6, the acceleration time histories have different characteristics. These records are chosen to be representative of the different earthquake excitation types that may be encountered. For this study, the earthquake records are scaled to 0.2g peak ground acceleration and their response spectra are shown in Figure 4.2.7.

By inspection of the earthquake records (Figure 4.2.6), it is not obvious what value of the DSC earthquake duration parameter  $S$  may be optimal for each earthquake. In this study,  $S$  is taken as 10 seconds for each earthquake, although longer values may be more appropriate especially for the for the El Centro and Orion records.

#### 4.2.5 Results from Regular Building Analysis

The story deflection, shear and overturning moment maximum envelope values resulting from the Pacoima Dam excitation are shown in

Figure 4.2.8. Note that the estimated maximum values using the SRSS, DSC and CQC methods are virtually identical. This is expected because the structural periods are well separated (Table 4.2.1) which produces very small DSC and CQC modal cross-correlation coefficients (Figure 4.2.1), justifying the SRSS assumption of statistically independent modal responses for this model. A comparison with the time history result indicates that the SRSS, DSC, and CQC methods all give good estimates of the peak response. However, the ABS combination appreciably overestimates the actual response at most story levels illustrating the important influence of the individual modal maximum response time phasing to the total response.

For each earthquake analysis, the accuracy of each combination rule, is presented in (Tables 4.2.3, 4.2.4, 4.2.5) in terms of a percentage error relative to the time history response (a negative value implies underestimation). Regarding the response in the building's lower stories, the SRSS, DSC, and CQC rules tend to overestimate the actual deflections and shears (by as much as 15 and 14% for deflection and shear, respectively), whereas the overturning moments are estimated within 5%. Upper story deflections are accurately predicted (within 5%); However, shears and overturning moments are both overestimated (Pacoima Dam) and underestimated (El Centro) at several levels by more than 10%. ABS combination is conservative being 30% greater than time history response for lower story deflections, upper and lower story shears, and upper story overturning moments.

In Table 4.2.6, the average error (calculated from absolute error values), the percentage of the response predictions over the height of the building that are underestimated when compared with total number of response predictions (error bias), and the error extremes for each combination rule considering all three earthquake inputs are shown. For reasons discussed previously, the SRSS, DSC and CQC rules yield

similar results with average errors in the response ranging from 6% to 8%. The error bias indicates generally conservative deflection (only about 20% of the responses are underestimated) and story shear (only about 30% underestimated), but slightly unconservative overturning moment predictions (about 60% underestimated). The ABS rule overestimates response at all levels with average errors of 24, 41 and 33% for deflection, shear and overturning moment, respectively.

#### **4.2.6 Results from Irregular Building Analyses**

Plots of story deflection, shear, overturning moment and torque envelopes from the Pacoima Dam excitation are shown in Figures 4.2.9, 4.2.10 and 4.2.11. These quantities are categorized as response parallel (East-West) to the earthquake excitation direction, orthogonal (North-South), and torsional about a vertical axis. For the parallel, orthogonal and torsional response quantities, the DSC and CQC rules yield similar values which provide the best estimates of the actual peak responses. The SRSS rule significantly underestimates the parallel responses, greatly overestimates the orthogonal responses, but gives a fairly good estimate of torsional responses. The upper bound ABS response values are extreme overestimates for the orthogonal and torsional response quantities.

The irregular building model study illustrates the importance of accounting for the correlation between coupled modes with closely spaced periods when combining modal responses in response spectrum analysis. Since the SRSS method neglects all cross-modal contributions, the significance of this effect may be assessed by comparison of the DSC and CQC results with the SRSS computed responses in Figures 4.2.9 and 4.2.10. For the parallel response quantities, the DSC and CQC rules estimate the cross-modal reinforcement to effectively account for more than 20% of the deflection, shear and

overturning response. On the other hand, the striking feature of cross-modal cancellation is apparent in the orthogonal response quantity estimations by a reduction greater than 60% in the DSC and CQC responses compared to the SRSS results (Figure 4.2.10). However, the cross-modal contributions are not significant for the torsional response since the SRSS method yields similar results to the DSC and CQC methods which estimate the actual response well (Figure 4.2.11).

The mechanism by which the DSC and the CQC methods provide the appropriate amounts of cross-modal reinforcement or cancellation may be explained by consideration of the individual modal responses. For the irregular building studied herein, the parallel and orthogonal responses are dominated by the first two modes, that is, their modal contributions to overall response are much larger than any of the higher modal contributions. Because the first two modes have closely spaced periods, it may be expected that each attains its maximum or minimum value at nearly the same time. The modal cross-correlation matrix accounts for this effect by scaling the cross-modal contributions. As discussed previously, this scaling is primarily dependent upon the relative spacing of the natural periods. Whether the modes are nearly in-phase (cross-modal reinforcement) or nearly  $180^\circ$  out-of-phase (cross-modal cancellation) is dependent upon the relative signs of the modal responses. These are set by the modal participation factors which include the earthquake directionality information. The parallel response modal components of the first two modes have the same sign, indicating cross-modal reinforcement. The orthogonal response modal components are of opposite signs, thus cross-modal cancellation results. This behavior can be visualized by inspection of the mode shapes in Figure 4.2.5. If the first two modes oscillate such that the X components are nearly in-phase, it is apparent that the Y components must be nearly  $180^\circ$  out-of-phase. Regarding the torsional response, the first and third modes have the

largest modal components; however, their natural periods are well separated which implies small cross-modal contributions. This explains the relatively small differences between the DSC, CQC, and SRSS results. Also, by inspection of Figure 4.2.5, if the first and third modes oscillate with the X components nearly in-phase, the torsional components will be nearly  $180^\circ$  out-of-phase, thus some cross-modal cancellation results and this is reflected in the story torque envelope plot by the reduced DSC and CQC values compared to SRSS results.

The accuracy of the combination methods in predicting the actual time history maxima of story deflection, shear and torques for each earthquake excitation is contained in (Tables 4.2.7 through 4.2.11). In general, the trends illustrated in the Pacoima Dam response plots discussed previously are the same for the El Centro and Orion results; that is, the DSC and CQC methods yield similar results that are the best estimates of the actual peak response. The SRSS method consistently underestimates the parallel response, greatly overestimates the orthogonal response, and reasonably predicts the torsional response. For the parallel response quantities, the DSC and CQC methods agree closely and generally do not show error trends consistent for all earthquakes regarding response overestimation or underestimation, that is, at a given floor level, the responses may be either overestimated or underestimated, depending upon the earthquake excitation. Regarding the orthogonal response predictions, the DSC and CQC methods have definite error trends whereby the DSC underestimates and the CQC overestimates the actual peak responses. As shown in Figure 4.2.1, the DSC method closely approximates the CQC method as the strong motion time duration parameter  $S$  approaches infinity. This implies that the DSC method with an  $S$  value longer than 10 seconds as used in this study would achieve superior orthogonal response predictions as compared to the CQC method. The

DSC results from the Pacoima Dam excitation have the smallest average errors (Tables 4.2.7 to 4.2.11) suggesting that  $S$  equal to 10 seconds may be a better value for Pacoima Dam excitation than for either the El Centro or Orion Blvd. records. The orthogonal responses as computed by the DSC and CQC methods have larger error percentages than the corresponding parallel responses. However, the orthogonal responses are much smaller than the parallel responses at any story level.

The combined results for all three earthquakes in terms of average error, error bias and error extremes are presented in Table 4.2.12. The parallel response predictions using the DSC and CQC methods yield the smallest average errors (6 to 8%). The SRSS method produces consistent underestimations with average errors of 18 to 25%, and the ABS method has overestimations of 27 to 49%. Regarding orthogonal response quantity predictions, the DSC and CQC methods have average errors 16 to 18% and 24 to 32%, respectively. The DSC underestimates whereas the CQC overestimates the actual peak response. The SRSS and ABS rules produce extreme overestimations with average errors of 217 to 251% and 491 to 528%, respectively. For story torques, the SRSS, DSC and CQC methods yield predictions with similar average errors (7 to 13%). The ABS rule considerably overestimates the actual peak torques with an average error of 137%.

It is of interest to note that the peak response quantity estimations by the DSC and CQC methods involve more numerical calculations than those as computed by the SRSS method; yet, for this study, the differences in execution times between analyses using the different methods are negligible. This is because relatively few response quantities are calculated. For the solution of large numbers of response quantities involving many modes, the DSC and CQC methods may require significantly more computational effort than the SRSS method. For these cases, the DSC and CQC double summation

calculations (equations 4.2.2 and 4.2.6) can be truncated when the value of  $P_{ij}$  becomes small, therefore avoiding unnecessary computations(15,38).

#### 4.2.7 Summary and Conclusions

The peak dynamic responses of two mathematical models of a fifteen-story steel moment resisting frame building subjected to three earthquake excitations are computed by the response spectrum and time history methods. The models examined are: a "regular" building in which the centers of stiffness and mass are coincident resulting in uncoupled modes with well separated periods in each component direction of response; and, an "irregular" building with the mass offset from the stiffness center of the building causing coupled modes with the translational modes having closely spaced periods. The building response quantities examined are the story deflections, shears, overturning moments and torques. These quantities are categorized as parallel and orthogonal response with respect to the earthquake direction and as torsional response about a vertical axis. Four response spectrum modal combination rules are discussed and are used to predict the peak responses: (1) the square root of the sum of the squares (SRSS) method, (2) the double sum combination (DSC) method, (3) the complete quadratic combination (CQC) method, and (4) the absolute sum (ABS) method. The response spectrum analysis results are compared to the corresponding peak time history analysis values to evaluate the accuracy of the different combination rules.

For the regular building, the SRSS, DSC, and CQC methods yield virtually identical peak response predictions, and agree well with the time history values. The calculated peak response values have average errors in the range of 6 to 8% (see Table 4.2.6) with respect to time history analysis. Depending upon the earthquake, the modal combination rules may overestimate or underestimate the peak response a given floor level over the height of the building. The ABS method

substantially overestimates the actual response at most story levels.

For the irregular building, the parallel, orthogonal, and torsional response quantity predictions by the DSC and CQC methods have similar values which agree well with the time history values. The DSC and CQC methods both predict nearly identical values for parallel and torsional response having average errors ranging from 6 and 8% and 7 to 9%, respectively (see Table 4.2.12, Parallel and Torsional Response). Both may overestimate or underestimate the parallel and torsional response values a given floor level over the height of the building depending upon the earthquake. The orthogonal response quantities as computed by the CQC method consistently overestimate the actual peak responses with average errors ranging from 24 to 32% (see Table 4.2.12, Orthogonal Response). Those computed by the DSC method consistently underestimate the peak responses with average errors ranging from 16 to 18% (see Table 4.2.12, Orthogonal Response). The magnitude of the DSC orthogonal estimation errors is influenced by the strong motion time duration parameter  $S$ . Because the DSC method closely approximates the CQC method if the strong motion duration parameter  $S$  is set to infinity, it is possible to select a value of  $S$  that achieves superior DSC orthogonal response predictions. The parallel, orthogonal and torsional response predictions as computed by the SRSS method have average errors 18 to 25%, 217 to 251%, and 13% (see Table 4.2.12), respectively. The parallel responses are consistently underestimated and the orthogonal responses are consistently overestimated for all earthquakes. The torsional responses at different floor levels over the height of the building, are either overestimated or underestimated depending upon the earthquake. The poor accuracy in the parallel and orthogonal response predictions is attributable to the effects of coupled translational modes with closely spaced periods. The ABS method substantially overestimates the actual response at most story levels,

especially the orthogonal response.

Based on the results of this study, the following conclusions are made:

(1) The DSC and the CQC methods provide good peak response estimates, for both regular and irregular building models irrespective of modal coupling. Both methods are recommended. In addition to the DSC and CQC rules, the SRSS method gives accurate response predictions for regular buildings and is recommended for systems where coupled modes with closely spaced periods do not dominate the response.

(2) The use of a modal cross-correlation matrix is an effective procedure for combining the results from coupled modes with closely spaced periods. Because the DSC modal cross-correlation matrix formulation includes the strong motion time duration (parameter  $S$ ), the DSC method has the potential to provide better peak response estimates than the CQC method. However, the selection of  $S$  is somewhat arbitrary when utilizing design or actual earthquake spectra. Furthermore, for the irregular building studied, only the DSC orthogonal response predictions could be significantly improved over those by the CQC method by adjustments of  $S$ . The difference between the DSC and CQC orthogonal response estimates may not be significant in design applications because the magnitude of the orthogonal responses is considerably less than the corresponding parallel values that may ultimately control the design. For design applications that involve independent designs in both building principal directions(20), the orthogonal responses probably would not govern. For these reasons, the DSC and CQC methods may be considered to yield results of equivalent accuracy.

(3) When interpreting response spectrum results utilizing the DSC, the CQC, and the SRSS (for regular type buildings) methods, it is important to recognize that underestimation of the actual peak response is possible. In situations where the possibility of under

estimation is unacceptable, the use of the ABS combination method or time history analysis should be considered.

Table 4.2.1: Regular Building Natural Periods

Mode Number	Period in seconds		Direction
	Analytical Model	Experimental Fall 1965-II	
1	1.113	1.1	E-W translational (all modes)
2	.386	.43	
3	.222	.22	
4	.154	-	

Table 4.2.2: Irregular Building Natural Periods

Mode Number	Period in seconds	Predominant Direction
1	1.167	First E-W mode
2	1.121	First N-S mode
3	.773	First torsional mode
4	.409	Second E-W
5	.390	Second N-S
6	.278	Second torsional
7	.238	Third E-W
8	.225	Third N-S
9	.166	Fourth E-W
10	.165	Third torsional
11	.156	Fourth N-S
12	.124	Fifth E-W

Table 4.2.3: Regular Building Story Deflection Results

Level (1)	Pacoima Dam							El Centro							Orion Blvd.						
	Time History Results			Response Spectrum % Error vs. Time History				Time History Results			Response Spectrum % Error vs. Time History				Time History Results			Response Spectrum % Error vs. Time History			
	D, in (2)	Time, in sec. (3)		SRSS (4)	DSC (5)	CQC (6)	ABS (7)	D, in (8)	Time, in sec. (9)		SRSS (10)	DSC (11)	CQC (12)	ABS (13)	D, in (14)	Time, in sec. (15)		SRSS (16)	DSC (17)	CQC (18)	ABS (19)
RF	3.60	4.16		-1	-1	-1	13	3.67	3.52		-1	-1	-1	10	4.90	11.88		-3	-3	-3	8
16	3.47			-1	-1	-1	10	3.50			1	0	1	9	4.72			-3	-3	-3	6
15	3.29			-1	-1	-1	7	3.28			2	2	2	8	4.48			-3	-3	-3	3
14	3.09			0	-1	0	5	3.02			4	4	4	9	4.19			-2	-2	-2	2
13	2.85			0	0	0	4	2.73			7	7	7	11	3.85			-1	-1	-1	2
12	2.58			1	1	1	9	2.42	3.52		10	10	10	17	3.48			-1	0	0	6
11	2.30	4.16		2	2	2	14	2.16	3.02		11	11	11	21	3.09			1	1	1	11
10	2.01	4.14		2	3	2	19	1.91			10	10	10	24	2.69			2	2	2	16
9	1.72			3	4	4	24	1.64			10	11	10	27	2.28			4	4	4	20
8	1.43			5	6	5	30	1.37			11	11	11	31	1.88			5	6	6	27
7	1.15			6	7	6	36	1.10			12	12	12	36	1.50			7	7	7	32
6	0.87			7	8	7	41	0.83	3.02		12	13	12	42	1.12			9	10	9	39
5	0.60			8	10	8	47	0.58	3.00		12	12	12	47	0.77			10	12	10	45
4	0.35			11	11	11	54	0.34	3.00		12	15	15	50	0.45			11	13	13	51
3	0.13	4.14		8	8	8	54	0.13	3.00		8	8	8	46	0.17	11.88		12	12	12	47
Average % Error				4	4	4	24				8	8	8	26				5	5	5	21

Table 4.2.4: Regular Building Story Shear Results

Level (1)	Pacoima Dam							El Centro							Orion Blvd.						
	Time History Results			Response Spectrum % Error vs. Time History				Time History Results			Response Spectrum % Error vs. Time History				Time History Results			Response Spectrum % Error vs. Time History			
	V, in kips (2)	Time, in sec. (3)		SRSS (4)	DSC (5)	CQC (6)	ABS (7)	V, in kips (8)	Time, in sec. (9)		SRSS (10)	DSC (11)	CQC (12)	ABS (13)	V, in kips (14)	Time, in sec. (15)		SRSS (16)	DSC (17)	CQC (18)	ABS (19)
RF	559	8.48		0	-2	-1	80	621	3.54		-17	-19	-18	51	636	11.84		7	5	6	91
16	968	8.48		6	4	5	82	1136	3.54		-17	-18	-17	44	1215			3	2	3	76
15	1223	4.76		15	13	14	82	1552	3.52		-15	-17	-16	32	1725			1	-1	0	57
14	1540	4.76		10	9	10	65	1891	3.52		-15	-16	-15	24	2165			-1	-2	-2	45
13	1803	4.16		8	7	7	52	2172	3.50		-14	-14	-14	17	2542	11.84		-2	-3	-3	35
12	2053			4	3	4	47	2347			-10	-10	-10	22	2863	13.12		-3	-3	-3	33
11	2269			2	1	2	36	2426			-4	-4	-4	25	3159	11.88		-4	-4	-4	25
10	2453			1	1	1	24	2441	3.50		4	4	4	26	3415			-4	-4	-4	15
9	2609			1	1	1	16	2495	3.54		9	9	9	25	3610			-2	-3	-2	10
8	2738			3	3	3	25	2666	3.04		8	8	8	29	3742			0	0	0	19
7	2843	4.16		5	5	5	30	2777	3.04		8	9	9	29	3816			3	3	3	24
6	2928	4.14		7	7	7	36	2840	3.02		10	11	11	35	3844			7	7	7	32
5	2991			8	9	9	46	2893	3.02		12	13	12	45	3846			10	11	11	44
4	3029			10	11	10	54	2945	3.00		12	13	13	52	3839	11.88		13	14	13	53
3	3044	4.14		10	11	11	57	2967	3.00		12	13	13	55	3890	12.48		12	13	13	55
Average % Error				6	6	6	49				11	12	12	34				5	5	5	41

Table 4.2.5: Regular Building Story Overturning Moment Results

Level (1)	Pacoima Dam						El Centro						Orion Blvd.										
	Time History Results			Response Spectrum % Error vs. Time History			Time History Results			Response Spectrum % Error vs. Time History			Time History Results			Response Spectrum % Error vs. Time History							
	M x 10 <sup>3</sup> k-in. (2)	Time, in sec. (3)		SRSS (4)	DSC (5)	CQC (6)	ABS (7)	M, in k-in. (8)	Time, in sec. (9)		SRSS (10)	DSC (11)	CQC (12)	ABS (13)	M, in k-in. (14)	Time, in sec. (15)		SRSS (16)	DSC (17)	CQC (18)	ABS (19)		
16	.87	8.48		0	-2	-1	80	.97	3.54		-18	-19	-19	51	.99	11.84		7	5	6	92		
15	238	8.48		4	2	3	81	274	3.54		-17	-18	-18	46	289			4	3	3	81		
14	426	8.48		9	7	8	83	572	3.54		-16	-17	-17	41	558			2	1	1	70		
13	631	4.78		15	13	14	84	804	3.52		-16	-17	-16	33	896			0	-1	0	58		
12	907	4.76		13	11	12	71	1137			-15	-16	-16	26	1292			-1	-2	-1	47		
11	1218	4.16		10	9	10	61	1495			-14	-15	-15	21	1739			-2	-3	-3	39		
10	1571			7	6	7	50	1868			-13	-13	-13	17	2227			-3	-4	-3	32		
9	1954			5	4	4	40	2248			-11	-11	-11	14	2748			-4	-4	-4	25		
8	2361			3	2	2	32	2632			-8	-9	-9	13	3295	11.84		-4	-5	-4	20		
7	2788			1	1	1	28	3017			-6	-6	-6	13	3876	11.88		-4	-5	-4	17		
6	3232			0	0	0	22	3402			-4	-4	-4	13	4471			-4	-5	-4	13		
5	3688			0	-1	-1	15	3788			-1	-1	-1	11	5071			-4	-4	-4	9		
4	4152			-1	-1	-1	9	4173			1	1	1	9	5670			-3	-3	-3	5		
3	4622			-1	-1	-1	5	4588			3	3	3	8	6269			-2	-2	-2	2		
2	5076	4.16		0	0	0	2	4930	3.52		5	5	5	8	6846	11.88		-1	-1	-1	1		
Average % Error				5	4	4	44					10	10	10	22					3	3	3	34

Table 4.2.6: Regular Building Compiled Error Results

% Error Results Compiled From 3 Earthquake Excitations					
		SRSS	DSC	CQC	ABS
Deflections	Average error	6%	6	6	24
	% underestimated*	22%	22	20	0
	Extreme errors	-3, 12%	-3, 15	-3, 15	2, 54
Shears	Average error	7	8	8	41
	% underestimated*	29	33	31	0
	Extreme errors	-17, 15	-19, 14	-18, 14	10, 91
Overturning Moments	Average error	6	6	6	33
	% underestimated*	56	62	60	0
	Extreme errors	-18, 15	-19, 13	-19, 14	1, 92

\* Number of underestimated responses expressed as a percentage of the total number of response predictions

Table 4.2.7: Irregular Building Story Deflection Results, East-West Response

Level (1)	Pacoima Dam						El Centro						Orion Blvd.					
	Time History Results			Response Spectrum % Error vs. Time History			Time History Results			Response Spectrum % Error vs. Time History			Time History Results			Response Spectrum % Error vs. Time History		
	D, in (2)	Time, in sec. (3)	SRSS (4)	DSC (5)	CQC (6)	ABS (7)	D, in (8)	Time, in sec. (9)	SRSS (10)	DSC (11)	CQC (12)	ABS (13)	D, in (14)	Time, in sec. (15)	SRSS (16)	DSC (17)	CQC (18)	ABS (19)
RF	3.54	4.18	-23	-1	-3	14	3.47	5.86	-22	1	-1	16	5.13	13.12	-26	-5	-7	8
16	3.42	4.16	-23	-1	-3	11	3.33		-22	2	0	14	4.94		-26	-5	-7	5
15	3.26		-24	-1	-3	8	3.14		-21	3	1	12	4.68		-25	-4	-6	4
14	3.06		-24	-1	-3	6	2.92		-20	4	2	12	4.37		-25	-4	-5	3
13	2.82		-23	0	-2	5	2.66		-19	6	4	13	4.01		-24	-3	-5	2
12	2.55		-22	1	-2	11	2.38		-17	8	6	19	3.61		-23	-1	-3	7
11	2.27		-22	2	0	16	2.09	5.86	-15	11	8	25	3.20		-22	0	-2	13
10	1.99		-21	3	1	20	1.80	3.04	-13	13	11	31	2.78		-21	1	-1	17
9	1.70		-20	4	2	25	1.55		-14	14	11	34	2.35		-20	3	1	22
8	1.41		-19	6	3	31	1.30		-13	14	11	39	1.94		-18	5	3	28
7	1.13		-18	7	4	37	1.04		-13	14	13	45	1.54		-17	7	5	34
6	0.85		-16	8	6	44	0.79	3.04	-13	15	13	51	1.15		-16	10	7	41
5	0.59		-17	8	7	49	0.55	3.02	-13	15	13	56	0.79		-14	11	9	47
4	0.35		-17	9	6	51	0.32	3.02	-9	19	16	63	0.46	13.12	-13	13	11	52
3	0.13	4.16	-15	8	8	54	0.12	3.02	-8	17	17	67	0.17	12.52	-12	12	12	53
Average % Error			20	4	4	25			15	10	8	33			20	6	6	22

Table 4.2.8: Irregular Building Story Shear Results, East-West Response

Level (1)	Pacoima Dam						El Centro						Orion Blvd.					
	Time History Results			Response Spectrum % Error vs. Time History			Time History Results			Response Spectrum % Error vs. Time History			Time History Results			Response Spectrum % Error vs. Time History		
	V, in kips (2)	Time, in sec. (3)	SRSS (4)	DSC (5)	CQC (6)	ABS (7)	V, in kips (8)	Time, in sec. (9)	SRSS (10)	DSC (11)	CQC (12)	ABS (13)	V, in kips (14)	Time, in sec. (15)	SRSS (16)	DSC (17)	CQC (18)	ABS (19)
RF	446	4.80	-12	13	12	122	580	3.56	-35	-18	-19	71	636	13.16	-21	0	-1	94
16	835	4.80	-13	11	10	103	1032	3.56	-34	-15	-16	61	1233		-24	-3	-5	73
15	1183	4.78	-16	8	7	81	1407	3.54	-34	-14	-15	46	1772		-27	-6	-7	53
14	1474	4.78	-17	7	5	70	1742	3.52	-34	-14	-16	38	2238	13.16	-28	-7	-9	44
13	1720	4.16	-19	5	4	57	1968	3.52	-32	-11	-13	31	2639	13.12	-29	-8	-10	33
12	1976		-22	2	0	48	2086	5.84	-28	-5	-7	37	2981		-29	-9	-10	29
11	2188		-24	0	-2	38	2233	5.84	-26	-2	-4	37	3263		-29	-8	-10	24
10	2359	4.16	-24	0	-2	28	2336	5.86	-23	2	0	34	3493		-28	-7	-9	17
9	2498	4.18	-23	1	-1	19	2419	5.86	-20	5	3	29	3669		-27	-5	-7	12
8	2617	4.18	-22	3	0	29	2463	5.86	-17	10	7	40	3789		-25	-2	-4	21
7	2705	4.18	-20	5	3	35	2490	3.04	-14	14	11	46	3855		-22	2	-1	27
6	2772	4.16	-18	8	5	41	2554	3.04	-13	16	13	51	3876		-19	5	3	35
5	2828	4.16	-17	10	7	50	2580	3.04	-11	19	16	61	3869		-17	9	6	46
4	2853	4.16	-16	11	8	59	2609	3.00	-10	20	17	73	3854		-15	12	9	56
3	2880	4.14	-16	12	9	63	2633	3.00	-10	20	17	77	3846	13.12	-14	13	10	61
Average % Error			19	6	5	56			23	12	12	49			24	6	7	42

Table 4.2.9: Irregular Building Story Deflection Results, North-South Response

Level (1)	Pacoima Dam							El Centro							Orion Blvd.						
	Time History Results			Response Spectrum % Error vs. Time History				Time History Results			Response Spectrum % Error vs. Time History				Time History Results			Response Spectrum % Error vs. Time History			
	D, in (2)	Time, in sec. (3)		SRSS (4)	DSC (5)	CQC (6)	ABS (7)	D, in (8)	Time, in sec. (9)		SRSS (10)	DSC (11)	CQC (12)	ABS (13)	D, in (14)	Time, in sec. (15)		SRSS (16)	DSC (17)	CQC (18)	ABS (19)
RF	0.56	6.14		304	-7	52	550	0.72	7.24		218	-26	19	407	0.87	14.52		253	-17	33	463
16	0.54			304	-7	52	535	0.70	7.24		216	-27	19	393	0.84			254	-17	33	451
15	0.51			308	-8	53	522	0.66	7.26		218	-27	20	385	0.81			249	-19	32	431
14	0.47	6.14		315	-6	55	521	0.63	7.26		214	-29	19	373	0.77			245	-19	31	417
13	0.44	5.58		311	-7	55	505	0.58	7.28		216	-28	19	371	0.71			246	-18	31	413
12	0.40	5.60		313	-8	55	533	0.54	7.28		209	-30	17	378	0.65			245	-20	31	429
11	0.36	5.60		311	-6	53	556	0.48	7.28		210	-29	17	396	0.59			241	-20	29	439
10	0.32	5.62		306	-6	53	572	0.43	7.30		205	-30	16	395	0.52			240	-19	29	452
9	0.28	5.64		300	-7	50	582	0.37	6.72		205	-30	16	408	0.45			238	-20	29	462
8	0.24			292	-8	50	592	0.32			197	-31	13	406	0.37			246	-16	32	492
7	0.20			285	-10	45	595	0.26			192	-31	12	419	0.30			260	-17	30	507
6	0.15			287	-7	47	627	0.20			190	-30	10	435	0.23			239	-17	30	522
5	0.11			273	-9	45	618	0.14			186	-29	7	450	0.16			244	-19	31	538
4	0.07			243	-14	29	571	0.08			200	-25	13	475	0.09			256	-11	33	578
3	0.02	5.64		350	0	50	800	0.03	6.72		200	-33	0	467	0.03	14.52		267	0	67	667
Average % Error				300	7	50	579				205	29	14	411				248	17	33	484

Table 4.2.10: Irregular Building Story Shear Results, North-South Response

Level (1)	Pacoima Dam							El Centro							Orion Blvd.						
	Time History Results			Response Spectrum % Error vs. Time History				Time History Results			Response Spectrum % Error vs. Time History				Time History Results			Response Spectrum % Error vs. Time History			
	V <sub>s</sub> in kips (2)	Time, in sec. (3)		SRSS (4)	DSC (5)	CQC (6)	ABS (7)	V <sub>s</sub> in kips (8)	Time, in sec. (9)		SRSS (10)	DSC (11)	CQC (12)	ABS (13)	V <sub>s</sub> in kips (14)	Time, in sec. (15)		SRSS (16)	DSC (17)	CQC (18)	ABS (19)
RF	144	8.46		133	-22	1	510	116	5.34		171	-9	17	639	153	10.52		173	-13	14	612
16	244	8.44		155	-20	6	526	194	4.06		199	-8	24	661	275			184	-16	16	595
15	335	8.98		155	-24	4	486	268	4.02		200	-14	21	601	357			204	-15	21	594
14	407	8.98		156	-28	2	457	344	4.02		189	-20	16	532	394	10.52		241	-9	34	633
13	436	8.98		174	-26	8	461	394	4.00		194	-21	17	496	443	15.04		254	-9	37	613
12	439	8.40		201	-23	17	505	421	4.00		211	-19	22	519	502	15.04		250	-14	34	591
11	424	8.38		238	-16	30	551	451	7.26		221	-18	26	518	561	15.08		244	-17	31	550
10	413	6.10		273	-10	43	565	498	7.28		215	-20	23	471	620	14.56		237	-21	28	494
9	421	6.12		291	-7	49	544	551	7.30		205	-24	19	478	674			232	-22	26	449
8	430	5.58		307	-3	55	617	600	7.30		196	-26	15	427	717			231	-23	25	478
7	467	5.66		296	-4	51	612	639	7.32		192	-27	14	421	751			232	-21	26	489
6	511	5.66		279	-6	46	600	675	6.74		188	-27	12	424	779			234	-20	27	506
5	549	5.64		266	-8	42	609	710	6.74		182	-28	11	440	800			236	-18	29	538
4	578	5.64		256	-9	38	621	754	4.42		171	-29	7	445	813			237	-17	30	568
3	590	5.64		252	-9	37	625	778	4.40		165	-31	4	443	818	14.56		238	-16	30	580
Average % Error				229	14	29	533				193	21	17	497				228	17	27	553

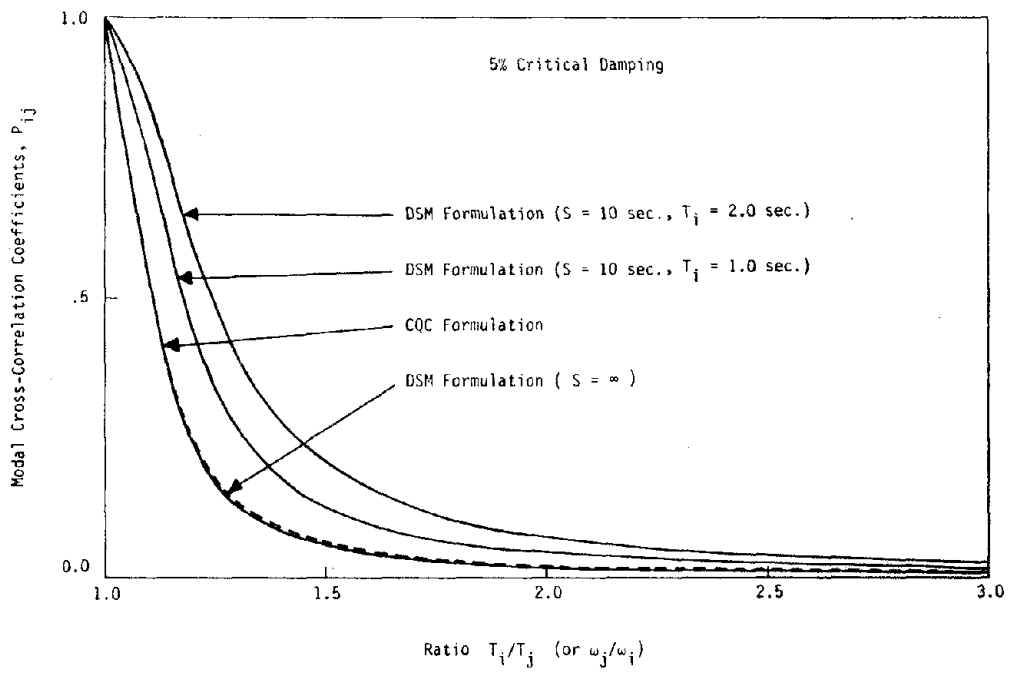
Table 4.2.11: Irregular Building Story Torque Results

Level (1)	Pacoima Dam							El Centro				Orion Blvd.						
	Time History Results		Response Spectrum % Error vs. Time History				Time History Results		Response Spectrum % Error vs. Time History		Time History Results		Response Spectrum % Error vs. Time History					
	T x 10 <sup>3</sup> k-in. (2)	Time, in sec. (3)	SRSS (4)	DSC (5)	CQC (6)	ABS (7)	T, in k-in. (8)	Time, in sec. (9)	SRSS (10)	DSC (11)	CQC (12)	ABS (13)	T, in k-in. (14)	Time, in sec. (15)	SRSS (16)	DSC (17)	CQC (18)	ABS (19)
16	73	4.82	15	-8	-5	227	117	3.58	-15	-27	-26	141	85	9.32	40	18	21	288
15	130		15	-8	-5	214	205	3.58	-14	-25	-23	135	161	12.52	35	15	19	259
14	168		15	-5	-2	201	266	3.56	-12	-23	-20	125	230		28	10	14	219
13	194	4.82	18	-3	2	187	311	2.70	-9	-20	-17	114	296		21	5	10	180
12	216	4.18	19	-2	3	161	359	2.72	-9	-19	-16	90	361		16	1	5	140
11	243	4.16	16	-5	0	156	388	2.72	-4	-16	-12	99	418		12	-2	2	133
10	267	4.16	14	-7	-2	155	404	3.10	2	-11	-7	114	462		12	-3	2	131
9	284	4.18	15	-7	-2	142	455		-2	-14	-10	97	491	12.52	14	-1	3	124
8	301	4.22	14	-7	-2	114	495		-3	-16	-12	76	526	12.48	14	-1	3	103
7	325	4.24	12	-9	-3	109	524	3.10	-4	-15	-12	73	558		14	-1	4	102
6	344		11	-8	-3	108	548	3.08	-4	-15	-11	71	589		13	-2	3	100
5	357		13	-7	-2	121	567		-3	-15	-11	79	620		12	-3	2	107
4	365	4.24	15	-6	-1	142	579		-2	-14	-10	94	647		11	-4	1	118
3	370	4.26	17	-5	0	159	587		-1	-14	-10	106	667		10	-5	0	126
2	371	4.26	18	-5	1	167	590	3.08	0	-13	-9	112	675	12.48	10	-6	-1	130
Average % Error			15	6	2	158			6	17	14	102			17	5	6	150

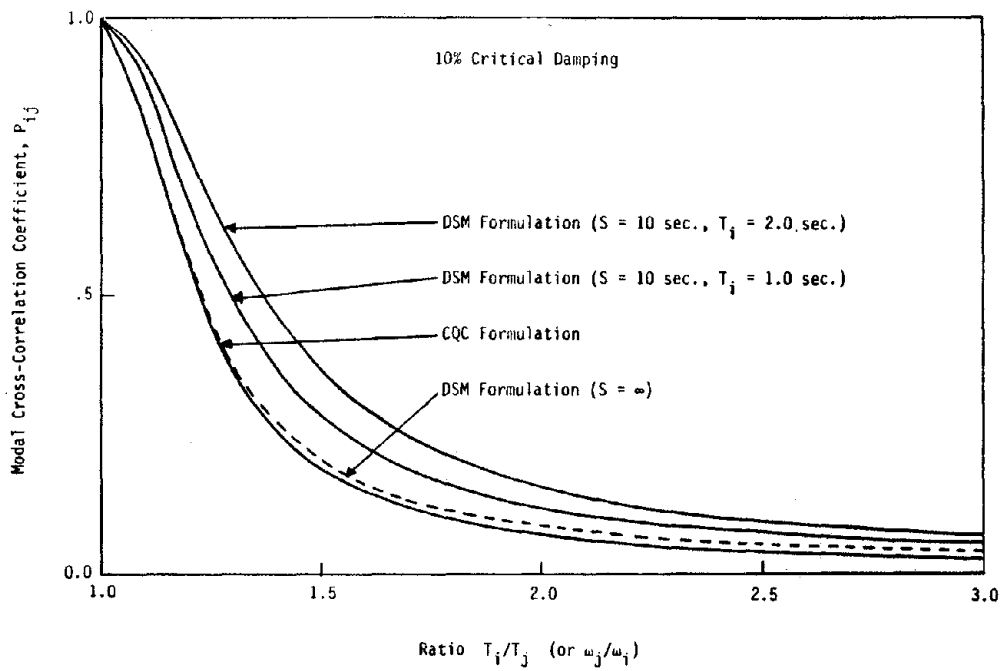
Table 4.2.12: Irregular Building Compiled Error Results

		% Error Results Compiled from 3 Earthquake Excitations			
		SRSS	DSC	CQC	ABS
Parallel (E-W) Response					
Deflections	Average error	18%	7	6	27
	% underestimated*	100%	22	33	0
	Extreme errors	-26, -8%	-5, 19	-7, 17	2, 67
Shears	Average error	22	8	8	49
	% underestimated*	100	36	47	0
	Extreme errors	-35, -10	-18, 20	-19, 17	12, 122
Overturning moments	Average error	25	6	7	39
	% underestimated*	100	56	76	0
	Extreme errors	-34, -11	-18, 12	-18, 11	2, 120
Orthogonal (N-S) Response					
Deflections	Average error	251	18	32	491
	% underestimated*	0	100	0	0
	Extreme errors	186, 350	-33, 0	0, 67	371, 800
Shears	Average error	217	17	24	528
	% underestimated*	0	100	0	0
	Extreme errors	133, 307	-31, -3	1, 55	418, 661
Overturning moments	Average error	218	16	25	520
	% underestimated*	0	100	0	0
	Extreme errors	136, 299	-25, -6	5, 51	366, 658
Torsional Response					
Torques	Average error	13	9	7	137
	% underestimated*	29	89	58	0
	Extreme errors	-15, 40	-27, 18	-26, 21	71, 288

\* Number of underestimated responses expressed as a percentage of the total number of response predictions



(a)



(b)

Figure 4.2.1: Comparison of DSC and CQC Modal Cross-Correlation Coefficients  
 (a) 5% Critical Damping  
 (b) 10% Critical Damping

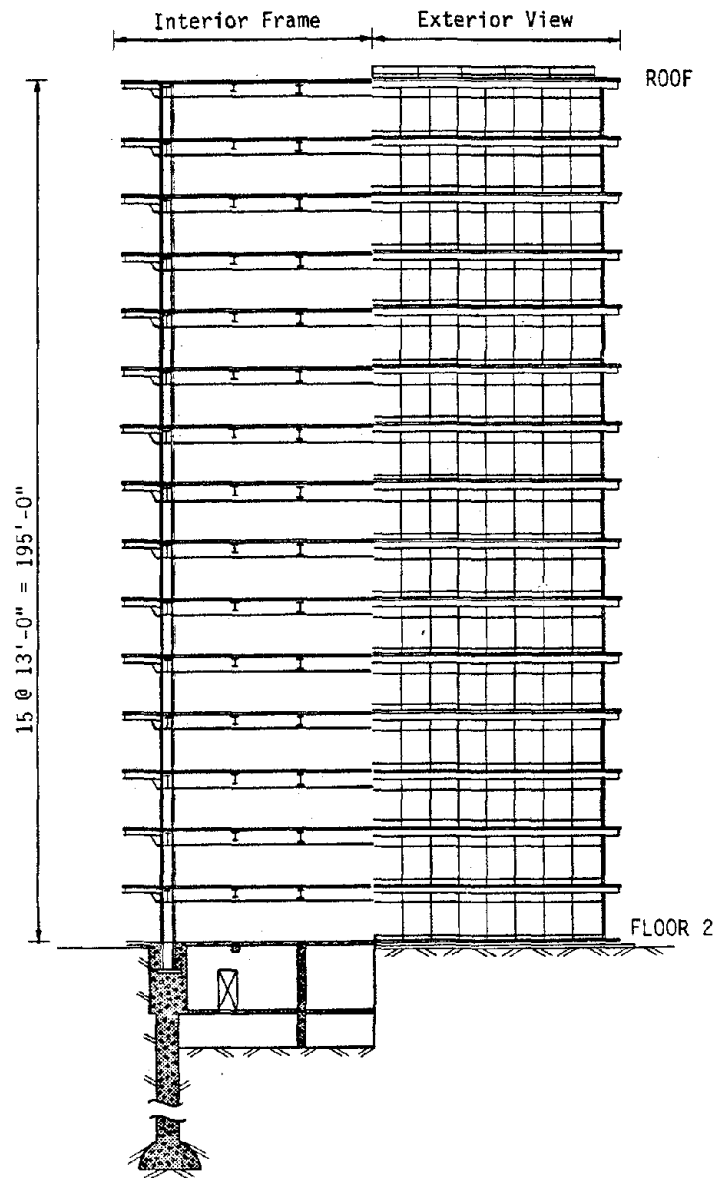


Figure 4.2.2: Example Building

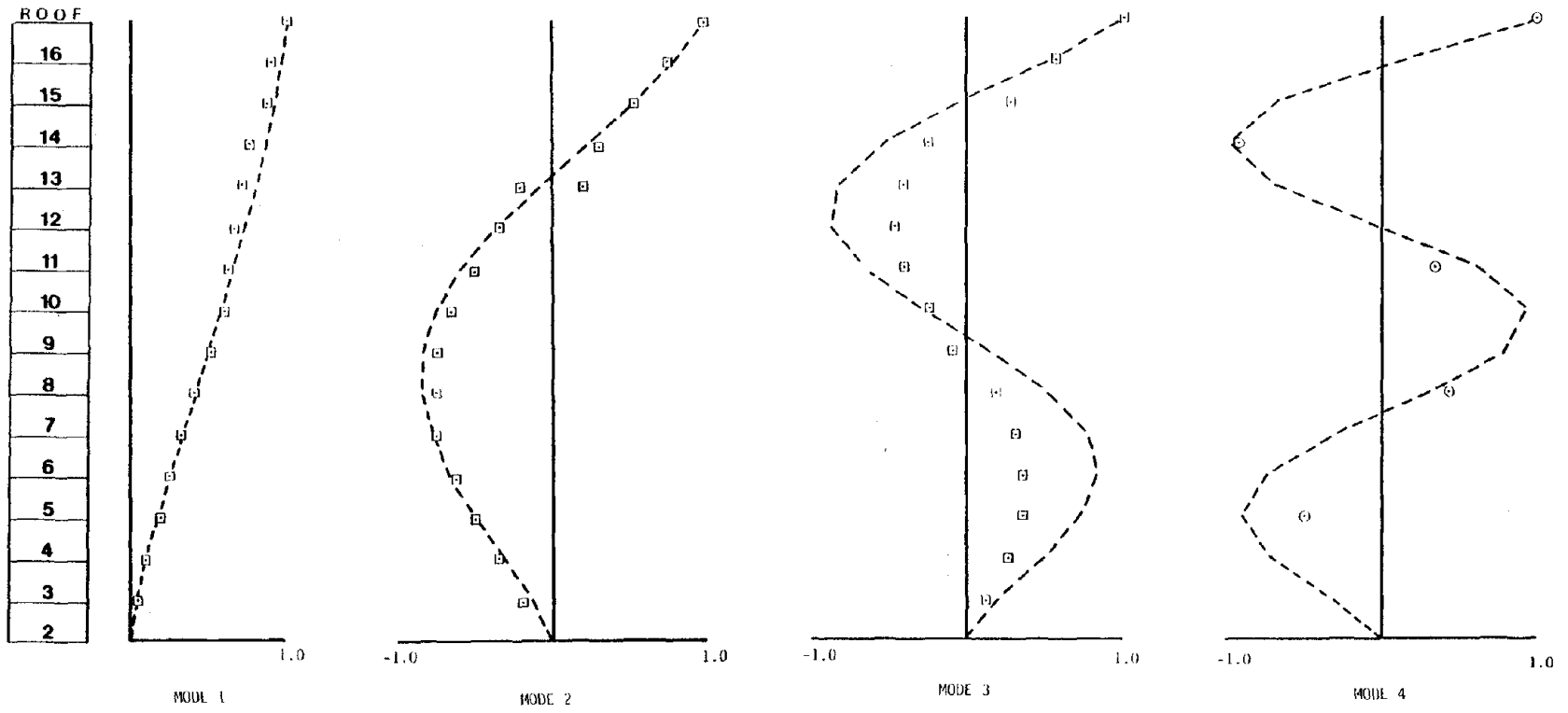


Figure 4.2.3: Regular Building Mode Shapes

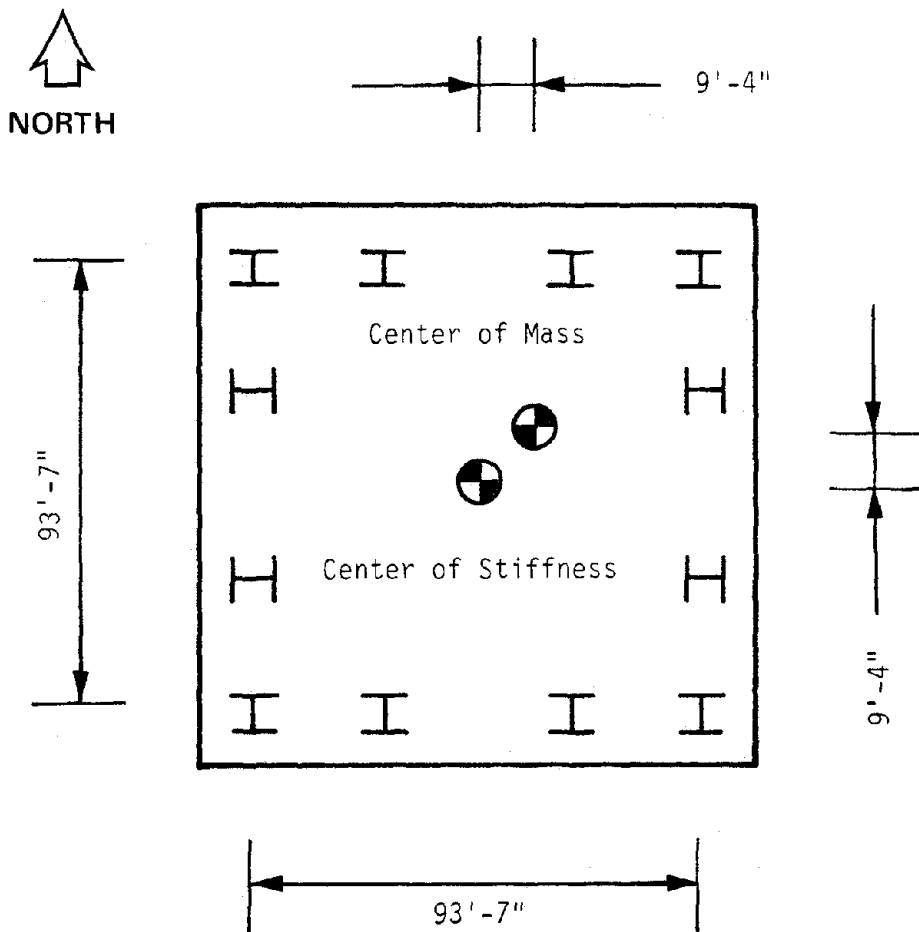


Figure 4.2.4: Irregular Building Plan View

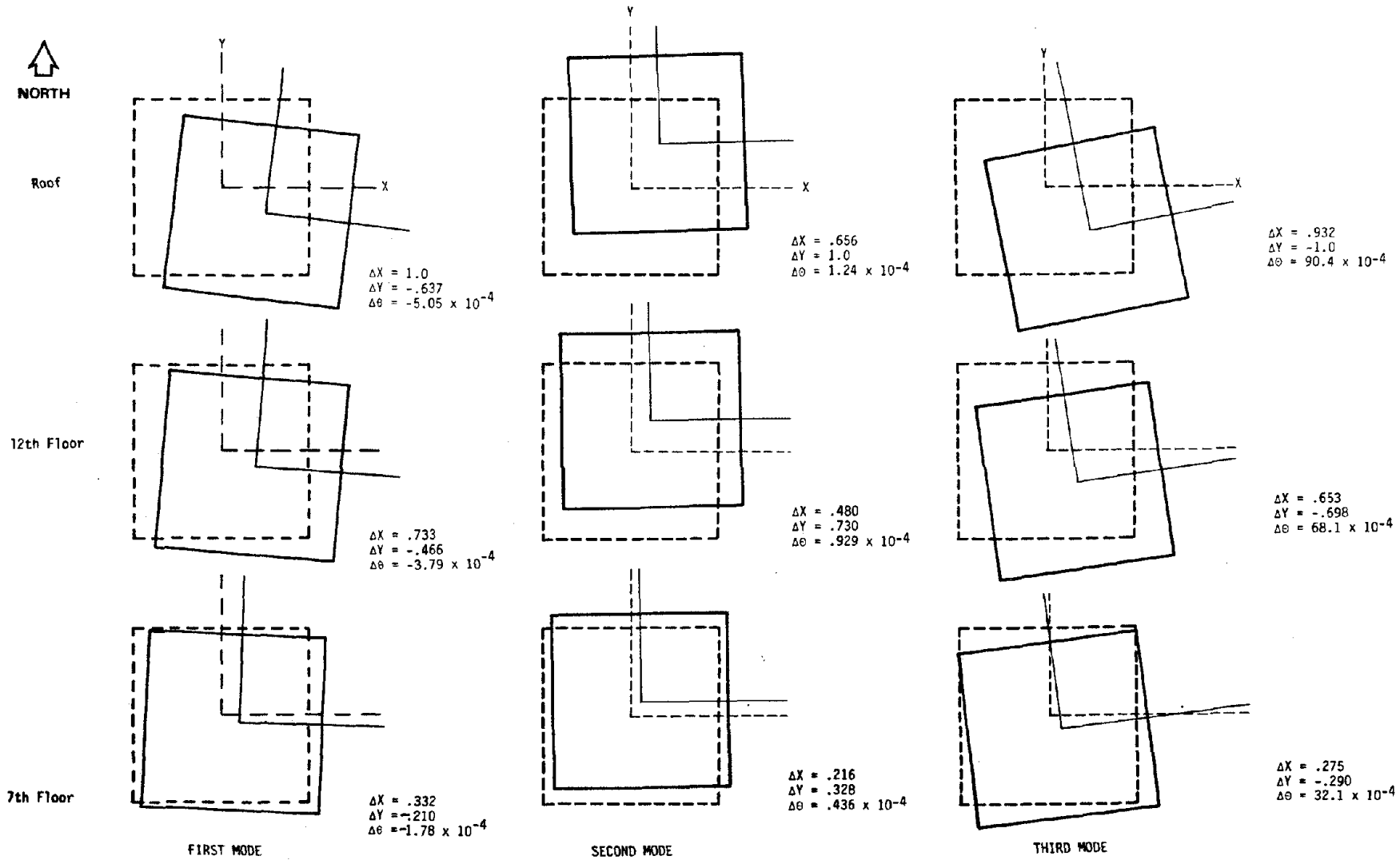


Figure 4.2.5: Irregular Building Mode Shapes

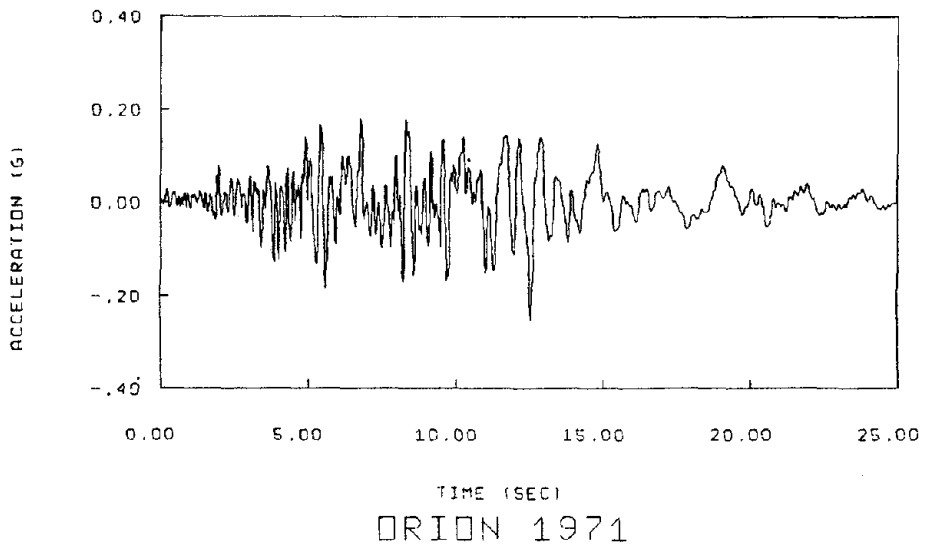
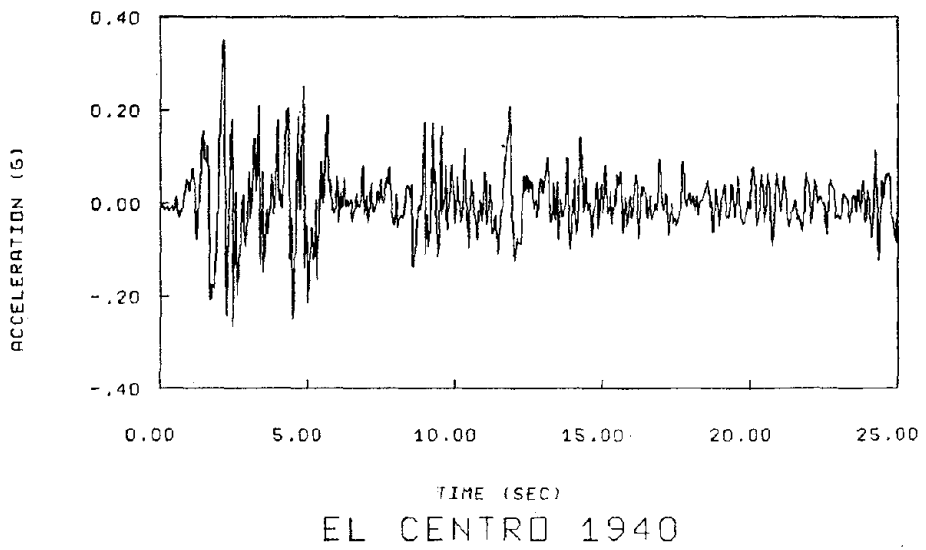
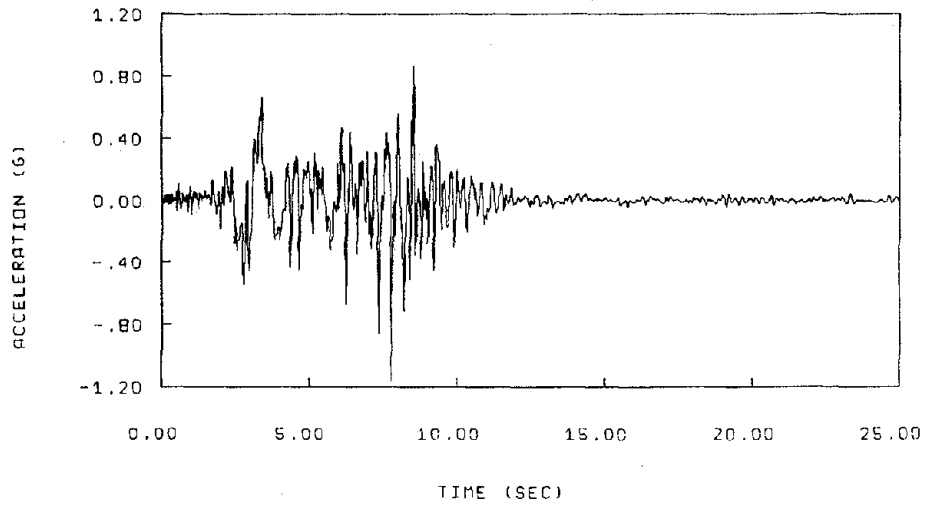


Figure 4.2.6: Example Earthquake Excitations

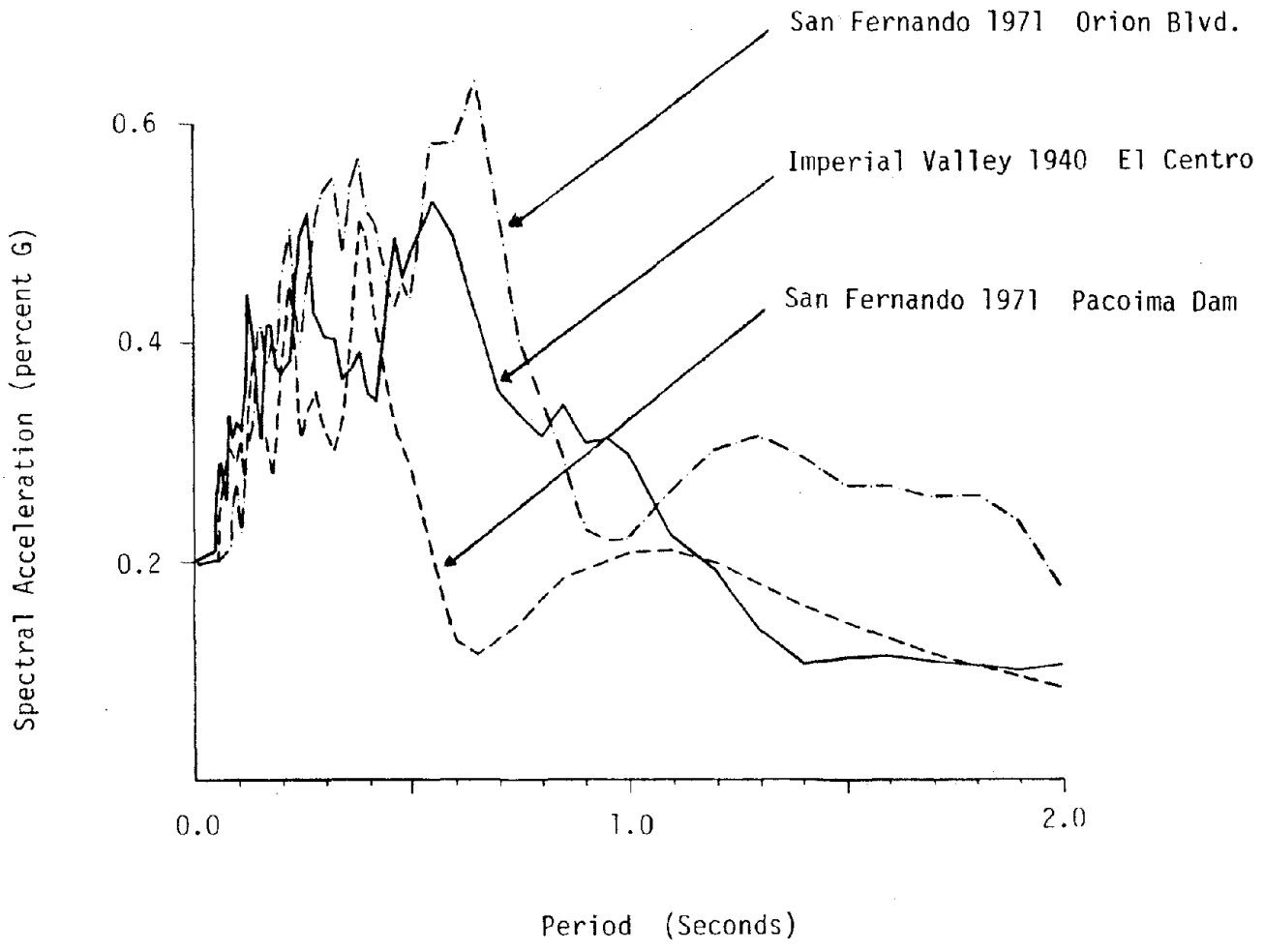


Figure 4.2.7: Example Earthquake Response Spectra

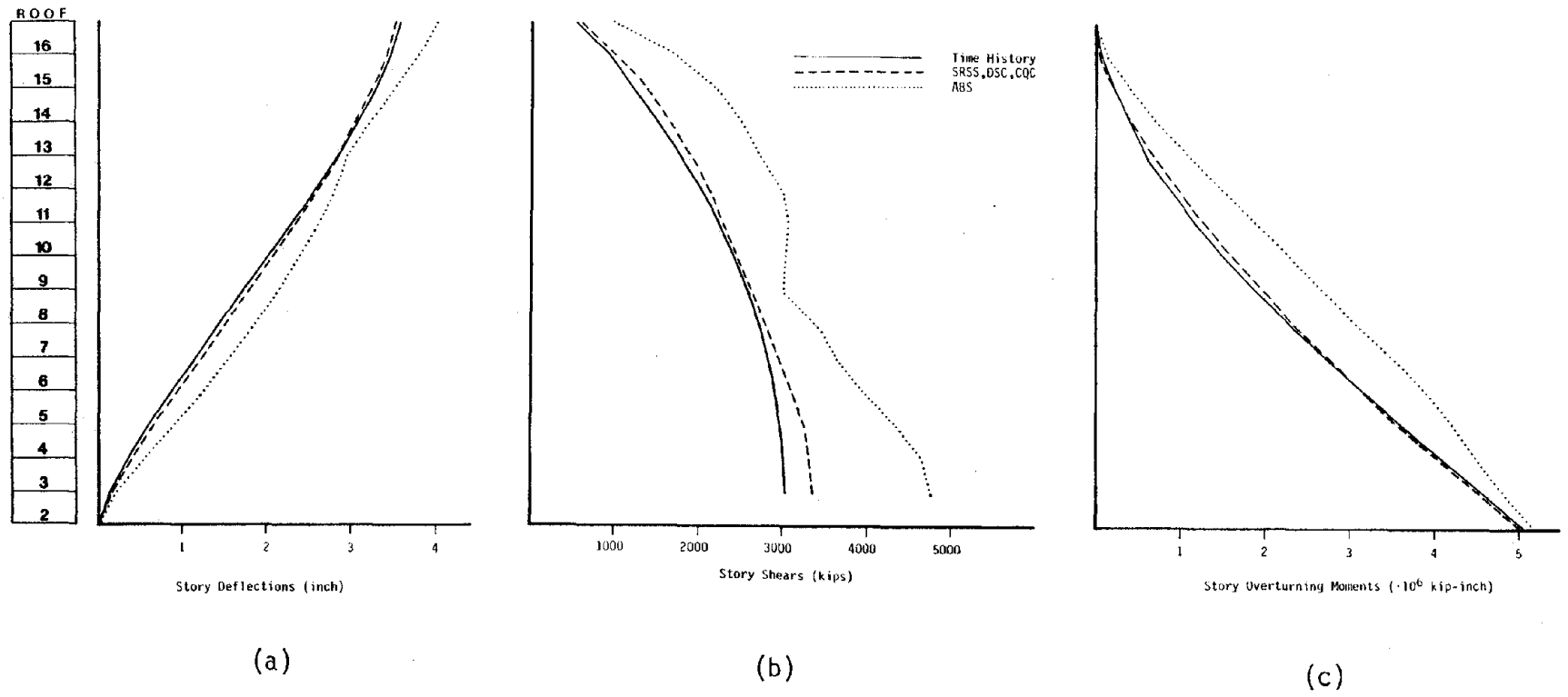


Figure 4.2.8: Regular Building Peak Response Envelopes from the Pacoima Dam Excitation  
 (a) Story Deflections  
 (b) Story Shears  
 (c) Story Overturning Moments

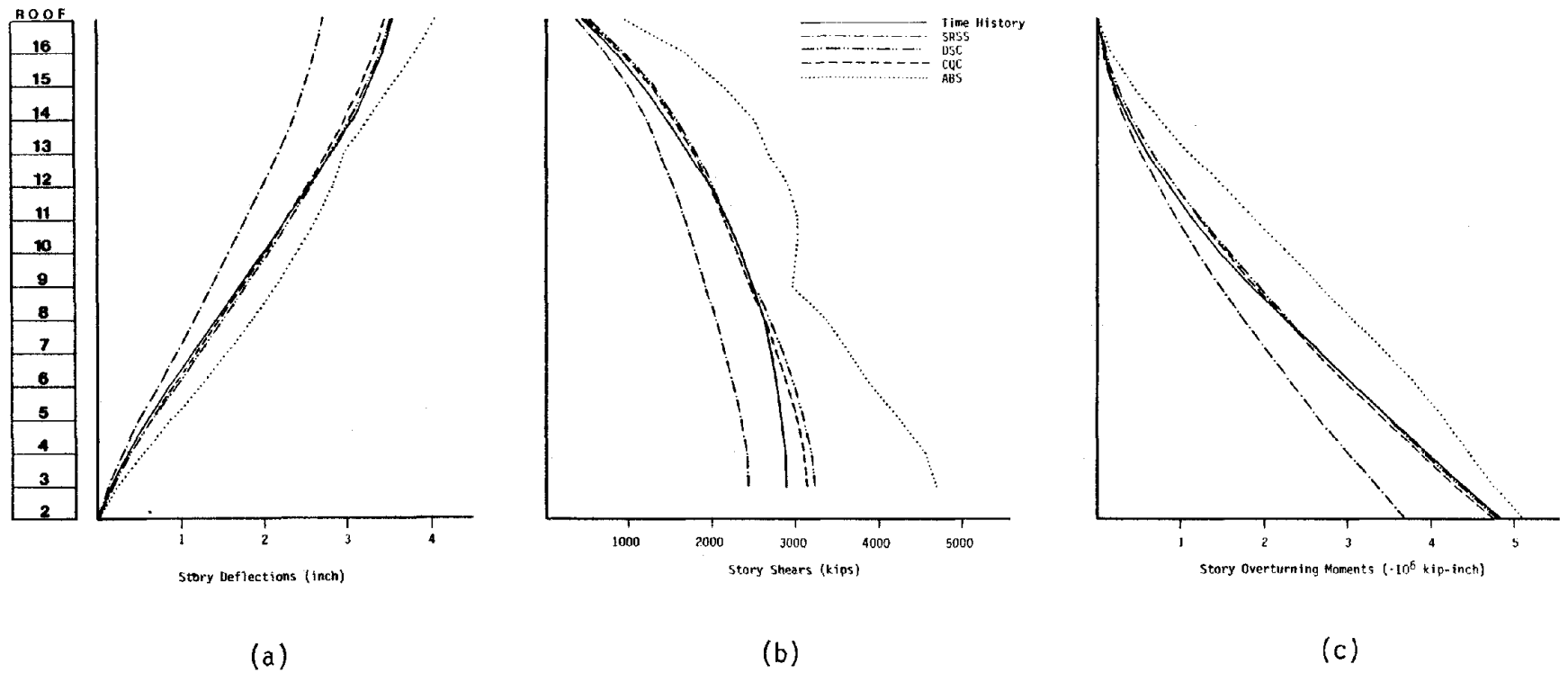


Figure 4.2.9: Irregular Building Peak Response Envelopes from the Pacoima Dam Excitation (East-West Response)

- (a) Story Deflections
- (b) Story Shears
- (c) Overturning Moments

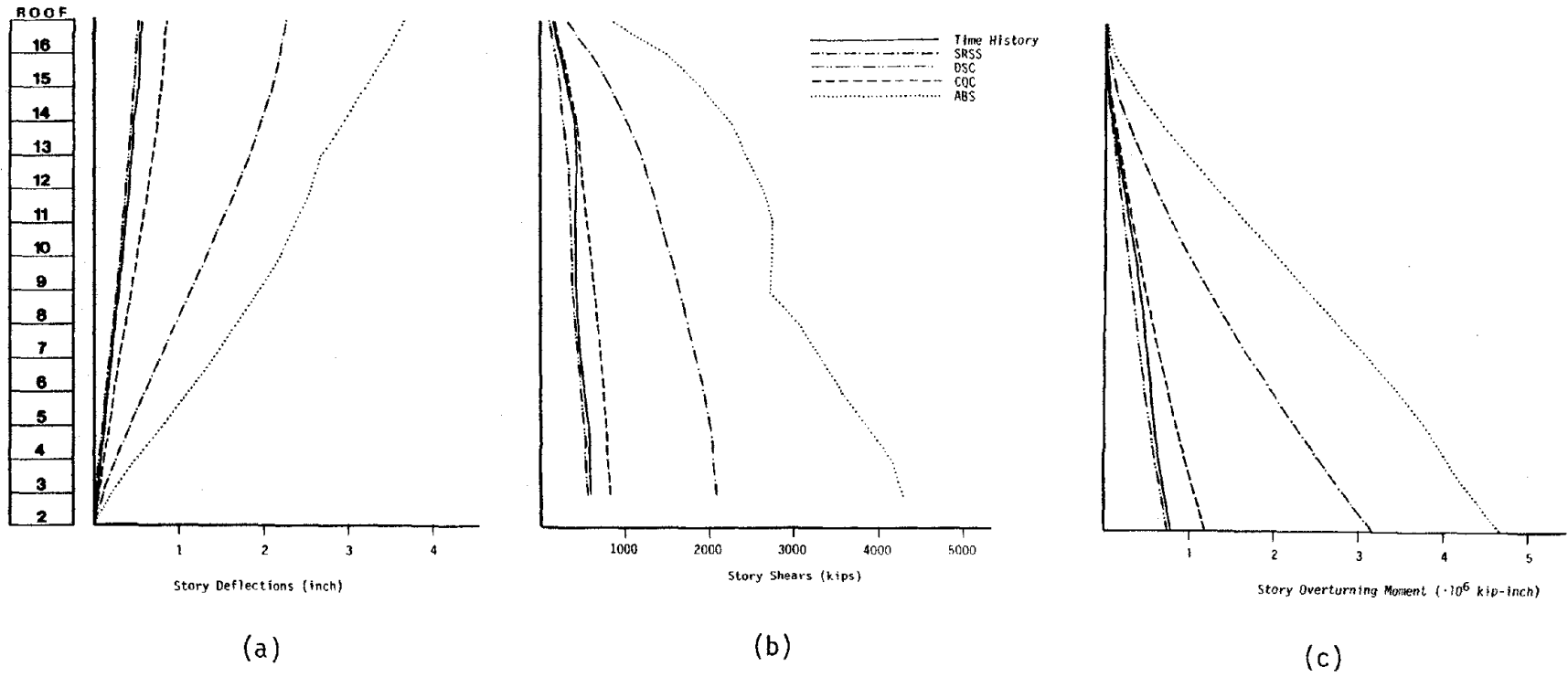


Figure 4.2.10: Irregular Building Peak Response Envelopes from the Pacoima Dam Excitation (North-South Response)  
 (a) Story Deflections  
 (b) Story Shears  
 (c) Story Overturning Moments

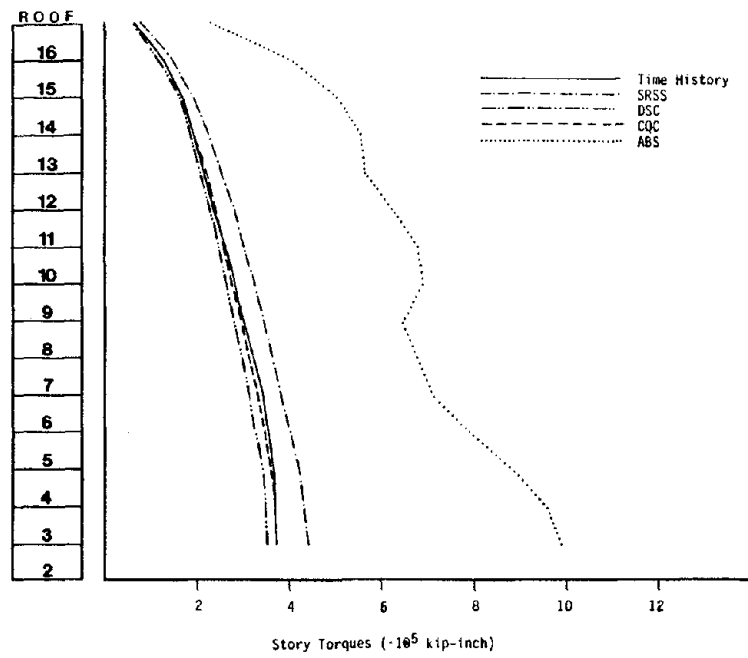


Figure 4.2.11: Irregular Building Peak Story Torque Envelope

Page Intentionally Left Blank

### 4.3 A METHOD FOR PERFORMING APPROXIMATE SEISMIC ANALYSIS OF MULTISTORY BUILDINGS

#### 4.3.1 Introduction

In the present state-of-the-art, the structural design of multistory buildings which are to be constructed in seismically active regions of the United States often requires a two stage seismic analysis approach. Typically, the first stage involves equivalent static seismic loading and analysis procedures as prescribed by current building codes. Determination of codebook seismic design loads at this stage of analysis allows initial sizing of the structural members leading to a preliminary design. The Uniform Building Code (UBC) (20) equivalent static procedure utilizes estimates of the building's fundamental period and mode shape to approximate seismic force magnitude and distribution, respectively. The resulting seismic load levels do not reflect the local seismicity or specific soil conditions of the site and are generally less than those that may be expected during a major earthquake event since working stress design criteria and stress formulae are generally used in this design phase.

After a preliminary design of the building has been completed, a more rigorous seismic analysis is often carried out as part of the final design process. At this second analytical stage, a detailed computer model of the structural system is developed and, usually, a response spectrum dynamic elastic analysis is performed. Here, a more accurate determination of periods and mode shapes is made based on the detailed structural characteristics of the building. Several modes, rather than the fundamental mode only, are used to determine the magnitude and distribution of seismic forces. Local seismicity and soil data may be incorporated in the development of a site-specific response spectrum curve to be used for final design which reflects refined estimates of critical ground motion characteristics and intensities that may occur. Since some inelastic response is

allowable in the event of a major earthquake, deformation levels resulting from this analysis are often beyond the elastic range. Accordingly, inelastic design criteria and stress formulae are applied using ductility factors to reduce elastic member forces for conformance to a maximum allowable degree of ductile response (2). Overstressed members (i.e., members having ductility demands in excess of the allowed ductility factor) are resized to meet the inelastic design criteria.

From the above description, it can be seen that the primary differences between the preliminary equivalent static and the final dynamic analysis approaches are:

- . A single (fundamental) mode idealization is used as the basis for the equivalent static approach to determine the magnitude and distribution of loading; whereas, in final dynamic analysis, multiple modes are used in response prediction.
- . In equivalent static analysis according to UBC, earthquake load intensity is based on categorization of the site into one of four general seismicity zones which may not necessarily reflect specific site conditions; whereas, in final dynamic analysis, more refined seismicity and soil characteristics of the particular site may be reflected in the shape and amplitude of the design spectrum.
- . In the equivalent static approach, seismic loads can be developed before structural characteristics are known making this method useful for preliminary design; whereas, in final dynamic analysis, the detailed structural characteristics are used as input in the development of a computer model whose dynamic properties determine seismic loading.

Because of these differences in analytical approach and the differences in design criteria, some member resizing is usually necessary to upgrade the preliminary design in order to meet final design requirements. If a substantial amount of redesign is required, an additional cycle of analysis and design may be necessary. In order to minimize the time and expense required for redesign and possible reanalysis at the final design stage, it would be advantageous to apply the multiple mode analytical procedures, site specific response spectrum data and inelastic design criteria typically used in the final dynamic analysis at the preliminary design stage.

In the discussion that follows, a technique is presented which demonstrates how initial estimates of natural periods and mode shapes can be used to predict gross force and displacement response quantities resulting from both response spectrum dynamic and equivalent static loading procedures at the preliminary design stage, before any detailed member design is undertaken. The estimation of dynamic properties is based on results of experimental and analytical studies which have been performed on several modern multistory buildings located in seismically active regions of the United States. Gross response quantities are calculated based on matrix methods commonly used in dynamic analysis of buildings. The technique has been implemented in a computer program and results of comparative analyses performed on an example building are presented to demonstrate the degree of accuracy that can be achieved in predicting final analytical response at the initial stages of the design process.

#### 4.3.2 Matrix Relationships for Gross Response Calculation Based on Dynamic Properties

In elastic analysis of buildings, gross response quantities such as story shears, story overturning moments, total deflections and interstory drifts can be calculated directly from the natural periods and mode shapes of the structure. This can be seen from the matrix equations that represent the individual modal force and displacement responses. In response spectrum dynamic analysis, the peak lateral inertia forces for a single mode are given by

$$\underline{F} = \underline{M} \underline{\phi} \frac{\underline{\phi}^T \underline{M} \underline{r}}{\underline{\phi}^T \underline{M} \underline{\phi}} S_a \quad (4.3.1)$$

and peak lateral displacements are given by

$$\underline{D} = \underline{\phi} \frac{\underline{\phi}^T \underline{M} \underline{r}}{\underline{\phi}^T \underline{M} \underline{\phi}} \frac{2\pi}{T^2} S_a \quad (4.3.2)$$

where, for planar analysis of a building with N stories,

$F$  = modal inertial force vector (N x 1)

$D$  = modal displacement vector (N x 1)

$\phi$  = a mode shape vector of lateral displacements (N x 1)

$M$  = diagonal (lumped) mass matrix (N x N)

$r$  = column vector of ones (N x 1)

$T$  = the modal natural period

and  $S_a$  = spectral acceleration for modal period,  $T$ .

(See Clough, et al. (11) for the derivation of equations (4.3.1) and (4.3.2). From the modal inertial force vector, modal shear and overturning moments acting at a given story,  $n$ , can be calculated by

$$V(n) = \sum_{k=n}^N F(k) \quad (4.3.3)$$

and

$$OTM(n) = \sum_{k=n}^N [F(k) \cdot (h(k) - h(n-1))] \quad (4.3.4)$$

where

$V(n)$  = modal cumulative shear at story  $n$

$OTM(n)$  = modal cumulative overturning moment at the base of story  $n$

and  $h(k)$  = the height of level  $k$  above the base of the building.

From the modal displacement vector, modal drifts can be calculated by

$$\Delta(n) = D(n) - D(n-1) \quad (4.3.5)$$

where  $\Delta(n)$  = modal interstory drift at story n.

The maximum total responses resulting from the combined effects of the individual peak responses of all modes can be approximated with the use of an appropriate modal combination rule such as the SRSS or CQC techniques (see section 4.2). For example, using the SRSS method, the maximum total story shear at story n is given by

$$V_{\text{Total}}(n) = \left( \sum_{i=1}^N [V_i(n)]^2 \right)^{1/2}$$

where

$V_i(n)$  = peak shear at story n contributed by mode i.

In this way, the maximum total dynamic response of the design quantities  $V$ ,  $OTM$ ,  $D$  and  $\Delta$  can be calculated at each story of the building.

In addition to their use in the calculation of dynamic response, the natural periods and mode shapes can also be used to calculate displacement and drift responses resulting from the application of equivalent static lateral loads. The matrix formulation for the static analysis problem is

$$\mathbf{K} \mathbf{D} = \mathbf{F} \quad (4.3.6)$$

where  $\mathbf{F}$  = the applied static lateral load vector ( $N \times 1$ )  
 $\mathbf{K}$  = the lateral stiffness matrix ( $N \times N$ )

and  $\underline{D}$  = the resulting lateral displacement vector ( $N \times 1$ ).

Since the mode shapes (eigenvectors) are linearly independent, the static displacement vector can be represented by

$$\underline{D} = \underline{\Phi} \underline{a} \quad (4.3.7)$$

where  $\underline{\Phi}$  = matrix of all mode shapes ( $N \times N$ )

and  $\underline{a}$  = an unknown vector of modal multipliers ( $N \times 1$ ).

Substituting equation (4.3.7) into equation (4.3.6) we have

$$\underline{K} \underline{\Phi} \underline{a} = \underline{F} \quad (4.3.8)$$

Note that the natural periods and mode shapes, by definition, must satisfy the eigenproblem

$$\underline{K} \underline{\Phi} = \underline{M} \underline{\Phi} \underline{\Lambda} \quad (4.3.9)$$

where  $\underline{\Lambda}$  = a diagonal matrix of eigenvalues ( $N \times N$ )

with  $\Lambda_i = (2\pi/T_i)^2$ ,  $i=1, \dots, N$ .

Thus, equation (4.3.9) can be substituted into equation (4.3.8) giving

$$\underline{M} \underline{\Phi} \underline{\Lambda} \underline{a} = \underline{F} \quad (4.3.10)$$

Premultiplying equation (4.3.10) by  $\underline{\Phi}^T$  we have

$$\underline{\Phi}^T \underline{M} \underline{\Phi} \underline{\Lambda} \underline{a} = \underline{\Phi}^T \underline{F} \quad (4.3.11)$$

and assuming a mass normalized eigensolution, where

$$\underline{\Phi}^T \underline{M} \underline{\Phi} = \underline{I} = \text{the identity matrix;}$$

equation (4.3.11) becomes

$$\underline{I} \underline{\Lambda} \underline{a} = \underline{\Lambda} \underline{a} = \underline{\Phi}^T \underline{F}$$

or

$$\underline{a} = \underline{\Lambda}^{-1} \underline{\Phi}^T \underline{F}. \quad (4.3.12)$$

Equation (4.3.12) may now be substituted into equation (4.3.7) giving

$$\underline{D} = \underline{\Phi} \underline{a} = \underline{\Phi} \underline{\Lambda}^{-1} \underline{\Phi}^T \underline{F}. \quad (4.3.13)$$

Using equations (4.3.13) and (4.3.5), the deflection and drift responses resulting from any set of applied static lateral loads can be calculated. Although, for theoretically exact displacement values, the periods and mode shapes corresponding to all N modes should be used in the formulation of  $\underline{\Phi}$  and  $\underline{\Lambda}$  in equation (4.3.13), use of only the first several modes generally will yield results of sufficient accuracy. However, note that if, for example, only the first 5 modes are used, the dimension of  $\underline{\Phi}$  becomes (N x 5) and the dimension of  $\underline{\Lambda}$  becomes (5 x 5).

As can be seen from the preceding formulations, the maximum dynamic force and deflection response quantities resulting at every story level can be determined directly from the natural periods and mode shapes. In addition, deflection response to a given set of static loads may also be determined. It should be noted that neither element stiffness properties nor formulation of the structural

stiffness matrix is required to produce these gross response quantity results. Other than the dynamic properties (natural periods and mode shapes), the only data required for this analysis is story mass values, story heights and the response spectrum design curve. The story masses and story heights are known or can be approximated from architectural plans at the initial stages of design and, in fact, are required as input for the UBC equivalent static procedure. The response spectra design curve(s) to be used may also be available prior to preliminary design. The only additional data needed to perform the analyses outlined above are approximations of the natural periods and mode shapes for the building. If good initial estimates of these dynamic properties can be made, accurate static and dynamic gross response analyses may be performed prior to detailed member design.

#### **4.3.3 Observed Dynamic Properties of Actual Buildings**

In Chapter 3, the results of experimental and analytical studies on the dynamic characteristics of several different multistory buildings are presented. The period and mode shape properties discussed in this section are based on refined analytical models which show close correlation with the experimentally observed dynamic properties. From these results, it can be seen that regular multistory building frames (i.e., those not having severe stiffness discontinuities over their heights) generally have several important similarities in their dynamic properties. These similarities were previously discussed in section 3.7.2 and are reviewed in this section.

In Table 4.3.1, ratios of fundamental translational period to higher translational periods are shown for several different buildings studied (i.e., Alcoa E-W, Alcoa N-S, Rainier Tower, U.C. Medical Center and Century City). As can be seen from this table, these

buildings which have essentially regular framing systems over their heights all have very similar period ratios. The average period ratios are 2.89 for  $T_1/T_2$ , 5.06 for  $T_1/T_3$  and 7.18 for  $T_1/T_4$ . Also shown in Table 4.3.1 are the percent variations of the individual periods ratios for each building with respect to the average values. Period ratios for the first four modes of all the buildings are within 8.8% of the average values indicating that these average ratios can be used to accurately represent the individual ratios for any of the sample buildings.

In Figure 4.3.1, the first four translational mode shapes of these same building frames are shown for comparison. As can be seen from this figure, some variations in mode shape exist among the different buildings. However, the following similar characteristics are apparent:

- (1) The number of node points (points of zero deflection) for a given mode is equal to the mode number. For example, the first mode has one node point (at the base); the second mode has two node points; etc. This result generally occurs in multistory buildings unless flexibility of the floor slab allows substantial in-plane diaphragm deformation. For tall multistory buildings, diaphragm deformation is usually not significant.
- (2) Except for the antinodes occurring at the top of the buildings, all antinodes (points of maximum relative deflection) of the 2nd, 3rd, and 4th modes have nearly equal relative deflection amplitudes for each building. The antinodes at the tops of the buildings tend to have a less predictable relative amplitude but are of the same general magnitude as those below.
- (3) The location of node points relative to total height are roughly coincident for the different buildings. For example, for each of the buildings shown in Figure 4.3.1, a node for the second mode occurs at a point located between approximately 0.75 and 0.81 times the total height. The third and fourth modes of the different buildings also have corresponding nodes that are within close proximity.
- (4) The distances between node points of higher modes tend to decrease with increasing height above the base. For example, for the fourth mode in Figure 4.3.1, the average distances between the first (base) to second, second to third, and third to fourth nodes are approximately 0.37, 0.29, and 0.24 times the total height, respectively.

It should be noted that the above similarities in dynamic properties result despite the significant differences that exist among

these buildings with regard to total height, plan layout and structural type. Considering these differences, it is reasonable to project that the dynamic properties of other multistory building frames which are basically regular over their heights will show similar characteristics.

#### 4.3.4 Comparison with Uniform Shear Beam Idealization

A cantilever shear beam with uniform mass and stiffness properties is often used to idealize the behavior of multistory buildings. For this reason it is of interest to compare the theoretical dynamic properties of this idealization with the actual properties observed for the buildings studied. The natural period ratios and mode shapes for a uniform shear beam (see Newmark, et al. (28) are

$$T_1/T_m = 2m-1 \quad (4.3.14)$$

and

$$\phi_m(x) = \sin \left[ \frac{(2m-1)\pi}{2} \frac{x}{H} \right] \quad (4.3.15)$$

where

- m = mode number
- x = height above base
- H = total height

Thus, according to equation (4.3.14),  $T_1/T_2 = 3.0$ ,  $T_1/T_3 = 5.0$ ,  $T_1/T_4 = 7.0$ , etc. Comparing these values with those in Table 4.3.1, it is seen that the uniform shear beam period ratios correlate quite closely with those of the actual buildings. However, based on average values, the actual buildings tend to have a slightly lower ratio of  $T_1/T_2$  (2.89 vs. 3.0) and a slightly higher ratio of  $T_1/T_4$  (7.18 vs. 7.0).

In Figure 4.3.1, the first four mode shapes for a uniform shear beam are plotted according to equation (4.3.15). As can be seen from this figure, these mode shapes vary significantly from the actual mode shapes. Comparing the characteristics of these shapes with those of the actual buildings it can be seen that they share two of the four characteristics listed previously; namely, the number of node points (described under (1) above) and relative amplitudes of antinodes ((2) above) are in agreement with the observed characteristics. However, regarding the location of node points in higher modes ((3) above), the uniform shear beam has its respective nodes at lower locations over the height. This can be seen in Table 4.3.1 where the relative locations of node points in the first four modes for both the actual buildings and the uniform shear beams are shown for comparison. For example, in the second mode, the actual buildings have node points between 0.747 and 0.805 times total height, whereas the node for the uniform shear beam occurs at 0.667 times total height. Regarding the distance between node points ((4) above), the actual buildings have decreasing inter-nodal distances with height for the higher modes, whereas the corresponding uniform shear beam inter-nodal distances are constant over height. In addition to these differences in the higher modes, the fundamental mode shape for the shear beam is substantially more convex than the observed fundamental mode shapes of the actual buildings having significantly larger relative deflections in the lower portions of the structure.

The differences mentioned above exist because multistory buildings behave more as shear beams with decreasing stiffness rather than uniform stiffness and, to a lesser extent, because some cantilever type behavior caused by axial flexibility of columns occurs. Because of these differences, use of a uniform shear beam analogy to approximate dynamic properties of actual buildings may lead to response predictions of limited accuracy.

#### 4.3.5 Development of Empirical Mode Shapes

By using the observed dynamic characteristics of the actual buildings as a basis for developing approximate mode shapes, improved preliminary estimates of dynamic response can be made. An empirical procedure has been developed based on the response characteristics of the buildings studied from which several mode shapes for an arbitrary building can be approximated. This procedure is described in the following.

For a given mode number 'm', the total height of the building is divided into m different regions represented by the vertical heights  $h_1, h_2, \dots, h_m$  as shown in Figure 4.3.2. These regions define the location of the m node points of the mode. Region  $h_1$ , the uppermost region, is bounded by the highest ( $m^{\text{th}}$ ) node point at its lower end and by the top of the building at its upper end. All other regions ( $h_2, \dots, h_m$ ) are bounded by two adjacent node points. As observed in the actual buildings, inter-nodal distances increase with increasing height above the base, that is

$$h_1 < h_2 < \dots < h_m.$$

Thus, the height,  $h_i$ , of each region i can be represented by

$$h_i = a_i h_1 \quad (4.3.16)$$

where  $a_i$  = scale factor for region i

with  $a_1 = 1.0$

and  $a_m > \dots > a_{i+1} > a_i > a_{i-1} \dots > a_2 > 1.0$

Since the sum of the heights of all regions must equal the total building height, we have

$$\sum_{k=1}^m h_k = h_1 \cdot \sum_{k=1}^m a_k = H$$

or

$$h_1 = H / \left( \sum_{k=1}^m a_k \right) \quad (4.3.17)$$

where  $H$  = the total building height.

Substituting equation (4.3.17) into equation (4.3.16), the height of any region  $i$  can also be represented as

$$h_i = \left[ a_i / \left( \sum_{k=1}^m a_k \right) \right] \cdot H = (a_i / a_T) \cdot H \quad (4.3.18)$$

where

$$a_T = \sum_{k=1}^m a_k$$

Using the node point data from the mode shapes of the actual buildings, the following empirical relationships were developed for representing  $a_i$  in equation (4.3.18):

$$a_i = 1.0 + [(\pi-1) \cdot \left( \sum_{n=1}^{i-1} \frac{1}{n} \right)] \quad \text{for } i \geq 2 \quad (4.3.19)$$

and  $a_1 = 1.0$ .

From equations (4.3.18) and (4.3.19), the locations of node points of a given mode  $m$  can be empirically determined. As an example of the application of these equations, the locations of node points in the fourth translational mode ( $m=4$ ) can be empirically determined as follows:

From equation (4.3.19), we have

$$a_1 = 1.0$$

$$a_2 = 1.0 + [(\pi-1) \cdot (1.00)] = 3.142$$

$$a_3 = 1.0 + [(\pi-1) \cdot (1.500)] = 4.212$$

$$a_4 = 1.0 + [(\pi-1) \cdot (1.833)] = 4.926$$

Applying equation (4.3.18), for  $m=4$ , we have

$$h_1/H = a_1/a_T = 1.0/(1.0 + 3.142 + 4.212 + 4.926) = 1.0 / (13.280) = 0.075$$

$$h_2/H = a_2/a_T = 3.142/13.280 = 0.237$$

$$h_3/H = a_3/a_T = 4.212/13.280 = 0.317$$

$$h_4/H = a_4/a_T = 4.926/13.280 = 0.371$$

Thus, node points above the base in the fourth mode are predicted to occur at locations of .371, .688 (= .371 + .317) and .925 (= .371 + .317 + .237) times the total height. The relative locations of node points for the first four modes as calculated by this empirical approach are shown in Table 4.3.2. Also shown in the table are the minimum and maximum relative node point locations observed for the actual buildings and for a uniform shear beam. As can be seen, the empirical method leads to node point locations that compare well with those of the actual buildings lying between the observed minimum and maximum values in all cases. The uniform shear beam shows poorer correlation with the observed values having node points which occur at points significantly below those observed in the actual buildings.

Having identified the node point locations and corresponding regions over the height of the building as described above, separate functions can be used to represent the mode shape variation in each region. It can be seen from Figure 4.3.1 that the second, third and fourth mode shapes of the actual buildings show smooth variations of relative displacement in the lower regions ( $h_2, h_3, h_4, \dots$ ) with antinodes occurring at approximately midway between the bounding nodes. This characteristic can be approximated by a half-sine curve defined separately over each of the lower regions with the mode shape variation being represented by (see Figure 4.3.2)

$$\phi_i(x_i) = (-1)^{i-1} \cdot \sin \frac{\pi x_i}{h_i} \quad (4.3.20)$$

where

$\phi_i$  = the mode shape function defined over region  $i$

$x_i$  = the vertical distance above the lower bounding node of region  $i$

$i$  = region number  $\geq 2$ .

However, closer inspection of the mode shapes in Figure 4.3.1 shows that in the lower most regions,  $h_m$ , of the 2nd, 3rd and 4th modes, the antinode occurs above midway between the bounding nodes at a point lying nearer to three-fifths times the region height ( $0.6 \times h_m$ ). In order to reflect this observed behavior, the relationship in equation 4.3.20 can be modified for region  $m$  so that the peak amplitude occurs at this point as follows:

$$\phi_m(x_m) = (-1)^{m-1} \cdot \sin \pi \left( \frac{x_m}{h_m} \right)^{1.357} \quad (4.3.21)$$

It can also be seen from 4.3.1, that the mode shapes in the uppermost regions ( $h_1$ ) of the actual buildings vary more as straight lines than as sine curves (e.g., see first mode in Figure 4.3.1). This mode shape characteristic can be approximated by

$$\phi_1(x_1) = \frac{x_1}{h_1} \quad (4.3.22)$$

In Figure 4.3.1, the empirical mode shapes determined from equations (4.3.20), (4.3.21) and (4.3.22) are shown for the first four modes. As can be seen from this figure, the empirical method leads to significantly improved mode shape estimates over the uniform shear beam approximations. The differences in the amplitudes of the empirical and actual antinodes result from the fact that the curves have been arbitrarily normalized with respect to the deflection at the top of the buildings. In the approximate analysis procedure, the mode shapes are normalized with respect to mass thereby mitigating any amplitude differences that may exist. Based on these empirical mode shapes and the average period ratios along with estimates of fundamental period, mass values and story heights, an approximate dynamic analysis according to the matrix formulation presented earlier can be performed. Satisfactory approximate preliminary analysis of multistory buildings can generally be performed using as few as 4 to 6 modes for a planar analysis. The empirical mode shape algorithm, however, can be used to generate higher modes as well.

#### 4.3.6 Example Analyses

The approximate static and dynamic analysis procedures outlined in section 4.3.2 have been implemented in a modified version of the ETABS computer program (23). In performing approximate analysis, the program user may input his/her own best estimates of all natural periods and mode shapes; or, alternatively, he/she may specify only the fundamental period and the program will automatically generate

higher periods and all mode shapes based on the uniform shear beam idealization or the empirical representation.

The Century City Theme Tower building (see section 3.6) has been reanalyzed for static and dynamic seismic loading using the approximate analysis procedures outlined in the previous sections. The Century City building is a 44 story moment resisting frame structure rising 590 feet above ground level. A novel design feature of the building is its triangular plan configuration. Elevation and plan views of the building are shown in Figure 4.3.3. The primary lateral force resisting moment frames are located at the outer walls along the triangular periphery. All columns except those at the three corners are terminated at the second floor where they frame into a deep girder which carries the intermediate column vertical loads to the corner columns. At this level, lateral forces are transferred from the peripheral frames through the second floor diaphragm to a shear wall system located in the building's core. At the 43rd level, the moment framing is discontinued and a 28-foot deep plate girder extending up to the roof caps the peripheral frames. Other than these structural irregularities existing above the 43rd floor and below the second floor, the building's framing system is basically regular over its height.

In performing approximate analysis, stiffness discontinuities caused by structural irregularities such as those noted above should be considered in the development of representative mode shapes of the building. However, in order to demonstrate the direct application of the uniform shear beam and empirical mode shape representations, no special mode shape refinements were made to account for these stiffness discontinuities in the approximate analyses performed on the Century City building. Analytical results of the approximate analyses are compared with results of "exact" analyses determined using a detailed numerical model whose dynamic properties correlate closely

with experimentally determined dynamic properties. A more complete description of the analytical model used for the exact analysis can be found in section 3.6.3 (Model 4). In order to separately assess the influence of inaccuracies in the mode shape approximations and in natural period estimates, the fundamental period of 3.94 sec. as determined from the exact analysis is used for the initial static and dynamic approximate analyses. In subsequent dynamic analyses, response variations that may result from the use of less accurate fundamental periods are illustrated. For all analyses (exact and approximate), the first four translational modes are included in prediction of response. The second, third and fourth periods are based on period ratios (fundamental mode period/higher mode period) of 3.0, 5.0, and 7.0, respectively, for the uniform shear beam idealization and on ratios of 2.89, 5.06, and 7.18, respectively, for the empirical representation (refer to Table 4.3.1).

#### Static Analysis

Lateral loads used for the static analyses were developed in accordance with UBC seismic load requirements (i.e.,  $V=ZICKS$  where  $Z=1.0$ ,  $I=1.0$ ,  $K=0.67$ ,  $C=0.0336$ ,  $S=1.2$ ). The resulting story shear and overturning moment envelopes are shown in Figures 4.3.4 (a) and (b), respectively. In Figures 4.3.5 (a) and (b), the deflection and drift responses resulting from the UBC loadings are shown for the exact model, the empirical model and the uniform shear beam model. In Table 4.3.3, response values at the 40th, 20th and 2nd floors are tabulated. As can be seen from Figure 4.3.5, the empirical model shows better correlation with the exact model over most of the building than does the shear beam model. At the 40th floor, the empirical model yields a lateral deflection of 8.05 in., only 0.4% larger than the exact value of 8.02 in. and, the shear beam model yields a 7.16 in. deflection or 10.7% less than the exact result (Table 4.3.1). At the 20th floor, the empirical model gives a deflection of 3.97 in. or 8.5% greater

than the exact result of 3.66 in. and the shear beam model gives a value of 4.32 in. which exceeds the exact value by 18%. The approximate results show poorest correlation with the exact values near the base of the building and in the uppermost stories due to the larger relative stiffnesses that exist in these portions of the structure. Note the larger errors in the drift values of the empirical model in these regions (Figure 4.3.5 (b)). The relatively stiff shear walls below the 2nd floor level cause the large relative errors in deflection predicted by approximate analysis at the 2nd floor where the empirical model indicates a deflection of 0.57 in. which is 159% greater than 0.22 in. exact value (Table 4.3.1). Also, the plate girder at the top of the building restrains drift response in the upper stories as is seen in Figure 4.3.5 (b). The empirical model drift response at the 40th story is 0.236 in. or 41.3% greater than the exact value of 0.167 in. At the 20th story, the empirical drift value of 0.187 in. shows better correlation with the 0.217 in. exact value being an underestimation of 13.8%. In general, drifts are the most difficult response values to predict with good accuracy in approximate analyses since they are more sensitive to the specific stiffness properties at a given story than are cumulative shear, overturning and deflection responses.

Overall, the empirical model demonstrates good correlation with the deflection response resulting from exact analysis. The uniform shear beam model yields deflection and drift responses having somewhat lesser overall accuracy than the empirical model. The greatest relative errors in the approximate analyses result near the base of the building and in the upper several stories where the empirical mode shapes do not accurately reflect the large relative stiffnesses which exist in these portions of the structure.

## Dynamic Analyses

A smoothed earthquake response spectrum recommended by Blume (9) scaled to a 0.4g peak acceleration value was used for performing the dynamic analyses. A plot of this spectrum is shown in Figure 4.3.6. A variation to the structural idealization used in the static analyses is made for performing the dynamic analyses. As seen from the results of the static analyses, the stiff concrete shear walls below the plaza level cause this lower portion of the structure to have relatively small deflection response. Therefore, for the approximate dynamic analyses, the two stories below the plaza level are eliminated from the model in order to yield approximate mode shapes which will better reflect actual response.

In Figures 4.3.7(a) and (b), the story shear and overturning moment responses are shown for the exact model, the empirical model and the shear beam model and, in Table 4.3.4, their respective response values at the 40th, 20th, and 2nd floors are tabulated. For these analyses, the "exact" fundamental period of 3.94 seconds has been used for all models. As can be seen from this figure, both the empirical and shear beam models predict shear and overturning response with fairly good accuracy. At the 40th story, the empirical model predicts a story shear of 3174k, only 1.2% greater than the exact value of 3136k and the shear beam model yields a value of 2922 or 6.8% less than the exact result (Table 4.3.4). At the 20th story, the empirical and shear beam models are 2.2% greater than and 0.3% less than the exact shear value of 7156k, respectively. Near the base of the buildings, the empirical model compares somewhat less favorably with the exact result than does the shear beam model; at the 2nd story, the empirical shear value is 10238k, which is 10% greater than the 9309k exact value and the shear beam value is 9494k or 2.0% greater than the exact value. Both the empirical and shear beam models predict overturning response with excellent accuracy over the

full height of the building. At the base of the 2nd story, the empirical and shear beam overturning values are only 1.4% and 3.2% greater than the exact value of  $39334 \times 10^3$  k-in., respectively. In Figure 4.3.8, the deflection and drift responses for the various models are shown. As can be seen from Figure 4.3.8 (a), the empirical model gives good estimates of deflection over most of the building's height and the shear beam model yields somewhat less accurate results. At the 40th floor, the empirical and shear beam deflection values are 0.3% greater than and 3.6% less than the exact value of 36.1 in., respectively (Table 4.3.4). For drift response, the empirical model yields better estimates than the shear beam model in the lower two-thirds of the building, as seen from Figure 4.3.8 (b). At the 2nd story, the empirical model yields a drift value of 0.94 in., only 3.3% greater than the exact value of 0.91 in. and the shear beam model gives a drift value of 1.31. or 44% greater than the exact value. The restraining effect of the stiff plate girder located at the top of the building causes the exact drift values in the upper third of the building to be significantly smaller than the values predicted by the empirical model.

Overall, the empirical model predicts the dynamic response of the building with good accuracy. The shear beam model predicts shear and overturning responses with good accuracy but predicts deflection and drift responses with lesser accuracy. As was also noted in the static analyses, the greatest relative errors of the approximate analyses result in the upper stories where the larger relative stiffness caused by the top story plate girder has not been accounted for in the empirical model mode shapes. Response predictions for this portion of the structure could have been improved if modifications to the approximate empirical mode shapes had been made to account for the stiffening effect of the top story plate girder.

For the static and dynamic analyses presented thus far, the approximate models (empirical and shear beam) have used the fundamental period value of 3.94 seconds which was determined from the exact analysis of a detailed numerical model of the building. Of course, when performing an approximate analysis prior to actual design, the exact fundamental period is not known. However, the engineer/analyst can usually make a good preliminary estimate of fundamental period based on knowledge of the gross dimensions of the building, the structural system that is to be used and past experience in performing dynamic analysis of buildings. To demonstrate how response predicted using approximate methods may be influenced by the use of inexact fundamental period estimates, approximate analyses using the empirical model with fundamental period values of 3.55 sec ( $0.9 \times 3.94$  sec) and 4.33 sec ( $1.1 \times 3.94$  sec) have been performed. Thus, the analyses performed using these two fundamental periods bound a range of responses resulting from period estimates that are within 10% of the exact period value.

In Figure 4.3.9(a) and (b), the shear and overturning responses for the exact model ( $T_1=3.94$  sec) and the approximate empirical models ( $T_1=3.55, 3.94$  and  $4.33$  sec) are shown; and, in Figure 4.3.10(a) and (b), corresponding deflection and drift responses are shown. In Table 4.3.5, comparative response values at the 40th, 20th, and 2nd stories are tabulated. At the 20th story, the empirical models predict story shears ranging from +10.9% to -5.6%, overturning moments ranging from -0.3% to -15.1%, deflections ranging from -11.5% to +12.0%, and drifts ranging from -20.0% to +1.0% of the exact values (Table 4.3.5). These error ranges are representative of those occurring at other levels of the building as well. Approximate analyses leading to dynamic response estimates having accuracies within these ranges can be useful in performing preliminary design. Of course, the degree of error that may result from inexact estimates of fundamental period will depend

upon the particular response spectrum being used. However, when using smoothed design spectra typically applied for dynamic seismic analyses of buildings, the engineer/analyst should be able to keep these response prediction inaccuracies within reasonable limits.

#### **4.3.7 Summary and Conclusions**

A method for performing approximate static and dynamic seismic analysis of multistory buildings based on assumed dynamic properties has been presented. The input data needed to perform the approximate analysis are same as that required for equivalent static seismic load determination according to current building codes. An empirical approach for estimating natural periods and mode shapes has been developed based on the observed dynamic characteristics of five actual multistory buildings. Empirically developed dynamic characteristics are contrasted with those based on a uniform shear beam idealization. The approximate analyses method has been implemented in a computer program and sample seismic analyses have been performed on a 44-story building. Analytical results based on the approximate empirical method are compared with results of an "exact" analysis and with results of approximate analyses based on the uniform shear beam idealization.

From the results of the example analyses performed, it is seen that accurate approximations for story shears, overturning moments, deflections and drifts can be determined prior to actual member design if a reasonably good estimate of fundamental period can be made. By making upperbound and lowerbound estimates of fundamental period, the engineer/analyst can generate approximate results which bound a range of probable response for a given seismic loading criterion. Application of the approximate method should lead to a more realistic representation of seismic response than do equivalent static methods recommended by current building codes. Thus, results of approximate analyses can be used effectively at initial design stages in order to

produce an improved preliminary design thereby helping to minimize the effort required for redesign and reanalysis at the final design stage.

Another aspect worth noting is the cost effectiveness of the approximate analysis technique as implemented in the modified version of the ETABS program (23). In the analyses for gross design quantity response performed on the Century City Theme Tower building presented herein, the ratio of computer processing time required for the exact analysis based on a member-by-member model to that required for an approximate analysis based on overall dynamic properties was greater than 400 to 1. In addition, the amount of data required for performing approximate analyses is much less than that required for an exact analysis. For example, for the Century City building, the exact analysis required about 1080 data cards to define the detailed structural properties whereas the approximate analyses, using internally generated mode shapes, required only 93 data cards. Thus, the approximate analysis procedure is very economical with respect to both computational and manpower costs.

Table 4.3.1: Translational Period Ratios Based on Correlative Analytical Studies

Building	No. of Stories	Height (ft)	First Period $T_1$	Period Ratios					
				$T_1/T_2$ (%)		$T_1/T_3$ (%)		$T_1/T_4$ (%)	
Alcoa E-W	28	358	2.12	3.03	(4.8)	5.37	(6.1)	7.71	(8.8)
Alcoa N-S	28	358	1.76	2.89	(0.0)	5.07	(0.0)	6.97	(2.9)
U.C. Med. Center	15	195	1.09	2.86	(1.0)	4.94	(2.4)	7.13	(0.7)
Rainer Tower	31	393	4.27	2.74	(5.2)	4.80	(5.1)	6.78	(5.6)
Century City	44	576	3.94	2.92	(1.0)	5.11	(1.0)	7.29	(1.5)
Average Period Ratios	--	---	----	2.89		5.06		7.18	
Uniform Shear Beam Period Ratios	--	---	----	3.0		5.0		7.0	

% = percent variation from average period ratios

425

Table 4.3.2: Comparative Locations of Node Points for Mode Shapes of the Actual Buildings, the Uniform Shear Beam and the Empirical Approximations

Node Point	Node Locations as Ratios of Total Height												
	Mode 1			Mode 2				Mode 3			Mode 4		
	Actual min., max.	Shear Beam	Empirical	Actual min., max.	Shear Beam	Empirical	Actual min., max.	Shear Beam	Empirical	Actual min., max.	Shear Beam	Empirical	
1 (base)	0. , 0.	0.	0.	0. , 0.	0.	0.	0. , 0.	0.	0.	0. , 0.	0.	0.	
2	- -	-	-	.747 .805	.667	.759	.482 ,.533	.400	.504	.345 ,.412	.286	.371	
3	- -	-	-	--- ---	---	---	.861 ,.902	.800	.880	.644 ,.693	.571	.688	
4	- -	-	-	--- ---	---	---	--- ---	---	---	.901 ,.929	.857	.925	

Table 4.3.3: Comparative Deflection Results for Exact and Approximate Static Analysis (UBC equivalent static loads)

Story	Response Quantity	Exact Analysis	Approximate Analyses	
			Empirical (%)	Shear Beam (%)
40	Shear (k)	739	739 -	739 -
	OTM(10 <sup>3</sup> k-in)	493	493 -	493 -
	Defl.(in.)	8.02	8.05 (+ 0.4)	7.16 (-10.7)
	Drift (in.)	0.167	0.236 (+41.3)	0.084 (-49.7)
20	Shear	1444	1444 -	1444 -
	OTM	3951	3951 -	3951 -
	Defl.	3.66	3.97 (+8.5)	4.32 (+18.0)
	Drift	0.217	0.187 (-13.8)	0.178 (-18.0)
2	Shear	1708	1708 -	1708 -
	OTM	8688	8688 -	8688 -
	Defl.	0.22	0.57 (-159.)	0.64 (+191.)
	Drift	0.184	0.188 (+2.2)	0.214 (+16.3)

% = percent variation from exact analysis results

Table 4.3.4: Comparative Results for Exact and Approximate Dynamic Analyses (for Blume Spectrum scaled to 0.4g peak ground acceleration)

Story	Response Quantity	Exact Analysis	Approximate Analyses	
			Empirical (%)	Shear Beam (%)
40	Shear (k)	3136	3174 (+1.2)	2922 (-6.8)
	OTM (10 <sup>3</sup> k-in)	1788	1921 (+8.0)	1646 (-7.4)
	Defl. (in.)	36.1	36.2 (+0.3)	34.8 (-3.6)
	Drift (in.)	0.71	1.08 (+52.1)	0.38 (-46.5)
20	Shear	7156	7310 (+2.2)	7137 (-0.3)
	OTM	18113	16646 (-8.1)	17164 (-5.2)
	Defl.	19.3	18.4 (-4.7)	22.2 (+15.0)
	Drift	1.05	0.95 (-9.5)	1.02 (-2.9)
2	Shear	9309	10238 (+10.0)	9494 (+2.0)
	OTM	39334	39880 (+1.4)	40582 (+3.2)
	Defl.	1.22	0.94 (-23.0)	1.31 (+7.4)
	Drift	0.91	0.94 (+3.3)	1.31 (+44.0)

% = percent variation from exact analysis results

Table 4.3.5: Comparative Results for Exact and Approximate Empirical Dynamic Analyses  
 (for Blume Spectrum scaled to 0.4g peak ground acceleration)

Story	Response Quantity	Exact Analysis $T_1=3.94$ sec.	Approximate Analyses (Empirical)					
			$T_1=3.55$ sec. (%)		$T_1=3.94$ sec. (%)		$T_1=4.33$ sec. (%)	
40	Shear (k)	3136	3446	(+9.9)	3174	(+1.2)	2935	(-6.4)
	OTM ( $10^3$ k-in)	1778	2086	(+17.3)	1921	(+8.0)	1777	(-0.1)
	Defl. (in.)	36.1	31.9	(-11.6)	36.2	(+0.3)	40.4	(+11.9)
	Drift (in.)	0.71	0.96	(+35.2)	1.08	(+52.1)	1.21	(+70.4)
20	Shear	7156	7937	(+10.9)	7310	(+2.2)	6753	(-5.6)
	OTM	18113	18068	(-0.3)	16646	(-8.1)	15376	(-15.1)
	Defl.	18.3	16.2	(-11.5)	18.4	(+0.6)	20.5	(+12.0)
	Drift	1.05	0.84	(-20.0)	0.95	(-9.5)	1.06	(+1.0)
2	Shear	9309	11109	(+19.3)	10238	(+10.0)	9462	(+1.6)
	OTM	39334	43286	(-10.1)	39880	(+1.4)	36833	(-6.4)
	Defl.	1.22	0.83	(-32.0)	0.94	(-23.0)	1.05	(-13.9)
	Drift	0.91	0.83	(-8.8)	0.94	(+3.3)	1.05	(+15.4)

% = percent variation from exact analysis results

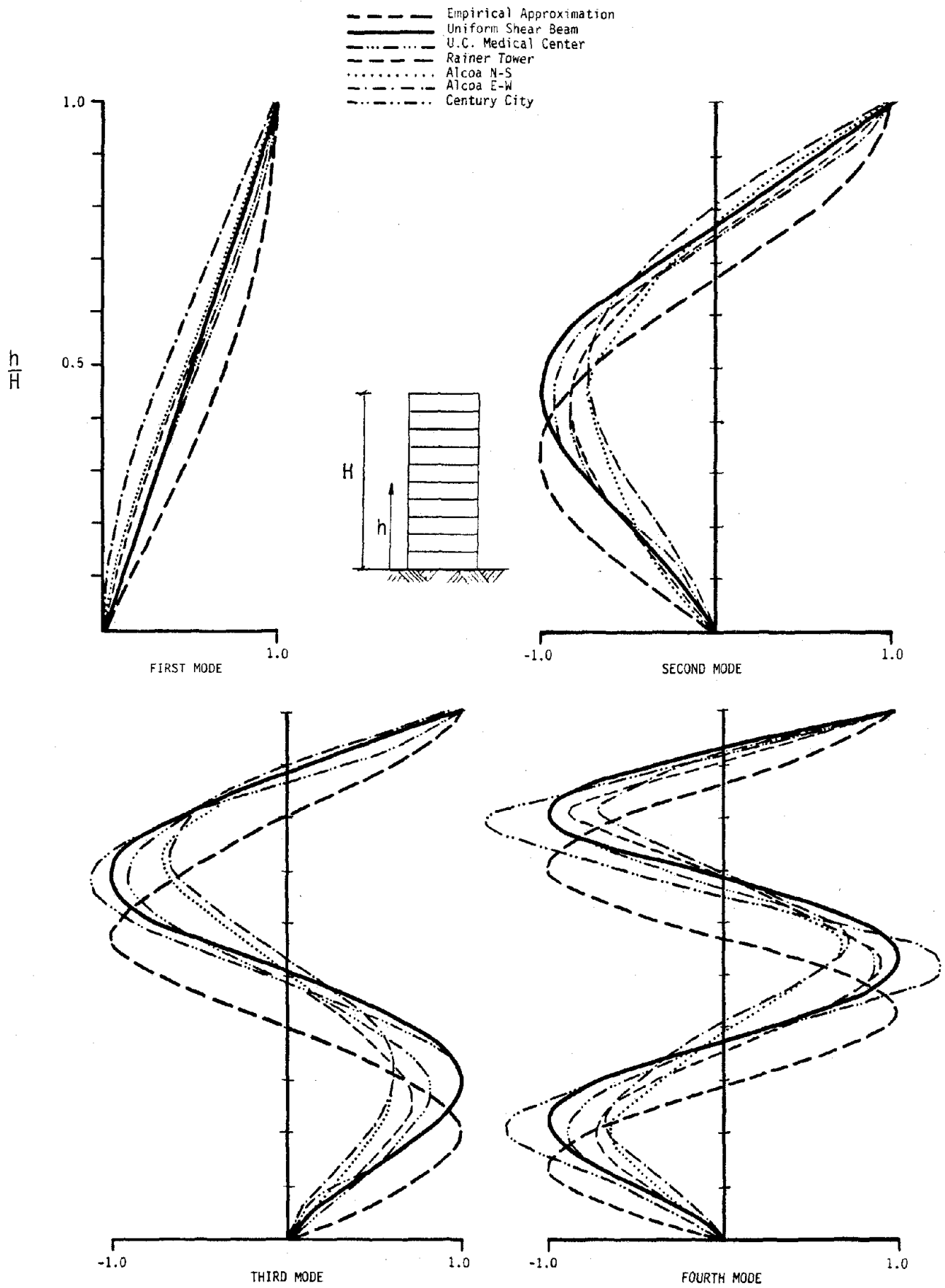
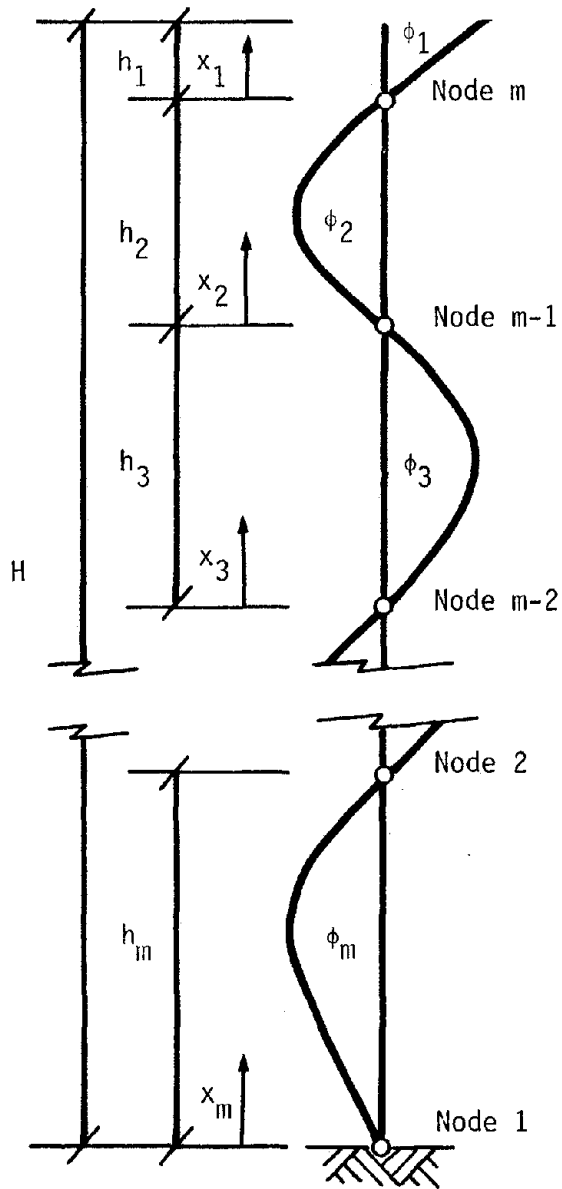


Figure 4.3.1: Approximate vs. Actual Mode Shapes of Multistory Buildings



$m^{\text{th}}$  Mode Shape defined by

$$\phi_1 = x_1/h_1$$

$$\phi_i = (-1)^{i-1} \cdot \sin(\pi x_i/h_i) \quad \text{for } 2 \leq i \leq m-1$$

$$\phi_m = (-1)^{m-1} \cdot \sin[\pi (x_m/h_m)^{1.357}]$$

$$h_i = a_i h_1 = (a_i/a_T) H$$

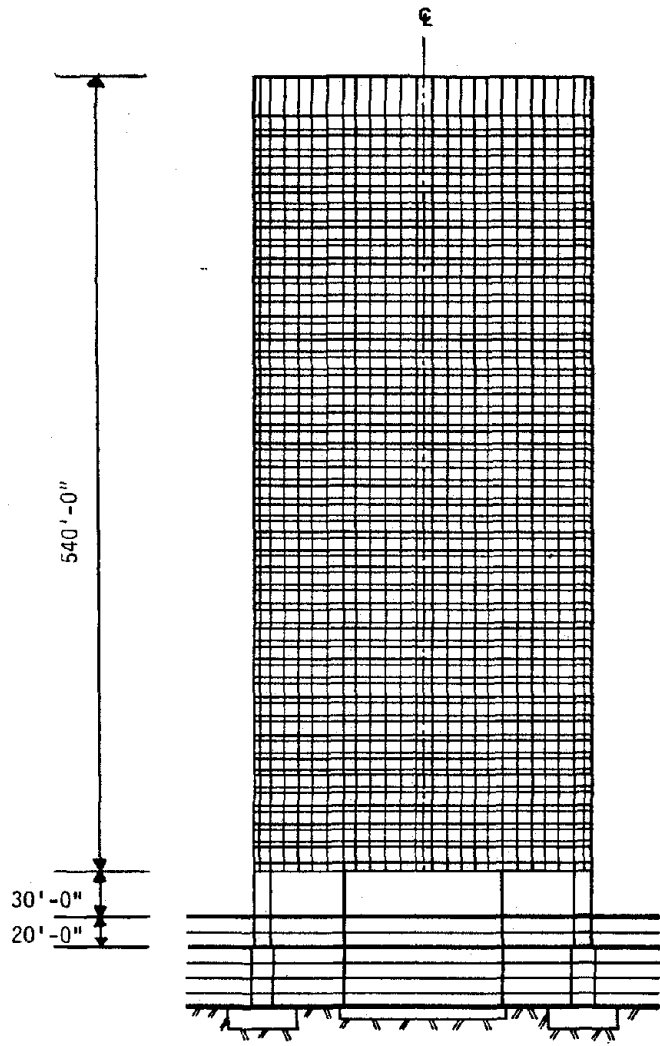
where

$$a_1 = 1.0$$

$$a_i = 1.0 + [(\pi-1) \cdot \left( \sum_{k=1}^{i-1} 1/k \right)] \quad \text{for } i \geq 2$$

$$a_T = \sum_{k=1}^m a_k$$

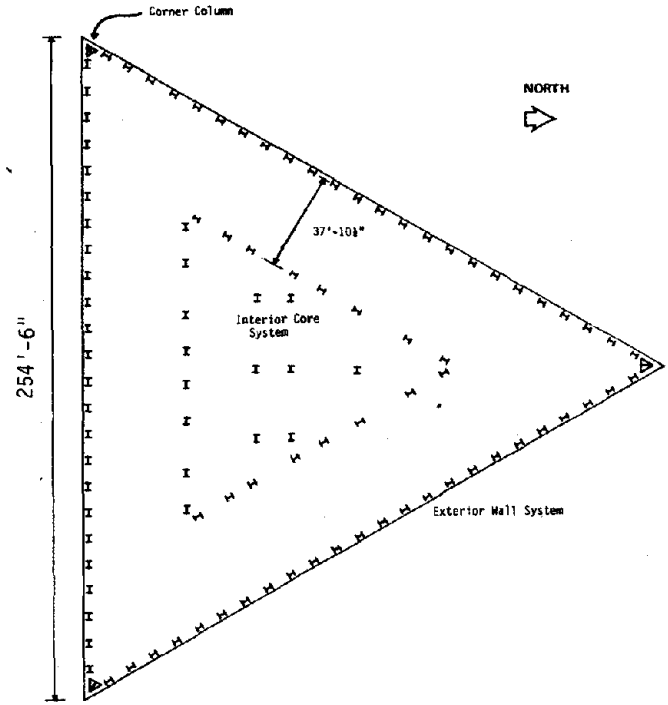
Figure 4.3.2: Empirical Mode Shape for  $m$ th Mode



Elevation

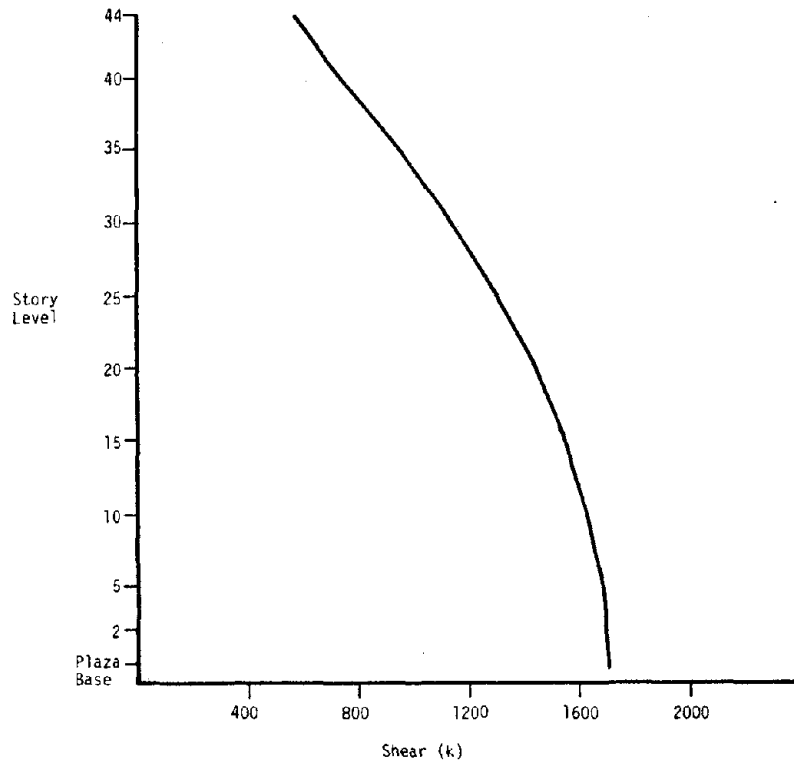
Roof  
42nd Floor

Second Floor  
Plaza Level  
Base Level  
Foundation Level

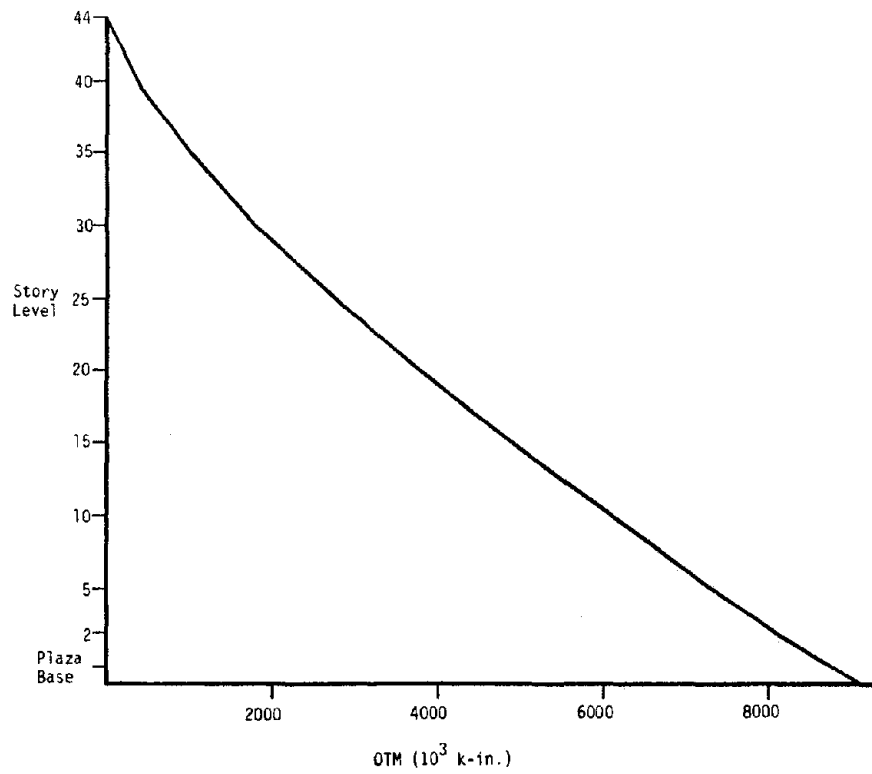


Plan

Figure 4.3.3: Century City Theme Tower Building



(a) Story Shears



(b) Story Overturning Moments

Figure 4.3.4: UBC Static Forces

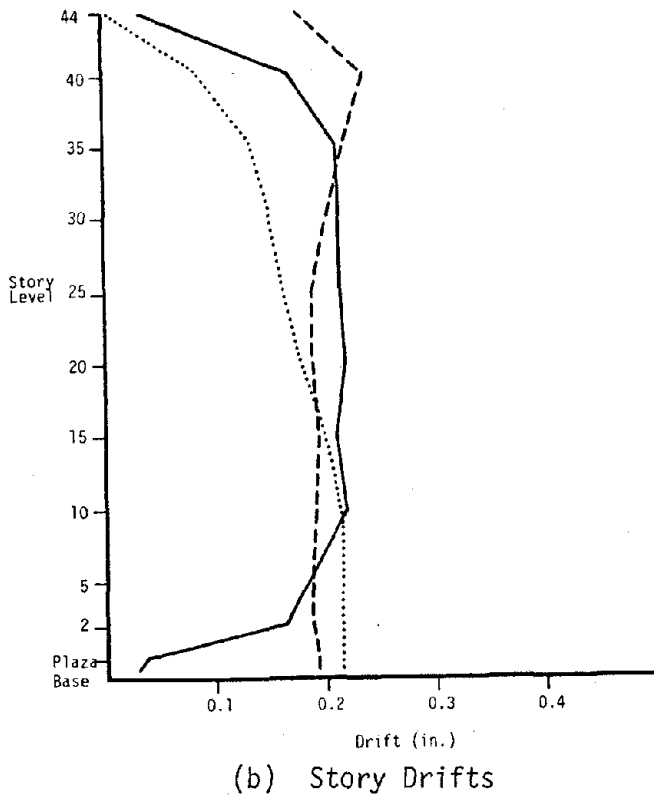
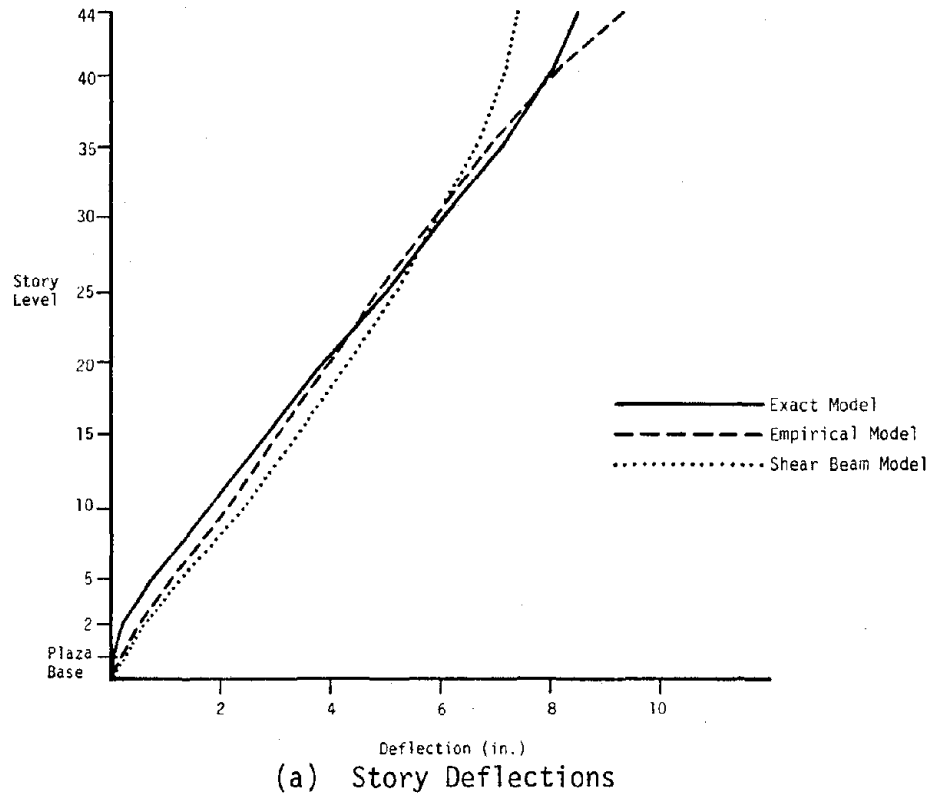


Figure 4.3.5: Approximate vs. Exact UBC Static Deflections

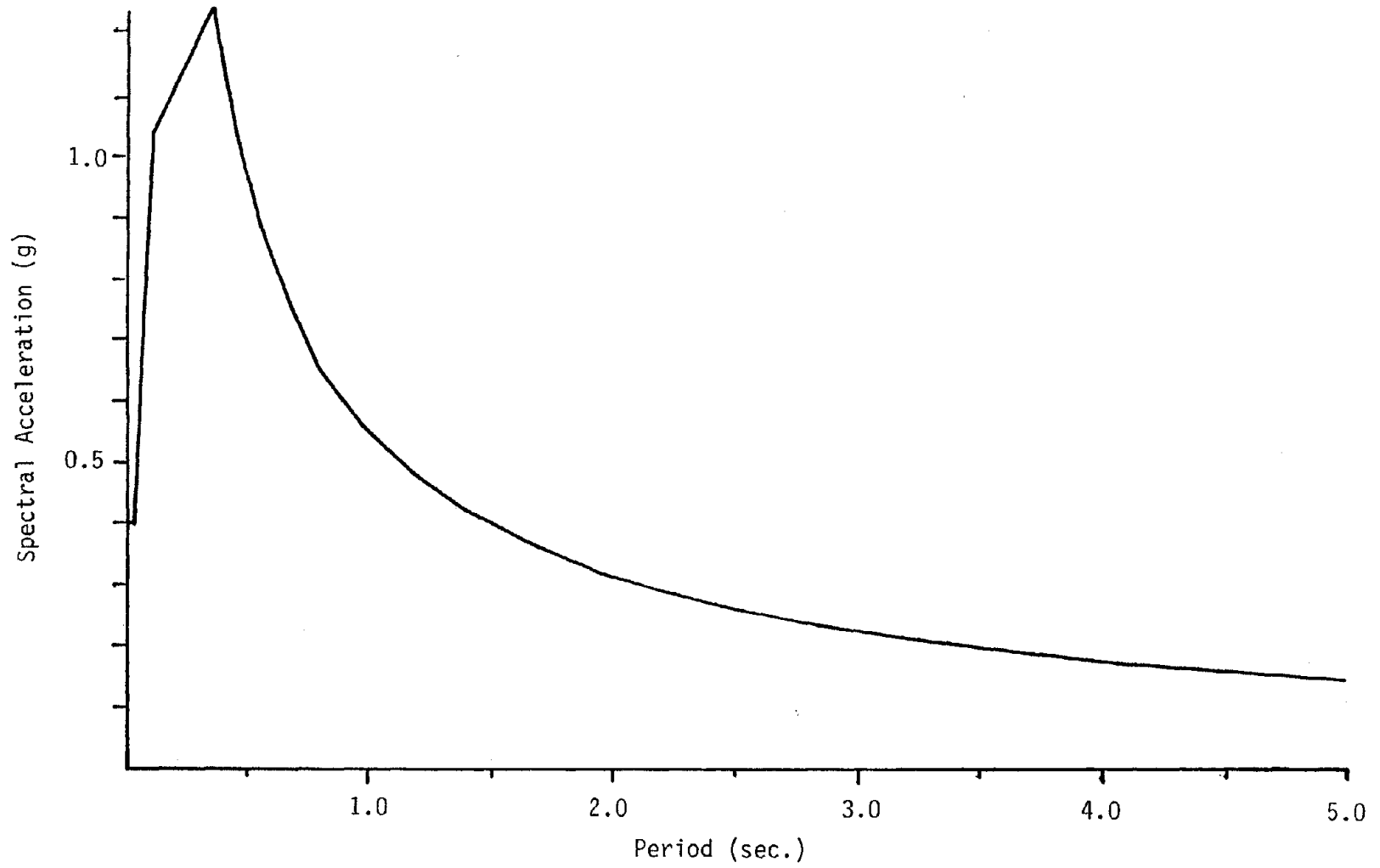
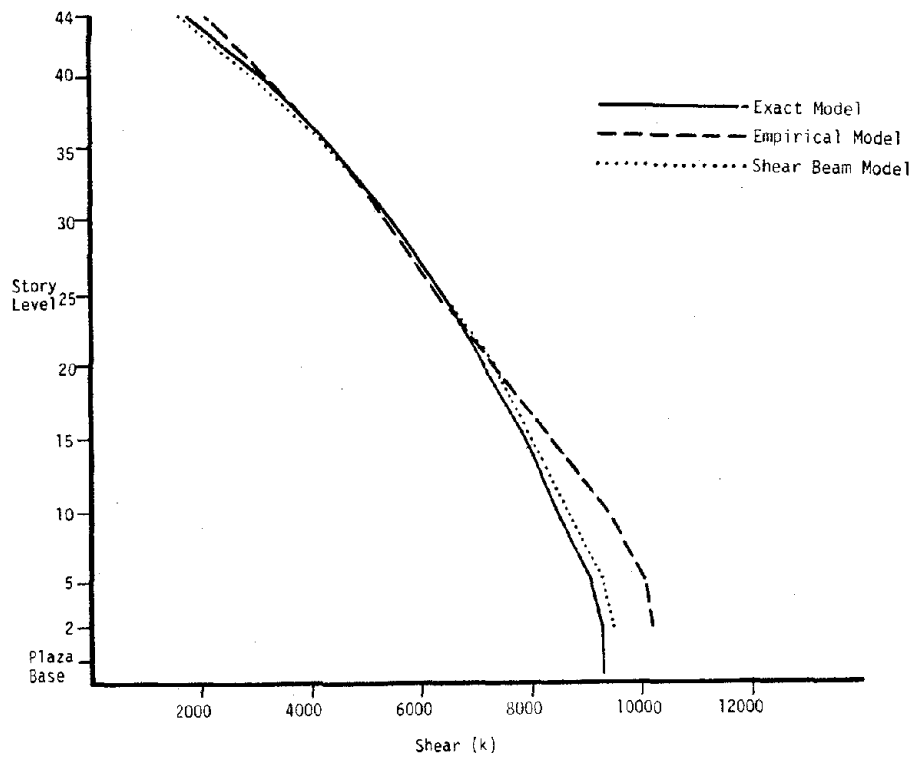
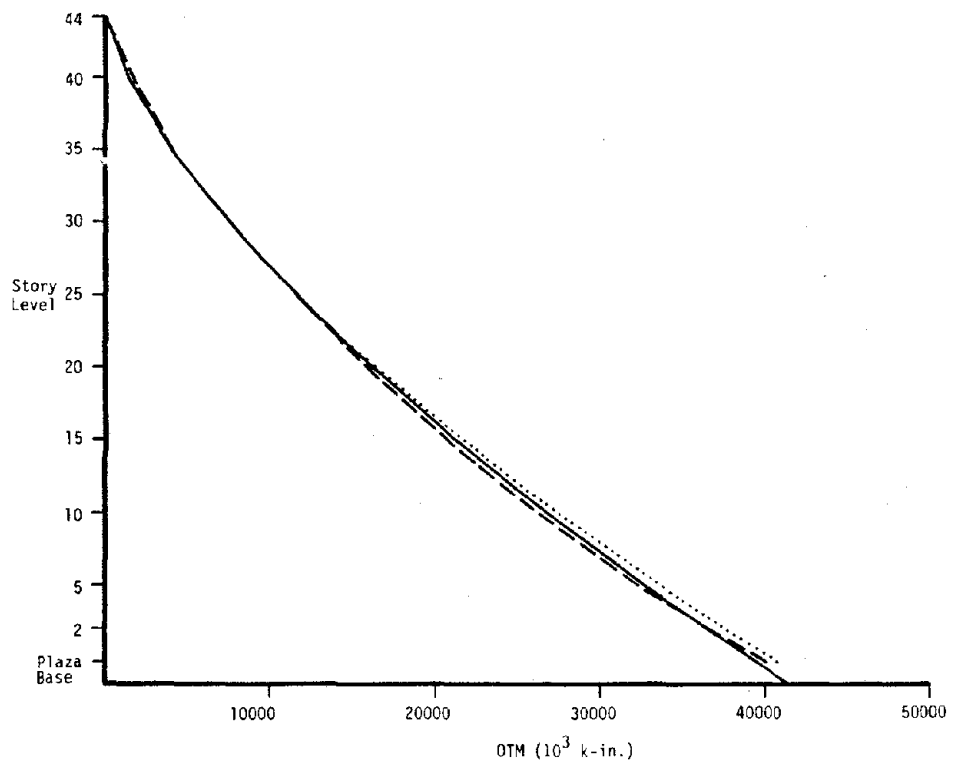


Figure 4.3.6: Blume Recommended Response Spectrum

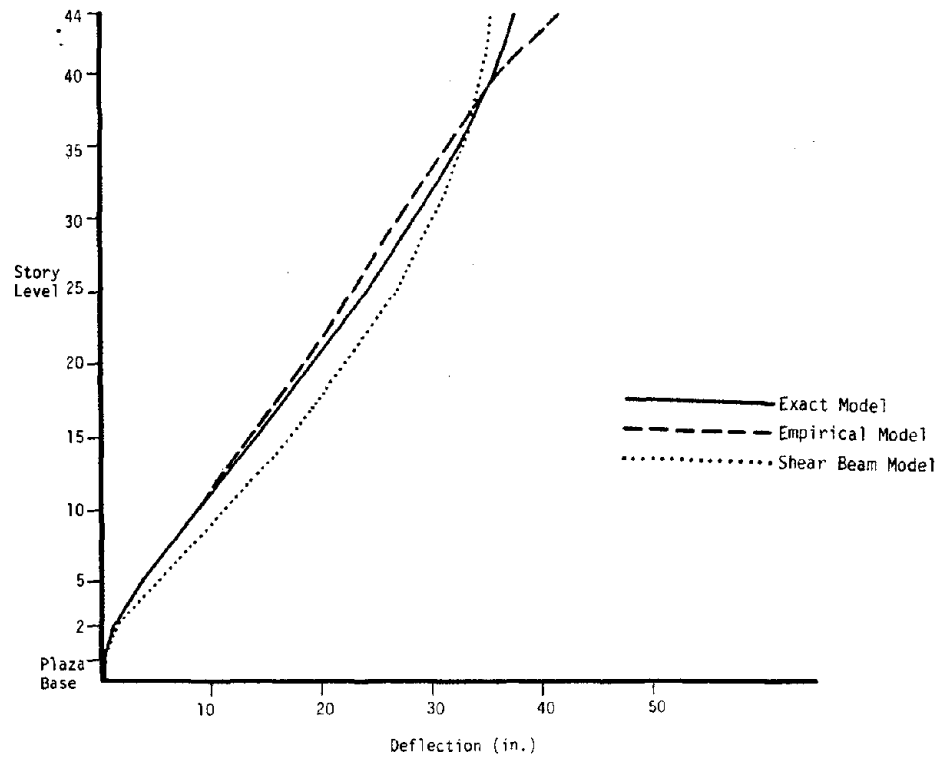


(a) Story Shears

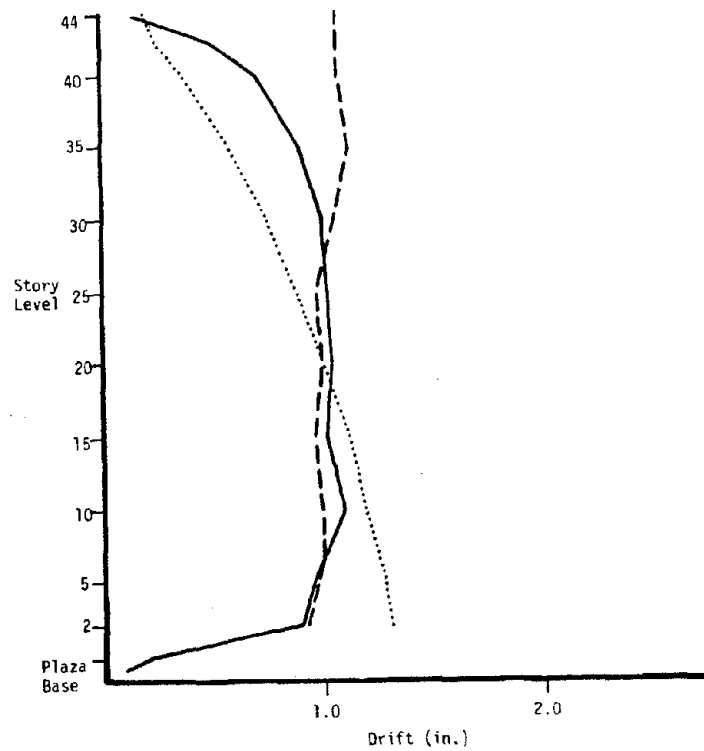


(b) Story Overturning Moments

Figure 4.3.7: Approximate vs. Exact Dynamic Force Response

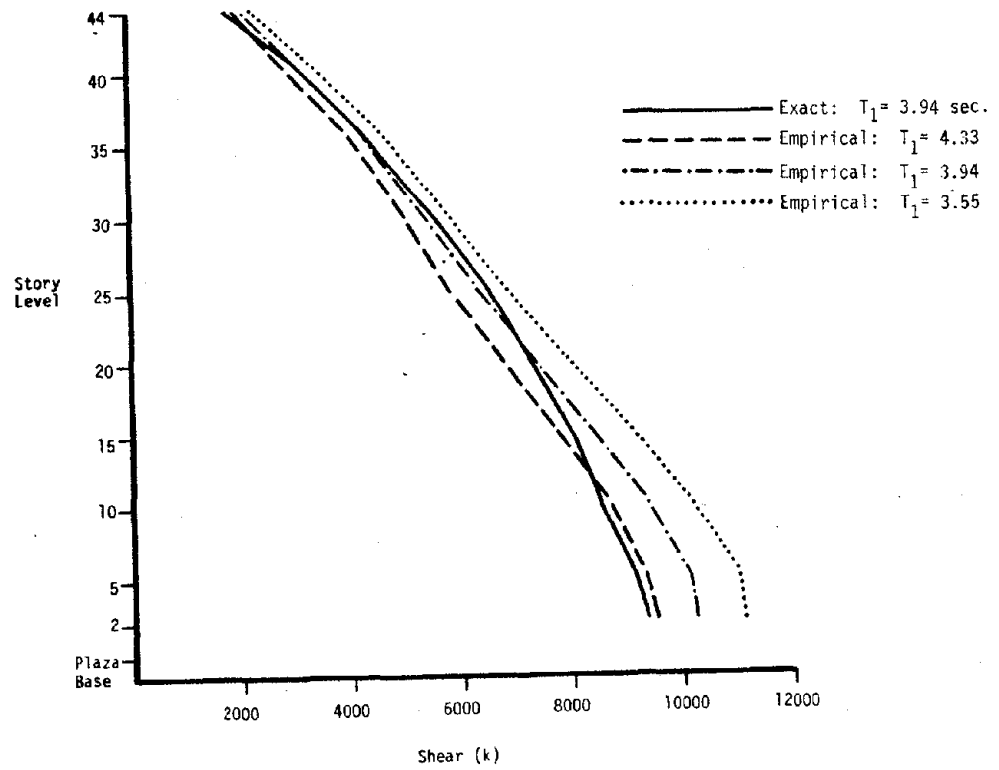


(a) Story Deflection

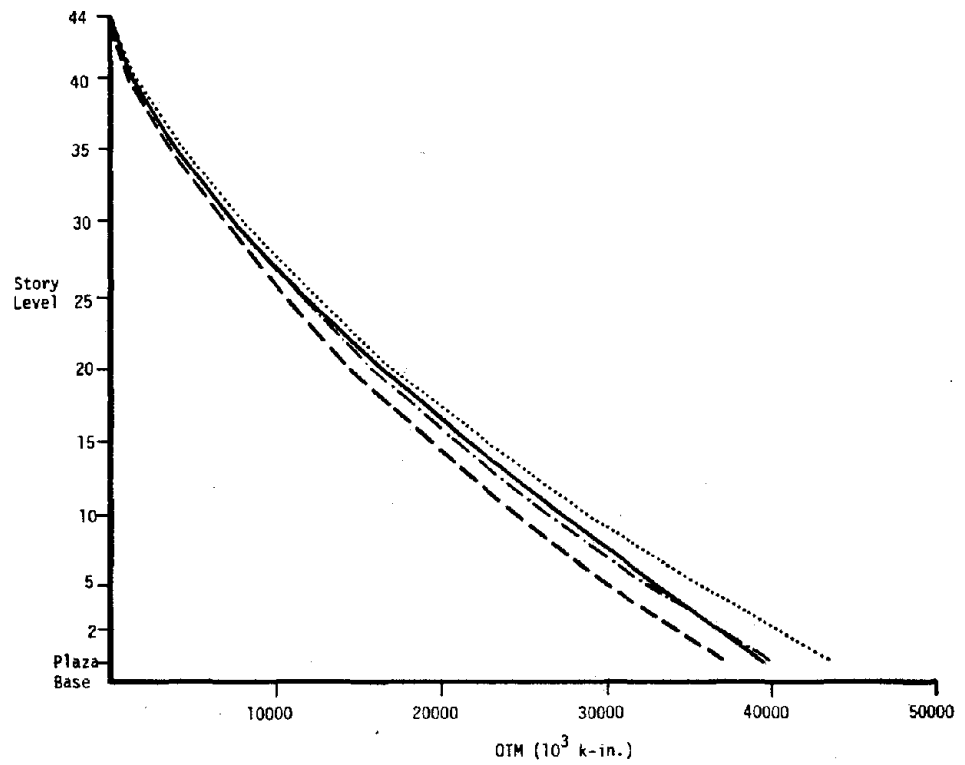


(b) Story Drifts

Figure 4.3.8: Approximate vs. Exact Dynamic Deflection Response

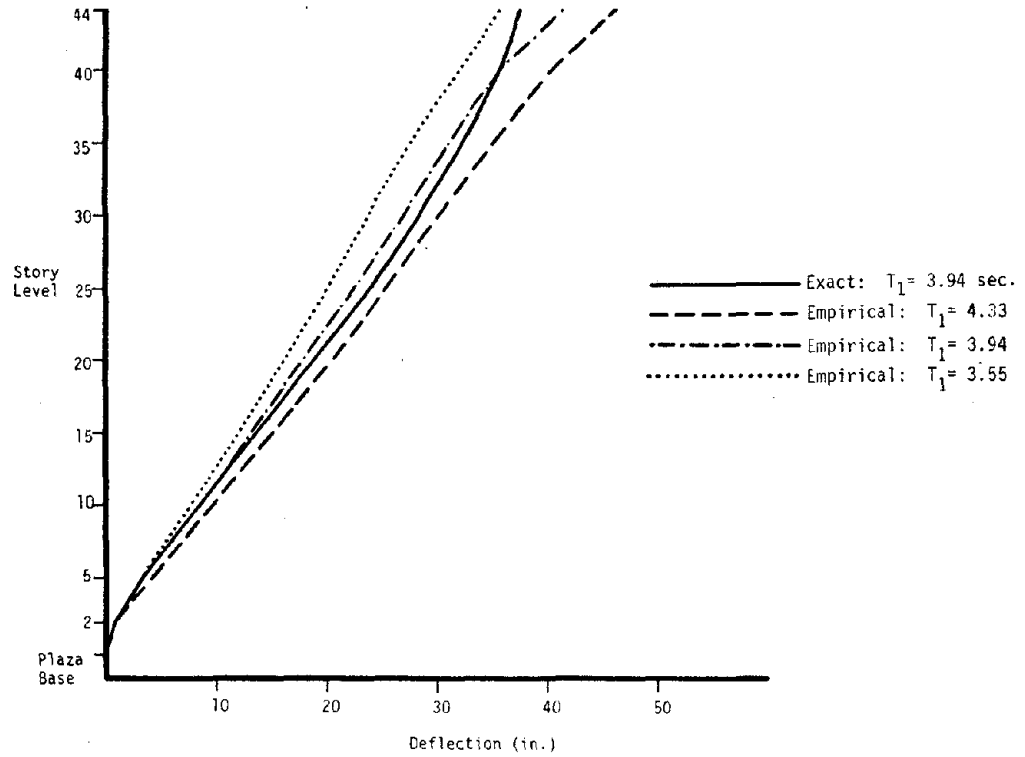


(a) Story Shears

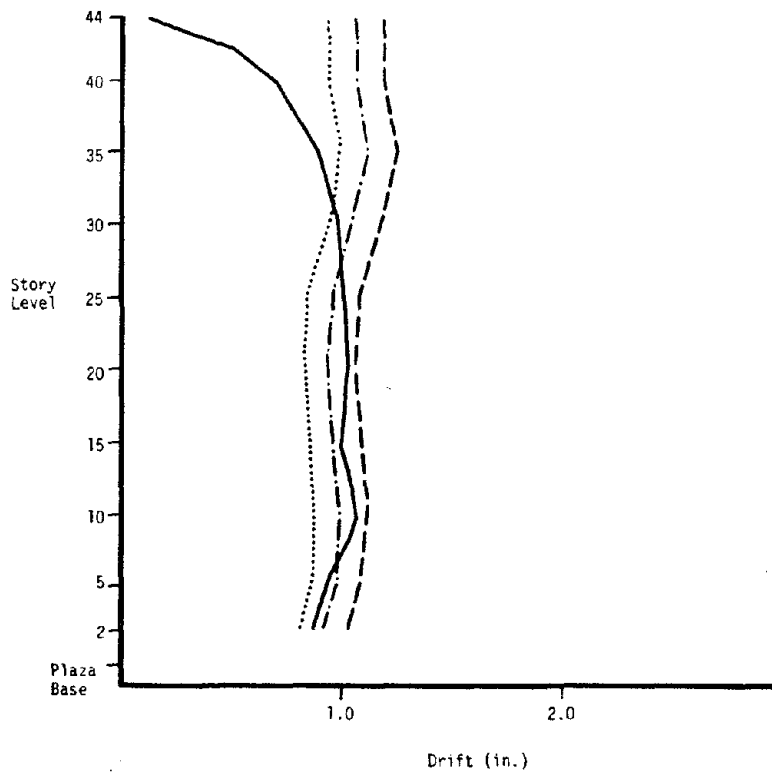


(b) Story Overturning Moments

Figure 4.3.9: Empirical Approximate vs. Exact Dynamic Force Response



(a) Story Deflections



(b) Story Drifts

Figure 4.3.10: Empirical Approximate vs. Exact Dynamic Deflection Response

Page Intentionally Left Blank

## CHAPTER 5

### GENERAL SUMMARY AND CONCLUSIONS

The primary objectives in earthquake resistant design of multistory buildings are: to provide a structure that remains relatively free of structural damage from a moderate earthquake which may be expected to occur at the building site during the design life; and, to ensure against collapse and associated possible loss of life from the largest credible earthquake that can occur at the site. To meet these design objectives, dynamic analysis by computer is often performed as part of the aseismic design process. State-of-the-art dynamic analysis of buildings for earthquake response involves the following general tasks: (1) development of ground motion characteristics which are believed to be representative of the local seismicity and soil conditions at the building site; (2) formulation of a numerical model which accurately reflects the dynamic properties of the building and application of analytical techniques which lead to good predictions of seismic response; and, (3) interpretation of response for conformance to the specific seismic design criteria being applied. These different analytical aspects are interrelated and must be integrated to produce an effective overall design approach. In developing representative ground motions for a particular site (task 1) which are to be consistent with the design objectives, two earthquakes of different intensities are often considered. The first is an earthquake which has only a moderate probability of being exceeded during the lifetime of the structure (a "maximum probable" earthquake); and, the second is an earthquake of greater intensity which has a small probability of being exceeded (a "maximum credible" earthquake). Generally, the structure is expected to resist the maximum probable earthquake with essentially elastic response; that is, with no significant yielding of the structural members. For the

maximum credible earthquake, substantial inelastic deformations may be allowed in the members but collapse must be avoided. In the development of numerical models and the application of analytical techniques for seismic analysis (task 2), a linear elastic formulation is usually used to predict response for both levels of earthquake intensity. However, the interpretations of the resulting responses differ in that separate design criteria are usually associated with each earthquake (task 3). Whereas elastic limit member design criteria are used for evaluating member performance for the maximum probable event, inelastic design criteria are used for evaluating member performance for the maximum credible event. Inelastic design procedures as applied in building design generally rely on the assumption that the inelastic deformations are well distributed throughout the structure and that the displacement levels resulting from the elastic analysis are reasonable estimates for the displacement levels that would actually occur during inelastic response to a maximum credible event. Based on this assumption, individual members can be checked for conformance to maximum allowable ductility demands using inelastic design criteria formulae.

The current study has focused primarily on the second general task relating to dynamic analysis mentioned above; that is, the development of numerical models and the application of analytical techniques to be used in linear elastic seismic analysis of multistory buildings. Since the foremost objective in the development of numerical models is to accurately represent actual building behavior, results obtained from full scale vibration tests have been used as a data base for performing correlative analytical studies on five modern multistory buildings. Several numerical models have been developed for each of the buildings wherein progressive modeling refinements have been made in order to produce improved estimates of the observed linear dynamic properties.

The correlative analyses performed show that the natural periods and mode shapes as determined from small amplitude vibration tests can be accurately predicted using practical analytical models of limited complexity developed based upon the actual detailed physical characteristics of the building. Fundamental natural periods calculated from the final numerical models are within 5% of the experimentally determined values for all of the buildings studied. However, the initial models based on simplified idealizations of the primary lateral force resisting systems have periods that are significantly larger than the experimentally observed values. In order to achieve correlation between experimental and analytical results, various secondary modeling aspects which might ordinarily be overlooked must be accounted for in the models. For the five buildings studied, secondary aspects that proved to be significant are: (1) allowance for the inherent rigidity in the beam-column connection regions (modeled with rigid joint zones); (2) modeling of nonplanar, intersecting frames allowing full three-dimensional compatibility; (3) inclusion of structural and nonstructural slab-girder composite action; (4) modeling of core frame systems which may be part of a secondary lateral and/or vertical force resisting system; and, (5) inclusion of nonstructural masonry block infill walls. The incorporation of these modeling aspects lead to increases in the fundamental mode generalized stiffnesses which range from 42% to 109% for the buildings studied. These large increases in stiffness indicate the importance of modeling the various secondary features in order to predict accurate small amplitude periods. In developing analytical models for larger amplitude motions, secondary nonstructural aspects such as slab-girder interaction (slabs not designed to act compositely) and infill walls may be neglected if it is judged that these components are unable to provide resistance at larger displacement levels. However, structural aspects such as rigid

joint zones, 3-D frame modeling and core frame modeling can be expected to contribute resistance at all displacement levels. Aspects such as these should be included in model development in order to obtain accurate period estimates. The use of an analytical model that neglects the above features will most likely lead to period estimates which are larger than those that would result during a moderate earthquake. Detailed modeling of structural and nonstructural systems extraneous to the lateral force resisting system (e.g. floor beams with non-moment connections, architectural cladding, electromechanical piping and ducts, etc.) was not required to achieve good period correlation. Unless these systems are composed of structurally non-isolated rigid elements of significant strength, they can be neglected in model development. The small influence of such systems may be more appropriately represented by use of an increased overall damping value in calculation of response spectrum amplitudes.

In addition to the excellent period correlation, the analytical mode shapes also compared well with those derived from the experimental studies. The location and relative deflection amplitudes of nodes and antinodes were predicted with good accuracy. In contrast to the natural periods, the analytical mode shapes were not significantly influenced by the various modeling refinements mentioned above. This result indicates that the secondary modeling aspects considered produce roughly uniform relative stiffening over the height of the building and suggests that it may be appropriate to represent the influence of secondary effects by simple factoring of the stiffness of the primary lateral force resisting system.

Similarities in the dynamic characteristics of the different buildings are apparent from the analytical studies performed. Ratios of fundamental to higher mode periods show close comparison among those study buildings having vertically regular framing systems. These ratios compare very well with the period ratios for a uniform

shear beam. Also, despite the differences in the total heights and framing systems of the buildings studied, striking similarities in the mode shapes exist among the different buildings. However, significant differences exist between the observed modes shapes of the buildings and those of a uniform shear beam. The similarities in the observed dynamic properties have led to the development of an empirical method for estimating higher mode periods given the fundamental period value and for estimating the corresponding mode shapes for regular multistory buildings of arbitrary height. These empirical formulations can be used to perform approximate static or dynamic analyses at the preliminary design stage prior to actual detailed member sizing as described in section 4.3.

In order to assess the influences of the various dynamic properties and modeling assumptions on the analytical response, dynamic seismic analyses have been performed on all buildings studied using the response spectrum method. From these analyses, it is observed that, although the fundamental mode is generally the most dominant contributor to earthquake response of multistory buildings, the contributions of higher modes are also significant. Greater relative contributions of higher modes are observed in taller, more flexible buildings. The relative importance of the higher modes on the total peak response depends upon the fundamental period of the building, the particular response quantity of interest, and the location being considered over the height of the building. For multistory buildings not having significant structural irregularities over their height, the first 4 to 6 modes for a single translational direction are usually adequate to capture all significant unidirectional response. However, if irregularities such as large stiffness discontinuities exist, several additional modes may be necessary to adequately capture response. Effective mass determinations should be made in order to insure that full

participation of the structure's mass is reflected in the analysis.

The response spectrum analyses also demonstrate the significant influence that the aforementioned secondary modeling aspects can have on the computed response. For the buildings studied, modeling of the various secondary features lead to increases in base shears ranging from +16% to +87%, increases in base overturning moment ranging from +13% to +112%, and decreases in roof deflection ranging from -1% to -27%. The degree of variation in the computed responses depend upon the amount of stiffness increase, the shape of the response spectrum used, the relative importance of the fundamental versus the higher modes, and the particular response quantity of interest. If a reasonable estimate of the stiffening effects of secondary modeling aspects can be made, the relationships presented in section 2.5 can be used to estimate the resulting variations in response quantities.

Results of equivalent static methods for seismic analysis as specified in current building code recommendations (UBC and ATC) have been compared with results of dynamic response spectrum analysis for all of the buildings studied. Three important observations relating to these two different approaches are noted. First, the results of the experimental and analytical studies indicate that the UBC and ATC empirical formulae have limited accuracy in predicting actual small amplitude fundamental periods. Since the natural period value ultimately controls response magnitude, the use of approximate periods calculated from codebook formulae can lead to large differences in seismic force values compared to those that would result from use of the actual small amplitude periods. Second, equivalent static response distributions may differ significantly from dynamic response distributions in some respects. Compared to dynamic analysis, the UBC equivalent static method tends to yield relative overestimations of story shear response in the mid- and upper-story regions and relative overestimations of overturning response in lower

story regions of multistory buildings. The ATC equivalent static method tends to overestimate response in the mid-story regions of the building but gives reasonably good estimates of overturning response by allowing application of an overturning reduction factor. In general, the differences between equivalent static and dynamic response distributions are amplified with increasing fundamental period and, consequently, are generally more pronounced for taller buildings. Third, although it is recognized that the equivalent static procedures as recommended by UBC and ATC base building design on force levels that are less than those expected during a major earthquake, the force levels as predicted by elastic analysis using spectra corresponding to major earthquakes indicate that, for multistory buildings, the difference in force levels are not as great as generally perceived. This results from conservatisms inherent in equivalent static procedures such as: fundamental period underestimation; response spectrum amplitude overestimations in the longer period range; fundamental modal mass overestimation; and , conservative mass estimates for dead weight and partition loads.

In addition to the correlative analyses performed for this study, certain selected topics have been addressed relating to seismic analysis of multistory buildings. These topics include: (1) analysis for P-  $\Delta$  effects in seismic response of buildings; (2) the comparative performance of different modal combination rules in response spectrum analysis; and (3) a method for performing approximate analysis of multistory buildings. It has been demonstrated how application of special analytical techniques relating to these topics can be used to give improved seismic response predictions in the analysis of multistory buildings. Detailed discussions of these topics and related analytical procedures are presented in Chapter 4 of this report.

In the performance of this study, several modifications to the

ETABS computer program have been made in order to extend its analytical capabilities and to produce results in a form most useful for building design purposes. It is felt that the added capabilities significantly enhance the ETABS program and will be useful to the practicing engineer in performing computer seismic analysis of multistory buildings. Therefore, this modified program, called SUPER-ETABS, has been made available for public distribution through the National Information Service for Earthquake Engineering.

Page Intentionally Left Blank

Page Intentionally Left Blank

## REFERENCES

1. American Institute of Steel Construction, Manual of Steel Construction, Eighth Edition, AISC, 1980.
2. American Petroleum Institute, "API Recommended Practice for Planning, Designing and Constructing Fixed Offshore Platforms," API-RP-2A, Twelfth Edition, January 1981.
3. Amrheim, J.F., Reinforced Masonry Engineering Handbook, Third Edition, Masonry Institute of America, Los Angeles, 1978.
4. Applied Technology Council, An Evaluation of a Response Spectrum Approach to Seismic Design of Buildings, ATC-2, September 1974.
5. Applied Technology Council, Tentative Provisions for the Development of Seismic Regulations for Buildings, NSF Publication 78-8, NBS Special Publication 510, U.S. Dept. of Commerce, Washington, D.C., June, 1978.
6. Arnold, P., Adams, P.F., and Lu, L.W., "Strength and Behavior of an Inelastic Hybrid Frame", Journal of the Structural Division, ASCE, Vol. 94, No. ST 1, January 1968, pp. 243-266.
7. Bathe, K.J., Wilson, E.L. and Peterson, F.E., "SAP IV - A Structural Analysis Program for Static and Dynamic Response of Linear Systems", Report No. EERC 73-11, Earthquake Engineering Research Center, University of California, Berkeley, 1973.
8. Bertero, V.V., Herrera, R.A., and Mahin, S.A., "Establishment of Design Earthquakes - Evaluation of Present Methods," Proceedings, International Symposium on Earthquake Structural Engineering, August 1976, pp. 551-580.
9. Blume, J.A., Sharpe, R.L. and Dalal, J., "Recommendations for Shape of Earthquake Response Spectra," report prepared for the Directorate of Licensing, United States Atomic Energy Commission, 1973.
10. Bouwkamp, J.G., "An Investigation for the Earthquake Resistant Design of Large-Size Welded and Bolted Girder to Column Connections", Proceedings, Third World Conference on Earthquake Engineering, Vol. 4, New Zealand, 1965.
11. Clough, R.W., Penzien, J., Dynamics of Structures, McGraw-Hill, New York, 1975.
12. Council on Tall Buildings and Urban Habitat, Structural Design of Tall Steel Buildings, ASCE, New York, 1979.
13. Degenkolb, H.J., "A Study of the P- $\Delta$  Effect", Structural Moments, Structural Engineers Association of Northern California, No. 9, June 1981.
14. Der Kiureghian, A., "On Response of Structures to Stationary Excitation," Report No. UCB/EERC-79/32, Earthquake Engineering Research Center, University of California, Berkeley, California, 1979.

Preceding pages blank

15. Der Kiureghian, A., "A Response Spectrum Method for Random Vibrations," Report No. UCB/EERC-80/15, Earthquake Engineering Research Center, University of California, Berkeley, California, 1980.
16. Driscoll, G. C., "Lehigh Conference on Plastic Design of Multistory Frames - A Summary", Eng. Journal, AISC, 3, No. 2, April 1966.
17. Goel, S.C., "P- $\Delta$  and Axial Column Deformation in Aseismic Frames," Journal of the Structural Division, ASCE, Vol. 95, No. ST 8, August 1969, pp. 1693-1717.
18. Goodman, L.E., Rosenblueth, E., and Newmark, N.M., "Aseismic Design of Firmly Founded Elastic Structures," Trans. ASCE Vol. 120, 1955, pp. 782-802.
19. Hartz, B.J., "Matrix Formulation of Structural Stability Problems", Journal of the Structural Division, ASCE, Vol. 91, No. ST 6, December 1965, pp. 141-157.
20. International Conference of Building Officials, Uniform Building Code, 1979.
21. Jennings, P.C. and Husid, R., "Collapse of Yielding Structures During Earthquakes", Journal of the Engineering Mechanics Division, ASCE, Vol. 94, No. EM 5, October 1968, pp. 1045-1066.
22. Mahin, S.A. and Bertero, V.V., "An Evaluation of Inelastic Seismic Design Spectra," Journal of the Structural Division, ASCE, Vol. 107, No. ST9, September 1981, pp. 1777-1795.
23. Maison, B.F. and Neuss, C.F., "SUPER-ETABS: An Enhanced Version of the ETABS Program," Technical Report to the National Science Foundation, J.G. Bouwkamp, Inc., January 1983.
24. Martin, P.P. and Seed, H.B. "MASH - A Computer Program for the Non-Linear Analysis of Vertically Propagating Shear Waves in Horizontally Layered Deposits," Report 78-23, Earthquake Engineering Research Center, University of California, Berkeley, 1978.
25. Meravich, A.T. and Nicoletti, J.P. "Eccentric Bracing in Tall Buildings", Journal of the Structural Division, ASCE, Vol. 108, No. ST9, September 1982, pp. 2066-2080.
26. Newmark, N.M., and Hall, W.J. "Procedures and Criteria for Earthquake Resistant Design," Building Practices for Disaster Mitigation, National Bureau of Standards, Building Science Series 46, February 1973.
27. Newmark, N.M., "A Study of Vertical and Horizontal Spectra," report prepared for the Directorate of Licensing, United States Atomic Energy Commission, Report WASH-1255, April 1973.
28. Newmark, N.M. and Rosenblueth, E., Fundamentals of Earthquake Engineering, Prentice Hall, Englewood Cliffs, N.J., 1971.

29. Petrovski, J., Stephen, R.M., Gartenbaum, E. and Bouwkamp, J.G., "Dynamic Behavior of a Multistory Triangular Shaped Building," Report No. EERC 76-3, Earthquake Engineering Research Center, University of California, Berkeley, 1976.
30. Przemieniecki, J.S., Theory of Matrix Structural Analysis, McGraw-Hill, New York, 1968.
31. Rea, D., Bouwkamp, J.G. and Clough, R. W., "The Dynamic Behavior of Steel Frame and Truss Buildings," American Iron and Steel Institute, Bulletin No. 9, 1968.
32. Rea, D., Shah, A.A., and Bouwkamp, J.G., "Dynamic Behavior of a High-Rise Diagonally Braced Building", Report No. EERC 71-5, Earthquake Engineering Research Center, University of California, Berkeley, 1971.
33. Rosenblueth, E., "Slenderness Effects in Buildings", Journal of the Structural Division, ASCE, Vol. 91, No. ST 1, February 1965, pp. 229-252.
34. Rosenblueth and Elorduy, J., "Response of Linear Systems to Certain Transient Disturbances," Proceedings, Fourth World Conference on Earthquake Engineering, Vol. 1, Santiago, Chile, 1969.
35. Schnabel, P.B., and Lysmer, J., "SHAKE - A Computer Program for Earthquake Response Analysis of Horizontally Layered Sites," Report 72-12, Earthquake Engineering Research Center, University of California, Berkeley, 1972.
36. Seed, H.B., Ugas, C. and Lysmer, J., "Site-dependent Spectra for Earthquake-resistant Design," Report No. UCB/EERC 74-12, Earthquake Engineering Research Center, University of California, Berkeley, California, 1974.
37. Seed, H.B., Ugas, C., and Lysmer, J., "Site Dependent Spectra for Earthquake Resistant Design," Bulletin of the Seismological Society of America, Vol. 66, No. 1, February 1976, pp. 221-244.
38. Singh, A.K., Chu, S.L. and Singh, S., "Influence of Closely Spaced Modes in Response Spectrum Method of Analysis," Proceedings of the Specialty Conference on Structural Design of Nuclear Plant Facilities, Vol. 2, Chicago, 1973.
39. Stephen, R.M., Hollings, J.P., Bouwkamp, J.G., "Dynamic Behavior of a Multistory Pyramid Shaped Building," Report No. EERC 73-17, Earthquake Engineering Research Center, University of California, Berkeley, 1973.
40. Stephen, R.M., Wilson, E.L., Bouwkamp, J.G., and Button, M., "Dynamic Behavior of a Pedestal-Base Multistory Building", Report No. EERC 78-13, Earthquake Engineering Research Center, University of California, Berkeley, 1978.
41. Structural Engineers Association of California, Recommended Lateral Force Requirements and Commentary, SEAOC Seismology Committee, 1980.
42. Structural Engineers Association of California, "Suggested Procedures for Developing Seismic Ground Motions," SEAOC Seismology Committee, April 1979.

43. Structural Engineers Association of Southern California, "Seismic Analysis by Computer", SEAOSC Electronic Computation Committee, 1977.
44. Timoshenko, S.P. and, Gere, J.M. Theory of Elastic Stability, McGraw-Hill, New York, 1961.
45. Trifunac, M.D., "Forecasting the Spectral Amplitudes of Strong Ground Motion," Sixth World Conference on Earthquake Engineering. New Delhi, India, 1977.
46. U.S. Nuclear Regulatory Commission, "Design Response Spectra for Seismic Design of Nuclear Power Plants," Regulatory Guide 1.60, Washington, D.C.: Directorate of Regulatory Standards, 1973.
47. U.S. Nuclear Regulatory Commission, "Combining Modal Responses and Spatial Components in Seismic Response Analysis," Regulatory Guide 1.92, Revision 1, 1976.
48. Veterans Administration, Office of Construction, "Earthquake Resistant Design Requirements for VA Hospital Facilities," Handbook H-08-8, 1973.
49. Wilson, E.L., Hollings, J.P. and Dovey, H.H., "Three Dimensional Analysis of Building Systems (extended version)", Report No. UCB/EERC 75-13, Earthquake Engineering Research Center, University of California, Berkeley, California, 1975.
50. Wilson, E. L., Der Kiureghian, A. and Bayo, E.P., "A Replacement for the SRSS Method in Seismic Analysis," Earthquake Engineering and Structural Dynamics, Vol. 9, 1981, pp. 187-194.